PROCESS REQUIREMENTS FOR PRECISON GRINDING

STEPHEN EBBRELL

A thesis submitted in partial fulfilment of the requirements of Liverpool John Moores University for the degree of Doctor of Philosophy

September 2003

PAGE/PAGES EXCLUDED UNDER INSTRUCTION FROM UNIVERSITY

PAGE NUMBERING AS ORIGINAL

ABSTRACT

An investigation into process requirements for precision grinding was undertaken. The work included a study of the technological requirements and their economic implications. A high technology prototype grinding machine was used, known as the Suprema, to establish the effects of grinding at high speed using a vitrified CBN wheel. Comparisons were made with results from work carried out using conventional abrasives and vitrified CBN at conventional speed on a standard CNC cylindrical grinding machine. The research was based on two workpiece materials, namely, AISI 52100 an easy-to-grind bearing steel and Inconel 718 a difficult-to-grind nickel based alloy.

The Suprema was designed to have high dynamic and static stiffness. Excitation tests revealed that the dynamic characteristics of the machine were good. However, it was found that the machine static stiffness was low. Despite this the performance of the machine was not noticeably impaired in terms of workpiece surface roughness or roundness. This was attributed to the good dynamic characteristics of the machine.

A two level experimental arrangement was used to establish the effects of process parameters. Grinding with CBN at a high wheelspeed was found to lead to improved workpiece quality, high G-ratio and long re-dress life. This had a significant effect on reducing process costs. A cost model, sensitive to the effects of process parameters and workpiece quality, was developed. Through this it was shown that high-speed grinding with vitrified CBN provides a step change in the performance and economics of the grinding process.

For both the easy and the difficult-to-grind workpiece material, significant advantages were gained using vitrified CBN compared with using aluminium oxide at conventional speed on a standard CNC cylindrical grinding machine. For the material AISI 52100, conventional speed vitrified CBN was more effective than a sol gel abrasive. However, for both workpiece materials high-speed grinding using a vitrified CBN wheel gave overwhelmingly superior workpiece quality at significantly lower cost. Wheel costs were found to be negligible and labour costs greatly reduced when grinding at high speed using vitrified CBN.

ACKNOWLEDGEMENTS

I would like to thank my director of studies, Professor W.B. Rowe for his invaluable guidance and help throughout the course of the work. Thanks are also given to Dr. Xun Chen for his guidance at the beginning of the project.

Acknowledgements are also extended to EPSRC for grant support and to the collaborating partners, Castrol, Dittel, Jones and Shipman, Rolls Royce, Timken and Wendt Boart for financial support, advice and practical assistance.

Finally I would like to thank everyone at AMTTREL especially Mr. P.D. Wright and Mr. P. Moran for their sustained enthusiasm, help and encouragement throughout.

NOMENCLATURE

a	Applied depth of cut
a_e	The true depth of cut
a_d	Depth of dressing increment
A_{max}	Resonance amplitude
b_d	Effective width of the dressing tool
b_s	Wheel width
c	Workpiece specific heat capacity
c_l	Labour cost per unit time including an overhead contribution
C_l	Labour cost per part including an overhead contribution
C_m	Machine cost per part
C_{mc}	The purchase cost of the machine tool
C_s	Wheel cost per part
C'_t	Total cost per part including machine tool purchase costs spread over the payback period
C_{wd}	Dressing cost per unit volume of material removed
C_{wh}	Handling cost per unit volume of material removed
C_{wl}	Labour cost per unit volume of material removed
C_{ws}	Wheel cost per unit volume of material removed
d_e	Equivalent wheel diameter
d_s	Wheel diameter
d_{ss}	Stand-off distance
d_w	Workpiece diameter
d_{smax}	Maximum wheel diameter
d_{smin}	Minimum wheel diameter
d_{ww}	Stock removed from workpiece diameter
e_c	Specific energy
e_{cc}	Specific energy convected by the grinding chips
e_{cf}	Specific energy convected by the fluid
E	Youngs modulus
F_t	Tangential grinding force

F_n	Normal grinding force
h_{eq}	Equivalent chip thickness
h_m	Maximum uncut chip thickness
I	Second moment of area
k_a	Contact stiffness
k_c	Grinding force coefficient
k_{dyn}	Dynamic stiffness
k_e	Effective stiffness
k_{mc}	Machine stiffness
k_r	Wheel wear resistance
k_s	Wheelhead stiffness
$k_{tailstock}$	Tailstock stiffness
k_w	Overall stiffness of workhead, workpiece and tailstock system
$k_{workhead}$	Workhead stiffness
$k_{workpiecep}$	Workpiece stiffness
l_e	Real contact length
L	Grain spacing
n_d	Number of dressing passes
N_d	Number of parts per dress
N_l	Number of parts per unit time
N_{mc}	The number of parts produced during a specified payback period
P	Grinding power
q_{ch}	Heat dissipated to grinding chips
q_f	Heat dissipated to grinding fluid
q_s	Heat dissipated to grinding wheel
q_t	Total heat generated in the grinding zone
q_w	Heat dissipated to workpiece
Q_w	Volumetric removal rate
Q'_w	Specific volumetric removal rate
r_o	Wear flat contact radius
r_s	Radial wheel wear per dress

s	Dwell time
t_d	Dressing time
t_s	The cycle time per part
u	Infeed
U_d	Dressing overlap ratio
v_d	Dressing feedrate
v_f	Infeed rate
v_r	Rotary dresser surface speed
v_s	Wheel surface speed
v_w	Workpiece surface speed
V_s	Volume of wheel wear
V_w	Volume of material removed
V'_w	Specific volume of material removed
w	Load
x	Displacement
$\ddot{x}$	Acceleration
y_a	Contact deflection
y_m	Machine deflection
y_s	Deflection of wheelhead
y_t	Payback period
y_w	Deflection of workpiece
β	Workpiece thermal contact coefficient = $(\kappa\rho c)_w^{1/2}$
δ_s	Radial amount of wheel wear
δ_w	Radial amount of workpiece material removed
θ_a	Workpiece ambient temperature
κ	Workpiece thermal conductivity
κ_g	Coefficient of thermal conductivity for abrasive
ρ	Density
τ_w	Time for one revolution of workpiece.
ω	Angular frequency

CONTENTS

CHAPTER 6. PROCESS REQUIREMENTS FOR COST EFFECTIVE PRECISION GRINDING OF AISI 52100

CHAPTER 7. PROCESS REQUIREMENTS FOR COST EFFECTIVE PRECISION GRINDING OF INCONEL 718

APPENDIX B

APPENDIX C

LIST OF FIGURES

LIST OF TABLES

CHAPTER 1. INTRODUCTION

1.1 Background

One of the greatest challenges when seeking to advance the technical and scientific aspects of a process is to overcome what has been termed the economic straight-jacket [1]. This has been a difficulty in advancing the application of the CBN grinding process. While it is now established as technically successful for some applications, it has not had the widespread impact on grinding practice once envisaged. At present there are some industries using CBN for specific applications. An example of this is the automotive industry where most camshafts are now ground using vitrified CBN [2]. However, many industries such as the bearing and aerospace industry have still to be convinced of the ability to produce the required quality and reduce costs. To accomplish economic viability, wheel and labour costs per part must be cut while maintaining or improving target quality. The process must be judged using a 'total cost accounting' philosophy and not by initial costs alone which are high. It is widely believed that high speed grinding is the key to technical and economic success with vitrified CBN. This has implications for increased costs of the grinding wheel, the machine tool and the delivery of coolant. To support a move to high-speed CBN grinding a detailed understanding of process and system requirements is needed. Only by gaining and applying such knowledge, can the vitrified CBN grinding process be tested and its performance appraised objectively. There is therefore a need to establish economic relationships between process parameters, grinding performance and system requirements. The hypothesis was that high-speed CBN grinding allows total costs to be reduced while maintaining or improving quality. In accordance with this, the following aims and objectives were set.

1.2 Aim

To establish if high speed grinding using vitrified CBN offers the benefits predicted by theory and leads to a reduction in process costs without losing target workpiece quality.

1.3 Objectives

a. To investigate the design, characteristics and performance of a purpose built high speed grinding machine.
b. To investigate how dressing and cycle parameters affect performance when grinding an easy-to-grind material with vitrified CBN.
c. To investigate how dressing and cycle parameters affect performance when grinding a difficult-to-grind material with vitrified CBN.
d. To determine if high-speed grinding offers a cost benefit to justify the increased complexity and cost of a suitable high-speed grinding machine.
e. Establish if step changes in the grinding process can be achieved when moving from:
    i. Grinding with aluminium oxide wheels to grinding with vitrified CBN wheels at conventional speeds.
    ii. Grinding with vitrified CBN wheels at conventional speed to grinding with vitrified CBN wheels at high speed.
f. To propose process requirements for cost effective precision grinding.

1.4 Scope

The first part of the thesis reviews previous work on CBN grinding, high-speed machine tool design and optimisation of process parameters for high-speed grinding. Theory is then presented defining the factors that affect process costs.

The experimental work was predominantly based on a purpose built high-speed precision grinding machine. The machine known as the Suprema, was designed and built as part of an earlier investigation by Jones and Shipman together with RWTH Aachen and other industrial collaborators. RWTH Aachen carried out an extensive study of the machine tool static, dynamic and thermal characteristics. In this project, an investigation was carried out to determine how the machine tool behaved from a performance and economic perspective. Major structural and system problems were experienced which caused considerable initial difficulty in using the machine. These problems were overcome and it was then possible to carry out experiments and consider machine tool requirements in relation to grinding

performance. Conclusions are reached on the characteristics necessary for economic success. Critical aspects of machine design were identified for high-speed performance in precision grinding.

The main experimental work was carried out on two workpiece materials, namely, the bearing steel AISI 52100 and the nickel based alloy Inconel 718. These workpiece materials were selected, for their contrasting grinding characteristics. AISI 52100 is widely used for manufacturing bearings and is considered an easy-to-grind material. In the bearing industry this material is ground successfully using conventional abrasives at conventional speeds. With regard to AISI 52100, the focus of this investigation was on determining if high speed grinding with vitrified CBN offers significant advantages leading to a step change in grinding development. This was judged in terms of performance and costs. Experimental work during this part of the investigation allowed the Suprema to be tested and its design assessed.

Inconel 718 is a very different material to AISI 52100 and is used throughout the aerospace industry. Inconel 718 is considered to be a difficult-to-grind material. Its mechanical properties allow it to remain creep resistant at high temperatures making it ideal for turbine blades. Inconel 718 is difficult to grind due to the formation of long continuous grinding chips that tend to load the wheel. Therefore, process requirements for grinding this material at conventional speed using conventional abrasives are included in this part of the investigation. A Jones and Shipman Series 10 machine was used to carry out research at conventional wheelspeeds, that is, up to 45m/s. Three aluminium oxide wheels were used during the investigation. These wheels were only tested on the Series 10 machine. Vitrified CBN was tested on both the Series 10 and Suprema, thus covering conventional and high speed grinding. The CBN wheels used for this part of the work were of higher porosity than usual. This was the result of work carried out in parallel with this research, where the effects of wheel porosity on grinding performance were investigated.

An economic analysis of the CBN grinding process was carried out and it was found that the economic success of the process is predominantly dependent on a balance between redress life and cycle time. Conditions were defined for success in the high-speed CBN grinding process.

CHAPTER 2. REVIEW OF PREVIOUS WORK

2.1 History and Background to Precision Grinding

The brief historical overview presented in this section shows how the grinding process has and continues to evolve. It highlights the motivating forces behind this progress and gives some focus to current and future developments required of the process.

Despite being one of the oldest processes known to man, the development of the grinding machine was slower than other common machine tools. The lathe, milling machine, planer and shaper were all in use in the early nineteenth century. Woodbury (1959) **[3]** attributes this delay to the lack of suitable materials to develop the grinding wheel in line with the machine tool. The first patent for a surface grinding machine was issued in 1831. A primitive universal grinding machine was proposed in 1834, the design of which was based on the lathe. However, it was not until 1875 that Browne and Sharp produced the first universal grinding machine capable of precision grinding metal components. This machine was similar to the modern universal grinding machine and is regarded as a milestone in the development of precision grinding. The machine had a swivelling wheelhead and an attachment for internal grinding. The headstock, tailstock, lead screws, structure and precision of the bed were all based on other machine tools such as the lathe. In this sense it has been stated **[3]** that the grinding machine did not undergo the same metamorphosis as other machine tools. The motivation for the grinding machines original development was to improve the quality of its product rather than to increase the rate of production. At the beginning of the twentieth century advances in grinding wheel technology made rapid production possible. Early man-made grinding wheels were made of emery, i.e. aluminium oxide, iron oxide and silica, bonded with either glue, baked clay, vulcanised rubber or vitrified silicate. It was soon realised that using naturally occurring stones, such as emery, would not suffice to exploit the possibilities of the grinding machine and process. It was not until the 1890's that synthetic abrasives were manufactured. In 1891, Acheson produced synthetic silicon carbide and in 1897, Jacobs produced a synthetic form of aluminium oxide **[3,4,5,6]**. This was another milestone in the development of the grinding process and the beginning of modern precision grinding. During the early twentieth century grinding wheels

were produced using vitrified, rubber, shellac and oxychloride bonds. In 1923 a resin bond was developed, adding to the abrasive and bond combinations available. With the growth in manufacturing and in particular mass manufacturing, that occurred in the early twentieth century, the grinding process became more widespread and essential for achieving the required precision. Instrumental in continuing the development of the grinding process was the automotive industry. This was largely due to the continual demand for reduced costs in the automotive industry. This demand provided the impetus for Charles Norton to demonstrate grinding machine capability, not only for precision, but also for rapid and economic metal removal. Norton achieved this by developing a Plain Grinder. The Plain Grinder was a simpler and more powerful machine than the Universal Grinder. Guest (1915) **[7]** states that compared with the Universal Grinder designed for the same size workpieces, the Plain Grinder had wider wheels, usually of greater diameter, a more copious supply of coolant and faster infeeds. The simpler construction also led to increased stiffness as there was no requirement for swivel arrangements on the table, workhead or wheelhead. Colvin and Stanley (1908) **[8]** record that Nortons Plain Grinder could do in fifteen minutes what had previously taken five hours of turning, filing and polishing. The process itself was regarded as one of the most difficult precision operations in making a car engine. Norton, however, proved that dimensional accuracy and surface finish standards could be achieved using a single operation, namely, plunge grinding.

Between 1900 and 1930 the automotive industry was the largest single customer of the machine tool industry **[3]**. This had a significant impact on the development of the grinding machine. A list of some of the machines developed commercially around this time gives an indication of the scope of application, i.e. Pratt & Whitney Ball Bearing Grinder (1899), Norton Crankpin Grinder (1905), Pratt & Whitney Gun Mount Grinder (1906), Landis Roll Grinder (1908-1910), Landis Crankshaft Grinder (1906), Heald Piston Ring Grinder (1904), Heald Cylinder (Planetary) Grinder (1905), Bryant Chucking Grinder (1908), Pratt & Whitney Automatic Sizing Grinder (1908). By the 1920's most of the previously mentioned machines were available in automatic form, e.g. Landis Automatic Crankpin Grinder (1923). In 1922 The Cincinnati Milling Machine Company introduced the first

commercially available centreless grinding machine. Car engine parts such as push rods and valve tappets were ideally suited for the centreless grinding process. By 1933 the Heald Company developed the internal Centreless Grinder. This was developed to solve the problems of eccentricity between external diameters and bores and found usage in the automotive and bearing industries.

Throughout the twentieth century developments in abrasive technology have continued. This has led to a number of different types of aluminium oxide abrasive and two types of silicon carbide abrasive. The defining characteristics of each type are hardness and friability. Toughness is another important parameter with tougher abrasives tending to wear rather than fracture. Increased friability indicates a lower toughness, yielding abrasives that tend to fracture and splinter rather than wear. This leads to sharp new cutting edges being produced, which give it a self-sharpening ability.

Continuing research into developing abrasives has seen the introduction of new products known as 'sol gel' and 'Altos' abrasives. The sol gel abrasive is an aluminium oxide grain produced by sintering rather than fusing **[9]**. Common aluminium oxide grains are produced by fusing, where the raw materials are melted together, cooled and then crushed. The resulting crystal structure is large and each grain comprises one to three crystals. By comparison a sol gel abrasive grain contains many sub-micron aluminium oxide crystals. Each of the sub-micron crystals is pore free and unusually tough. The resulting abrasive grain has the characteristics of high toughness and high friability. This seemingly contradictory characteristic is due to individual grains shedding worn sub-micron crystals allowing sharp new crystals to engage in the grinding process. Thus, the abrasive grain does not wear or fracture in the typical way of common aluminium oxide abrasives. It has been reported that, providing the grinding force is sufficient to maintain a re-sharpening process, increased wheel life and removal rates can be achieved using sol gel abrasives **[9,10,11]**. Jackson and Mills (2000) **[12]** state that sol gel wheels bridge the gap between conventional aluminium oxide wheels and CBN wheels. They also state that an advantage of sol gel over CBN is that cost reductions can be achieved without a new or modified machine tool.

More recently the emphasis on grinding wheel development has moved to grinding wheel structure. Controlled and uniform wheel porosity is difficult to achieve in practice without the use of artificial pore inducers. However, this can lead to increased bond contact and reduced numbers of cutting points. To overcome this, elongated aluminium oxide grains have been developed **[13]**. The shape of the grains allows a wheel to be manufactured that has increased and uniform porosity. A disadvantage with increasing porosity is that the grain is supported by less bond. This results in weaker bond bridges and consequently a weaker wheel structure. With elongated grains this problem is overcome. The shape of the grain leads to a natural loose pack density with sufficient abrasive/bond bridging to provide a strong wheel structure. Recent developments in this wheel design have led to the Altos abrasive. Aspect ratios of abrasive grains are usually around one, the Altos abrasive grain has a length to diameter aspect ratio of eight. Jackson (2001) **[14]** reports that performance tests on the Altos abrasive have shown that wheel wear was reduced, power consumption was less and greater material removal rates could be achieved, when compared to other abrasives.

The abrasive form of CBN has been commercially available since the late 1960's. Its development was a later outcome of the successful research into developing synthetic diamonds **[6]**. The stimulus for this research was largely due to the high cost of using natural diamond, which made it prohibitive in many cases. The development of CBN provided a superabrasive which, unlike diamond, could be used on ferrous materials. The first natural diamond wheels were developed in the 1930's. This was largely to satisfy the demand for grinding tungsten carbide cutting tools. Since their successful development in 1955 synthetic diamonds tended to become more and more popular for use in industry. Diamond wheels provide a superabrasive that has filled the role of grinding cemented carbides, ceramics, glasses and fibre-reinforced composites. As diamond is a form of carbon it is not suitable for grinding ferrous materials as excessive wear occurs. In 1957 the continuation of the research that led to the production of synthetic diamonds finally resulted in producing CBN, a synthetic material second only to diamond in hardness, but with no affinity to carbon. CBN was identified as a superabrasive suitable for grinding ferrous

materials. However, due to its perceived high cost its acceptance in production grinding has been slow. This was acknowledged by McKeown in 1986 **[15]**. However, McKeown also put forward an optimistic outlook for CBN based on new manufacturing methods for grinding wheels. These new methods were leading the way in producing vitrified bonded CBN wheels. Vitrified bonded wheels have a higher degree of porosity than other bonds, which allows for increased coolant access and chip clearance. A disadvantage with increased porosity is that the wheel structure may be weaker. Consequently, until recently, vitrified bonds have not been considered suitable for high speed applications. McKeown also points out that vitrified CBN wheels can be dressed and opened up in a way that cannot be achieved with resin or metal bonded wheels. This leads to a free-cutting wheel that allows high material removal rates while maintaining high grinding ratios (known as G-ratio, i.e. ratio of volume of material removed over volume of wheel wear). Additionally, the wheel surface can be modified by dressing to suit workpiece surface texture requirements.

During the 1980's the automotive industry was undergoing radical changes in its management and manufacturing methods. The need to change was forced by new environmental legislation, global competition and a need to gain a greater share of the market. To achieve this a new manufacturing philosophy was introduced known as lean production, a term coined by the International Motor Vehicle Program (IMVP) **[16]**. Lean production is a manufacturing philosophy which advocates that less of everything is used, i.e. human effort, manufacturing space, investment in tools, engineering hours etc. to develop and produce more. This is achieved by employing teams of multi-skilled workers, at all levels in the organisation, supporting and using highly flexible and increasingly automated machines, to manufacture products in volume and variety. It is the flexibility of both the workforce and technology that overcomes the rigidity of mass production. Also those manufacturers that survived were those that modernised their production methods with increased use of automation, robots and CNC machines **[16]**.

A further requirement for the automotive industry was higher precision. This was due to the demand for increased performance and economy. However, lower production costs were also demanded. One of the areas targeted to increase performance and economy was a reduction in engine friction. However, improving the accuracy and surface integrity of rotating engine parts (camshafts, crankshafts etc.) was difficult to achieve while reducing production costs, using conventional methods. A step change in production was required. These requirements coincided with new developments in CBN grinding wheel technology. After much research and development work, Toyoda Machine Works produced a CNC cam-grinding machine for use with CBN wheels. This machine had the following features: **[17,18]**

- Hydrostatic slideways.
- Hydrostatic spindle bearings.
- A small diameter wheel.
- A high speed (for 1985) of 80m/s.
- High-speed, high-response servosystem (important to allow workhead speed to be increased while maintaining cam geometry).
- Use of CBN grinding wheels.
- Rotary dresser.

The machine was designed to meet the automotive industry needs. Toyoda attributed the success of this machine to the integration of the seed technologies such as CBN technology, cam grinding technology and CNC technology. Hanard (1985) **[19]** of Caterpillar Tractor Company reports that the change over to CBN using the Toyoda machine had the following benefits:

- 70% increase in feed rate compared with aluminium oxide wheels without excessive heat generation.
- 100 times less wheel conditioning.
- Wheel life increased by 20 to 30 times.
- Increased output.
- Production requirements attained with fewer machines.

- Reduced labour costs.
- Reduced floor space required.

2.2 Using Vitrified CBN

2.2.1 Dressing Strategies

Klocke and König (1995) **[20]** point out that the terms dressing and conditioning can be both used to describe the sub-processes of truing, sharpening and cleaning the grinding wheel. This work will use the term 'dressing' to embrace all three sub-processes. The two sub-processes of sharpening and cleaning will be referred to as 'conditioning'. Truing the wheel is carried out to eliminate run-out errors and machine the wheel to the correct profile. Conditioning the wheel is carried out to produce a suitable wheel surface topography to achieve high removal rates and the specified workpiece surface roughness.

The dressing process affects the macroscopic characteristics of the wheel, i.e. wheel shape, and the microscopic characteristics, i.e. wheel surface topography. Lewis and Schleicher (1976) **[21]** state that the aims, methods and effects of truing and conditioning operations overlap. While this is true for conventional abrasives it has led to many problems in the dressing of CBN wheels. Only recently has a single method, i.e. the rotary diamond dresser, gone some way to achieving truing and dressing in the same operation **[22,23,24]**.

For many years truing and dressing have been considered as two separate operations in the preparation of a CBN wheel. This has been blamed as a reason for the slow rise in demand for CBN. Metzger (1986) **[1]** states that ignorance and lack of attention to the dressing of CBN wheels is the most common reason why CBN grinding has failed to gain wider use in industry. The dressing of a CBN wheel cannot be underestimated and a very different approach to wheel dressing is required compared with conventional abrasives. Following truing of a CBN abrasive, the wheel surface is closed. It is necessary to open up the wheel surface by an operation known as conditioning. When this has been achieved an open wheel surface may be maintained by 'touch-dressing' taking very fine cuts of 1 to 5 microns from the wheel surface **[22,23,24]**.

Over the last two decades a number of dressing tools and techniques have been researched. Much of this work is contradictory as to the best method to dress a vitrified CBN wheel. However, in recent years the general trend is towards touch-dressing using a rotary dresser to carry out truing and conditioning in one operation **[22,23,24]**. The benefits of touch dressing are that only a small amount is dressed off the wheel and that it can produce a wheel surface with the correct topography to match the cycle requirements. The single operation also reduces the time where no production is being undertaken. This method would seem to alleviate the main problem with CBN, which is, making it cost effective.

Other techniques used for truing the wheel to an acceptable roundness include:

a) Multi-point diamonds: Benefits include sharing of diamond wear over multiple diamonds in the tool. It has been reported that this method is successful for truing vitrified or resin bonded wheels **[25]**.

b) Single-point diamond: Successful when used to true vitrified or resin bonded wheels provided the wheel is run at a slower speed to reduce diamond wear. It is generally considered bad practice to dress at a different speed to that at which the cycle is to be run. Different stress systems are set up in the wheel at different speeds leading to changes in the wheel surface **[26]**.

c) Rotary powered diamond truing device: This device is suitable for dressing vitrified and resin bonded CBN wheels. By the mid 1980's this method accounted for 23% of dressing methods **[25]**. The high volume of diamonds on the dresser increases its life over using a single point diamond. It can also dress the wheel at high speed and avoid the problems mentioned in point b. One of the problem areas associated with rotary dressers is what speed ratio to the wheel should they be run at? Also, which direction should the dresser rotate in relation to the wheel? These questions have been at the heart of much research over the years and will be discussed in more detail in Section 2.2.2.

d) Brake-controlled truing: A brake-controlled truing device uses an abrasive wheel pushed into contact with the CBN wheel. The CBN wheel drives the brake dresser. The dressing wheel can be either aluminium oxide or silicon carbide. It has been

reported that the most success with this method has been achieved with resin bonded CBN wheels **[25]**. However, Malkin (1988) **[9]** states that this method will leave a vitrified CBN wheel in a sharper state than a resin bonded wheel. This is due to greater dislodgment and grain fracture. Some degree of conditioning is also achieved.

e) Electroplated/metal bond diamond block: The wheel is moved across a diamond truing block. The wheel can be dressed straight or into a desired profile. This is a simple method for surface grinding applications and does not require any ancillary equipment as do rotary and brake dressers.

Where the wheel is blunt after truing, the following methods have been used to condition the wheel.

a) Aluminium oxide stick: This is sometimes considered to be a simple way of opening up a wheel after truing has taken place. A soft (grade 'G') fine grit (220 grit or finer) aluminium oxide stick is fed into the wheel while coolant is applied. To provide an even load across the wheel surface it is recommended to hold the stick in a vice. However, it is not uncommon to see the stick held by hand. There are several problems with this method. Firstly it has little effect on sharpening the CBN grains. It wears away the bond material and it wears the CBN grains. Malkin **[9]** carried out an experiment to confirm this where the grinding force was measured before and after stick dressing. Even after stick dressing high initial forces were recorded. In a CIRP paper by Klocke and König (1995) **[20]** the opposite was reported. They attributed this to the increased chip space created by wearing away the bond. It was also found that aggressive application of the stick caused grain pull out. A further problem is that stick dressing can lead to an uneven wheel surface. This can cause problems such as uneven wheel wear and poor workpiece geometry.

b) Loose abrasive: Abrasive grits (aluminium oxide or silicon carbide) are fired at the wheel. The grits can be carried in a jet of compressed air or coolant. This method has only limited success with resin bonded wheels **[25,27]**.

c) Mild steel block: Prior to grinding the workpiece material, preliminary grinding is carried out on a mild steel block. It has been stated that this method exploits the self

sharpening properties of vitrified CBN wheels **[20]**. Klocke and König **[20]** reported that sharpening the wheel with a free-cutting operation gave better results than using the stick-sharpening method. This was attributed to less grain pull out when free cutting. Thus, there are more active grains engaged in the actual grinding process. This method of conditioning was also recommended by Malkin (1985) **[28]**.

Over the last decade many of the above techniques have become redundant. This is largely due to the success of the rotary dresser, especially for vitrified CBN **[22,23,24]**. The high volume of diamonds on the dresser increases its life over using a single-point diamond. It can also dress the wheel at high speed and avoid the problems resulting from having to reduce the wheelspeed to dress. Two new parameters result when using a rotary dresser, namely, dressing disc direction and dressing speed ratio. Research on the effect of these parameters found that **[22,23,24,28]**:

- Up dressing (where the disc is running in the same direction as the wheel and, therefore, opposes the wheel at the point of contact) tends to generate a smoother wheel surface and has the effect of making the wheel act hard. This is generally used for operations where a low surface roughness is required. Up dressing allows very high G-ratios to be achieved.
- Down dressing (where the disc runs in the opposite direction to the wheel and, therefore, at the point of contact the wheel and disc are running in the same direction) leaves the wheel with a more open surface and has the effect of making the wheel act softer than up dressing. This allows increased stock removal rates to be achieved. As the wheel behaves 'softer', G-ratio is lower than when up dressing.

Brinksmeier and Çinar (1995) **[29]** investigated the number of collisions between the wheel grits and the diamond grits of the dresser. The dresser used was a cup dresser and the application was internal grinding. The number of collisions was dependent on dressing direction, ratio and overlap. In up dressing, increasing the dressing ratio from 0 to 1, the number of collisions increases. With down dressing, as the ratio is increased from 0 to 1 the number of collisions decreases. When down-dressing at a ratio of 1, collisions are

assumed not to occur, instead the action is one of rolling and crushing. This condition is to be avoided as a direct transfer of the dresser topography is transferred on to the wheel surface. As the ratio is increased above 1 the number of collisions increases. In both up and down dressing, increasing the overlap increases the number of collisions. Brinksmeier and Çinar present graphs showing that as the number of collisions increases, the normal force increases and the surface roughness decreases. This work also confirms that up dressing is best for finish grinding and down dressing best for rapid stock removal.

In a more recent CIRP cooperative technical report various investigators researched the grinding performance of vitrified CBN wheels **[30]**. Each laboratory involved dressed the wheel with its own preferred method and parameter settings. The workpiece material ground was AISI 52100 and a finish grinding process was required of specific volumetric removal rate, $Q'_w = 1$ mm^3/mm·s. A roughing operation was also tested where $Q'_w = 3$ mm^3/mm·s. In each case the specific volume of material removed $V'_w = 1000$ mm^3/mm. The process was internal grinding. Of all the parameter levels tested the following parameters gave the best results:

dressing tool:	cup wheel	wheel diameter:	50 mm
cup diameter:	15 mm	wheelspeed:	35 m/s
diamond layer width:	1 mm	workpiece bore diameter:	70 mm
dressing increment:	4 µm	workpiece speed:	1 m/s
total amount dressed:	16 µm	coolant:	mineral oil
dressing ratio:	0.7 (up dressing)		
overlap:	3 (roughing) 20 (finishing)		

This work highlighted the importance of small dressing increments. This is due to the reduced load on the grains causing small fractures rather than large fractures or break-out as with larger infeeds and higher loads.

To achieve small dressing increments the technique of touch dressing is employed. This is seen as a key area to using CBN successfully. The reasons for this are as much to do with economics as with technical requirements. Touch dressing requires the use of an acoustic emission sensor, ideally, integrated with the control of the machine. The acoustic emission sensor detects initial contact between the wheel and dresser and allows dressing to begin without a heavy and unknown depth of first cut. More advanced machines use the acoustic emission signal to hunt for the surface of the wheel, thus, reducing the amount of time dressing 'fresh air'.

Touch dressing was found to produce an open wheel surface without requiring a subsequent conditioning process. This is discussed in a number of papers **[22,23,24,28,29]** and is accredited to the dresser cutting through the grains rather than pulling them out or leaving them flattened. By cutting the grains, grain splintering also occurs leaving them in a sharp condition. The degree to which splintering occurs depends on the aggressiveness of the dressing action. This was also observed by Brinksmeir and Çinar in their previously discussed work, where, as the number of collisions between grain and diamond increases, so to does the amount of splintering. The reason that smaller dressing increments have this effect is due to the high mechanical strength of the vitrified bond. With CBN wheels the bond is designed to have a higher wear resistance than with aluminium oxide wheels **[23]**. This is to complement the increased hardness and wear resistance of the CBN grit. Thus, smaller increments are less likely to pull out the grits and leave an excess of wear resistant bond on the dressed wheel surface.

Manufacturers list dimensional stability and lower grinding temperatures as particular advantages of CBN wheels. These benefits become more obvious when a wheel has been touch dressed rather than conventionally dressed. This is not only due to the wheel having increased sharpness but also increased roundness. Chen, Rowe and Cai (2002) **[24]** show roundness measurements made on wheels dressed using 10 µm increments and 3 µm increments. The out of roundness was 5 µm and 1 µm respectively. The improved roundness allows more grits to be active in the grinding action. Along with increased

sharpness this leads to more efficient grinding. In the work carried out by Chen et al. wheel sharpness, roundness and efficient coolant delivery were shown to be the main factors in reducing wheel wear, wheel loading and the risk of thermal damage.

The work carried out by Chen et al. was based on internal grinding using a rotary cup dresser. From the results, the following values were shown to be optimum **[22,24]**:

dressing speed ratio:	-0.7 (up dressing for finish grinding)
	0.4 (down dressing for stock removal)
dressing overlap:	3 to 5
dressing increment:	2 μm to 3 μm

In summary, this section has established that touch dressing using a rotary diamond dresser is now the preferred technique for dressing a vitrified CBN wheel. The following section is a more detailed review of previous research focused solely on the effects of dressing parameters when using a rotary diamond dresser.

2.2.2 Rotary Dressing Parameters

The rotary dresser introduces two new parameters to the dressing operation, namely dressing speed ratio and dressing direction, i.e. up or down dressing. Dressing speed ratio is simply the dresser surface speed over the wheel surface speed, the value being proceeded by a minus or plus sign to represent up or down dressing respectively. Up and down dressing refer to the direction of the dresser relative to the wheel. It is said to be up dressing when, at the point of contact, the wheel and dresser are in opposite directions. Down dressing is when, at the point of contact, the wheel and dresser are rotating in the same direction. In recent years the trend on dressing direction has tended towards down dressing according to wheel manufacturers literature which advises down dressing for most cases. This is despite much research that has advocated the use of up dressing particularly where low surface roughness is the priority.

Work carried out by Klocke and König **[20]** found that during down dressing the diamond grit meets the CBN grit at a significantly steeper angle than in up dressing. This has the effect of producing a high compressive load and increases the likelihood of splitting the CBN grit. This leads to a rougher and sharper wheel surface. With regard to up dressing Klocke and König report that shearing is the principle mechanism which occurs as the diamond and CBN grits collide coming from opposite directions. This leads to a smoother and dull wheel surface. The shearing action also pulls out any loosely bonded grits from the wheel. These effects are intensified as the speed of the rotary dresser is increased. For up dressing Klocke and König show that grinding force continues to increase as the dressing speed ratio increases to –0.7. For down dressing the opposite effect is shown with grinding forces reducing as the speed ratio is increased to 0.7. Results presented in a final technical report by Aachen University from a Brite/Euram project based on the Suprema grinding machine **[26]**, show that the dressing speed ratio becomes less significant as dressing overlap increases. This is particularly true for up dressing.

The rougher and sharper wheel topography produced by down dressing leads to a freer cutting wheel. As a result grinding forces are lower leading to reduced power and, therefore, specific energy. Where high material removal rates are required down dressing offers the greatest advantage. Noichle (2000) **[31]** also points out that for grinding nickel based alloys such as inconel 718 it is important to choose grinding conditions which will lead to lower temperatures. However, as pointed out by Chen et al. **[24]**, the benefits of up dressing should not be ignored if workpiece quality is a priority, particularly surface roughness. This point is also emphasised by Klocke and König who state that dressing parameters should be selected according to the requirements of a particular grinding process.

Dressing overlap is the ratio of the effective width of the dressing tool and the axial feedrate per revolution of the wheel. Thus, the lower the axial feed rate per revolution of the wheel the higher the overlap will be. It has long been established **[7]** that high overlaps lead to a smoother wheel surface. In this way rotary dressers behave in the same way as single point diamonds. Klocke and König found that as the overlap increases lower dressing forces

occur. The resulting grit is smoother and less sharp. During grinding both tangential and normal forces increase to increases in overlap. It is shown that normal forces increase more severely than tangential forces. According to Klocke and König the wheel topography generated using a high overlap not only increases the number of cutting edges available but also gives a greater overlap between cutting edge contact paths. This leads to a reduction in chip thickness resulting in lower workpiece surface roughness.

As discussed touch dressing is recommended when grinding with vitrified CBN. There is no agreement on the ideal dressing increment. Most research suggests that the dressing increment should not exceed 10 μm **[22,23,24,26,29,30]**. In general lower increments have been found to lead to lower workpiece surface roughness **[26]**. However, the effect of dressing increment has also been shown to diminish as grit size increases **[26]**.

The number of dressing passes required is usually dependent on the condition of the wheel. Malkin **[9]** states that the number of dressing passes serves two purposes, firstly to true the wheel and secondly to remove debris from previous grinding. Thus, if the dressing increment is reduced the number of passes required may necessarily increase.

In summary, for finish grinding where workpiece quality is the priority up dressing with a high overlap and speed ratio will produce a suitable wheel surface topography. For an open, sharper and rougher wheel topography to suit high material removal rates, down dressing with a low overlap and high speed ratio are recommended. In both cases the dressing increment should be below 10μm and the number of passes as required to true the wheel.

2.3 Some Effects of Grinding at High Speed

Tönshoff, Karpuschewski and Mandrysch (1999) **[32]** summarised the effects of wheelspeed on the grinding process as shown in Figure 2.1:

Figure 2.1. Effects of increasing wheelspeed on the grinding process **[32]**.

While this is a simplified view of the high speed grinding process it draws attention to the fact that improved quality comes at the cost of constant material removal rate. This is a real cost as higher material removal rates, leading to shorter cycle times, are an important factor in reducing total process costs. King and Hahn (1986) **[33]** stress that the economic benefits of grinding with CBN are lower labour and overhead costs. Reduction in these costs can be achieved through cutting down cycle times.

Increasing wheelspeed leads to higher specific energy, the bulk of which is in the form of heat **[9]**. This results in higher grinding temperatures. Contrary to this, research by Tawakoli (1993) **[34]** has suggested that beyond a threshold value of workspeed, temperature should drop. This is partly due to the extremely short contact time between abrasive wheel and workpiece material. Before the heat generated has time to be absorbed by the workpiece it is removed, in the form of a chip, by a following abrasive grit.

In theory the thermal stability of the abrasive, limits the maximum temperature at which the abrasive acts effectively. Metzger [1] gives 1400°C as the limit of thermal stability for CBN in air. By contrast the limit of thermal stability for diamond is given as 700°C. This has serious consequences for grinding at high wheelspeeds. Due to the low limit of thermal stability of diamond Metzger observed accelerated thermal attrition of diamond grit beyond a certain wheelspeed. This led to a significant drop in wheel life. Similar trials carried out using CBN found that as wheelspeed was increased, the advantages of longer wheel life, improved profile stability and surface finish were realised without damaging the workpiece. The reason given for this was the high thermal stability of CBN. Malkin [9] reports that the high thermal stability of CBN allows it to be fired at much higher temperatures resulting in a much broader range of vitreous bonds that can be considered for manufacture.

Increased grinding temperatures impart higher residual stresses to the workpiece. Chen, Rowe and McCormack (1999) [35] show that the nature and magnitude of the residual stress is determined by the thermal stress developed in the workpiece. They also show that a transitional temperature exists beyond which, unwanted tensile residual stresses will develop. Increasing wheelspeed exacerbates these effects. However, Chen et al. point out that compared to aluminium oxide abrasives, grinding with CBN conducts more heat away from the grinding zone. Thus, the thermal properties of CBN make it the most suitable abrasive for high speed applications.

High speed grinding with vitrified CBN offers significant potential benefits. However, this may be offset by the increased complexity in machine tool design. Further to this, increasing wheelspeed has a negative effect on coolant application. The following sections review some of the previous research findings on these two subjects.

2.4 Machine Tool Design and High Speed Grinding

Grinding at high speed has several implications for machine tool design. As the operating range increases there is greater risk of exciting one of the natural frequencies of the machine, thus causing resonance. As a machine tool is the sum of many parts it has many

natural frequencies which may lie in its operating range. In a recent study by Noichle **[31,36]** the detrimental effects of resonance are clearly shown. A surface grinding process was carried out comparing the effects of dressing the grinding wheel at different wheelspeeds, i.e. 60 m/s and 80 m/s. Grinding results show that wheel wear and surface roughness were far worse after dressing at 60 m/s. Further investigation into the difference in these results revealed that the wheelspeed of 60 m/s coincided with a natural frequency of the machine.

With reports of grinding machines now operating at 250 m/s it is crucial to know the dynamic characteristics of the machine **[37,38]**. This is accomplished by using modal analysis techniques. Pearce (1998) **[39]** recommends that this is best achieved using experimental methods such as impulse testing using an impact hammer or by applying harmonic excitation through a shaker. In both cases the response of the system is measured by an accelerometer. With knowledge of the dynamic characteristics of a machine tool and the natural frequencies of the wheel spindle, workhead/workpiece/tailstock system and the dressing spindle, process parameters can be selected judiciously.

To run at wheelspeeds above 100 m/s heavy demands are imposed on the grinding wheel spindle bearings. Webster (1990) **[37]** lists the following criteria for a high-speed wheel spindle:

- Low friction to reduce temperature effects, maintain accuracy and reduce power input.
- Long maintenance free life.
- High radial and axial stiffness.
- Low rotational and geometric errors.
- Moderate cost.

High-speed spindles that satisfy the above criteria have taken conventional rolling element bearings to their limit. However, hybrid ceramic ball bearings, using advanced lubrication systems, are proving capable of operating at high speeds and in a demanding environment **[40]**. These are silicon nitride ceramic balls running in steel inner and outer races and are

specifically designed for high speed applications. Aramaki, Shoda, Morishita and Sawamoto (1988) **[41]** report that using bearings with silicon nitride ceramic balls for machine tool spindles resulted in 30% to 50% less friction loss at high speeds compared with conventional bearings. For the hybrid bearings it was also found that the temperature rise was lower while higher speeds could be achieved. With an angular contact configuration the bearings are preloaded offering a stiff design. For thermal stability at high speed the bearings require a sophisticated lubrication system, usually an oil/air mixture or continuous oil feed. An advantage of using angular contact bearings is that they are fairly economical as they are a standard product. The main disadvantage is that they have a limited life although this may be many thousands of hours.

Hydrostatic bearings have several attractive benefits for use on machine tools. They offer high stiffness, allow high speed, have extremely high rotational accuracy and have unlimited life. During the development of the Toyoda CNC/CBN Full Automatic Crankpin Grinder **[17]**, an initial design specification identified the following requirements as prerequisite for successful grinding using vitrified CBN: increased static rigidity, improved rotational accuracy. To achieve this, hydrostatic bearings were used. While satisfying the initial design criteria, hydrostatic bearings also allowed wheelspeeds to be increased. Increased damping is also a characteristic of hydrostatic bearings. This is due to the pressurised oil film between the bearing surfaces. It has been reported recently that practically all cam grinding is carried out with CBN **[2]**. This success has partly been attributed to the characteristics of hydrostatic bearings. Since the work by Toyoda, many machine tool manufacturers and research engineers strongly advocate the use of hydrostatic bearings for high speed grinding using vitrified CBN **[2,14,17,18,19,26,37]**.

More recently active magnetic bearings have been used for grinding wheel spindles. This is particularly true for internal grinding spindles where extremely high rotational speeds are required due to the small diameter of the wheel. This bearing has several advantages over conventional fluid film and rolling element bearings:

- No lubricant required.

- No contact.
- No elaborate seals required.
- Control of dynamic characteristics, i.e. stiffness and damping controlled by external control algorithm.
- Compensation for wheel unbalance or eccentricity.

The main disadvantage is the extremely high cost and sophisticated control system required. Webster **[37]** quotes a figure of $50,000 just for the bearings without the control system.

Air bearings have been used in grinding machines with some success. Rowe (1967) **[42]** reported excellent results when using this type of bearing with the only disadvantage being the necessity for a supply of clean pressurised air. Also it is imperative not to exceed the load bearing capacity. Webster **[37]** lists stiffness as a disadvantage, considering high speed CBN grinding to take air bearings to their limit. As air does not provide the same degree of damping as oil lubricated or rolling element bearings the dynamic stiffness is not as high. For successful CBN grinding high static and dynamic stiffness, which varies with frequency, are seen as imperative **[43]**.

Traditionally tapered roller bearings have been used in lower speed applications where axial and radial loads are high. It was generally accepted that the design of tapered roller bearings was unsuitable for high speed applications due to the excessive heat generated. This is due to rubbing at the ends of the roller as well as the larger contact area along its length. However, one of the main characteristics of tapered roller bearings is its high axial and radial stiffness, a prerequisite for CBN grinding. As with rolling ball bearings the demands of industry to move to ever higher speeds have driven research into high speed tapered roller bearing design. With the added attribute of higher stiffness than angular contact bearings, tapered roller bearings become an attractive option for high speed applications. In a recent study in the USA by the National Centre for Manufacturing Sciences **[44]** tapered roller bearings have been successfully used for heavy general purpose machining. The

speed range was from 2500rpm to 12000rpm. Up until recently these high speeds would not have been considered possible with tapered roller bearings.

Klocke and Muckli (1999) **[43]** make the following recommendations, which summarise the essential machine features required for precision CBN grinding:

- High positioning performance and repeatability.
- High static and dynamic stiffness.
- Few resonance frequencies.
- Good thermal stability.
- True roundness of grinding wheel.

Many of the above points have serious implications on each other. For example Furukawa and Yokogawa (1990) **[45]** make the point that without high static and dynamic stiffnesses dressing accuracy and roundness of the wheel is seriously affected. Also without good thermal stability it becomes impossible to attain high positioning performance and repeatability.

At present the greatest success with using vitrified CBN has been in the automotive industry grinding cam shafts **[2,46]**. Hitchener (2002) **[47]** reports that this success is largely due to the material being ground, i.e. chilled cast iron. While this material is suitable for small, low powered engines, its mechanical strength is too low for the high powered engines demanded by the US market. Consequently, new cam shaft materials present new challenges for high speed grinding with vitrified CBN. Hitchener also points out that as wheelspeed increases effective coolant application becomes more difficult. It is reported that matching coolant velocity to wheelspeeds between 80 m/s and 160 m/s leads to enormous hydrodynamic pressure. This creates high normal forces, leading to profile or roundness errors. Much research has been carried out on coolant application and this is the subject of the following section.

2.5 Coolant Application

This work does not intend to look at coolant application directly. However, grinding at high speed has implications on how effective coolant delivery is. Coolant application has been the subject of much research and an overview is presented below. Much of this previous work is the basis for the high pressure coolant system design used on the Suprema.

Conventional methods of coolant delivery generally fall into two categories, namely, low pressure flood delivery or high velocity jet delivery. Work by Engineer, Guo and Malkin (1992) **[48]** has shown that, due to the presence of a boundary layer, flood delivery is ineffective. This investigation revealed that the percentage of applied fluid passing through the grinding zone, i.e. the useful flow rate, varied from 4% to 30%. Generally with flood delivery methods the kinetic energy of the coolant is not sufficient to penetrate the boundary layer of air surrounding the wheel. The percentage of fluid utilization was found to significantly increase with more porous wheels and a closer positioning of the nozzle to the grinding zone. A theoretical study by Guo and Malkin (1992) **[49]** based on results by Engineer et al. **[48]**, concluded that the useful flow rate equalled the amount of fluid retained in the grinding wheel pores from the point of application to the point where grinding commences. A theoretical model for fluid flow through a porous medium was proposed based on experimental results. Webster (1995) **[50]** found that water based emulsions were more effective for higher porosity wheels, while neat oils were more effective for denser wheel structures. This may be due to the different properties of the two types of coolant. As emulsions are largely water based, they tend to cool more by convection, thus transporting heat away from the process. Neat oils have better lubrication properties than emulsions. This reduces friction allowing chip formation to be more significant compared with ploughing, rubbing and sliding. The surfaces between the swarf and grits are also lubricated. The overall effect of this is to lower grinding temperatures. Conventional methods of fluid delivery tend to supply high volumes of cutting fluid of which only a small percentage may be considered as useful flow rate. This has led to work by Klocke et al. (2000) **[51,52]** on delivering the minimum quantity of coolant required for optimum grinding conditions. This approach is known as 'minimum quantity lubrication'.

The motivation for this work was predominantly due to tighter legislation controlling the use of coolants in the workplace. The coolant is delivered as an aerosol with typical flow rates less than 50ml/hour. Some difficulty was found with regard to achieving low surface roughness and it was concluded that more research was required before the method could be recommended to industry.

Webster, Cui, and Mindek (1995) **[6]** carried out research on the effects of a coherent jet of coolant as opposed to a dispersed jet. The need for high fluid velocities to penetrate the air boundary layer make the application of water based coolants much more difficult in terms of a coherent jet. Measuring the grinding temperature Webster et al. showed that where a coherent jet is maintained the grinding temperature is reduced compared with a dispersed jet. To maintain a coherent jet, a round nozzle was used with concave internal nozzle walls prior to exit. Flow conditioners were used to reduce fluid turbulence.

Effective coolant delivery can be achieved by using a coolant shoe **[54]**. The shoe follows the wheel curvature, disturbing the boundary layer and allowing improved coolant flow into the grinding zone. For CBN wheels, where wheel wear is minimal Klocke, Baus and Beck (2000) **[54]** showed that this method can lead to improved workpiece quality. However, as Webster, Brinksmeier, Heinzel, Wittman and Thoens (2002) **[55]** point out, coolant shoes are not practical when wheel wear is significant. This has led to jet delivery being the preferred method in the workplace.

Work carried out at AMTTREL **[56,57]** showed that the effects of the boundary layer entrained around a rotating grinding wheel are stronger than initially thought. This is illustrated in the following photograph which shows a reservoir of coolant, analogous to flood delivery, backed up from the rotating wheel. The wheel is rotating in a clockwise direction and conventional wisdom would assume it to pump the coolant through the 80 μm gap between the wheel and workpiece. What is actually happening is that, on approaching the minimum gap, the boundary layer of air reverses and opposes the reservoir of coolant.

The kinetic energy of the reversed boundary layer is greater than the potential energy of the reservoir.

Figure 2.2. Photograph showing how the boundary layer of air entrained around the grinding wheel, which is rotating in a clockwise direction at 33m/s, holds the coolant back rather than pumping it through the 80μm gap between wheel and workpiece [57].

Pressure measurements were taken on the workpiece surface, either side of the minimum gap. The results revealed a high pressure region just prior to the minimum gap and a low pressure region just after the minimum gap. This accords with bearing theory as predicted using Reynolds equation for a converging and diverging wedge. A computational fluid dynamics (CFD) analysis using the finite element code FIDAP was used and the pressure distribution shown in Figure 2.3 determined.

Figure 2.3. Experimental Pressure Contours [57].

Experimental measurements were recorded of the velocity of the boundary layer. This was achieved using a laser doppler anemometer. A theoretical analysis was carried out using CFD to model the boundary layer. The results of the CFD analysis are shown in Figure 2.4 This work supported using a nozzle to deliver a jet of coolant to the grinding zone. Delivery of cutting fluid via a nozzle in the form of a jet can have two benefits. Firstly the fluid can be delivered with a velocity great enough to penetrate the boundary layer of air and secondly, if applied at a high enough velocity, it may be used to clean the wheel mechanically by removing adhered metal **[58]**.

Figure 2.4. Predicted Velocity Directions **[57]**.

The angle at which the coolant is delivered has been the subject of much research in recent years. Delivering the coolant as near to tangential to the grinding wheel as possible, is a common approach with the fluid directed straight towards the grinding zone. This approach is supported by Akiyama, Shibata and Yonetsu (1984) **[59]** who investigated the film thickness of the coolant in the micro gap of the contact area between wheel and workpiece. Two delivery methods were investigated, firstly where the fluid was carried into the grinding zone by the boundary layer and secondly, where the fluid was directed towards the wheel/workpiece interface prior to entry into the grinding zone. For the first delivery method where the coolant was directed at some angle to the wheel periphery and the boundary layer of air carried the fluid into the grinding zone, the maximum film thickness was estimated to be 40 μm. Delivering the same volume of fluid at the same velocity but with the nozzle positioned so that the coolant was directed straight towards the grinding

zone a film thickness of 80 μm was estimated. Increased film thickness was found to lead to lower grinding temperatures. However, this is contrary to other investigations which have suggested the nozzle be positioned at an angle to the wheel periphery **[60,61]**. This was the subject of an extensive study by Trmal and Kaliszer (1976) **[60]** who found that, providing the velocity of the coolant matched the velocity of the boundary layer, the boundary layer could be overcome and the coolant carried into the grinding zone. The coolant was delivered at an angle of 15°. Trmal and Kaliszer also show the benefits of using scraper plates. Using a pitot tube to measure the velocity of the boundary layer, a decrease in air velocity occurred as the scraper plate was moved towards the wheel periphery. This was supported by Campbell (1995) **[61]** who investigated the hydrodynamic pressure at the wheel/workpiece interface caused by the passage of coolant beneath the wheel. At a critical wheelspeed this pressure measured zero, i.e. the boundary layer of air prevented coolant from passing beneath the grinding wheel. Introducing a scraper plate allowed the grinding wheelspeed to be increased by 20% before the hydrodynamic pressure again measured zero. Campbell found the optimum angle of delivery to be 5° when using a neat oil. Campbell pointed out that the optimum angle at which to position the nozzle may depend on the viscosity of the cutting fluid and its velocity at nozzle exit.

Research **[56,57]** has found that delivery of coolant via a tangential nozzle position with a low velocity jet, i.e. 3.5 m/s compared to a wheel surface speed of 27 m/s, led to increased side leakage. It is shown in Figure 2.3, that pressure decreases from the centre of the wheel towards the sides. Also from Figure 2.3 it is shown that just prior to the minimum gap a high pressure region exists. This high pressure corresponds approximately to the stagnation point on the workpiece surface where the kinetic energy of the boundary layer is converted into pressure energy. As coolant is directed towards this point of high pressure some of the fluid flows to the lower pressure regions at the grinding wheel sides, hence side leakage and reduced useful flow rate. From an understanding of the flow mechanisms, the tangential nozzle position was raised by approximately 12 mm. By doing this the coolant may be delivered to the wheel surface at a point above the area of reversed flow. The low velocity jet of fluid is redirected by the grinding wheel so that it is coincident with the boundary layer direction. Enough energy exists in the boundary layer to carry the coolant towards the

minimum gap. The effects of reversed flow aid this process as the coolant rides over the high pressure stagnation points and is taken through the minimum gap. The mechanism of flow is a combination of velocity induced (Couette) flow provided by the grinding wheel and pressure induced (Poiseuille) flow due to the pressure difference either side of the minimum gap. As the coolant flows in above the region of high pressure, side leakage is reduced as flow runs to the negative pressure on the exit side of the minimum gap; the useful flow rate is increased.

The benefits of increasing the useful flow rate have been shown by research carried out at AMTTREL **[56,57]**. In this work, knowledge of the mechanisms of flow occurring around the grinding zone allowed a low velocity jet of coolant to be applied critically, leading to increased through flow under the wheel, i.e. useful flow rate, and improved workpiece quality. This work highlights the importance of how, by understanding the flow mechanisms involved in the process, significant improvements can be made. Initially these improvements were thought to be primarily due to increased lubrication in the grinding zone. However, more recent work by Rowe and Jin (2001) **[58]** has shown that extremely high convection coefficients apply as long as the flow rate is useful and sufficient to ensure grinding temperature is kept below the boiling point of the fluid. This discovery implies a new approach to coolant delivery. It has also been shown by Rowe and Jin **[58]** that increased wheel porosity is beneficial when grinding long chipping materials such as inconel 718. This material is difficult to grind with rapid wheel loading a particular problem. By increasing the porosity of the wheel, workpiece quality was improved, G-ratio increased and the onset of wheel loading delayed. A contributing factor to this success may be the increased presence of coolant in the wheel pores.

The previous work outlined in this chapter forms the background on which the strategies for successful high speed grinding are based. In the following chapter some of the theoretical consequences of high speed grinding are reviewed. This includes the effects on chip thickness, grinding temperature and stability.

CHAPTER 3. MATHEMATICAL RELATIONSHIPS

3.1 Introduction

This chapter introduces the theoretical basis for the increasing use of high speeds in grinding. Mathematical relationships are presented as required for the discussion of machine tool characteristics required for high speeds and as essential background to the techniques employed in the investigation.

3.2 Chip Thickness Effects

It has been understood for many years that chip thickness is an important parameter for the consideration of the effects of wheelspeed on process performance. Chip thickness is inversely proportional to wheelspeed. The geometric relationships between wheel and workpiece were discussed by Alden (1914) **[62]** and Guest (1915) **[7]**. Alden made the following statements:

a. Increased workspeed increases grain depth of cut and makes the wheel act softer.
b. Decreased wheelspeed increases grain depth of cut.
c. Diminishing the diameter of the grinding wheel increases grain depth of cut, and increasing the diameter of the wheel decreases grain depth of cut.
d. Making the workpiece diameter smaller increases grain depth of cut. Conversely, making the workpiece diameter larger makes grain depth of cut smaller.

Where Alden used grain depth of cut, the term uncut chip thickness is now generally used. The analysis carried out by Alden required the number of cutting particles per unit length to be determined. This made the chip thickness difficult to evaluate with any certainty. However, this work is important as it was the first to show a relationship between wheel and workpiece with regard to speed and size. The effect of wheelspeed on chip thickness from the Alden equation is:

$$h_m = \frac{v_w}{v_s n} \sin(A + B) \tag{3.1}$$

where h_m = grain depth of cut (uncut chip thickness)

v_w = workspeed

v_s = wheelspeed

n = number of cutting particles per unit length of circumference of wheel

$A+B$ = The angle made by tangents from the wheel and workpiece, struck from the point of intersection between the two peripheries

Since this work, many further investigations have been carried out with the aim of estimating chip thickness more accurately **[63]**. For simplicity, the argument can be related to the simplest forms of expression. The wheelspeed is seen to be a significant factor for the chip thickness and in recent years, much of the research on CBN grinding has concentrated on the benefits of increasing wheelspeeds.

An even simpler expression is the equivalent chip thickness given by,

$$h_{eq} = a_e \cdot \frac{v_w}{v_s} \tag{3.2}$$

where h_{eq} = equivalent chip thickness

a_e = the true depth of cut

v_w = workspeed

v_s = wheelspeed

While equivalent chip thickness does not represent real chip thickness in the grinding process it is regarded as a measure of the order of magnitude and avoids argument about wheel topography. Equation 3.2 is not a model for an individual grinding chip, instead it represents a sheet of grinding chips removed by the wheel. Consequently no account is given to grain spacing. Equation 3.2 is widely used for presenting empirical grinding results where the wheel topographical parameters remain unspecified.

The maximum uncut chip thickness may be defined in the more usual form in terms of the depth of cut and the equivalent wheel diameter,

$$h_m = 2L \cdot \frac{v_w}{v_s} \cdot \sqrt{\frac{a_e}{d_e}} \tag{3.3}$$

where L = grain spacing

$d_e = \dfrac{d_s}{1 \pm d_s/d_w}$ = equivalent wheel diameter, for surface grinding $d_e = d_s$

d_s = wheel diameter

d_w= workpiece diameter

The plus sign in the equivalent diameter, is for external grinding, the minus sign for internal grinding. Equation 3.3 is still difficult to evaluate in that L is not precisely defined.

From both Equations 3.2 and 3.3, it is clear that an increase in wheelspeed reduces chip thickness. By reducing chip thickness, workpiece roughness is reduced and cutting forces on the abrasive grains are reduced. As a consequence, wheel life tends to be increased. Alternatively, depth of cut and hence volume removal rate may be increased as wheelspeed is increased, maintaining chip thickness constant. Thus, production time can be reduced. In summary, it is claimed that either quality can be improved or production rate can be increased through increased wheelspeed or a compromise can be achieved between these two aims. This summarises the main argument for increasing wheelspeeds in grinding.

It appears from the above equations that chip thickness is proportional to workspeed. In practice, chip thickness is not directly proportional to workspeed, since depth of cut is inversely proportional to workspeed in cylindrical grinding. Chip thickness is therefore proportional to the square root of workspeed in Equation 3.3 and independent of workspeed in Equation 3.2. According to Equation 3.3, increased workspeed, offsets to some extent the benefit of increased wheelspeed on reducing roughness and grain forces. It might therefore appear to be a benefit to reduce workspeed. More usually, it is argued that workspeed should be increased in proportion to wheelspeed, maintaining chip thickness constant and hence the material removed in each grain–workpiece interaction. This increases the wheel

wear rate but is consistent with increasing removal rates. One of the questions that needs to be addressed is how to determine the best combination of cycle parameters for a particular industrial requirement.

One of the problems with reducing workspeed is that it can lead to an increase in grinding temperature. This is because the heat source due to grinding remains in contact with a location on the workpiece for a longer duration **[64]**. The effect of grinding conditions on temperatures is discussed in the next section.

3.3 Temperatures in Grinding

Increasing wheelspeed tends to increase the risk of thermal damage. This is due to the increase in specific energy, caused by reducing chip thickness **[65,66]**. Almost all of the energy in grinding is converted to heat. The specific energy is defined as,

$$e_c = \frac{P}{Q_w} \tag{3.4}$$

where e_c = specific energy

$P = F_t (v_s \pm v_w)$ = grinding power

F_t = tangential force

Q_w = volumetric removal rate

- for surface grinding, $Q_w = v_w a_e b$ where b = grinding width
- for cylindrical grinding, $Q_w = \pi d_w v_f b$ where v_f = infeed rate

Shaw (1996) **[65]** states that, in general, specific energy varies exponentially with uncut chip thickness,

$$e_c = \frac{1}{h_m{}^x} \tag{3.5}$$

where e_c = specific energy

h_m = maximum uncut chip thickness

x is approximately equal to 0.3 for stock removal grinding and approaches 1.0 for finish grinding

This is known as the 'size effect'. Rowe and Chen (1997) **[66]** explained this using an analogy to sliced bread. Basically, as the number of slices in which the bread is to be cut increases, the energy expended increases. More chips per unit volume will be produced during a fine grinding operation than when using high stock removal rates. Shaw also states that, in coarse grinding the chips convey more heat away from the workpiece than in fine grinding, where a greater proportion of the heat is transferred to the workpiece. Thus, a balance between removal rate, workspeed and wheelspeed is required for efficient grinding. This has led some researchers to propose an optimum value of q-ratio (ratio of wheel surface speed over workpiece surface speed). Krar and Ratterman (1990) **[67]** recommend a q-ratio of 100 for stock removal and 150 for finish grinding. Higher wheelspeeds have led to q-ratios above 200.

Unlike milling and turning there are no widely accepted recommendations for wheelspeeds, workspeeds and feedrates. This makes the choice of speeds and feedrates difficult. Workpiece material, removal rate, workpiece tolerances and G-ratio requirements should all be considered when deciding on q-ratio.

Increasing specific energy leads to higher grinding temperatures. The total heat, q_t, generated in the grinding zone is dissipated between the workpiece, q_w, grinding wheel, q_s, grinding chips, q_{ch}, and grinding fluid, q_f, i.e.

$$q_t = q_w + q_s + q_{ch} + q_f \qquad 3.6$$

The workpiece partition ratio, R_w, is defined as the proportion of the total heat conducted into the workpiece, i.e.

$$R_w = \frac{q_w}{q_t} \qquad 3.7$$

The wheel-workpiece partitioning is a subsystem of the total heat partitioning system and may be determined using the Rowe/Morgan **[68]** model given by Equation 3.8. The workpiece partition ratio, R_w, is the fraction of total grinding heat entering the workpiece. The wheel-workpiece partition ratio, R_{ws}, is the faction of heat which enters the workpiece of that heat shared by the workpiece and wheel.

$$\frac{1}{R_{ws}} = 1 + \frac{\kappa_g}{(r_o v_s)^{1/2} (\kappa\rho c)_w{}^{1/2}} \qquad (3.8)$$

where κ_g = coefficient of thermal conductivity for abrasive

r_o = wear flat contact radius (typically 15μm)

κ = workpiece thermal conductivity

ρ = workpiece density

c = workpiece specific heat capacity

$\beta = (\kappa\rho c)_w{}^{1/2}$ = workpiece thermal contact coefficient

The thermal properties of the workpiece can be determined from data handbooks, e.g. Woolman & Mottram **[69]**. For the material AISI 52100, $(\kappa\rho c)_w{}^{1/2} = 10{,}830\ \mathrm{Js^{-1/2}m^{-2}K^{-1}}$.

The thermal conductivity of aluminium oxide is typically between 20 and 45 $\mathrm{W(mK)^{-1}}$. Reported values of thermal conductivity for CBN vary widely. The theoretical value for pure CBN given by DeVries (1972) **[70]** is 1300 $\mathrm{W(mK)^{-1}}$. However, measured values for polycrystalline CBN are as low as 87 $\mathrm{W(mK)^{-1}}$, as reported by DeVries **[70]** and Shaw (1990) **[71]**. A more recent study by Rowe, Black, Mills, Morgan and Qi (1997) **[72]** using the bond/grit combination of vitrified CBN gave the effective thermal conductivity as 290 $\mathrm{W(mK)^{-1}}$.

Equation 3.8 assumes steady-state conditions and tends to slightly over predict the partition ratio. However, it can be seen that increasing wheelspeed leads to a higher partition ratio. Based on values reported by Rowe et al. **[72]** of 36 $W(mK)^{-1}$ and 290 $W(mK)^{-1}$ for aluminium oxide and vitrified CBN respectively, and using typical parameter values in Equation 3.8, the following values of R_{ws}, have been determined for a range of wheelspeeds:

Wheelspeed	R_{ws} (Al_2O_3)	R_{ws} (vitrified CBN)
30m/s	0.86	0.44
60m/s	0.9	0.53
90m/s	0.92	0.58
120m/s	0.93	0.61
150m/s	0.93	0.64

It can be seen that wheelspeed has a less dramatic effect on the partition ratio for low values of grain thermal conductivity, as in the case of aluminium oxide.

To determine how wheelspeed affects grinding temperature it is useful to consider the specific energies. The maximum grinding zone temperature, θ_m, is given by **[73]**:

$$\theta_m = 0.8\frac{R_{ws}(e_c - e_{cc} - e_{cf})a_e}{(\kappa\rho c)_w^{1/2}}\left(\frac{v_w}{l_e}\right)^{1/2} + \theta_a \qquad (3.9)$$

where e_c = total specific energy due to grinding

e_{cc} = specific energy convected by the grinding chips

e_{cf} = specific energy convected by the fluid

l_e = real contact length

θ_a = workpiece ambient temperature

In shallow-cut grinding, the deflections of a vitrified grinding wheel are substantial compared with the depth of cut. For shallow cut grinding, the contact length, l_e, is

sometimes taken approximately as twice the geometric value, l_g, in order to achieve greater accuracy than obtained by simply ignoring the significant deflection effect **[74]**.

$$l_e = 2l_g = 2(ad_e)^{1/2} \tag{3.10}$$

The specific energy convected by the grinding chips, e_{cc}, is estimated as the energy required to melt the chips. For steels this is typically 6 J/mm^3, which is often a small proportion of the total grinding energy **[72]**. Often, the effect of convection to the grinding fluid is ignored in Equation 3.9. However, despite this Rowe et al. **[72]** have shown close correlation between predicted and experimental results. This is because, the grinding temperatures are usually considerably higher than the fluid boiling temperatures for shallow cut grinding limiting fluid convective effects to bulk cooling **[72,75]**. This is particularly true when water-based emulsions are employed. The results presented by Rowe et al. were achieved using a water-based emulsion as the grinding fluid. According to Howes (1987) **[75]** boiling temperatures for emulsions range between 110°C and 140°C. Boiling temperatures of neat oils tend to be in excess of 300°C. However, the thermal conductivity of mineral oils is 0.13 W/mK as opposed to 0.6 W/mK for water, the main constituent of emulsion type grinding fluids **[54]**. This offsets the benefits of the higher boiling temperature of neat oil when used as a grinding fluid. In general, neat oils limit the amount of heat generated by providing increased lubrication to the process rather than by convection **[76]**.

Wheelspeed has a significant effect on the specific energy as shown by Equation 3.5. Higher wheelspeeds lead to increased specific energy and, consequently, to increased grinding temperature as shown by Equation 3.9.

Higher grinding temperatures are experienced when there is a higher wheel-workpiece partition ratio. Reducing the wheel-workpiece partition ratio not only reduces the amount of heat absorbed by the workpiece but also leads to a lower grinding temperature. CBN has a much higher thermal conductivity than conventional abrasives. This provides a strong case for the use of CBN at high wheelspeeds. However, to achieve high wheelspeed and

precision grinding, there are several implications with regard to machine tool design considered as follows.

3.4 Process stability

Grinding wheelspeed plays an important role in the stability of the grinding process. This is clearly indicated by stability charts **[33]** for the grinding process. Chatter occurs when the machining process becomes unstable. This may be due either to a regenerative effect of the workpiece or of the grinding wheel. The first case is known as work-regenerative chatter and the second as wheel-regenerative chatter. Chatter is instigated by the process regenerating the growth of waves around and along the periphery of the wheel or of the workpiece. The amplitude of the waves increases with every pass or revolution. In work-regenerative chatter, the growth of periodic waves is rapid; with wheel-regenerative chatter the growth is slower. The wheel-regenerative effect is much slower with CBN wheels compared with aluminium oxide wheels. This is due to the reduced wear rate with CBN, which slows the growth of the periodic waves.

Snoeys and Brown (1969) **[77]** carried out an investigation on the dominant parameters in wheel and work-regenerative chatter. The block diagram, Figure 3.1, describes the regenerative effects in the process and the contributing parameters. The analysis begins with the statement that at any instant of time, the total amount of workpiece material removed plus wheel wear, must equal the total infeed minus system deflections. This may be expressed as:

$$\delta_w(t) + \delta_s(t) = u(t) - y_a(t) - y_m(t) \qquad (3.11)$$

where δ_w = radial amount of workpiece material removed

δ_s = radial amount of wheel wear

u = infeed

y_a = contact deflection

y_m = machine deflection

Equation 3.11 is in the time domain. In Laplace notation this becomes:

$$\delta_w(s) + \delta_s(s) = u(s) - y_a(s) - y_m(s) \tag{3.12}$$

The desired depth of cut is the increment of infeed during one revolution of the workpiece. This may be written as:

$$\Delta u(t) = u(t) - u(t - \tau_w) \tag{3.13}$$

where: τ_w = time for one revolution of workpiece.

Transforming into the Laplace domain, the depth of cut becomes:

$$\Delta u(s) = u(s) - u(s)e^{-\tau_w s} \tag{3.14}$$

$$\frac{u(s)}{\Delta u(s)} = \frac{1}{1 - e^{-\tau_w s}} \tag{3.15}$$

The instantaneous wear of the workpiece and of the wheel can be described in a similar fashion. The instantaneous wear equals the total wear minus the total wear one revolution earlier, i.e.

$$\Delta\delta_w(t) = \delta_w(t) - \delta_w(t - \tau_w) \tag{3.16}$$

$$\Delta\delta_s(t) = \delta_s(t) - \delta_s(t - \tau_s) \tag{3.17}$$

Carrying out the Laplace transformation as shown by Equations 3.14 and 3.15, yields the following expressions:

$$\frac{\delta_w(s)}{\Delta\delta_w(s)} = \frac{1}{1 - e^{-\tau_w s}} \tag{3.18}$$

$$\frac{\delta_s(s)}{\Delta\delta_s(s)} = \frac{1}{1-e^{-\tau_s s}} \tag{3.19}$$

Snoeys and Brown assumed that the instantaneous depth of cut or wear amount is proportional to the cutting force. In their analysis the cutting force is the resultant of the normal and tangential force components. Thus,

$$F_c(t) = k_c \Delta\delta_w(t) \tag{3.20}$$

$$F_c(t) = k_r \Delta\delta_s(t) \tag{3.21}$$

In Laplace notation:

$$F_c(s) = k_c \Delta\delta_w(s) \tag{3.22}$$

$$F_c(s) = k_r \Delta\delta_s(s) \tag{3.23}$$

Snoeys gives the machine structure compliance as,

$$\frac{y_m(s)}{F_c(s)} = \frac{1}{k_m} G_m(s) \tag{3.24}$$

G_m(s) is a function relating the relative compliance of the structure to the rotational frequency. When the frequency is zero the compliance is simply the inverse of the static stiffness k_m.

The contact stiffness is expressed as:

$$\frac{y_a}{F_n} = \frac{1}{k_a} \tag{3.25}$$

Snoeys and Brown show the inter-relationships of the equations in the form of a block diagram as shown in Figure 3.1.

Figure 3.1. Closed loop representation of the plunge grinding operation **[77,78]**.

The block diagram shows the system deflections y_a and y_m and cutting force which result from the total infeed, u. From this an instantaneous depth of cut of the workpiece and wear of the wheel will arise. It can be seen that the feedback paths for the wheel and workpiece operate in the same manner. Hence, a description of the workpiece return path will suffice for both. The feedback loop returns as the total wear of the workpiece. As described by Equation 3.16, this is the summation of the instantaneous depth of cut and total wear of the workpiece one revolution earlier. As shown in the block diagram this is where the regenerative effect occurs, i.e. if the process is unstable the amplitude of the waves on the workpiece will grow.

The next step in the analysis is to identify the dominant parameters. The transfer function for the block diagram is given as,

$$\frac{\Delta\delta_w(s)}{\Delta u(s)} = \frac{1}{1+(k_c/k_r)(1-e^{-\tau_w s}/1-e^{-\tau_s s})+(1-e^{-\tau_w s})[(1/k_a)+(1/k_m)G_m(s)]k_c} \tag{3.26}$$

By setting the denominator to zero the characteristic equation may be written, thus,

$$1+\frac{k_c}{k_r}\frac{1-e^{-\tau_w s}}{1-e^{-\tau_s s}}+(1-e^{-\tau_w s})\left[\frac{1}{k_a}+\frac{1}{k_m}G_m(s)\right]k_c=0 \tag{3.27}$$

In the frequency domain, Equation 3.27 becomes:

$$-\frac{k_m}{k_c}\frac{1}{1-e^{-j\tau_w\omega}}-\frac{k_m}{k_r}\frac{1}{1-e^{-j\tau_s\omega}}-\frac{k_m}{k_a}=G_m(j\omega) \tag{3.28}$$

Snoeys and Brown show that the real part of Equation 3.28 is a straight line crossing the abscissa at a point equal to:

$$-k_m\left(\frac{1}{2k_c}+\frac{1}{2k_r}+\frac{1}{k_a}\right)=\mathrm{Re}(G_m(j\omega)) \tag{3.29}$$

The limit of stability is reached when the two sides of Equation 3.29 are equal. If the real part of Equation 3.29 is greater than the left hand side the system is stable. If the real part of Equation 3.29 is less than the left hand side the system is unstable. Thus, for stability, it may be written:

$$\mathrm{Re}(G_m(j\omega))\geq -k_m\left(\frac{1}{2k_c}+\frac{1}{2k_r}+\frac{1}{k_a}\right) \tag{3.30}$$

This is illustrated in Figure 3.2.

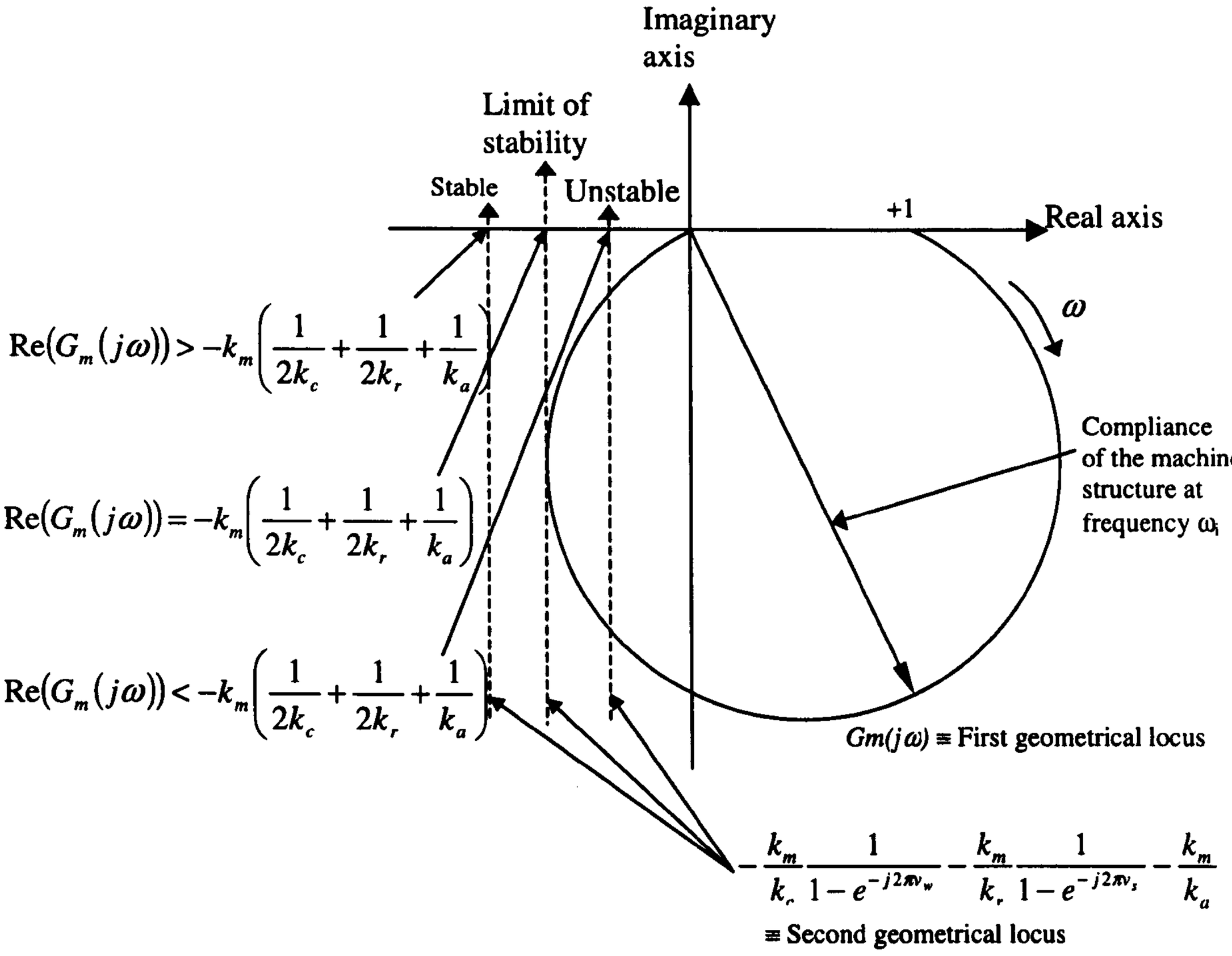

Figure 3.2. Graphical interpretation of stability equations [77,78].

The above analysis illustrates the basic functions of the parameters involved in the chatter process. Other investigators have modified this analysis. However, the effect of the parameters shown above is consistent [79].

From the analysis, it can be seen that a high value of static machine stiffness is desirable with low values for contact stiffness, grinding force coefficient and wheel wear resistance. Damping is also an important parameter affecting the dynamic characteristics of the machine tool. These factors will be discussed individually in the following sections.

3.5 Machine Stiffness

A high machine static stiffness is desirable for stability as shown by the previous analysis. High stiffness is also important to offset the tendency to increased amplitudes of forced vibrations due to wheel unbalance and vibrations due to other machine parts rotating at increased speeds. High stiffness also improves accuracy and repeatability of workpiece size. The machine static stiffness is the combined stiffness of the wheelhead and the workhead/workpiece/tailstock system. This is shown in Figures 3.4 and 3.5

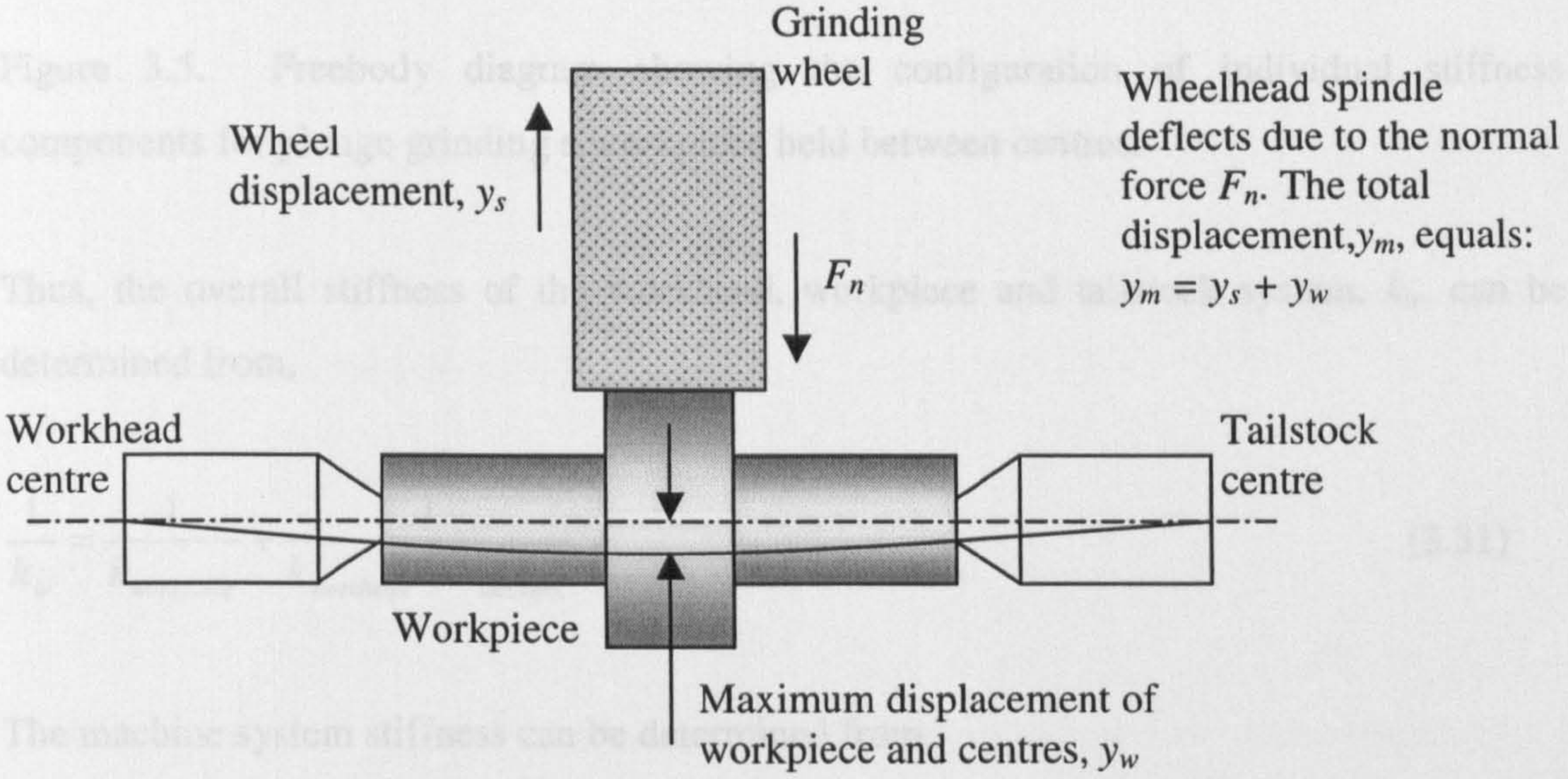

Figure 3.4. System deflections arising from the infeed of the wheel and the resulting force.

The stiffness of the workhead and tailstock centres, $k_{workhead}$ and $k_{tailstock}$, act in parallel with each other and in series with the workpiece stiffness, $k_{workpiece}$, as shown in Figure 3.5.

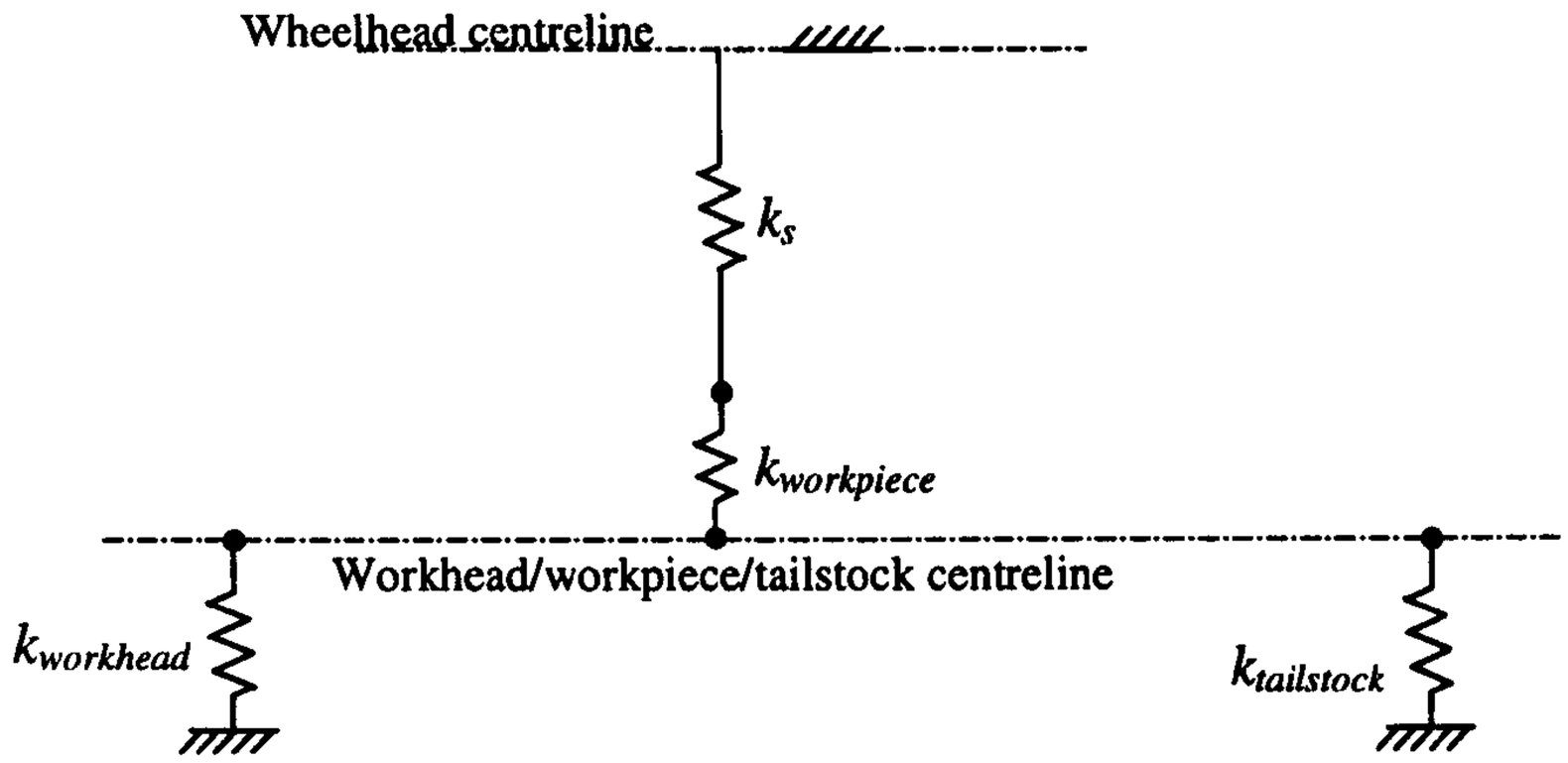

Figure 3.5. Freebody diagram showing the configuration of individual stiffness components for plunge grinding a workpiece held between centres.

Thus, the overall stiffness of the workhead, workpiece and tailstock system, k_w, can be determined from,

$$\frac{1}{k_w} = \frac{1}{k_{workpiece}} + \frac{1}{k_{workhead} + k_{tailstock}} \tag{3.31}$$

The machine system stiffness can be determined from,

$$\frac{1}{k_m} = \frac{1}{k_w} + \frac{1}{k_s} \tag{3.32}$$

The overall effective stiffness is determined when the wheel contact stiffness, k_a, is included, i.e.

$$\frac{1}{k_e} = \frac{1}{k_m} + \frac{1}{k_a} \tag{3.33}$$

The deflection, y_m, in the grinding system is determined by:

$$y_m = \frac{F_n}{k_e} \tag{3.34}$$

Inasaki, Karpuschewski and Lee (2001) **[79]** gave 20 N/μm as a typical effective stiffness for external cylindrical grinding machines. This figure was established from a survey of the characteristics of universal grinding machines.

The effective static stiffness may be related to the dynamic stiffness, k_{dyn}, in the following way,

$$k_{dyn} = 2\zeta k_e \tag{3.35}$$

Tobias (1965) **[80]** defines dynamic stiffness at resonance as the ratio between disturbing force and the resonance amplitude, A_{max}, thus,

$$k_{dyn} = \frac{F_n}{A_{\max}} \tag{3.36}$$

It can be seen, from Equation 3.36, that damping plays a crucial role in the magnitude of dynamic stiffness. This is due to the influence of damping on the resonance amplitude. Königsberger and Tlusty (1970) **[81]** found that 0.05 is a typical damping ratio for a mounted machine tool spindle. Merritt (1965) **[82]** concluded that the lack of adequate dynamic stiffness was the principal cause of chatter. This was attributed to the lack of damping inherent in structures. According to Merritt, if damping ratios of 0.5 were characteristic of structures, chatter would still be possible but it would be a relatively minor problem.

3.6 Contact Stiffness

The contact stiffness is the relationship between the normal force and the elastic deformation of the grinding wheel. Various investigations have found it to be non-linear with the relationship between the force and deformation described by,

$$y_a = F_n^{\,x} \tag{3.37}$$

where $x < 1$ and y_a is the elastic deformation of the wheel.

Thus, contact stiffness may be determined by differentiating Equation 3.37, yielding,

$$k_a = \frac{dF_n}{dy_a} \tag{3.38}$$

The stability analysis shows that a low contact stiffness contributes to moving the response locus (1st geometric locus in Figure 3.2) to the right. One of the easiest methods to reduce contact stiffness is to reduce force. This is achieved when wheelspeed is increased.

CBN wheels are generally harder than aluminium oxide wheels. While this has the advantage of increasing wheel life due to reduced wheel wear it is seen as a disadvantage in terms of stability. This was investigated by Sexton, Howes and Stone (1982) **[83]** where a more flexible inner layer between the CBN rim and the wheel hub material was found to suppress chatter. This method increased radial flexibility without compromising the wear resistance of the CBN. In terms of the stability analysis, it had the effect of adding a massless spring between the machine tool and the excitation point. The effect was that a positive in-phase quantity was added to the response at every frequency. Thus, the response locus was moved in the positive direction favouring greater stability. Examples of how increased radial flexibility can improve performance have been reported for other processes. For example, swan-neck tools used for turning operations such as screw cutting and parting-off have been found to benefit from increased radial flexibility. Rowe (1974) **[84]** reported that under conditions of geometric instability in centreless grinding, a rigid machine will regenerate waviness more strongly than a flexible machine. This was supported by evidence where rubber, and more flexible, control wheels gave improved roundness during the centreless grinding process. By increasing the elastic flexibility the resilience was increased. Resilience may be defined as the amount of strain energy, which

can be stored in a structure when it is deformed elastically and then, on unloading, to have this energy recovered. Thus, a lower contact stiffness will cushion a sudden blow by an undulation, by deforming elastically under the load, so that the transient forces and stresses, which result, are reduced. As the hardness of the grinding wheel (or control wheels in centreless grinding) increases more violent interchanges between potential and kinetic energy occur every time an undulation is encountered. By increasing the resilience, an energy reservoir is provided which allows potential energy to be stored temporarily as strain energy, thus, smoothing the process. At present there is no easy way to determine the best compromise between required static stiffness and resilience. However, as described by Equation 3.30, a low contact stiffness contributes to increased stability.

3.7 Grinding Force Coefficient

The grinding force coefficient may be defined as the normal force required to achieve a unit depth of cut, thus,

$$k_c = \frac{F_n}{a_e} \tag{3.39}$$

The term cutting stiffness is frequently used as its units are those of stiffness and it is often considered to represent the resistance to grinding, due to the wheel condition. However, it is not a stiffness in the true sense of the term, since the movement cannot be recovered. The lower the grinding force coefficient is, the more efficient the grinding action. As shown by Equation 3.30, a lower grinding force coefficient is desirable for stability.

Snoeys found that for the most common workspeed to wheelspeed ratios, $v_w/v_s<0.1$, the grinding force coefficient was linear. However, as k_c is affected by wheel condition, the coefficient constantly varies to some degree. Snoeys reports that from practical experience, increased workspeed tends to lead to chatter while increased wheelspeed contributes to better dynamic stability. This is partly attributed to an effect on grinding force coefficient as, when wheelspeed is increased, the normal force reduces for the same programmed depth of cut, and the grinding force coefficient is reduced.

3.8 Wheel Wear Resistance

The wheel wear resistance is the ratio of normal grinding force to depth of wheel wear.

$$k_r = F_n \,/\, depth\ of\ wheel\ wear\ per\ revolution \tag{3.40}$$

k_r is usually large enough in relation to the grinding force coefficient, to be considered of little consequence in the stability equation, i.e. $1/k_r << 1/k_c$. This is particularly true when applied to CBN wheels where wheel wear is generally far less than for aluminium oxide wheels. However, wheel-regenerative vibration builds up slowly over a long period and is generally significant for the redress life of the wheel.

The parameters, which contribute to the stability of the grinding process, have been outlined. It has been shown that contact stiffness and grinding force coefficient tend to reduce as wheelspeed increases. Increased grinding wheelspeed has been regarded as a key factor for successful use of CBN for many years, as reported by Malkin (1985) **[28]**, Tönshoff and Grabner (1984) **[85]**, Smith and Tsujigo (1977) **[86]**.

It can be argued that high initial costs of vitrified CBN wheels favour grinding at higher speeds. Higher wheelspeeds lead to higher G-ratios and shorter cycle times reducing production costs. It is this conclusion, which led research into the field of high speed grinding machines, their requirements and their problems. Based on this and the preceding considerations, the Suprema grinding machine was developed for wheelspeeds up to 150m/s. Later chapters detail the characteristics of the Suprema machine and assesses the design of the machine for the role of high precision grinding at high speed.

CHAPTER 4. ECONOMIC ANALYSIS

4.1 Introduction.

The purpose of this analysis is to provide a basis to assess the hypothesis that total process costs can be reduced and quality improved or maintained by grinding with vitrified CBN wheels at high surface speeds.

The technological principles presented in the previous chapter show that high-speed grinding with vitrified CBN has the potential to increase production rate and there is some industrial experience to show that the process can be technologically acceptable. At present, there is evidence of success in the use of high speed grinding with vitrified CBN, most notably in the automotive industry for grinding chilled cast iron camshafts and crankshafts **[87]**. It is important to note, however, that not all attempts to introduce the process in industry have been successful. This is particularly true of the bearing and aerospace industry. This is evident from the support for this research by two leading manufacturers from these industries. Later chapters will investigate the detailed technological requirements for success of the process.

The next step in the theoretical analysis, however, is to examine the economic merits of the process, taking the high costs of the technology into account. Further aims are to establish the economic benefits of high-speed grinding with vitrified CBN for wider application in the manufacturing community and to identify potential directions for further reducing costs.

The costs of producing parts by a process vary with process conditions. The costs consist of constant and variable costs. When considering a change in process conditions, it is only necessary to consider costs changes to determine whether there is a reduction in cost per part. In the case of a change in grinding conditions, the variable contributions to the total cost per part are wheel cost per part, machine cost per part, and labour cost per part and overhead contribution per part. Material cost per part remains constant when changing grinding conditions unless there is a significant change in the number of scrapped parts.

Wheel cost per part depends on the number of parts produced per wheel. Thus, abrasive lost through dressing, wheel wear, re-dress life and parts per dress, all affect wheel cost per part.

Labour cost per part is a time based cost and is affected by handling cost, down time, dressing and cycle time, inspection time and re-work time. Labour costs may also be increased to include the overhead contribution. Overheads include costs of buildings, estates and other services incurred by non-producing operations and staff. In the following analysis, the increased purchase costs of a high technology machine tool are identified by dividing the cost of the machine by the number of parts produced during a predetermined payback period.

Assuming that wheel costs are affected by abrasive lost through dressing, wheel wear and re-dress life, the controlling factors are the dressing and cycle parameters. Time dependent costs will be reduced by increased production rate. Costs related to down time and inspection time are reduced if greater consistency in quality is introduced. Since increased productivity through higher removal rates can have an adverse effect on wheel wear and part quality an in-depth study of the controlling factors affecting total cost is required.

From an economic perspective, attempts have been made to develop models that optimise the grinding process **[63, 88-92]**. However, as pointed out by Malkin **[9]** they generally yield results contrary to practical experience and have been found to be unreliable. This is largely due to the models not being sensitive to factors such as dressing conditions. They also rely heavily on empirically derived data, which are often not available. It is also pointed out by Malkin that these problems are exacerbated for precision grinding operations. The following analysis follows the classic simplified approach **[63, 88-91]**. A second approach is then presented which makes more realistic assumptions.

4.2 A Simplified Cost Analysis. The following approximate cost analysis is presented to show that it is possible to determine an optimum removal rate for minimum cost per part. This analysis considers only the variable costs and introduces simplifications to avoid the

complication of second order effects such as the cost of the abrasive removed by dressing, the labour involved in dressing and the effect of improved process reliability on cost per part. The total variable cost per unit volume of material removed may be assumed to be of the form,

$$C_{wt} = C_{wh} + C_{wl} + C_{wd} + C_{ws} \tag{4.1}$$

where C_{wh} = handling cost per unit volume of material removed.

C_{wl} = labour cost per unit volume of material removed.

C_{wd} = dressing cost per unit volume of material removed.

C_{ws} = wheel cost per unit volume of material removed.

The following substitutions can be made:

$$C_{wl} = c_l / Q_w$$

i.e. labour rate divided by workpiece volumetric removal rate ($Q_w = \pi d_w v_f$).

$$C_{wd} = a / \Delta V$$

i.e. cost per dressing operation divided by the volume of workpiece material removed per dress. Snoeys **[63]** states that dressing costs are almost exclusively due to the consumption of dressing time during which no material is ground.

$$C_{ws} = b / G$$

i.e. cost per unit volume of wheel divided by G-ratio, i.e. $G = V_w/V_s$ = volume of material removed divided by volume of wheel wear. The wheel cost in this approximate analysis neglects the effect of the wheel volume removed by dressing. In practice, the volume of abrasive removed by dressing is usually larger than the wear volume.

Handling costs are independent of the grinding process parameters. Consequently handling costs need only be included when considering lead times. As this cost analysis is in terms

of the process parameters and how they affect total costs, handling costs will be ignored. Thus, Equation 4.1 may be re-written as,

$$C_{wt} = \frac{c_l}{Q_w} + \frac{a}{\Delta V} + \frac{b}{G} \tag{4.2}$$

Since the volume of material removed per dress varies in an inverse relationship with the removal rate the following empirical relationships have been suggested for ΔV and G **[63,88-91]**:

$$\Delta V = V_0 \left(\frac{Q_w}{\nu_s} \right)^{-\nu} \tag{4.3}$$

where V_0 and ν are empirically derived constants. For a particular wheelspeed, Equation 4.3 can be re-written in the form,

$$\Delta V = V_1 Q_w^{-\nu} \tag{4.4}$$

where, V_1 and ν are empirically derived constants. For the G-ratio, the following empirical relationship has been suggested.

$$G = G_0 Q_w^{-g} \tag{4.5}$$

where G_0 and g are empirically derived constants.

Thus, the equation for total cost per unit material removed may be written,

$$C_{wt} = \frac{c_l}{Q_w} + \frac{a Q_w^{\nu}}{V_1} + \frac{b Q_w^{g}}{G_0} \tag{4.6}$$

Equation 4.6 ignores several cost terms, e.g. labour cost while dressing is performed, dressing tool cost, wheel cost for wheel volume removed by dressing and set-up costs at the start of each batch.

Equation 4.6 can be modified to suit two particular conditions. Condition 1 is met when the wheel-wear cost given by the last term of Equation 4.6 is negligible compared with other factors. It is often assumed that this condition is satisfied for precision grinding carried out using conventional abrasives. The second condition is met when wheel cost is significant relative to dressing cost which may be negligible or non-existent. This condition is said to be met for heavy-duty operations such as snagging (removal of surface defects from slabs or billets) and wheel cut-off. Grinding with superabrasives is also said to satisfy condition two. Where either of these conditions is met a simple expression for the optimum removal rate can be obtained by differentiating Equation 4.6 with respect to Q_w. Setting dC_{wt}/dQ_w to zero, the removal rate can be determined for minimum cost. This is shown, for both conditions, below:

Condition 1. When wheel costs are negligible, the optimum removal rate is given by,

$$\frac{dC_{wt}}{dQ_w} = -\frac{c_l}{Q_w^2} + \frac{vaQ_w^{v-1}}{V_1} = 0 \tag{4.7}$$

$$Q_w = \left(\frac{c_l V_1}{av}\right)^{1/(1+v)} \tag{4.8}$$

Condition 2. When dressing costs are negligible, the optimum removal rate is given by,

$$\frac{dC_{wt}}{dQ_w} = -\frac{c_l}{Q_w^2} + \frac{gbQ_w^{g-1}}{G_0} = 0 \tag{4.9}$$

$$Q_w = \left(\frac{c_l G_0}{gb}\right)^{1/(1+g)} \tag{4.10}$$

In summary, the classical costing analysis for optimum removal rates has been shown for two cases. However, Malkin **[9]** questions the practicality and reliability of this method. This is due to its reliance on experimentally derived data, and the fact that the optimum removal rates calculated are independent of process parameters. This is particularly problematic for precision grinding operations, the success of which is heavily dependent on correct parameter selection. It is also pointed out that no consideration is given to the limitations of the machine tool or target workpiece quality.

To overcome some of these issues the following cost analysis has been developed.

4.3 A Full Variable Cost Analysis. The limitations of the economic analysis described above make it necessary to use a more realistic and sensitive model and to include the machine cost if required. The model should be sensitive to input data such as dressing and cycle conditions, while relating to output results such as workpiece quality which can be used to determine re-dress life. Finally, the economic analysis should not only give total cost per part but also account for the constituent parts, i.e. wheel costs per part, labour cost per part, machine cost per part and the governing factors.

Since handling and material costs per part are constant, these are ignored as previously. The constituent parts of the total variable cost per part are assumed to be,

$$C_t = C_s + C_l + C_m \tag{4.11}$$

where C_s = wheel cost per part.

C_l = labour cost per part including an overhead contribution.

C_m = machine cost per part.

Each of the three cost contributions are defined in greater detail in the following sections.

4.3.1 Wheel Costs

Wheel cost per part may be written,

$$C_s = \frac{c_s}{N_w} \tag{4.12}$$

where c_s = the cost of the grinding wheel, i.e. purchase cost.

N_w = number of parts produced per wheel.

The number of parts produced per wheel is,

$$N_w = \left[\left(\frac{d_{s\max} - d_{s\min}}{2}\right) \Big/ (r_s + a_d n_d)\right] N_d \tag{4.13}$$

where d_{smax} = maximum wheel diameter.

d_{smin} = minimum wheel diameter.

r_s = radial wheel wear per dress.

a_d = depth of dressing increment.

n_d = number of dressing passes.

N_d = number of parts per dress.

Thus, C_s including the previously neglected effect of the cost of abrasive removed by dressing is,

$$C_s = \frac{2 \cdot c_s (r_s + a_d n_d)}{(d_{s\max} - d_{s\min}) N_d} \tag{4.14}$$

The effects of r_s, a_d, n_d and N_d on wheel cost per part can be seen from Equation 4.14. The sensitivity of wheel costs per part to different values of r_s, a_d, n_d and N_d depends on the relative sizes of the various factors. Typical variations in wheel cost per part are shown in the graphs presented below. Wheel cost is a contentious issue when comparing

conventional abrasives with CBN. To show how aluminium oxide and CBN wheels are affected, graphs are presented showing wheel cost per part based on assumed conditions. The assumptions made in each case are listed with the relevant figure. This analysis shows only how wheel costs per part are affected and is not a basis for wheel selection which should be based on total cost per part.

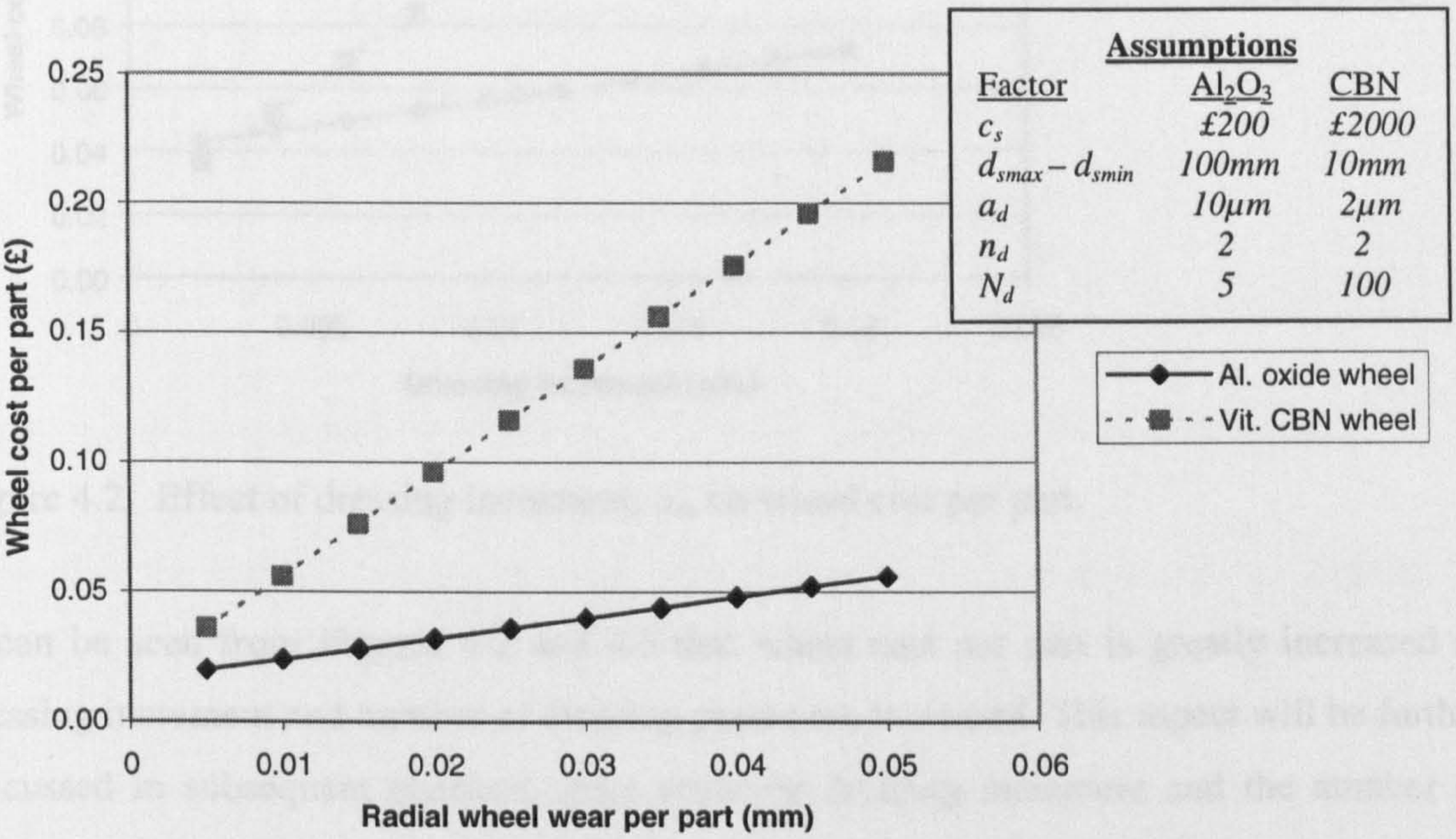

Figure 4.1. Effect of wheel wear per dress, r_s, on wheel cost per part.

The wheel cost per part for CBN is several times greater than the wheel cost per part for aluminium oxide despite the greater number of parts per dress. Based on wheel cost per part alone, this would suggest that CBN is more expensive. However, it will be shown later that the total cost per part may be reduced.

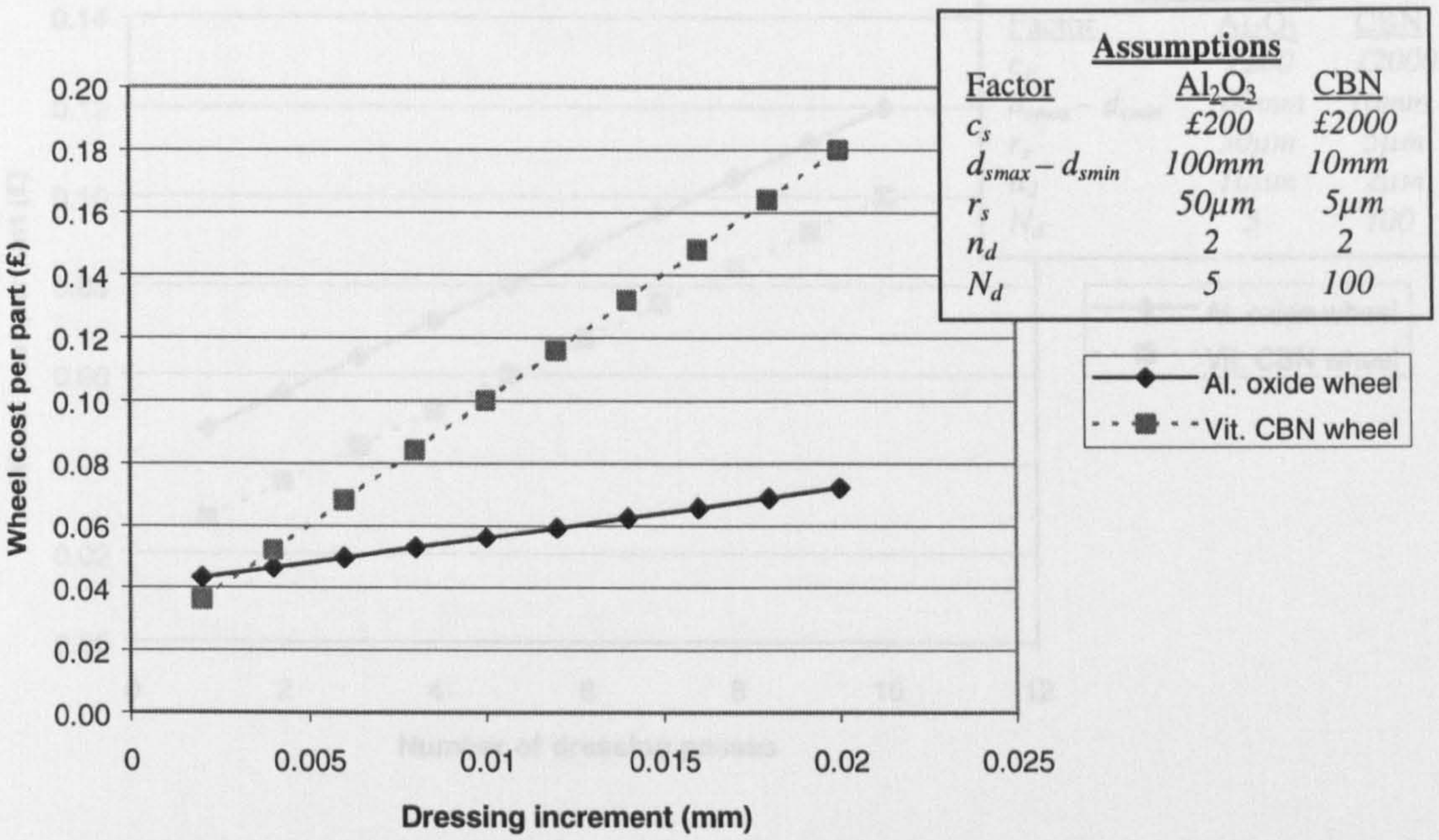

Figure 4.2. Effect of dressing increment, a_d, on wheel cost per part.

It can be seen from Figures 4.2 and 4.3 that wheel cost per part is greatly increased as dressing increment and number of dressing passes are increased. This aspect will be further discussed in subsequent chapters, since reducing dressing increment and the number of dressing passes with vitrified CBN helps to maintain a more efficient cutting action.

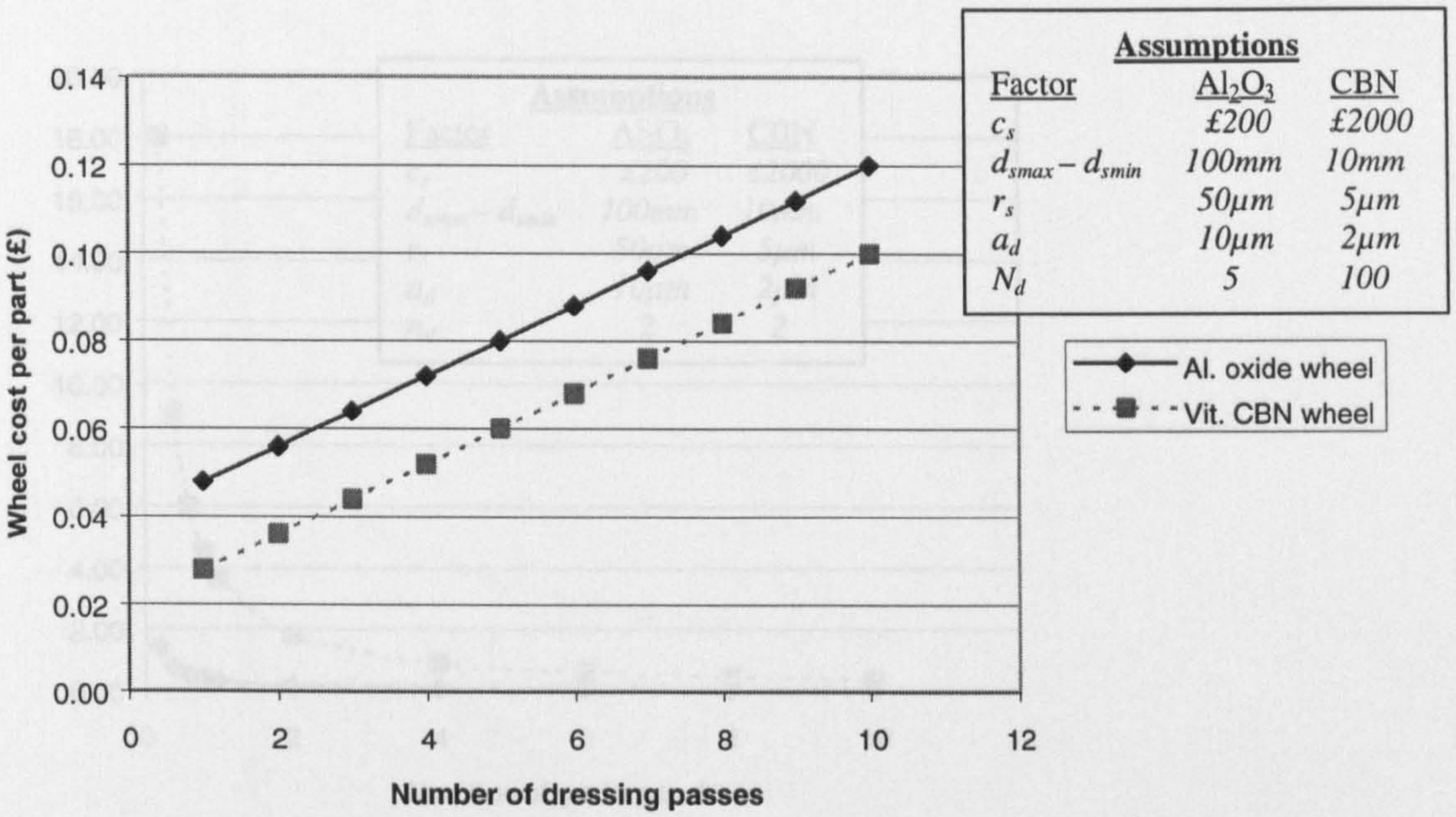

Figure 4.3. Effect of number of dressing passes per dress, n_d, on wheel cost per part.

Increasing the number of dressing passes consumes time and abrasive. At this stage in the analysis this effect has only been considered from the point of view of wheel cost per part. This does not include time dependent costs. This will be considered in the next section. The following chapters also show how the number of dressing passes affects performance and workpiece quality.

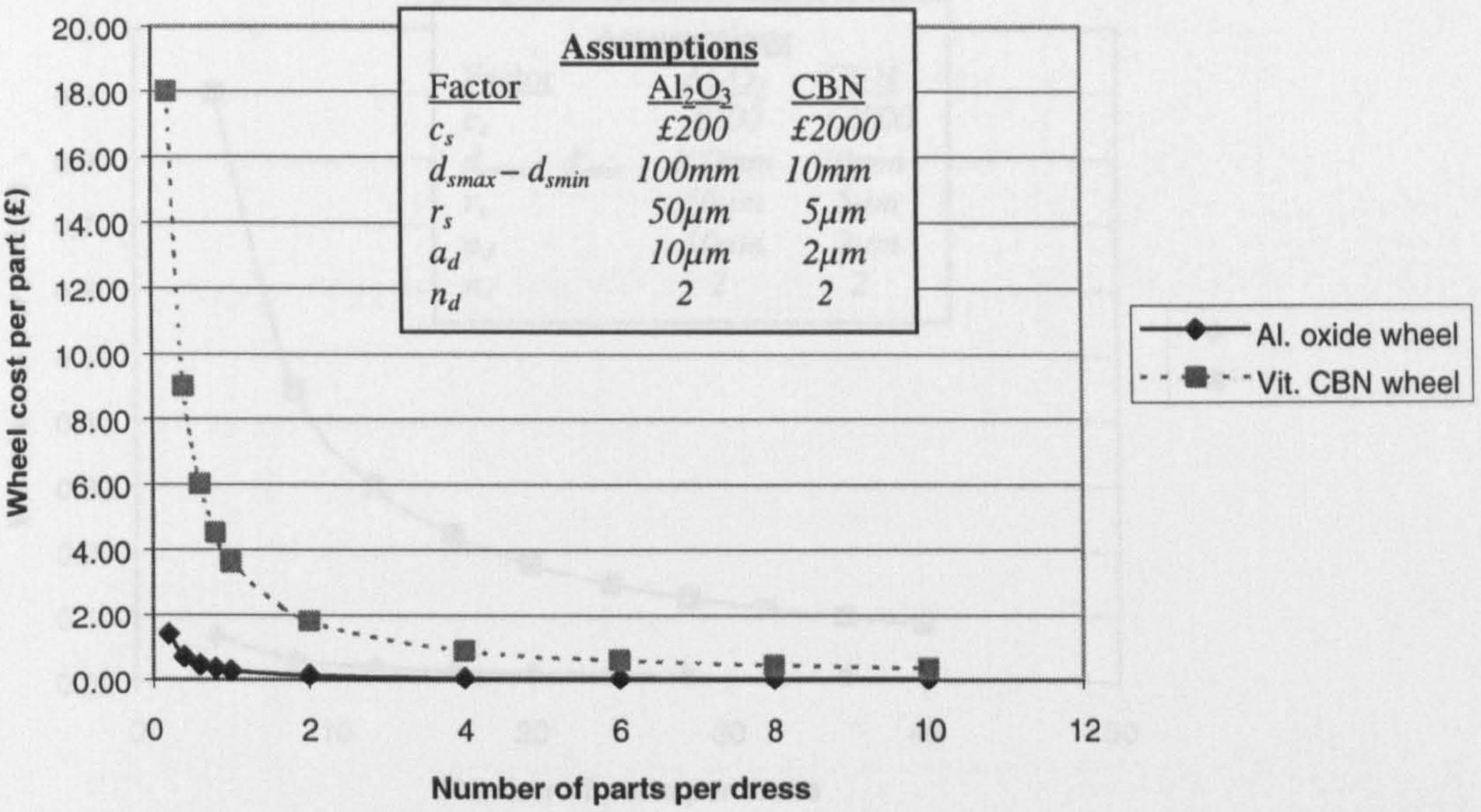

Figure 4.4. Effect of re-dress life in terms of number of parts per dress, N_d, on wheel cost per part. For precision grinding re-dress life is based on workpiece quality.

Figure 4.4 shows that the wheel cost per part is greatly reduced as the number of parts per dress is increased. This highlights one aspect of the critical importance of redress life.

Figure 4.5 extends the results shown in Figure 4.4 for a larger number of parts per dress. It can be seen that when the number of parts per dress reaches 40, the wheel cost per part is a small fraction of the value for a small number of parts per dress. This shows that, if the redress life is greatly increased with CBN the wheel cost per part reduces to a point where it is not much greater than for aluminium oxide. It should also be pointed out that, in practice, the re-dress life for both processes would not be equal. Thus, a large re-dress life for CBN compared to a low re-dress life for aluminium oxide could, in theory, lead to lower wheel costs per part for the CBN process.

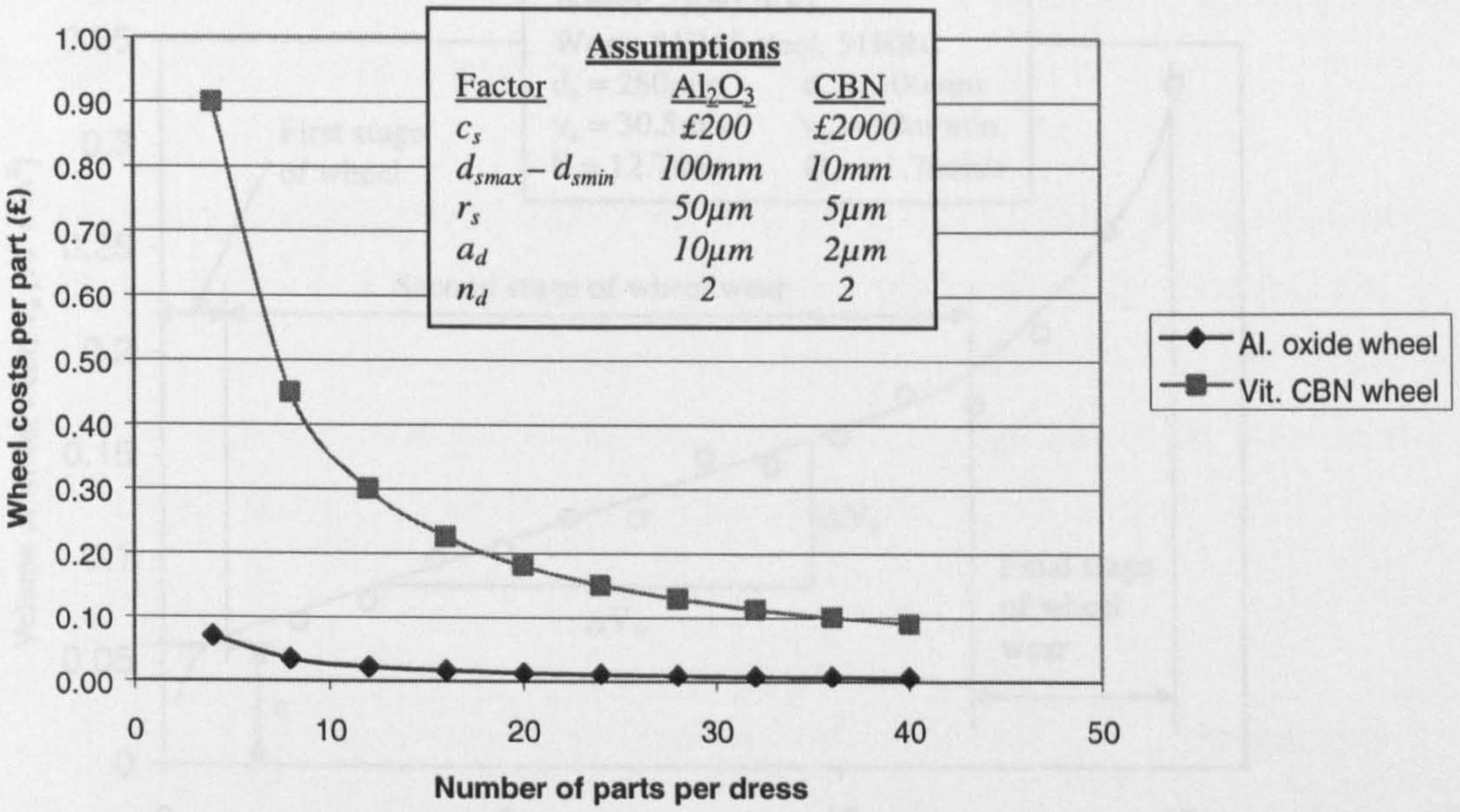

Figure 4.5. Effect of extended re-dress life in terms of number of parts per dress, N_d, on wheel cost per part. For precision grinding re-dress life is determined by workpiece quality.

The effects shown in Figures 4.4 and 4.5 have been based on wheel wear per dress, r_s, remaining constant even though re-dress life has been increased. The following analysis re-considers the affect of re-dress life with a corresponding increase in wheel wear.

Grinding wheel wear is a complex process. Wheel wear is usually greatest immediately after dressing. Beyond this initial stage the rate of wheel wear tends to become constant before reaching a final stage of excessive wear. A result from Backer and Krabacher (1956) **[93]** demonstrates this effect with an aluminium oxide wheel as shown in Figure 4.6.

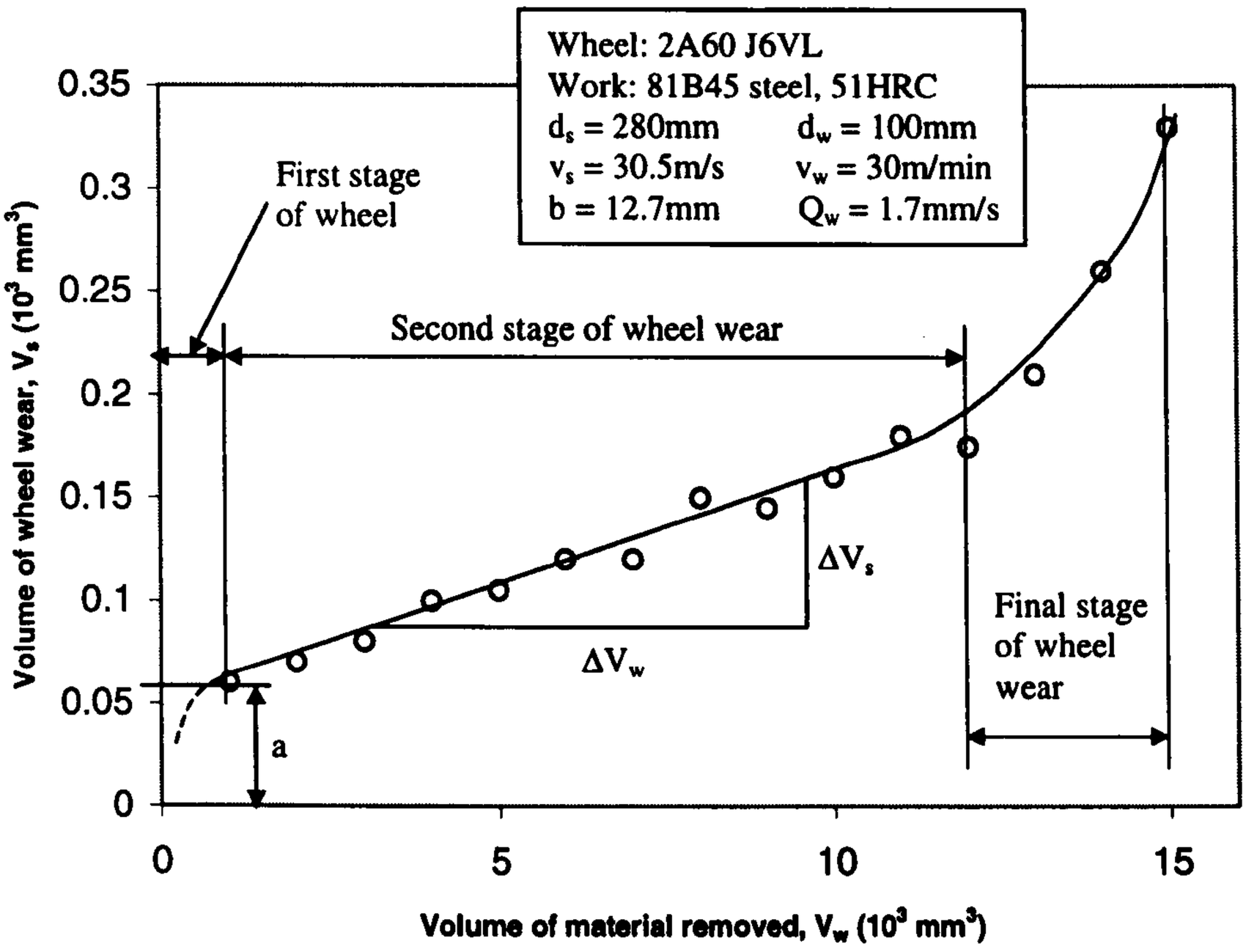

Figure 4.6. Typical grinding wheel wear curve for plunge grinding between centres using an aluminium oxide wheel **[93]**.

Using the following series it is possible to model the first two stages of wheel wear per unit volume of material removed,

$$a\ ,\ (a + d)\ ,\ (a + 2d)\ ,\ (a + 3d)\ ,\ \ldots.\text{etc.} \qquad (4.15)$$

where a = the initial volume of wheel wear.

d = the steady wheel wear per unit volume of workpiece material removed.

Each term in the series represents an increment of volume of material ground, or number of parts ground. 'a' is equal to the initial amount of wheel wear in the first stage and 'd' is equal to the constant rate of wheel wear during the second stage, i.e. $\Delta V_s / \Delta V_w$. If number of parts ground is used rather than volume of material removed, the effects shown in Figures 4.4 and 4.5 can be re-considered with an increase in wheel wear corresponding to

an increase in re-dress life. Thus, the following graph shows how the positive effects of increased re-dress life are affected by increased wheel wear per dress.

The following assumptions have been made. For an aluminium oxide wheel an initial radial wheel wear of 50 μm is assumed after 4 parts have been ground. Beyond this the rate of radial wheel wear is constant at 5 μm for every 4 parts ground. For a CBN wheel the initial radial wheel wear is assumed to be 5 μm after 4 parts ground. Thereafter the constant rate of radial wheel wear is 0.25 μm for every 4 parts ground.

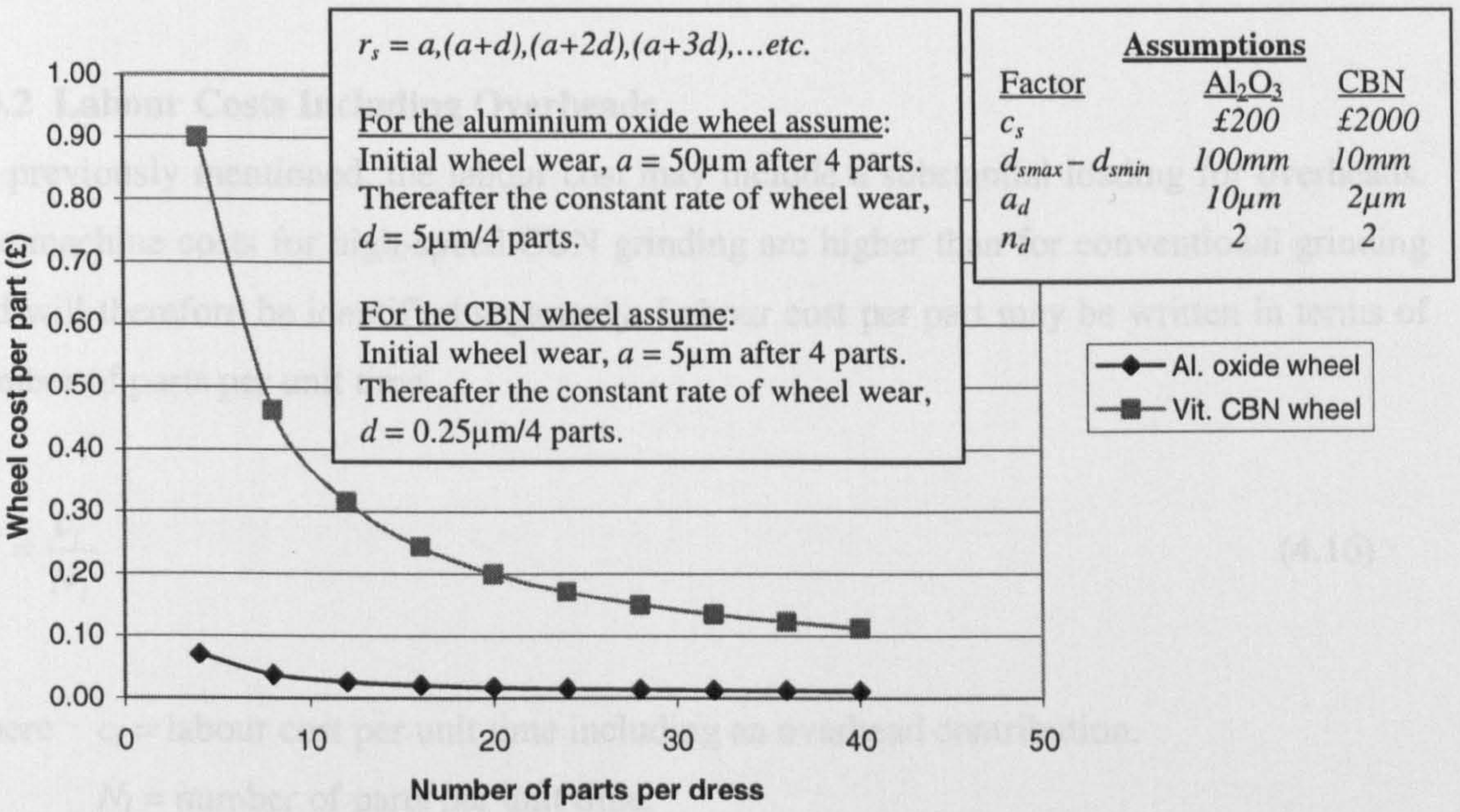

Figure 4.7. Effect of extended re-dress life on wheel cost per part with a corresponding increase in wheel wear.

It can be seen that the increase in wheel wear has a negligible effect on the wheel costs of the aluminium oxide wheel and a minimal effect on the CBN wheel. This is due to the stronger effect that an increased number of parts per dress has on reducing the wheel cost per part.

It has been shown that for a CBN wheel, an increase in wheel wastage through wear, dressing and/or reduced re-dress life, affects wheel cost per part. However, of these factors re-dress life appears to have the strongest affect. The analysis reveals that an aluminium oxide wheel is not as sensitive to these factors as CBN. This has implications for the performance requirements of the CBN wheel, as it appears to be cost sensitive to dressing parameters. This is directly through wheel wastage and indirectly through the influence of dressing parameters on re-dress life. To offset this cost, an increase in production rate may offer a solution. However, increased production rate usually leads to higher wheel wear or reduced re-dress life. The following analysis outlines the controlling factors with regard to labour costs.

4.3.2 Labour Costs Including Overheads

As previously mentioned, the labour cost may include a substantial loading for overheads. The machine costs for high-speed CBN grinding are higher than for conventional grinding and will therefore be identified separately. Labour cost per part may be written in terms of number of parts per unit time,

$$C_l = \frac{c_l}{N_l} \tag{4.16}$$

where c_l = labour cost per unit time including an overhead contribution.

N_l = number of parts per unit time.

The number of parts produced per unit time is based on a modified cycle time which includes the dressing time divided by the number of parts produced per dress, i.e. re-dress life,

$$N_l = \frac{1}{t_t} \tag{4.17}$$

where t_t = the modified total cycle time including dressing time given by,

$$t_t = t_s + \frac{t_d}{N_d} \tag{4.18}$$

and t_s = the cycle time per part.

t_d = dressing time.

N_d = number of parts per dress.

The cycle time per part includes the time to feed the stand-off distance and the dwell time,

$$t_s = \frac{d_{ww} + d_{ss}}{v_f} + s \tag{4.19}$$

where d_{ww} = stock removed from workpiece diameter.

d_{ss} = stand-off distance.

s = dwell time.

v_f = infeed rate.

Since, the specific volumetric removal rate, $Q'_w = v_f \pi d_w$,

$$t_s = \frac{(d_{ww} + d_{ss})\pi d_w}{Q'_w} + s \tag{4.20}$$

From Equation 4.18, dressing time is determined by,

$$t_d = \frac{b_s n_d}{v_d} \tag{4.21}$$

where b_s = wheel width.

n_d = number of dressing passes per dress.

v_d = dressing feedrate.

Dressing feedrate, v_d, is calculated from a specified dressing overlap. Thus, the dressing feedrate is dependent on the effective width of the dressing tool,

$$v_d = \frac{b_d}{U_d} \times \frac{v_s}{\pi d_s} \tag{4.22}$$

where b_d = the effective width of the dressing tool.

U_d = the dressing overlap ratio.

The effective width of the diamond(s) in a dressing tool is usually dependent on the dressing depth. Generally, as the dressing depth is increased, the effective width increases. This is due to the diamond tool geometry. To determine this accurately, it is necessary to measure the dressing tool using a profile-measuring instrument. Where rotary dressers are used, i.e. with multiple diamonds, an average should be taken from the profile measurements of a number of diamonds.

Substituting Equations 4.20 and 4.21 into Equation 4.18, the cycle time is,

$$t_t = \frac{(d_{ww} + d_{ss})\pi d_w}{Q'_w} + s + \frac{b_s n_d}{v_d N_d} \tag{4.23}$$

The labour cost per part in Equation 4.16 is therefore,

$$C_l = c_l \left[\frac{(d_{ww} + d_{ss})\pi d_w}{Q'_w} + s + \frac{b_s n_d}{v_d N_d} \right] \tag{4.24}$$

It can be seen from Equation 4.24 that factors such as volumetric removal rate, dwell time, number of dressing passes, dressing feed rate and the number of parts per dress affect labour cost per part. As the number of parts per dress increases, the final term becomes smaller reaching a point where it is negligible. Conversely, if a number of dressing

operations are called for during the production of every part the final term can have a significant effect.

The graphs presented below show how strongly the different factors of Equation 4.24 affect labour cost per part. Several assumptions have been made and are listed on the relevant figures. The analysis compares an aluminium oxide process on a standard CNC grinding machine, i.e. the J&S Series 10, with a CBN process on a high-speed grinding machine, i.e. the J&S Suprema. The dressing feedrate used for Figures 4.9 to 4.12 was based on the following values:

	Al_2O_3 wheel	Vit. CBN wheel
b_d	0.120mm (a_d = 0.01mm)	0.04mm (a_d = 0.002mm)
U_d	2	2
d_s	450mm	250mm
v_s	45m/s	120m/s

The above values give, v_d of 2mm/s for dressing the aluminium oxide wheel and 3mm/s for dressing the CBN wheel.

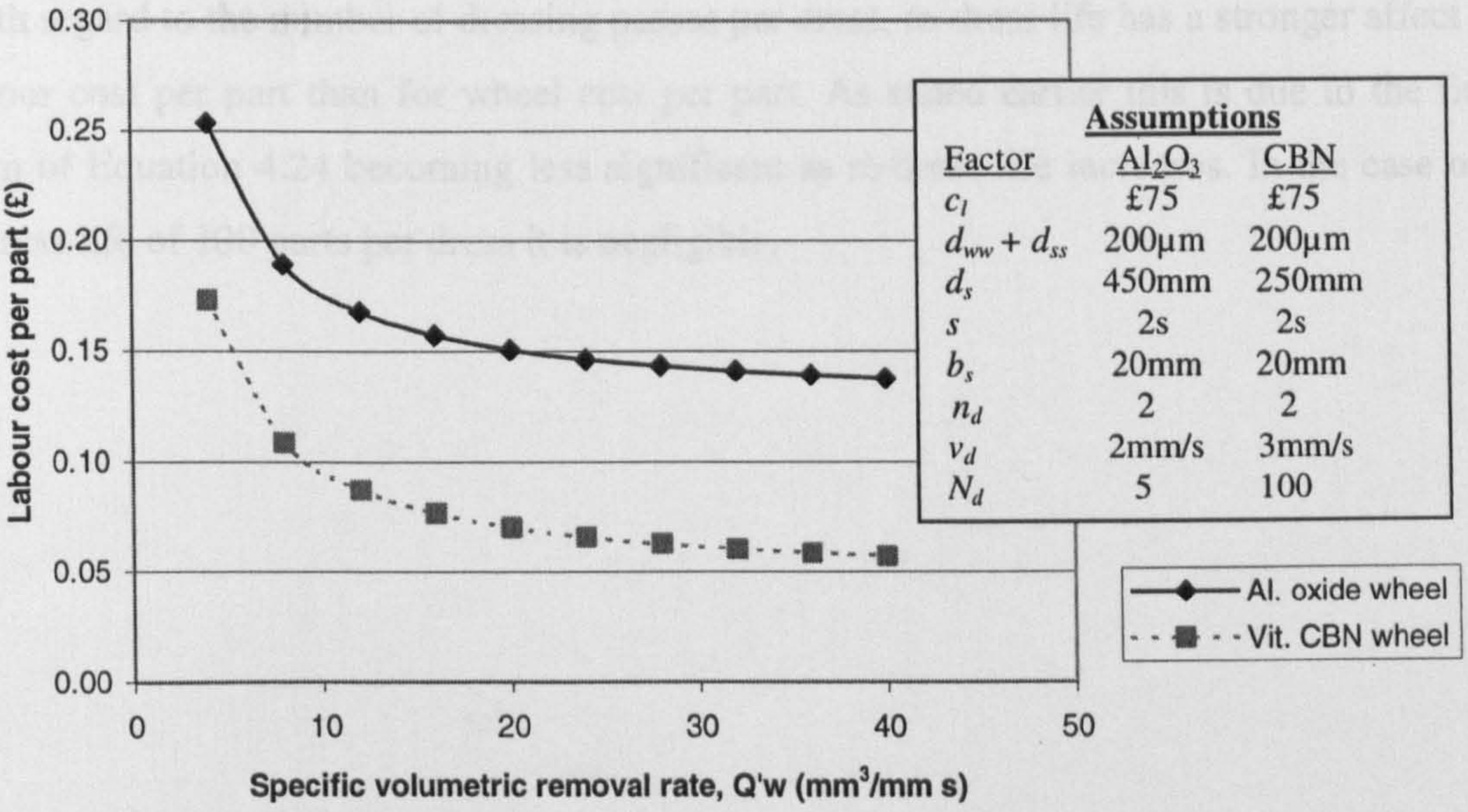

Figure 4.8. Effect of material removal rate, Q'_w, on labour cost per part.

Figure 4.9 shows how despite equal removal rates, a significantly high re-dress life can lead to lower labour cost per part for the CBN process. This highlights the importance re-dress life has on labour cost per part as well as wheel cost per part.

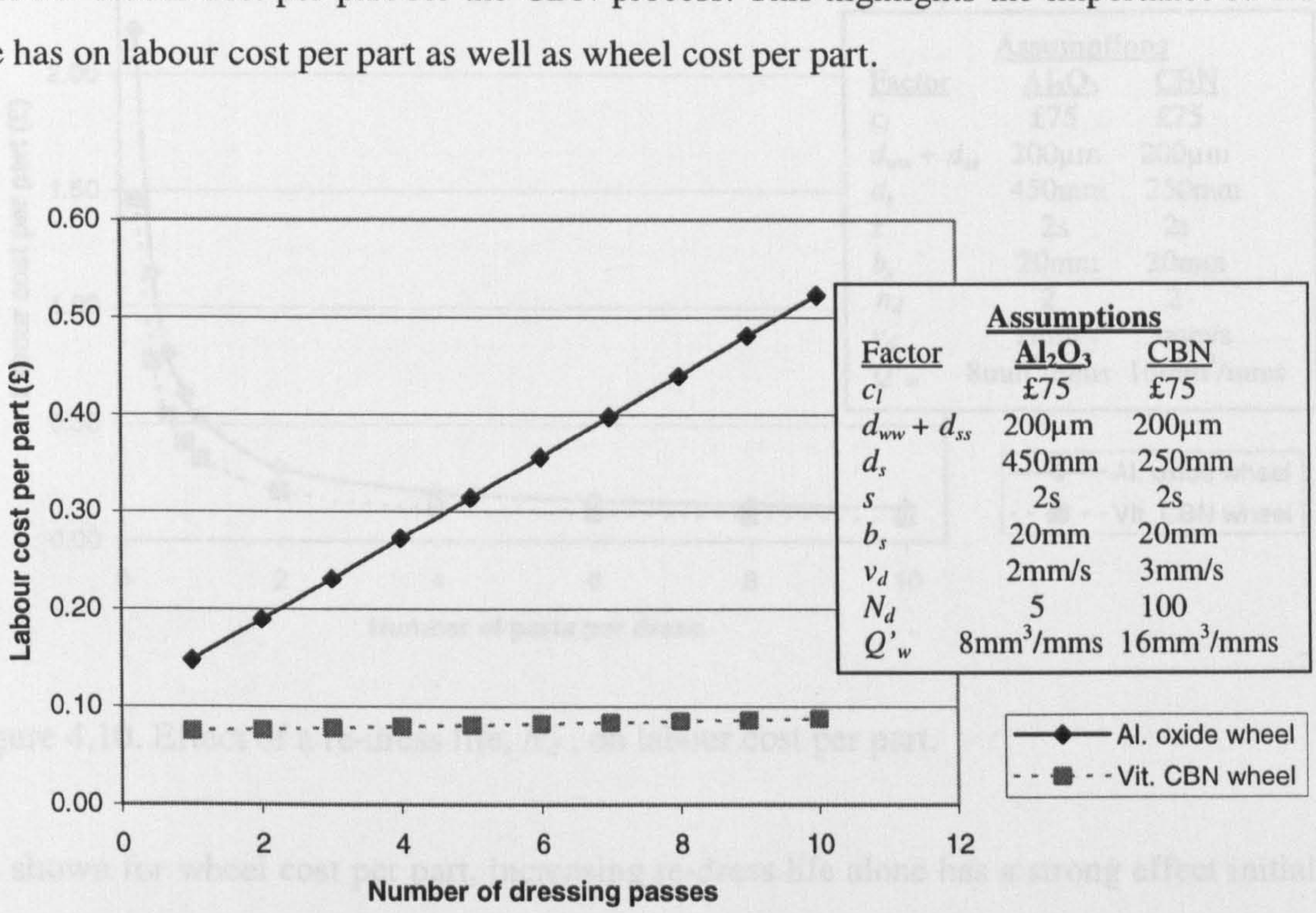

Figure 4.9. Effect of the number of dressing passes per dress, n_d , on labour cost per part.

With regard to the number of dressing passes per dress, re-dress life has a stronger affect on labour cost per part than for wheel cost per part. As stated earlier this is due to the final term of Equation 4.24 becoming less significant as re-dress life increases. In the case of a redress life of 100 parts per dress it is negligible.

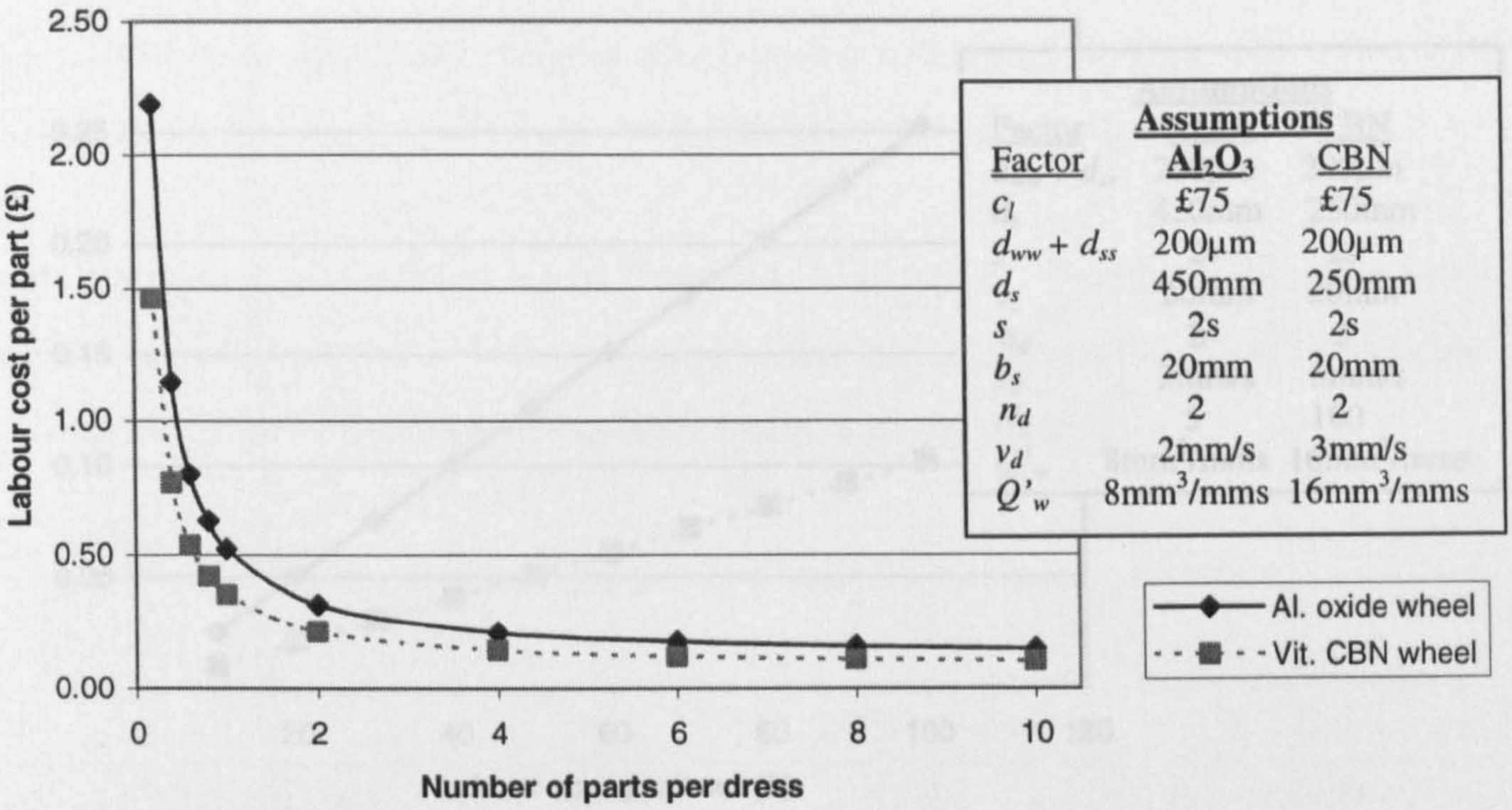

Figure 4.10. Effect of a re-dress life, N_d , on labour cost per part.

As shown for wheel cost per part, increasing re-dress life alone has a strong effect initially. However, beyond 4 parts per dress this effect is less marked. This is again due to the affect on the final term of Equation 4.24 which for the conditions used in this analysis becomes negligible for a re-dress life of 4 parts per dress and thereafter.

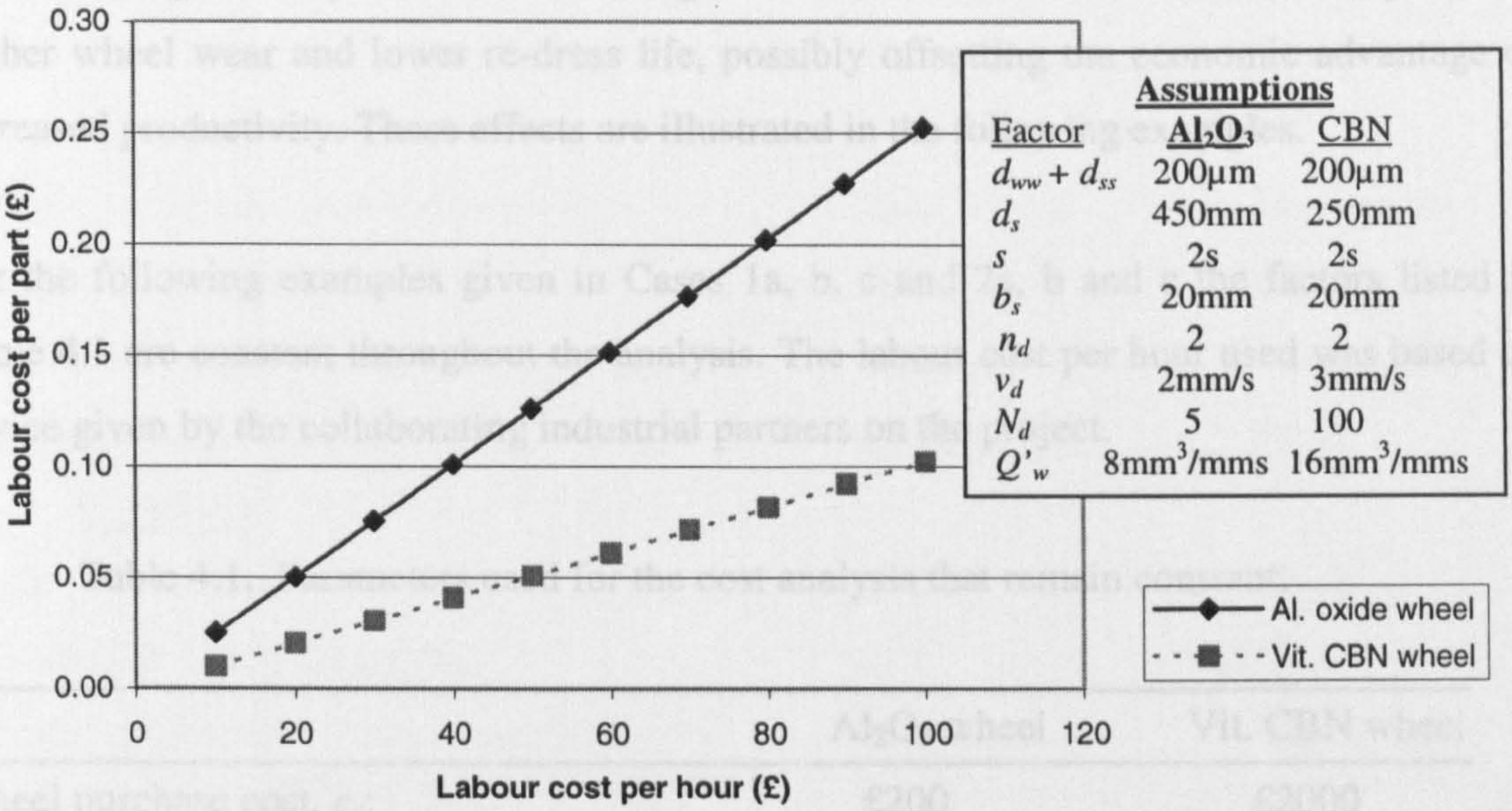

Figure 4.11. Effect of labour cost per hour, c_l, on labour cost per part.

As the high re-dress life for the CBN process makes the final term of Equation 4.24 negligible, increased removal rate is the primary factor for lowering labour cost per part with respect to labour cost per hour.

The total cost per part including labour cost and wheel cost may be written as,

$$C_t = \frac{2c_s(r_s + a_d n_d)}{(d_{s\max} - d_{s\min})N_d} + c_l\left[\frac{(d_{ww} + d_{ss})\pi d_w}{Q'_w} + s + \frac{b_s n_d}{v_d N_d}\right] \qquad (4.25)$$

From Equation 4.25 it can be seen that re-dress life, represented by the number of parts per dress, affects both the wheel and labour costs per part. The number of dressing passes affects both parts of the equation but is an input of dressing rather than an outcome. As a result the number of dressing passes can be kept low and its overall effect minimized.

By increasing wheelspeed, removal rate Q'_w can be increased. However, this may lead to higher wheel wear and lower re-dress life, possibly offsetting the economic advantage of increased productivity. These effects are illustrated in the following examples.

For the following examples given in Cases 1a, b, c and 2a, b and c the factors listed in Table 4.1 are constant throughout the analysis. The labour cost per hour used was based on advice given by the collaborating industrial partners on the project.

Table 4.1. Parameters used for the cost analysis that remain constant.

	Al_2O_3 wheel	Vit. CBN wheel
Wheel purchase cost, c_s:	£200	£2000
Dressing increment, a_d:	0.01mm	0.002mm
No. of dressing passes, n_d:	2	2
$d_{smax} - d_{smin}$:	100mm	10mm
Labour cost per hour, c_l:	£75	£75
$d_{ww} + d_{ss}$:	0.2mm	0.2mm
Workpiece diameter, d_w:	40mm	40mm
Dwell time, s:	2s	2s
Wheel width, b_s:	20mm	20mm
Dressing feedrate, v_d:	2mm/s	3mm/s

The effects of wheel wear, re-dress life and removal rate are illustrated in the following examples. Cases 1a, b and c compare CBN with aluminium oxide when the difference in re-dress life is high, i.e. for an easy-to-grind material such as AISI 52100. Cases 2a, b and c compare the two processes when re-dress life is low, i.e. for a difficult-to-grind material such as Inconel 718. The range of values used for radial wheel wear, re-dress life and specific volumetric removal rate differs between Case 1 and Case 2 to reflect the two different materials considered.

CASE 1a	Al_2O_3 wheel	Vit. CBN wheel
Radial wheel wear, r_s:	20µm	5µm
Re-dress life (parts/dress), N_d:	5	100
Specific volumetric removal rate, Q'_w:	5mm^3/mm·s	5mm^3/mm·s
Wheel cost per part, C_s:	**£0.03**	**£0.04**
Labour cost per part, C_l:	**£0.23**	**£0.15**
Total cost per part, C_t:	**£0.26**	**£0.19**

CASE 1b		
Radial wheel wear, r_s:	20µm	10µm
Re-dress life (parts/dress), N_d:	5	50
Specific volumetric removal rate, Q'_w:	5mm^3/mm·s	10mm^3/mm·s
Wheel cost per part, C_s:	**£0.03**	**£0.11**
Labour cost per part, C_l:	**£0.23**	**£0.10**
Total cost per part, C_t:	**£0.26**	**£0.21**

CASE 1c			
Radial wheel wear, r_s:	(20µm)	40µm	5µm
Re-dress life (parts/dress), N_d:	(5)	2.5	100
Specific volumetric removal rate, Q'_w:		10mm^3/mm·s	5mm^3/mm·s
Wheel cost per part, C_s:	(£0.03)	**£0.1**	**£0.04**
Labour cost per part, C_l:	(£0.22)	**£0.26**	**£0.15**
Total cost per part, C_t:	(£0.25)	**£0.36**	**£0.19**

Case 1a compares the aluminium oxide and CBN process when the difference in re-dress life is high and removal rate equal. For the CBN wheel the high re-dress life is important for reducing wheel cost per part. As the aluminium oxide wheel is relatively cheap a high re-dress life has a less significant effect on wheel cost per part. For Case 1b the removal rate for the CBN wheel has been doubled. Corresponding adjustment to radial wheel wear and re-dress life has been made. The overall effect on total cost per part is minimal. In Case 1c the removal rate for the aluminium oxide wheel has been doubled. Even without making an adjustment to wheel wear and re-dress life (figures in brackets of Case 1c) it can be seen that the CBN process remains the most cost effective.

CASE 2a	Al_2O_3 wheel	Vit. CBN wheel
Radial wheel wear, r_s:	60µm	10µm
Re-dress life (parts/dress), N_d:	1	5
Specific volumetric removal rate, Q'_w:	$5mm^3/mm \cdot s$	$5mm^3/mm \cdot s$
Wheel cost per part, C_s:	**£0.32**	**£1.12**
Labour cost per part, C_l:	**£0.56**	**£0.20**
Total cost per part, C_t:	**£0.88**	**£1.32**

CASE 2b		
Radial wheel wear, r_s:	60µm	10µm
Re-dress life (parts/dress), N_d:	1	5
Specific volumetric removal rate, Q'_w:	$5mm^3/mm \cdot s$	$20mm^3/mm \cdot s$
Wheel cost per part, C_s:	**£0.32**	**£1.12**
Labour cost per part, C_l:	**£0.56**	**£0.12**
Total cost per part, C_t:	**£0.88**	**£1.24**

CASE 2c		
Radial wheel wear, r_s:	60µm	5µm
Re-dress life (parts/dress), N_d:	1	10
Specific volumetric removal rate, Q'_w:	$5mm^3/mm \cdot s$	$2mm^3/mm \cdot s$
Wheel cost per part, C_s:	**£0.32**	**£0.36**
Labour cost per part, C_l:	**£0.56**	**£0.33**
Total cost per part, C_t:	**£0.88**	**£0.69**

The examples given in Case 2a, b and c show clearly that for CBN, wheel costs per part become significant when re-dress life is low. Case 2b highlights the minimal effect of increasing removal rate using CBN when the difference in re-dress life is small. To illustrate how important re-dress life is in affecting the total cost per part, an assumed set of conditions is given in Case 2c. Even when removal rate is less than half that of the aluminium oxide process the CBN process is economically viable providing re-dress life is increased and wheel wear reduced. In reality the removal rate of the aluminium oxide wheel could be reduced and economic advantage regained. However, the above examples

show firstly the importance of re-dress life when grinding with CBN and secondly how maximum production rate may not necessarily yield minimum cost per part.

4.3.3 Machine Costs

A move to high speed grinding will generally require a new machine tool. The costs of a machine tool are usually spread over a pay back period. The purchase cost can then be divided into cost per part for the payback period. Thus, Equation 4.25 becomes:

$$C_t' = \frac{2c_s(r_s + a_d n_d)}{(d_{s\max} - d_{s\min})N_d} + c_l\left[\frac{(d_{ww} + d_{ss})\pi d_w}{Q_w'} + s + \frac{b_s n_d}{v_d N_d}\right] + \frac{C_{mc}}{N_{mc}} \qquad (4.26)$$

where C'_t = total cost per part including machine tool purchase costs spread over the payback period.

C_{mc} = the purchase cost of the machine tool.

N_{mc} = the number of parts produced during the payback period.

The number of parts produced during the pay back period is,

$$N_{mc} = y_t N_l = \frac{y_t}{t_s + \frac{t_d}{N_d}} \qquad (4.27)$$

where y_t = payback period.

N_l = number of parts per unit time, i.e. $1/t_t$.

Substituting for t_s and t_d from Equations 4.20 and 4.21, the modified total cost per part is,

$$C_t' = \frac{2c_s(r_s + a_d n_d)}{(d_{s\max} - d_{s\min})N_d} + \left[\frac{(d_{ww} + d_{ss})\pi d_w}{Q_w'} + s + \frac{b_s n_d}{v_d N_d}\right]\left(c_l + \frac{C_{mc}}{y_t}\right) \qquad (4.28)$$

It can be seen that re-dress life is the only factor common to all three terms, i.e. wheel, labour and machine tool costs per part.

By including machine tool cost, total cost per part for the high-speed process may be higher than the conventional process, for the duration of the payback period. This will possibly be the case if a high-speed machine tool is bought to replace an existing conventional machine tool. However, providing the total cost per part after the payback period is sufficiently low enough, the initial investment may be justified.

The following graphs presented in this section show how the wheel, labour and machine tool costs contribute to the total cost per part. The graphs also show the effects of removal rate and re-dress life on total cost per part.

Figures 4.11 – 4.14 are based on the parameters listed in Table 4.1. The parameters not listed in Table 4.1 are as discussed below.

For the conventional process, the machine cost used was £100,000. For the high-speed process the machine cost used was £250,000. This increase was based on the high level of technology required for the high-speed machine tool. A short payback period of six months was assumed for both cases in order to highlight the differences. Assuming an average of 20 working days a month and sixteen hours per day, this equates to a payback period of 1,920 hours.

For Figures 4.12 and 4.13 the redress life was assumed to be 5 and 100 respectively and wheel wear was increased with each increase in removal rate. For the aluminium oxide wheel, wheel wear was increased from 0.01 mm to 0.1 mm in steps of 0.01 mm for each increase in removal rate of $4mm^3/mm{\cdot}s$. For the vitrified CBN wheel the increase was from 0.005 mm to 0.05 mm in steps of 0.005 mm for each increase in removal rate of $4mm^3/mm{\cdot}s$.

For Figures 4.14 and 4.15 the specific removal rate assumed was 8 $mm^3/mm{\cdot}s$ and 16 $mm^3/mm{\cdot}s$ respectively. Wheel wear was kept constant at 0.05 mm for the aluminium oxide wheel and 0.005 mm for the CBN wheel. This was seen as logical in that a constant value of removal rate was being used and that Figure 4.7 shows increased wheel wear to have a minimal effect on wheel cost per part when re-dress life is also increased.

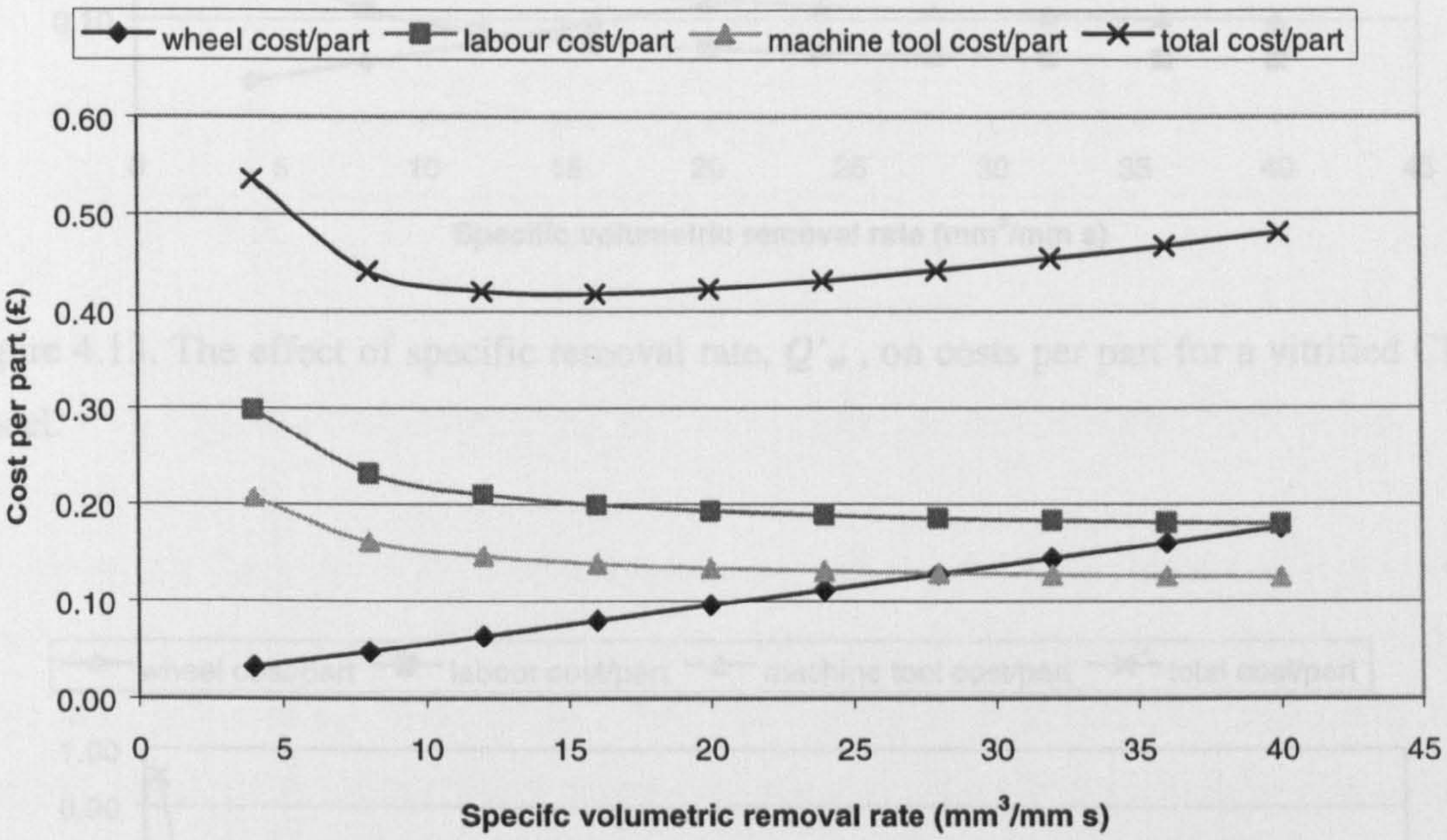

Figure 4.12. The effect of specific removal rate, Q'_w , on costs per part for an aluminium oxide wheel.

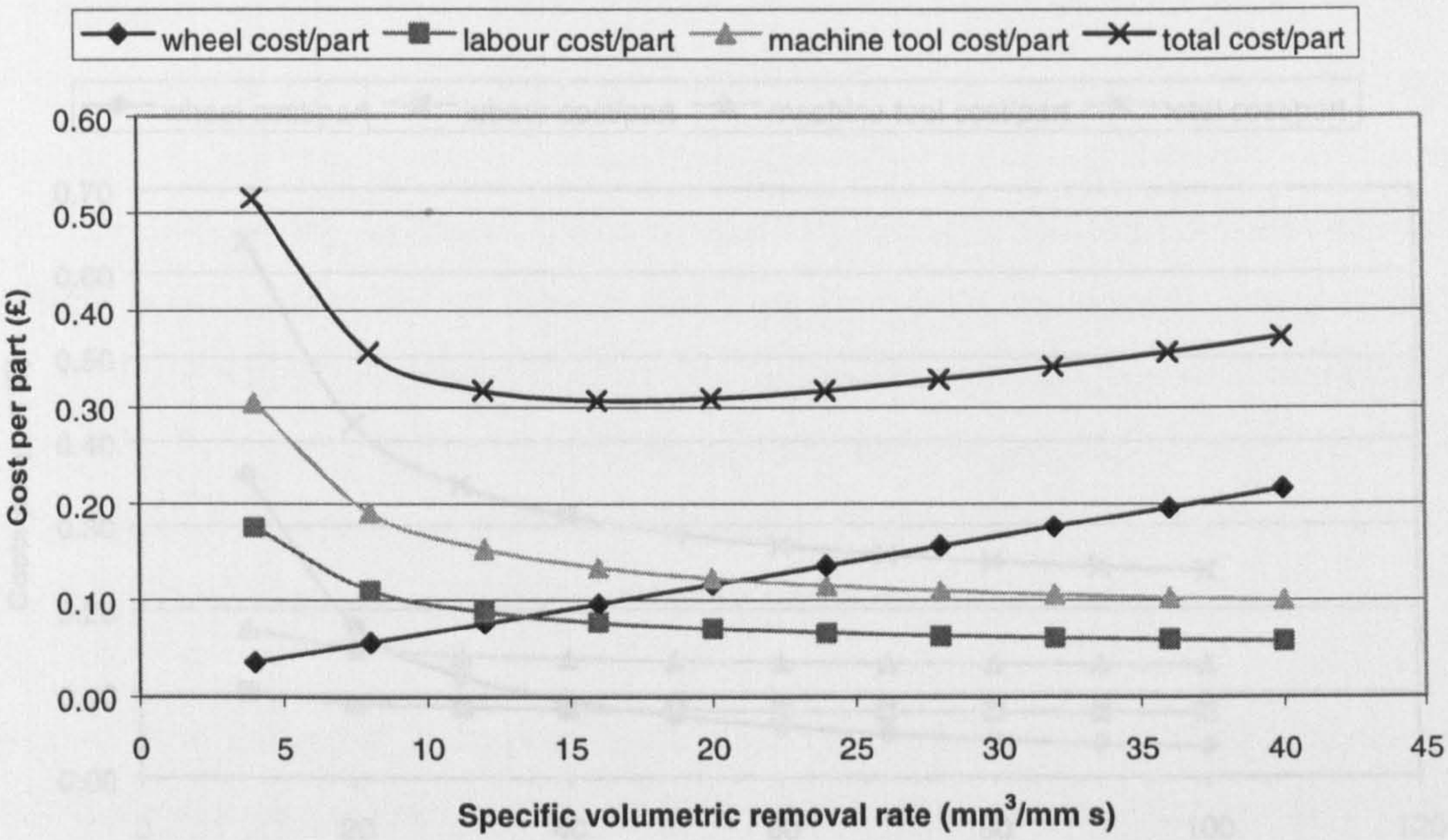

Figure 4.13. The effect of specific removal rate, Q'_w , on costs per part for a vitrified CBN wheel.

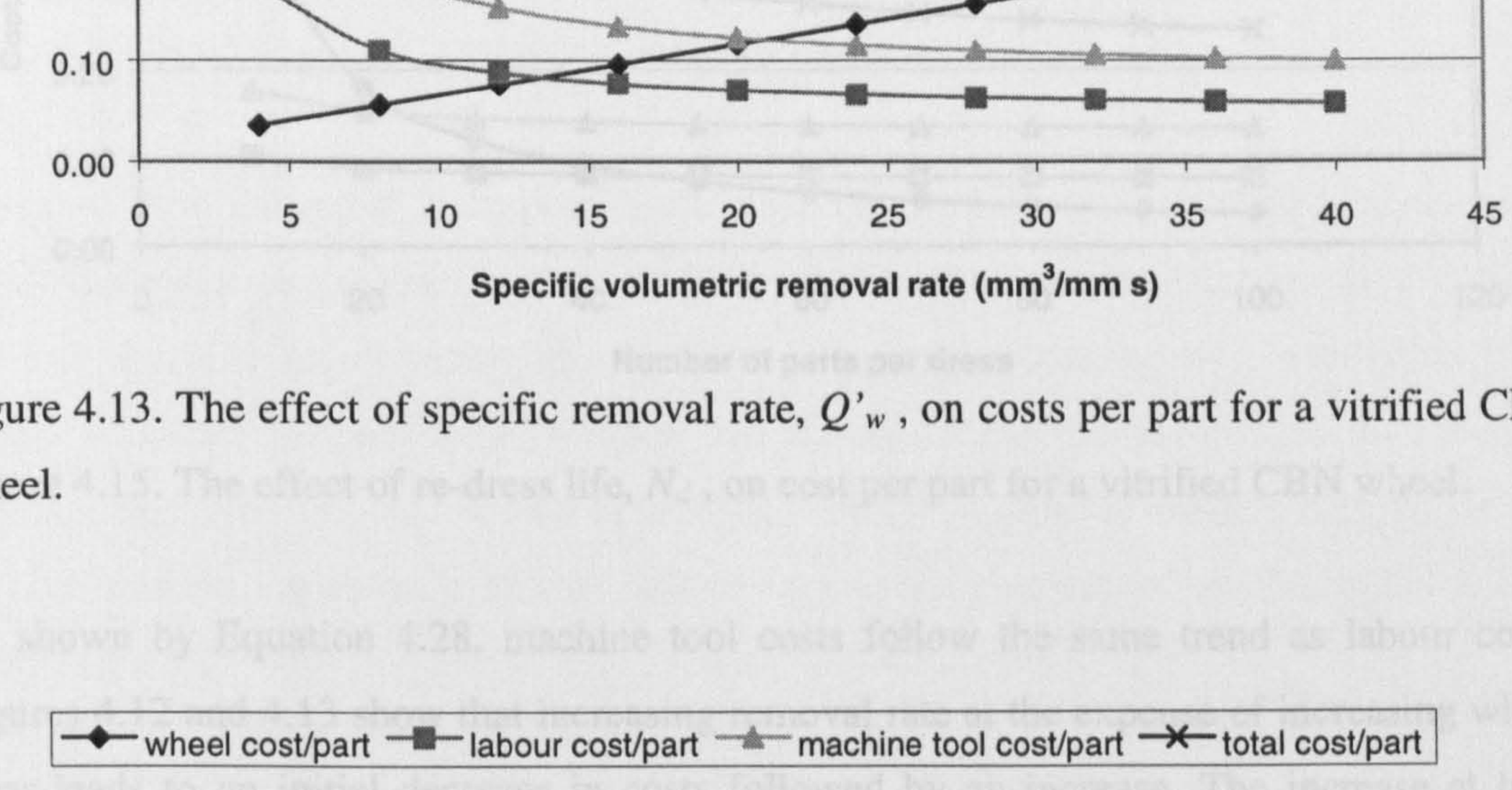

Figure 4.14. The effect of re-dress life, N_d, on cost per part for an aluminium oxide wheel

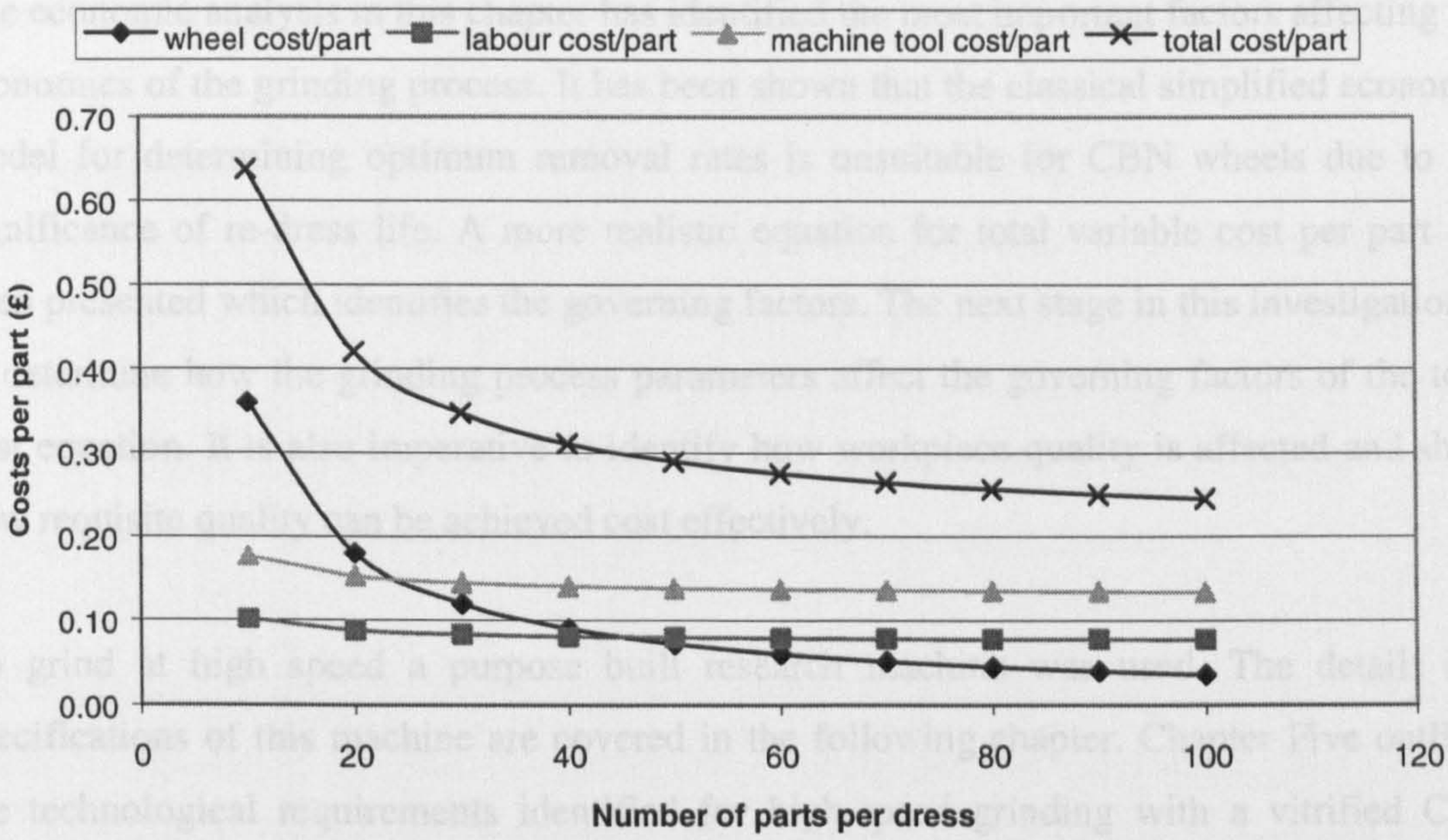

Figure 4.15. The effect of re-dress life, N_d , on cost per part for a vitrified CBN wheel.

As shown by Equation 4.28, machine tool costs follow the same trend as labour costs. Figures 4.12 and 4.13 show that increasing removal rate at the expense of increasing wheel wear leads to an initial decrease in costs followed by an increase. The increase at high removal rates is due to increasing wheel cost per part. The effect of re-dress life on total cost is strong initially but levels off as the number of parts per dress increases.

In terms of costs, if the assumptions are reasonable, the preceding graphs indicate a removal rate of between $10mm^3/mm{\cdot}s$ and $20mm^3/mm{\cdot}s$ for both wheels. For precision grinding a lower removal rate may be necessary, particularly for the aluminium oxide wheel. For the CBN wheel the cost analysis requires a re-dress life in excess of 40 parts per dress. For the aluminium oxide wheel, a re-dress life in excess of 5 parts per dress is required.

4.4 Summary

The economic analysis in this chapter has identified the most important factors affecting the economics of the grinding process. It has been shown that the classical simplified economic model for determining optimum removal rates is unsuitable for CBN wheels due to the significance of re-dress life. A more realistic equation for total variable cost per part has been presented which identifies the governing factors. The next stage in this investigation is to determine how the grinding process parameters affect the governing factors of the total cost equation. It is also imperative to identify how workpiece quality is affected and show how requisite quality can be achieved cost effectively.

To grind at high speed a purpose built research machine was used. The details and specifications of this machine are covered in the following chapter. Chapter Five outlines the technological requirements identified for high-speed grinding with a vitrified CBN wheel. Chapters Six and Seven outline the effects of process parameters on precision grinding and their implications on economic viability. Using the models outlined in this chapter, namely Equations 4.25 and 4.28, the economic potential of vitrified CBN will be identified.

CHAPTER 5. RESEARCH RIG - THE SUPREMA: A HIGH-SPEED PRECISION GRINDING MACHINE

5.1 Introduction

The Suprema grinding machine was built for an earlier project between Aachen University and a number of manufacturers. Its aim was to establish a step change in the precision grinding process. To achieve this, a high technology machine tool was developed to match the latest technology in grinding wheel design. This provided the foundation for the development of a high-speed vitrified CBN precision grinding machine.

The machine resulting from this work was known as the Suprema. However it was not tested sufficiently to confirm the concept of a special-purpose high-speed CBN grinding machine as an economic way forward in grinding practice. As a result, the present project was set up and the Suprema forms the basis of the research rig for this investigation. This chapter is in two parts. It will be seen that the mathematical models described in Chapter 3 provide the theoretical foundation on which the machine design and application is based.

The first part of this chapter is an overview of the materials, design, and application of the Suprema precision grinding machine. The second part discusses important features of the Suprema that affect its performance as a high precision grinding machine.

5.2 The Suprema Grinding Machine

The design of the Suprema is introduced by considering firstly how the machine tool elements collectively form a whole. A later discussion deals with how the design of the elements affects dynamic, static and thermal characteristics. Photographs of the Suprema can be found in Appendix A.

The base of the Suprema machine was solid granite. The worktable was bolted to a second granite block bolted to the base block. The workhead and tailstock were mounted on the worktable. The workhead centre was live when grinding between centres. The dresser unit

was mounted on a third granite block bolted to the second granite block. The worktable remained stationary during grinding. The wheelhead was fixed to the x-axis slideway mounted on the z-axis slideway. This allowed a working envelope within the footprint of the machine tool. The grinding wheel was mounted in a patented location system within the wheelhead arrangement and was at an angle of 30° to the worktable.

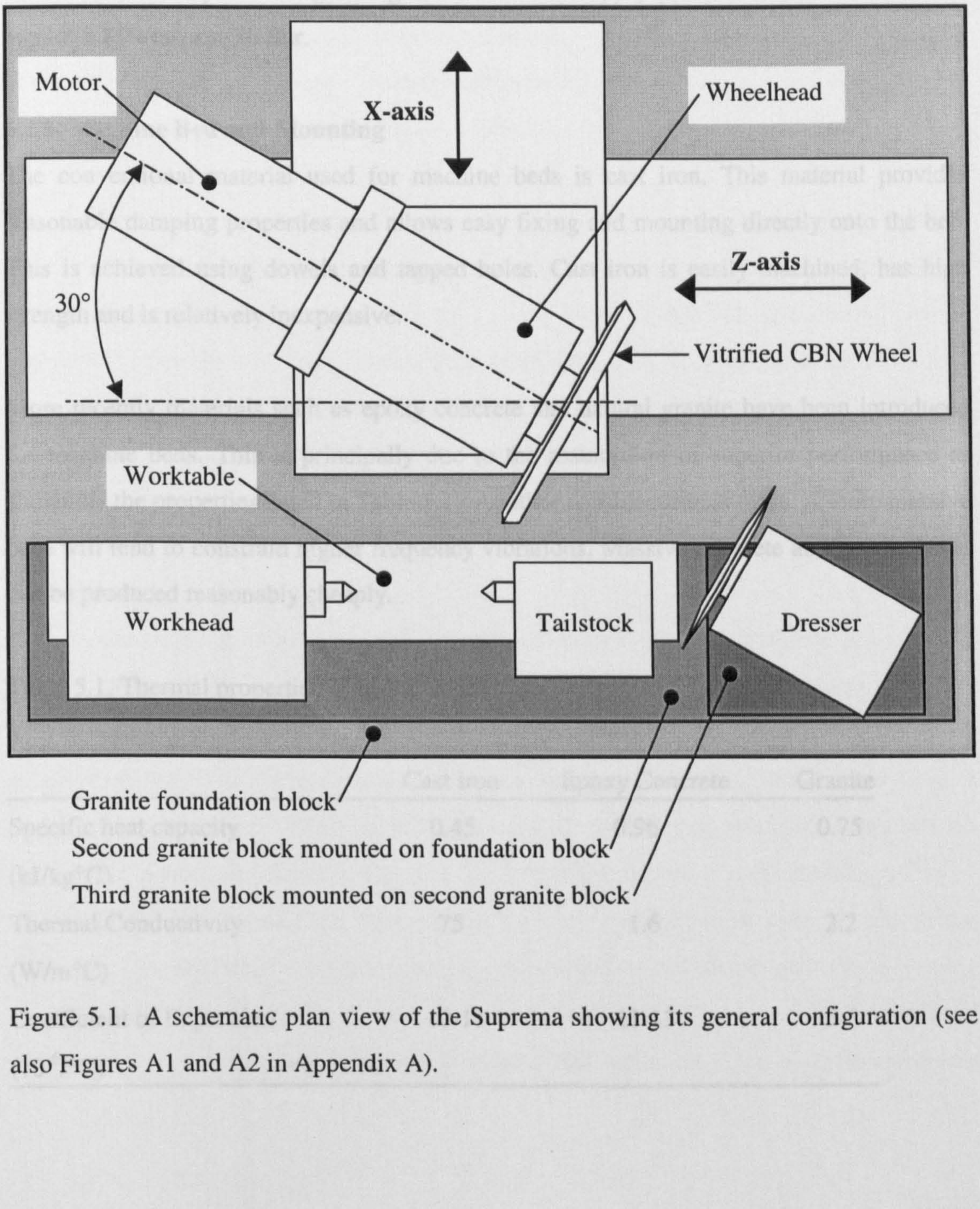

Figure 5.1. A schematic plan view of the Suprema showing its general configuration (see also Figures A1 and A2 in Appendix A).

The bearings of the workhead, dresser and wheelhead were hydrostatic. For all three spindles the oil used for the bearings was Mobil Velocite Number 3. The oil was pumped from a tank at a supply pressure of 14 MN/m^2. The oil tank was refrigerated for thermal stability. The configuration of the machine is summarised in Figure 5.1. Coolant was supplied to the grinding zone from a nozzle overhanging the grinding wheel. The design is conventional for cylindrical grinding machines. The supply pressure for the coolant was high at 3 MN/m^2, i.e. 30 Bar.

5.2.1 Machine Bed and Mounting

The conventional material used for machine beds is cast iron. This material provides reasonable damping properties and allows easy fixing and mounting directly onto the bed. This is achieved using dowels and tapped holes. Cast iron is easily machined, has high strength and is relatively inexpensive.

More recently materials such as epoxy concrete and natural granite have been introduced for machine beds. This is principally due to the assumption of superior performance as shown by the properties listed in Table 5.1. Another consideration is mass. A more massive base will tend to constrain higher frequency vibrations. Massive concrete and granite bases can be produced reasonably cheaply.

Table 5.1. Thermal properties of bed materials.

	Cast Iron	Epoxy Concrete	Granite
Specific heat capacity (kJ/kg°C)	0.45	0.96	0.75
Thermal Conductivity (W/m°C)	75	1.6	2.2
Coefficient of Expansion (10^{-6}/°C)	10-11	11-13	5-8

The material used for the Suprema was granite. As granite cannot be easily formed into a specific shape, as can the other materials, the bed was constructed using three blocks. This was not seen as a disadvantage as the increased number of mating surfaces provides increased dissipation of energy and results in improved damping. The three blocks were of the following dimensions:

Main bed:	1600mm x 1000mm x 300mm
Table support:	1600mm x 240mm x 225mm
Dresser support:	275mm x 240mm x 110mm

The granite blocks were bolted and bonded together. Parts mounted on the granite blocks, such as the machine table and the dressing unit, were bolted to the granite using steel inserts in the granite. The steel inserts were glued into holes drilled into the granite. Where appropriate, dowels were also fitted in the same way. The steel inserts were positioned away from the edges of the granite so as to reduce the risk of fracture due to the stresses arising from bolting. The granite bed sat on a steel frame supported by anti-vibration pads at three points.

5.2.2 Slideways

The standard configuration for slideways of a cylindrical grinding machine is to have a moving table in the z axis, with the wheelhead moving in and out on the x axis slideway. The movement of the table requires that the machines working envelope is larger than its actual footprint. This is also true of surface grinding machines, which also have a reciprocating work-table. When shop floor space is divided up into unit costs, it can be seen that having a work envelope greater than the machine footprint is a disadvantage. One of the design specifications of the Suprema was for it to require no more space than its actual footprint. This was achieved by mounting the wheelhead on both the x and z axis. By doing this, the worktable remains fixed and the movement of the wheelhead is within the footprint of the machine. Jones and Shipman developed this technology for a surface grinding

machine. Liverton (2001) **[94]** reports the following advantages, which also apply to the Suprema for cylindrical grinding:

- Stiff cuboid bed.
- Small footprint.
- Reciprocating mass is small and constant.
- Large non-working zone area for mounting auxiliary equipment.
- Good operator ergonomics for set up and component loading/unloading.

X and z axis slideways both ran on pre-loaded rolling element linear bearings. The classification of the bearings was Q4 specifying a 0.004 mm per 1000 mm maximum parallelism error between the bearing tracks and locating face. Whilst linear bearings have a higher stiffness than equivalent rotary ball bearings they do not have particularly good damping properties compared with plain bearing slideways. To overcome this, the bearing manufacturers, INA, developed a viscous damping element. To utilise this property, the carriage, which runs on the guideway, is in three parts with the central section acting as a damper. This was achieved by matching the profile of the carriage and guideway to within a clearance of 20 μm to 30 μm. The gap was filled with lubricating oil to provide damping without compromising stiffness or greatly increasing friction. The two end carriages ran on the rolling element linear bearings. Both axes of the machine were driven by continuously lubricated recirculating ballscrews.

Linear encoders were used to measure axis position. To minimise the effects of Abbé errors the encoders were positioned as close to the grinding wheel as possible. The resolution of the measuring system on the z axis was 0.1μm; on the x axis was 0.05 μm.

5.2.3 Worktable, Workhead and Tailstock

The worktable was mounted directly onto the granite and was manufactured from cast iron. Both the workhead and tailstock were located and fastened to the worktable by mating dovetails and clamping bolts. The tailstock was made from cast iron and was bolted to the worktable. It included a Number 3 Morse taper. The tailstock was a standard design where

the centre was spring-loaded to apply an axial force. Where the error in workpiece parallelism was large it is necessary to adjust the angular position of the worktable on its mounting. This is a standard set-up procedure for cylindrical grinding. However, incorporated in the tailstock design was an adjusting mechanism allowing fine radial movement. This was used to remove slight tapers in the workpiece, thus easing set-up.

To provide increased stiffness, hydrostatic bearings were used for the workhead spindle. Cooled oil was supplied to the bearings with a supply pressure of 14 MN/m^2. Traditional workhead designs have used either plain bearings or roller bearings. These bearing designs allowed the workhead to operate in one of two states allowing grinding to be carried out either between centres or using a chuck. When grinding between centres it is usual to use dead centres. This minimises roundness errors due to any eccentricity in the workhead spindle. To achieve this an outer sleeve on the workhead spindle rotates while the actual workhead spindle remains stationary. Guest [7] called this design the 'running spindle'. The outer sleeve is used to drive a carrier fastened to the workpiece, providing rotation of the workpiece on dead centres. It was assumed that the greater accuracy of hydrostatic bearings would allow a live spindle to be employed. As a result grinding between centres on the Suprema was carried out with a live centre. It was found later, that this led to run out errors of the centre. This is discussed in more detail in Section 5.18.

5.2.4 Dresser Unit

Dressing was carried out on the Suprema using a 150 mm diameter diamond dressing disc. The dresser was capable of speeds up to 15,000 rpm in either direction. The bearings, spindle and motor were all contained in a cylindrical steel cartridge. The cartridge was mounted in a cast iron housing bolted to the worktable. The bearings of the dresser were hydrostatic. The oil tank was refrigerated for thermal stability. The dresser was driven by a 3 phase asynchronous motor mounted between the hydrostatic bearings. This is known as an integrated design and is useful when space is limited. The motor had a continuous power rating of 2 kW and an intermittent duty cycle of 3 kW. The motor was cooled by a continuous flow of water passing through a surrounding cooling jacket.

5.2.5 Wheelhead Spindle

The wheelhead was a cast iron housing bolted to the x and z-axis slideways, containing a steel cylindrical cartridge. The cartridge contained the wheelhead spindle, bearings and balancing unit. The wheelhead spindle was supported by conical hydrostatic journal bearings. The supply pressure was 14 MN/m^2 and radial film thickness between the bearing and journal was 10 μm. The maximum speed of the spindle was 10,000 rpm equivalent to a surface speed of 130 m/s for a 250 mm diameter wheel. The wheel head was mounted at 30° to the worktable. This allowed a smaller diameter wheel to be used. The benefits of this were lower cost. However, a disadvantage was that a higher speed motor was required to achieve the high surface speed of the wheel. The motor selected for this purpose was manufactured by AMK and was a 3 phase asynchronous type, mounted directly to the wheelhead. The motor was water-cooled and had a continuous power rating of 10 kW and an intermittent duty cycle of 15 kW.

Wheel balancing was carried out by an automatic balancing unit (auto-balancer) located inside the spindle shaft. This was a separate unit to the CNC controller and was supplied by Dittel GmbH. The auto-balancer was controlled via a non-contacting transmitter and receiver. The receiver rotated with the shaft while the transmitter was fixed. An accelerometer monitored the vibration generated by the rotating wheelhead spindle. The magnitude of the vibration was analysed by a Dittel control unit. If the magnitude of the vibration was unacceptable a signal was sent to the auto-balancer, via the transmitter and receiver, to adjust until the vibration subsided to an acceptable level. A second feature of the Dittel control unit was its function for monitoring acoustic emission. This gave the machine an instrument with the sensitivity to allow touch dressing.

To minimise wheel wastage through truing the wheelhead incorporated a Wendt Boart patent wheel location system. The wheel body was located through a spring-loaded collet into a taper in the wheelhead. On bolting the wheel to the wheel spindle, the spring-loaded collet was compressed and brought the wheel to within a radial run-out of 2 μm.

5.3 Dynamic Characteristics of the Suprema

The aim of this work was to determine the natural frequencies of the principal machine elements. The workhead, workpiece and tailstock were considered as a single system surrounding the grinding contact. Two other systems investigated were the wheelhead and the dresser. Each system was tested individually using a vibration exciter to provide an oscillating input force. The force was measured using a force transducer. The response of the system was measured using an accelerometer. The transducers were calibrated as follows.

5.3.1 Calibration of Transducers

The input force was measured using a Kistler force transducer. As part of the calibration procedure a Keyence inductive gauge was used to measure displacement. Acceleration was calculated from the displacement measurements using the relationship between displacement and acceleration, for simple harmonic motion.

$$\ddot{x} = -\omega^2 x \tag{5.1}$$

where: $\ddot{x}$ = acceleration

ω = angular frequency

x = displacement

The response of the accelerometer was calibrated against a known mass. However, before this was undertaken, the inductive gauge and force transducer were calibrated in the following way.

5.3.2 Calibration of Keyence Inductive Gauge

The Keyence inductive gauge used was an EX 305 sensor head with the EX 201 controller. The sensor had a working range of 1mm equivalent to 5 V full scale. This correlates to 5mV/μm. The resolution was given as 0.04% of full scale equivalent to 0.4 μm. The response break frequency was given as 1.3 kHz (-3dB). Linearity was given as ±1% of full scale, i.e. 50 mV (10 μm). For calibration purposes, the inductive gauge was securely fixed into a Talymin comparator stand. This allowed the sensor to be accurately positioned and

slip gauges passed beneath it for setting and calibration. Results were recorded using a Tektronix TDS3054 oscilloscope and a Fluke volt-meter. The Tektronix oscilloscope was factory calibrated and self-calibrated. The Fluke volt-meter provided a secondary check. Results are presented in Figure 5.2, showing that the measured sensitivity agreed with the specified sensitivity of 5 mV/μm.

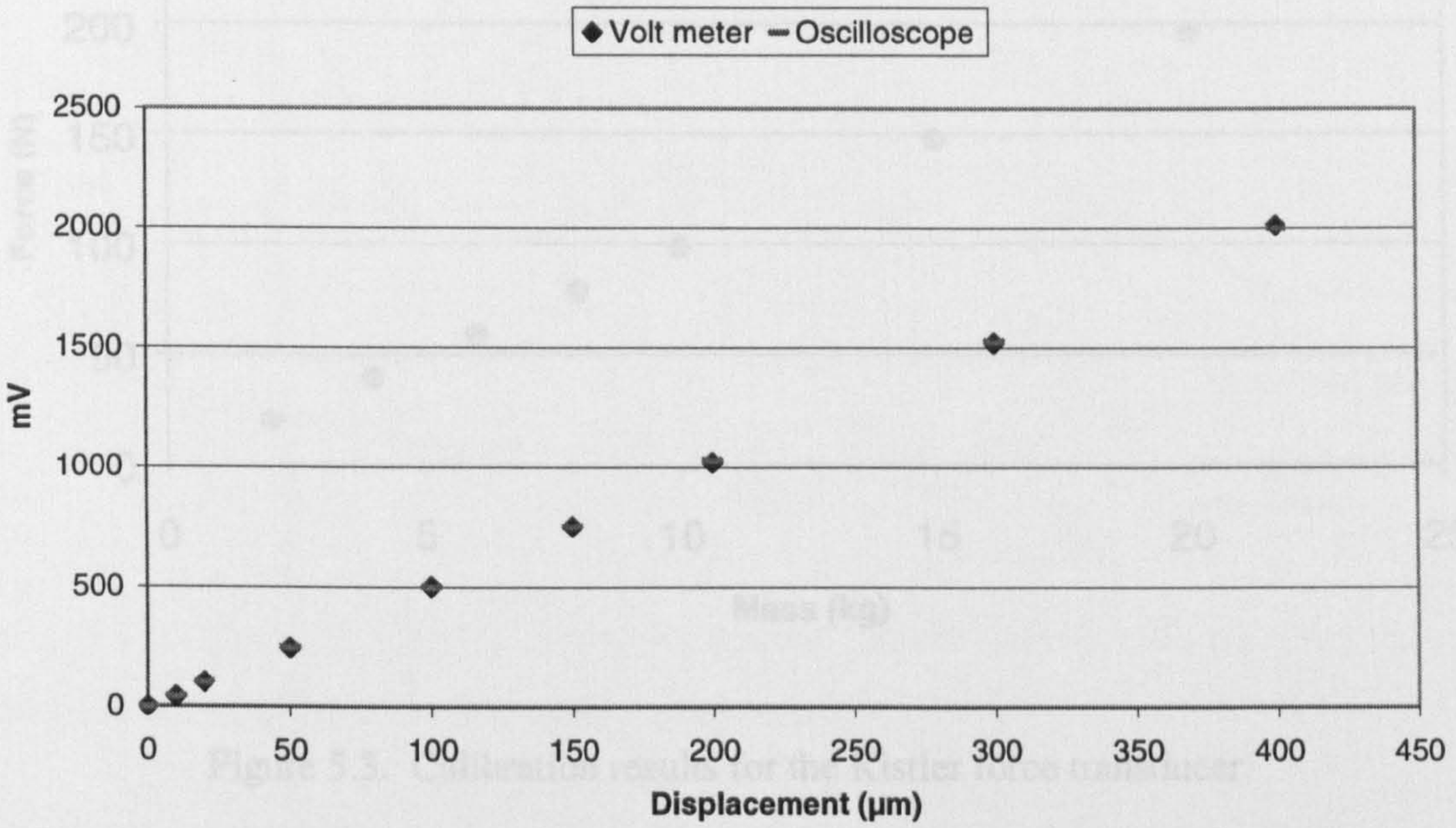

Figure 5.2. Calibration results for Keyence 200-Series inductive gauge. The factory calibration constant was given as 5mV/μm. The measured calibration constant was 5 mV/μm.

5.3.4 Calibration of Kistler Force Transducer

The Kistler force transducer used was Type 9601A31. The force transducer was a force washer usually used in the pre-loaded condition. In this instance the force measured was in the same direction as the pre-load, i.e. the z direction. This is the direction normal to the faces of the force washer and, therefore, measured compressive and tensile forces. The transducer was specified to behave linearly up to a pre-load force of 25 kN. The maximum load, with pre-load of 25 kN, was ±5 kN. The stiffness in the z direction was 1.25 kN/μm.

The force transducer was connected to a Kistler charge amplifier, module Type 5036. The amplifier was set to give an output equivalent to 3.8 mV/N. To check the calibration, the

force transducer was loaded and unloaded using a known mass. The results are shown in Figure 5.3 and agree with the specified 3.8 mV/N.

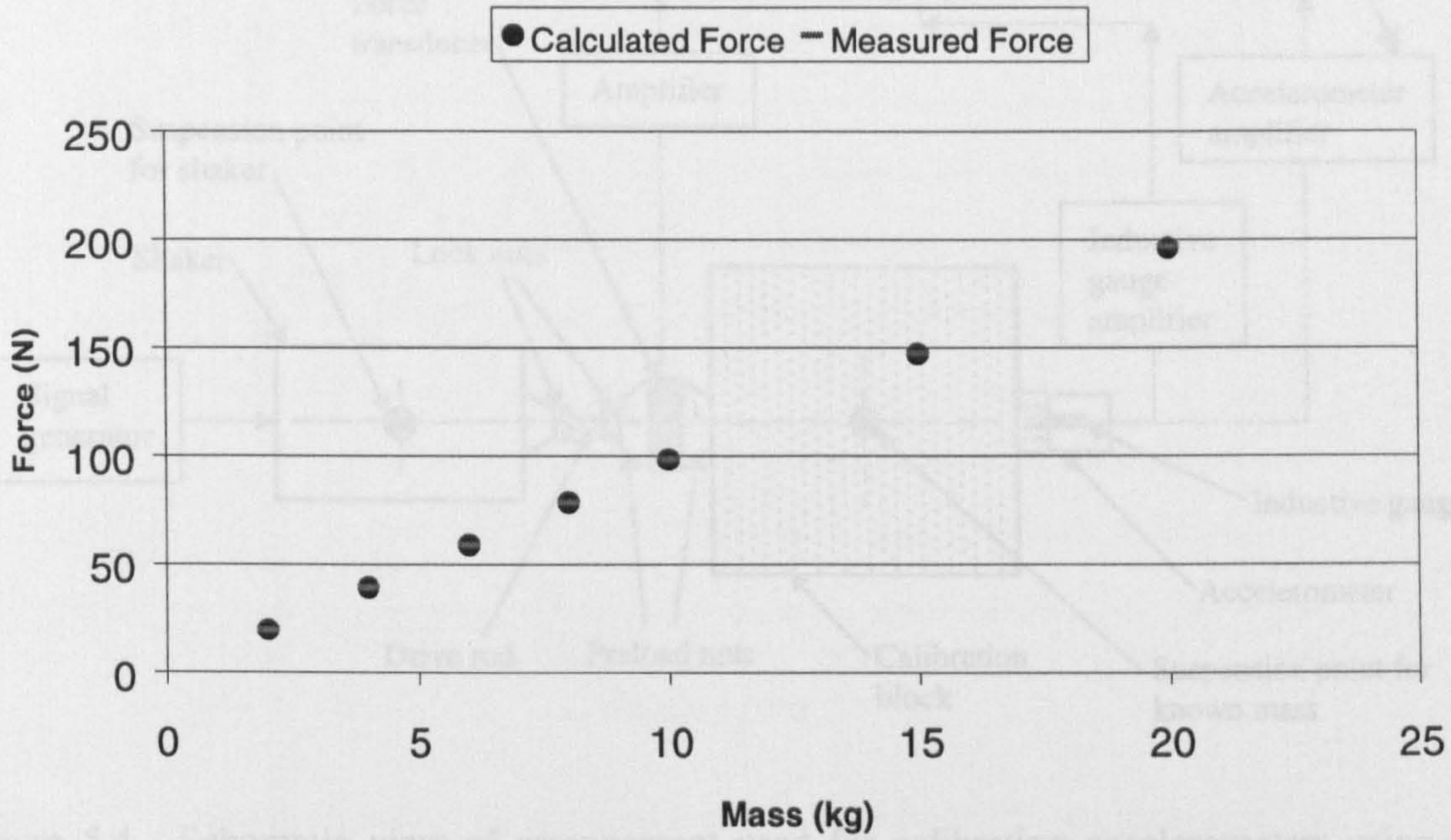

Figure 5.3. Calibration results for the Kistler force transducer.

5.3.3 Calibration of Accelerometers

Sensonics PZP1 accelerometers were used for the research. These accelerometers were of the conventional piezo-electrical type. The specific voltage sensitivity was 40 mV/g for a range up to 600 g and between 0.5 Hz and 20 kHz. The resonant frequency of the accelerometer was stated as 58 kHz.

Figure 5.4 shows the calibration set-up for the accelerometers. The mass of the calibration block was found to be 497 g. This was measured using a Sartorius universal scale, which was calibrated in position at zero, i.e. unloaded. The scales have a resolution of 0.01 g and are maintained in a stable environment.

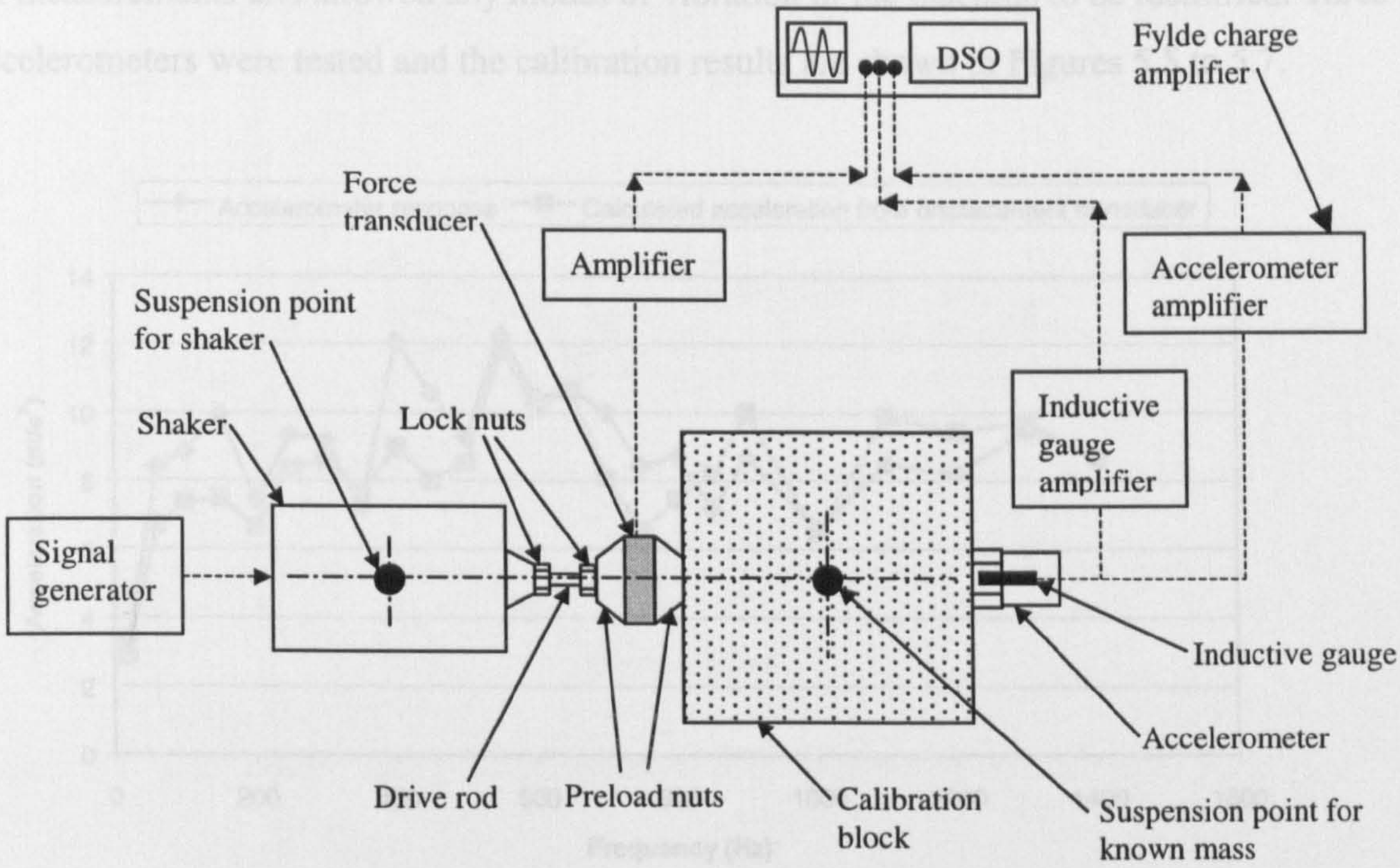

Figure 5.4. Schematic view of arrangement used for calibrating accelerometers using a known mass and an inductive displacement transducer.

For the calibration test the inductive gauge was positioned in the same plane as the accelerometer. The shaker was driven by a signal generator allowing a sinusoidal force to be applied at set frequencies. The frequency of the input force was checked using the force, acceleration and displacement signals captured on the Tektronix TDS3054 oscilloscope. The magnitude of the signals was also measured using the oscilloscope. A photograph of the general arrangement of the vibration testing equipment is shown in Appendix A, Figure A3. Also shown in Figure A4 is the set-up of the shaker, force transducer and accelerometer for testing the workhead/workpiece/tailstock system.

Equation 5.1 was used to calculate acceleration from the displacement results. This allowed a direct comparison to be made with the acceleration results measured from the accelerometer. Three accelerometers were used for the investigation. This provided a check

on measurements and allowed any modes of vibration of the machine to be identified. Three accelerometers were tested and the calibration results are shown in Figures 5.5 to 5.7.

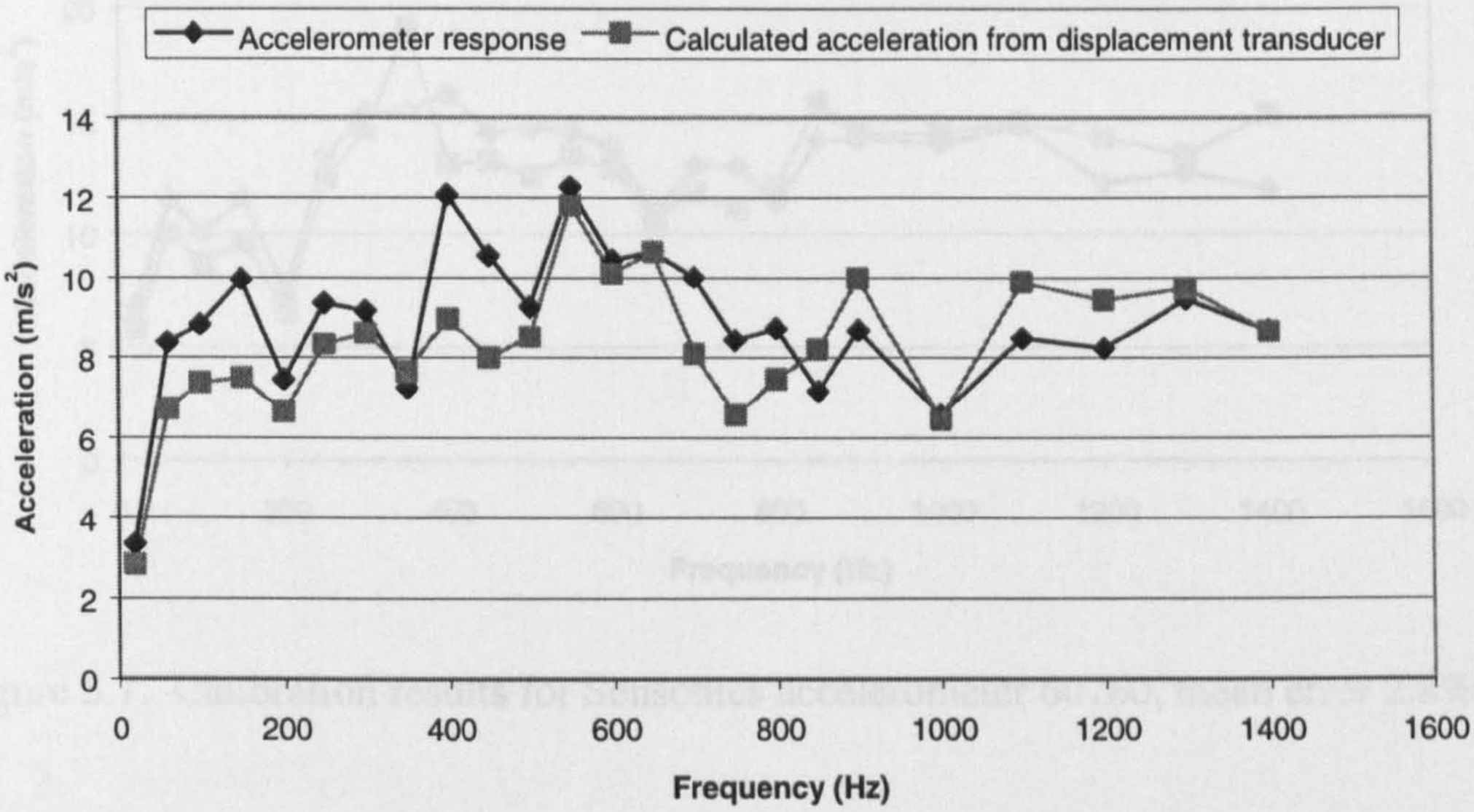

Figure 5.5. Calibration results for Sensonics accelerometer 60758, mean error 6.7%.

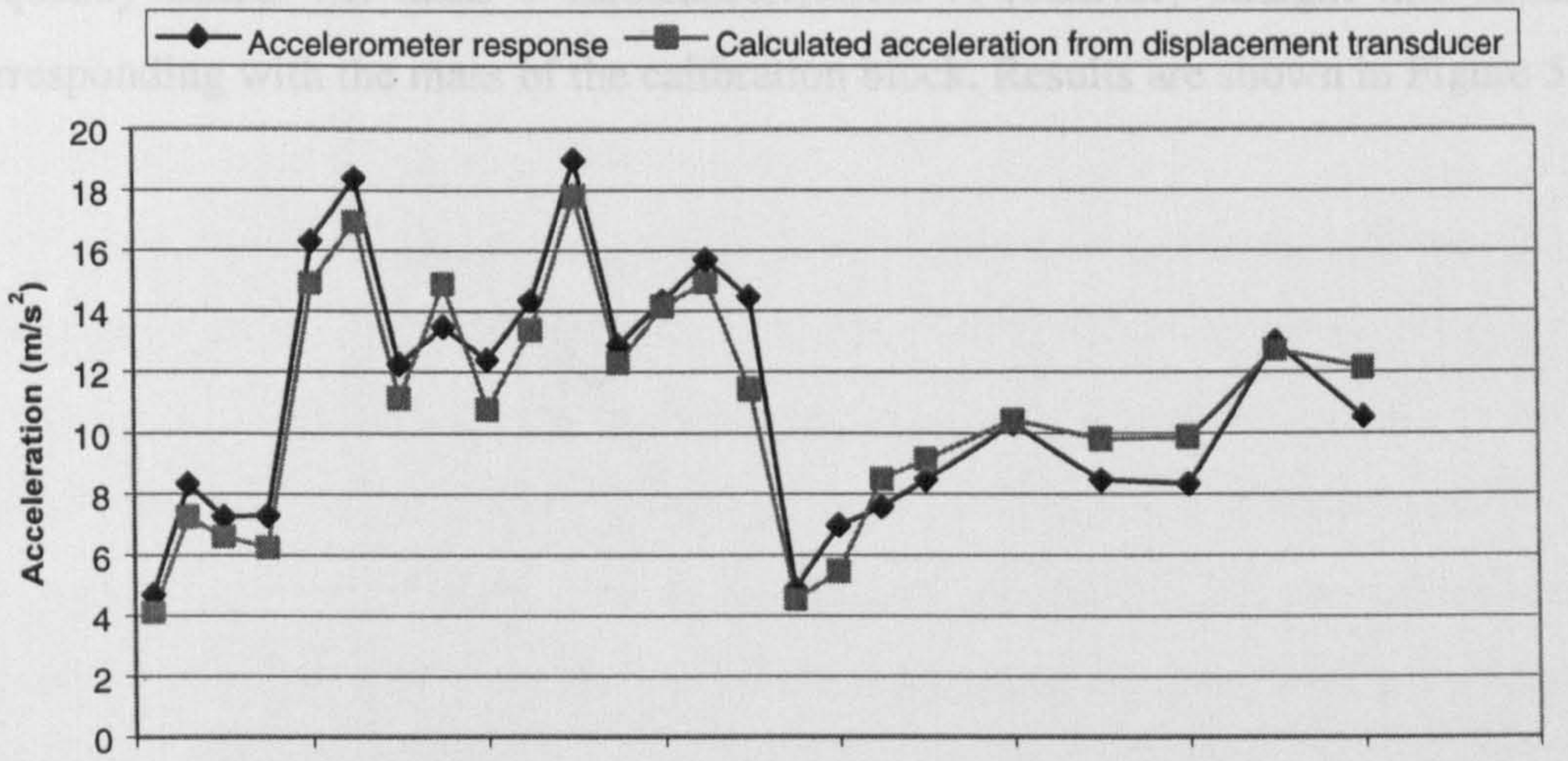

Figure 5.6. Calibration results for Sensonics accelerometer 60759, mean error 3.5%.

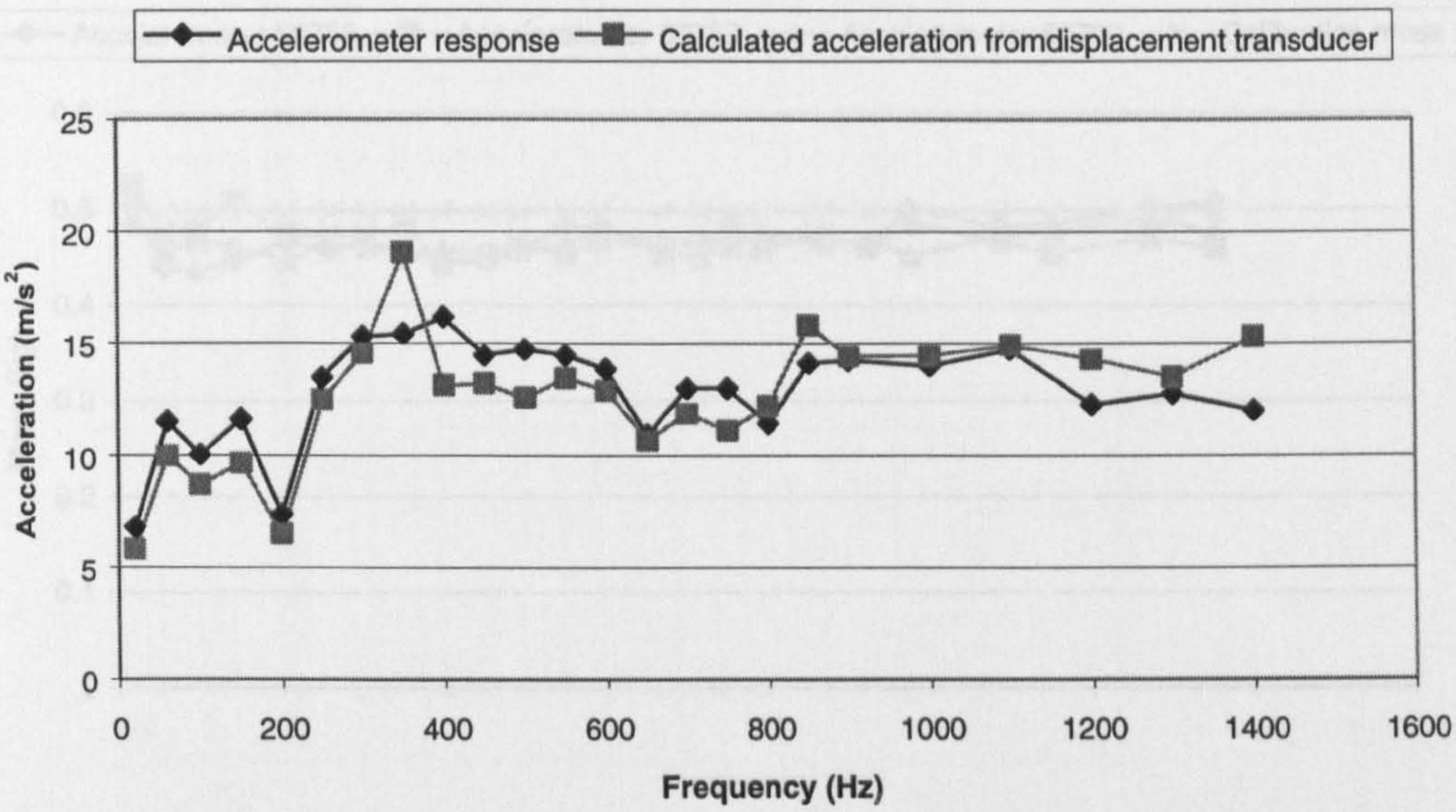

Figure 5.7. Calibration results for Sensonics accelerometer 60760, mean error 2.8%.

The calibration method recommended by Ewins (2000) **[95]** requires the mass of the calibration block to be known. Providing the force measurement is reliable and the specified sensitivity of the accelerometer is known, the mass can be calculated at each frequency tested, i.e. mass = force/acceleration. A relatively straight line should result corresponding with the mass of the calibration block. Results are shown in Figure 5.8.

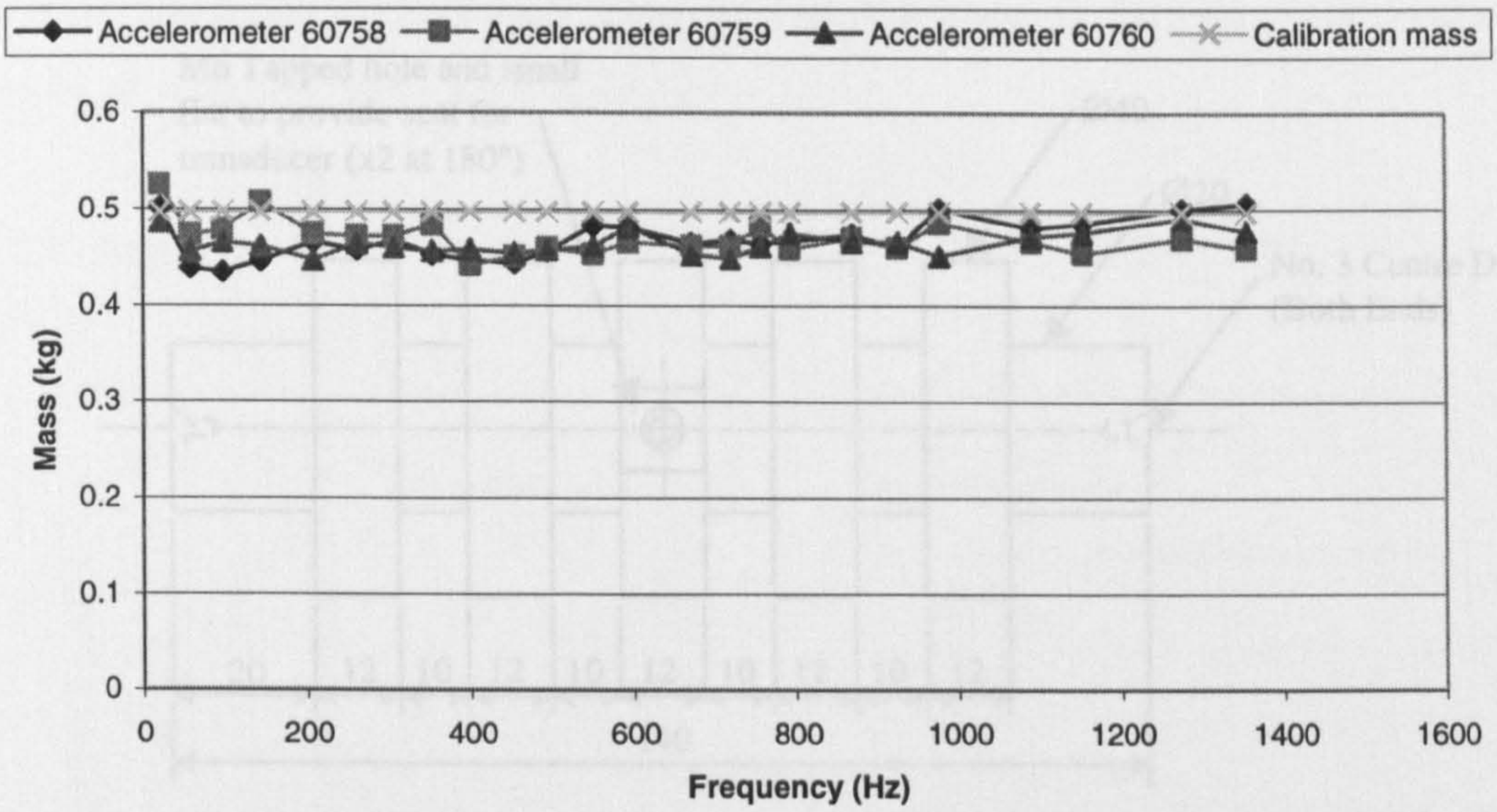

Figure 5.8. Calibration results with respect to the calibration block with a known mass of 497 g. Mean error 5.8%.

It can be seen that the calibration results for all the transducers tested gave reasonable agreement with specifications. Thus, the system tested was considered suitable for the vibration analysis of the Suprema.

5.3.5 Experimental Set-up and Procedure

The exciter, force transducer and accelerometer were set-up as shown in Figure 5.4 with the mass representing either the wheelhead, dresser or workhead/workpiece/tailstock system. It was required to securely fix the exciter, force transducer and accelerometer to the vibrated system. Consequently, a dummy grinding wheel and dressing disc were used. In each case the dummy part was of equal mass to the original. An AISI 52100 workpiece was used to represent the grinding system. The workpiece dimensions are shown in Figure 5.9.

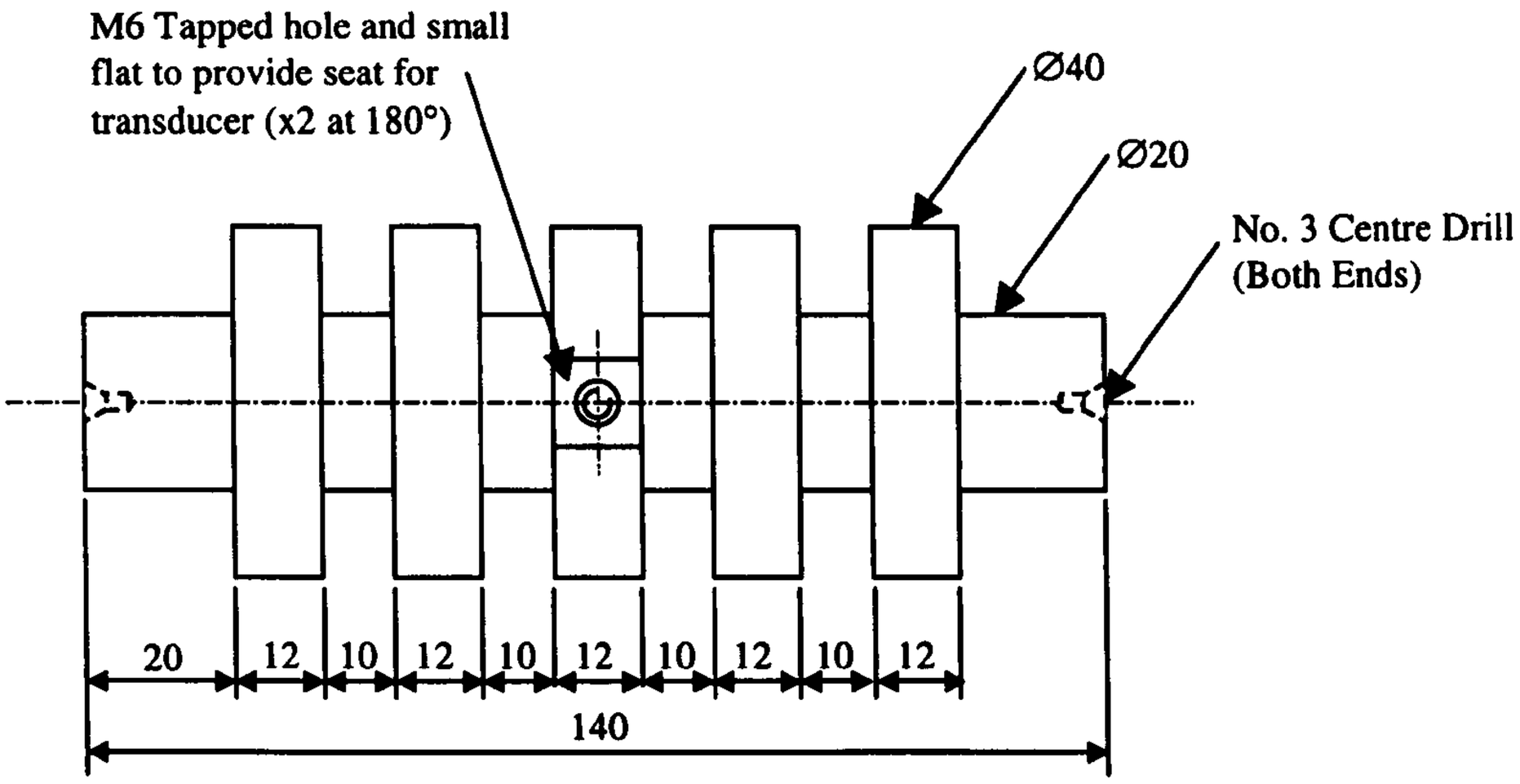

Figure 5.9. Modified AISI 52100 workpiece.

The workpiece was modified slightly to facilitate fixing the force transducer and accelerometer to it. This included machining a small flat for the transducers to sit on and an M6 tapped hole for attachment. The force transducer and accelerometer were set at 180° to each other. It can be seen from Figure 5.4 that a driving rod transmits the input force from the exciter to the force transducer mounted directly on the workpiece, dummy wheel or dummy dressing disc. The accelerometer was mounted directly opposite the input force. The exciter was suspended from an overhead crane. In each case the direction of the oscillating input force was in the grinding direction. The accelerometer was connected to a Fylde charge amplifier from which the response signal was recorded on the Tektronix oscilloscope. The input force to the system was also measured on the Tektronix oscilloscope. The frequency range tested was from 10 Hz to 1400 Hz. For the wheelhead no significant response was recorded above 700 Hz. The response of each system tested is shown in the following section. During testing, one accelerometer was used to measure the response of the system being excited. The other two accelerometers were mounted on magnetic bases enabling them to be positioned around the machine. Depending on their positions the response measurement could be checked or alternatively the response of other

parts of the machine measured. This method was used to determine any characteristic modes of vibration between the three systems.

5.3.6 Results

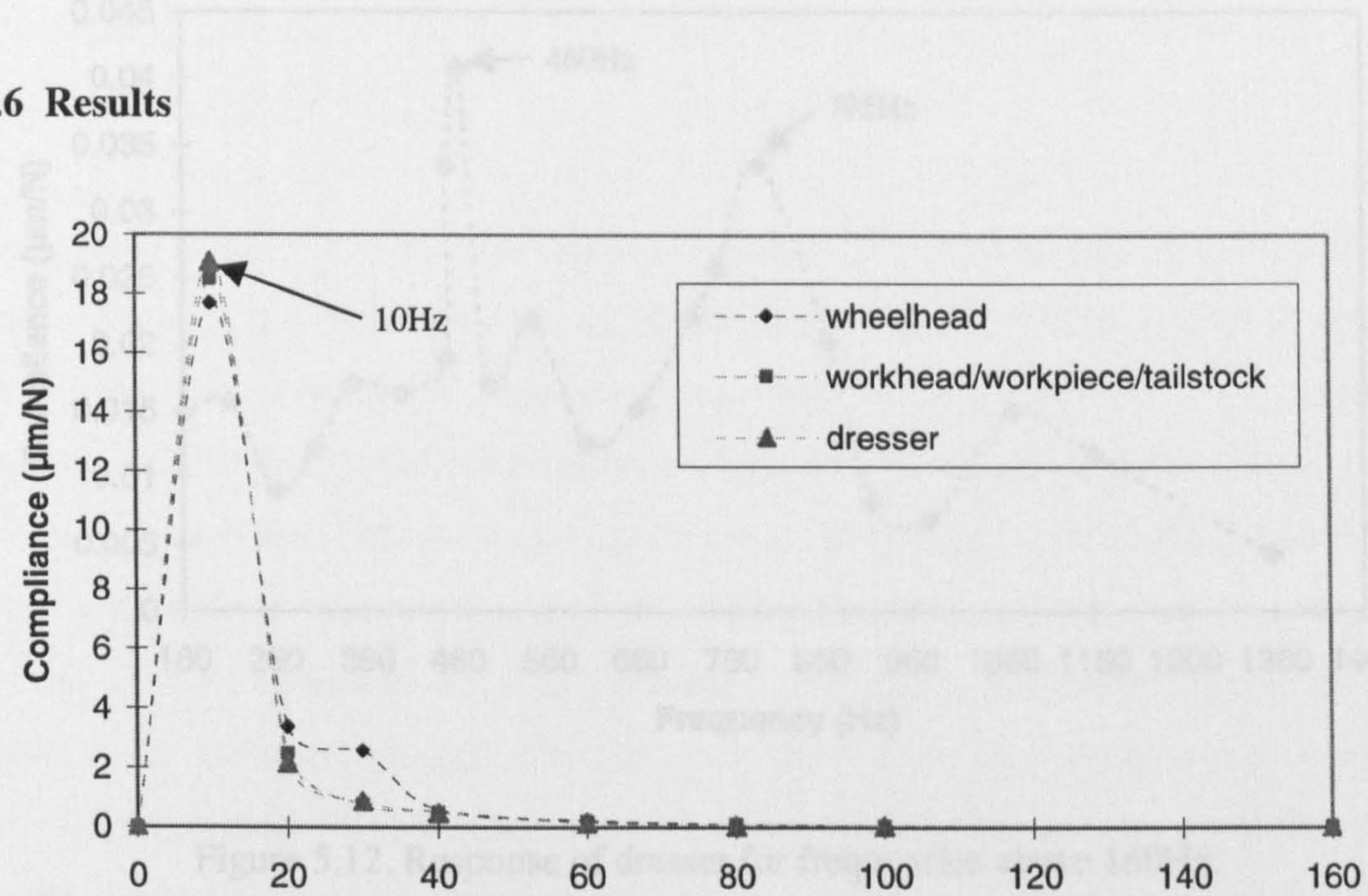

Figure 5.10. Response curves for frequencies up to 160Hz

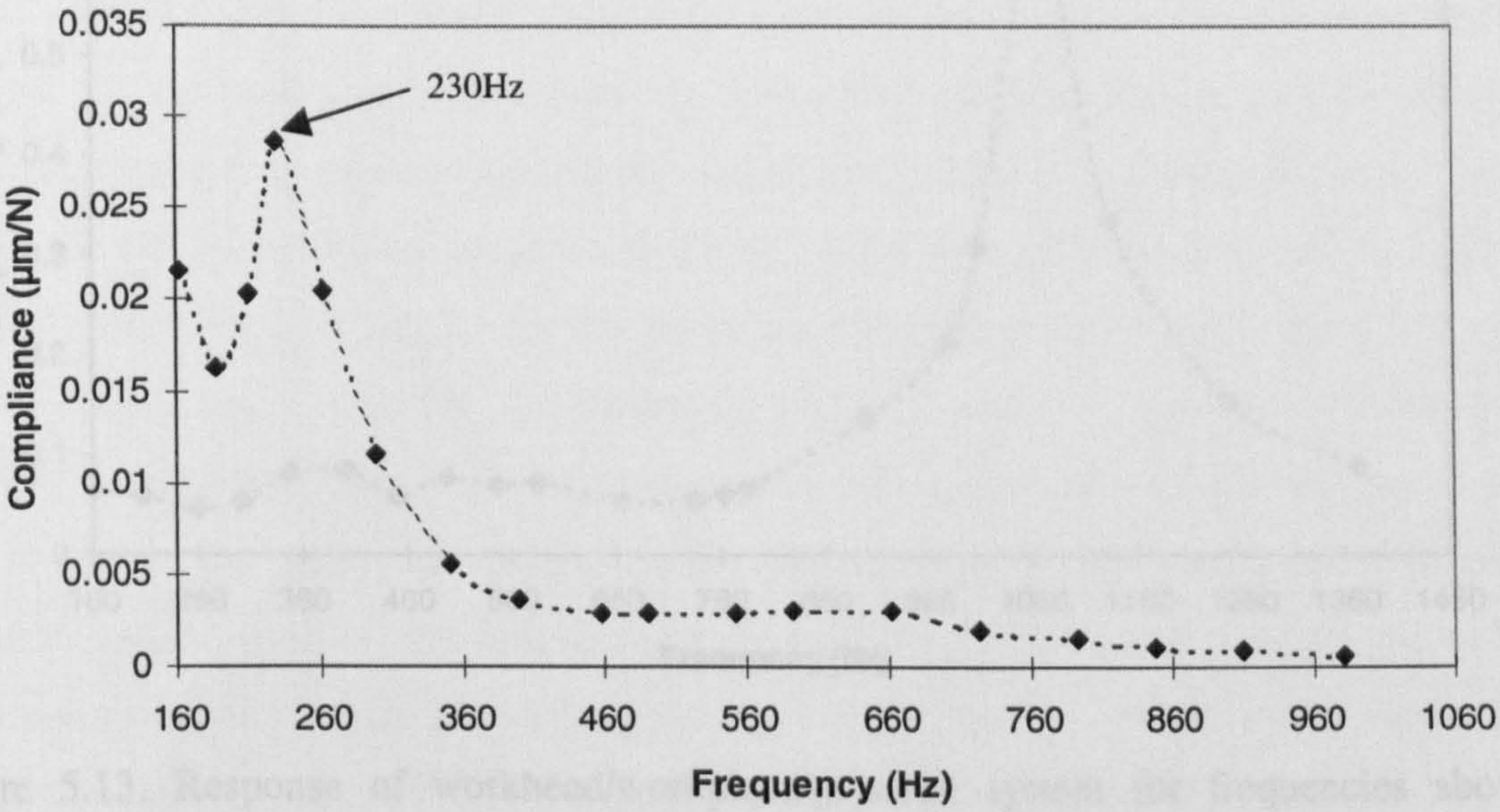

Figure 5.11. Response of wheelhead for frequencies above 160Hz.

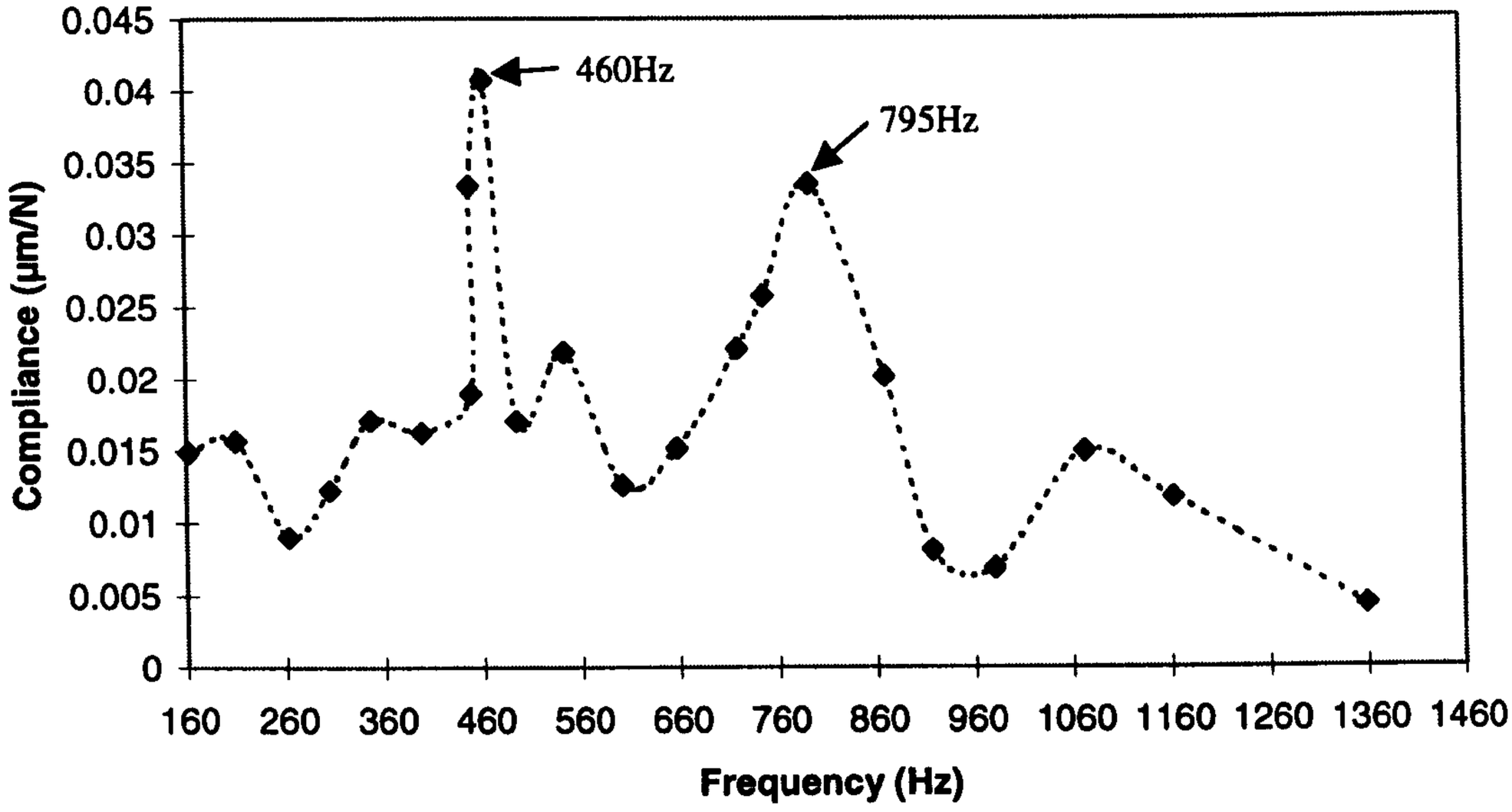

Figure 5.12. Response of dresser for frequencies above 160Hz.

Figure 5.13. Response of workhead/workpiece/tailstock system for frequencies above 160Hz.

5.3.7 Discussion of Results

The main area of interest in the dynamic tests was from 0 Hz to 250 Hz, where 250 Hz corresponds to a rotational speed of 15,000 rpm. This range includes all the rotation speeds of the machine.

From Figure 5.10, it is seen that a natural frequency exists in the vicinity of 10 Hz. Measurements below 10 Hz were not made due to the limitations of the exciter. It can also be seen that each system tested followed the same trend. This is a rocking frequency common to all machine tools and dependent on the floor mounting conditions. Rowe (1964) **[96]** and Tobias (1965) **[80]** show that this frequency is usually below 20 Hz. Generally, the better the mounting conditions the lower the rocking frequency. At very low frequencies the machine is less vulnerable to shape distortion that can cause machining errors. The Suprema was mounted on anti-vibration pads. Its granite base construction gave it a relatively large mass. This produces the low rocking frequency. The magnitude of this response swamped other important lower frequency responses, in particular the first tuning fork mode of vibration at 35 Hz. This mode was picked up using a second accelerometer on the workhead slide while the wheelhead was excited. The phase difference between the accelerometers on the wheelhead and workhead slide was 180 degrees at 35 Hz. This mode of vibration is common to many machine tools due to the configuration of two opposing systems, i.e. tool and work **[80]**. Thus, the tuning fork analogy. Tobias gave results that show the tuning fork mode to be independent of floor mounting conditions and to occur around 30 Hz. A significant response at 35 Hz would be a problem for machine speeds around 2,100 rpm. This was above the workpiece speeds tested and below the wheel and dresser speeds used. However, the frequency could influence workpiece roundness. For example a workpiece speed of 300 rpm correlates with 7 undulations per revolution if the amplitude is significant. The frequency was not evident on any workpiece roundness measurements. Therefore, the first tuning fork mode of 35 Hz was not considered to be excited substantially during any of the trials undertaken. This does not mean that this mode had no effect on workpiece roundness errors. It can only be stated that other frequencies and vibrations in the system were more significant.

With regard to the wheelhead, a minor resonant frequency seemed to occur at 230 Hz. However, the magnitude of the response was relatively small. While this response characteristic should not be discounted, there were no roundness errors on any of the workpieces to suggest the vibration was large enough to be considered problematic. The wheelhead frequency of 230 Hz correlates with 13,800 rpm. This is not within the wheelspeed range but is within the dresser speed range. It would therefore be inadvisable to dress with a dressing disc rotational speed close to 13,800 rpm. The maximum dressing disc rotational speed was 15,000 rpm. For this investigation the maximum dressing disc speed used was 9,170 rpm. Between 260 Hz and 1000 Hz, no resonant frequencies of the wheelhead were found.

The dresser system had resonant frequencies at 460 Hz and 795 Hz which are above any of the operating speeds of the machine. For the workhead/workpiece/tailstock system the natural frequency was found to be 1070 Hz. Thus, there appears to be good dynamic stability in the operating range of the machine.

In summary the following points may be highlighted:

- The resonant frequency of the wheelhead was 230 Hz.
- Resonant frequencies of the dresser were 460 Hz and 795 Hz.
- The resonant frequency of the workhead, workpiece and tailstock system was 1070 Hz.
- Dressing at a dresser speed of 13,800 rpm (230 rev/s) should be avoided.
- For all grinding trials carried out there were no operating speeds corresponding to a resonant frequency.
- To increase the resonant frequency of the wheelhead above the operating range of the dresser, a lower mass wheel body could be used, i.e. aluminium rather than steel.

5.4 Static Characteristics of the Suprema

Analysis carried out by Aachen University **[26]** revealed the following static stiffness values:

	Static stiffness	Static compliance
Wheelhead	24.4 N/μm	0.041 μm/N
Workhead	12.5 N/μm	0.08 μm/N
Tailstock	5.25 N/μm	0.19 μm/N

Aachen stated that the average static stiffness of the wheelhead for an external cylindrical grinding machine was of the order of 23 N/μm. For comparison, a Jones and Shipman Format 15 had a wheelhead stiffness of 38.5 N/μm. To measure this value for the Suprema a simple loading test was carried out. The static stiffness tests were carried out using an AISI 52100 workpiece of the dimensions shown in Figure 5.9.

The workpiece was mounted between the centres of the Suprema. A dummy wheel mounted with the Kistler load cell was moved into contact with the middle diameter of the workpiece. At this stage, the stiffness of the workpiece was unknown. Using dial test indicators the displacement of the workpiece was measured independent of the displacement of the centres. The force was measured using the load cell and applied by moving the wheel in the direction of the x-axis. The resulting workpiece stiffness was 62.7 N/μm.

To check if this value is reasonable, the maximum displacement equation for a simply supported beam may be used. Thus,

$$x = \frac{wl^3}{48EI} \tag{5.2}$$

where x = maximum displacement.

w = load.

E = Youngs modulus (200 GN/m^2).

I = second moment of area, i.e. $I = \frac{\pi d^4}{64}$ and d = workpiece diameter.

As the diameter of the workpiece was not constant, the second moment of area was difficult to calculate. However, if the displacement per unit force is known, i.e. 1/62.7 N/μm, the second moment of area may be determined, and from this an equivalent workpiece diameter. The equivalent workpiece diameter should be slightly larger than the core diameter, of 20 mm, to allow for the larger diameters.

From Equation 5.2 a value for the second moment of area was calculated as 1.71×10^{-8} m^4. For this value of second moment of area, the equivalent workpiece diameter was calculated to be 24.3 mm. Considering the shape of the workpiece used this value is reasonable.

The overall stiffness, k_w, of the workhead, workpiece and tailstock system consists of three stiffness values. The stiffness of the workhead and tailstock centres act in parallel with each other and in series with the workpiece. Thus, Equation 5.3 may be written as:

$$\frac{1}{k_w} = \frac{1}{k_{workpiece}} + \frac{1}{k_{workhead} + k_{tailstock}} \tag{5.3}$$

$$\frac{1}{k_w} = \frac{1}{62.7} + \frac{1}{12.5 + 5.3}$$

$k_w = 13.9$ N/μm

The machine system stiffness 'k_{mc}' consists of two stiffness values in series, i.e. k_w and the wheel stiffness k_s, thus, the machine system stiffness using the five diameter workpiece is equal to:

$$\frac{1}{k_{mc}} = \frac{1}{k_w} + \frac{1}{k_s} \tag{5.4}$$

$$\frac{1}{k_{mc}} = \frac{1}{13.9} + \frac{1}{24.4}$$

$k_{mc} = 8.9$ N/μm

To check this value, a static stiffness test was carried out. This was achieved by moving the dummy wheel into contact with the workpiece and then by an amount measured using the linear scale of the x-axis. The force was measured using the Kistler load cell. The following graph shows the results obtained.

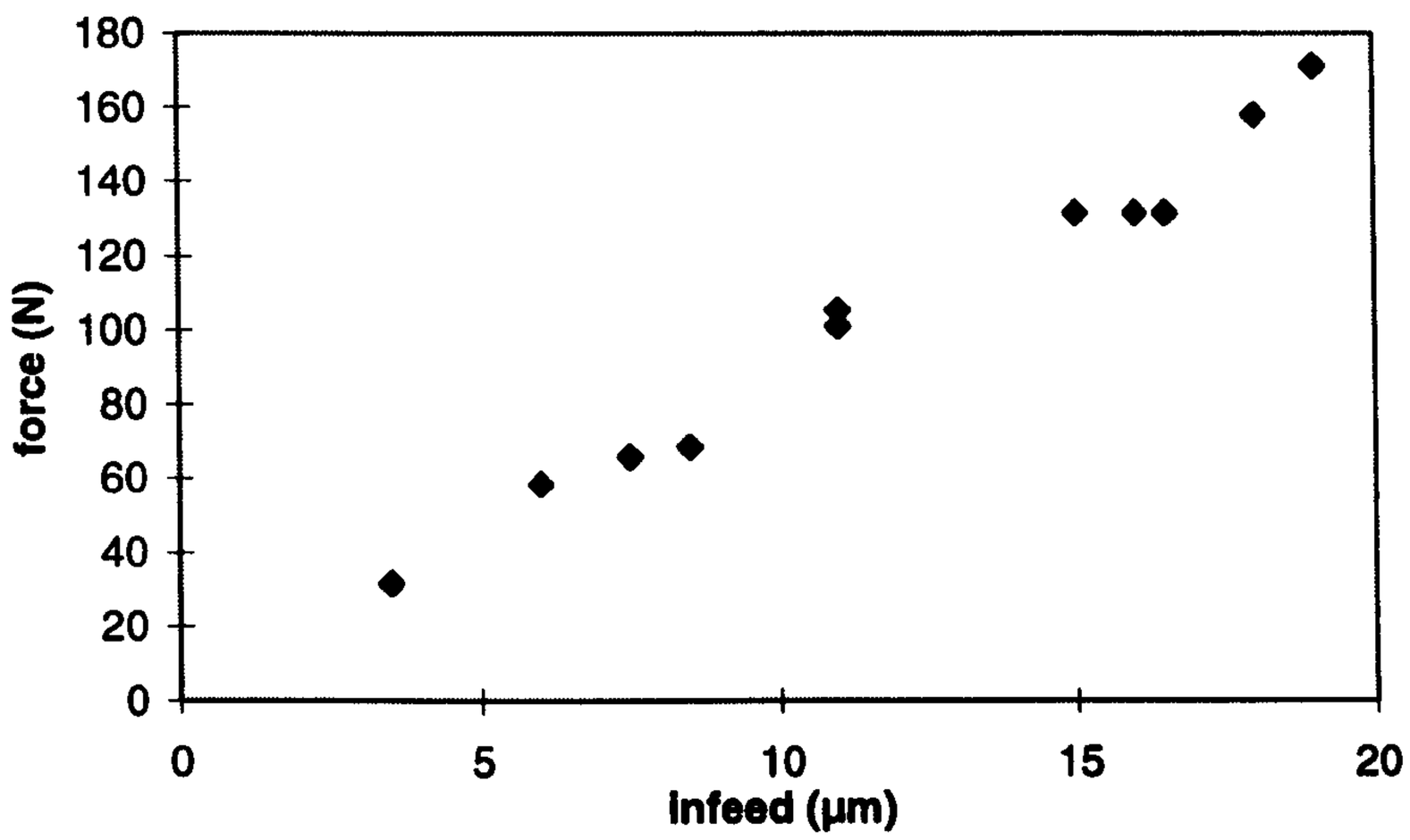

Figure 5.14. The force and infeed relationship for the Suprema using the AISI 52100 workpiece.

The gradient of the line through the experimental points of Figure 5.14, gives a machine system stiffness of 9 N/μm. This value was for the infeed recorded by the linear scale and is the actual machine system stiffness for the particular workpiece used. It can be seen that this value closely agrees with the calculated system stiffness of 8.9 N/μm.

5.5 Thermal Characteristics of the Suprema

The high speed spindles, spindle cooling jackets, hydrostatic spindle oil supplies, and refrigerated coolant all have a thermal effect on the machine structure and slideways. The

following graph shows the drift in the x-axis position from when the machine is run up to an operating speed of 95 m/s.

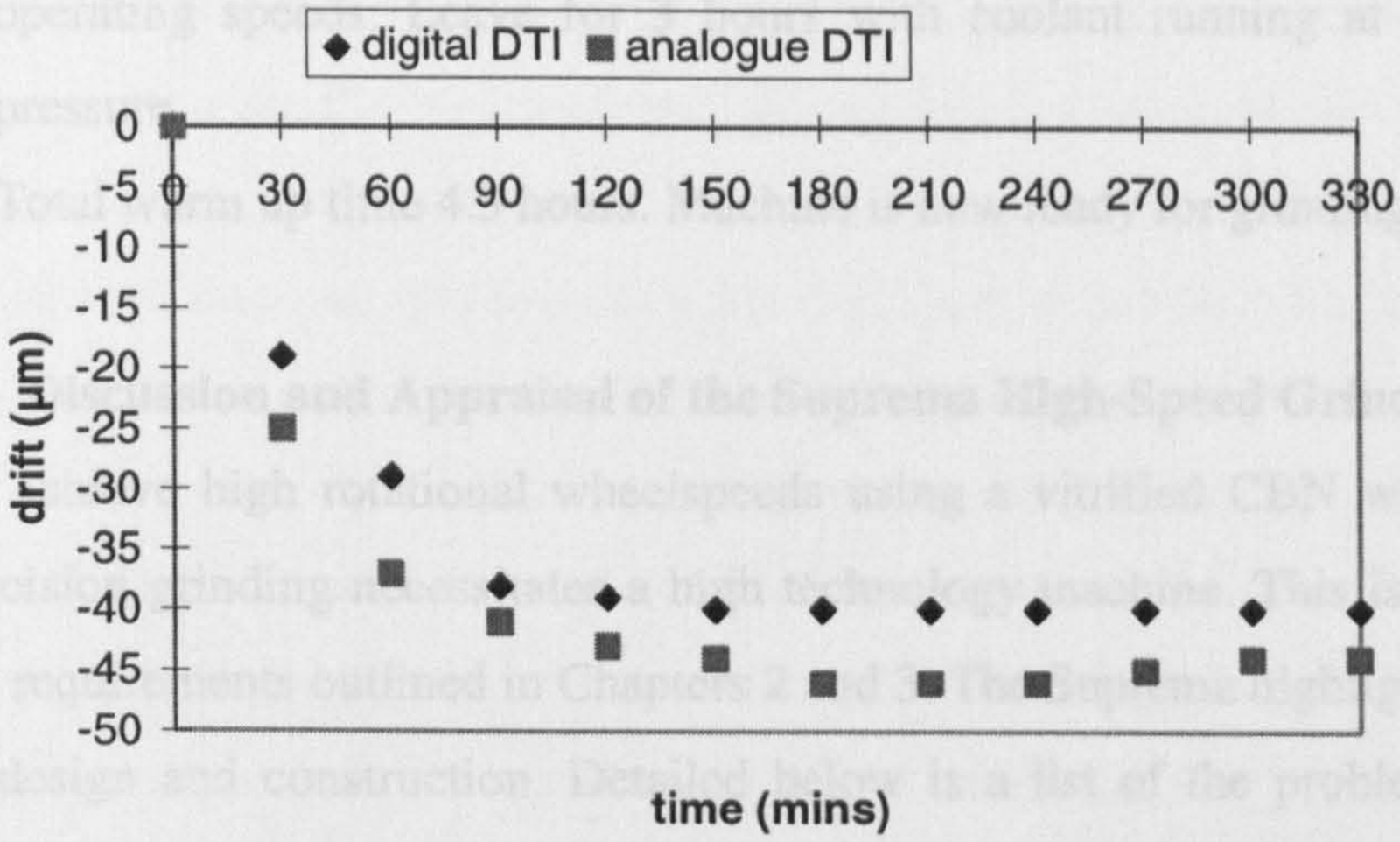

Figure 5.15. Displacement of x-axis over time at an operating speed of 95 m/s.

Figure 5.15 shows that a serious size error would result if grinding was carried out without compensation before a warm-up period of 150 minutes. Thermocouples were mounted on various parts of the machine tool to determine, firstly, how great the temperature increase was and secondly, how long it took for thermal stability to be achieved. The results of this test are shown in Figure A11 in Appendix A. It can be seen that the general trend at all points where temperature was monitored is the same. The oil returning from the wheelhead spindle has the greatest temperature increase of about 14°C after 150 minutes.

It is clear that a warm-up period of at least 150 minutes is required before grinding. This warm-up period should be run with the wheel at its operating speed. Prior to running up the wheel, a warm-up period is required to stabilise the temperature of the hydrostatic bearings as well as flushing out the system. The following warm-up procedure was followed prior to every trial undertaken:

1. Switch on machine tool hydraulics feeding spindles. Leave for 30 minutes.

2. Run spindles at idling speeds, i.e. wheel 1000 rpm, workhead 100 rpm, dresser 4000 rpm. Leave for 1 hour.
3. Run a dummy cycle and put machine in a feed hold with all spindles at required operating speeds. Leave for 3 hours with coolant running at required flow rate and pressure.
4. Total warm up time 4.5 hours. Machine is now ready for grinding trials.

5.6 Discussion and Appraisal of the Suprema High-Speed Grinding Machine

To achieve high rotational wheelspeeds using a vitrified CBN wheel for the purpose of precision grinding necessitates a high technology machine. This is predominantly to fulfil the requirements outlined in Chapters 2 and 3. The Suprema highlighted some of the pitfalls in design and construction. Detailed below is a list of the problems encountered on the Suprema over the course of this investigation. The list includes simple faults easily overcome as well as some more fundamental design flaws. The purpose of this appraisal is to provide comment on the problems that can be encountered when increasing the level of technology to gain an improvement in performance. For the buyer of a high technology machine tool, higher cost might be expected to indicate higher quality. Many of the problems encountered over the course of this investigation would be unacceptable on a machine of this specification. The list is as follows:

- Corrupted software: This required the controller for the machine to be replaced. As the software was unique to the machine this required many months of work in building up an earlier version of the software for compatibility with the Suprema.
- Crash control sensitivity: During the commissioning stage of the machine problems were encountered with the crash control unit. Even at its minimum sensitivity, the crash control was triggered during dressing. This required modification to the hardware of the unit and was successfully carried out.
- Misalignment between workhead and tailstock: A discrepancy between the height of the workhead and tailstock centres was found. Shimming was carried out to correct the fault.
- Out of roundness of the workhead: To reduce the risk of out of roundness errors, most external grinding machines have a dead centre in the workhead. As discussed in Section

5.5, the Suprema workhead requires a live centre for grinding between centres. This is due to the hydrostatic bearings used which made it impossible to change the workhead arrangement. As hydrostatic bearings were used the outside diameter of the workhead spindle runs true. Providing the bore of the spindle is true with the outside diameter, the centre mounted in it should also run true when rotating. However, it was found that the bore of the workhead ran out by 4 µm to 5 µm. Attempts to re-grind the bore did not improve concentricity to within 3 µm. This error translated to an out of roundness of 3 µm to 4 µm on the centre. To overcome this a modified centre had been made for the machine by its original users at Aachen University. The modified centre located off the outside diameter of the spindle. The basic design is shown in Figure 5.16. The internal diameter was manufactured to suit the external diameter of the workhead spindle, on which it located. The modified centre was bolted to the face of the workhead spindle. With the modified centre it was not possible to achieve an out of roundness less than 2 µm. As this was an improvement on the originally intended method the modified centre was used throughout the investigation.

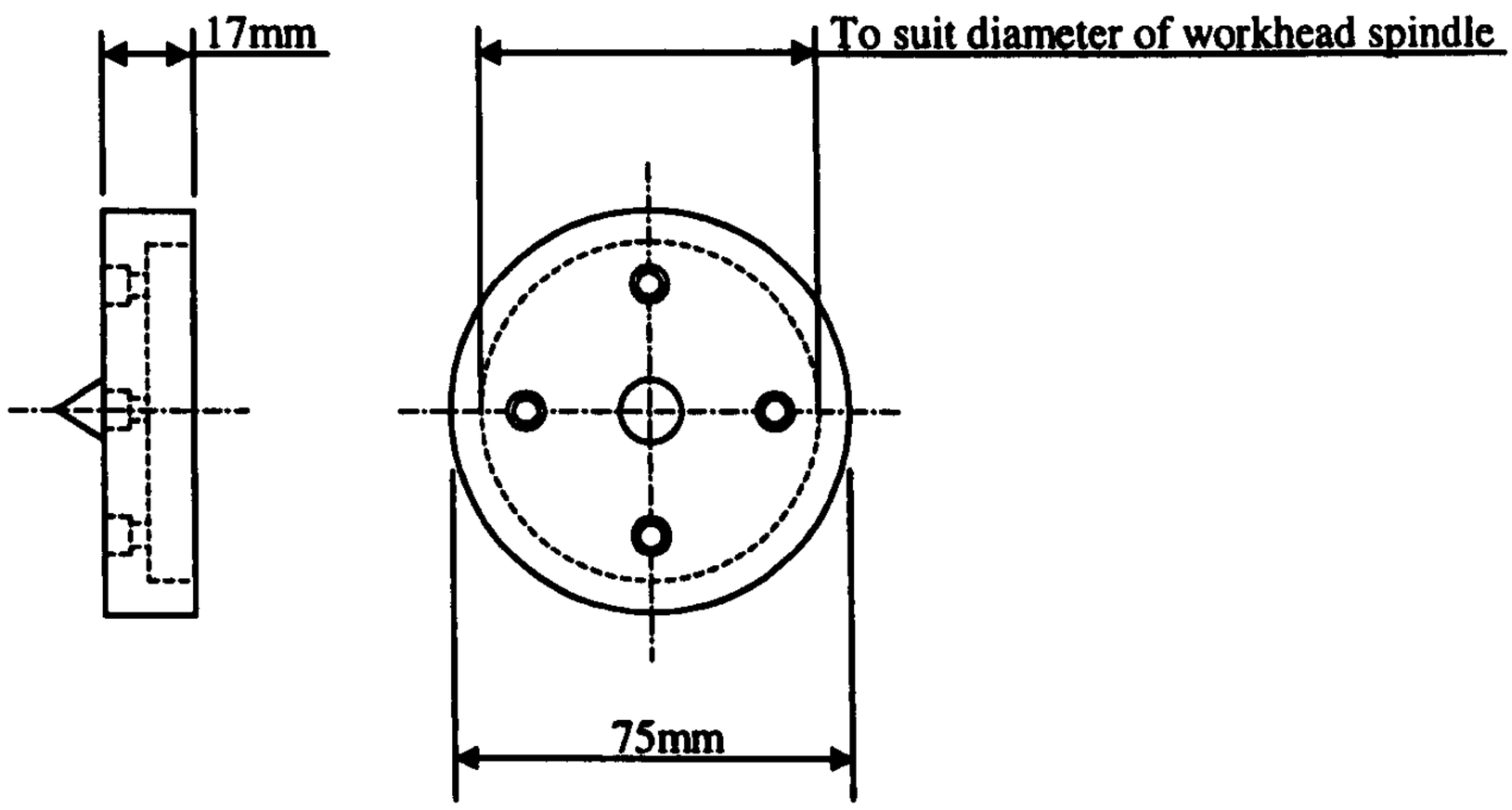

Figure 5.16. Modified centre for location on workhead spindle.

- Loose inserts in the granite: As discussed in Section 5.3, three granite blocks formed the basic structure of the machine. To fasten parts to the structure, steel inserts were glued

into holes drilled in the granite. This is due to the fact that granite cannot be tapped directly and is not an uncommon practice. However, due to the non-repeatability of the dresser contact position, the soundness of the structure was investigated. It was found that several of the steel inserts had become loose. To correct this, the granite block on which the dresser was mounted was replaced with a cast iron block. A further investigation was carried out by Jones & Shipman to check other inserts in the structure. Other parts of the machine were found to be sound. Figure A5 of Appendix A shows how flaking had occurred in the granite surrounding the steel inserts of the dresser block. Some of the steel inserts are also shown to be proud of the surface, indicating they had moved.

- AMK spindle motor failure: During one of the grinding trials the bearings of the grinding wheel spindle motor burnt out. A strip-down of the motor revealed that one of the radial bearings had burnt out leading to catastrophic failure. A photograph of the motor is presented in Appendix A, Figure A6, shows the burnt-out bearing.
- Hydrostatic bearing failure: Due to the failure of the AMK motor the second motor/wheel spindle assembly was fitted to the machine. The spindle was flushed out over a period of days and allowed to warm up at 1000 rpm for a period of time. The spindle was then gradually run up to maximum speed. Before reaching maximum speed the spindle went out of balance. This resulted in contact between bearing surfaces and failure. Inspection of the spindle revealed that a broken wire between the balance unit and the receiver had prevented the balance unit receiving the signal to adjust. Figures A7 to A10, in Appendix A, show the various part of the wheelhead spindle arrangement and the hydrostatic bearings damaged through contact.
- Dressing problems: Software errors prevented the correct speed control of the dresser. To overcome this the dresser was powered independently by a separate power supply. This voltage was used to control the dresser speed. A positioning problem was also encountered when dressing during a cycle. After dressing during set-up, the cycle is called and executed. If during that cycle a dressing procedure is carried out the dresser was found to move in 100 μm more than had been set during set-up. Consequently, all dressing had to be carried out in set-up mode rather than in the cycle mode.

- x-axis over-travel limit: A software problem led to problems with the x-axis over-travel limit being hit at intermittent times during grinding trials. As the procedure to manually move the wheelhead off the x-axis over-travel limit required a partial strip down of the machine guarding, trials had to be abandoned. J&S investigated the problem and advised on software alterations to prevent the problem occurring.
- Cabinet temperature: An intermittent problem existed with regard to the temperature of the machines electrical cabinet. If the temperature exceeded a certain limit, it was flagged up on the controller and the machine shut down.
- Hydraulic oil pipes: The high-pressure oil delivery to the hydrostatic bearings required high-pressure piping. Despite this, pipes burst on a number of occasions. The pipes now installed are of a specification exceeding the pressure used.
- Lubrication oil contaminated: Perished seals led to water, from the spindle cooling jackets, to leak into the lubrication circuit. The lubrication circuit had to be made open loop, so that polluted oil did not return into the system. Jones and Shipman stripped down the z-axis of the machine and replaced all seals which cured the problem.
- Hydraulic oil contaminated: Due to perished seals in the dressing unit the same problem was encountered as described previously with the hydraulic oil circuit. Seals were replaced solving this problem.
- Cooling water float switch: An intermittent problem existed with the float switch in the refrigeration unit for the hydrostatic bearing cooling water. This was overcome with regular maintenance.
- AMK drive unit failure: The servomotor drive unit in the electrical cabinet for the workhead failed. This was replaced with a spare unit.
- Workhead proximity switch: Workhead speeds were found to be slower than those programmed. This was due to a fault which developed on the workhead proximity switch due to the workhead belt shredding through rubbing against a bolt within the guarding. The proximity switch, belt and bolt were replaced overcoming the problem.
- Cooling unit failures: A leakage from the coolant refrigeration unit was encountered. This required the attention of an outside company to re-fill the unit with the correct refrigerant.

Despite the problems encountered, the general machine concept was appropriate for the requirements of high-speed machining.

Many of the problems listed were superficial rather than fundamental design flaws. For example, although software problems were a considerable cause of problems over the course of the project they do not mean the machine was badly designed. These are problems that would be expected with a concept machine. Further development and testing of the software, would be undertaken by the machine tool builder before incorporation into a production machine and problems would be overcome.

Other problems such as burst pipes, problematic float switches and proximity switches would be easily corrected and are not significant to the potential cost of the machine.

However, problems such as motor and bearing failures were serious issues incurring expenses to the user through repair costs and down time. These failures were a consequence of the high rotational speed demanded of the wheelhead, i.e. 10,000 rpm, to achieve the surface speed of 130 m/s and insufficient prototype development. For a wheel of 450 mm diameter the rotational speed required to achieve 130 m/s is 5,500 rpm. The lower rotational speed reduces the demand on the wheelhead motor and bearings. The design challenges and complexity associated with high speeds will necessarily be reflected in a high-cost machine and higher maintenance costs. Without substantial design development, high speeds may also be reflected in a less reliable machine.

Providing the initial wheel costs can be divided sufficiently by the number of parts produced, true wheel costs may be very low. Thus, larger wheel diameters may allow a less complex and more reliable machine system to be employed.

A more fundamental problem is the workhead design. To overcome this, improved accuracy of the workhead bore is required. Alternatively as the workhead speeds are relatively low, a

standard workhead design could be used using roller bearings. However, this could lead to lower resonant frequencies of the workhead. If these lie within the speed range of the wheelhead there is an increased risk of resonance. However, the question remaining was whether using the current set-up, economic precision grinding could be achieved.

As a prototype high-speed grinding machine the general design concept appeared to be suitable for high-speed precision grinding. The next two chapters are concerned with the performance of the Suprema in grinding trials.

CHAPTER 6. PROCESS REQUIRMENTS FOR COST EFFECTIVE PRECISION GRINDING OF AISI 52100

6.1 Introduction

The following chapter details the research carried out for the characterisation of the high-speed grinding process using a vitrified CBN wheel on the Jones and Shipman Suprema. The workpiece material used was AISI 52100. This is classed as an easy to grind material. Benchmark results were also established for this material using aluminium oxide, sol gel and vitrified CBN wheels at conventional wheelspeeds, i.e. <45m/s, on the Jones and Shipman Series 10 grinding machine. This allowed a comparison of process costs to be made. Thus, high-speed grinding was characterised in terms of performance and cost. The dominant factors affecting both performance and cost were established.

6.2 Aim

To investigate how the high-speed grinding process, using a vitrified CBN wheel, compares with conventional speed grinding processes in terms of performance and cost when grinding an easy to grind material such as AISI 52100.

6.3 Specific Objectives

- To characterise the high-speed grinding process using a two level experimental arrangement and show how strongly dressing and cycle parameters affect specific energy, surface roughness, workpiece roundness, size holding and G-ratio.
- To determine process requirements for low cost high precision grinding.

6.4 Equipment

6.4.1 Grinding Machines Used

Two grinding machine tools were used. The bulk of the investigation was carried out on the Jones and Shipman Suprema. On this machine the high-speed characterisation trials were carried out and the effects of process parameters at high speed established.

To provide comparative results for the high-speed trials to be judged against, benchmark trials were carried out using the Jones and Shipman Series 10 machine. The grinding wheels used throughout the investigation are detailed in the following section.

6.4.2 Grinding Wheels Used

Grinding wheels used for the high-speed trials carried out on the Suprema were of the following specification: B91 VR150. The wheels were supplied by Wendt Boart. Due to the large amount of dressing carried out, two wheels were used over the course of the investigation. The first wheel was used for trials 1 to 8. The second wheel, of the same specification, was used for trials 9 to 16 plus the confirmation trials.

Wheels used for the benchmark trials on the Series 10 machine were as follows:

1. WA801 J6V Aluminium oxide wheel manufactured and supplied by Universal.
2. A465 K5V Aluminium oxide wheel manufactured and supplied by Carborundum.
3. 73A 601 J8V Sol gel wheel manufactured and supplied by Universal.
4. B91 ABN500 Vitrified CBN wheel manufactured and supplied by Saint Gobain.

6.4.3 Coolant Used

For all trials carried out the coolant used was Castrol Hysol X. This is an emulsion type coolant. According to manufactures guidelines the recommended water to coolant ratio for grinding is 10:1. The following pump pressures and delivery flow rates were used:

All Suprema grinding trials:

Pump pressure = 30 bar

Coolant delivery rate = 36 l/min

All Series 10 grinding trials:

Pump pressure = 0.4 bar

Coolant delivery rate = 33 l/min

6.4.4 Workpiece Specifications

The workpiece material was AISI 52100 (also known as EN31) hardened to 62 HRC. The composition of the workpiece material is given in Table 6.1.

Table 6.1. Composition of the alloy steel AISI 52100.

Element	C	Si	Mn	P	S	Cr
% Content	0.98	0.27	0.36	0.013	0.016	1.55

The dimensions of the workpieces used are shown in Figure 6.1.

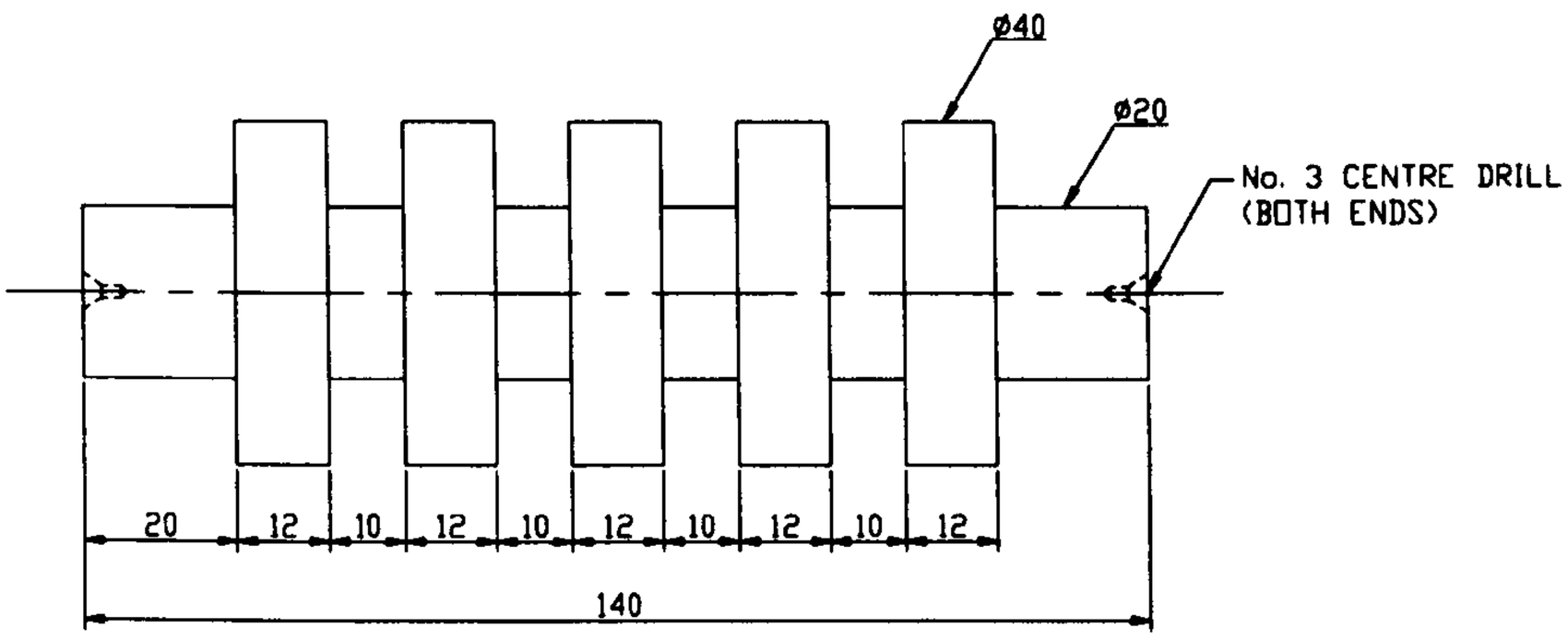

Figure 6.1. AISI 52100 workpiece, 62 HRC. All sizes are shown in mm.

6.5 Measuring Equipment Used and its Calibration

The performance indicators used to assess the performance of each trial were:

- Specific energy
- Surface roughness, i.e. Ra
- Roundness
- Size holding
- G-Ratio

For the first eight grinding trials 550 diameters were ground consecutively, i.e. 110 workpieces. The grinding power for each diameter was measured and the specific energy determined. The measuring frequency for surface roughness and roundness was the first five workpieces, i.e. 25 diameters, followed by every fifth workpiece. For size holding every diameter was measured. Due to the unreasonable amount of time required to carry out the first eight grinding trials and complete measuring, the trials and measuring frequency had to be modified. For all remaining trials, including the confirmation trials, 540 diameters were ground using 36 workpieces. This required all five diameters of each workpiece to be ground three times. This simulated the grinding of three workpieces as carried out in the first eight trials. Grinding power was measured for every diameter ground. For roughness and roundness the first two workpieces were measured followed by every other workpiece. For size holding all 36 workpieces were measured. For the conventional speed grinding trials the measuring frequency can be seen from the result graphs shown in Appendix B4.

The measurement of the performance indicators was carried out using the equipment described in the following sections. Calibration details are also discussed.

6.5.1 Determining Specific Energy from Power Measurement

Specific energy was calculated from grinding power measurements recorded over the course of the trial. The relationship between power and specific energy is given by equation 3.4. The power was measured using a Siemens Function Meter, model B1081, which was connected to one phase of the wheelhead motor. The Function meter measures the voltage and current used by the wheelhead motor during the cycle, from which power is determined. The arrangement is shown in Figure 6.2.

Grinding power was measured by subtracting the no load power from the maximum power recorded for each plunge grinding operation. The no load power was the power required by the wheelhead motor to run the grinding wheel at the programmed speed. Also included in the no load power was the power induced by the high velocity coolant acting on the wheel. The oscilloscope allowed the power profiles to be tracked.

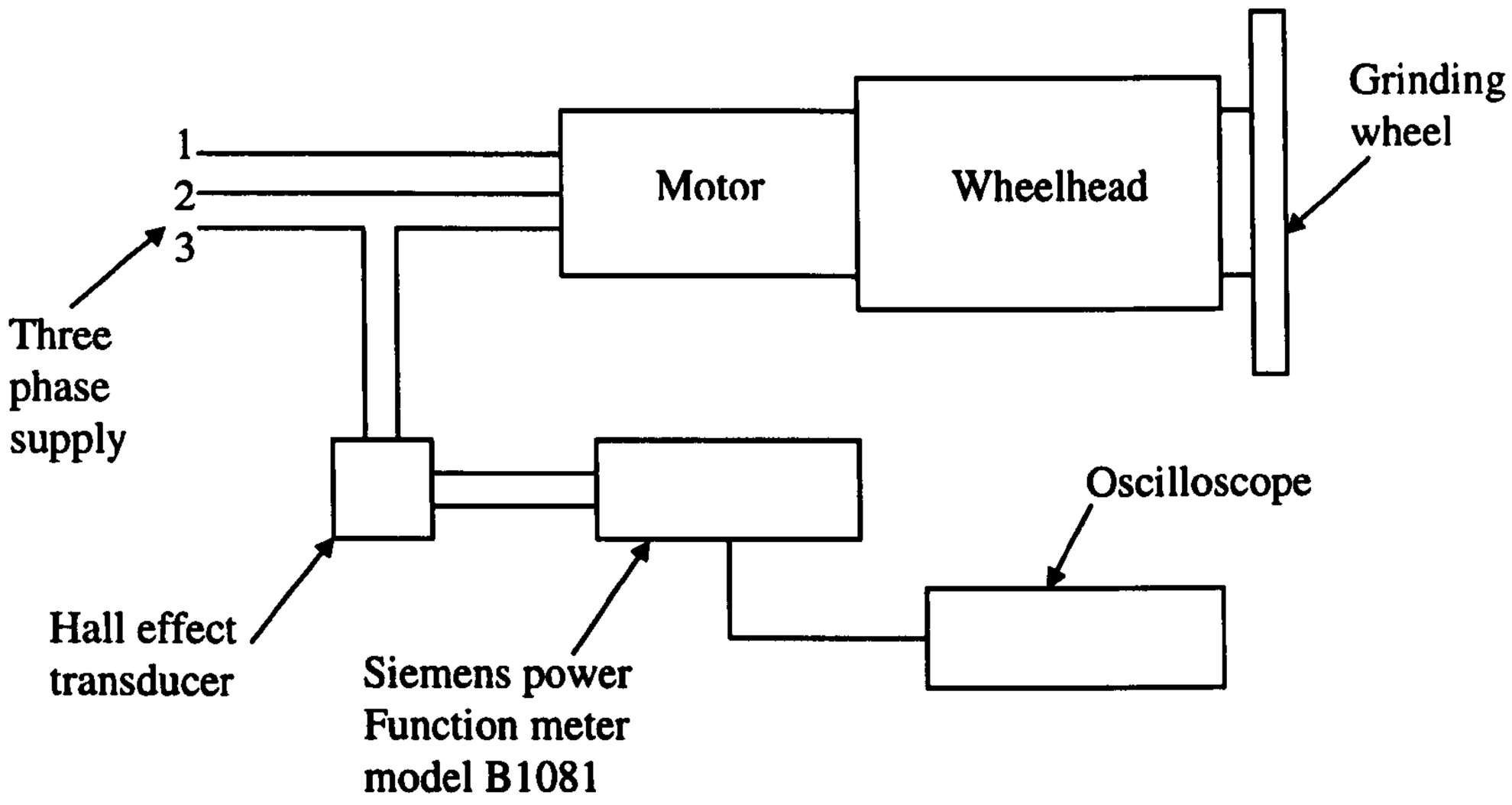

Figure 6.2. Arrangement for grinding power measurement.

The Siemens Function Meter is of calibration standard. However, to check its accuracy power measurements were compared with power calculated from measurements of tangential force. This was carried out on a surface grinding machine where tangential force could be measured directly using a Kistler force table. The force table had a calibration constant of 45.87 mV/N. This was confirmed by testing using weights of known mass. The relationship between power and force is given by Equation 6.1 and 6.2.

$$P = F_t(v_s \pm v_w) \tag{6.1}$$

where: P = power.

F_t = tangential force.

v_s = wheelspeed.

v_w = workpiece speed. The plus sign is for up grinding, i.e. v_s and v_w act in opposite directions and the minus sign for down grinding, i.e. v_s and v_w acting in the same direction.

As v_s is usually much higher than v_w, Equation 6.1 is simplified to:

$$P = F_t v_s \tag{6.2}$$

The results of grinding trials where the tangential force was measured using the Kistler force table and the power measured using the Function meter are presented in figure 6.3.

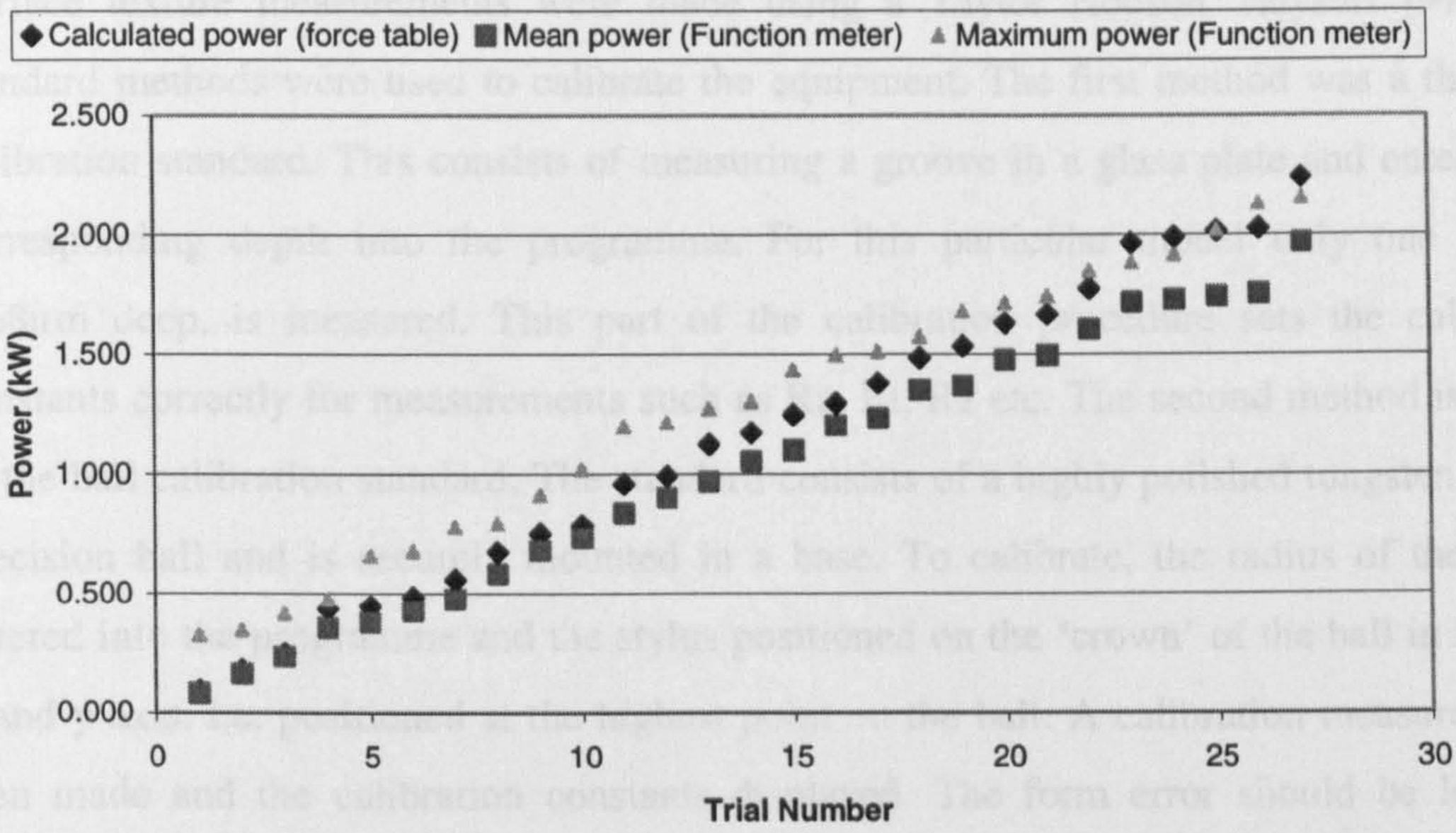

Figure 6.3. Comparison of measured power (mean and maximum) with power calculated from force measurement.

To determine if the maximum power was subject to spikes a mean power was taken from the Function meter and read from the Tektronix oscilloscope. Figure 6.3 shows that the Function meter gives a power reading comparable to the calculated power from the force measurement. For higher power measurements the maximum power from the Function meter gives a more reliable reading. Thus, for power induced by grinding the maximum power appears to be the most appropriate measurement to take. For lower power measurements the mean power gives closer readings to the calculated power. Thus, for

measurements of no load power the mean power may be more reliable. This discrepancy is due to spikes in the power signal. At higher power, the spikes tend to be less significant. To ensure readings were as reliable as possible all power measurements were read as maximum from the Function meter and compared visually with the power curve on the oscilloscope. This method allowed spikes in the signal to be seen visually and removed from the maximum power measurement.

6.5.2 Surface Texture Measurement and Calibration of Equipment

Surface texture measurements were made using a Taylor Hobson Talysurf **[97]**. Two standard methods were used to calibrate the equipment. The first method was a three-line calibration standard. This consists of measuring a groove in a glass plate and entering the corresponding depth into the programme. For this particular model only one groove, 2.68µm deep, is measured. This part of the calibration procedure sets the calibration constants correctly for measurements such as Ra, Rt, Rz etc. The second method is known as the ball calibration standard. The standard consists of a highly polished tungsten carbide precision ball and is securely mounted in a base. To calibrate, the radius of the ball is entered into the programme and the stylus positioned on the 'crown' of the ball in both the x and y axis, i.e. positioned at the highest point on the ball. A calibration measurement is then made and the calibration constants displayed. The form error should be less than 0.3µm. The ball standard calibration is particularly relevant for wheel wear measurements due to the relatively large step that may be measured.

6.5.3 Roundness Measurement and Calibration of Equipment

Roundness measurements were carried out using a Taylor Hobson Talyrond **[98]**. The equipment runs an automatic calibration procedure each time a measurement is made. However, a standard calibration procedure was also carried out before measuring. This comprised of measuring two steps using three slip gauges of 2.5 mm, 2.8 mm and 3.0 mm. The slip gauges are mounted on a 'glass flat' so that two steps could be measured, i.e. steps of 0.5 mm and 0.2 mm. The steps are measured three times each and the average taken. Values are then used to calculate the gain correction factor that is then entered into the

program. The gain correction factor is the ratio of actual step height to measured step height.

6.5.4 Size Measurement and Calibration of Equipment

For all size measurements a Mitutoyo LSM506 laser scan micrometer was used **[99]**. The laser micrometer was calibrated using two Mitutoyo calibration gauges, one of diameters 0.9996 and the second 60.0046mm. For stability, the laser micrometer was mounted on a granite base and maintained in a temperature controlled room.

6.5.5 Determining G-ratio and Measurement of Wheel Wear

To determine G-ratio, the radial depth of wheel wear had to be accurately determined. This was achieved by transferring the wheel wear profile onto a Stanley knife blade. The blade was plunge ground gently using manual control immediately after each grinding trial.

To determine the depth of wheel wear the profile was measured using the Taylor Hobson Talysurf. From the radial depth of wheel wear the volume of wheel wear was calculated. By dividing the volume of workpiece material removed by the volume of wheel wear G-ratio was determined.

6.6 Experimental Procedure

From an experimental study using a two-level orthogonal array, it was possible to show the effects of process parameters on a set of performance indicators graphically. From the graphs produced and experimental results, predictions were made to determine if and how target workpiece quality was achieved and economic advantage gained using vitrified CBN wheels. These results formed the confirmation trials for this part of the investigation and provided the data required for the costing analysis.

6.6.1 Machine Warm Up Procedure

To ensure all trials were carried out while the machine was in a thermally stable condition a warm up procedure was followed. This was based on the results presented in chapter five,

Figure 5.15 where the thermal drift of the x-axis over a period of time was established. The warm up procedure followed was follows.

1. Switch machine hydraulics on and leave for 30 minutes.
2. Run all spindles at idling speed for 1 hour.
3. Put machine in a feed hold with wheel, workhead and dressing spindle at the speeds to be used for the subsequent trial. Leave in feed hold for 3 hours.
4. Measure coolant flow rate and set to specified flow rate.
5. Commence trial.

6.6.2 Grinding Procedure

All workpieces were ground between centres using a plunge grinding process. The stock removed from each diameter for each plunge was 0.2mm.

A feature of the Suprema is that the workhead centre is live and rotates with the drive plate. It is not possible to operate the workhead with the centre not running. The centre mounted in the tailstock is a dead centre. For the Series 10 trials both the workhead and tailstock were dead centres.

The five diameters of the workpiece were ground consecutively starting with the diameter nearest the workhead moving towards the final diameter at the tailstock end. The process parameters used, and the experimental arrangement followed, are discussed in the following section.

6.7 Experimental Arrangement

Eight process parameters were selected for the characterisation of the high speed grinding process. Each parameter was tested at two levels to determine its effect on performance indicators. The parameters investigated and the levels used are listed in Table 6.2.

Table 6.2. Parameters and levels tested for process characterisation trials.

Parameter	**Level**	
	1	**2**
A. Dressing direction	down	up
B. Dressing overlap (U_d)	2	10
C. Dressing increment (a_d)	2μm	10μm
D. Number of dressing passes (n_d)	2	10
E. Wheelspeed (v_s)	60m/s	120m/s
F. Workpiece speed (v_w)	36m/min	54m/min
G. Dwell (s)	10μm off diameter at1μm/s	10s
H. Dresser speed (v_r)	42m/s	72m/s

For all trials the specific volumetric removal rate was, $Q'_w = 10\ mm^3/mm{\cdot}s$.

To carry out a full factorial test on eight parameters at two levels would require 2^8 trials, i.e. 256. This requires an excessive amount of time and labour. The most economical fractional factorial experimental plan for this number of parameters follows the $L_{16}2^8$ orthogonal array, i.e. sixteen trials with eight parameters at two levels. This design allowed all parameters to be tested against each other at both levels. The orthogonal array is shown in Table 6.3. According to Taguchi **[100,101]** the plan may be checked for reliability by running confirmation trials based on the results collected. If the results from the confirmation trials agree with the expected results, then the experimental plan may be considered to be reliable. A table showing the experimental arrangement is shown in Table 6.3.

Table 6.3. The $L_{16}2^8$ orthogonal array.

Parameter:	A	B	C	D	E	F	G	H
Test	Level							
1	1	1	1	1	1	1	1	1
2	1	1	1	2	2	2	2	1
3	1	2	2	1	1	2	2	1
4	1	2	2	2	2	1	1	1
5	2	1	2	1	2	1	2	1
6	2	1	2	2	1	2	1	1
7	2	2	1	1	2	2	1	1
8	2	2	1	2	1	1	2	1
9	2	2	2	2	2	2	2	2
10	2	2	2	1	1	1	1	2
11	2	1	1	2	2	1	1	2
12	2	1	1	1	1	2	2	2
13	1	2	1	2	1	2	1	2
14	1	2	1	1	2	1	2	2
15	1	1	2	2	1	1	2	2
16	1	1	2	1	2	2	1	2

In accordance with the experimental design sixteen trials were carried out with the process parameters set at levels indicated in Table 6.3.

To show the effect of each parameter direct effects charts have been generated. The direct effects charts show clearly how each parameter affects the performance indicators. This is achieved by determining a mean value for each performance indicator at each parameter level. The difference between mean values for each parameter is the direct effect. For example, from Table 6.3 it can be seen that parameter H is set at level 1 for the first eight trials and level 2 for trials 9 to 16. Thus, for each performance indicator, the mean from the

first eight trials is determined and compared with the mean from the last eight trials. The difference shows the effect of H on the performance indicator.

Results showing the direct effects of process parameters on specific energy, surface roughness (Ra), roundness, size holding and G-ratio are presented in Section 6.8. A further set of direct effects charts for variance is included in Appendix B1. The charts show a line for each parameter and the effect of the parameter level, on the performance indicator. This shows clearly how increasing or decreasing the parameter affects the performance indicator. The direct effects chart for G-ratio is based on absolute values of G-ratio from each trial. There is no mean G-ratio or variance within a trial. Therefore, a single direct effect chart for G-ratio based on absolute values is included. Graphs showing the results and trends of performance indicators for each trial are located in Appendix B2.

The parameters selected for the confirmation trials are presented in the following section. A summary of the results of the confirmation trials is also included in the following section supporting corresponding graphs located in Appendix B3.

Note on Specific Energy Results

During the investigation a wheelhead motor failure occurred. This was due to a bearing failure on the motor spindle. Failure occurred on set-up for Trial 6. A spare motor was installed and grinding trials resumed from Trial 6 onwards. From power measurements made with the new motor it became apparent that the power measurements made for the first five grinding trials were unreliable. This was due to grinding power measurements being made while the motor power was unstable. Consequently, the direct effects charts for specific energy are based on the last eight trials and not the full sixteen. This is to avoid the risk of including spurious results. This action is valid due to the second half of the experimental plan being the reverse of the first half. This is known as a reflection in the experimental plan. It can be seen that the experimental plan is a combination of two $L_8 2^7$ orthogonal arrays with the second half, i.e. Trials 9 to 16 being a reflection of the first eight trials where both $L_8 2^7$ arrays have the same pattern with the levels the opposite way around.

As a result of this, the effect of parameter H is not included in the specific energy results. This is due to it being set at level 2 for all of the last eight trials. A photograph showing the failed wheelhead motor is shown in Appendix A, Figure A6.

6.8 Results

6.8.1 Direct Effects Charts for Grinding AISI 52100 with Vitrified CBN

Figures 6.4 to 6.8 presented in this section are the direct effects chart generated from grinding trials carried out following the orthogonal array shown and discussed in Section 6.7. Additional direct effects charts for variance can be found in Appendix B1.

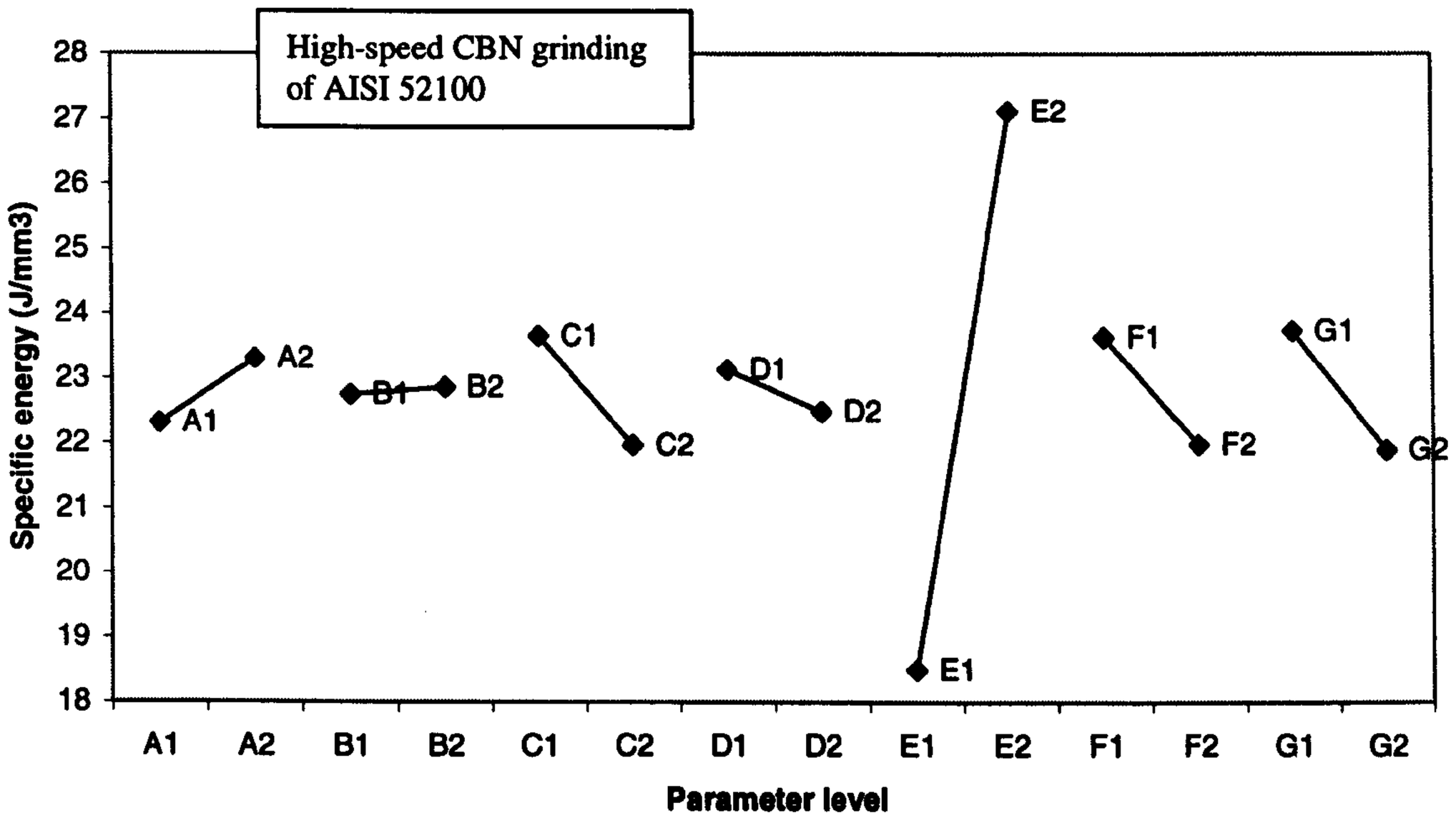

Figure 6.4. Direct effects of process parameters on specific energy.

Where:

A = dressing direction, **A1 = down, A2 = up**. B = dressing overlap, **B1 = 2, B2 = 10**. C = dressing increment, **C1 = 2µm, C2 = 10µm**. D = number of dressing passes, **D1 = 2, D2 = 10**. E = wheelspeed, **E1 = 60m/s, E2 = 120m/s**. F = workspeed, **F1 = 36m/min, F2 = 54m/min**. G = dwell, **G1 = 10µm off diameter at1µm/s, G2 = 10s**. H = dresser speed, **H1 = 42m/s, H2 = 72m/s**.

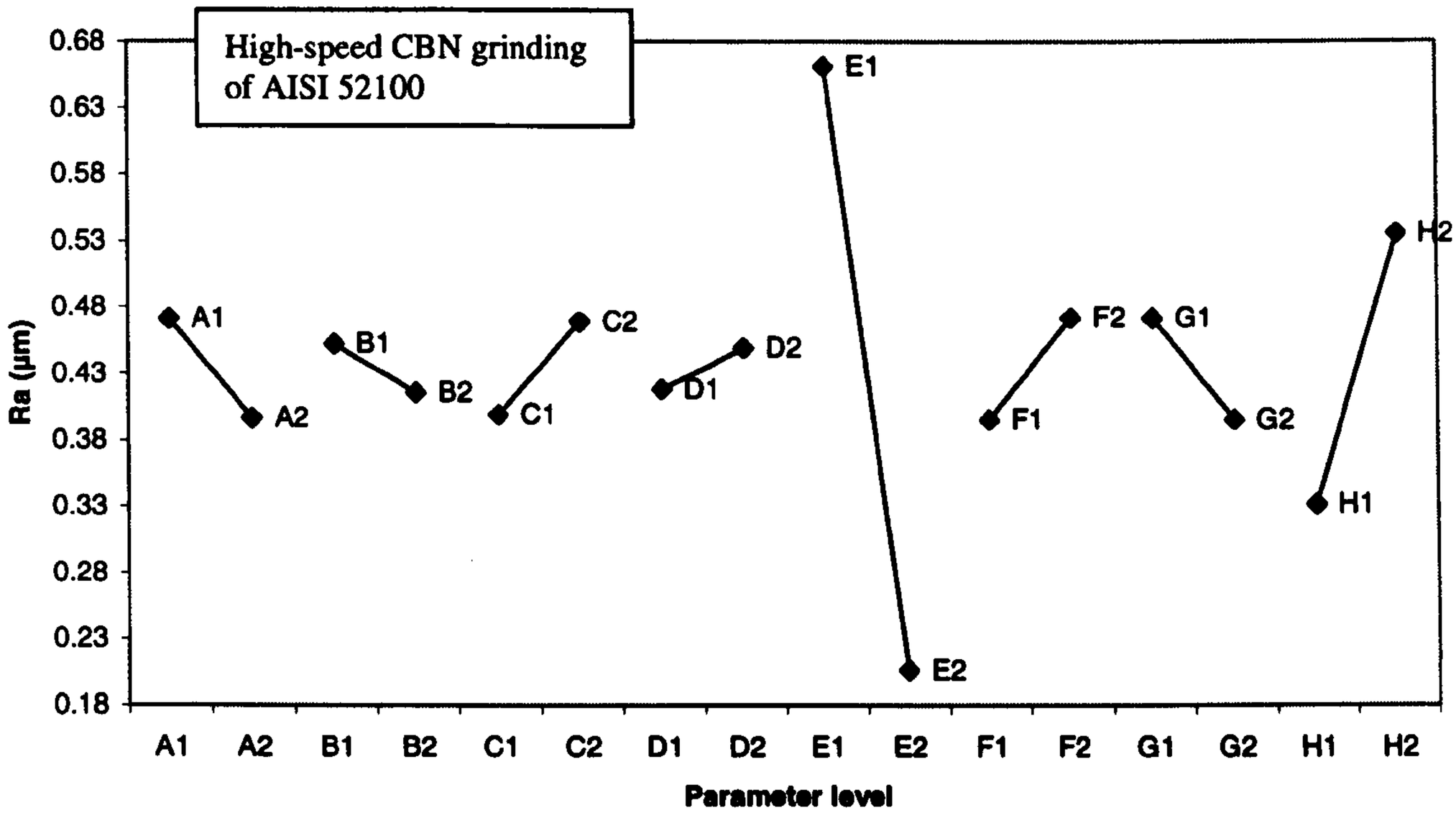

Figure 6.5. Direct effects of process parameters on surface roughness, i.e. Ra. A is down/up dressing, B dressing overlap, C dressing increment, D number of dressing passes, E wheelspeed, F workspeed, G dwell and H dresser speed.

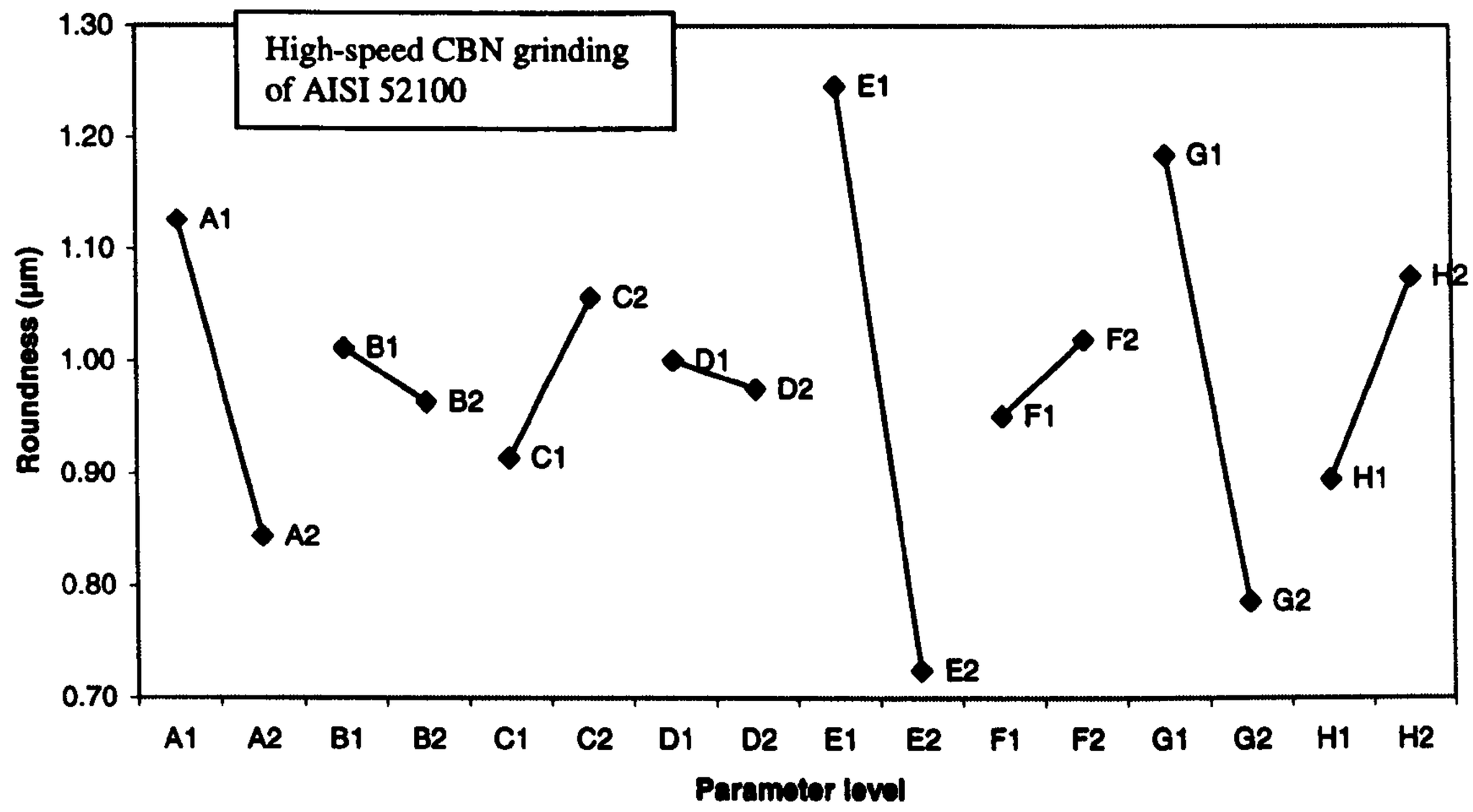

Figure 6.6. Direct effects of process parameters on roundness. A is down/up dressing, B dressing overlap, C dressing increment, D number of dressing passes, E wheelspeed, F workspeed, G dwell and H dresser speed.

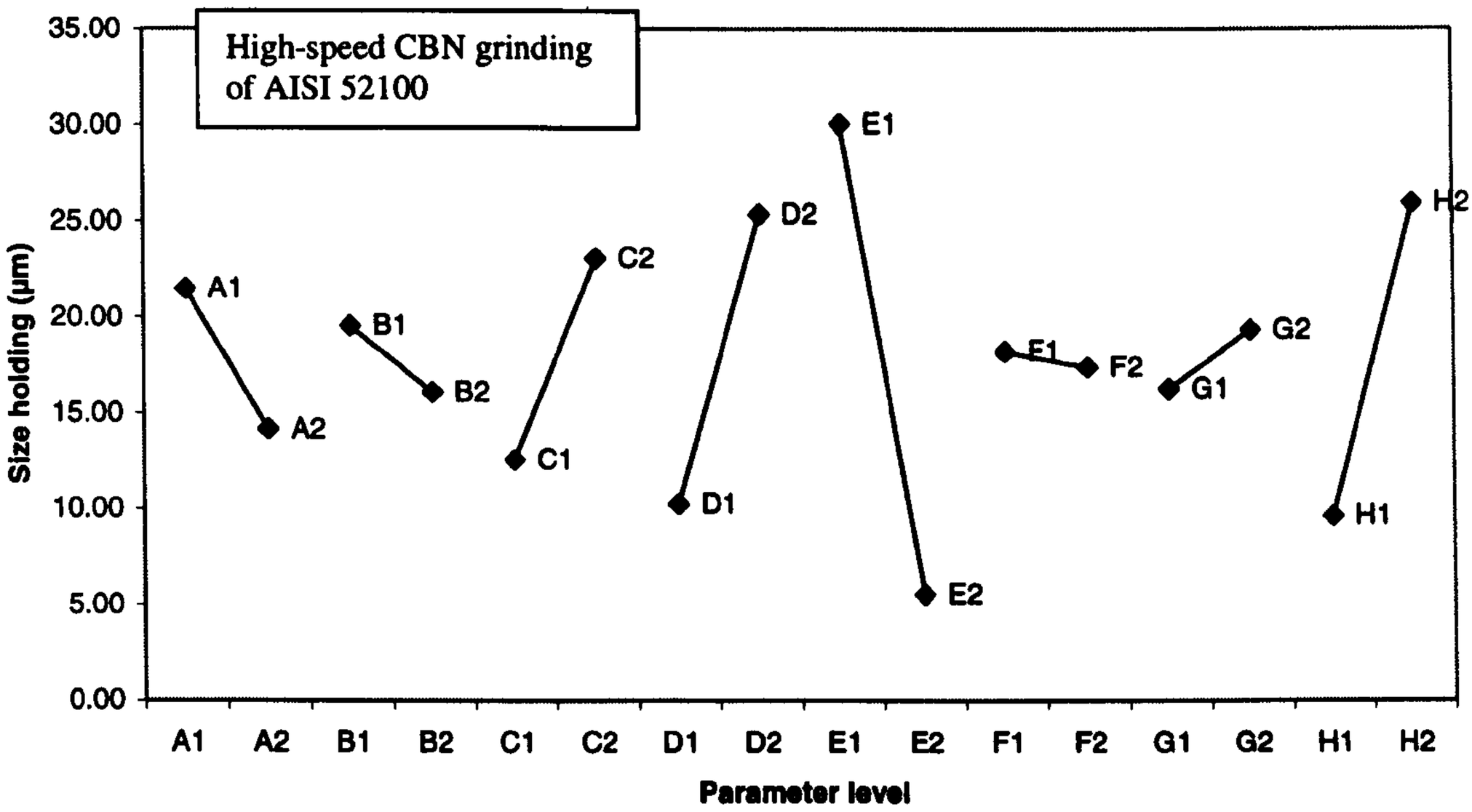

Figure 6.7. Direct effects of process parameters on size holding. A is down/up dressing, B dressing overlap, C dressing increment, D number of dressing passes, E wheelspeed, F workspeed, G dwell and H dresser speed.

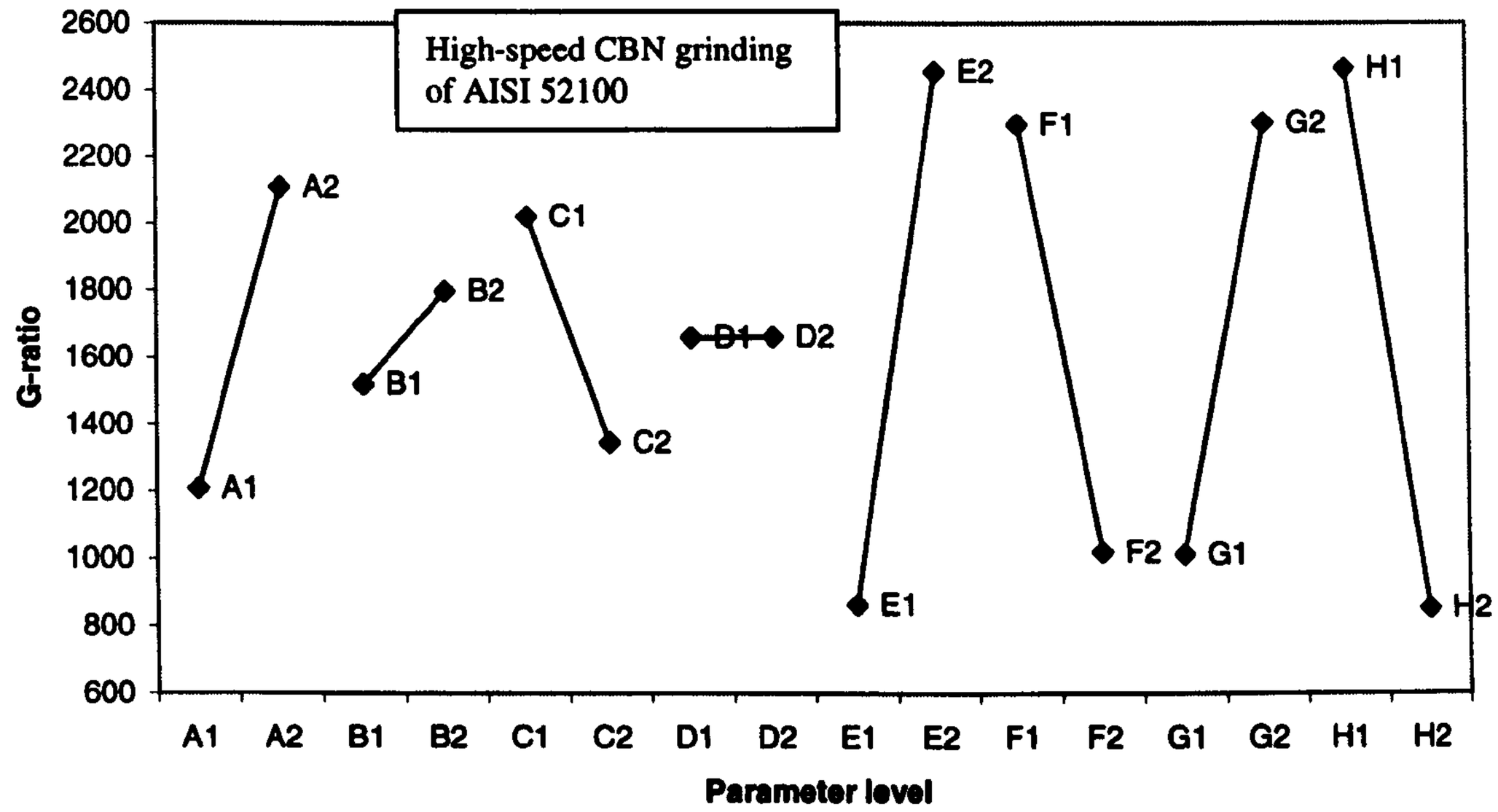

Figure 6.8. Direct effects of process parameters on G-ratio. A is down/up dressing, B dressing overlap, C dressing increment, D number of dressing passes, E wheelspeed, F workspeed, G dwell and H dresser speed.

The direct effects charts shown clearly indicate the direction in which each parameter affects the performance indicators. A discussion on the direct effects charts is given in Section 6.9. To check if a significant difference exists between the parameter levels and their effect on the performance indicator Students t-test, Equation 6.3, was used. A description of this analysis is given in the following section.

6.8.2 Analysis of Results Using Students t-Test

If a null hypothesis, denoted H_0, is taken then the means of the samples being compared are said to equal each other, i.e. H_0: $x_1 = x_2$. For a significant difference to exist it is required to show that this hypothesis can be rejected. To do this, a value of 't' is calculated from the experimental results, denoted t_{obt}, and compared with a value of 't' determined from statistical tables, denoted t_{crit}. If $t_{obt} > t_{crit}$ the hypothesis is rejected and a significant difference between means does exist.

The equation for Students t-test is given as:

$$t_{obt} = \frac{x_1 - x_2}{\sqrt{\frac{s_1^{\,2}}{n_1} + \frac{s_2^{\,2}}{n_2}}} \qquad (6.3)$$

where: t_{obt} = the value of t determined for the sample

x = the mean of the sample

s^2 = the variance of the sample

n = the sample size

The subscripts 1 & 2 represent the sample for the parameter level

For the null hypothesis to be rejected t_{obt} must be greater than t_{crit}, which is determined from tables. To determine t_{crit} from tables the degrees of freedom and significance level must be established. The degrees of freedom is calculated as,

$$df = n_1 + n_2 - 2 \tag{6.4}$$

The maximum degrees of freedom given in tables is 120. For degrees of freedom in excess of this the final row of the table is used which is denoted by the symbol, ∞ in the degrees of freedom column. For this analysis the degrees of freedom was always above 120.

Two types of error can occur when carrying out a significance test known as Type I and Type II errors. A Type I error occurs if a null hypothesis is rejected when it is actually true. A Type II error occurs if a null hypothesis is not rejected when it is actually false. To determine t_{crit} a significance level must be decided upon. If the significance level selected is too large there is an increased risk of a Type I error occurring. If the significance level is too small there is an increased risk of a Type II error occurring. If t_{obt} is smaller than t_{crit}, the null hypothesis is not rejected and it is unproven whether a significant difference exists. The null hypothesis is never accepted. The significance level most widely accepted as the best compromise to avoid making a Type I or Type II error is 0.05. This value was used for this investigation.

The test is two tailed as it is non-directional, i.e. the direction of the difference has not been assumed. From tables of the t distribution, for a two tailed test with over 120 degrees of freedom and a significance level of 0.05, $t_{crit} = 1.96$

Table 6.4 gives the results for the t-test carried out. Due to the problems encountered on the first five trials, with regard to specific energy, the t-test results have been calculated using the final eight trials, i.e. $L_8 2^7$ orthogonal array. Consequently, the effects of dresser speed on specific energy could not reliably be determined. Results for all other performance indicators have been determined using the full $L_{16} 2^8$ orthogonal array.

Note: The negative values are from results where the mean for 'sample 2' was greater than the mean of 'sample 1', i.e. the results of the parameter at level 2 are higher than at level 1 for that performance indicator. For example, results for parameter A set at level 2 gave

higher specific energy than when set at level 1. However, the opposite occurs for this parameter with regard to Ra.

Table 6.4. Results of Students t-test on performance indicators.

Parameter		Value of t_{obt} for performance Indicators			
		Specific Energy	Ra	Roundness	Size Holding
A	(down/up dress)	-10	8	13	14
B	(U_d)	**-1.2**	4	2	5
C	(a_d)	18	-8	-7	-20
D	(n_d)	7	-3	**1.3**	-29
E	(v_s)	-91	49	23	46
F	(v_w)	18	-8	-3	**1.6**
G	(s)	19	8	17	-6
H	(v_r)	-	-22	-8	-31

As can be seen, values for t_{obt} are higher than t_{crit} (= 1.96) in all but three instances, which are shown in bold type. This shows that the parameter levels tested were of the correct magnitude to determine the direction in which they influence the performance indicators. The values in the table are also a good indication as to how strongly a parameter affects a particular performance indicator. The greater t_{obt}, the greater is the influence of that parameter on the performance indicator relative to the other parameters. This is clearly shown by the direct effects charts. As G-ratio measurements are based on the final wheel wear and a single measurement rather than a sample of a population, there is no variance making it unsuitable for Students t-test.

A summary of the results from the characterisation trials is given in Table 6.5. The results shown are mean values for each performance indicator. Read in isolation Table 6.5 does not give a full picture of the results. However, it may be used to support the full set of graphs for each trial shown in Appendix B2. The values of G-ratio are for a fixed volume of

material removed, i.e. $V_w = 80{,}000\ mm^3$. This provided an objective comparison of G-ratio, reflecting the performance of each trial. Re-dress life is also included in the summary and is based on achievement of target workpiece quality. Re-dress life is given as the number of parts (number of diameters) per dress and is the point when either the target Ra of ≤0.25μm or target roundness of ≤1.0μm is exceeded. It can be seen from the graphs of individual performance indicators that for some trials re-dress life is exceeded immediately after dressing when the trial commences. Beyond this the trial produces good results. In these cases re-dress life has been given as the number of parts within target workpiece quality criteria.

Table 6.5. Mean results for all sixteen Suprema characterisation trials grinding.

Trial No.	Specific Energy (J/mm^3)	Ra (μm)	Roundness (μm)	Size Holding (μm)	G-Ratio	Re-dress life (pts/dress)
1	-	0.41	1.37	2.9	876	5
2	-	0.12	0.71	-1.3	2919	540
3	-	0.53	1.25	10.4	486	3
4	-	0.22	0.75	3.7	2189	540
5	-	0.09	0.62	-9.8	5837	>550
6	20.45	0.58	1.19	29.5	302	50
7	32.69	0.26	0.68	-6.7	2502	175
8	19.12	0.45	0.59	13.1	4608	150
9	24.76	0.15	0.49	-11.7	1425	>540
10	20.28	0.71	1.58	24.5	252	30
11	29.83	0.20	0.85	-0.7	1711	5
12	18.36	0.74	0.77	17.4	244	90
13	18.67	0.90	1.85	55.1	71	15
14	27.76	0.12	0.5	3.4	2851	535
15	16.69	0.97	1.35	87.8	59	0
16	26.14	0.50	1.21	7.2	209	0

Parameter levels for the confirmation trials were selected from visual inspection of the direct effects charts. To test a range of conditions seven confirmation trials were carried out. Listed in Table 6.6 are the parameters selected for each of the confirmation trials. Results are presented in two formats. In this section the results for each confirmation trial are shown statistically, see Tables 6.7 to 6.13. The corresponding graphs showing the trend of performance indicators are presented in Appendix B3. For ease of reference the mean results for each performance indicator (from Tables 6.7 to 6.13) have been summarised at the end of Table 6.6.

Table 6.6. Parameters selected for the seven confirmation trials and summary of mean results.

Confirmation Trial No. **Parameter level**	C1	C2	C3	C4	C5	C6	C7
Dressing direction	up	up	up	up	down	down	down
Dressing overlap, U_d	10	10	10	10	2	2	2
Dressing increment, a_d (μm)	2	2	2	2	10	10	10
No. of dressing passes, n_d	2	2	2	2	2	2	2
Wheelspeed, v_s (m/s) 120	120	120	120	120	120	120	
Workpiece speed, v_w (m/min)	36	36	36	72	36	36	72
Dwell, s (s)	10	2	2	2	2	2	2
Dresser speed, v_r (m/s)	42	42	42	42	42	42	42
Specific volumetric removal rate, Q'_w ($mm^3/mm{\cdot}s$)	10	10	20	20	10	20	20
Summary of Mean Results							
Mean specific energy (J/mm^3)	*26.5*	*27*	*18.4*	*17.5*	*20.8*	*16.2*	*15.8*
Mean surface roughness, Ra, (μm)	*0.14*	*0.2*	*0.22*	*0.5*	*0.54*	*0.5*	*0.67*
Mean roundness (μm)	*0.5*	*0.56*	*0.7*	*0.82*	*0.9*	*1.0*	*0.85*
Mean size holding (μm)	*-0.5*	*-10*	*4.7*	*-3.8*	*-3.4*	*3.2*	*13.8*
G-ratio (for $V_w = 80{,}000mm^3$)	*5700*	*4280*	*2850*	*1220*	*780*	*720*	*475*

The aim of trials C1, C2, C3 and C4 was to achieve low cost high precision grinding. Trials C5, C6 and C7 were carried out with the aim of trying to minimise specific energy and in doing so validate the direct effects charts from a different perspective. The parameter levels used for trials C1 and C5 allow direct comparison with the direct effects charts. Parameter levels for the remaining five confirmation trials have been refined in order to show how they affect performance and, depending on the results, process costs. The refinement of process parameters has been carried out judiciously using the direct effects charts. Consideration has also been given to how process parameters affect costs and how costs can be minimised. This was based on the analysis carried out in Chapter 4.

Table 6.7. Results for Confirmation Trial C1.

	Specific Energy	Ra	Roundness	Size Holding
Mean	26.5 J/mm^3	0.14µm	0.5µm	-0.5µm
Median	25.5	0.14	0.5	-1
Mode	25.3	0.13	0.5	-3
Maximum	49	0.18	0.65	10
Minimum	21.5	0.1	0.3	-6
Range	27.5	0.08	0.35	16
Variance	11.3	0.0003	0.008	14
Standard deviation	3.4	0.017	0.09	3.7

G-ratio = 5,700 (G-ratio is for a fixed volume of material removed, i.e. V_w = 80,000mm^3, not re-dress life).

Table 6.8. Results for Confirmation Trial C2.

	Specific Energy	Ra	Roundness	Size Holding
Mean	27 J/mm^3	0.2µm	0.56µm	-10µm
Median	26.5	0.2	0.55	-11
Mode	26.3	0.18	0.5	-14
Maximum	46.5	0.25	0.9	9
Minimum	23.0	0.16	0.4	-17
Range	23.5	0.09	0.5	26
Variance	7.7	0.0004	0.01	22
Standard deviation	2.8	0.02	0.1	5

G-ratio = 4,280 (G-ratio is for a fixed volume of material removed, i.e. V_w = 80,000mm^3, not re-dress life).

Table 6.9. Results for Confirmation Trial C3.

	Specific Energy	Ra	Roundness	Size Holding
Mean	18.4 J/mm^3	0.22µm	0.7µm	4.7µm
Median	18.25	0.2	0.65	4
Mode	18.25	0.19	0.65	3
Maximum	31.1	0.42	1.25	14
Minimum	14.0	0.1	0.35	-2
Range	17.13	0.32	0.9	16
Variance	5.16	0.0076	0.034	14
Standard deviation	2.27	0.09	0.18	3.8

G-ratio = 2850 (G-ratio is for a fixed volume of material removed, i.e. V_w = 80,000mm^3, not re-dress life).

Table 6.10. Results for Confirmation Trial C4.

	Specific Energy	Ra	Roundness	Size Holding
Mean	17.5 J/mm^3	0.5µm	0.82µm	-3.8µm
Median	17.4	0.46	0.75	-3
Mode	17.8	0.6	0.6	-3
Maximum	27.4	1.04	1.8	9
Minimum	14	0.12	0.3	-15
Range	13.4	0.9	1.5	24
Variance	3.6	0.1	0.11	30
Standard deviation	1.9	0.32	0.33	5.5

G-ratio = 1,220 (G-ratio is for a fixed volume of material removed, i.e. V_w = 80,000mm^3, not re-dress life).

Table 6.11. Results for Confirmation Trial C5.

	Specific Energy	Ra	Roundness	Size Holding
Mean	20.8J/mm^3	0.54µm	0.9µm	-3.4µm
Median	20.75	0.53	0.85	-4
Mode	21.0	0.56	0.85	-8
Maximum	23.25	0.66	1.95	9
Minimum	18.0	0.46	0.5	-10
Range	5.25	0.2	1.45	19
Variance	0.69	0.0019	0.06	16.8
Standard deviation	0.83	0.044	0.24	4.1

G-ratio = 780 (G-ratio is for a fixed volume of material removed, i.e. V_w = 80,000mm^3, not re-dress life).

Table 6.12. Results for Confirmation Trial C6.

	Specific Energy	Ra	Roundness	Size Holding
Mean	16.2 J/mm^3	0.5µm	1.0µm	3.2µm
Median	16.3	0.5	0.95	2
Mode	16.5	0.6	0.8	-
Maximum	20.5	0.7	2.7	15
Minimum	11.4	0.4	0.6	-5
Range	9.1	0.3	2.1	20
Variance	2	0.004	0.1	27.5
Standard deviation	1.4	0.06	0.32	5.24

G-ratio = 720 (G-ratio is for a fixed volume of material removed, i.e. V_w=80,000mm^3, not re-dress life).

Table 6.13. Results for Confirmation Trial C7.

	Specific Energy	Ra	Roundness	Size Holding
Mean	15.8 J/mm^3	0.67µm	0.85µm	13.8µm
Median	15.9	0.64	0.8	13
Mode	16.5	0.53	0.7	13
Maximum	19.8	1.0	1.55	32
Minimum	11.0	0.46	0.45	0
Range	8.8	0.54	1.1	32
Variance	1.6	0.02	0.05	60.8
Standard deviation	1.3	0.14	0.23	7.8

G-ratio = 475 (G-ratio is for a fixed volume of material removed, i.e. V_w=80,000mm^3, not re-dress life).

6.9 Discussion of Direct Effects

The direct effects charts generated from this work are presented in Section 6.8.1 with additional direct effects charts for variance in Appendix B1. The results from Student's t-test show that in all but three cases the parameter levels selected resulted in a significant difference between the means of performance indicators.

Workpiece quality is defined by three performance indicators, namely, surface roughness, roundness and size holding. From the direct effects charts it can be seen that most of the process parameters affect these three performance indicators in the same way. The only parameters that do not agree in all three cases are:

i. The effect of the number of dressing passes (parameter D) is shown to have an opposite effect on roundness to that on surface roughness and size holding.
ii. The effect of workpiece speed (parameter F) is shown to have an opposite effect on size holding to that on surface roughness and roundness.
iii. The effect of dwell (parameter G) is shown to have an opposite effect on size holding to that on surface roughness and roundness.

It was shown in Table 6.4 that for parameter D on roundness and parameter F on size holding the null hypothesis could not be rejected. However, this is consistent with a weak effect and further testing was not considered necessary. For the levels tested, roundness and size holding are insensitive to the number of dressing passes and workspeed respectively.

The effect of dwell on size shows that a fine infeed dwell leads to slightly closer size holding with less variance. However, for reducing surface roughness and out of roundness the static dwell is shown to lead to better results. Firstly, it should be pointed out that the duration of the static dwell was 10 s while the duration of the fine infeed dwell was 5 s, i.e. 10 µm off diameter at 1 µm/s. This increase in dwell time allows form errors to be reduced. However, low values of surface roughness usually lead to higher specific energies. Long dwell periods are often associated with wheel glazing where an increasing size of wear flats reduces wheel sharpness and reduces chip formation. This can lead to low wheel wear but not necessarily high G-ratio as the volume of material removed is reduced. This may also be

accompanied by increasing degrees of wheel loading, chatter and thermally damaged workpieces indicating the end of re-dress life. It can be seen that the static dwell is one of the dominant parameters leading to a high G-ratio. A possible reason for this is that specific energy and hence grinding forces were lower. The direct effects charts show that lower mean values of specific energy were recorded when a static dwell was used. However, should improved size holding also result from lower grinding forces? As lower forces cause smaller system deflections this would seem to be reasonable. Lower grinding forces are the result of a sharper wheel. The high G-ratios show that wheel wear was low for trials where the static dwell was used. The direct effects chart of variance in specific energy indicates that the grinding force of trials using the static dwell was more consistent. From these results it may be concluded that size-holding should be improved when a long static dwell is used. However, the direct effects chart for size shows the opposite. Based on the above arguments it may be that this is a spurious result. Alternatively, a stronger thermal effect may occur during the increased dwell period leading to larger size errors.

An objective for this work was to determine how strongly wheelspeed affects each performance indicator. It can be seen from the results that it is the dominant parameter for achieving low surface roughness, roundness and size scatter. It is also one of the most dominant parameters for achieving high G-ratio. This is in accordance with the theory of Chapter 3 and supports the use of high wheelspeed for effective grinding. The higher specific energy is expected due to the size effect. As outlined in an earlier chapter this is due to the reduced chip thickness and increased number of chips produced. The direct effects charts for variance also show increased wheelspeed to have the greatest effect on reducing the variance of the results over the course of the trial. Thus, the combined effect of improved workpiece quality with lower variance shows high wheelspeed to be an important step forward for the development of the grinding process.

The direct effects charts show that increasing workspeed leads to lower specific energy and G-ratio and higher surface roughness and out of roundness. The effect on size holding was

not established as discussed earlier. Increasing workspeed leads to a smaller depth of cut as shown by Equation 6.4

$$a = \pi d_w v_f / v_w \qquad (6.4)$$

By decreasing depth of cut the overall grinding force is reduced. This is supported by the lower mean specific energy for increased workspeed as shown by the direct effects charts. However, lower grinding forces should lead to less wheel wear. The direct effects chart for G-ratio does not support this. This may be due to the proportional relationship shown by Equation 3.3 where chip thickness is proportional to the square root of workspeed. Thus, higher workspeed leads to increased chip thickness. An increased chip thickness would cause a greater force on the individual grits engaging in the grinding action. However, as chip thickness is increased fewer grains are required at any instant to engage in the grinding action to remove the material. This allows the overall force to be lower while individual forces acting on abrasive grains may be larger than when a lower workspeed is used. This higher force acting on the grains leads to greater wheel wear as shown by the direct effects chart for G-ratio. The poorer results for surface roughness and roundness also support the argument that fewer abrasive grains engage in the grinding action. This argument is also supported by the size effect. When workspeed is reduced chip thickness is also reduced. Therefore more grains engage in the grinding action leading to higher specific energy, i.e. energy is proportional to the number of grinding chips produced per unit volume of material. The smaller chip thickness and increased number of grains engaging in the grinding action also results in lower surface roughness and roundness errors.

Initial inspection of the direct effects charts indicates that dressing direction is consistent with the general opinion that up dressing gives improved workpiece quality with higher specific energy. It is also shown that up dressing has a strong effect on increasing G-ratio. Down dressing tends to crush the CBN grits leaving them splintered and sharp. In general this results in lower specific energy with poorer workpiece quality. The lower G-ratios indicate that the crushing action leaves the grains in a weakened condition in the bond. This

could be due to the fact that the grains have splintered and are not fully supported by bond material. This is particularly true when the higher dressing speed of 72 m/s was used. The lower dresser rotational speed of 42 m/s is shown to give, on average, the best workpiece quality and have a dominant effect on increasing G-ratio. This is true for both down and up dressing. Up dressing tends to shear the grits yielding a smoother wheel surface. This is supported by the higher specific energies recorded, better workpiece quality and higher G-ratios. In effect the wheel is in a blunter condition after up dressing with the shearing action leading to flats on the grains. However, the direct effects charts indicate that if workpiece quality is the priority, i.e. for precision grinding operations, up dressing should be used. Re-dress life was also found to be higher when up dressing was used. For Trials 5, 9 and C1 the grinding trial finished before re-dress life was exceeded. In all three cases up dressing was used. Trial 5 also had the highest G-ratio of 5837. The highest G-ratio for a trial where down dressing was used was Trial 2 at 2919. For rough grinding operations where high removal rates are employed down dressing offers potential benefit due to the tendency towards a lower specific energy.

Increasing dressing overlap produces a smoother wheel surface. The direct effects charts show that this leads to the expected result of improved workpiece quality. However, in comparison with other parameters the effect is fairly small. It has also been shown that according to Student's t-test there is not a significant effect on specific energy.

In recent years much has been made of touch dressing. This was discussed in some detail in Chapter 2. The grinding trials undertaken for the production of the direct effects charts compared dressing increments of 2 µm and 10 µm. It can be seen that the smaller increment leads to improved workpiece quality with reduced variance and higher G-ratio. This may also be significant for the cost analysis for reducing wheel costs per part by less wheel wastage through dressing. The direct effects charts show that a larger dressing increment leads to lower specific energy with lower G-ratio. This may be due to the more aggressive dressing action which leaves more fractured grains. The fractured grains provide a greater

number of sharper edges to engage in the grinding action. However, the fractured grains are less securely fixed in the wheel bond resulting in greater wheel wear.

On the whole the number of dressing passes appears to have less effect on performance than any of the other parameters. Where its effect is largest, i.e. on the mean size holding and its variance, the lower number of dressing passes is recommended. This also suits the costing analysis where less wheel wastage through dressing is desirable.

Finally with regard to the direct effects charts it is useful to compare the parameter levels used which produced the best and worst during the sixteen characterisation trials. This provides a convenient check on some of the findings. The best results were achieved from Trial 5. The worst results were recorded from Trial 15. The results are summarized in Table 6.14. The specific energy is not given for Trial 5 due to the motor problem. However, in general trials which give low surface roughness and high G-ratio tend to have a high specific energy. Thus it may be assumed that the specific energy for Trial 5 was greater than for Trial 15. The results are interesting in that they reveal the enormous difference between the best and worst cases. This highlights the improvements in performance that can be achieved by selecting appropriate process conditions.

Table 6.14. Results for Trials 5 and 15

Conditions

Trial 5: Up dress, U_d= 2, a_d=10µm, n_d= 2, v_s=120m/s, v_w=36m/min, s=10s, v_r=42m/s

Trial 15: Down dress, U_d= 2, a_d=10µm, n_d= 10, v_s=60m/s, v_w=36m/min, s=10s, v_r=72m/s

	Trial 5	Trial 15
Specific energy (J/mm3)	-	16.7
Ra (µm)	0.09	0.97
Roundness (µm)	0.62	1.35
Size holding (µm)	10	88
Radial wheel wear (µm)	1.5	145
G-ratio	5837	59
Re-dress life (no. of parts)	>550	0

As Trial 15 failed immediately to meet target workpiece quality for re-dress life G-ratio is based on a fixed volume of material removed, i.e. V_w = 76,140 mm^3. For Trial 5 the opposite is true in that re-dress life was not determined as the trial finished with the wheel still in condition. Thus, G-ratio is for the same volume of material removed.

The parameter levels for Trial 5 are consistent with the direct effects charts for good workpiece quality and high G-ratio. The main factors contributing to the poor performance of Trial 15 are low wheelspeed and high dresser speed. Out of the sixteen trials undertaken Trials 10, 12, 13 and 15 produced the worst workpiece quality and highest G-ratio. It is interesting to point out that the only common factors to all four trials were low wheelspeed and high dresser speed. The four best results achieved overall from the characterisation trials were Trials 2, 5, 9 and 14. The only common factors to all four of these trials is high wheelspeed and a 10s static dwell.

6.10 Discussion of Confirmation Trials

A series of Confirmation Trials were carried out to validate the direct effects charts. The parameters selected for Confirmation Trials C1 to C4 were for improved workpiece quality and explore the effects of process parameters on costs. The parameters used for Confirmation Trials C5 to C7 were selected with the aim of achieving a low specific energy while using a high wheelspeed. This has two purposes, firstly it tests the robustness of the direct effects charts and secondly, it is analogous to a roughing process. Although the direct effects charts cannot be used to make exact predictions, by using them in conjunction with each other, general predictions for the tendencies of performance indicators can be made. The following is a discussion on the performance of each confirmation trial. The discussion on how process costs are affected can be found in Section 6.11.

Confirmation Trial 1 is the only confirmation trial which has a 10s dwell. Thus, this trial provides a direct comparison with the characterisation trials and the direct effects charts. It can be seen that the values of surface roughness are lower than the range indicated on the direct effects charts and that the variance is also low. This is also true for roundness. The

high value of G-ratio given is for a fixed volume of material removed. Re-dress life was not exceeded. High specific energy is recorded. However, for the parameters used the results are in accordance with the direct effects charts.

Confirmation Trial C2 uses the same parameters as Trial C1 except that the dwell is reduced from 10s to 2s. The intention of this trial was to achieve high workpiece quality and G-ratio while reducing cycle time. It is shown that workpiece quality and G-ratio are slightly reduced while a high specific energy is maintained. This result agrees with the point made earlier which highlighted the fact that the four best results from the characterisation trials were achieved using high wheelspeed and a 10s dwell. Results for the surface roughness for this trial indicate that further grinding would have led to a value of Ra above the re-dress limit of 0.25 μm. The G-ratio for this trial is for the same volume of material removed as all other trials but is also for the re-dress life.

The results from Confirmation Trial C3 are of particular interest as advantage is taken of the high wheelspeed by doubling the infeed rate. It can be seen that the mean values for workpiece quality compare well with Trial C2. However, the results for workpiece quality also show increased variance. The higher infeed leads to reduced specific energy and lower G-ratio. Trial C3 indicates that the direct effects charts can be used to select process parameters judiciously and reduce cycle time. Although workpiece quality is reduced slightly, the result was achieved using a short dwell of 2s and with infeed rate doubled. The re-dress life for this trial was still relatively high at 330 parts per dress.

Confirmation Trial C4 was carried out with an increased workspeed. Other parameters are the same as Trial C3. As discussed previously increased workspeed causes chip thickness to increase. The direct effects charts have shown this to offset the benefits of high wheelspeed. Results from this trial agree with this. As chip thickness is increased specific energy should reduce. The size effect theory and the direct effects charts both predict this effect. The specific energy recorded for Trial C4 is shown to be lower than that of Trials C1, C2 and C3. Results for surface roughness, out of roundness and G-ratio are consistent with the

direct effects charts and show a worsening effect. Re-dress life for this trial is also lower than for Trials C1, C2 and C3. For the workspeeds tested during this investigation the lower workspeed of 36 m/min leads to the best performance.

Confirmation Trials 5 to 7 are high wheelspeed grinding with down dressing. The parameters used were selected with the aim of reducing specific energy and cycle time. This allowed the direct effects charts to be tested from a different perspective. It can be seen that the parameters selected are not ideally suited to achieving precision workpiece quality or high G-ratio. As the aim of these trials was low cycle time the dwell for each one has been set at 2s.

Trial C5 has the same removal rate as that used for the characterisation trials. The purpose of this trial was to provide a direct comparison of specific energy. It can be seen that the parameters selected do lead to low specific energy grinding, further validating the direct effects charts. However, workpiece quality and G-ratio are significantly poorer. It is believed that this is a direct result of a short dwell being used. Graphs of the performance indicators for this trial (see Appendix B2) show it to be reasonably stable over the course of the trial. This is particularly true for specific energy where steady state power is achieved immediately. Considering a 2s dwell has been used the results compare reasonably well to other trials from the characterisation set where low specific energies were recorded. Target workpiece quality was not achieved for this trial and, therefore, there is no re-dress life. A positive feature of this trial was that the variance for all performance indicators is very low. It appears that the wheel was in almost the same condition at the end of the trial as at the start. From the original characterisation trials, Trial 8 has a comparable specific energy and a re-dress life of 150 parts per dress. This was a low wheelspeed trial with a 10s dwell and has large variance of performance indicators. The lowest specific energy achieved for a high wheelspeed trial from the original sixteen characterisation trials was trial 9 of 24.8 J/mm^3.

Trial C6 is a repeat of Trial C5 with removal rate doubled. It can be seen that despite this the results are similar. As removal rate has increased specific energy is lower. G-ratio is

similar to Trial C5. Variance of performance indicators has increased slightly due to increased removal rate. The parameters used for Trial C7 provide a direct comparison with Trial C6 with increased workspeed

From the original sixteen characterisation trials, Trials 2, 5, 9 and 14 gave the best results. To provide a clear comparison the parameters used along with corresponding results are re-written in a summarized form as follows:

Parameter levels set for Trials 2, 5, 9 and 14

	Dressing direction	U_d	a_d	n_d	v_s	v_w	s	v_r
Trial 2:	Down	2	2µm	10	120m/s	54m/min	10s	42m/s
Trial 5:	Up	2	10µm	2	120m/s	36m/min	10s	42m/s
Trial 9:	Up	10	10µm	10	120m/s	54m/min	10s	72m/s
Trial 14:	Down	10	2µm	2	120m/s	36m/min	10s	72m/s

Summary of results for Trials 2, 5, 9 and 14

	Trial 2	Trial 5	Trial 9	Trial 14
Mean specific energy	-	-	24.8J/mm^3	27.8J/mm^3
Mean surface roughness, Ra	0.12µm	0.09µm	0.15µm	0.12µm
Mean roundness	0.71µm	0.62µm	0.49µm	0.5µm
Mean size holding	-1.3µm	-9.8µm	-11.7µm	3.4µm
G-ratio (for V_w = 80,000mm^3)	2919	5837	1425	2851
Re-dress life (parts per dress)	540	>540	>540	535

These results show some interesting characteristics. Firstly, Trials 2 and 14 show that precision grinding can be achieved when down dressing is used. Also, Trials 2 and 9 were carried out using the high workpiece speed. Re-dress life for all trials is high and Trials 9 and 14 use the higher dressing speed. The investigation has shown that high workspeed and high dressing speed both tend to lead to lower G-ratio. These effects are coupled together

for Trial 9 which explains the lower G-ratio. The results show that high wheelspeed and a long static dwell appear to dominate over the effects of all other parameters. How this affects process costs is discussed in the following section.

6.11 Discussion of Process Costs

The following cost analysis is based on the theory outlined in Chapter 4. Where the cost analysis is based only on wheel and labour costs Equation 4.25 has been used. For Figure 6.11 the cost analysis includes machine tool purchase costs paid over a pay back period. Thus, Equation 4.28 has been used. The pay back period used is 6 months in duration, equating to 1920 hours, i.e. assuming an average of 20 days worked each month and two 8 hour shifts per working day. Once the cost of the machine tool has been paid back, i.e. after the payback period, the costs would be based on Equation 4.25 where total cost per part consists of wheel and labour costs per part.

Table 6.15 gives the results for the wheel and labour costs per part for all sixteen characteriation and seven confirmation trials carried out on the Suprema. The radial amount of wheel lost through dressing, radial wheel wear and re-dress life are also shown in Table 6.15. The process parameters for these trials are given in previous tables in this chapter. For the cost analysis of the Suprema trials the factors shown in Table 6.8 were constant throughout:

Table 6.15. Factors remaining constant throughout cost analysis of Suprema trials.

Factor remaining constant	Cost
Wheel purchase cost, c_s	£1,700
Maximum wheel diameter, d_{smax}	250mm
Minimum wheel diameter, d_{smin}	240mm
Labour costs per hour, c_l	£75
Stock removed, $d_{ww}+d_{ss}$	0.2mm
Workpiece diameter, d_w	40mm
Wheel width, b_s	17mm

Table 6.16. Comparison of process costs for Suprema characterisation and confirmation trials.

Trial	$a_d \times n_d$	r_s	N_d	C_s	C_l	C_t
1	2µm×2	10µm	5	£0.952	£0.19	£1.142
2	2µm×10	3µm	540	£0.015	£0.262	£0.277
3	10µm×2	18µm	3	£4.307	£0.452	£4.759
4	10µm×10	4µm	540	£0.066	£0.159	£0.225
5	10µm×2	1.5µm	550	£0.013	£0.261	£0.274
6	10µm×10	29µm	50	£0.877	£0.168	£1.045
7	2µm×2	3.5µm	175	£0.015	£0.159	£0.174
8	2µm×10	2µm	150	£0.05	£0.289	£0.339
9	10µm×10	6µm	540	£0.067	£0.263	£0.33
10	10µm×2	34µm	30	£0.61	£0.18	£0.79
11	2µm×10	5µm	5	£1.7	£0.24	£1.94
12	2µm×2	35µm	90	£0.147	£0.263	£0.41
13	2µm×10	120µm	15	£3.173	£0.435	£3.608
14	2µm×2	3µm	535	£0.004	£0.262	£0.266
15	10µm×10	145µm	0	-	-	-
16	10µm×2	41µm	0	-	-	-
C1	2µm×2	1.5µm	540	£0.004	£0.261	£0.265
C2	2µm×2	2µm	540	£0.004	£0.095	£0.099
C3	2µm×2	3µm	330	£0.007	£0.069	£0.076
C4	2µm×2	7µm	180	£0.021	£0.07	£0.091
C5	10µm×2	11µm	0	-	-	-
C6	10µm×2	12µm	0	-	-	-
C7	10µm×2	18µm	0	-	-	-

The results shown in Table 6.16 are shown graphically in Figure 6.9. Costs for Trials 15, 16, C5, C6 and C7 are not given as none of the workpieces ground during these trials satisfied the re-dress life criteria of Ra ≤ 0.25μm and out of roundness ≤ 1μm.

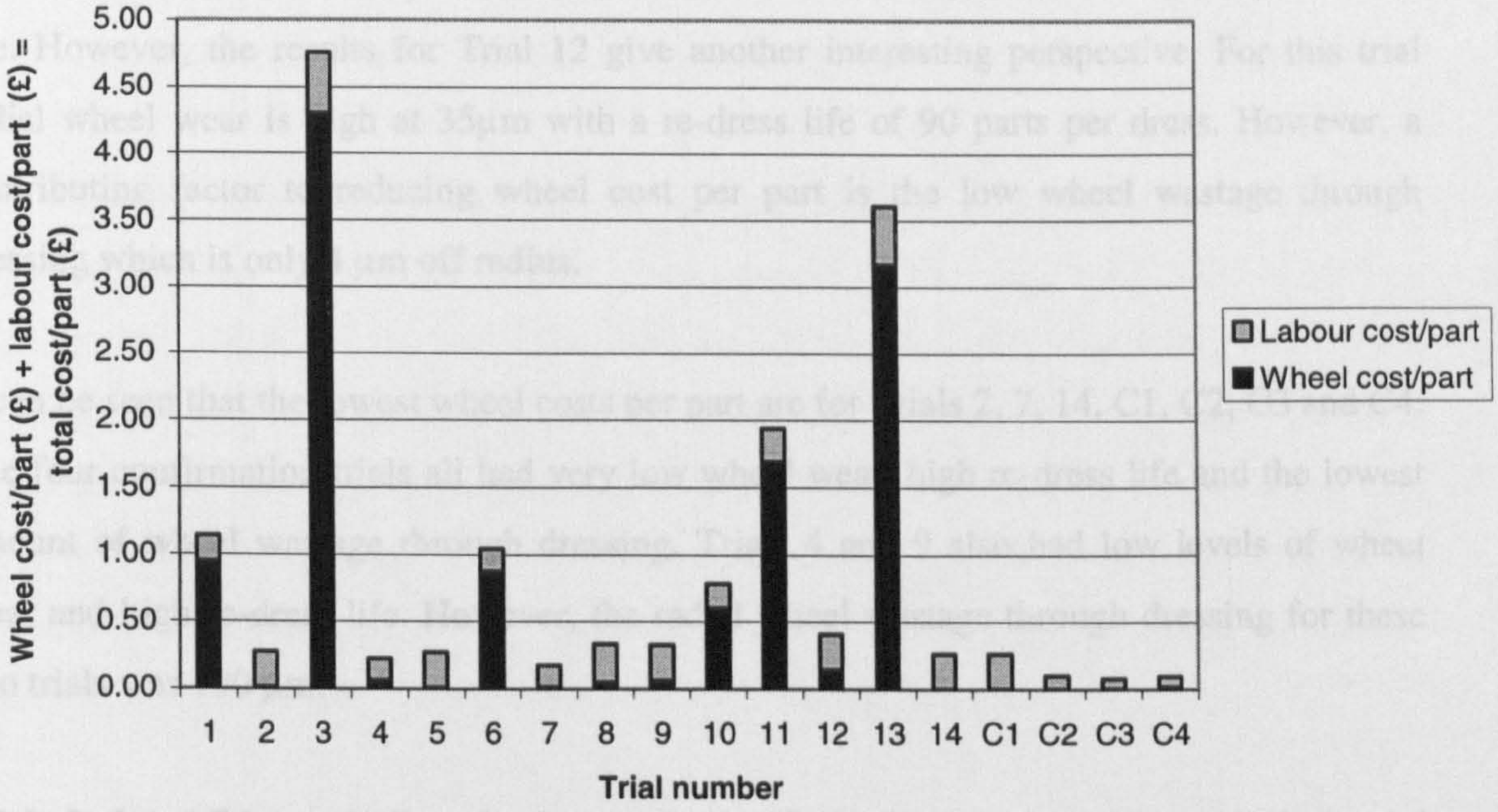

Figure 6.9. Comparison of costs for results from Suprema characterisation and confirmation trials.

From Figure 6.9 the following points are highlighted:

- Trial 3 has the greatest wheel cost per part. The characteristics of this trial are the lowest recorded re-dress life of 3 parts per dress, moderate radial wheel wear of 18 μm and radial wheel wastage through dressing of 20 μm.
- Trial 13 has the second greatest wheel cost per part. The characteristics of this trial are very high radial wheel wear of 120 μm (only Trial 15, with no re-dress life, had greater radial wheel wear of 145 μm), low re-dress life of 15 parts per dress and radial wheel wastage through dressing of 20 μm.

- Trial 11 also has a low re-dress life of 5 parts per dress. This is partly offset by a low level of radial wheel wear of 5µm. Radial wheel wastage through dressing equalled 20µm.

It can be seen by the above points that there is a trade off between wheel wear and re-dress life. However, the results for Trial 12 give another interesting perspective. For this trial radial wheel wear is high at 35µm with a re-dress life of 90 parts per dress. However, a contributing factor to reducing wheel cost per part is the low wheel wastage through dressing which is only 4 µm off radius.

It can be seen that the lowest wheel costs per part are for Trials 2, 7, 14, C1, C2, C3 and C4. The four confirmation trials all had very low wheel wear, high re-dress life and the lowest amount of wheel wastage through dressing. Trials 4 and 9 also had low levels of wheel wear and high re-dress life. However, the radial wheel wastage through dressing for these two trials was 100 µm.

Trials 2, 5 and 7 have similar wheel cost per part. Radial wheel wear is 3 µm, 1.5 µm and 3.5 µm respectively. Trials 2 and 5 have a similar re-dress life of 540 and 550 parts per dress respectively while Trial 7 has a re-dress life of 175 parts per dress. However, Trial 7 has less wheel wastage through dressing which offsets the lower re-dress life.

Wheel costs per part have been shown to be significantly affected by three main factors, namely, re-dress life, wheel wear and wheel wastage through dressing. It has been found that there is a trade off between factors and one can offset the positive effects of another. From the direct effects charts and confirmation trials, it has been shown that a small dressing increment is more likely to lead to lower wheel wear, improved workpiece quality and high re-dress life. It has also been found that the number of dressing passes has minimal effect on performance. Thus, as few dressing passes as possible should be used. These dressing parameters offer the most favourable conditions for reducing wheel cost per part, i.e. low wheel wastage through dressing, low wheel wear and high re-dress life.

With regard to labour costs the following points may be made:

- For all characterisation and confirmation trials the labour cost per hour, stock removed and workpiece diameter were constant.
- For the sixteen characterisation trials the volumetric removal rate was constant at 10 $mm^3/mm{\cdot}s$. For the confirmation trials shown in Figure 6.9 the volumetric removal rate was 10 $mm^3/mm{\cdot}s$ for Trial C1 and 20 $mm^3/mm{\cdot}s$ for Trial C2, C3 and C4.

Trial 3 has the highest labour cost per part of £0.452. This trial has the lowest re-dress life of 3 parts per dress. The second highest labour cost per part of £0.435 is for Trial 13 which has a re-dress life of 15 parts per dress. From the sixteen characterisation trials, Trials 4 and 7 have the lowest labour cost per part of £0.159. Re-dress life is 540 and 175 parts per dress respectively. Considering all characterisation and confirmation trials the lowest labour cost per part is £0.069 for Trial C3. To illustrate how labour costs are broken down, Equation 4.24 has been re-written and the individual terms for Trials 3, 4, 7, 13 and C3 shown. Labour cost per hour is £75. As the unit time is in seconds, c_l equals:

£75 / 3600 = £0.021 per second

$$C_l = c_l\left[\frac{(d_{ww}+d_{ss})\pi d_w}{Q'_w} + s + \frac{b_s n_d}{v_d N_d}\right] \tag{4.25}$$

After multiplying throughout by c_l the three terms in brackets representing removal rate, Q'_w, dwell time, s, and re-dress life, N_d, respectively become:

Trial 3: C_l = £0.452 = £0.052 + £0.208 + £0.192

Trial 4: C_l = £0.16 = £0.052 + £0.104 + £0.003

Trial 7: C_l = £0.159 = £0.052 + £0.104 + £0.002

Trial 13: C_l = £0.435 = £0.052 + £0.104 + £0.279

Trial C3: C_l = £0.069 = £0.026 + £0.042 + £0.001

The first term in brackets is the same for all the characterisation trials as the removal rate remained constant. For Trial C3 the removal rate was doubled. The effect of this is clearly shown in Equation 4.24. Trial 3 had a static dwell of 10s, Trials 4, 7 and 13 a fine infeed dwell which was 5s in duration. Trial C3 had a 2s dwell. It can be seen that reducing dwell has a fairly strong affect on the labour cost equation. Trials 4, 7 and C3 show that despite different dressing conditions a high re-dress life dominates and the final term becomes negligible. For Trials 3 and 13 where re-dress life is low the final term becomes a significant part of the labour cost equation.

The analysis has shown that dwell time has a significant affect on labour cost per part independent of re-dress life. When re-dress life is high labour cost per part is not significantly affected by dressing parameters. However, dressing parameters become significant as re-dress life reduces.

Confirmation Trial C3 is shown to be the most cost effective trial undertaken. This was achieved by compromise where the high re-dress life of 540 parts per dress for Trial C1 and C2 was sacrificed, i.e. to 330 parts per dress, in order to gain the benefits of doubling removal rate and reducing dwell time to 2s. It is interesting to point out that the greater reduction in cost is achieved by the lower dwell period rather than the increased removal rate. Trial C1 and C2 show how dwell time affects labour cost per part, dwell for C1 is 10s and 2s for C2. Trial C2 and C3 show how removal rate affects labour cost per part, i.e. specific volumetric removal rate for C2 is 10 $mm^3/mm{\cdot}s$ and 20 $mm^3/mm{\cdot}s$ for C3. The parameter selection for Trial C3 shows how the direct effects charts coupled with an increased understanding of the factors affecting costs can lead to low cost high precision grinding.

6.11.1 Comparison of Costs With Conventional Speed Grinding

Figure 6.10 shows how high speed grinding with vitrified CBN, compares with more conventional grinding processes. This includes comparisons with results from trials using two aluminium oxide wheels (A465 K5V, WA801 J6V), a sol gel wheel (73A 601 J8V)

and a vitrified CBN wheel (B91 ABN500). These trials were all carried out on the Jones and Shipman Series 10 machine at conventional wheelspeeds, i.e. between 42 m/s and 45 m/s. The parameters used for these trials are listed on the graphs of results presented in Appendix B4. The costs for Trial C3 have been used to represent the Suprema high-speed results.

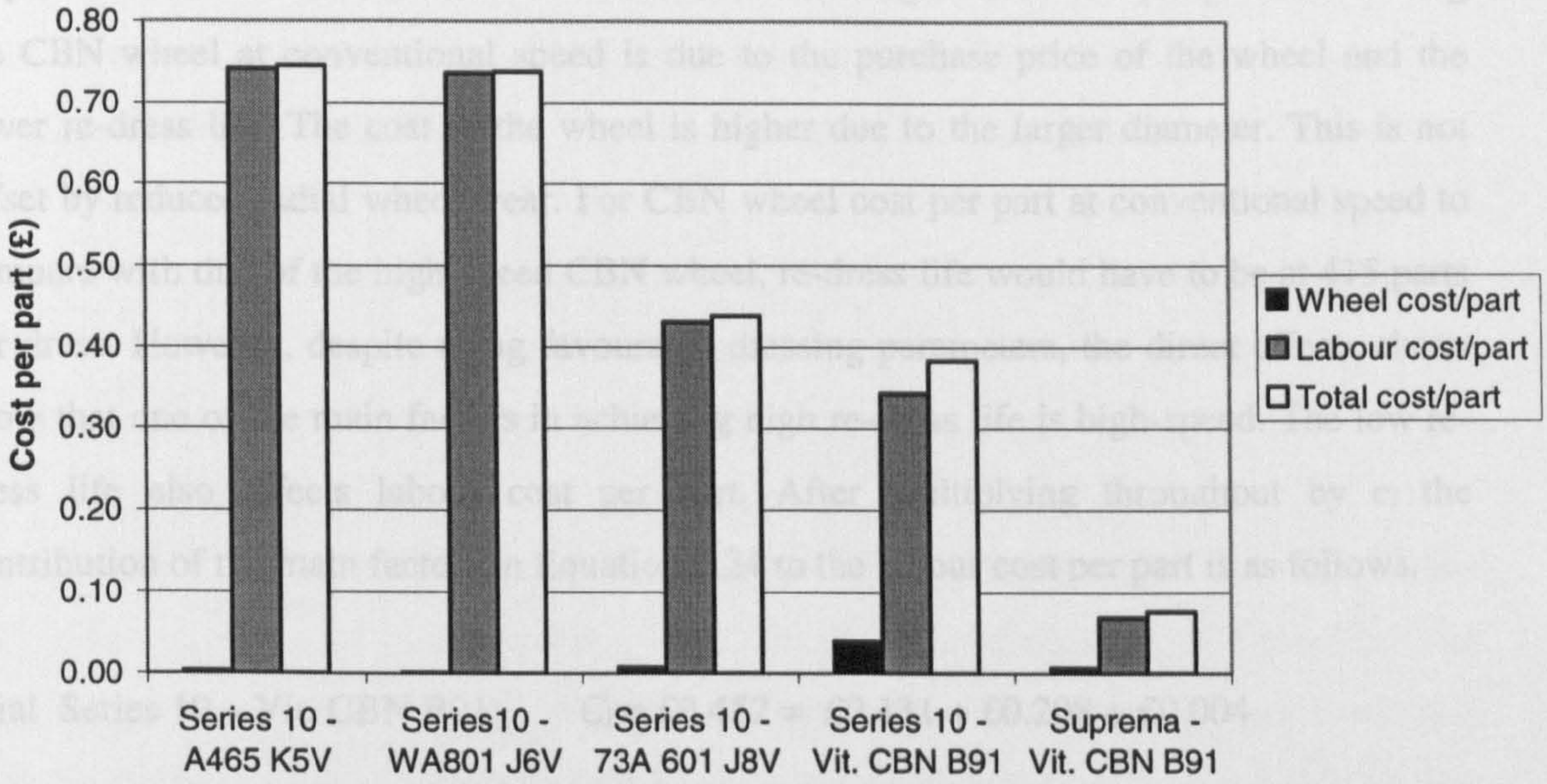

Figure 6.10. Comparison of costs for grinding AISI 52100.

It can be seen clearly that the high-speed results from the Suprema lead to considerably lower total cost per part. This is due to the significant reduction in labour cost per part through using a shorter dwell, high re-dress life and increased removal rate. This was achieved at the expense of marginally increasing wheel cost per part as discussed in the previous section. It has been shown that reducing dwell and increasing removal rate had a significant effect on reducing labour cost per part despite reducing G-ratio and re-dress life. When re-dress life is high this trade off is a key factor in cost effective high-speed precision grinding as predicted by the theory outlined in Chapter 4, see Figure 4.14 where it is shown that as re-dress life increases its effect of on altering total cost diminishes. Results for the

Series 10 CBN trials show that wheel costs are high in comparison to the wheel costs of other results. As has been clearly shown by the direct effects charts this is predominantly due to the low wheelspeed used. Despite this, Figure 6.10 shows that the most cost effective process for precision grinding at conventional speed is with vitrified CBN.

A comprehensive breakdown of the costs shown in Figures 6.9 and 6.10 is presented in Appendix B5. It can be seen that the main reasons for high wheel cost per part when using the CBN wheel at conventional speed is due to the purchase price of the wheel and the lower re-dress life. The cost of the wheel is higher due to the larger diameter. This is not offset by reduced radial wheel wear. For CBN wheel cost per part at conventional speed to compare with that of the high-speed CBN wheel, re-dress life would have to be at 415 parts per dress. However, despite using favourable dressing parameters, the direct effects charts show that one of the main factors in achieving high re-dress life is high-speed. The low re-dress life also affects labour cost per part. After multiplying throughout by c_l the contribution of the main factors in Equation 4.24 to the labour cost per part is as follows.

Trial Series 10 – Vit. CBN B91: C_l = £0.452 = £0.131 + £0.208 + £0.004

The contribution of re-dress life is shown to be negligible at £0.004. For the CBN wheel at conventional speed the effects of removal rate and dwell are greatest in terms of labour cost per part.

For the aluminium oxide wheels and the sol gel wheel, wheel costs per part are negligible. This is due to a number of effects. Firstly, the re-dress life is relatively high for the low purchase price of the wheels. The increased difference between maximum and minimum wheel diameter also has an affect on reducing wheel costs per part as shown by equation 4.14. Wheel wear was found to be relatively low for the aluminium oxide and sol gel wheels. To minimise the effects of dressing, a small dressing increment of 0.01 mm was used with two dressing passes. The selection of these parameters contributed to lower wheel costs per part and a tougher yardstick against which the CBN results had to compare. For

the two aluminium oxide wheels the greatest effect on labour costs per part was the low removal rate. It can be seen from chapter four that labour costs rise steeply below removal rates of 10 $mm^3/mm{\cdot}s$. For the sol gel wheel the contribution of removal rate and dwell is about equal. The break down of labour costs per part is shown below in the same format as previously explained.

Trial Series 10 – A465 K5V: $C_l = £0.741 = £0.524 + £0.208 + £0.009$

Trial Series 10 – WA801 J6V: $C_l = £0.736 = £0.524 + £0.208 + £0.004$

Trial Series 10 – 73A 601 J8V: $C_l = £0.431 = £0.209 + £0.208 + £0.013$

As can be seen in all three cases re-dress life is sufficient to render the final term negligible. Thus, for the CBN wheel at conventional speed increased removal rate is an important factor in reducing labour cost per part and overall total cost per part.

The effect of including machine tool costs spread over a pay back period is shown in Figure 6.11. The machine tool costs used are, £100,000 for a conventional speed machine and £250,000 for a high-speed machine. Figure 6.11 illustrates how the costs are distributed over the pay back period. Beyond the pay back period the distribution of costs would be that shown by Figure 6.10. It can be seen that the benefits gained by grinding at high wheelspeeds minimise the machine tool purchase costs in comparison to the other processes. Equation 4.28 shows that machine tool cost per part is affected by the same factors as labour cost per part.

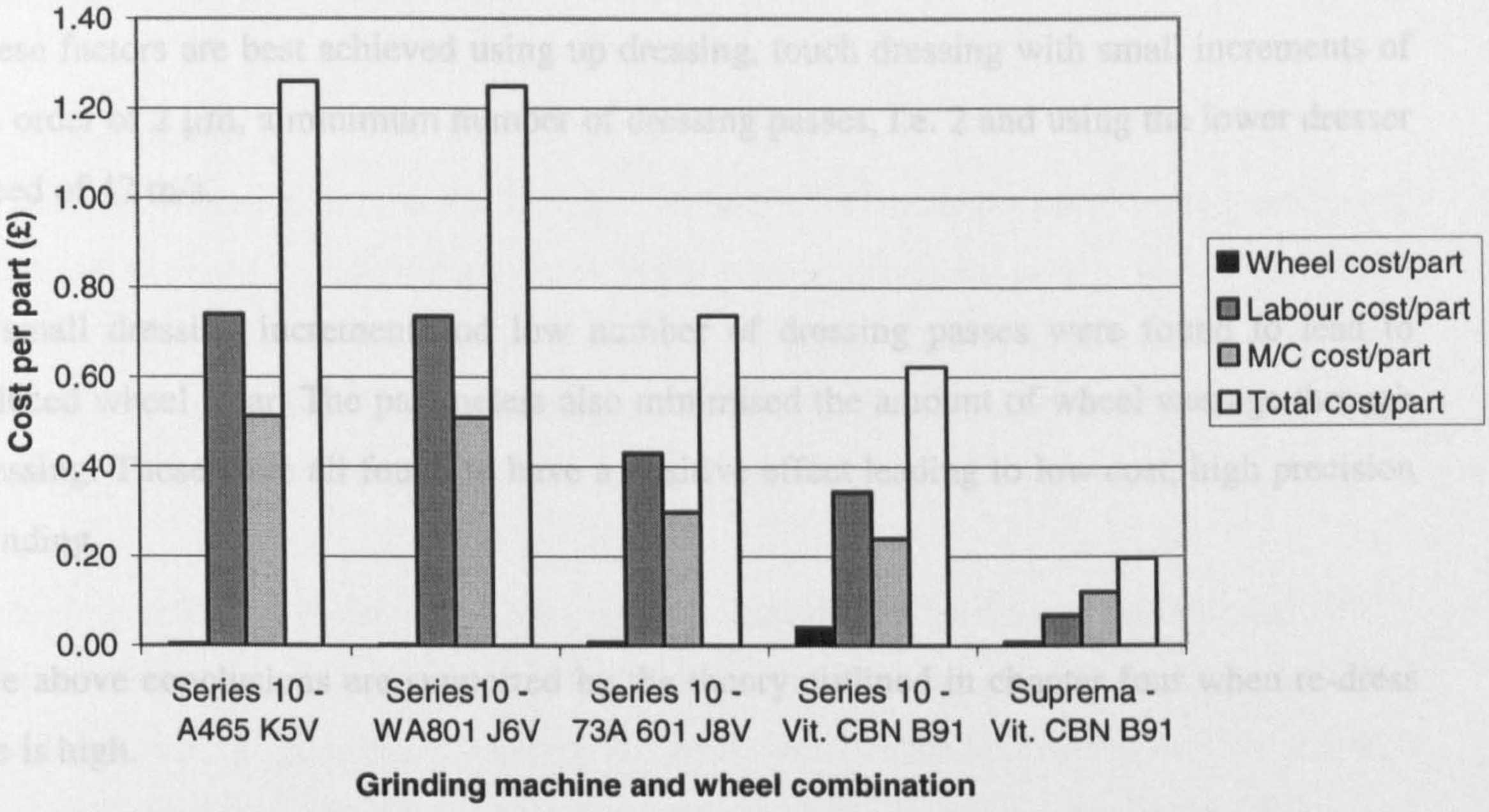

Figure 6.11. Comparison of costs for grinding AISI 52100 including machine tool costs.

The analysis has shown that high speed grinding using a vitrified CBN wheel to grind an easy to grind material such as AISI 52100 leads to significantly lower total costs while achieving high precision.

6.12 Conclusions

Direct effect charts have been produced which show how each of the performance indicators is affected by process parameters. High wheelspeed had by far the greatest affect all round on improving process performance. A long static dwell has also been shown to have a strong effect on improving performance.

In terms of process costs it has been shown that high wheelspeed leads to significantly reduced total cost per part even when machine tool costs are included over a pay back period. The important factors for achieving this are:

- High re-dress life.
- Increased removal rate.

- Reduced dwell time.

These factors are best achieved using up dressing, touch dressing with small increments of the order of 2 μm, a minimum number of dressing passes, i.e. 2 and using the lower dresser speed of 42 m/s.

A small dressing increment and low number of dressing passes were found to lead to reduced wheel wear. The parameters also minimised the amount of wheel wastage through dressing. These were all found to have a positive effect leading to low cost, high precision grinding.

The above conclusions are supported by the theory outlined in chapter four when re-dress life is high.

CHAPTER 7. PROCESS REQUIREMENTS FOR COST EFFECTIVE PRECISON GRINDING OF INCONEL 718

7.1 Introduction

Inconel 718 is used mainly in the aerospace industry. Its mechanical properties, particularly resistance to creep at high temperatures, make it appropriate for turbine blades. However, Inconel 718 is considered a difficult material to grind. This is largely due to the long continuous chips generated during grinding. The chips tend to block the pores of the wheel and hot ductile material tends to adhere to the wheel. Both effects cause loading.

In tandem with this research on process requirements for precision grinding, Cai (2002) **[104]** carried out an investigation on the effects of wheel porosity. Cai used vitrified CBN wheels for internal grinding of Inconel 718 workpieces. Wheel porosities of 35% and 40% were compared at a wheelspeed of 50m/s. Results showed that workpiece roughness was higher using the high-porosity wheel. Using the low-porosity wheel for Inconel 718, workpieces suffered thermal damage and wheel failure due to excessive loading. It was concluded that although workpiece roughness was higher, surface integrity was better when using the 40% porosity wheel for a difficult-to-grind material. This was supported by an increase in re-dress life from 40 mm^3/mm to 600 mm^3/mm. G-ratio was not reported for the 35% porosity wheel due to wheel failure. For the 40% porosity wheel, G-ratio was 2000. Based on this work, the vitrified CBN grinding wheels used for the high-speed and conventional speed trials, on the Suprema and Series 10 machines, had a porosity of 40%.

Research has shown that CBN has the potential to offer the aerospace industry the same gains as it has the automotive industry **[31, 105-107]**. However, some manufacturers in the aerospace industry have yet to be convinced. This is predominantly due to the high initial cost of the CBN wheel. Therefore, effects of process parameters were also investigated for three aluminium oxide wheels. This allowed comparison to be made between costs of precision grinding using aluminium oxide and CBN. To achieve this an $L_8 2^7$ orthogonal array experimental plan was used to characterise each grinding wheel. Confirmation trials were carried out and the most favourable results used for the cost analysis.

7.2 Aim

To establish process requirements for cost effective precision grinding of Inconel 718 using CBN and aluminium oxide wheels at conventional and high speeds.

7.3 Specific Objectives

- To produce direct effects charts for a vitrified CBN wheel at high wheelspeeds.
- To produce direct effects charts for a vitrified CBN wheel at conventional wheelspeeds.
- To produce direct effects charts for three aluminium oxide wheels at conventional wheelspeeds.
- To validate all direct effects charts through confirmation trials.
- To compare costs for each process using the analysis presented in Chapter 4.

7.4 Equipment

7.4.1 Grinding Machines Used

Two grinding machine tools were used. High-speed grinding trials with CBN wheels were carried out using the Jones and Shipman Suprema machine. Conventional speed grinding trials with CBN and alumina wheels were carried out using a Jones and Shipman Series 10 machine.

7.4.2 Grinding Wheels Used

Five grinding wheels were used for this part of the investigation. The specification for each wheel is listed below:

1. WA 801 J6V MRAA — A Universal aluminium oxide wheel (42% porosity).
2. 53A80 L15VPMF — A Winterthur aluminium oxide wheel (52% porosity).
3. 53A180 L13VPMF — A Winterthur aluminium oxide wheel (50% porosity).
4. B151-VR150J — A Wendt vitrified CBN wheel (40% porosity).
5. B151-VR150J — A Wendt vitrified CBN wheel (40% porosity).

The CBN wheels used for this work were based on the wheel characterisation study carried out by Cai **[104]**. However, there was some ambiguity as to which was the most suitable aluminium oxide wheel to use. This was due to the experience of one of the collaborating industrial partners. The two Winterthur wheels were the recommended choice due to their

high porosity. However, in practice the industrial partner had found the Universal wheel to be more effective. As a result of this, the opportunity was taken to test all three aluminium oxide wheels. This allowed the effects of process parameters to be identified and the performance of each wheel to be compared.

7.4.3 Coolant Used

For all trials the coolant used was Castrol Hysol X. This is an emulsion type coolant. According to the manufacturer's guidelines the recommended water to coolant ratio for grinding was 10:1. The following pump pressures and delivery flow rates were used:

All Suprema grinding trials:

Pump pressure = 30 bar

Coolant delivery rate = 36 l/min

All Series 10 grinding trials

Pump pressure = 0.4 bar

Coolant delivery rate = 33 l/min

7.4.4 Workpiece Specifications

The workpiece material was Inconel 718 hardened to 62 HRC. The main elements are given in Table 7.1.

Table 7.1. The main elements of Inconel 718 by percentage weight.

C	Si	Mn	Al	Co	Cr	Cu	Fe	Mo	Nb	Ni	Ti
0.03	0.12	0.1	0.48	0.16	19.13	0.06	17.3	3.01	5.18	53.54	0.94

Workpiece dimensions are shown in Figure 7.1.

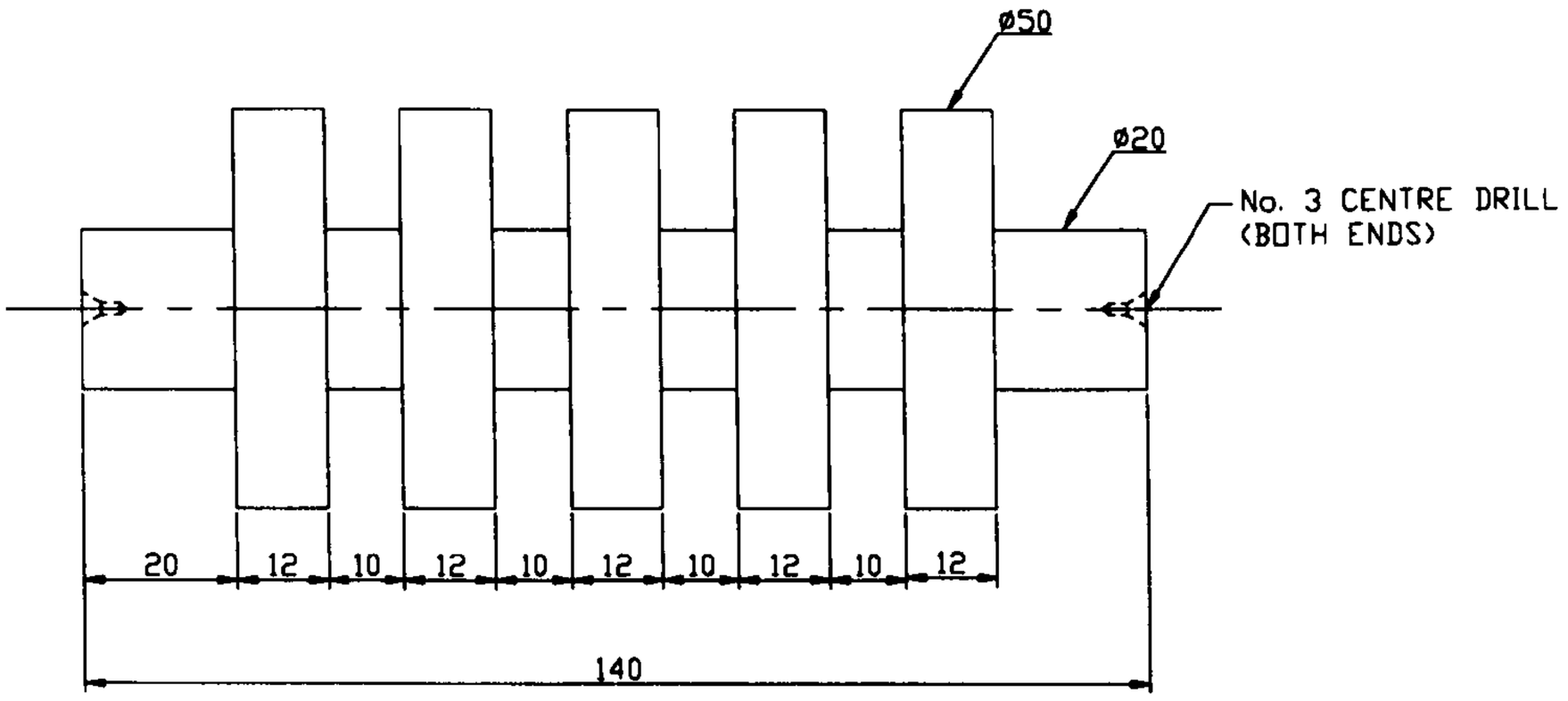

Figure 7.1. Inconel 718 workpiece, 62 HRC. All sizes are shown in mm.

7.4.5 Measuring Equipment

Details of the equipment and its calibration are given in Section 6.5.

7.5 Experimental Arrangement

The indicators used to assess performance of each trial were:

- Specific energy
- Surface roughness, i.e. Ra
- Roundness
- Size holding
- G-Ratio

For each wheel seven parameters were investigated. To test five wheels, a full two level factorial arrangement requires 5×2^7, i.e. 640 grinding trials. To minimise the number of trials a $L_8 2^7$ orthogonal array was used, requiring eight trials for each wheel and allowing seven parameters to be evaluated at two levels. Thus, using this method only forty trials were required in total. The experimental arrangement is shown in Table 7.2. The full set of eight trials was repeated for each wheel. Grinding conditions are listed in Tables 7.3 – 7.5. for CBN and alumina trials.

Table 7.2. The $L_8 2^7$ experimental plan.

Parameter:	A	B	C	D	E	F	G
Trial	Level						
1	1	1	1	1	1	1	1
2	1	1	1	2	2	2	2
3	1	2	2	1	1	2	2
4	1	2	2	2	2	1	1
5	2	1	2	1	2	1	2
6	2	1	2	2	1	2	1
7	2	2	1	1	2	2	1
8	2	2	1	2	1	1	2

Table 7.3. High-speed CBN trials on the Suprema.

	Level	
Parameter	1	2
A - Dressing direction	down	up
B - Dressing overlap	2	10
C - Dressing increment	2µm	10µm
D - No. of dressing passes	2	10
E - Wheelspeed	60m/s	120m/s
F - Workpiece speed	36m/min	54m/min
G - Dwell	2s	10s

Table 7.4. Conventional-speed CBN trials on the Series 10.

	Level	
Parameter	1	2
A - Dressing direction	down	up
B - Dressing overlap	2	10
C - Dressing increment	2μm	10μm
D - No. of dressing passes	2	10
E - Wheelspeed	33m/s	45m/s
F - Workpiece speed	10m/min	20m/min
G - Dwell	2s	10s

Table 7.5. Conventional-speed aluminium oxide trials on the Series 10 machine.

	Level	
Parameter	1	2
A - Dressing tool	chisel edge diamond	single point diamond
B - Dressing lead	0.05mm/rev	0.3mm/rev
C - Dressing increment	4μm	24μm
D - No. of dressing passes	2	10
E - Wheelspeed	33m/s	45m/s
F - Workpiece speed	10m/min	20m/min
G - Dwell	2s	10s

Conventional methods were used to dress the aluminium oxide wheels. This included using either a chisel edge or single point diamond rather than a rotary dresser.

For all trials the specific volumetric removal rate Q'_w was 2 mm^3/mm s. The stock removed from each diameter was 0.2 mm.

The results are illustrated using direct effects charts as described for the AISI 52100 material in Section 6.7. At least two confirmation trials were carried out to validate each set of results. Where necessary an extra confirmation trial was carried out. The aim of each

confirmation trial was to confirm a desired outcome predicted by the direct effects charts. The same experimental procedure was followed as described in Section 6.6.

7.6 Results

For each wheel the mean results from eight characterisation trials are shown in tabular form. Direct-effects charts are then presented showing how process parameters affect each performance indicator. Two confirmation trials for each wheel were carried out and are denoted as C1 and C2. Selection of grinding conditions for confirmation trials was based on the direct effects charts. For the high-speed CBN trials on the Suprema a third confirmation trial, denoted as C3, was carried out to determine re-dress life. Statistical measures have been used to summarise each confirmation trial. Graphs of performance indicators for all confirmation trials are presented in Appendix C. The results presented in this chapter follow the format listed below for each wheel tested:

- Table of mean results of performance indicators for eight characterisation trials.
- Direct effects charts for each performance indicator based on table of mean results.
- List of parameter levels for confirmation trials based on direct effects charts.
- Statistical measures summarising the results of each confirmation trial.

As the results are extensive, some discussion has been included where appropriate to help maintain clarity.

7.6.1 High-Speed Grinding of Inconel 718 Using Vitrified CBN on the J&S Suprema

Eight characterisation trials were carried out and the mean results for each performance indicator determined as shown in Table 7.6. These results provide the data on which the direct effects charts are based.

Table 7.6. Mean results from characterisation trials for high-speed CBN grinding of Inconel 718.

	Specific energy	Surface roughness	Roundness	Size holding	G-Ratio
Trial 1	67.0J/mm^3	0.45µm	0.94µm	12.9µm	29
Trial 2	96.0	0.29	0.53	-4.9	63
Trail 3	72.7	0.28	0.65	3.6	73
Trial 4	92.9	0.27	0.45	0.8	72
Trial 5	123.0	0.26	0.56	1.3	124
Trial 6	91.0	0.23	0.62	-2.3	62
Trial 7	144.0	0.1	0.43	-4.5	214
Trial 8	121.0	0.1	0.49	-15.9	142

It is tempting to compare the values in Table 7.6 with the values for the AISI 52100 material in Table 6.4. However, the removal rates for AISI 52100 were five times greater than with Inconel. This was necessary to achieve a satisfactory grinding process with Inconel. The specific energy values are several times higher for Inconel, while roughness, roundness and size variations fall within a smaller range due to the lower removal rates. However, the most significant differences are in the values of G-ratio. Maximum values of G-ratio when grinding Inconel 718 were an order of magnitude lower than with AISI 52100. These results illustrate the difficulty of grinding Inconel and the greatly increased rate of wheel wear.

There are large differences between the values for different trials in Table 7.6. Specific energy, roughness, size and G-ratio are all sensitive to the particular grinding conditions. In production, size variations can be limited by in-process gauging. It was therefore decided to pay greater attention to roughness, roundness and redress life, since roughness and

roundness are critical for component acceptance and redress life is critical for productivity and costs.

Direct effects charts for high-speed CBN grinding of Inconel 718.

Direct effects charts were generated from Table 7.6. To determine the direct effect of dressing direction on specific energy, the mean value of specific energy for each direction can be compared. From Table 7.2, Trials 1 to 4 are for down dressing. Thus, the direct effect of down dressing on specific energy is:

$(67.0\ J/mm^3 + 96.0\ J/mm^3 + 72.7\ J/mm^3 + 92.9\ J/mm^3) / 4 = 82.2\ J/mm^3$

For up dressing, Trials 5 to 8 are appropriate. The direct effect of up dressing on specific energy is:

$(123.0\ J/mm^3 + 91.0\ J/mm^3 + 144.0\ J/mm^3 + 121.0\ J/mm^3) / 4 = 119.8\ J/mm^3$

The mean results for specific energy are labelled A1 and A2 on Figure 7.2. For each parameter, Level 1 is a low value and Level 2 a high value.

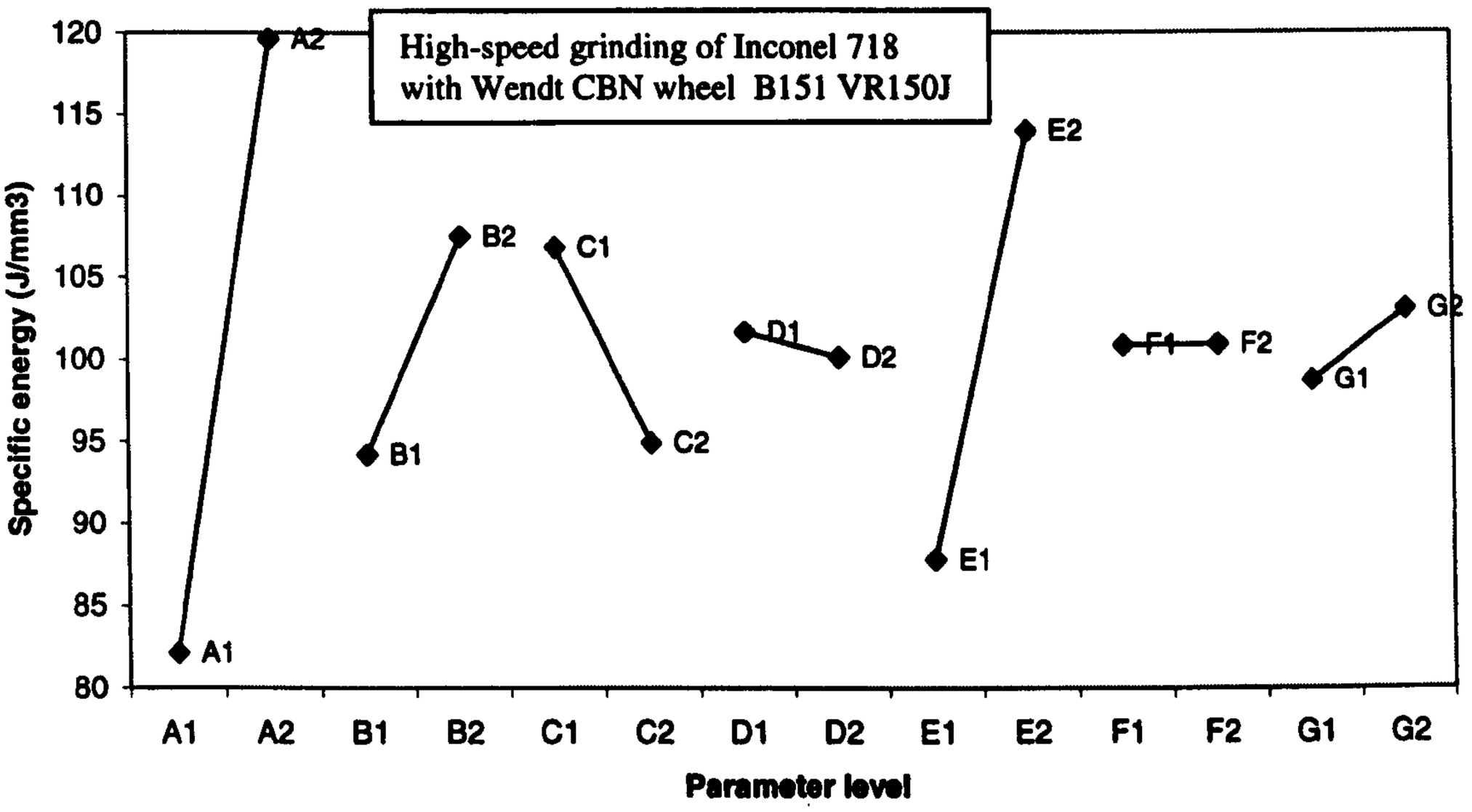

Figure 7.2. Direct effects on specific energy. A - down/up dressing, B - dressing overlap, C - dressing increment, D - number of dressing passes, E - wheelspeed, F - workspeed and G - dwell.

The results in Figure 7.2 illustrate that dressing has a strong effect on specific energy. The effect of dressing direction is particularly strong. Down dressing gives a much lower specific energy than up dressing. This is expected from the kinematic effects of dressing on the roughness of the wheel surface. Down dressing produces a much rougher wheel surface. This leads to fewer grains of the wheel actively involved in grinding. A lower number of active grains increases the mean uncut chip volume which reduces specific energy due to the size effect. The effect of the number of dressing passes on specific energy is relatively small since it is the first dressing pass which has the main effect on the number of active number of active grains.

The results illustrated in Figure 7.2 are as expected from the theoretical discussion of Chapter 3 and previous results presented in Chapter 6. Wheelspeed has a strong effect, explained by the effects of wheelspeed on the size effect. Workspeed and dwell have a weak effect on specific energy under the particular set of grinding conditions. Results for other performance indicators are shown in the figures below.

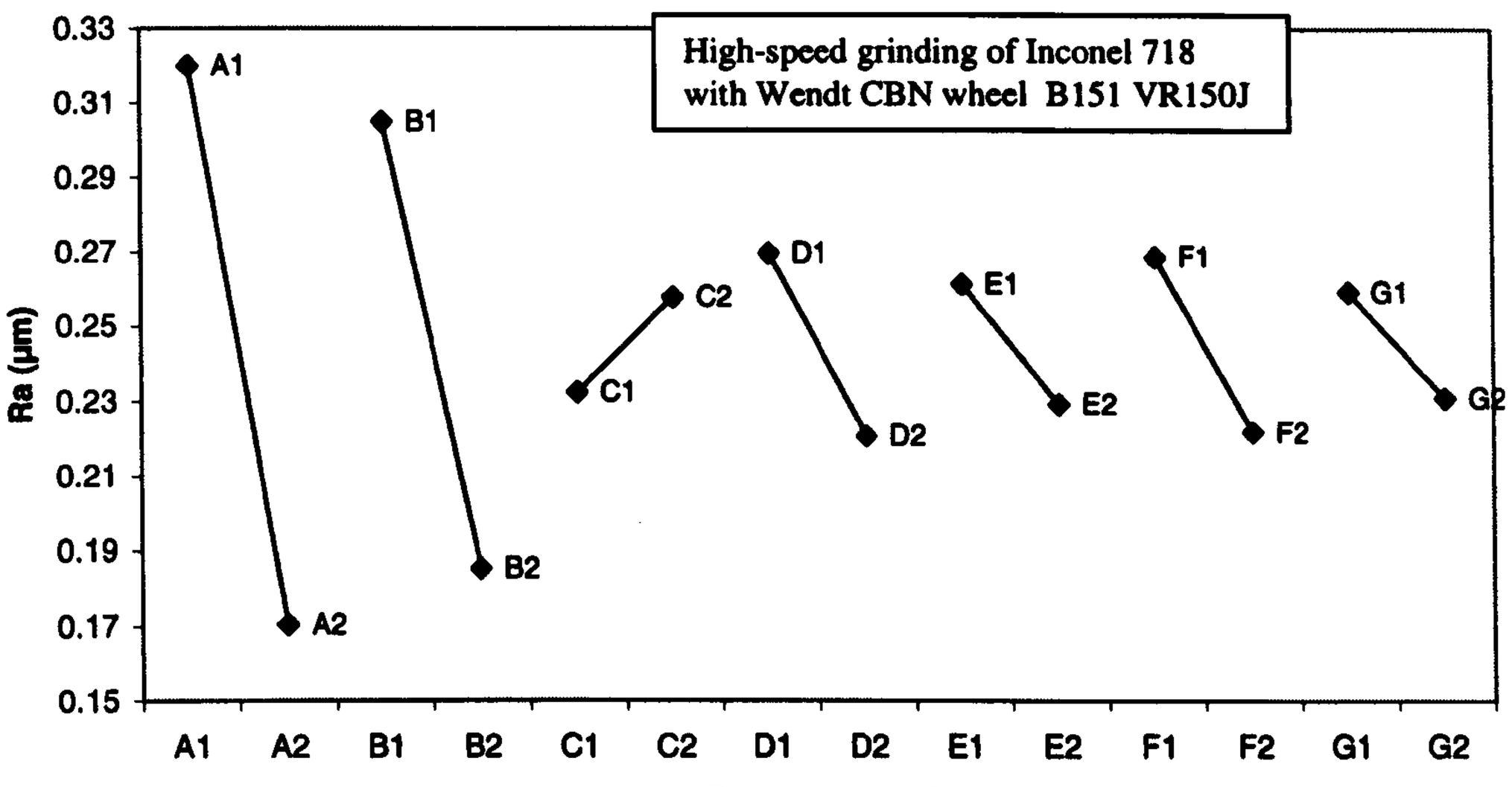

Figure 7.3. Direct effects on surface roughness. A - down/up dressing, B - dressing overlap, C - dressing increment, D - number of dressing passes, E - wheelspeed, F - workspeed and G - dwell.

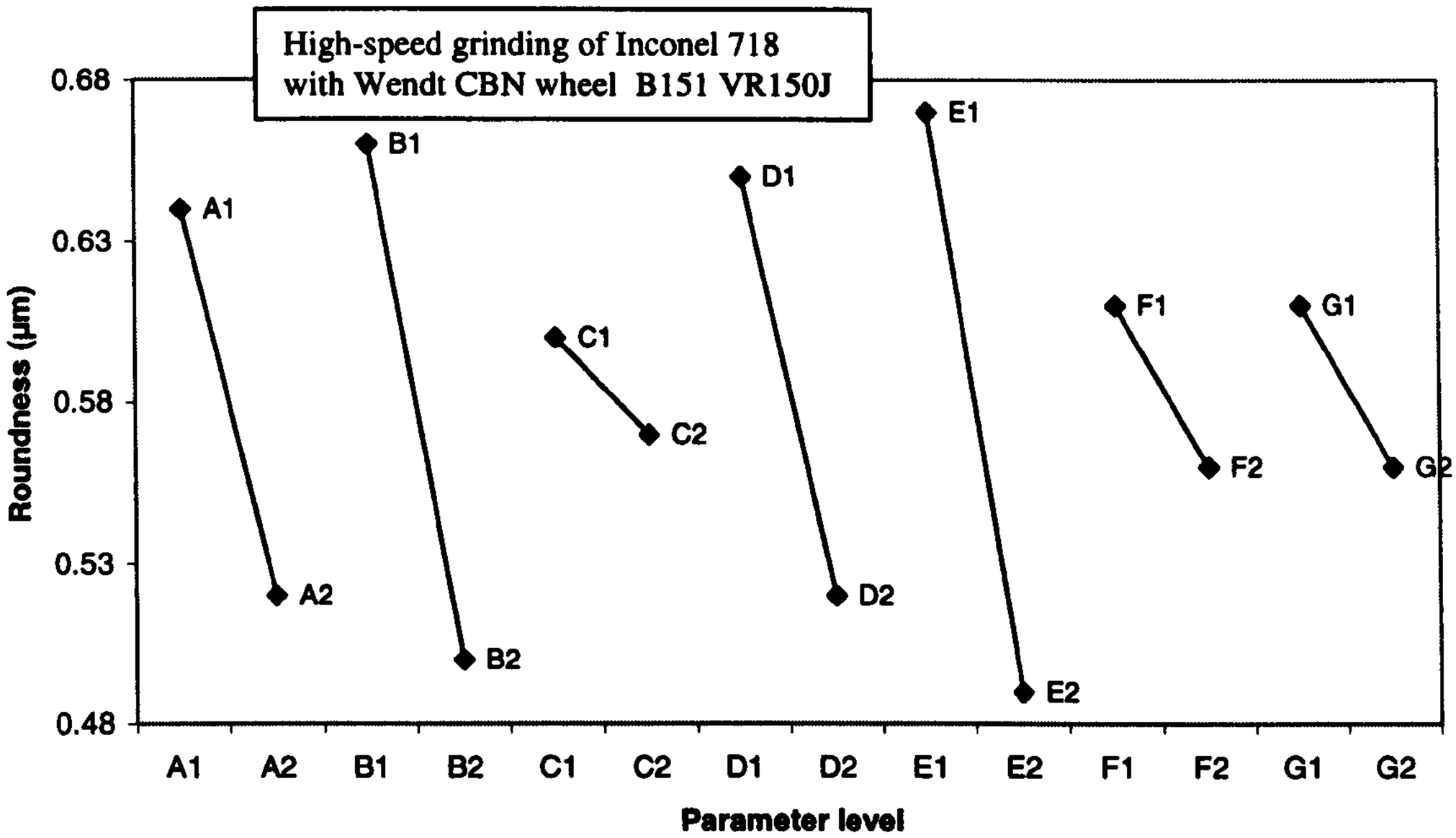

Figure 7.4. Direct effects on roundness. A - down/up dressing, B - dressing overlap, C - dressing increment, D - number of dressing passes, E - wheelspeed, F - workspeed and G - dwell.

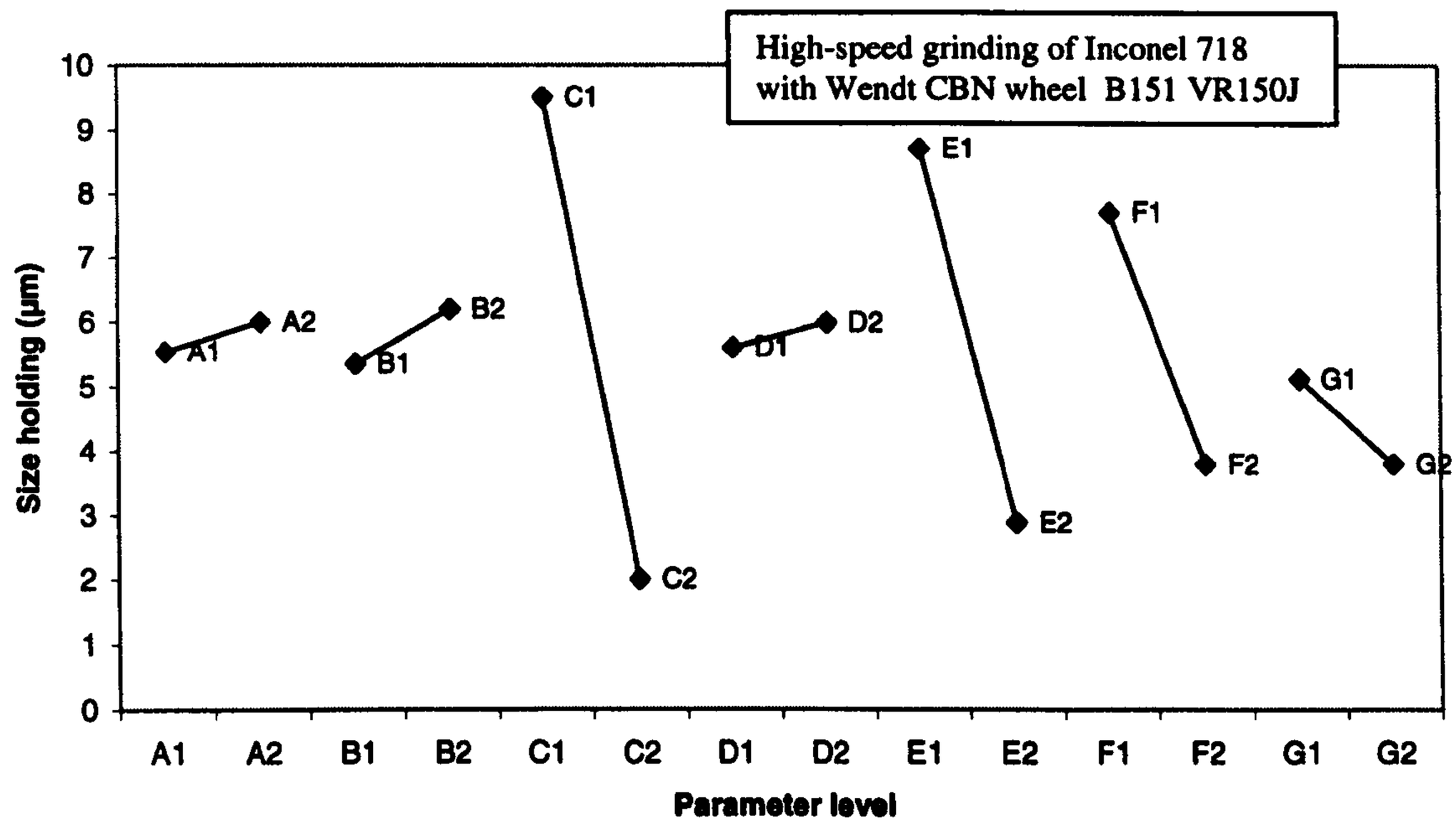

Figure 7.5. Direct effects on size holding. A - down/up dressing, B - dressing overlap, C - dressing increment, D - number of dressing passes, E - wheelspeed, F - workspeed and G - dwell.

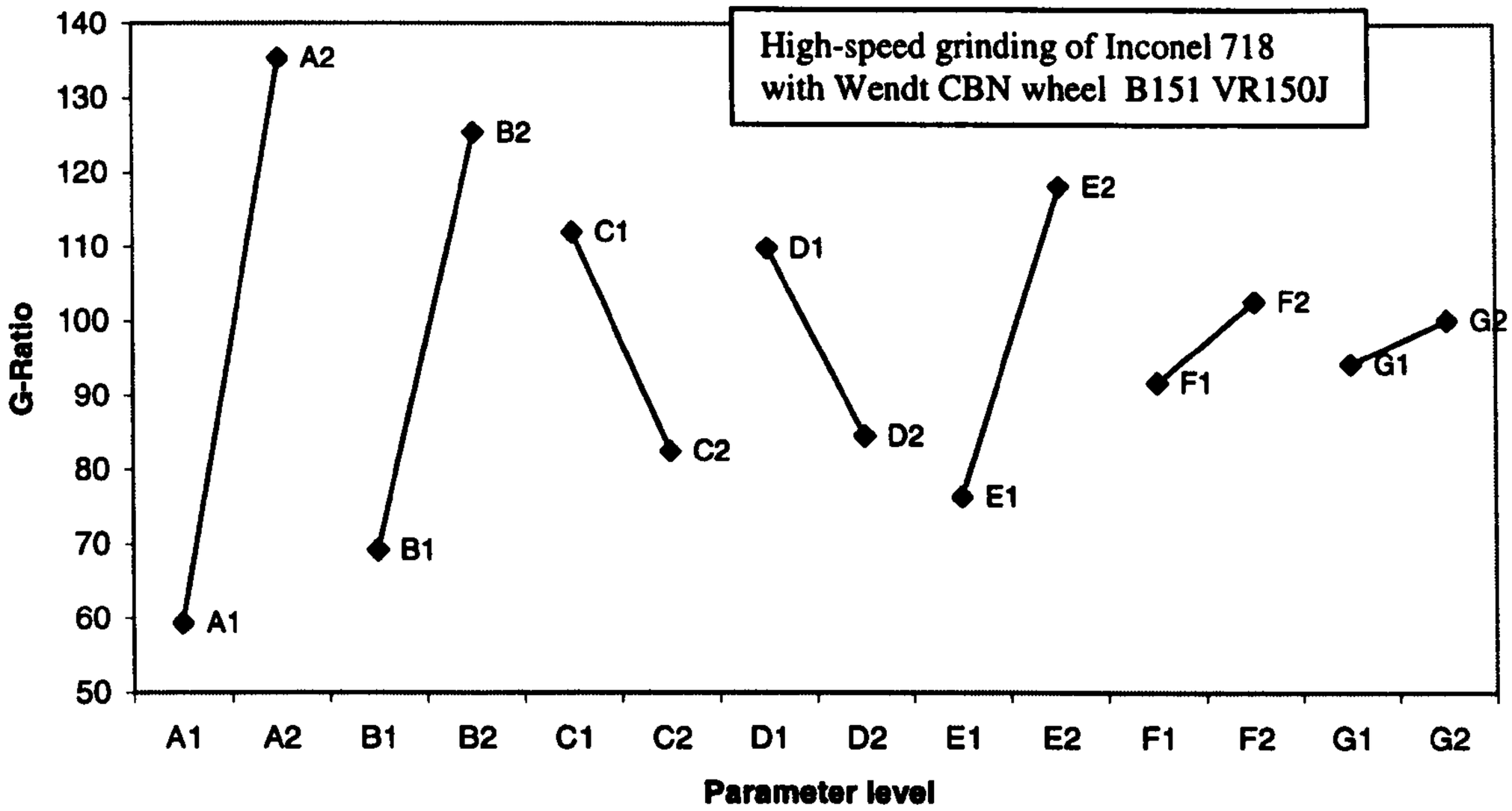

Figure 7.6. Direct effects on G-ratio. A - down/up dressing, B - dressing overlap, C - dressing increment, D - number of dressing passes, E - wheelspeed, F - workspeed and G - dwell.

By examining direct effects charts, it is possible to pick out values of each parameter tending to favour a particular result, i.e. low surface roughness. In this way, values were selected for confirmation trials.

Confirmation trials for high-speed CBN grinding of Inconel 718.

Three confirmation trials were carried out. Confirmation Trial C1 aimed at achieving good workpiece quality mainly through low roughness. Confirmation Trial C2 aimed at low specific energy. Confirmation Trial C3 was carried out to determine wheel life under conditions providing low roughness and short cycle time. The main difference in Trial C3 was that the dwell time was reduced to 2s. This is supported by Figure 7.3 which indicates that roughness is relatively insensitive to dwell. Parameters used for the three confirmation trials are listed in Table 7.7.

Table 7.7. Parameters for confirmation trials for high-speed grinding of Inconel 718 using vitrified CBN

Parameter	Confirmation Trial C1	Confirmation Trial C2	Confirmation Trial C3
A - Dressing direction	up	down	up
B - Dressing overlap	2	2	2
C - Dressing increment	2µm	10µm	2µm
D - No. of dressing passes	10	2	10
E - Wheelspeed	120m/s	120m/s	120m/s
F - Workpiece speed	36m/min	36m/min	36m/min
G - Dwell	10s	10s	2s

Dresser rotational speed, 42m/s

Q'_w=2 mm^3/mm s

V_w = 4,500 mm^3 for Confirmation Trials C1 and C2

V_w = 12,230 mm^3 for Confirmation Trial C3

The results of the confirmation trials are summarised in the following tables. Graphs for the confirmation trials can be found in Appendix C.

Table 7.8. Summary of results for Confirmation Trial C1 for high-speed CBN grinding of Inconel 718.

	Specific Energy	Ra	Roundness	Size Holding
Mean	121.7 J/mm^3	0.18µm	0.54µm	-4.8µm
Median	222.5	0.18	0.53	-4.0
Mode	125.0	0.17	0.40	-2.0
Maximum	128.8	0.21	0.80	3.0
Minimum	113.8	0.17	0.35	-13.0
Range	15.0	0.04	0.45	16.0
Variance	15.2	0.00	0.02	17.6
Standard deviation	3.9	0.01	0.14	4.2

G-ratio = 85 (G-ratio is for a fixed volume of material removed, i.e. $V_w = 4{,}100\ mm^3$, not re-dress life).

Table 7.9. Summary of results for Confirmation Trial C2 for high-speed CBN grinding of Inconel 718.

	Specific Energy	Ra	Roundness	Size Holding
Mean	73.3 J/mm^3	0.45µm	0.64µm	2.0µm
Median	76.3	0.43	0.60	2.0
Mode	77.5	-	0.55	1.0
Maximum	81.3	0.65	1.10	8.0
Minimum	58.8	0.38	0.35	-2.0
Range	22.5	0.27	0.75	10.0
Variance	32.6	0.01	0.04	7.6
Standard deviation	5.7	0.08	0.21	2.8

G-ratio = 35 (G-ratio is for a fixed volume of material removed, i.e. $V_w = 4{,}100\ mm^3$, not re-dress life).

Table 7.10. Summary of results for Confirmation Trial C3 for high-speed CBN grinding of Inconel 718.

	Specific Energy	Ra	Roundness	Size Holding
Mean	119.9 J/mm^3	0.25µm	0.67µm	4.0µm
Median	118.8	0.24	0.65	3.0
Mode	118.8	-	0.60	5.0
Maximum	133.8	0.34	1.25	12.0
Minimum	110.0	0.18	0.40	-3.0
Range	23.8	0.16	0.85	15.0
Variance	24.5	0.002	0.03	14.9
Standard deviation	5.0	0.05	0.18	3.9

G-ratio = 710 (G-ratio is for a fixed volume of material removed, i.e. $V_w = 12{,}230\ mm^3$, not re-dress life).

It can be seen that the results validate the direct effects charts. Low roughness is achieved under conditions tending to minimise grinding wheel roughness. This includes a small dressing increment with up dressing. Low specific energy is achieved under opposite conditions.

7.6.2 Conventional-Speed Grinding of Inconel 718 Using Vitrified CBN on the J&S Series 10

Results for grinding Inconel 718 at conventional speeds using CBN are illustrated below. Grinding Inconel 718 at conventional speeds, it was found that G-ratio was greatly reduced. Lower wheelspeed implies increasing mean uncut chip volume for the same removal rate. It appears that increasing chip volume increases the tendency for wheel loading with a difficult-to-grind material, Cai **[104]**. This is consistent with the reduction in G-ratio found in these results. The cause of wheel loading in grinding Inconel was further validated by Cai from microscopic and topographical examinations of the wheel surface.

Table 7.11. Mean results from characterisation trials for conventional-speed CBN grinding of Inconel 718.

	Specific energy	Surface roughness	Roundness	Size holding	G-Ratio
Trial 1	100.2J/mm^3	0.41µm	4.11µm	-13.9µm	28
Trial 2	101.3	0.24	2.63	-9.8	28
Trail 3	94.0	0.16	0.80	-1.6	49
Trial 4	93.2	0.75	3.75	0.9	35
Trial 5	108.5	0.29	1.15	4.6	82
Trial 6	77.5	0.46	2.92	8.8	19
Trial 7	109.0	0.18	1.31	-9.19	98
Trial 8	108.2	0.15	0.88	-1.6	70

Direct effects charts for conventional-speed CBN grinding of Inconel 718.

Direct effects at conventional speeds using CBN are given below. Parameters are listed in Table 7.4. Level 1 is low value and Level 2 is high.

A difference from the high-speed results is the increased sensitivity of some of the grinding results to dressing increment. A large dressing increment produces a rougher wheel surface with increased workpiece roughness and reduced specific energy. This is the same tendency as in the previous results but sensitivity to dressing increment was increased. The results were also more sensitive to dwell. Again the tendency was the same as in the high-speed results, but sensitivity was increased. No clear explanation was found for the changes in relative sensitivity for the different parameters. However, it was reassuring that for a large number of experiments, the differences in results for the various parameters were consistent with expectations from theoretical considerations. It was therefore assumed that the process was reasonably under control and formed a sound basis for testing the fundamental hypothesis stated in Chapter 1. This was confirmed from the confirmation trials.

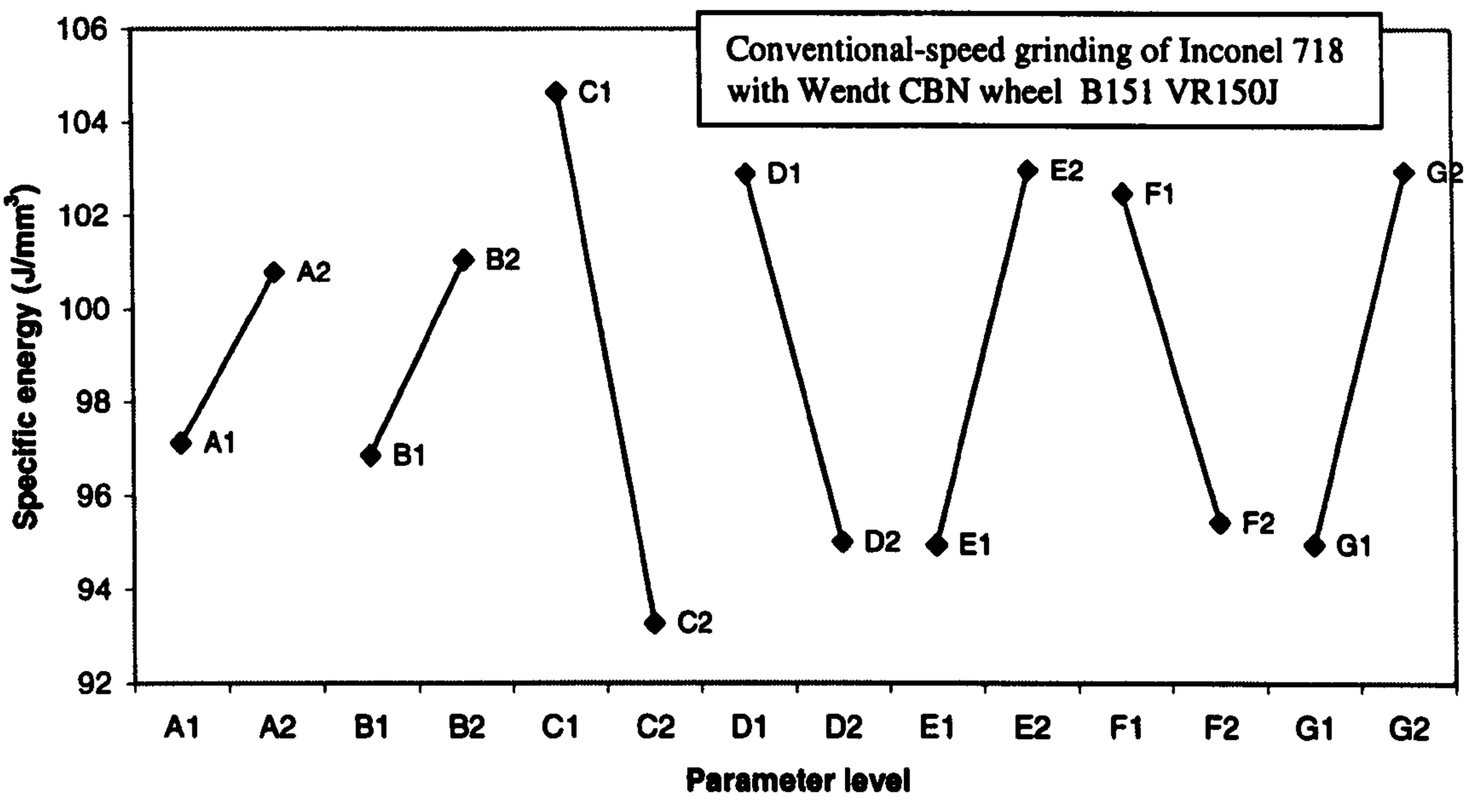

Figure 7.7. Direct effects on specific energy. A - down/up dressing, B - dressing overlap, C - dressing increment, D - number of dressing passes, E - wheelspeed, F - workspeed and G - dwell.

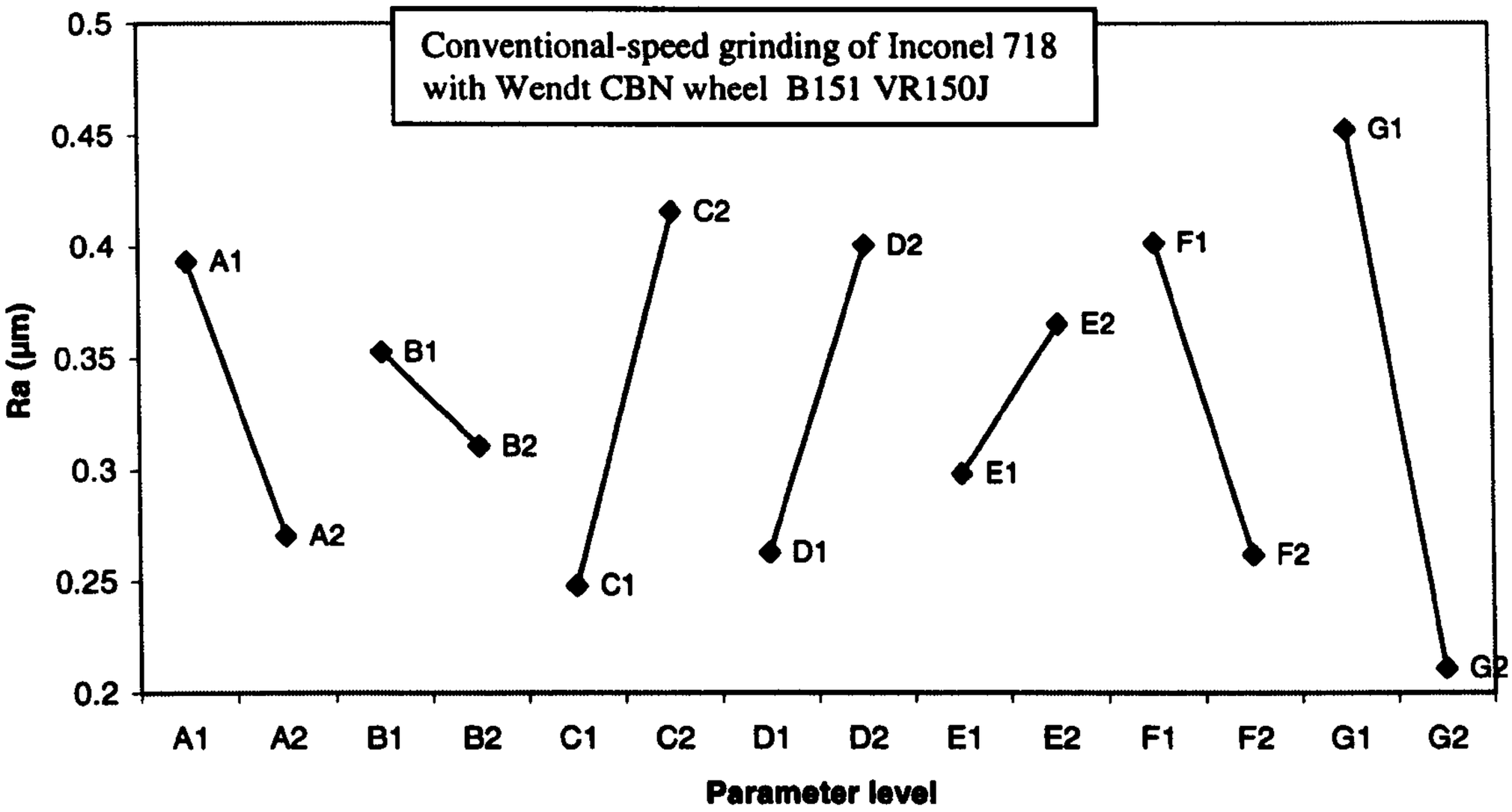

Figure 7.8. Direct effects on surface roughness. A - down/up dressing, B - dressing overlap, C - dressing increment, D - number of dressing passes, E - wheelspeed, F - workspeed and G - dwell.

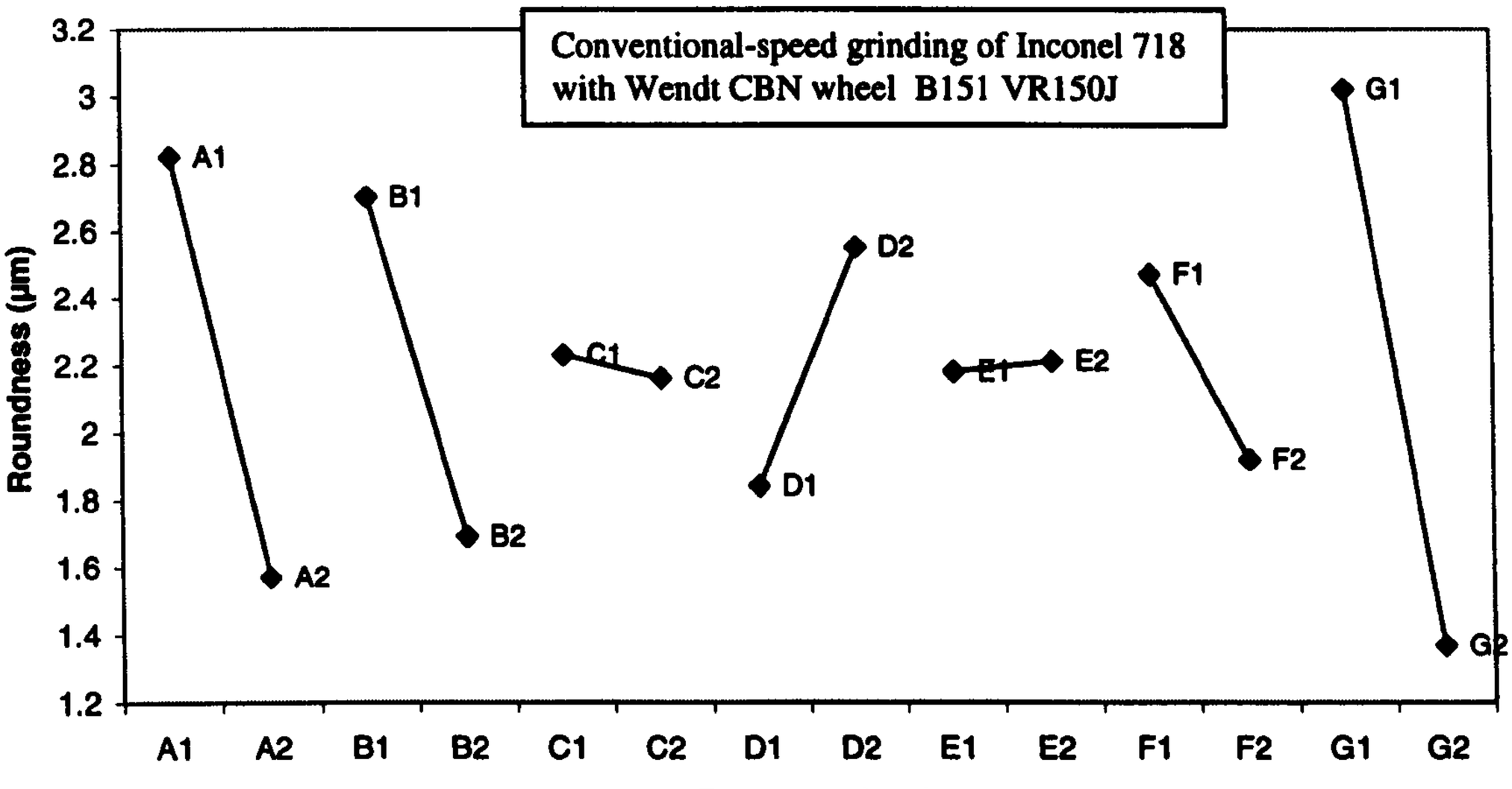

Figure 7.9. Direct effects on roundness. A - down/up dressing, B - dressing overlap, C - dressing increment, D - number of dressing passes, E - wheelspeed, F - workspeed and G - dwell.

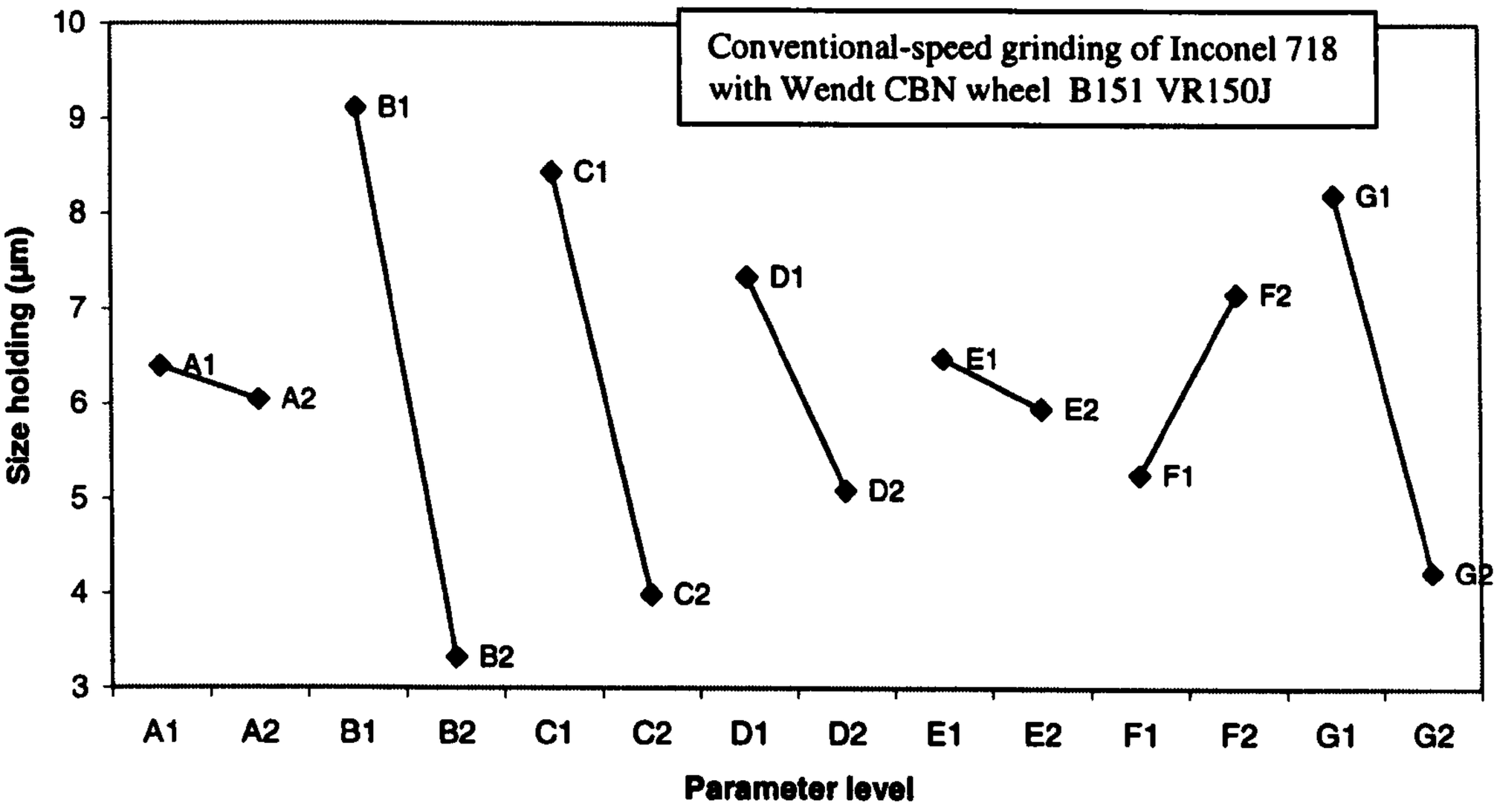

Figure 7.10. Direct effects on size holding. A - down/up dressing, B - dressing overlap, C - dressing increment, D - number of dressing passes, E - wheelspeed, F - workspeed and G - dwell.

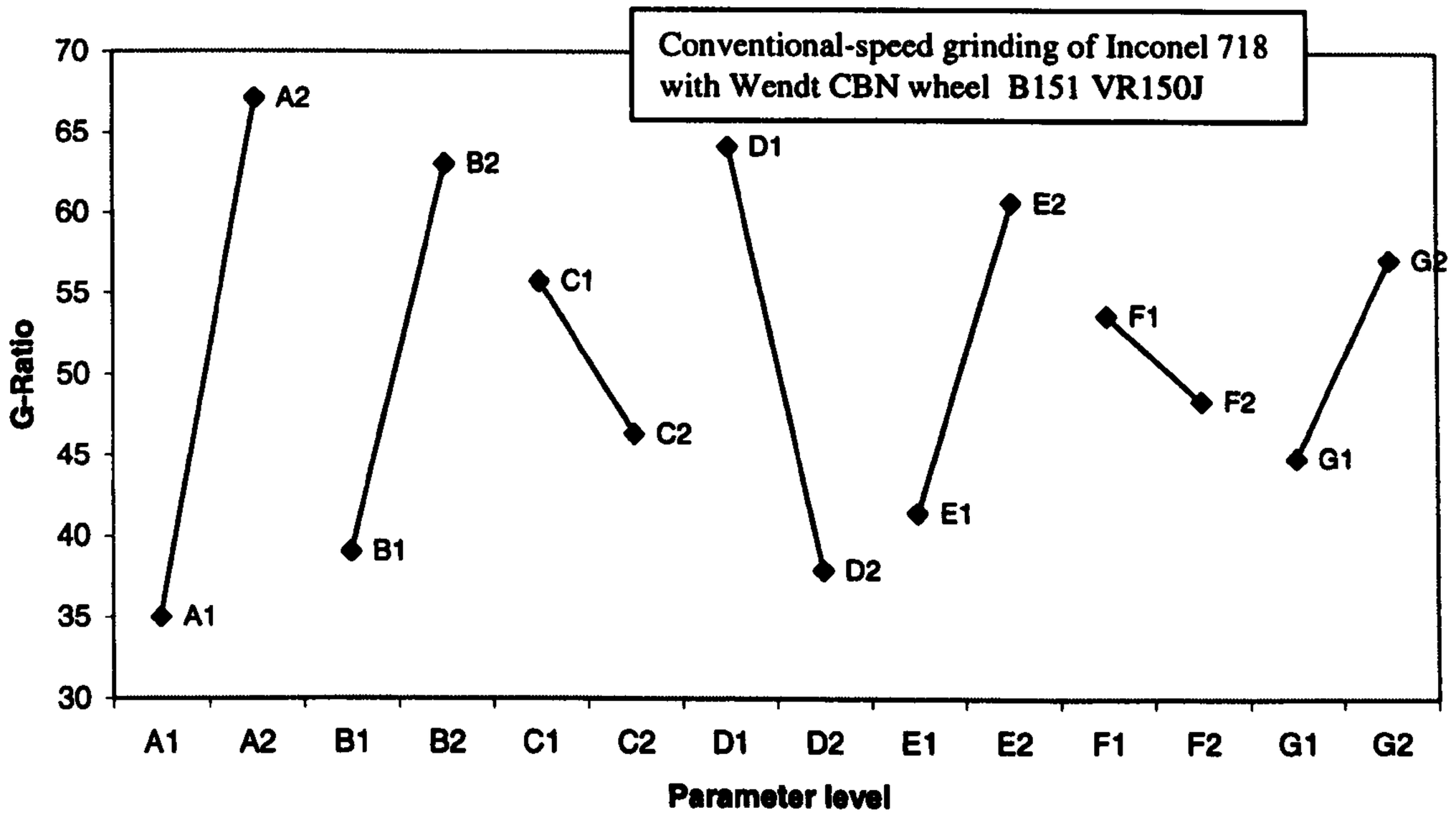

Figure 7.11. Direct effects on G-ratio. A - down/up dressing, B - dressing overlap, C - dressing increment, D - number of dressing passes, E - wheelspeed, F - workspeed and G - dwell.

Confirmation Trials for Conventional-speed CBN Grinding of Inconel 718.

Confirmation Trial C1 was aimed at high workpiece quality and C2 at reduced cycle time and cost. The results are in line with expectation and validate the direct effects charts. They also form a sound basis for the cost analysis carried out in Section 7.8. The parameters used for the two confirmation trials are listed in Table 7.12.

Table 7.12. Parameters for confirmation trials for conventional-speed CBN grinding of Inconel 718.

Parameter	Confirmation Trial C1	Confirmation Trial C2
A - Dressing direction	up	down
B - Dressing overlap	10	2
C - Dressing increment	2 μm	10 μm
D - No. of dressing passes	2	2
E - Wheelspeed	45 m/s	45 m/s
F - Workpiece speed	20 m/min	20 m/min
G - Dwell	10 s	2 s

Dresser rotational speed, 12.4m/s.

Q'_w=2 mm^3/mm s.

V_w=4,100 mm^3

The results of the confirmation trials are summarised in the following tables (see Appendix C for graphs).

Table 7.13. Summary of results for Confirmation Trial C1 for conventional-speed CBN grinding of Inconel 718.

	Specific Energy	Ra	Roundness	Size Holding
Mean	117.0 J/mm^3	0.07µm	0.5µm	0.5µm
Median	113.8	0.07	0.5	1.5
Mode	106.3	-	0.4	2.0
Maximum	148.8	0.10	1.1	6.0
Minimum	102.5	0.06	0.4	-7.0
Range	46.3	0.04	0.7	13.0
Variance	163.8	0.00	0.03	11.0
Standard deviation	12.8	0.01	0.16	3.3

G-ratio = 120 (G-ratio is for a fixed volume of material removed, i.e. V_w = 4,100 mm^3, not re-dress life).

Table 7.14 Summary of results for Confirmation Trial C2 for conventional-speed CBN grinding of Inconel 718.

	Specific Energy	Ra	Roundness	Size Holding
Mean	99.7 J/mm^3	0.12µm	1.1µm	-2.0µm
Median	97.5	0.10	1.0	-2.0
Mode	92.5	-	1.3	-4.0
Maximum	120.0	0.19	2.4	5.0
Minimum	91.3	0.07	0.4	-10.0
Range	28.8	0.11	2.0	15.0
Variance	65.3	0.00	0.3	14.3
Standard deviation	8.1	0.03	0.5	3.8

G-ratio = 80 (G-ratio is for a fixed volume of material removed, i.e. V_w = 4,100 mm^3, not re-dress life).

7.6.3 Conventional-Speed Grinding of Inconel 718 Using the Winterthur Aluminium Oxide wheel 53A180 L13VPMF on the J&S Series 10

This is a pure aluminium oxide wheel with an average grit size of 70µm and is graded medium to hard. It has a lower than average induced porosity with medium to fine pores. The wheel has a vitrified bond.

Table 7.15. Mean results from characterisation trials for conventional-speed grinding of Inconel 718 using Winterthur Al_2O_3 wheel 53A180 L13VPMF.

	Specific energy	Surface roughness	Roundness	Size holding	G-Ratio
Trial 1	100.0J/mm^3	0.75µm	12.65µm	39.4µm	1.6
Trial 2	71.4	0.64	10.83	42	1.2
Trail 3	68.6	0.53	4.75	46	1.1
Trial 4	76.8	0.79	6.95	23	1.6
Trial 5	77.9	0.44	3.36	27.6	2.1
Trial 6	65.2	0.81	8.88	29.2	1.4
Trial 7	53.1	1.01	14.54	59.8	1.2
Trial 8	71.6	0.54	3.49	31.0	1.7

The results in Table 7.15 show large roundness errors. This was due to chatter leading to wheel breakdown. This was probably the result of using a wheel which was too hard coupled with a fine grain size **[108]**.

Direct Effects charts for conventional-speed grinding of Inconel 718 using Winterthur Al_2O_3 wheel 53A180 L13VPMF.

The grinding conditions are given in Table 7.5. Level 1 relates to a low value and Level 2 to a high value except that A1 is for a chisel edge dressing tool and A2 for a single point dressing tool.

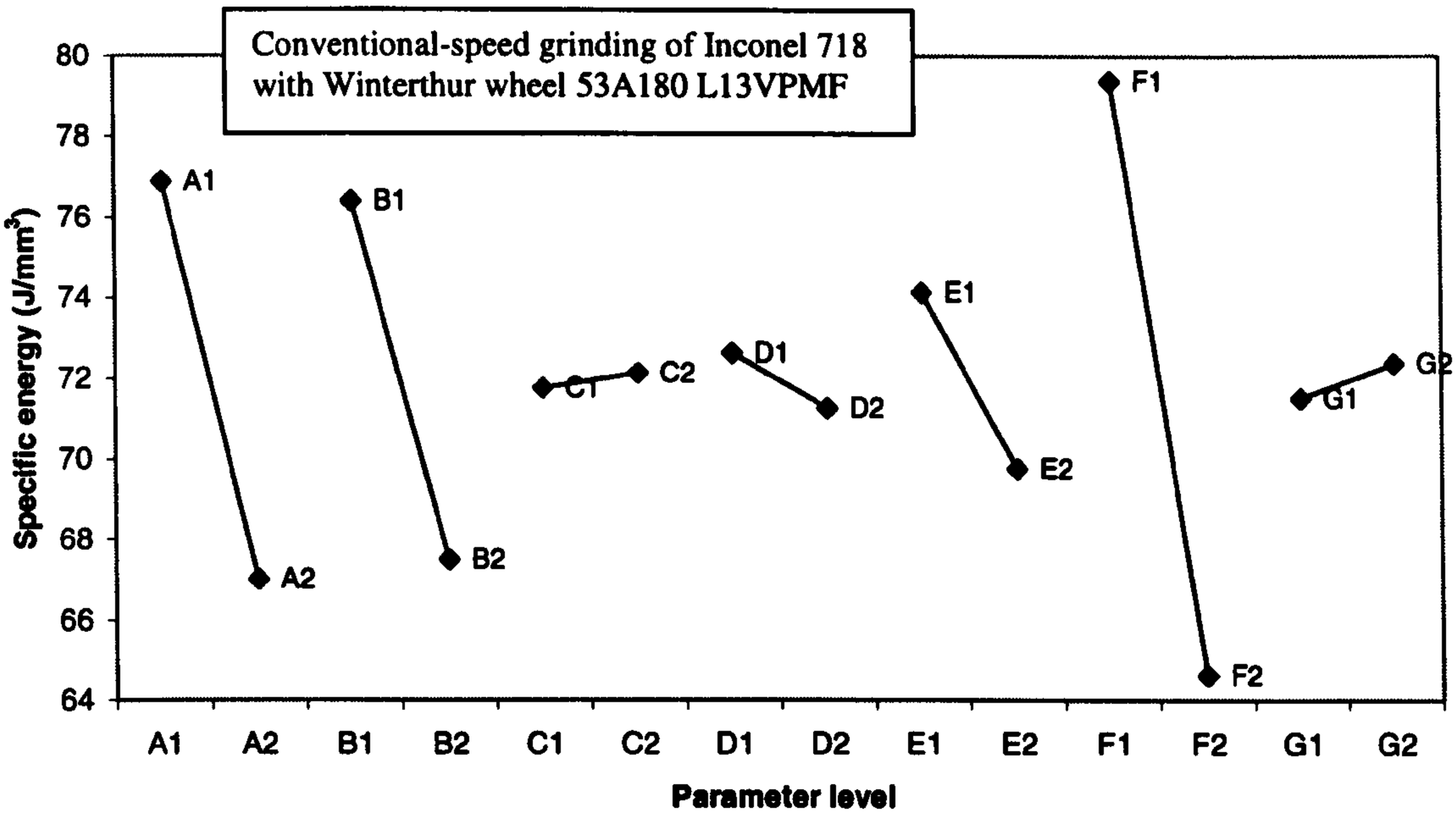

Figure 7.12. Direct effects on specific energy. A - dressing tool, B - dressing lead, C - dressing increment, D - number of dressing passes, E - wheelspeed, F - workspeed, G - dwell.

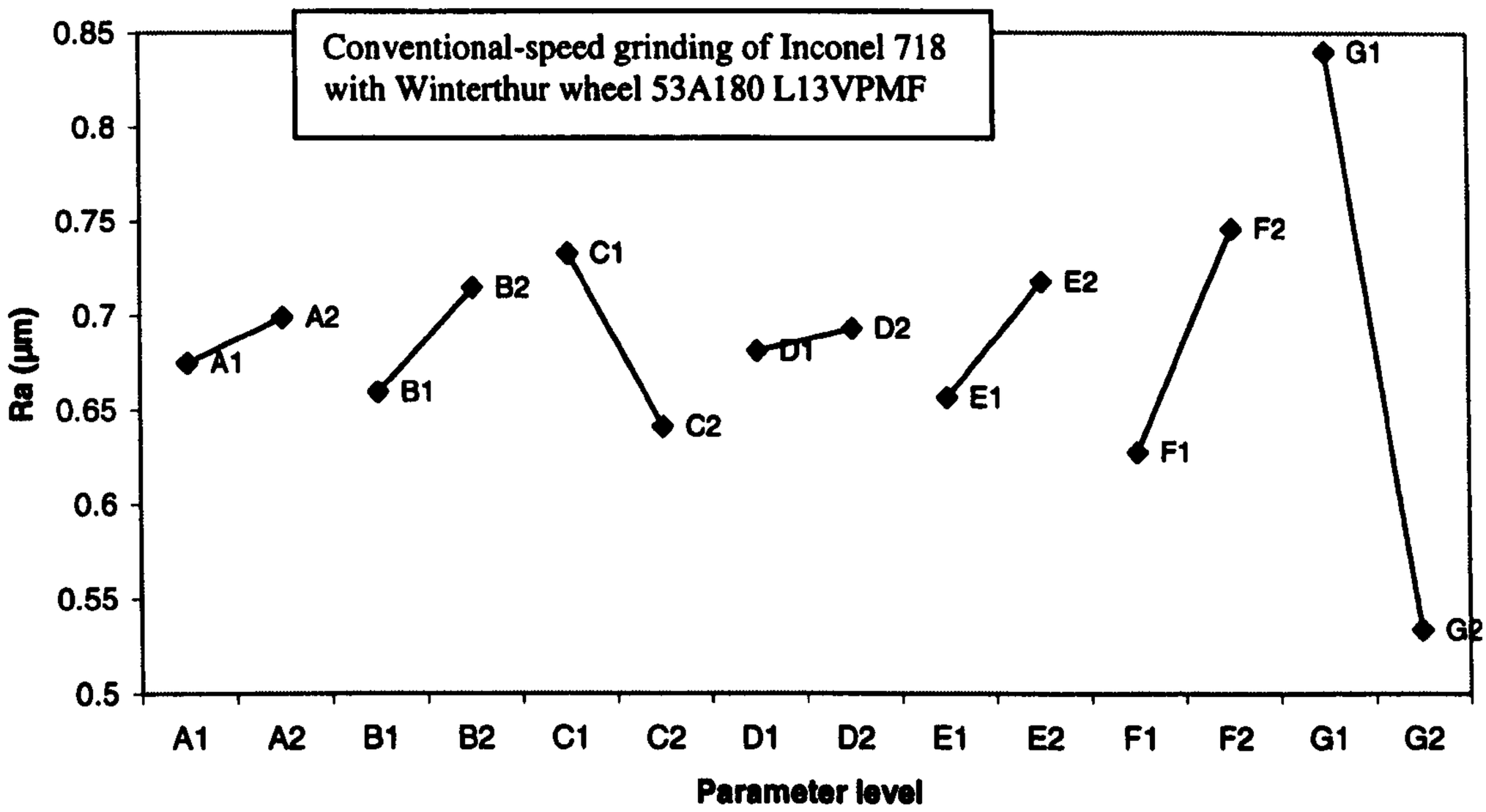

Figure 7.13. Direct effects on roughness. A - dressing tool, B - dressing lead, C - dressing increment, D - number of dressing passes, E - wheelspeed, F - workspeed, G - dwell.

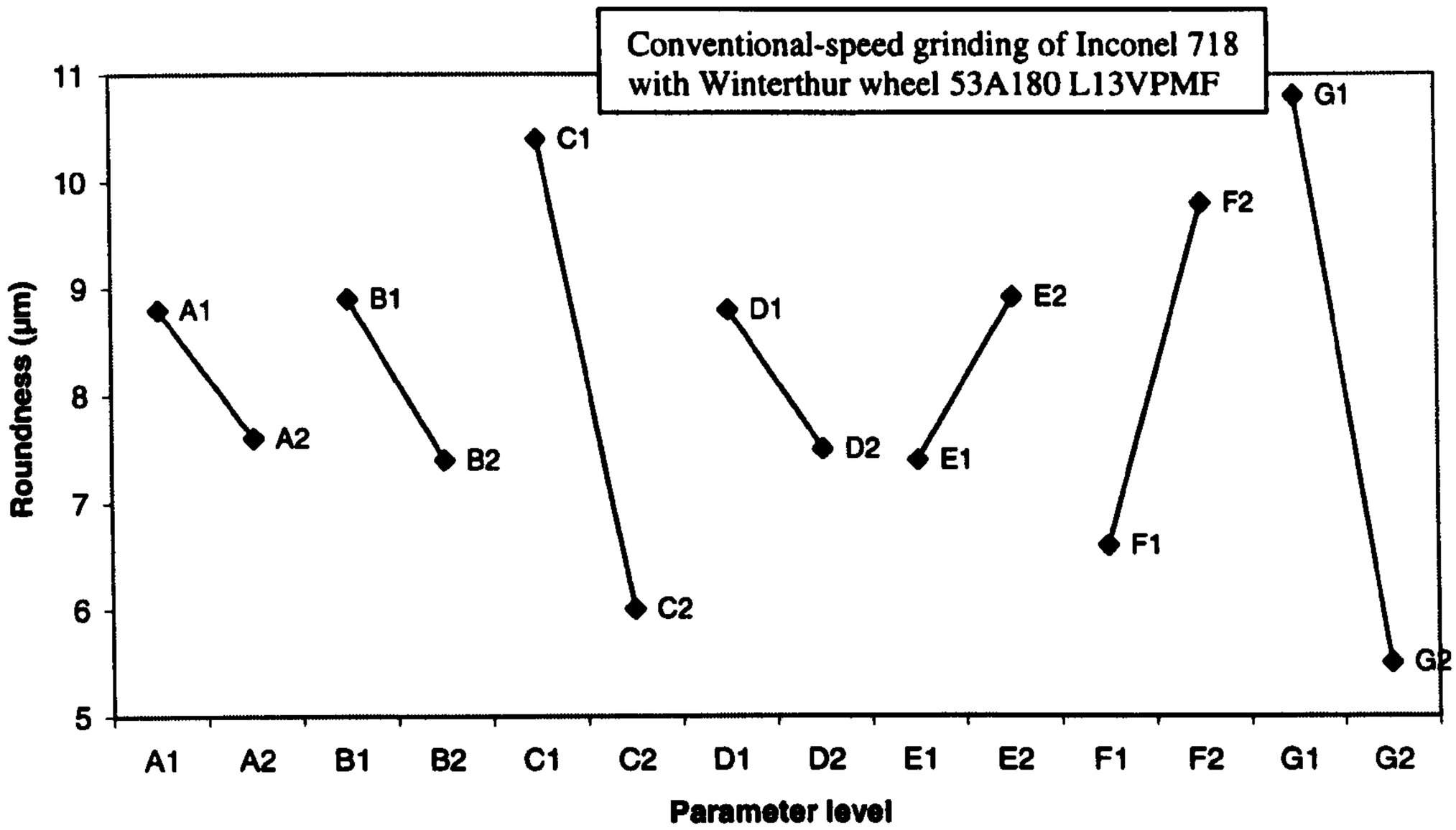

Figure 7.14. Direct effects on roundness. A - dressing tool, B - dressing lead, C - dressing increment, D - number of dressing passes, E - wheelspeed, F - workspeed, G - dwell.

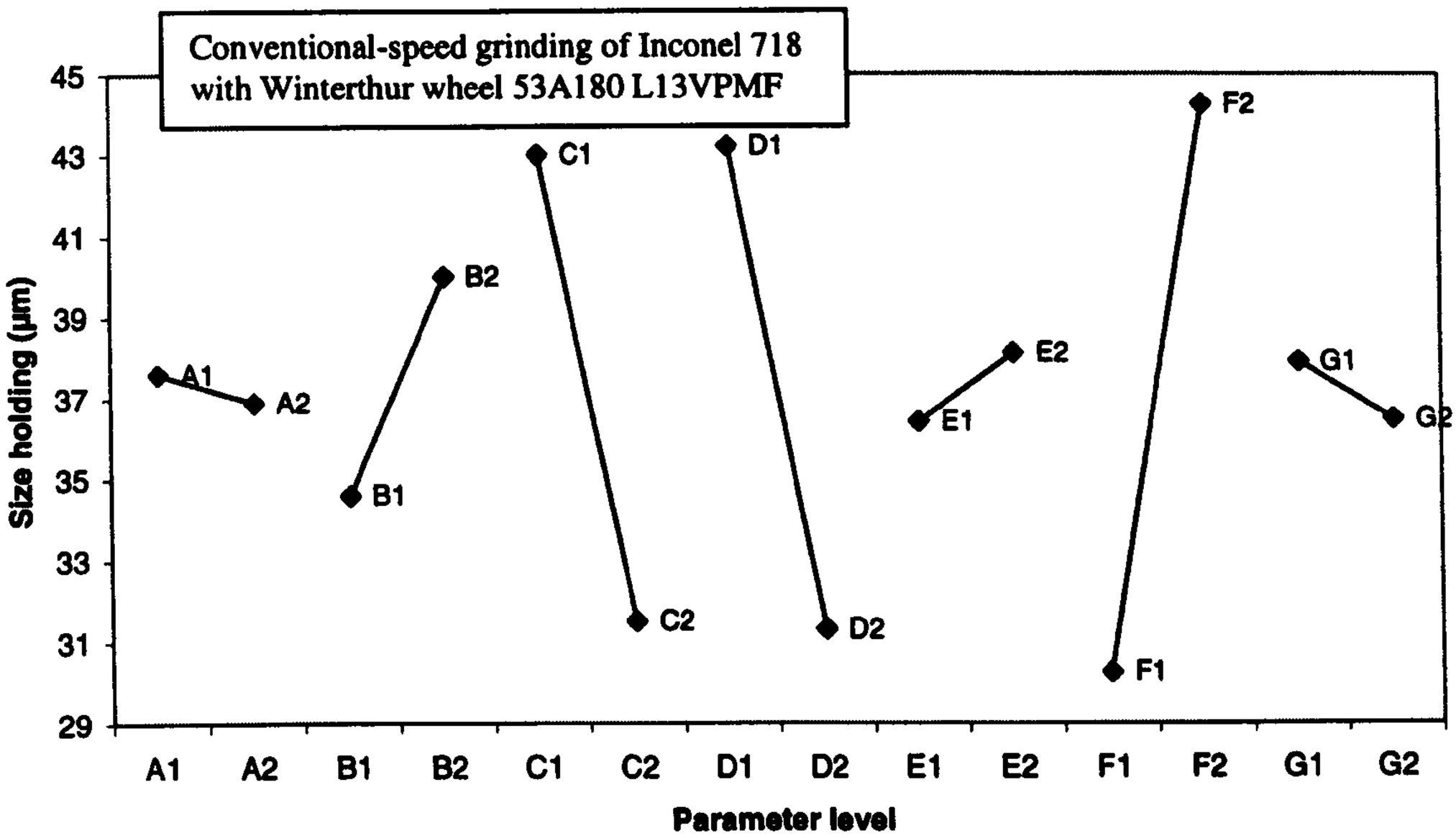

Figure 7.15. Direct effects on size holding. A - dressing tool, B - dressing lead, C - dressing increment, D - number of dressing passes, E - wheelspeed, F - workspeed, G - dwell.

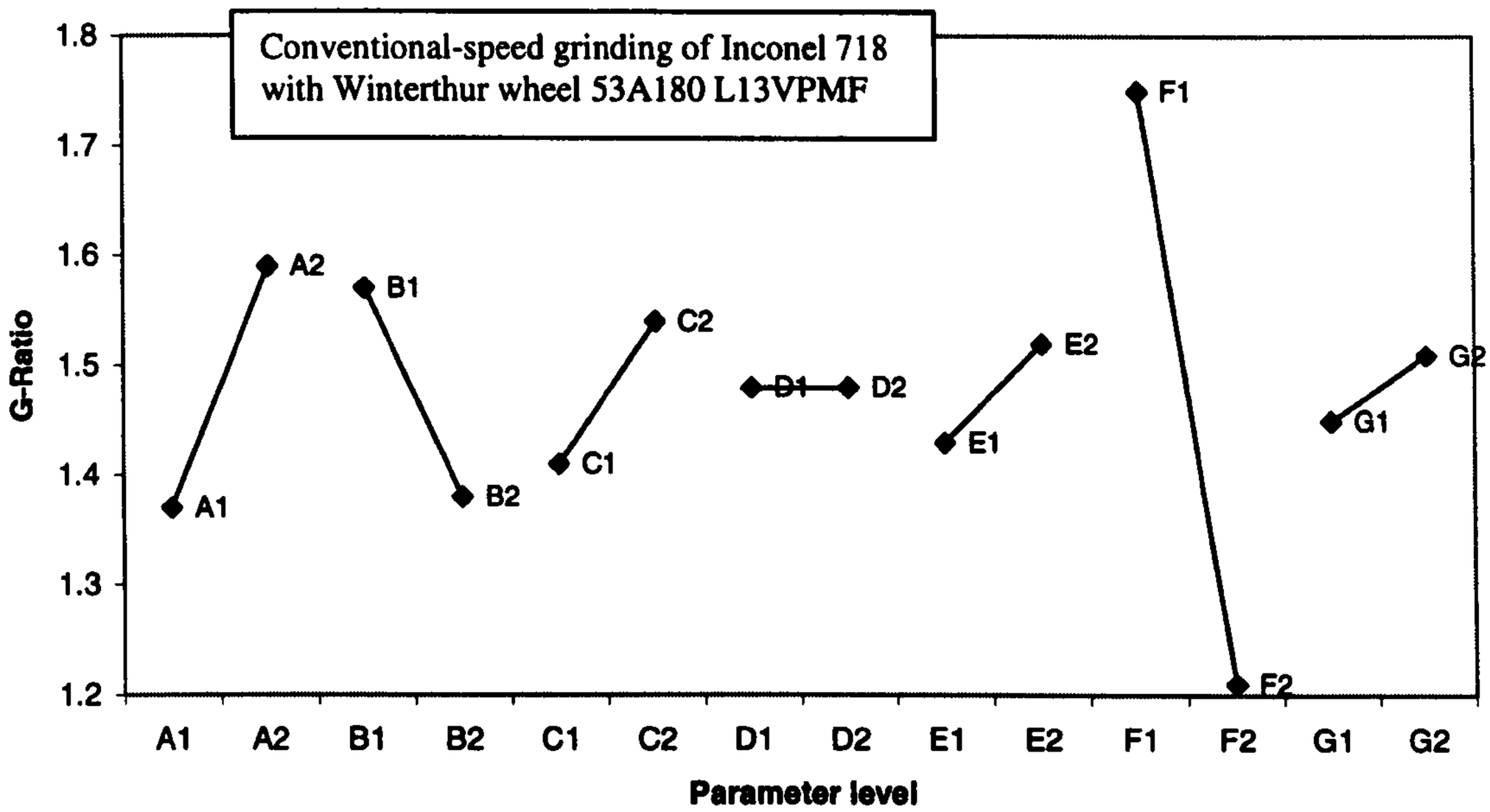

Figure 7.16. Direct effects on G-ratio. A - dressing tool, B - dressing lead, C - dressing increment, D - number of dressing passes, E - wheelspeed, F - workspeed, G - dwell.

Confirmation Trials for conventional-speed grinding of Inconel 718 using Winterthur Al_2O_3 wheel 53A180 L13VPMF.

Confirmation Trial C1 was carried out with the aim of achieving improved workpiece quality. From the direct effects charts the lower wheelspeed of 33m/s is recommended. Results for this trial show an improvement in surface roughness, however roundness is not improved. This is due to the fine dressing lead, which the direct effects charts recommend for surface roughness but not roundness. For Confirmation Trial C2 the faster dressing lead was used along with the higher wheelspeed. According to the direct effects charts this should lead to improved roundness and lower specific energy compared to Confirmation Trial 1. It can be seen from the results in Tables 7.17 and 7.18 that this is achieved.

A trial for the achievement of low specific energy grinding was not carried out as the parameter selection based on the direct effects charts, corresponded to the parameter configuration used for Trial 7. Trial 7 gave the lowest specific energy results for this wheel. Parameters used for both confirmation trials are listed in Table 7.16.

Table 7.16. Parameters for confirmation trials for conventional-speed grinding of Inconel 718 using Winterthur Al_2O_3 wheel 53A180 L13VPMF.

Parameter	Confirmation Trial C1	Confirmation Trial C2
A - Dressing tool	single point diamond	single point diamond
B - Dressing lead	0.05 mm/rev	0.3 mm/rev
C - Dressing increment	24 µm	24 µm
D - No. of dressing passes	10	2
E - Wheelspeed	33 m/s	45 m/s
F - Workpiece speed	10 m/min	10 m/min
G - Dwell	10 s	10 s

The results of the confirmation trials are summarised in the following tables (see Appendix C for graphs):

Table 7.17. Summary of results for Confirmation Trial C1 for conventional-speed grinding of Inconel 718 using Winterthur Al_2O_3 wheel 53A180 L13VPMF.

	Specific Energy	Ra	Roundness	Size Holding
Mean	66.2 J/mm^3	0.48µm	9.7µm	35.8µm
Median	75.1	0.35	4.2	20.0
Mode	-	-	-	-
Maximum	88.0	0.86	24.2	95.0
Minimum	38.8	0.21	1.1	0
Range	49.3	0.65	23.1	95.0
Variance	429.1	0.09	114.7	1746.7
Standard deviation	20.7	0.3	10.7	41.8

G-ratio = 1.6 (G-ratio is for a fixed volume of material removed, i.e. V_w = 855 mm^3, not re-dress life). Q'_w=2 mm^3/mm s.

Table 7.18. Summary of results for Confirmation Trial C2 for conventional-speed grinding of Inconel 718 using Winterthur Al_2O_3 wheel 53A180 L13VPMF.

	Specific Energy	Ra	Roundness	Size Holding
Mean	62.6 J/mm^3	0.62µm	4.1µm	39.2µm
Median	58.6	0.63	3.7	38.0
Mode	-	-	-	-
Maximum	79.0	0.87	7.8	74.0
Minimum	51.1	0.45	1.3	0
Range	27.9	0.42	6.5	74.0
Variance	139.9	0.03	5.5	819.2
Standard deviation	11.8	0.17	2.34	28.62

G-ratio = 1.3 (G-ratio is for a fixed volume of material removed, i.e. V_w = 855 mm^3, not re-dress life). Q'_w=2 mm^3/mm s.

7.6.4 Conventional-Speed Grinding of Inconel 718 Using the Winterthur Aluminium Oxide wheel 53A80 L15VPMF on the J&S Series 10

This is a pure aluminium oxide wheel with an average grit size of 180µm and is graded medium to hard. It has an average induced porosity with medium to fine pores. The wheel has a vitrified bond.

Table 7.19. Mean results from characterisation trials for conventional-speed grinding of Inconel 718 using Winterthur Al_2O_3 wheel 53A80 L15VPMF.

	Specific energy	Surface roughness	Roundness	Size holding	G-Ratio
Trial 1	56.1J/mm^3	1.20µm	9.83µm	33.4µm	1.6
Trial 2	63.1	0.69	2.84	29.2	1.7
Trail 3	45.2	1.14	4.18	45.2	1.1
Trial 4	56.7	1.11	5.77	40.2	1.2
Trial 5	58.6	0.80	4.11	37.8	1.4
Trial 6	59.1	1.31	8.79	39.2	1.5
Trial 7	42.8	1.55	7.30	51.6	1.1
Trial 8	47.4	1.02	8.43	38.2	1.1

The Winterthur wheel used for this part of the research has a larger grain size compared to the previous Winterthur wheel. Both wheels are the same hardness grade. This wheel also has a slightly higher porosity at 52% compared to 50% for the previous Winterthur wheel. From Table 7.15 it can be seen that roundness remains poor. Compared to the previous wheel, roughness results are worse. This is mainly due to the increased grain size.

Unlike the previous wheel, the direct effects charts show that improved roughness and roundness result when the higher wheelspeed is used (Figures 7.18 and 7.19). This may be due to the larger grain size used, which appears to be more sensitive to changes in wheelspeed. The direct effects charts for this wheel are as follows.

Direct Effects charts for conventional-speed grinding of Inconel 718 using Winterthur Al_2O_3 wheel 53A80 L15VPMF.

The grinding conditions are given in Table 7.5. Level 1 relates to a low value and Level 2 to a high value except that A1 is for a chisel edge dressing tool and A2 for a single point dressing tool.

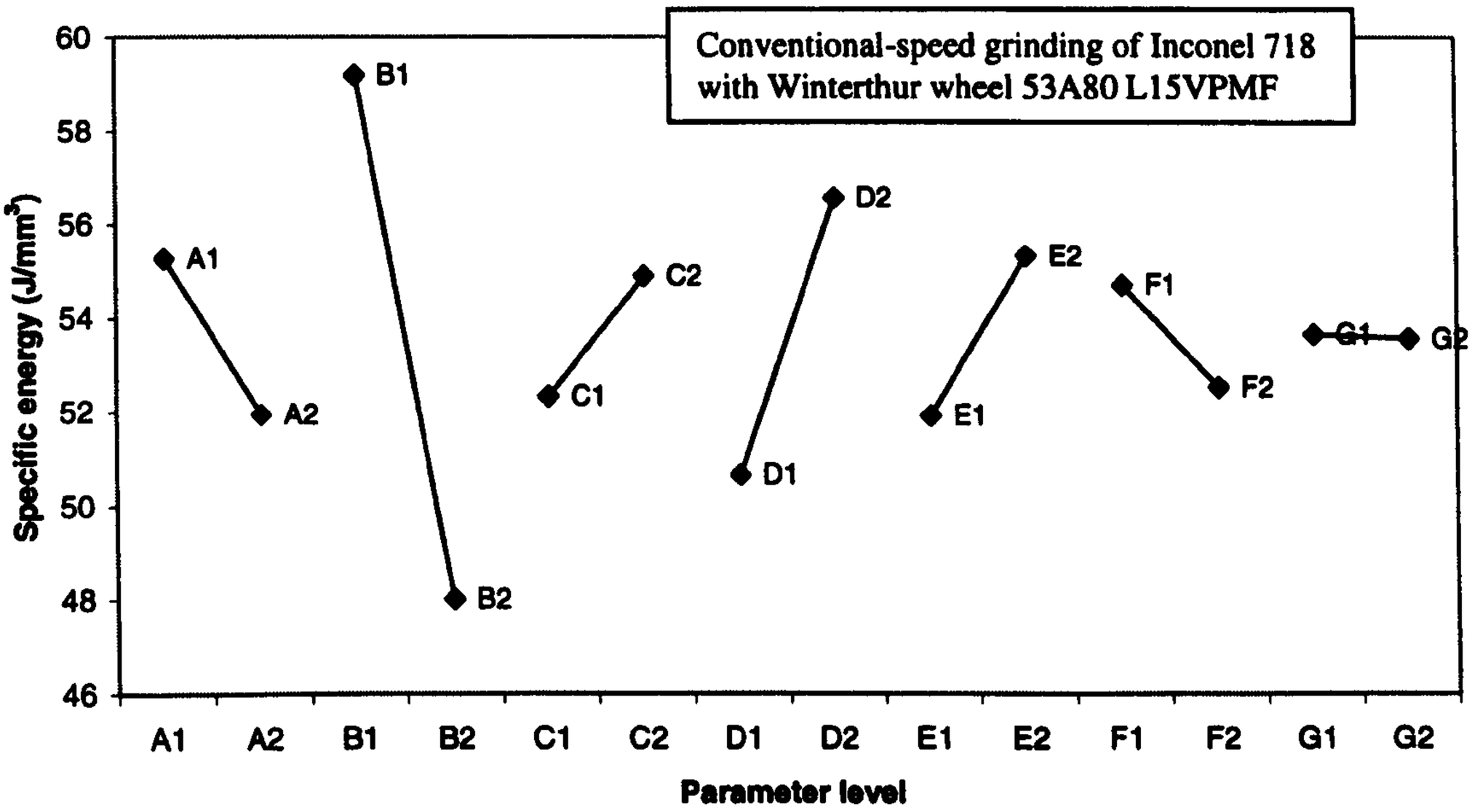

Figure 7.17. Direct effects on specific energy. A - dressing tool, B - dressing lead, C - dressing increment, D - number of dressing passes, E - wheelspeed, F - workspeed, G - dwell.

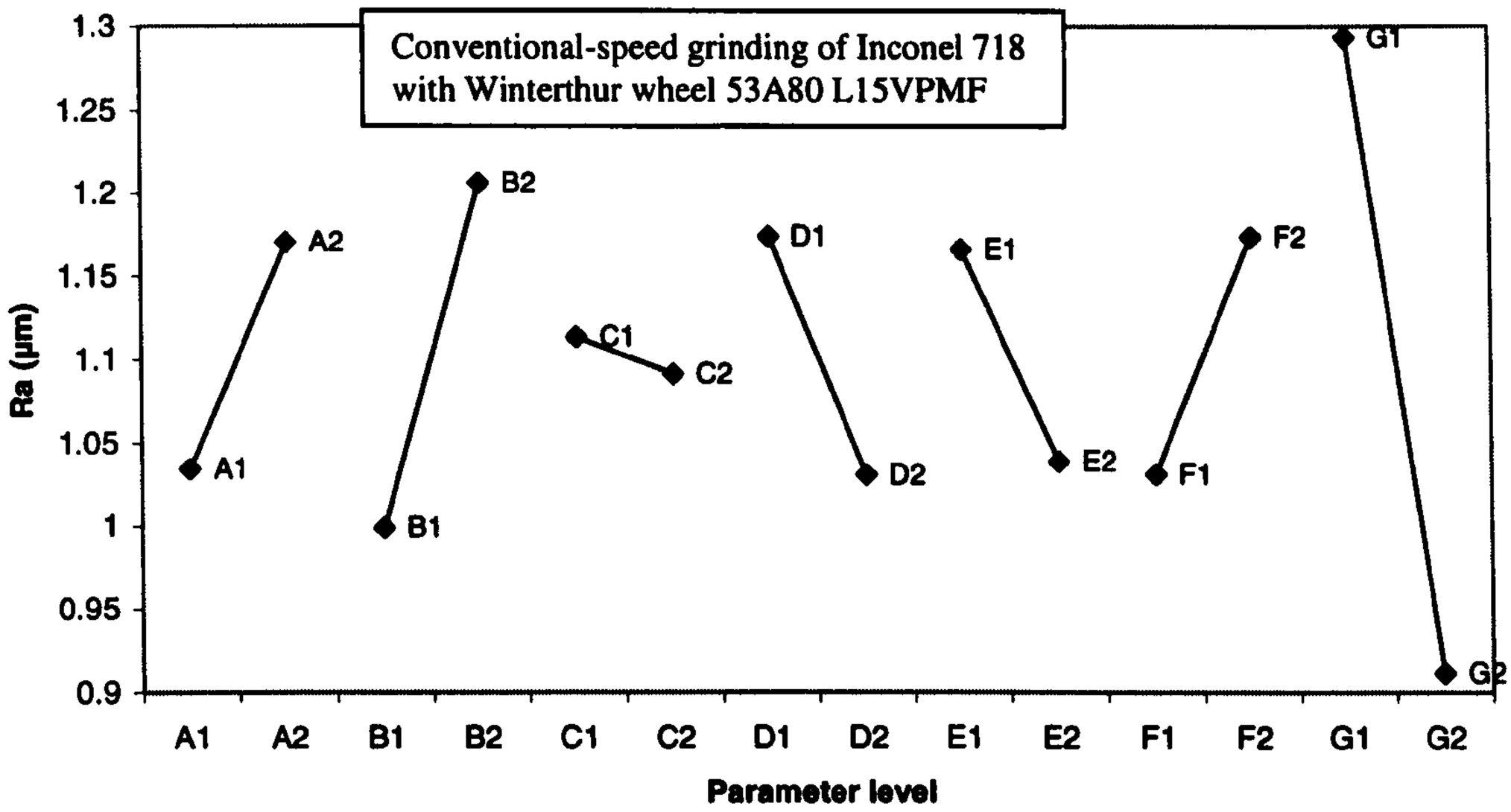

Figure 7.18. Direct effects on surface roughness. A - dressing tool, B - dressing lead, C - dressing increment, D - number of dressing passes, E - wheelspeed, F - workspeed, G - dwell.

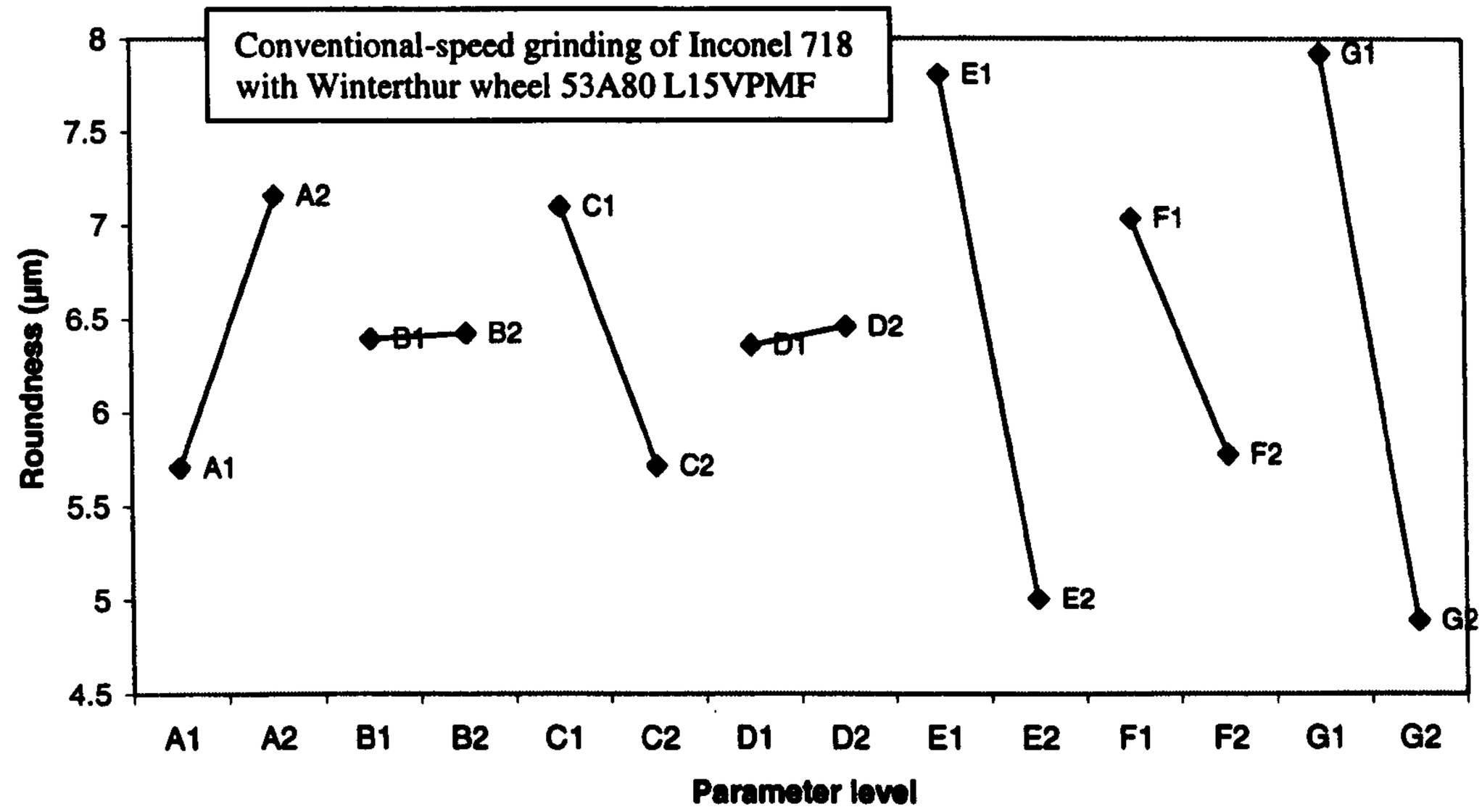

Figure 7.19. Direct effects on roundness. A - dressing tool, B - dressing lead, C - dressing increment, D - number of dressing passes, E - wheelspeed, F - workspeed, G - dwell.

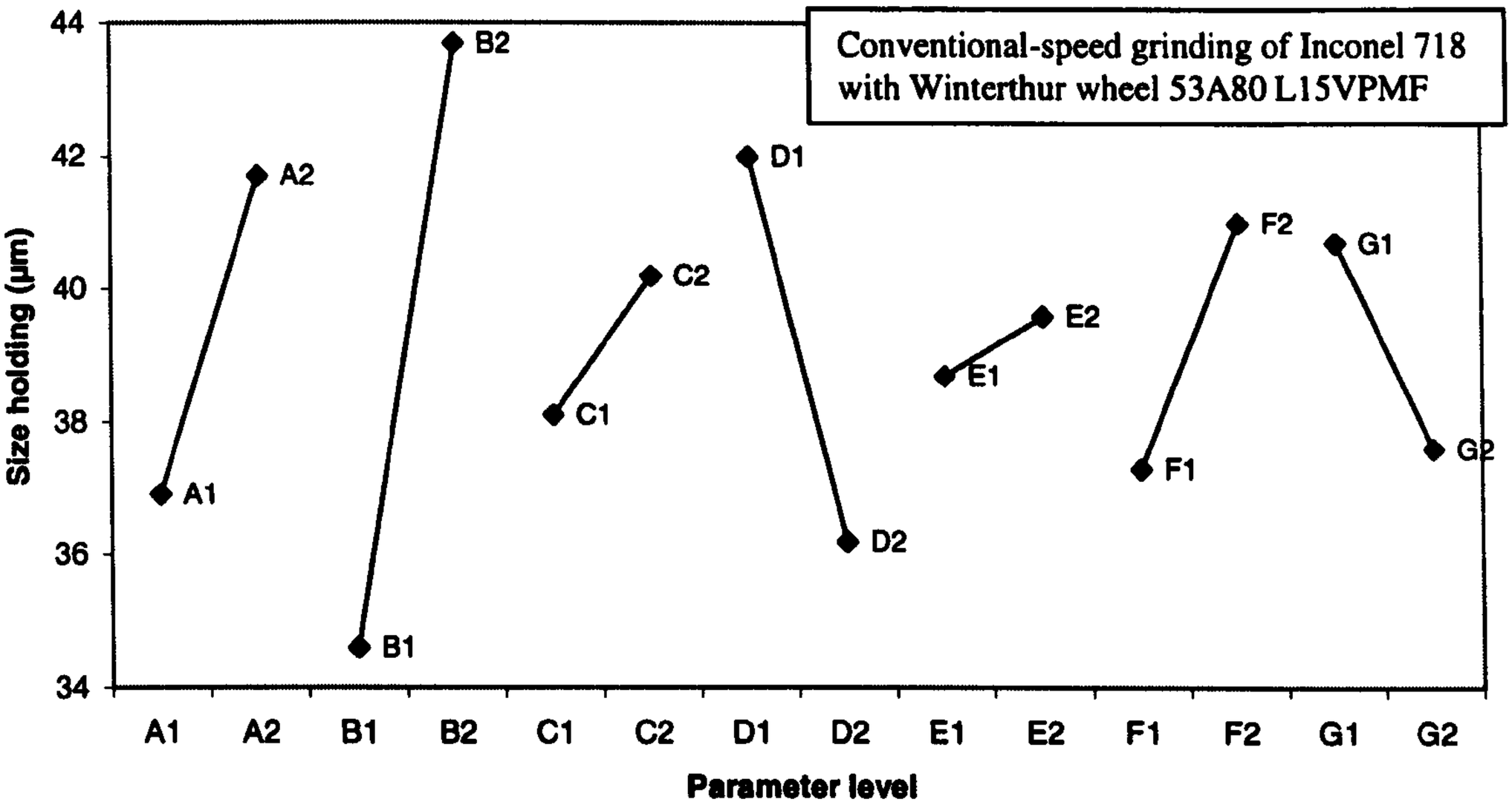

Figure 7.20. Direct effects on size holding. A - dressing tool, B - dressing lead, C - dressing increment, D - number of dressing passes, E - wheelspeed, F - workspeed, G - dwell.

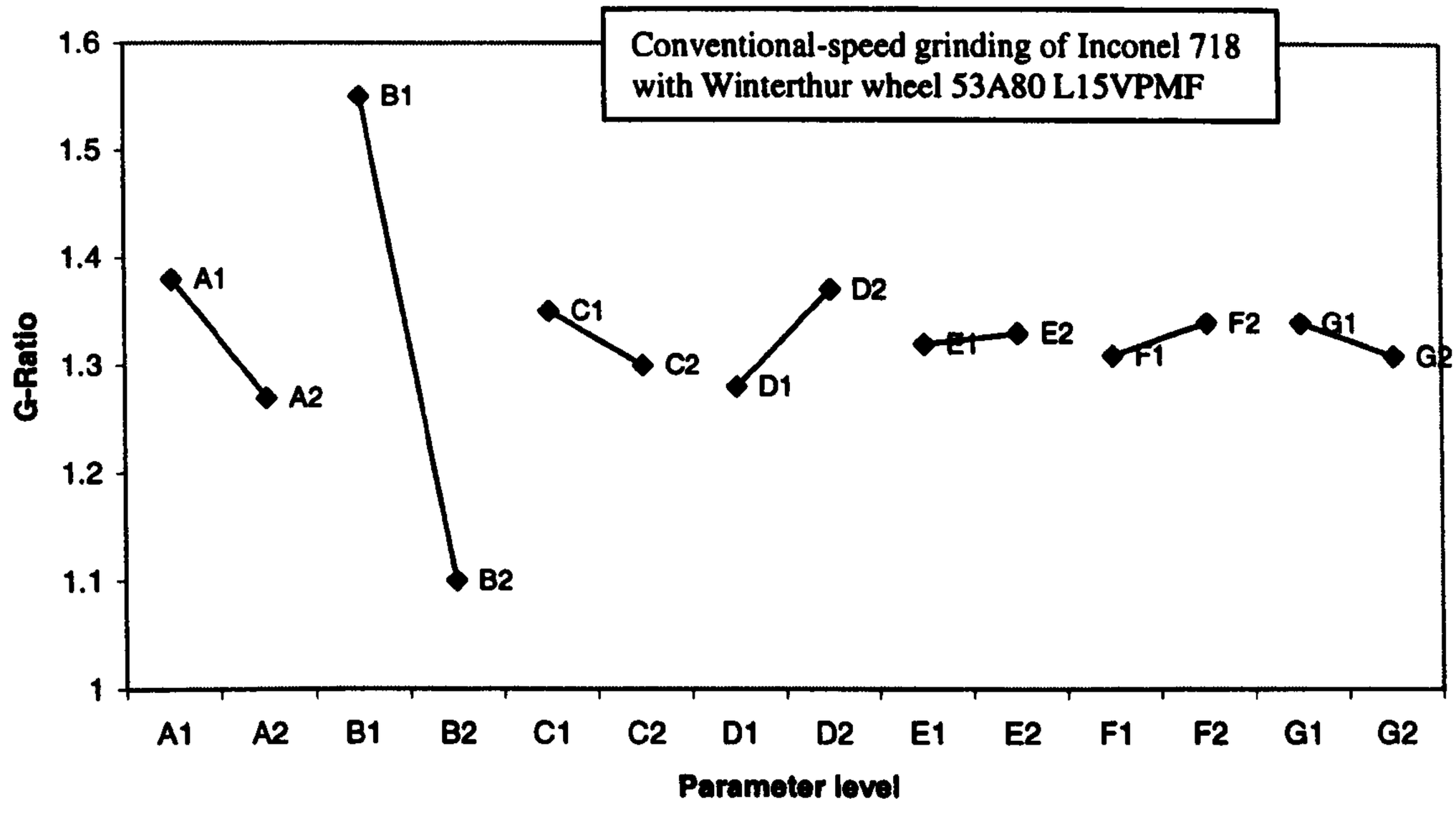

Figure 7.21. Direct effects on G-ratio. A - dressing tool, B - dressing lead, C - dressing increment, D - number of dressing passes, E - wheelspeed, F - workspeed, G - dwell.

Confirmation Trials for conventional-speed grinding of Inconel 718 using Winterthur Al_2O_3 wheel 53A80 L15VPMF.

The results for Trial 7 and Trial 8 from the characterisation trials gave low specific energy grinding, see Table 7.2. It can be seen that the parameters for these two trials are in accordance with the direct effects charts. Thus, the confirmation trials undertaken where for workpiece quality. It can be seen that only difference between Trial C1 and C2 is dressing lead and the number of dressing passes used. From the direct effects charts this should have a negligible affect on roundness. For Trial C2 dressing lead is decreased and the number of dressing passes increased. According to the direct effects this should have a cancelling affect on roughness. Thus, Trials C1 and C2 should give similar results for roughness and roundness. This is shown in the Confrimation Trial results Tables 7.21 and 7.22 as well as the graphs shown in Appendix C.

Table 7.20. Parameters for confirmation trials for conventional-speed grinding of Inconel 718 using Winterthur Al_2O_3 wheel 53A80 L15VPMF.

Parameter	Confirmation Trial 1	Confirmation Trial 2
A - Dressing tool	chisel edge diamond	chisel edge diamond
B - Dressing lead	0.3mm/rev	0.05mm/rev
C - Dressing increment	24µm	24µm
D - No. of dressing passes	2	10
E - Wheelspeed	45m/s	45m/s
F - Workpiece speed	20m/min	20m/min
G - Dwell	10s	10s

Results from the confirmation trials are summarised in the following tables (see Appendix C for graphs):

Table 7.21. Summary of results for Confirmation Trial C1 for conventional-speed grinding of Inconel 718 using Winterthur Al_2O_3 wheel 53A80 L15VPMF.

	Specific Energy	Ra	Roundness	Size Holding
Mean	54.1 J/mm^3	0.56µm	5.4µm	36.6µm
Median	59.0	0.52	4.4	38.0
Mode	-	-	-	-
Maximum	72.5	0.82	12.2	70.0
Minimum	35.6	0.4	2.8	0
Range	36.9	0.43	9.4	70.0
Variance	229.0	0.03	15.3	659.8
Standard deviation	15.1	0.18	3.9	25.7

G-ratio = 1.5 (G-ratio is for a fixed volume of material removed, i.e. V_w = 855 mm^3, not re-dress life). Q'_w=2 mm^3/mm s.

Table 7.22. Summary of results for Confirmation Trial C2 for conventional-speed grinding of Inconel 718 using Winterthur Al_2O_3 wheel 53A80 L15VPMF.

	Specific Energy	Ra	Roundness	Size Holding
Mean	63.6 J/mm^3	0.58µm	4.0µm	36µm
Median	57.6	0.59	2.7	29.0
Mode	-	-	-	-
Maximum	90.0	1.0	10.9	74.0
Minimum	36.3	0.22	1.1	0
Range	53.8	0.82	9.8	74.0
Variance	613.6	0.12	16.2	778.5
Standard deviation	24.8	0.35	4.0	27.9

G-ratio = 1.5 (G-ratio is for a fixed volume of material removed, i.e. V_w = 855 mm^3, not re-dress life). Q'_w=2 mm^3/mm s.

7.6.5 Conventional-speed Grinding of Inconel 718 Using the Universal Aluminium Oxide Wheel WA801 J6VMRAA on the J&S Series 10

This is a medium grade white aluminium oxide wheel with an average grain size of 180μm. The wheel structure is classed as regular and the bond type is vitrified.

Table 7.23. Mean results from characterisation trials for conventional-speed grinding of Inconel 718 using Universal Al_2O_3 wheel WA801 J6VMRAA.

	Specific energy	Surface roughness	Roundness	Size holding	G-Ratio
Trial 1	84.2J/mm^3	0.73μm	7.59μm	14.6μm	3.5
Trial 2	85.3	0.45	6.51	18.3	2.6
Trail 3	65.4	0.77	3.70	31.3	1.6
Trial 4	80.6	1.01	7.50	32.0	2
Trial 5	91.7	0.34	1.87	37.0	2.6
Trial 6	79.0	0.77	6.43	42.4	2.9
Trial 7	68.9	1.01	6.81	34.7	2.1
Trial 8	76.1	0.60	5.66	31.2	2.1

Table 7.23 indicates that lower roughness and roundness may be achieved with this wheel compared to the previous two aluminium oxide wheels. This is particularly true of the parameters used for Trial 5. This trial gives the lowest roughness and roundness results out of all the characterisation trials undertaken with aluminium oxide wheels to grind Inconel 718. The direct effects charts for this wheel are as follows.

Direct Effects charts for conventional-speed grinding of Inconel 718 using Universal Al_2O_3 wheel WA801 J6VMRAA.

The grinding conditions are given in Table 7.5. Level 1 relates to a low value and Level 2 to a high value except that A1 is for a chisel edge dressing tool and A2 for a single point dressing tool.

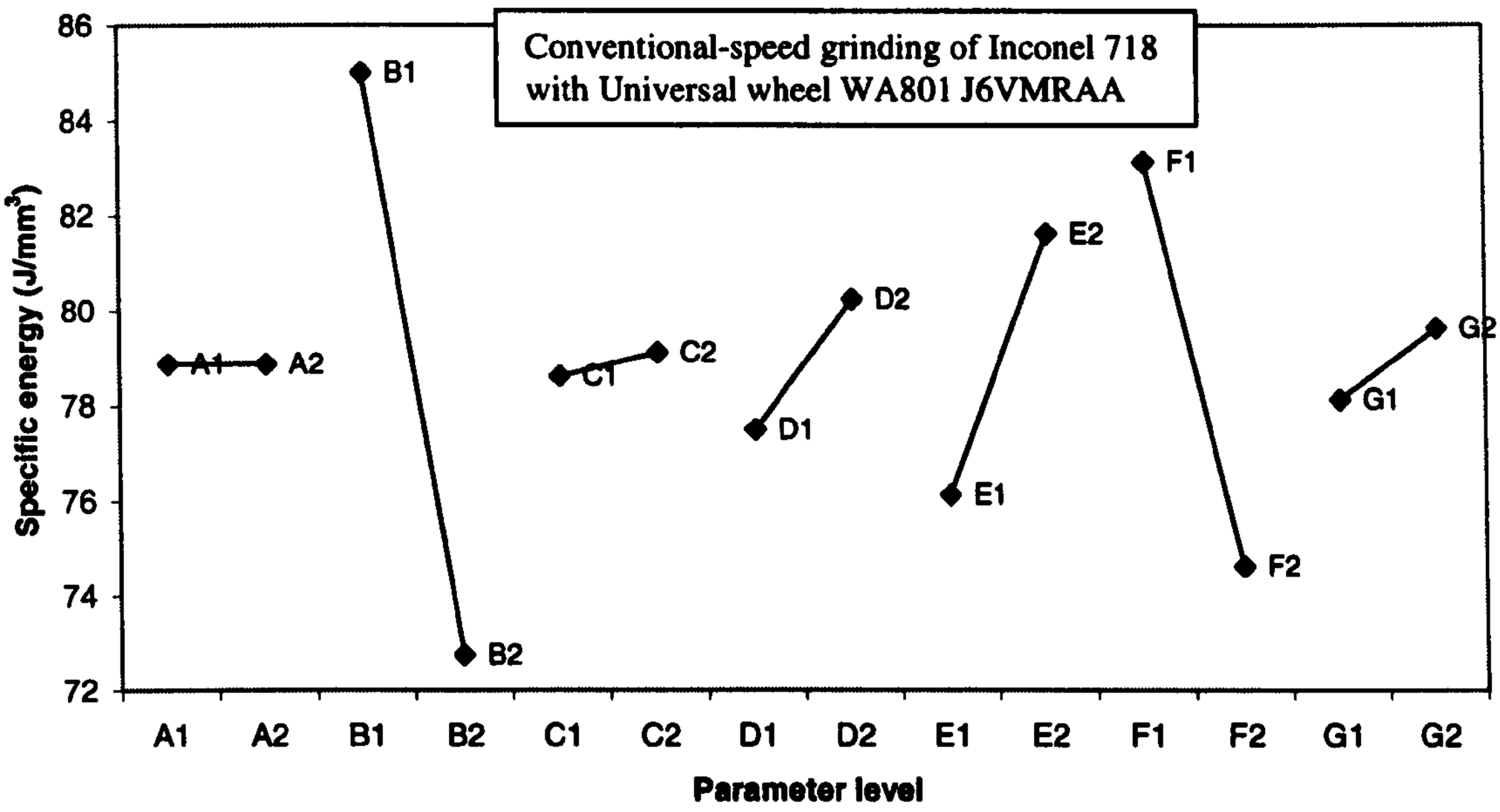

Figure 7.22. Direct effects on specific energy. A - dressing tool, B - dressing lead, C - dressing increment, D - number of dressing passes, E - wheelspeed, F - workspeed, G - dwell.

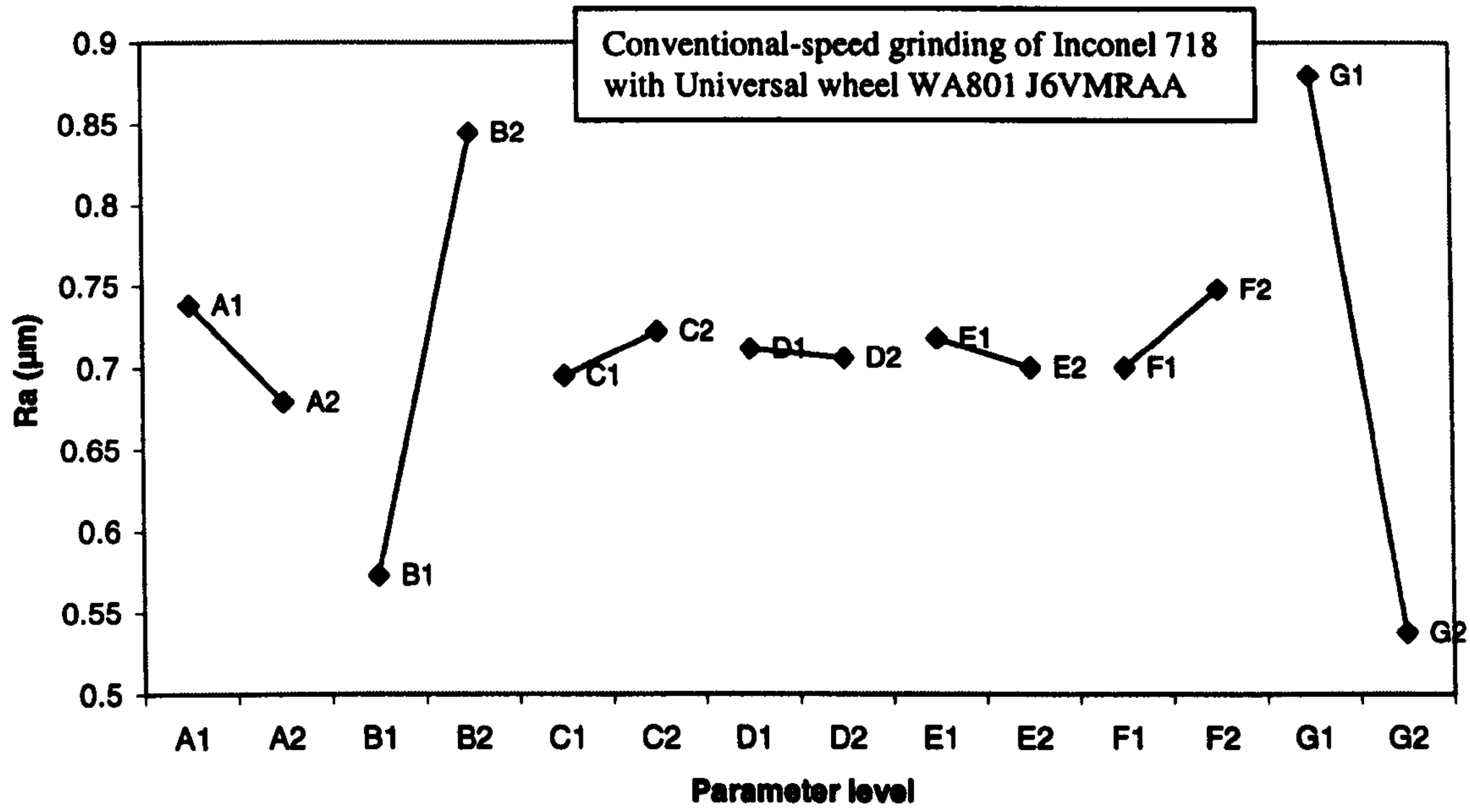

Figure 7.23. Direct effects on surface roughness. A - dressing tool, B - dressing lead, C - dressing increment, D - number of dressing passes, E - wheelspeed, F - workspeed, G - dwell.

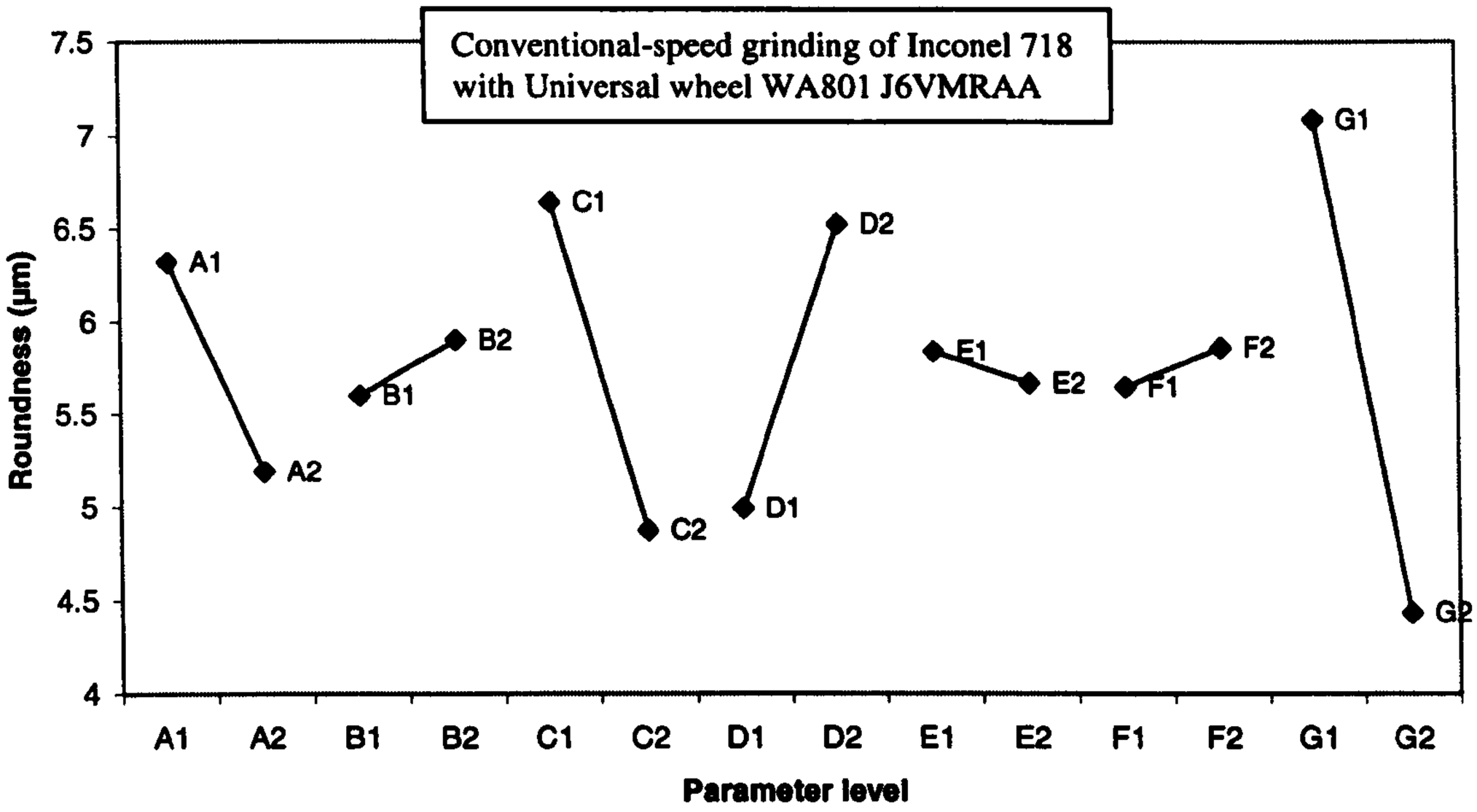

Figure 7.24. Direct effects on roundness. A - dressing tool, B - dressing lead, C - dressing increment, D - number of dressing passes, E - wheelspeed, F - workspeed, G - dwell.

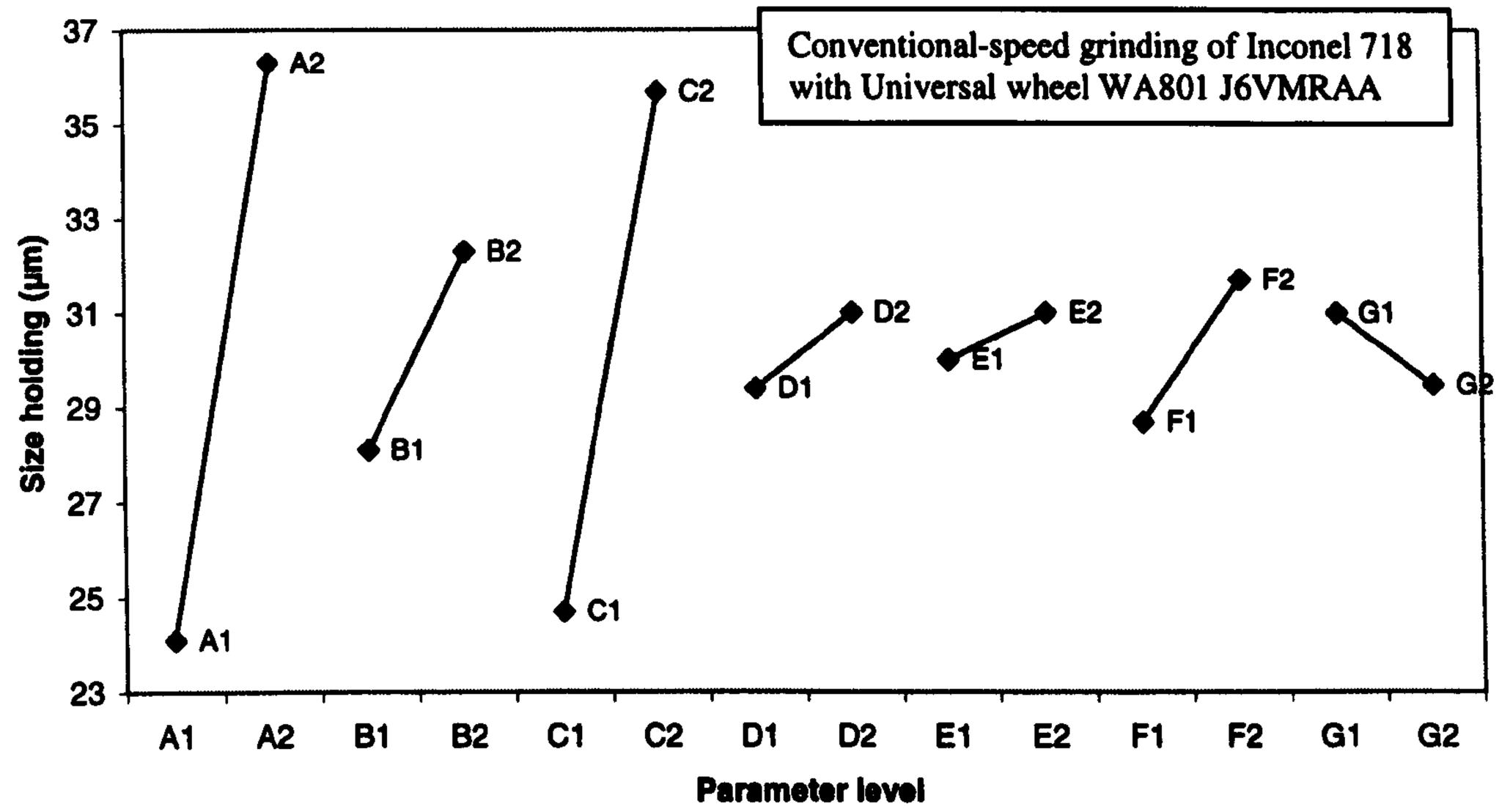

Figure 7.25. Direct effects on size holding. A - dressing tool, B - dressing lead, C - dressing increment, D - number of dressing passes, E - wheelspeed, F - workspeed, G - dwell.

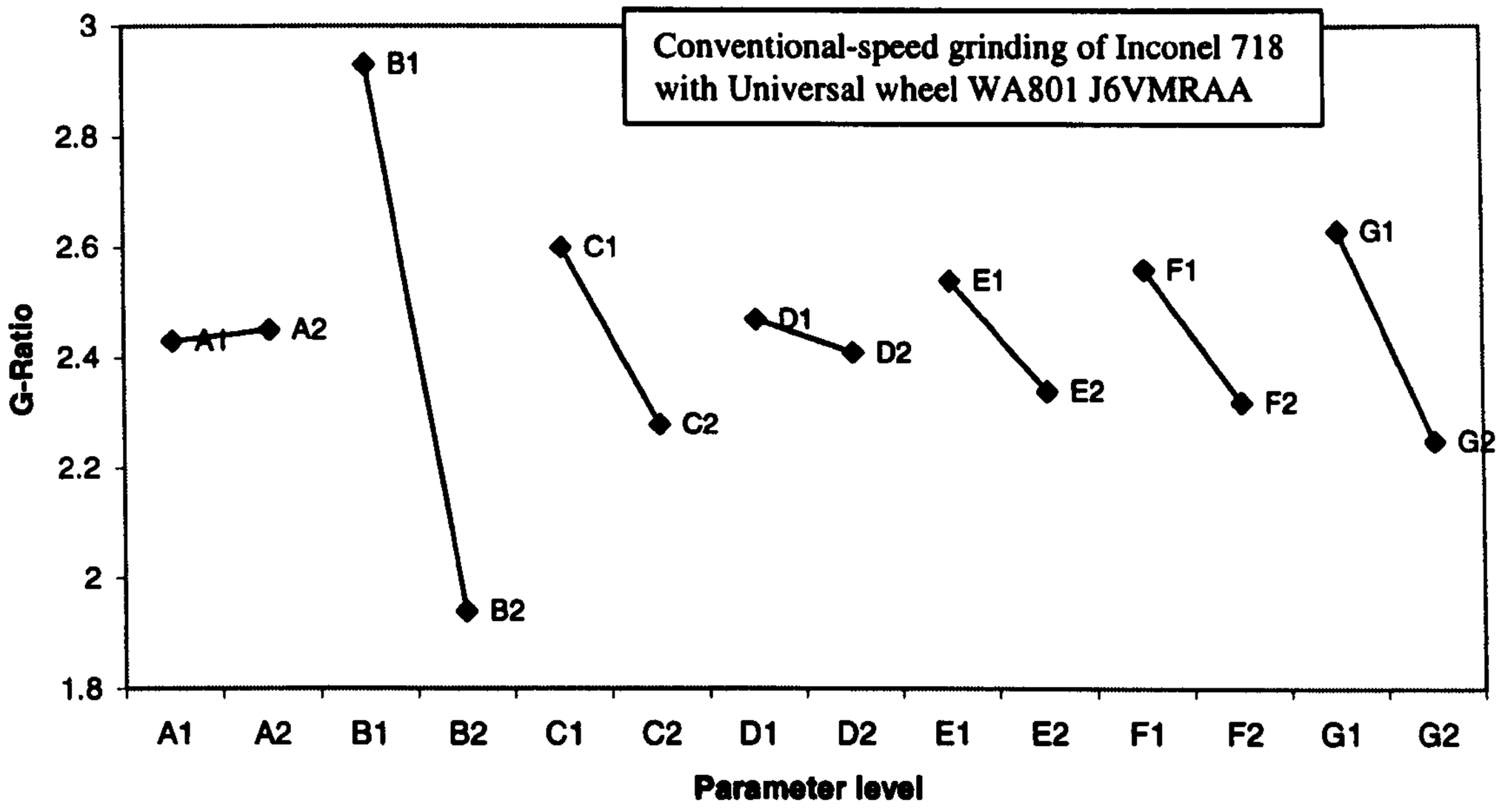

Figure 7.26. Direct effects on G-ratio. A - dressing tool, B - dressing lead, C - dressing increment, D - number of dressing passes, E - wheelspeed, F - workspeed, G - dwell.

Confirmation Trials for conventional-speed grinding of Inconel 718 using Universal Al_2O_3 wheel WA801 J6VMRAA.

According to the direct effects charts the parameters for low specific energy grinding are the same as those used for Trial 3 from the characterisation trials, see Table 7.2. So as not to repeat this trial, confirmation trials were carried out with the aim of improving workpiece quality. The direct effects charts for roughness and roundness show that increasing wheelspeed had a negligible affect. However, the lower wheelspeed led to lower specific energy and higher G-ratio. Thus, the lower wheelspeed of 33m/s was used for both confirmation trials.

From the direct effects charts it can be seen that a slow dressing lead is important for surface roughness but has negligible affect on roundness. For improved roundness, the larger dressing increment is important but has negligible affect on roughness. To show these effects, Trial C1 was run using the fast dressing lead and low dressing increment. Trial C2 was run with slow dressing lead and large dressing increment. Thus, roughness and roundness results should be better for Trial C2. This effect is shown by results

presented for Trials C1 and C2 in Tables 7.25 and 7.26 respectively. It can also be seen that, apart from wheelspeed, the parameters for Trial C2 are the same as those for Trial 5.

Table 7.24. Parameters for confirmation trials for conventional-speed grinding of Inconel 718 using Universal Al_2O_3 wheel WA801 J6VMRAA.

Parameter	Confirmation Trial 1	Confirmation Trial 2
A - Dressing tool	single point diamond	single point diamond
B - Dressing lead	0.3mm/rev	0.05mm/rev
C - Dressing increment	4µm	24µm
D - No. of dressing passes	2	2
E - Wheelspeed	33m/s	33m/s
F - Workpiece speed	20m/min	20m/min
G - Dwell	10s	10s

The results of the confirmation trials are summarised in the following tables (see Appendix C for graphs):

Table 7.25. Summary of results for Confirmation Trial C1 for conventional-speed grinding of Inconel 718 using Universal Al_2O_3 wheel WA801 J6VMRAA.

	Specific Energy	Ra	Roundness	Size Holding
Mean	66.0 J/mm^3	0.33µm	1.9µm	23.6µm
Median	67.4	0.33	1.6	27
Mode	-	-	-	-
Maximum	74.9	0.35	3.6	34.0
Minimum	56.1	0.31	1.2	0
Range	18.8	0.03	2.5	34.0
Variance	56.1	0	1.0	184.3
Standard deviation	7.5	0.01	1.0	13.6

G-ratio = 2.8 (G-ratio is for a fixed volume of material removed, i.e. V_w = 855 mm^3, not re-dress life). Q'_w=2 mm^3/mm s.

Table 7.26. Summary of results for Confirmation Trial C2 for conventional-speed grinding of Inconel 718 using Universal Al_2O_3 wheel WA801 J6VMRAA.

	Specific Energy	Ra	Roundness	Size Holding
Mean	68.6 J/mm^3	0.31µm	1.3µm	21.8µm
Median	69.8	0.31	1.2	25.0
Mode	-	-	-	-
Maximum	77.1	0.34	2.0	32.0
Minimum	61.1	0.27	0.9	0
Range	16.0	0.07	1.2	32.0
Variance	43.2	0	0.2	160.7
Standard deviation	6.6	0.03	0.5	12.7

G-ratio = 2.3 (G-ratio is for a fixed volume of material removed, i.e. V_w = 855 mm^3, not re-dress life). Q'_w=2 mm^3/mm s.

7.7 Discussion of Direct Effects Charts and Confirmation Trials

Results from the confirmation trials have validated the direct-effects charts for each wheel. It has been shown that in each case grinding conditions can be selected to achieve an improvement in workpiece quality. Some discussion was included with the results as they were presented. Before discussing the economic implications of the results, the main points from Section 7.6 are highlighted..

High-speed CBN grinding of Inconel 718 on the J&S Suprema.

From the direct effects charts and confirmation trials the following points are highlighted:

- High wheelspeed leads to increased specific energy, improved workpiece quality and high G-ratio. However, for surface roughness the effect is not particularly strong.
- Dressing direction and overlap strongly affect specific energy and have a dominant effect on surface roughness, roundness and G-ratio.
- With the exception of dressing increment the direct effects show that process parameters act in the same direction for surface roughness as they do on roundness.

The direct effects charts for the Suprema show that increased wheelspeed leads to higher specific energy, lower surface roughness, improved roundness and higher G-ratio. These results are in agreement with theory.

With regard to surface roughness in the direct effects chart, Figure 7.3, for the high-speed results show the dominant parameter to be dressing direction followed by dressing overlap. This may be a consequence of the increased porosity of the wheel where the effect of dressing parameters that close or open the wheel up are enhanced. This is also reflected in the direct effects charts for specific energy, Figure 7.2, where parameters leading to low surface roughness tend towards high specific energy. With the exception of dressing increment the direct effects of parameters for roundness, Figure 7.4, are the same as those for surface roughness. This effect is also shown for the conventional speed results from the Series 10 CBN trials, Figures 7.8 and 7.9.

Conventional-speed CBN grinding of Inconel 718 on the J&S Series 10.

From the direct effects charts and confirmation trials the following points are highlighted:

- Direct effects charts indicate that the lower wheelspeed leads to reduced specific energy, surface roughness and G-ratio.
- Dwell has the dominant effect on improving workpiece surface roughness and roundness.
- With the exception of dressing increment the direct effects show that process parameters act in the same direction for surface roughness as they do on roundness.
- The effects of dressing direction are consistent with the high-speed results.

The direct effects chart for surface roughness, Figure 7.8, shows that a lower roughness is achieved with the lower wheelspeed. To explain this effect it is necessary to look at the mean results from the characterisation trials shown in Table 7.11, page 169. It is shown that for Trial 4 the surface roughness is very high. Trial 4 is a high wheelspeed trial. However, as the roughness results for this trial are particularly poor, it has a dominating effect on the mean result used for the direct effects chart. The reason that roughness is poor for this trial is due to the stronger effects of parameters such as dressing direction, dressing increment, number of dressing passes and dwell time. For Trial 4 they are set at levels which lead to

high roughness. In this case these parameters have a more dominant effect on surface roughness than the high overlap and high wheelspeed used. However, Figures 7.7 and 7.11 show that high wheelspeed leads to higher specific energy and G-ratio respectively. This result is consistent with high-speed grinding. Results for the two confirmation trials, shown in Tables 7.13 and 7.14, show that improved workpiece quality was achieved when grinding at the higher wheelspeed. This is consistent with theory.

Conventional-speed grinding of Inconel 718 using Winterthur Al_2O_3 wheel 53A180 L13VPMF on the J&S Series 10.

From the direct effects charts and confirmation trials the following points are highlighted:

- Direct effects charts indicate the lower wheelspeed leads to higher specific energy, lower surface roughness and roundness.
- Workspeed has a stronger effect than wheelspeed with the lower workspeed leading to improved workpiece quality and higher G-ratio.
- Increased dwell time is the dominant parameter leading to improved surface roughness and roundness.

Chatter was encountered during all characterisation trials for this wheel. This can be seen by the roundness results shown in Table 7.15, page 175. In general chatter was worse at the higher wheelspeed, leading to rapid wheel loading and breakdown. This explains the higher surface roughness also encountered at higher wheelspeeds. The specific energy is consistent with the high surface roughness and is shown to be lower at the higher wheelspeed. Workspeed has a dominant effect on specific energy. It can be seen that the lower workspeed leads to higher specific energy, improved workpiece quality and higher G-ratio. This is due to the lower workspeed leading to reduced chip thickness. For wheelspeed the positive effects of increased wheelspeed were more than offset by the increase in chatter and wheel loading.

Conventional-speed grinding of Inconel 718 using Winterthur Al_2O_3 wheel 53A80 L15VPMF on the J&S Series 10.

Compared to the previous wheel, this wheel has increased grain size and porosity. The direct effects charts show that this changes the way in which some process parameters affect performance indicators. The following points are highlighted:

- The effect of workspeed is not as dominant for this wheel compared to the previous wheel and favours the high workspeed for roundness and size holding.
- For the previous fine grain wheel surface roughness is improved with a fast dressing lead. For this wheel a fine dressing lead leads to improved surface roughness.
- The higher wheelspeed appears to have a strong affect on improving workpiece roundness.
- From Table 7.19 it can be seen that, out of all the wheels tested, this wheel consistently gives a low specific energy and poor surface roughness.

Conventional-speed grinding of Inconel 718 using Universal Al_2O_3 wheel WA801 J6VMRAA on the J&S Series 10.

Results for this wheel are more consistent than for the other aluminium oxide wheels used to grind inconel 718. This is reflected in the relatively low values of variance shown in Tables 7.25 and 7.26 for the confirmation trials. The following points are highlighted:

- Dressing lead and dwell have a dominant effect on surface roughness favouring a fine dressing lead and long dwell. This is consistent with the previous wheel, which also had the same grit size.
- Dressing overlap has the most dominant effect on G-ratio favouring a fine dressing lead. This is consistent with the previous wheel. For both wheels the longer dwell time favourable to surface roughness leads to lower G-ratio.
- Dressing increment has a strong effect on roundness. Roundness is improved when the larger increment is used. However, this leads to lower G-ratio. This effect is true for all five wheel investigated including the CBN wheels.

It has been shown that the direct effects charts for each wheel can be successfully used to select process parameters with regard to their effect on performance indicators. From

achieving this, the next step is to establish if the parameters required to accomplish target workpiece quality lead to cost effective precision grinding.

7.8 Discussion of Process Costs

A cost analysis was performed using results from the confirmation trials. Confirmation Trial C2 using the Universal wheel WA801 J6VMRAA, was selected to represent the aluminium oxide wheels. This was based on the superior results for surface roughness and roundness recorded for this trial. Results on which the cost analysis is based are:

- Confirmation Trial C3 – Suprema – wheel B151 VR150J
- Confirmation Trial C1 - Series 10 - wheel B151 VR150J
- Confirmation Trial C2 - Series10 - wheel WA801 J6VMRAA

The re-dress life for each trial was based on the target workpiece quality criteria of:

Surface roughness, Ra ≤ 0.25μm

Roundness ≤ 1μm

It can be seen that target roughness is not achieved with the aluminium oxide wheel. However, for the cost analysis a re-dress life of 1 part per dress has been used. In reality to achieve this a slight reduction in removal rate would be required. For the cost analysis the re-dress life used for each trial is:

- Suprema CBN Confirmation Trial C3: 30 parts per dress
- Series 10 CBN Confirmation Trial C1: 25 parts per dress
- Series 10 Al_2O_3 Confirmation Trial C2: 1 part per dress

A comparison of costs per part for the three grinding processes is given in Figure 7.27.

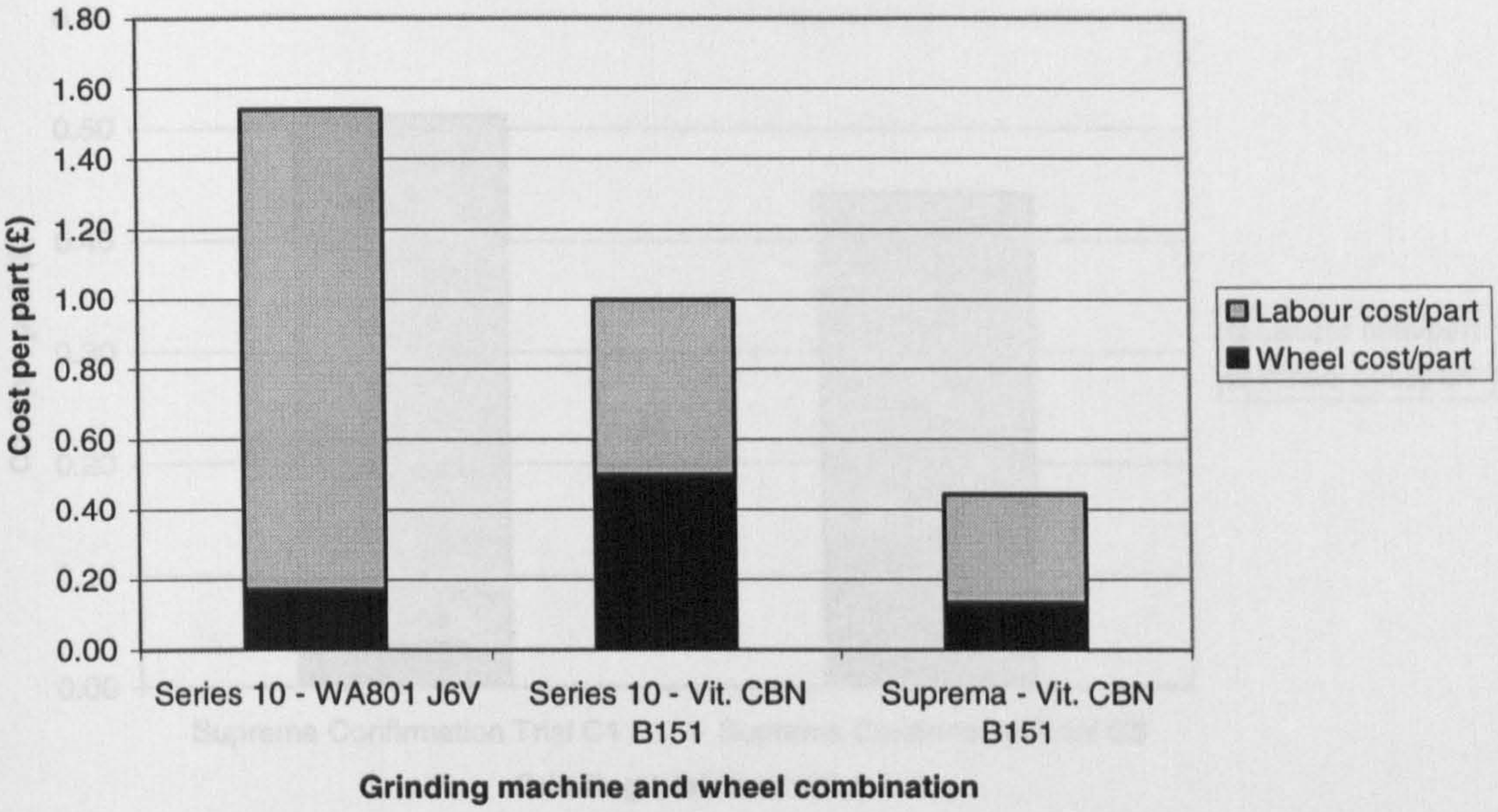

Figure 7.27. Basic cost comparison between different machine and wheel combinations for grinding Inconel 718.

It can be clearly seen that step changes occur when moving from aluminium oxide to vitrified CBN when grinding at conventional speed. However, the results also show that a further step change occurs when moving to high speed grinding with vitrified CBN. This is largely due to the fact that grinding at high speed allows a shorter dwell to be used while achieving the target workpiece quality over a reasonable re-dress life.

The effect of dwell on cost is further illustrated when the results of the Suprema high-speed Confirmation Trials C1 and C3 are compared. From Table 7.7 it can be seen that the only difference in parameters is the dwell time. For Suprema Confirmation Trial C1 a dwell of 10s was used. For Suprema Confirmation Trial C3 the dwell time was reduced to 2s. Re-dress life was not established for the Suprema Confirmation Trial C1. Consequently, for the cost analysis it was estimated. Based on the results graphs which show the specific energy, roughness and roundness to be stable, re-dress life was estimated to be 100 parts per dress. The effect on the process costs is shown in Figure 7.28.

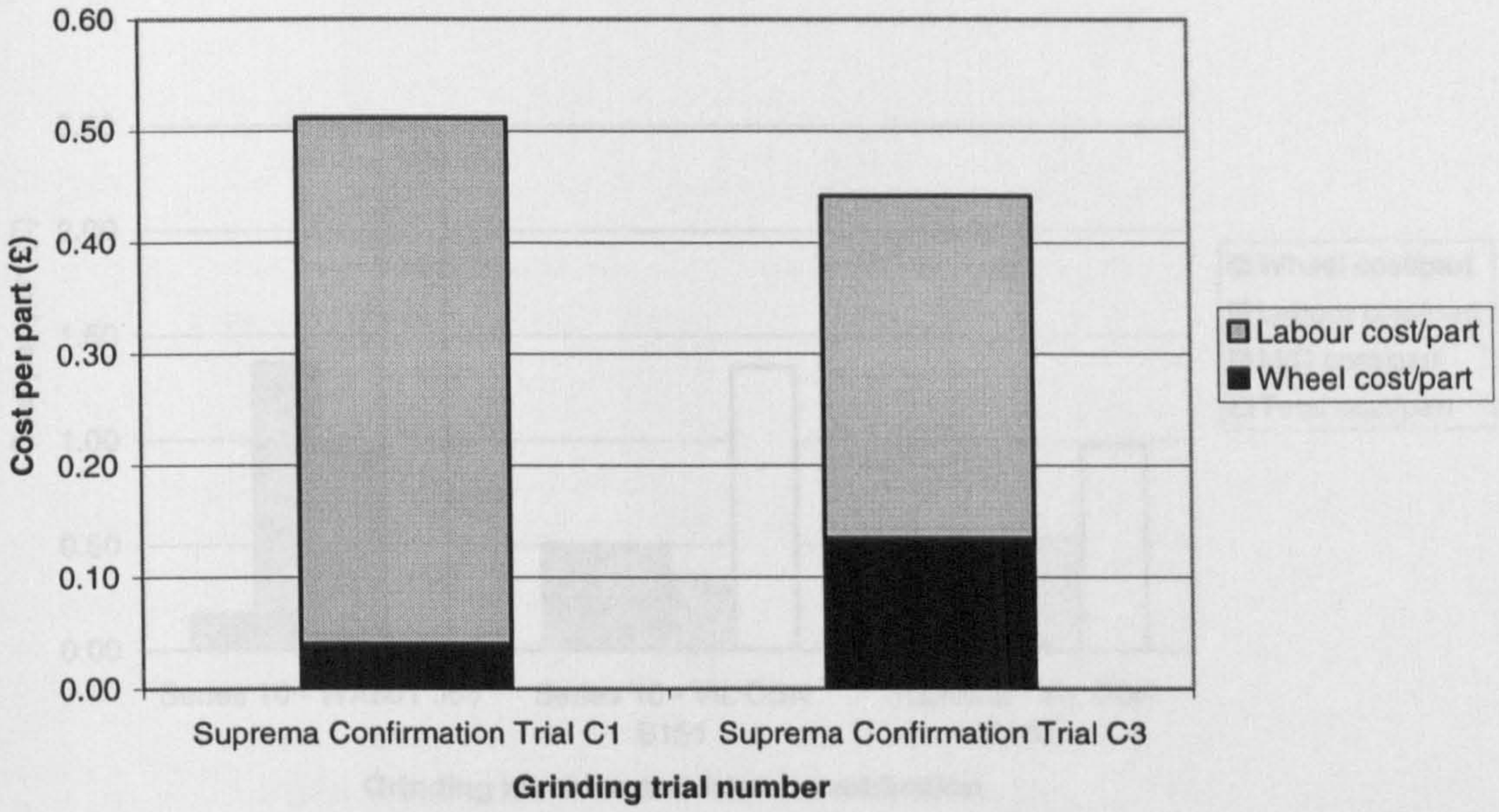

Figure 7.28. Comparison of costs for Suprema Confirmation Trials C1 and C3. For Suprema Confirmation Trial C1 re-dress life was estimated at 100 parts per dress.

From Figure 7.28 it can be seen that the higher re-dress life estimated for Suprema Confirmation Trial C1 would lead to a significantly lower wheel cost per part. However, re-dress life does not have the same impact on labour cost per part which is significantly higher due to the long dwell period of 10s.

The effect of including machine tool costs for the trials shown in Figure 7.27 is shown in Figure 7.29. A cost of £100,000 has been used for the conventional machine and £250,000 for the high-speed machine. The payback period is six months. The analysis is based on the same three trials shown in Figure 7.27. It can be seen that for the duration of the payback period the total cost per part for high speed CBN grinding, including machine tool cost, is lower despite the higher initial purchase cost.

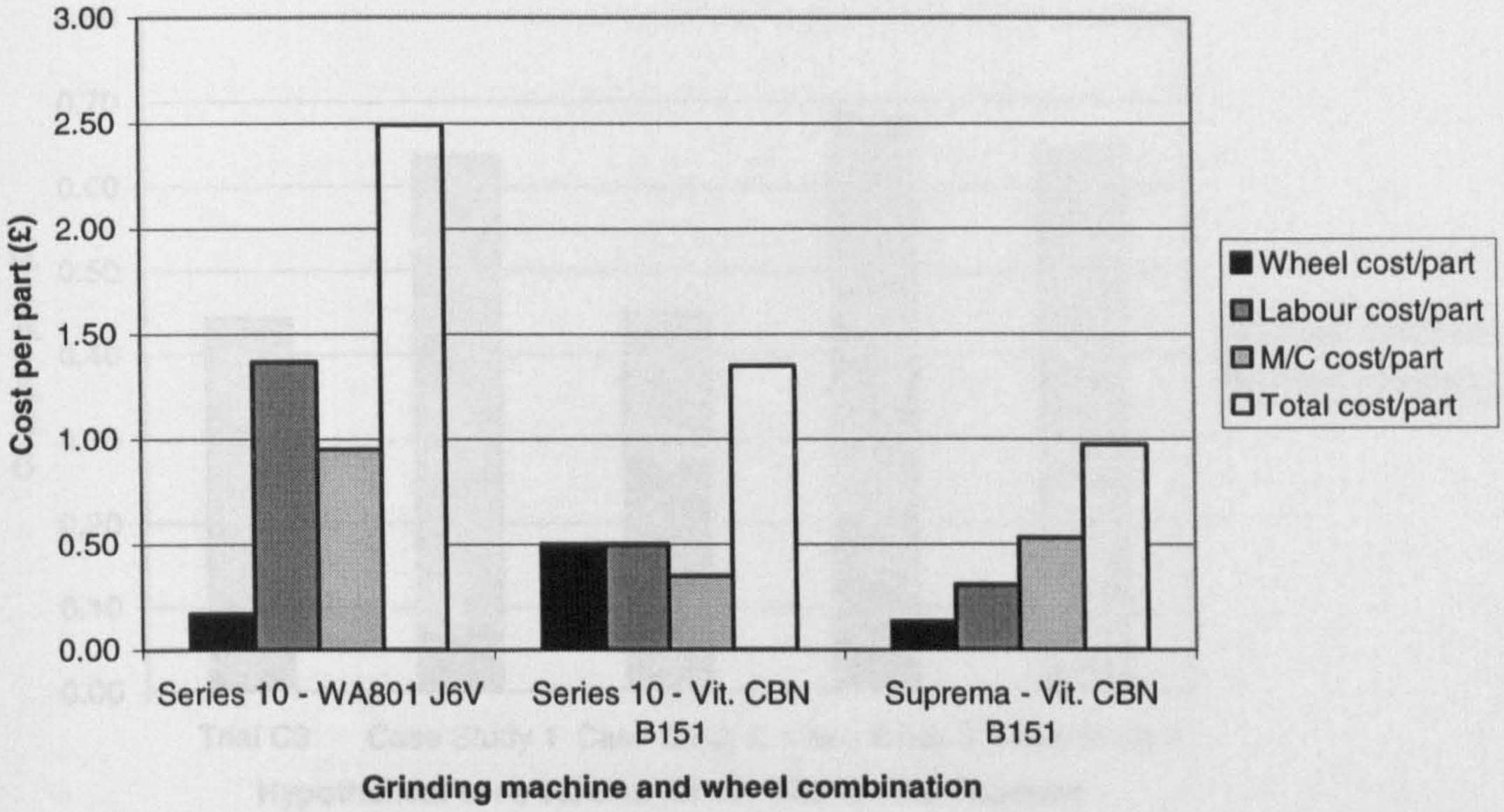

Figure 7.29. Modified cost analysis including machine tool costs over a payback period of six months, i.e. 1920hours.

The results from the three wheels discussed previously have been compared with some hypothetical case studies. In each case the following changes were made and the effect on cost compared with the actual result achieved. Assumptions were made as follows:

Case Study 1: Specific volumetric removal rate was halved and re-dress life doubled.

Case Study 2: Specific volumetric removal rate was doubled and re-dress life halved.

Case Study 3: Specific volumetric removal rate and dwell were halved, re-dress life remains the same.

Case Study 4: Specific volumetric removal rate was halved and dwell doubled, re-dress life was increased by four times.

Figure 7.30 demonstrates how costs would be affected if the above changes were made to Suprema Confirmation Trial C3. Figure 7.31 compares the costs determined for the Series 10 CBN Confirmation Trial C1, i.e. at conventional wheelspeed, with the hypothetical costs of the case studies. Figure 7.32 shows how costs are affected when grinding using an aluminium oxide wheel.

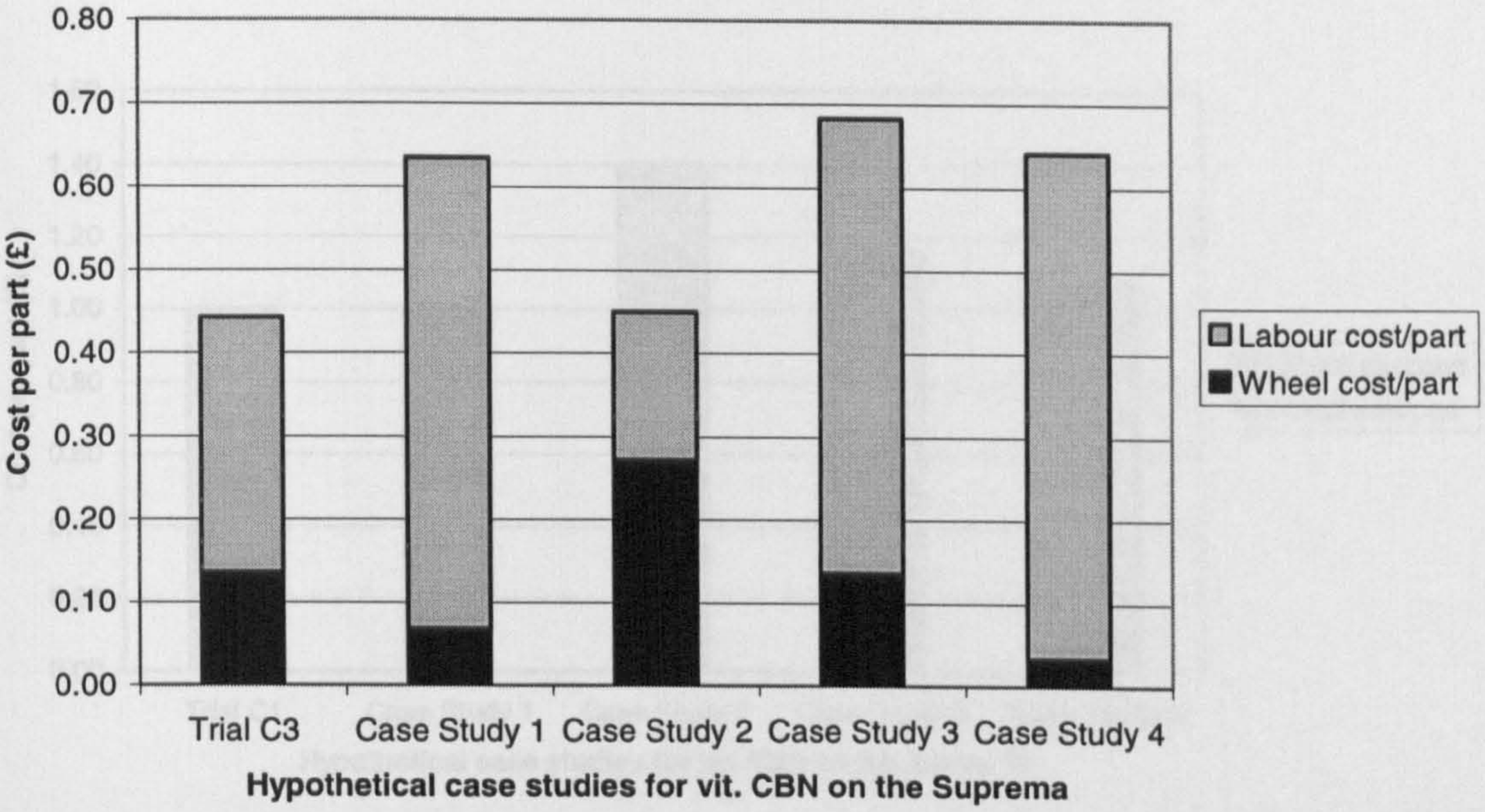

Figure 7.30. Comparison of costs between case studies and Confirmation Trial C3 for the vitrified CBN wheel B151 VR150J on the Jones and Shipman Suprema machine.

It can be seen from Figure 7.30 that the direct effects charts have allowed parameters to be selected which lead to cost effective precision grinding. A finding of the work presented in Chapter 4 was that there is a compromise between re-dress life, removal rate and dwell time. This is clearly supported by Figure 7.30. It is shown that attempts to reduce wheel cost per part can be offset by larger increases to labour cost per part and vice versa.

For grinding with CBN at a conventional wheelspeed on the Series 10 machine wheel costs make a greater contribution to the total cost per part. This is due to the higher initial cost of the wheel compared to the high-speed CBN wheel, along with a modest re-dress life. This is reflected in the analysis of Figure 7.31. As with the high-speed CBN process the results shown in Figure 7.31 indicate that using the direct effects charts has allowed appropriate parameters to be selected keeping costs low while achieving workpiece quality. The speculative results from the case studies indicate that there is no advantage gained by increasing re-dress life or removal rates. Again it can be seen that to attempt to lower wheel costs per part without due consideration to labour cost per part can lead to higher total cost per part as shown by Case Study 4.

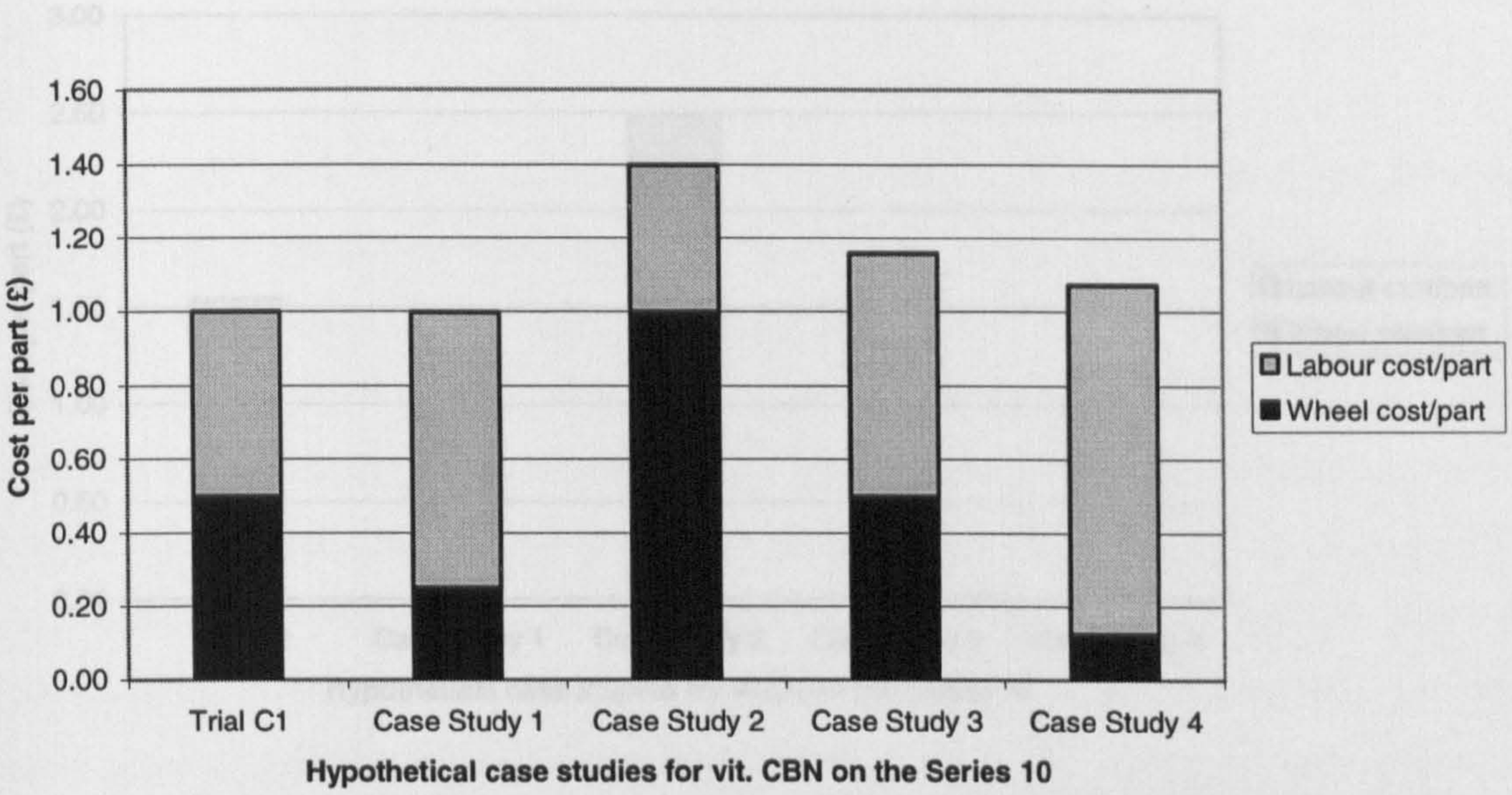

Figure 7.31. Comparison of costs between case studies and Confirmation Trial C1 for the vitrified CBN wheel B151 VR150J on the Jones and Shipman Series 10 machine.

Figure 7.32 indicates that for aluminium oxide wheels the greatest difficulty with regard to process costs is reducing labour cost per part. This is most successfully achieved in Case Study 4 where removal rate is reduced by half and dwell time doubled. However, re-dress life is increased by four times. As shown by Figure 4.13 in chapter four an increase in re-dress life for processes where the number of parts per dress is low, i.e. <5, has a significant effect. This effect is also shown for Case Study 1. The converse is also true as shown by the result of Case Study 3 where re-dress life is reduced.

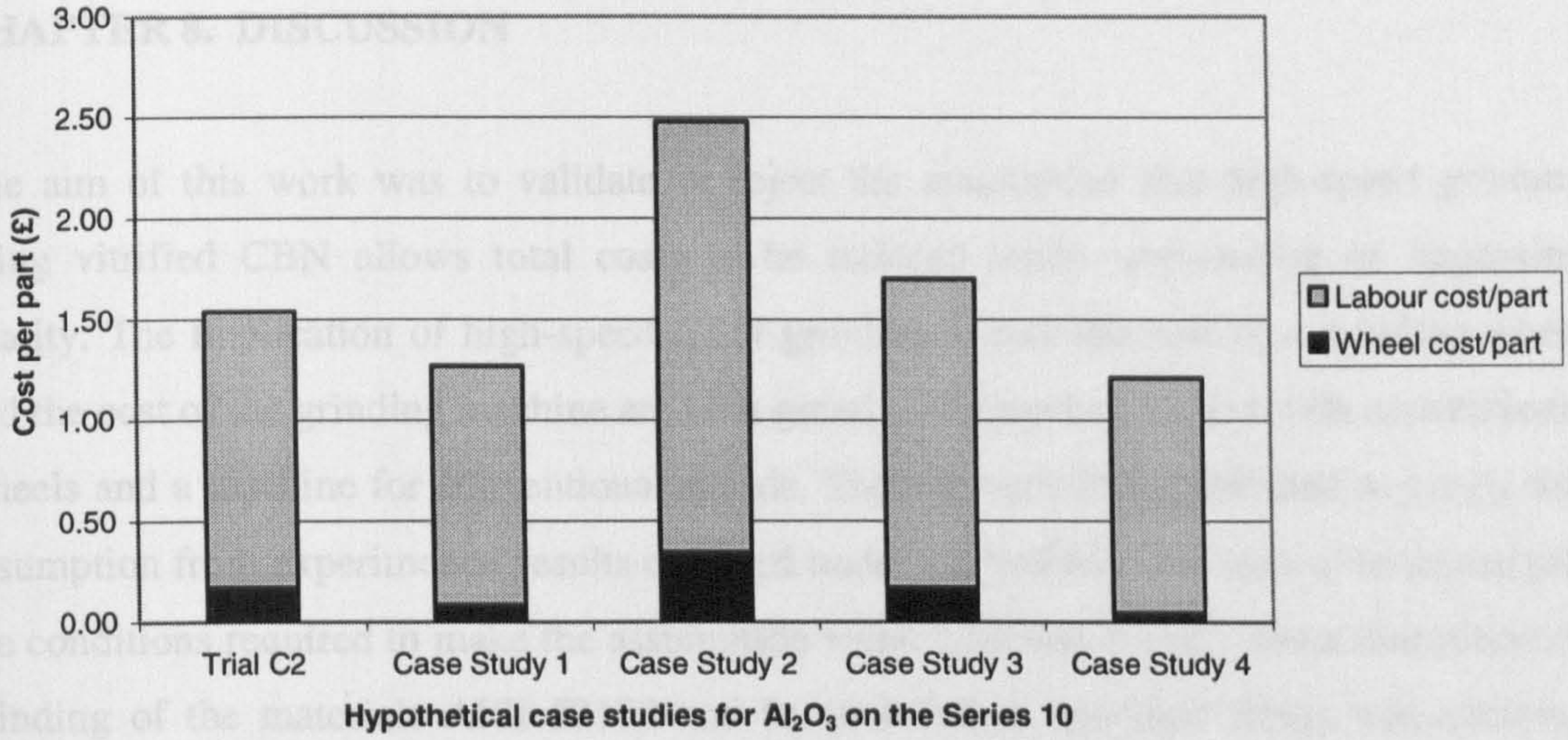

Figure 7.32. Comparison of costs between case studies and Confirmation Trial C2 for the aluminium oxide wheel WA801 J6V on the Jones and Shipman Series 10 machine.

The above cost analyses have also shown that wheel cost per part for high speed CBN grinding process is comparable to conventional speed grinding with an aluminium oxide wheel. However, when grinding a material such as Inconel 718 the high-speed CBN process gives far higher re-dress life, i.e. in this case higher by 30 times. The high-speed process also allows a shorter dwell time, i.e. in this case shorter by five times. This has a dramatic effect on reducing labour cost per part and, therefore, total cost per part. This is despite removal rates being equal.

7.9 Conclusions

Direct effects charts have been produced for each wheel investigated when grinding Inconel 718. The direct effects charts have been validated and shown to be a reliable description of how process parameters affect performance.

Process requirements for cost effective precision grinding have been determined. For grinding Inconel 718 the most cost effective way to achieve precision is to use high-speed vitrified CBN grinding as shown by Suprema Confirmation Trial C3.

CHAPTER 8. DISCUSSION

The aim of this work was to validate or reject the assumption that high-speed grinding using vitrified CBN allows total costs to be reduced while maintaining or improving quality. The implication of high-speed CBN grinding is that the cost of a grinding wheel and the cost of the grinding machine are both greatly increased compared with conventional wheels and a machine for conventional speeds. There is very little published to justify this assumption from experimental results obtained under controlled conditions or to investigate the conditions required to make the assumption valid. Chapters 6 and 7 show that precision grinding of the materials AISI 52100 and Inconel 718 to specified limits was achieved using a range of grinding wheels and two different grinding machines. A large number of experimental results and basic theoretical arguments have been advanced to support the hypothesis. The purpose of this chapter is to summarise the results and to consider the reliability of the findings.

A statistical approach was employed for testing the effects of process parameters. The results were shown to be repeatable and differences for most parameters were found to be significant. The method employed allowed the reliability of the results to be demonstrated beyond reasonable doubt. This is shown by the repeated reliability of the confirmation trials in validating the direct effects charts. It is therefore suggested that based on the conditions investigated, conclusions can be reliably achieved.

The basis for deciding whether a process is successful or not, is achievement of target quality at a competitive cost. Global competition tends to increase with time due to increased ease of transport and increased global sourcing of goods. Labour costs, environmental legislation, health and safety regulations and employment responsibilities remain parochial and tend to become more demanding. Consequently the achievement of cost effective manufacturing in the developed world becomes increasingly difficult. Nevertheless, previous chapters show that for equal labour-cost rates, total costs per part can be significantly reduced through the use of improved technology, built on an understanding of the process. However, comparing costs from a global viewpoint,

comparative process costs depend both on labour-cost rate and on the level of technology used.

Significant advantages were found using vitrified CBN wheels at conventional speed on a standard CNC machine compared with aluminium oxide wheels. For conventional-speed CBN grinding, wheel cost per part was higher but this was countered by much lower labour costs. For the AISI 52100 material conventional-speed CBN outperformed a sol gel abrasive. The biggest cost reductions, however, were made when grinding at high-speed. Compared to aluminium oxide wheels at conventional speed, CBN wheel cost per part was comparable for the AISI 52100 material and lower for the Inconel 718 material. In both cases, labour cost per part was reduced significantly when moving from conventional speed aluminium oxide to high-speed CBN.

Intrinsic to the cost analysis is achievement of workpiece quality. This is due to its controlling influence on re-dress life. For this work, re-dress life was given as the number of parts ground before a specified surface roughness or out of roundness was exceeded. In practice, any parameter used to assess workpiece quality can be used to determine re-dress life. The economic model developed in Chapter 4 presented the factors contributing to process costs. Re-dress life was shown to be one of the contributory factors. However, as re-dress life increases its influence in the cost analysis diminishes as shown for AISI 52100. For high-speed CBN grinding, costs were reduced by increasing removal rate even though this resulted in re-dress life reduced from 540 to 330 parts per dress. For Inconel 718, re-dress life had a stronger effect. This was a result of the material being difficult to grind and re-dress life tending to be low. It was shown that the high-speed CBN process was far more cost effective despite removal rates being the same as for the aluminium oxide wheel trials. The high wheel speed also allowed dwell time to be reduced making a significant contribution to lowering costs.

The cost analysis was based on a single plunge-grinding operation with a short cycle time as used in the automotive industry for diesel injector parts. This allowed the effects of re-dress life to be explored across a wide range. However, in many applications, cycle time

duration may be hours and require the wheel to be re-dressed a number of times per workpiece. Such applications exist in the aerospace industry in particular. A further difference between the aerospace industry and industries such as the automotive industry is the volume of production. For the automotive industry many parts are mass-produced. In the aerospace industry, manufacturing is often based around families of parts that are produced in small batches. It is therefore appropriate to question whether the findings in this work would be applicable to very small batch quantities with frequent changes of set-up. However, the investigation on the grinding of Inconel 718 shows the advantages of increasing wheel speed for shorter values of redress life. It has been shown that economic advantage can be gained without increasing removal rates when re-dress life is short. Thus, if the short re-dress life work is analogous to small batch production, results suggest that high-speed CBN grinding offers great potential. This is particularly true for difficult to grind materials such as Inconel 718 which are widely used in the aerospace industry.

The economic model highlighted the main factors contributing to process costs. The results for Inconel 718 provide an insight into the dominant factors for low re-dress life work. It was shown that increased re-dress life resulting from using high-speed vitrified CBN can lead to large cost savings. In Figure 7.27 it was shown that the high-speed CBN process was cost effective as re-dress life was increased and dwell time reduced. However, even if dwell time had not been reduced the high-speed CBN process was still more cost effective due to increased re-dress life. This is due to the large savings made in wheel cost per part where dwell time has no influence. Labour cost per part was increased from £0.31 to £0.47 when the dwell time of the high-speed CBN process was increased from 2s to 10s. Despite this increase, the high-speed process was still far more cost effective. Thus, it may be argued that a move from a low re-dress life conventional speed aluminium oxide process to a high-speed vitrified CBN process will maximise cost savings.

In Chapter 5 the possibilities of using a larger wheel were discussed. It was stated that a larger wheel diameter would allow machine tool complexity to be reduced. This would be favourable if machine reliability was improved. Using the cost model presented in Chapter 4, it is possible to show how increasing wheel size affects costs. It can be seen that if the

wheel purchase cost and re-dress life are increased in proportion to the increase in wheel diameter, wheel cost per part remains the same. However, a higher re-dress life will reduce labour cost per part by some degree. As shown by Figure 4.10 this effect may be minimal as re-dress life increases above 5 parts per dress. This effect is shown in Figure 8.1 for grinding Inconel 718 where Suprema Confirmation Trial C3 is compared with a modified version for increased wheel diameter. It was assumed that the wheel purchase cost and re-dress life are increased in proportion to the increase in wheel diameter, i.e. by 1.8 times. The assumption that re-dress life increases in proportion to wheel diameter is due to the increased number of grains sharing the workload during grinding.

For Suprema Confirmation Trial C3 shown in Figure 8.1 the process costs are based on the following:

Wheel purchase cost:	£1700	Maximum wheel diameter:	250mm
Radial wheel wear:	0.008mm	Minimum wheel diameter:	240mm
Dressing increment:	0.002mm	Number of dressing passes:	2
Labour cost:	£75 / hour	Re-dress life:	30parts/dress
Stock removed:	0.2mm	Workpiece diameter:	40mm
Dwell time:	2s	Specific volumetric removal rate:	$2mm^3/mm \cdot s$
Wheel width:	17mm	Dressing lead:	8.5mm/s

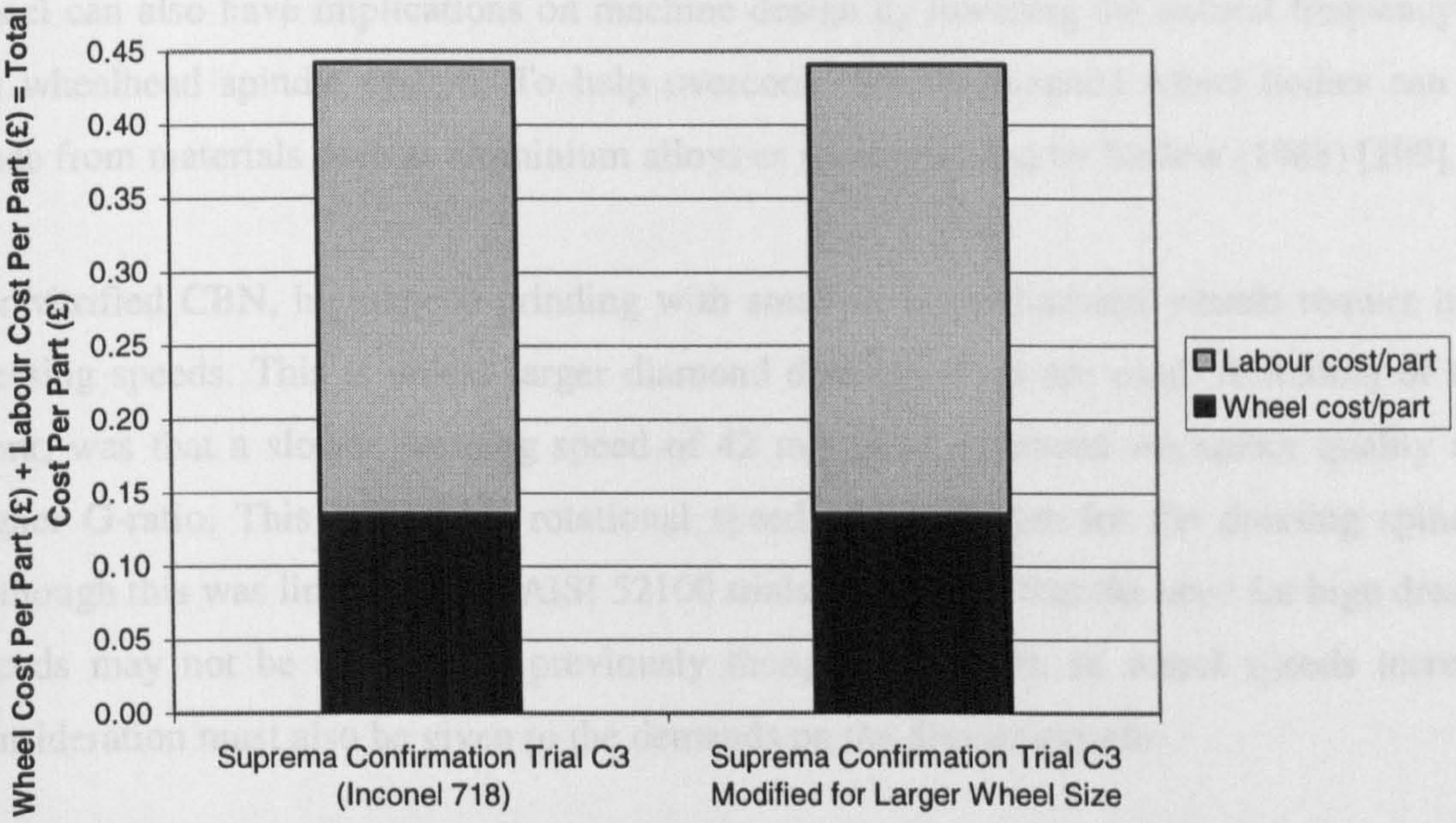

Table 8.1. Comparison of costs for different wheel size when grinding Inconel 718.

The modifications made to Confirmation Trial C3 (Inconel 718) in Figure 8.1 are:

- Maximum wheel size increased from 250mm to 450mm.
- Minimum wheel size increased from 240mm to 440mm.
- Wheel purchase cost increased from £1,700 to £3,060.
- Re-dress life increased from 30 parts per dress to 54 parts per dress.

It can be seen that increasing wheel diameter has virtually no effect on process costs per part providing there is a proportional increase in re-dress life. However, to maintain an equal dressing overlap ratio, dressing lead would have to be reduced as wheel diameter increases, see Equation 4.22. This could lead to increased costs through increased time without production. However, providing there is a corresponding increase in re-dress life, costs incurred through longer dressing times will be spread over an increased production rate per dress. Based on these assumptions, it might appear that the use of small wheel diameters offers little advantage from a cost perspective. From the machine tool design perspective, higher rotational speeds required for smaller diameter wheels is a disadvantage. This has implications on spindle design, motor selection and the required dynamic characteristics of the machine. However, the increased mass of a large diameter

wheel can also have implications on machine design by lowering the natural frequency of the wheelhead spindle system. To help overcome this, high-speed wheel bodies can be made from materials such as aluminium alloys as recommended by Barlow (1988) **[109]**.

For vitrified CBN, high-speed grinding with small or large diameter wheels require high dressing speeds. This is unless larger diamond dressing discs are used. A finding of this work, was that a slower dressing speed of 42 m/s gave improved workpiece quality and higher G-ratio. This required a rotational speed of 5,348 rpm for the dressing spindle. Although this was limited to the AISI 52100 trials it indicates that the need for high dresser speeds may not be as great as previously thought. However, as wheel speeds increase consideration must also be given to the demands on the dresser system.

For the type of batch production investigated in this research, high-speed grinding with vitrified CBN has been shown to be the most cost effective form of precision grinding. Direct effects charts show how a range of parameters affect the process. Dressing direction has a strong influence at high-speed. At present, manufacturers tend to recommend down dressing for most vitrified CBN applications. This is due to the freer cutting characteristics endowed to the wheel. Up dressing is associated with low surface roughness but increased risk of thermal damage. However, these opinions are based on work carried out when using CBN at conventional speed. In this work at high-speed, it was found that the wheel surface after down dressing was too open and sharp leading to higher surface roughness. Some reasonable results were achieved using down dressing as discussed in Chapter 6. But based on the large number of trials undertaken, up dressing is recommended for high-speed applications for low surface roughness. Up dressing was also found to lead to higher values of G-ratio. The dressing increments used for the high-speed trials were small, i.e. 2 μm and 10 μm. In both cases, touch dressing was required using acoustic emission techniques. This is important to limit the risk of heavy contact or collision and to reduce wheel wastage.

For the AISI 52100 trials, direct-effects charts showed how parameters affect the variance of a performance indicator, see Appendix B1. It can be seen that high wheel speed is dominant in reducing the variance of surface roughness, roundness and size holding over

the duration of a trial. This is a further advantage offered by high-speed grinding, as reducing variance can play an important role in helping to maintain target workpiece quality and increasing re-dress life.

In summary, direct effects charts show how precision grinding can be achieved for each application investigated whether it involves conventional speed aluminium oxide or high-speed CBN. However, high-speed grinding with vitrified CBN offers the greatest opportunity for cost effective precision grinding. It has been shown that cost advantages apply when grinding an easy-to-grind material in large batch quantities. It has also been shown that high-speed grinding with vitrified CBN can offer cost advantages when grinding a difficult-to-grind material with smaller batch quantities. Most importantly, it has been demonstrated that cost reductions are achieved despite a requirement for a much more expensive grinding machine and a grinding wheel many times more expensive than a conventional wheel.

To achieve cost effective grinding, it is necessary to select near-optimal values of process parameters. The work has demonstrated a combination of process conditions that allows the process to be brought into an approximately optimal state. It could be argued that increasing wheelspeeds to even higher values would reduce costs further. This is beyond the scope of the present study but is worthy of further investigation.

CHAPTER 9. CONCLUSIONS

High-speed grinding with vitrified CBN offers a cost advantage in precision batch grinding compared with conventional speeds using conventional abrasives. The conditions for a cost reduction particularly lie in the case where labour costs are high. In this case, the savings in labour costs far outweigh increased machine costs and increased wheel costs. However, in a low labour cost environment such as currently exists in some countries of the World, there might be no cost advantage.

The increased level of technology required for a high-speed machine is more than justified by its performance. High-speed grinding using vitrified CBN offers enormous benefits and the further development of reliable high-speed grinding machines is recommended.

In principle, the machine design of the Suprema was justified for precision grinding at high speed. However, further development is required to overcome premature failure of some crucial and ancillary parts. The live centre used in the workhead was unsatisfactory. A more standard design using a dead centre is recommended. Alternatively if a live centre is to be used, tighter tolerances are required to minimise eccentric running.

High wheelspeeds are the key to improved workpiece quality, increased removal rates and reduced cycle times. G-ratio is also significantly increased when grinding at high speed.

For both an easy and a difficult-to-grind workpiece material, significant advantages are gained when using vitrified CBN compared with aluminium oxide at conventional speed on a standard CNC cylindrical grinding machine. For the material AISI 52100, conventional speed vitrified CBN was more effective than a sol gel abrasive. However, for both workpiece materials the use of high-speed grinding using a vitrified CBN wheel on a special-purpose machine was overwhelmingly superior allowing workpiece quality to be achieved at significantly lower cost.

For the material AISI 52100, the main advantages of high wheelspeed leading to lower costs were increased re-dress life, increased removal rate and reduced dwell time. For the material Inconel 718, the main advantages of high wheelspeed leading to lower costs were increased re-dress life and reduced dwell time. These conditions were most effectively achieved when grinding on the Suprema. For both materials, wheel costs per part using high-speed vitrified CBN were comparable to wheel costs per part using aluminium oxide wheels at conventional-speed. Labour costs per part were considerably lower when using high-speed vitrified CBN.

CHAPTER 10. RECOMMENDATIONS FOR FURTHER WORK

The following areas are suggested for further investigation:

- All three spindles on the Suprema run on hydrostatic bearings. To simplify the design, the use of rolling element bearings should also be investigated. While machine tools move towards utilising higher technology the fundamental design structure should be as simple as possible. This may lead to a more robust design and greater reliability in the field. Hybrid angular contact bearings are designed for high-speed applications where accuracy is also of great importance. The use of these bearings requires testing for high-speed grinding using vitrified CBN, and the implications for performance and cost determined.

- The Suprema was designed for a small diameter CBN wheel. Further work is required to investigate the effects of using a larger grinding wheel. This may also have implications for the type of bearings that can be used due to the need for lower rotation speeds. The research has shown that high-speed grinding leads to very low wheel costs per part. The higher initial cost of a larger wheel may be offset by the longer re-dress life that should result due to the increased number of active abrasive grains around the larger periphery. Larger wheel diameters could also become more attractive if a simpler machine design could be used.

- This work has revealed how direct effects charts can be used to select process parameters to grind AISI 52100 and Inconel 718 using vitrified CBN. With the introduction of high aspect ratio abrasive grains such as Altos and Optimos a similar programme of research work is required to compare them objectively with vitrified CBN.

- The work has shown the benefits of CBN grinding up to a wheelspeed of 120 m/s. Further work is required to establish the effects of grinding at higher wheelspeeds. This should include research on machine tool development, grinding wheel design and coolant application. The technological aspects of such research should also be supported by a study on the economic implications.

REFERENCES

[1] J.L. Metzger (1986) Superabrasive Grinding. Butterworths.

[2] I. Tomoyasu (2000) High-Speed Grinding Using CBN Wheels. Proceedings of the Intertech 2000 Conference, British Columbia, Canada, July 17-21.

[3] R.S. Woodbury (1959) History of the Grinding Machine. The Technology Press, Massachusetts Institute of Technolgy.

[4] F.B Jacobs (1919) Abrasives and Abrasive Wheels. Henley, New York.

[5] A.F. Burstall (1963) A History of Mechanical Engineering. Faber and Faber, London.

[6] H.F.G. Ueltz (1972) Abrasive Grains – Past, Present and Future. Proceedings of the International Grinding Conference.

[7] J.J. Guest (1915) Grinding Machinery. Edward Arnold.

[8] F.H. Colvin and F.A. Stanley (1908) American Machinist Grinding Book. New York

[9] S. Malkin (1988) Grinding Technology: Theory and Applications of Machining with Abrasives. Ellis Horwood Limited.

[10] Institute of Grinding Technology (1996) Grinding Manual. University of Bristol.

[11] M.C. Shaw (1996) Principles of Abrasive Processing. Oxford University Press.

[12] M. Jackson and B. Mills (2000) Materials Selection Applied to Vitrified Alumina and CBN Grinding Wheels. Journal of Materials Processing Technology, vol. 108, pp. 114-124.

[13] D. Jackson (2000) Grinding Wheel Developments for High Stock Removal. Proceedings of the Institute of Grinding Technology Annual Seminar. March 2001, Bristol.

[14] M.J. Jackson, C.J. Davis, M.P. Hitchiner and B. Mills (2001) High-Speed Grinding with CBN Grinding Wheels – Applications and Future Technology. Journal of Materials Processing Technology, vol. 110, pp. 78-88.

[15] P.A. McKeown (1986) High Precision Manufacturing and the British Economy. Proceedings of the Institute of Mechanical Engineers, vol. 200 no. 76.

[16] J.P. Womack, D.T. Jones & D. Roos (1990) The Machine that Changed the World. Macmillan Publishing Company.

[17] I. Suzuki (1984) Development of Camshaft and Crankshaft Grinding Technology Using Vitrified CBN Wheels. Proceedings of the Society of Manufacturing Engineers. Paper MR84-526.

[18] M. Tsujichi (1988) CNC Camshaft Grinder with small Diameter CBN Wheels. Proceedings of the 3rd International Grinding Conference. SME paper MR88-609.

[19] M.R. Hanard (1985) Production Grinding of Cam Lobes with CBN. Proceedings of the Society of Manufacturing Engineers, pp. 4-1 - 4-11.

[20] F. Klocke & W. König (1995) Appropriate Conditioning Strategies to Increase the Performance Capabilities of Vitrified Bond CBN Grinding Wheels. Annals of the CIRP, vol. 44/1 pp. 305-310.

[21] K.B. Lewis and W.F. Schleicher (1976) The Grinding Wheel. The Grinding Wheel Institute, Cleveland, Ohio, 3rd Edition.

[22] W.B. Rowe, X Chen & D.R. Allanson (1997) The Coolant Coupling Method Applied to Touch Dressing in High Frequency Internal Grinding. Proceedings of the 32nd International MATADOR Conference. Manchester, UK, pp. 337-340.

[23] W.B. Rowe & X. Chen (2000) Application and Performance of CBN Wheels for Precision Grinding. Abrasives Magazine, October/November 2000, pp. 36-41.

[24] X. Chen, W.B. Rowe & R. Cai (2002) Precision Grinding Using CBN Wheels. International Journal of Machine Tools & Manufacture, vol. 42, pp. 585-593.

[25] A.C. Carius (1984) Preliminaries to Success - Preparation of Grinding Wheels Containing CBN. SME Technical Paper MR84-547.

[26] Final Technical Report (1996) Computerized System for the Coordinated Design of Machine, Tool and Process Parameters in Superabrasive Precision Machining. BRITE/EURAM Project BREU-CT90-0304.

[27] E. Salje & H.G.v. Mackensen (1984) Dressing of Conventional and CBN Grinding Wheels with Form Rollers. Annals of the CIRP, vol. 33/1, pp. 205-209

[28] S. Malkin (1985) Current Trends in CBN Grinding Technology. Annals of the CIRP, vol. 34/2, pp. 557-563.

[29] E. Brinksmeier & M. Çinar (1995) Characterization of Dressing by Determination of the Collision Number of the Abrasive Grits. Annals of the CIRP, vol. 44/1, pp.299-304.

[30] H.K. Tönshoff, B. Karpuschewski, P. Andrae & A. Türich (1998) Grinding Performance of Superhard Abrasive Wheels. Annals of the CIRP, vol. 47/2, pp. 723-732.

[31] H. Noichl (2000) CBN Grinding of Nickel Alloys in the Aerospace Industry. Proceedings of the Intertech 2000 Conference, British Columbia, Canada, July 17-21.

[32] H.K. Tönshoff, B. Karpuschewski and T. Mandrysch (1999) Grinding Process Achievements and their Consequences on Machine Tools Challenges and Opportunities. Annals of the CIRP, vol. 48/2 pp. 651-668.

[33] R.I. King and R.S. Hahn (1986) Handbook of Modern Grinding Technology. Chapman and Hall Advanced Industrial Technology Series.

[34] T. Tawakoli (1993) High Efficiency Deep Grinding. Mechanical Engineering Publications Limited, London.

[35] X. Chen, W.B. Rowe, D.F. McCormack (1999) Transitional Temperature for Tensile Residual Stress in Grinding. Proceedings of the 15th International Conference on Computer-Aided Production Engineering. April 19-21. University of Durham, UK.

[36] H. Noichle (1999) Developments in Grinding Wheel Technology to Minimise Heat Generation. Proceedings of the IGT Annual Seminar, Advances in Grinding Technology.

[37] J.A. Webster (1990) Design of a 250m/s CBN Grinding Machine. 4th International Grinding Conference. October 9-11, Dearborn, Michigan. SME paper MR90-551.

[38] I. Inasaki, H.K. Tönshoff and T.D. Howes (1993) Abrasive Machining in the Future. Annals of the CIRP, vol 42/2, pp.723-732.

[39] T.R.A. Pearce (1998) Does Vibration in Grinding Matter? Technical Meeting of the Institute of Grinding Technology. November 4, University of Bristol.

[40] M. Weck and A. Koch (1993) Spindle-Bearing Systems for High-Speed Applications in machine Tools. Annals of the CIRP, vol. 42/1, pp. 445-448.

[41] H. Aramaki, Y. Shoda, Y. Morishita and T. Sawamoto (1988) The Performance of Ball Bearings with Silicone Nitride Ceramic Balls in High Speed Spindles for Machine Tools. ASME Journal of Tribology, October, vol. 110, pp. 693-698.

[42] W.B. Rowe (1967) Experience with Four Types of Grinding Machine Spindle. Proceedings of the 8th International M.T.D.R. Conference. pp. 453-476.

[43] F. Klocke & J. Muckli (1999) Grinding at its Limits - High Speed Grinding. 3rd International Machining and Grinding Conference. SME paper MR99-232.

[44] R.B Aronson (1998) Spindles for 2000 and Beyond. Manufacturing Engineer, vol. 7/98, pp. 106-113. USA.

[45] Y. Furukawa & M. Yokogawa (1990) Effects of Machine Rigidity on the Dressing Accuracy of CBN Grinding Wheels. Annals of CIRP, vol. 39/1, pp. 305-308.

[46] J. Webster and M. Hitchiner (2000) Recent Advances in Camshaft and Crankshaft Grinding. Proceedings of the Intertech 2000 Conference, British Columbia, Canada, July 17-21.

[47] M. Hitchiner (2002) Practical Challenges to the Application to High Wheel Speeds to Grinding. Contribution to San Sebastion CIRP STC. 'G' meeting, August 2002.

[48] F. Engineer, C. Guo & S. Malkin (1992) Experimental Measurement of Fluid Flow Through the Grinding Zone. Transactions of ASME, vol. 114, pp. 61-66.

[49] C. Guo, S. Malkin (1992) Analysis of Fluid Flow Through the Grinding Zone. Journal of Engineering for Industry, vol. 114, pp. 427-434.

[50] J. Webster (1995) Selection of Coolant Type and Application Technique in Grinding, Supergrind 1995 – Grinding and Polishing with Superabrasives. Connecticut, USA, November 2-3, pp. 205 – 220.

[51] F. Klocke, T. Beck, G. Eisenblatter and D. Lung (2000) Minimal Quantity Lubrication (MQL) in Cutting and Grinding. 12th International Colloquium Industrial and Automotive Lubrication, Techbische Akademie Essligen.

[52] F. Klocke, T. Beck, G. Eisenblatter, R. Fritsch, D. Lung and M. Pohls (2000) Applications of Minimal Quantity Lubrication – Motivation, Fundamentals, Vistas.

12th International Colloquium Industrial & Automotive Lubrication, Techbische Akademie Essligen.

[53] J.A. Webster, C. Cui, & J.B. Mindek (1995) Grinding Fluid Application System Design. Annals of the CIRP, vol. 44/1.

[54] F. Klocke, A. Baus and T. Beck (2000) Coolant Induced Forces in CBN High Speed Grinding with Shoe Nozzles. Annals of the CIRP, vol. 49/1.

[55] J. Webster, E. Brinkmeier, C. Heinzel, M. Wittmann and K. Thoens (2002) Assessment of Grinding Fluid Effectiveness in Continuous-Dress Creep Feed Grinding. Annals of the CIRP, vol. 51/1.

[56] S. Ebbrell, N.H. Woolley, Y.D. Tridimas, D.R. Allanson, & W.B. Rowe (1997) The Effects of Cutting Fluid Application During the Grinding Process. Proceedings of 13th National Conference of Manufacturing. Glasgow, pp.486-490.

[57] S. Ebbrell, N.H. Woolley, Y.D. Tridimas, D.R. Allanson, & W.B. Rowe (2000) The Effects of Cutting Fluid Application Methods on the Grinding Process. International Journal of Machine Tools and Manufacture, vol. 40, No. 2. pp. 209-223.

[58] W.B. Rowe and T. Jin (2001) Temperatures in High Efficiency Deep Grinding (HEDG). Annals of the CIRP, vol. 50/1.

[59] T. Akiyama, J. Shibata & S. Yonetsu (1984) Behaviour of Grinding Fluid in the Gap of the Contact Area between a Grinding Wheel and Workpiece. Proceedings of the 5th International Conference of Production Engineering, Tokoyo.

[60] G. Trmal & H. Kaliszer (1976) Delivery of Cutting Fluids in Grinding, Institute of Mechanical Engineers, Sept. pp. 95-100.

[61] J.D. Campbell (1995) Optimised Coolant Application, 1st International Machining and Grinding Conference Michigan. USA. 12-14 Sept. Society of Manufacturing Engineers.

[62] G.I. Alden (1914) Operation of Grinding Wheels in Machine Grinding. Trans. ASME paper no. 1446, pp. 451-460.

[63] R. Snoeys, J. Peters & A. Decneut (1974) The Significance of Chip Thickness in Grinding. Annals of the CIRP vol. 23/2.

[64] W.B. Rowe (2001) Temperature Case Studies in Grinding Including an Inclined Heat Source Model. Proceedings of the Institute of Mechanical Engineers, vol. 215, part B.

[65] M.C. Shaw (1996) Energy Conversion in Cutting and Grinding. Annals of the CIRP, vol 45/1 pp.101-104.

[66] W.B. Rowe & X. Chen (1997) Characterisation of the Size Effect in Grinding and the Sliced Bread Analogy. International Journal of Production Research, vol. 35 no. 3, pp. 887-899.

[67] S.F. Krar & E. Ratterman (1990) Grinding and Machining with CBN and Diamond. McGraw Hill.

[68] W.B. Rowe, M.N. Morgan and D.R. Allanson (1991) An Advance in the Modelling of Thermal Effects in the Grinding Process. Annals of the CIRP, vol. 40/1, pp. 339-345.

[69] J. Woolman and R.A. Mottram (1966) The Mechanical and Physical Properties of the British Standard En Steels. The British Iron and Steel Research Association. Pergamon, Oxford.

[70] R.C. DeVries (1972) Cubic Boron Nitride: Handbook of Properties. General Electric Report No. 72CRD178.

[71] M.C. Shaw (1990) A Simplified Approach to Workpiece Temperatures in Fine Grinding. Annals of the CIRP, vol. 39, pp. 345-347.

[72] W.B. Rowe, S.C.E. Black, B. Mills, M.N. Morgan and H.S. Qi (1997) Proceedings of the Royal Society, part A 543, pp. 1083-1104.

[73] W.B. Rowe, J.A. Pettit, A. Boyle and J.L. Moruzzi (1988) Avoidance of Thermal Damage in Grinding and Prediction of the Damage Threshold, Annals of the CIRP, vol. 37/1, pp.557-559.

[74] H.S. Qi (1996) A Contact Length Model for Grinding Wheel-Workpiece Contact. Liverpool John Moores University. UK.

[75] T.D. Howes, K. Neailey and A.J. Harrison (1987) Fluid Film Boiling in Shallow-Cut Grinding. Annals of the CIRP, vol. 36, pp. 223-226.

[76] E. Brinksmeier, C. Heinzel and M. Wittman (1999) Friction, Cooling and Lubrication in Grinding. Annals of the CIRP, vol. 48/2, pp.1-18.

[77] R. Snoeys and D. Brown (1969) Dominating Parameters in Grinding Wheel and Workpiece Regenerative Chatter. Proceedings of the 10th International Machine Tool Design Research Conference, University of Birmingham, September, pp. 325-348.

[78] R. Snoeys (1971) Dominating Parameters of Grinding Machine Stability. Het Ingenieursblad, 40e, no. 4.

[79] I. Inasaki, B. Karpuschewski and H.S. Lee (2001) Grinding Chatter – Origin and Suppression. Annals of the CIRP, vol. 50/2, pp. 1-20.

[80] S.A. Tobias (1965) Machine Tool Vibration. Blackie and Son Ltd.

[81] F. Koenigsberger and J.F. Tlusty (1970) Machine Tool Structures. Pergamon Press.

[82] H.E. Merritt (1965) Theory of Self-Excited Machine Tool Chatter. Contribution to Machine Tool Chatter Research 1. Transactions of ASME, Journal of Engineering for Industry, vol. 87, pp. 447-454.

[83] J.S. Sexton, T.D. Howes and B.J. Stone (1982) The Use of Increased Wheel Flexibility to Improve Chatter Performance in Grinding. Proceedings of the Institute of Mechanical Engineers, vol. 196, pp. 291-300.

[84] W.B. Rowe (1974) An Experimental Investigation of Grinding Compliances and Improvements in Productivity. Proceedings of the 14th International Machine Tool Design and Research Conference. University of Birmingham, pp. 479-486.

[85] H.K. Tönshoff & T. Grabner (1984) Cylindrical and Profile Grinding with Boron Nitride Wheels. Proceedings of the 5th International Conference on Production Engineering. pp. 326-344.

[86] L.I. Smith & Y.Tsujigo (1977) An Analysis of CBN Grinding. Cutting Tool Engineering - Diamond / Superabrasive Directory 1977-1978, pp. 49-60. USA.

[87] W. Hinz, H. Hottek and M. Roth (2000) Economic Centreless Grinding of Camshafts with CBN. Industrial Diamond Review, vol. 60, no. 585, pp.102-106.

[88] M.C. Shaw (1975) Cost Reduction in Stock Removal Grinding. Annals of the CIRP, vol. 24/2.

[89] D.A. Farmer and M.C. Shaw (1967) Abrasive Machining Economics. ASTME Paper No. MR67-595.

[90] J. Peters (1972) Economic Selection of Grinding Wheels: Introduction of Wheel Efficiency Parameter. Proceedings of the International Grinding Conference, Pittsburgh.

[91] G.S. Reichenbach and L. Coes (1972) The Mechanics and Economics of Steel Conditioning. Proceedings of the International Grinding Conference, Pittsburgh.

[92] B. N. Colding (1959) Machining Economics: A Wear Relationship for Turning, Milling and Grinding. Hakan Ohlssons Boktryckeri, Stockholm.

[93] W.R. Backer and E.J. Krabacher (1956) New techniques in Metal-Cutting Research. Transactions of ASME, October.

[94] J.W. Liverton (2001) New Developments in CNC Surface Grinding. Proceedings of the 4th International Machining and Grinding Conference, Troy, Michigan, USA 7-9 May.

[95] D.J. Ewins (2000) Modal Testing: Theory, Practice and Application. Research Studies Press Ltd. England. Second Edition.

[96] W.B. Rowe (1964) Some Studies of the Centreless Grinding Process with Particular Reference to the Roundness Accuracy. Ph.D. Thesis, The Victoria University of Manchester. UK.

[97] Taylor Hobson Ltd. Form Talysurf Series Operators Handbook. Publication No. RTH-HB-100.

[98] Taylor Hobson Ltd. Talyrond 210 Operators Handbook. Issue 1, Revision 1.10 PR.

[99] Mitutoyo. LSM-6000/6000S Laser Scan Micrometer User's Manual. No. 99MBC014A, Series No. 544.

[100] D.M. Grove & T.P. Davis (1992) Engineering, Quality and Experimental Design. Longman Scientific and Technical.

[101] P.J. Ross (1996) Taguchi Techniques for Quality Engineering. McGraw-Hill, Second Edition.

[102] G.M. Clarke and R.E. Kempson (1997) Introduction to the Design and Analysis of Experiments. Arnold.

[103] D.C. Montgomery and G.C. Runger (1999) Applied Statistics and Probability for Engineers. John Wiley and Sons, Second Edition.

[104] R.Cai (2002) Assessment of Vitrified CBN Wheels for Precision Grinding. Ph.D. Thesis. Liverpool John Moores University. UK.

[105] P.L. Tso (1995) Study on the Grinding of Inconel 718. Journal of Materials Processing Technology, vol. 55 pp. 421-426

[106] S.G. Hess, P.D. Redington, R. Li and M. Cooper (2000) Vitrified CBN Superabrasives: A Brand-New, Proven Technology for Aerospace Applications. Proceedings of the Intertech 2000 Conference, British Columbia, Canada, July 17-21.

[107] M.W. Bailey and M.W. Cook (2000) The Future of Ultrahard Machining in the Aerospace Industry. Proceedings of the Intertech 2000 Conference, British Columbia, Canada, July 17-21.

[108] Universal (1992) The Grinding Data Book. Published by Unicorn Abrasives Ltd.

[109] N. Barlow (1988) High-Rate Grinding Wheel Design. Ph.D. Thesis, Liverpool Polytechnic. UK.

APPENDICES

APPENDIX A

Supplementary Figures for Chapter 5

Figure A1. Photograph of the Suprema high-speed precision grinding machine.

Figure A2. Photograph showing the wheelhead, workhead tailstock and dresser unit.

Figure A3. Photograph showing the general arrangement of the vibration testing equipment.

Figure A4. Photograph showing the application of harmonic excitation to the workhead/workpiece/tailstock system and measurement of response.

Figure A5. Photograph of the granite block support for the dresser unit showing the effect loose inserts.

Figure A6. Photograph showing the wheelhead motor stripped down after a bearing failure.

Figure A7. Photograph of the wheelhead spindle stripped down after failure of rear hydrostatic bearing.

Figure A8. Photograph showing close up view of rear journal showing burn marks from contact with bearing surface.

Figure A9. Photograph showing rear hydrostatic bearing of wheelhead spindle.

Figure A10. Photograph showing front hydrostatic bearing of wheelhead spindle.

Figure A11. Graph showing the trend of temperatures of various parts of the Suprema during warm up.

Figure A1. Photograph of the Suprema high-speed precision grinding machine.

Figure A2. Photograph showing the wheelhead, workhead, tailstock and dresser unit.

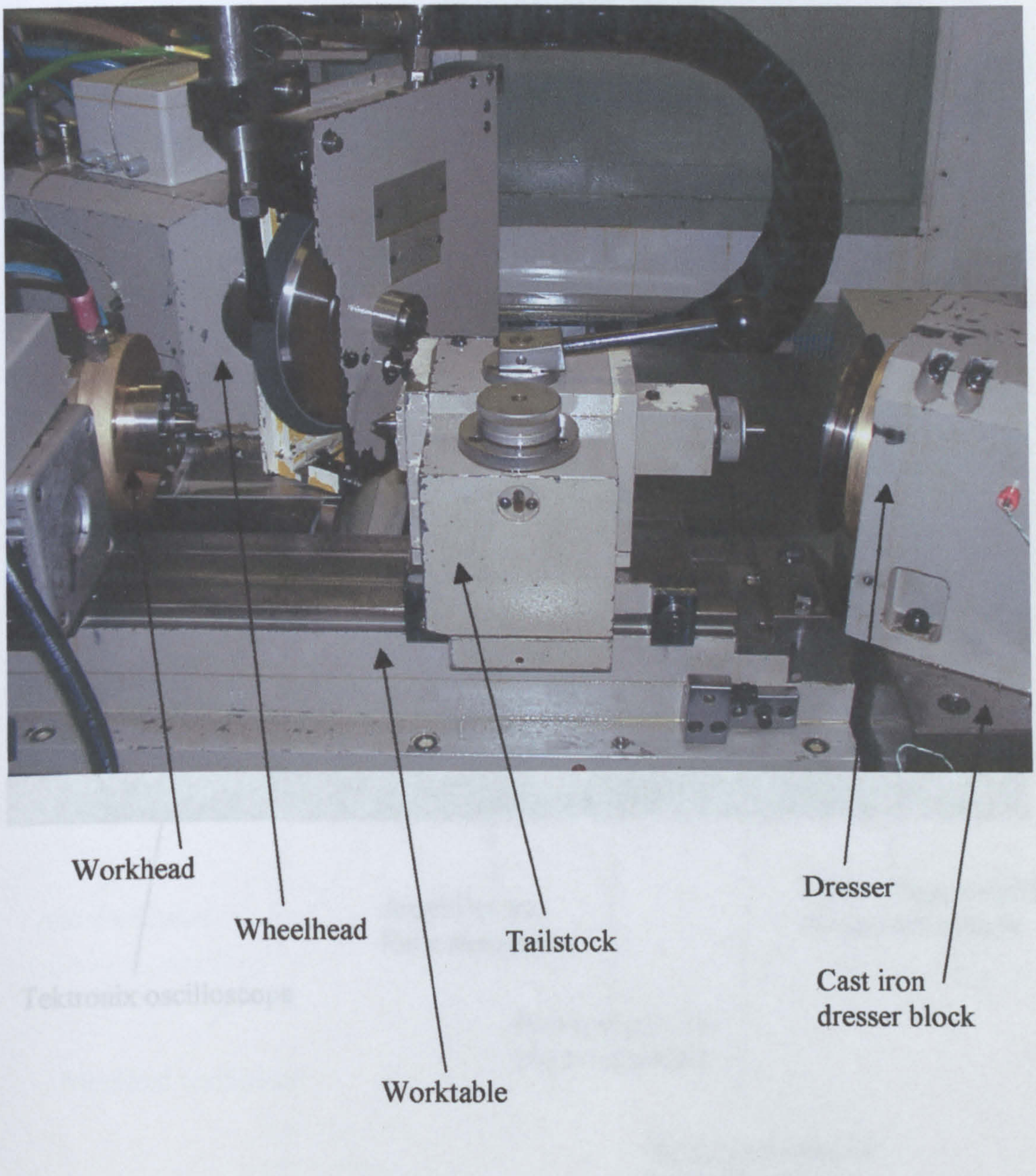

Figure A3. Photograph showing the general arrangement of the vibration testing equipment.

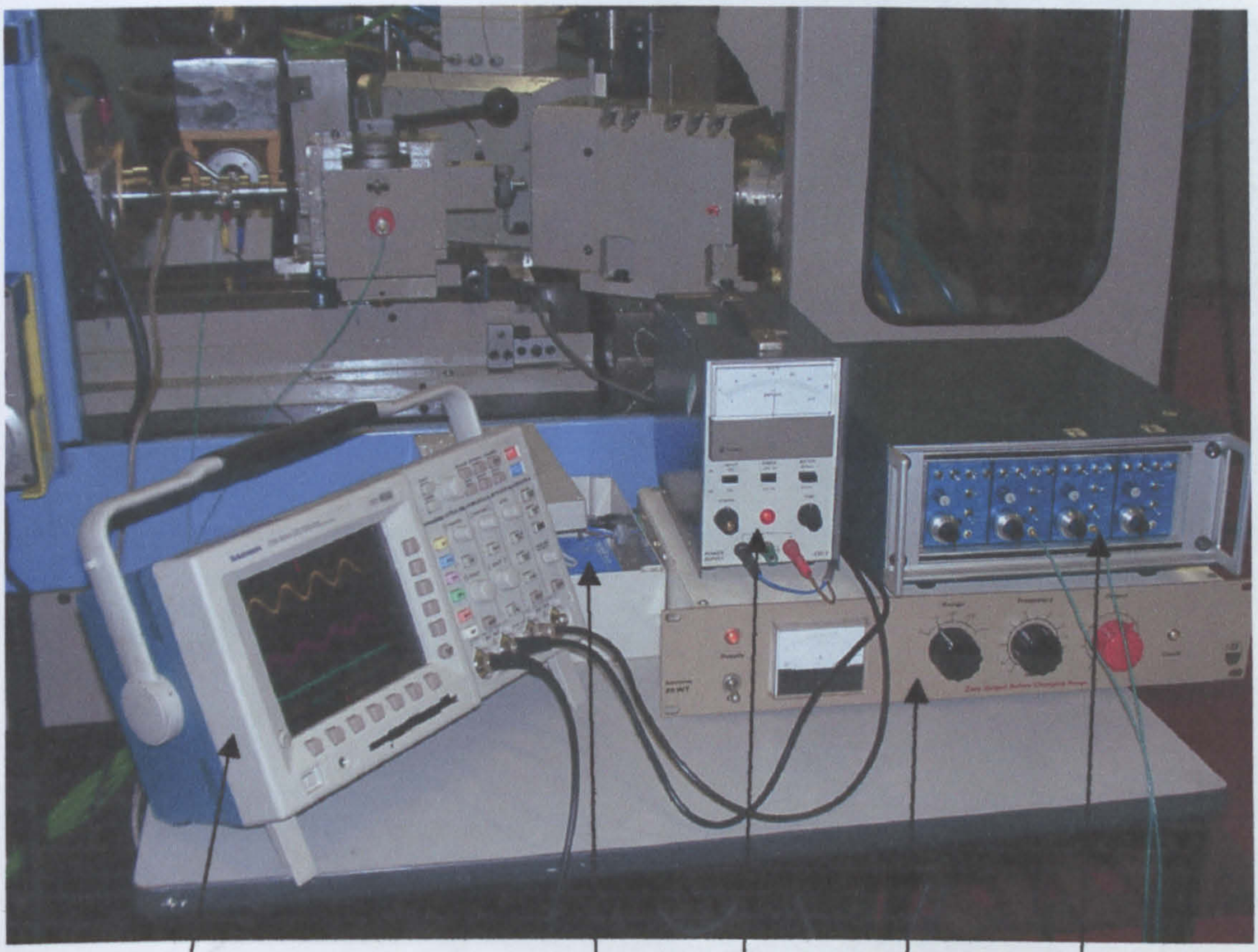

Figure A4. Photograph showing the application of harmonic excitation to the workhead/workpiece/tailstock system and measurement of response.

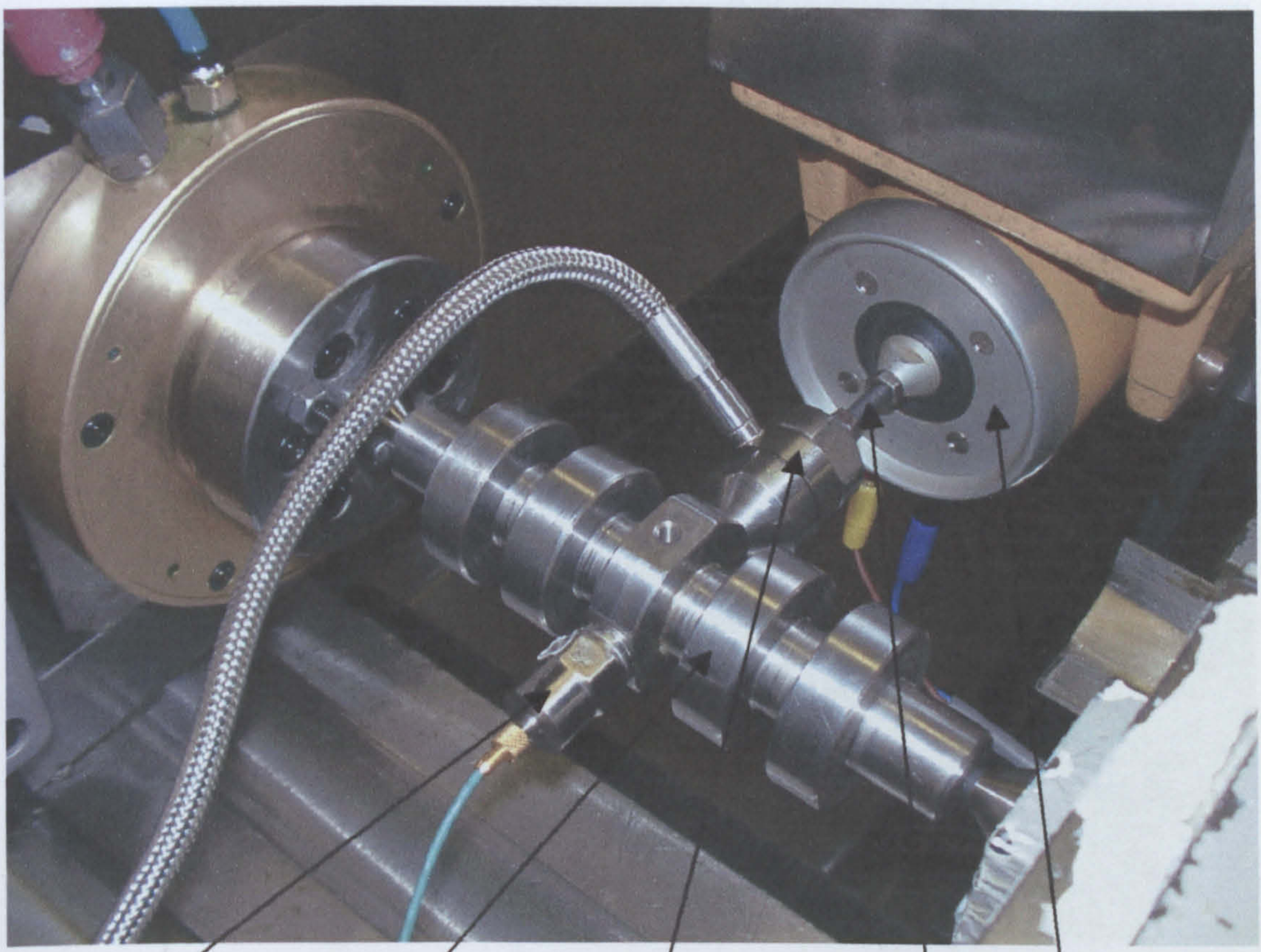

Figure A5. Photograph of the granite support block for dresser unit showing the effect of loose inserts.

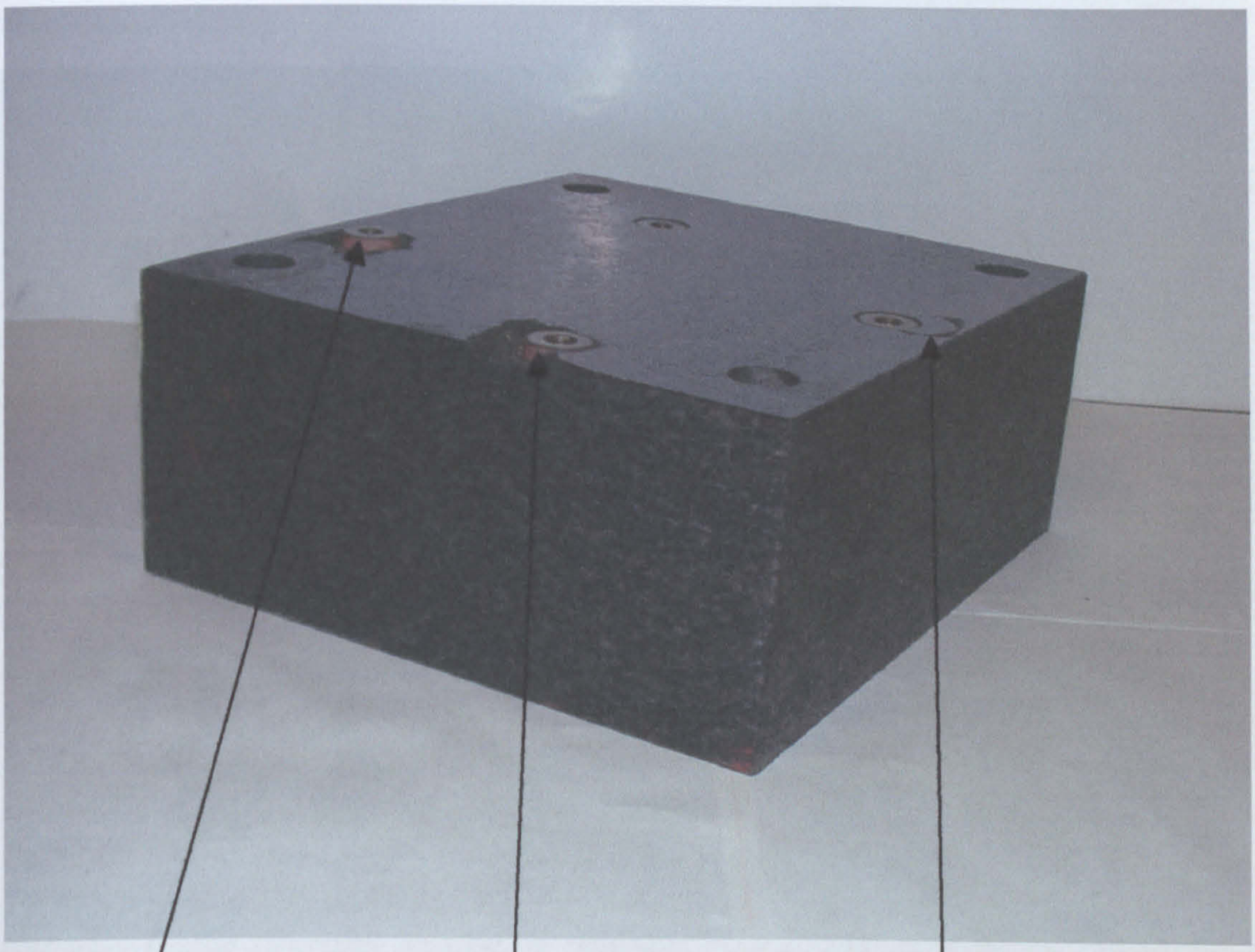

Figure A6. Photograph showing the wheelhead motor stripped down after a bearing failure.

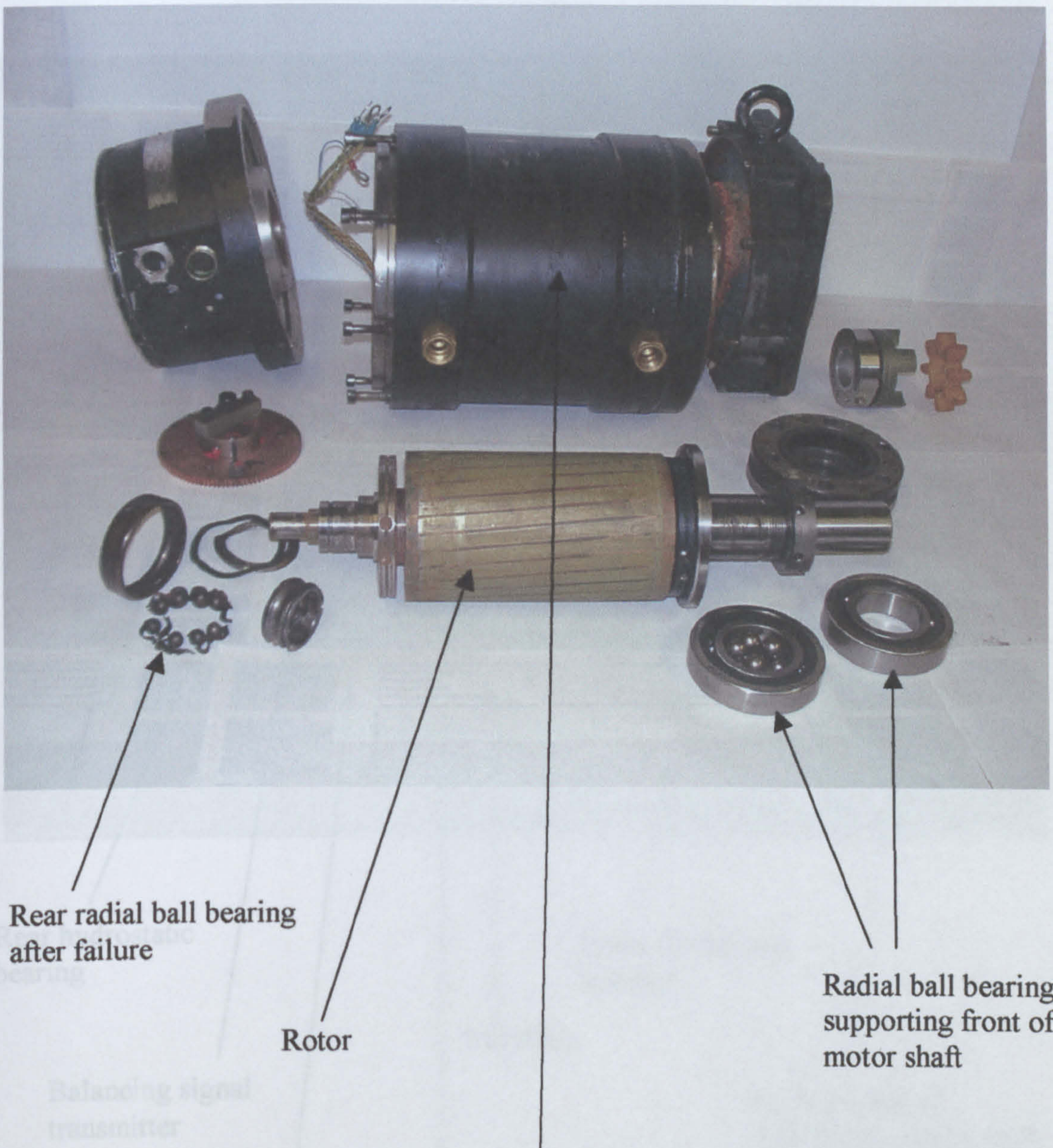

Figure A7. Photograph of the wheelhead spindle stripped down after failure of rear hydrostatic bearing.

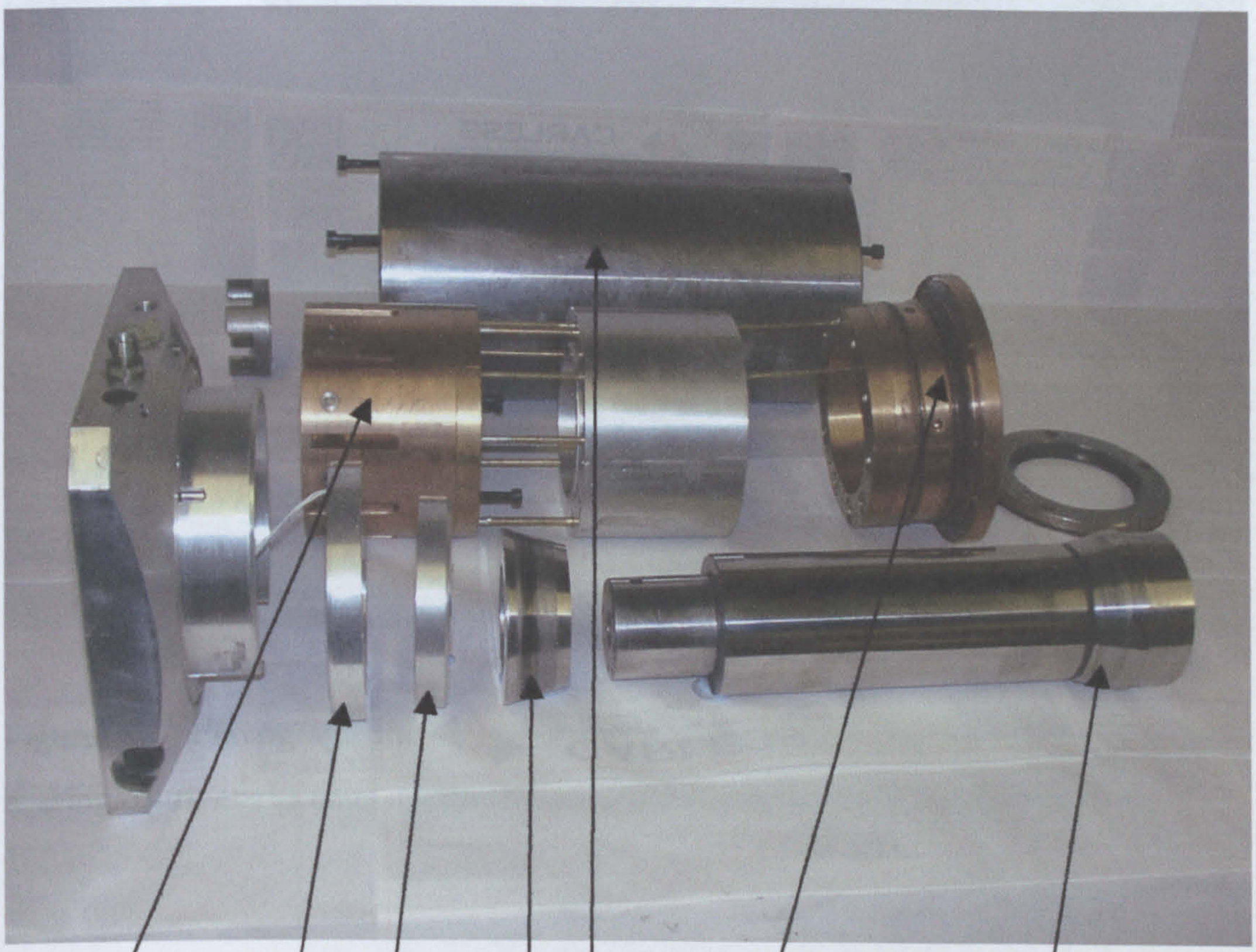

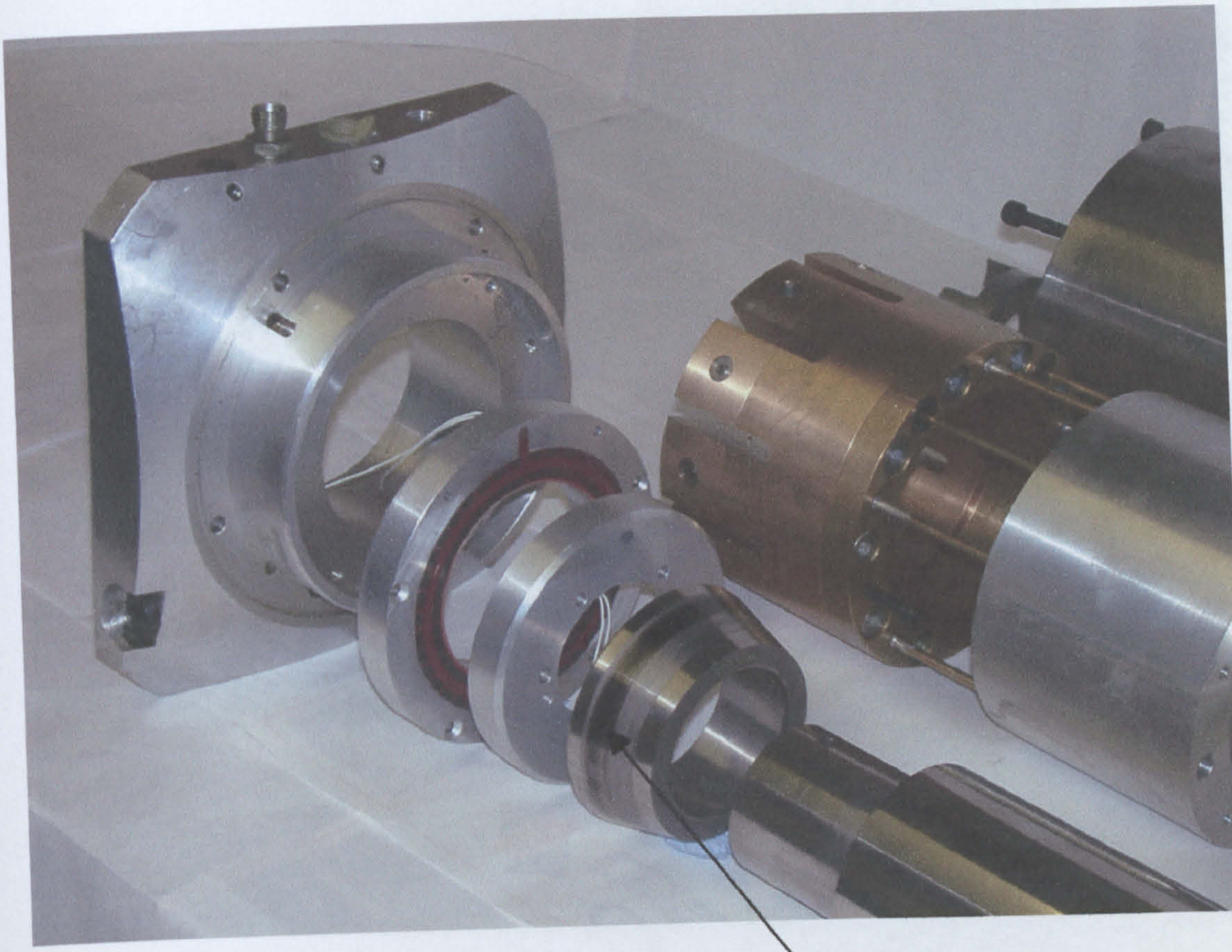

Figure A8. Photograph showing a close up view of rear journal of the hydrostatic bearing. Burn marks can be seen caused by contact with the bearing surface.

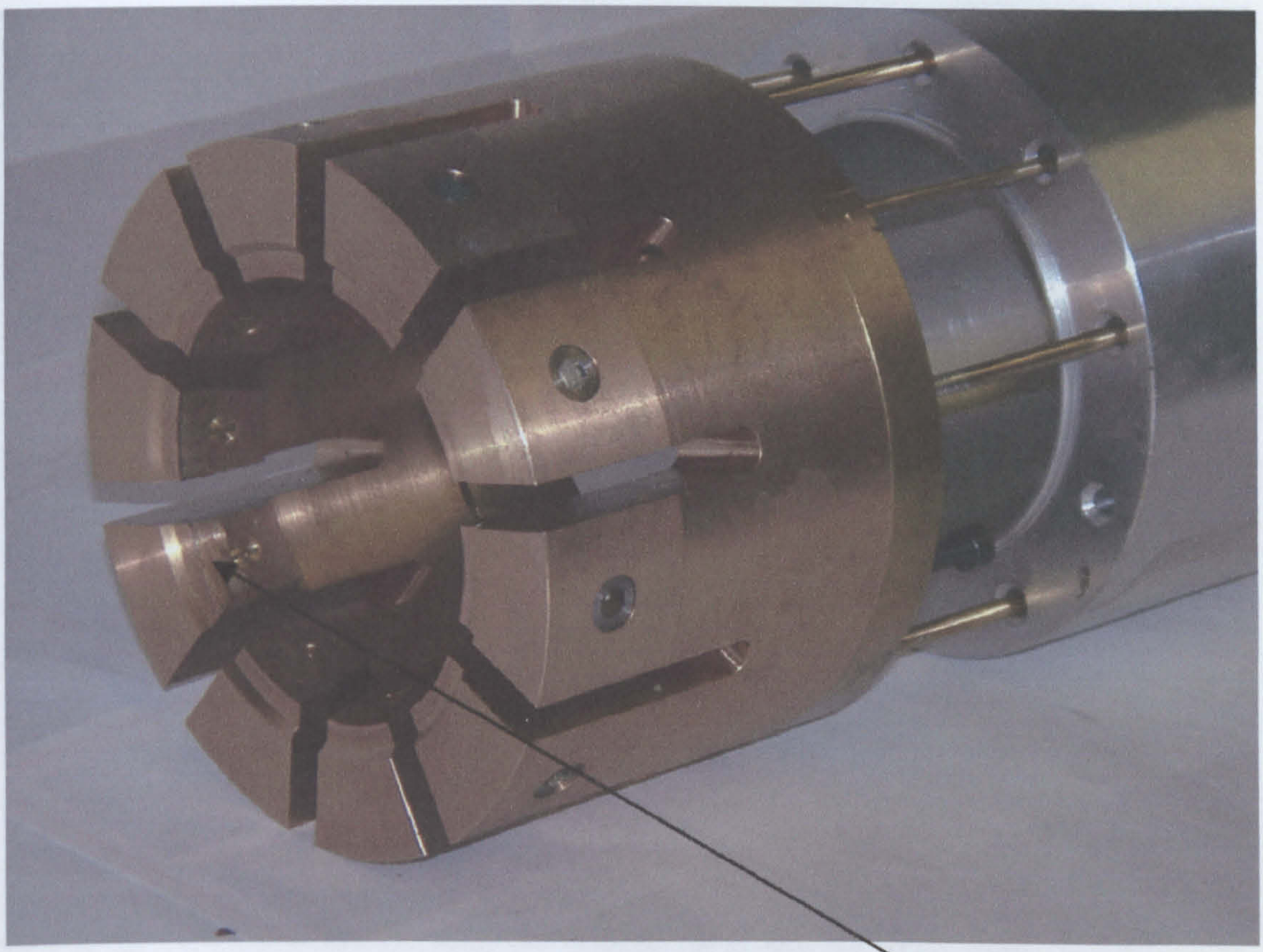

Figure A9. Photograph showing rear hydrostatic bearing of wheelhead spindle. The bearing surfaces are scuffed where contact with the rear journal was made.

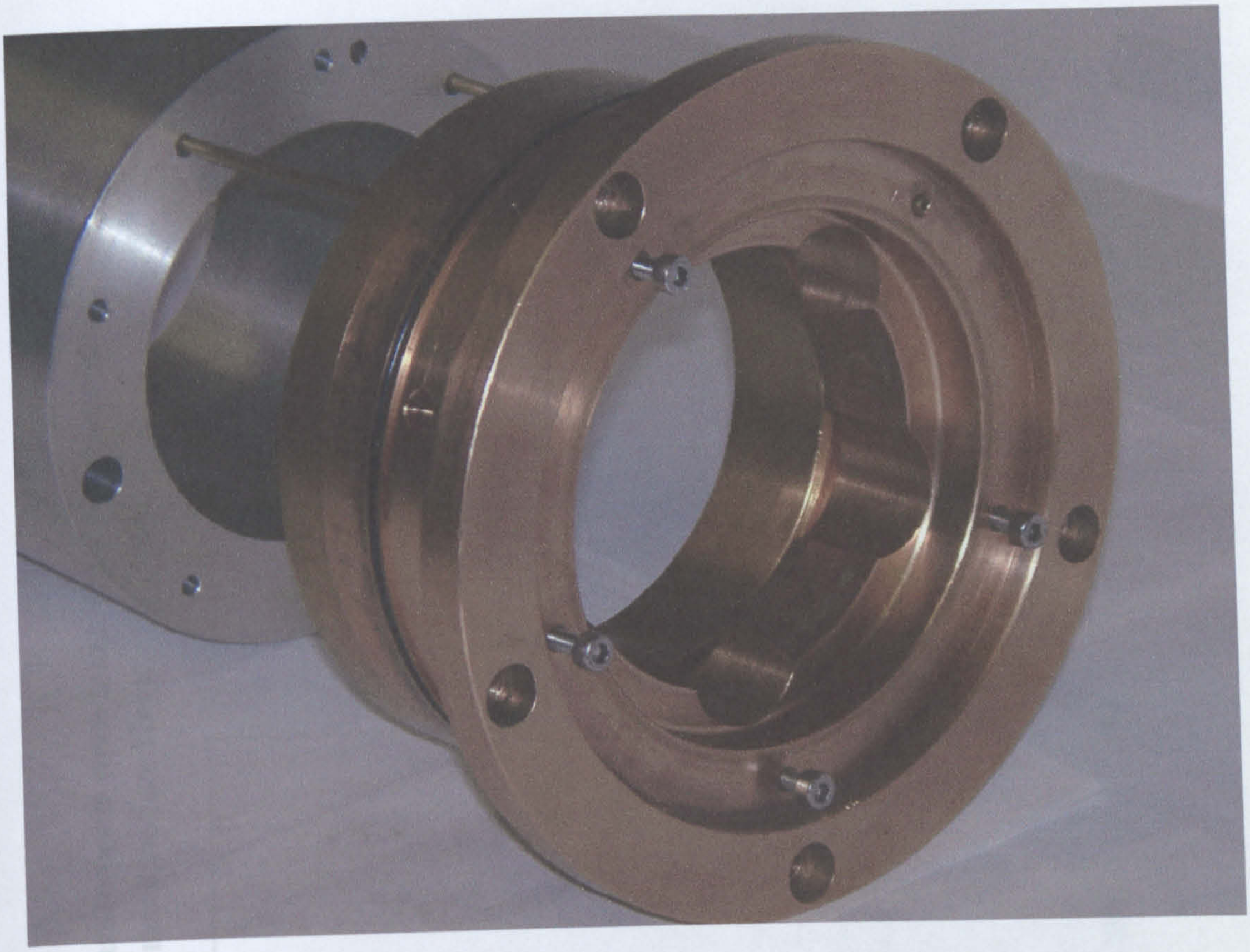

Figure A10. Photograph showing front hydrostatic bearing of wheelhead.

Figure A11. Temperature of Suprema during warm up. Measurements were taken from thermocouples mounted at various locations on the machine (see Key).

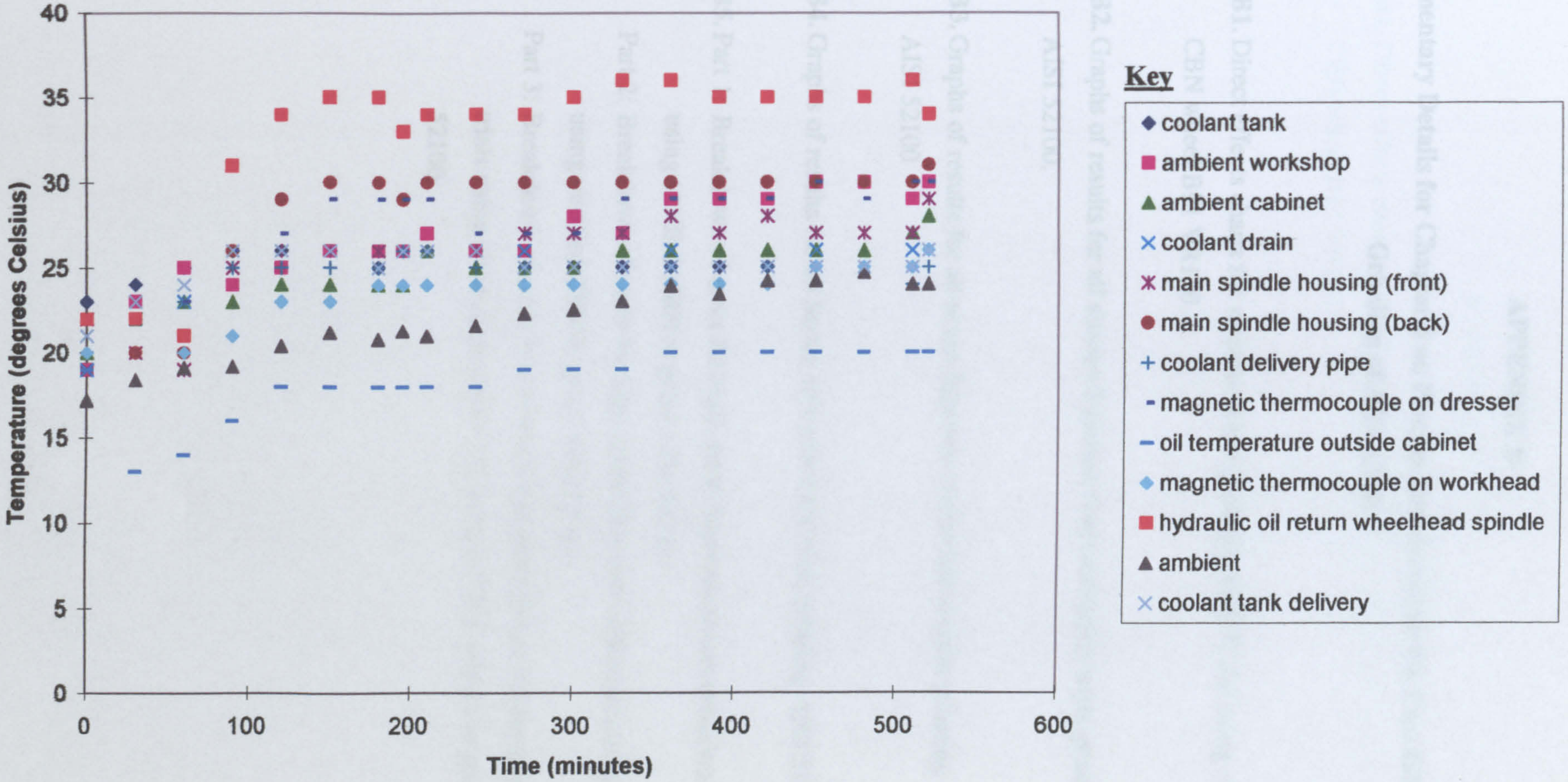

APPENDIX B

Supplementary Details for Chapter 6 on Process Requirements for Cost Effective Grinding of AISI 52100

Appendix B1. Direct effects charts for variance when grinding AISI 52100 using vitrified CBN wheel B91 VR150.

Appendix B2. Graphs of results for all sixteen Suprema characterisation trials grinding AISI 52100.

Appendix B3. Graphs of results for all seven Suprema confirmation trials grinding AISI 52100

Appendix B4. Graphs of results for all Series 10 benchmark trials grinding AISI 52100.

Appendix B5. Part 1: Breakdown of costs for high-speed Suprema characterisation trials using vitrified CBN to grind AISI 52100.

Part 2: Breakdown of costs for high-speed Suprema conformation trials using vitrified CBN to grind AISI 52100.

Part 3: Breakdown of costs for conventional-speed Series 10 Benchmark trials using aluminium oxide, sol gel and CBN wheels to grind AISI 52100.

APPENDIX B1

Appendix B1. Direct effects charts for variance when grinding AISI 52100 using vitrified CBN wheel B91 VR150.

Direct Effects of Process Parameters on Variance Using a CBN Grinding Wheel to Grind AISI 52100

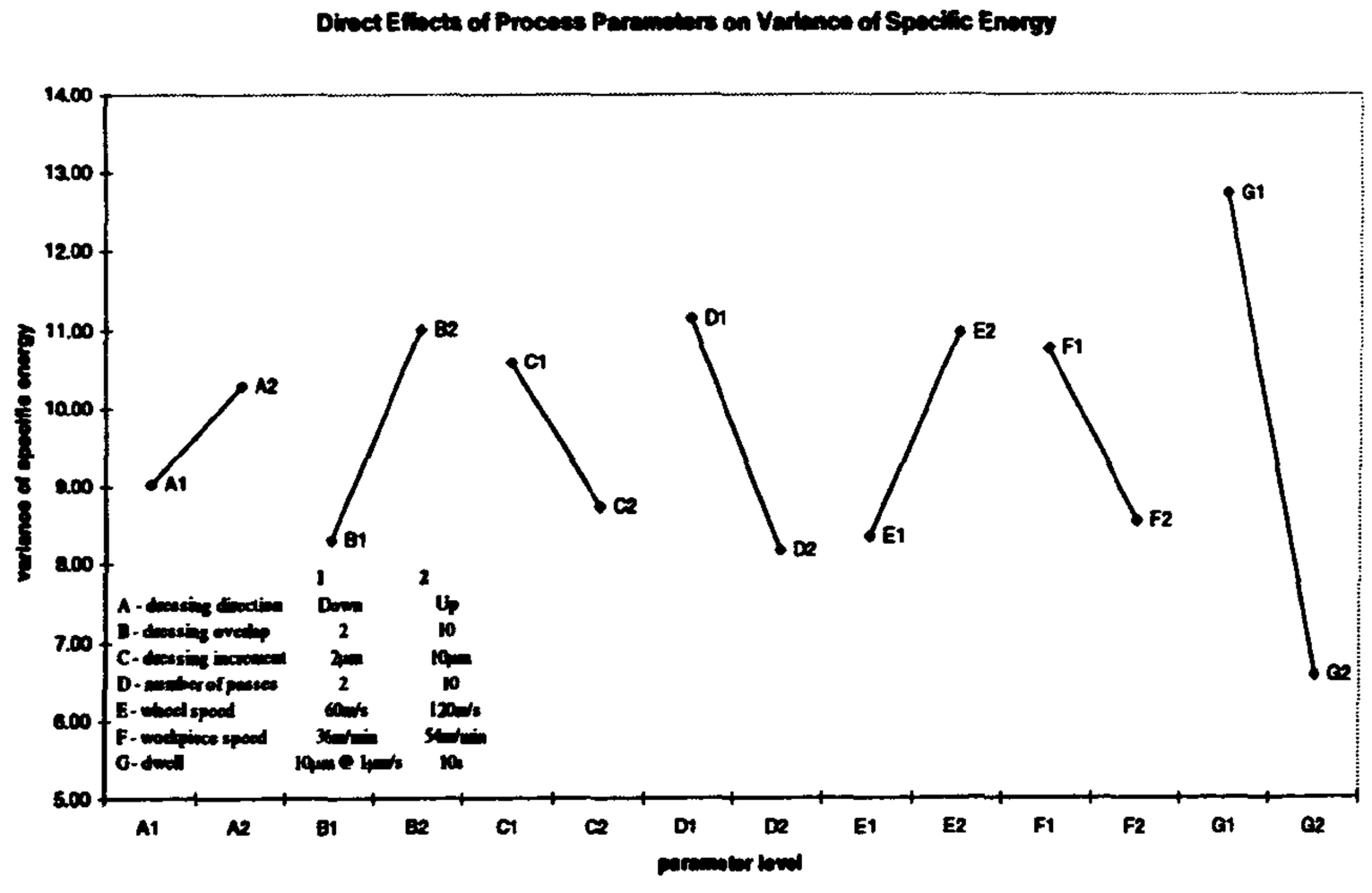

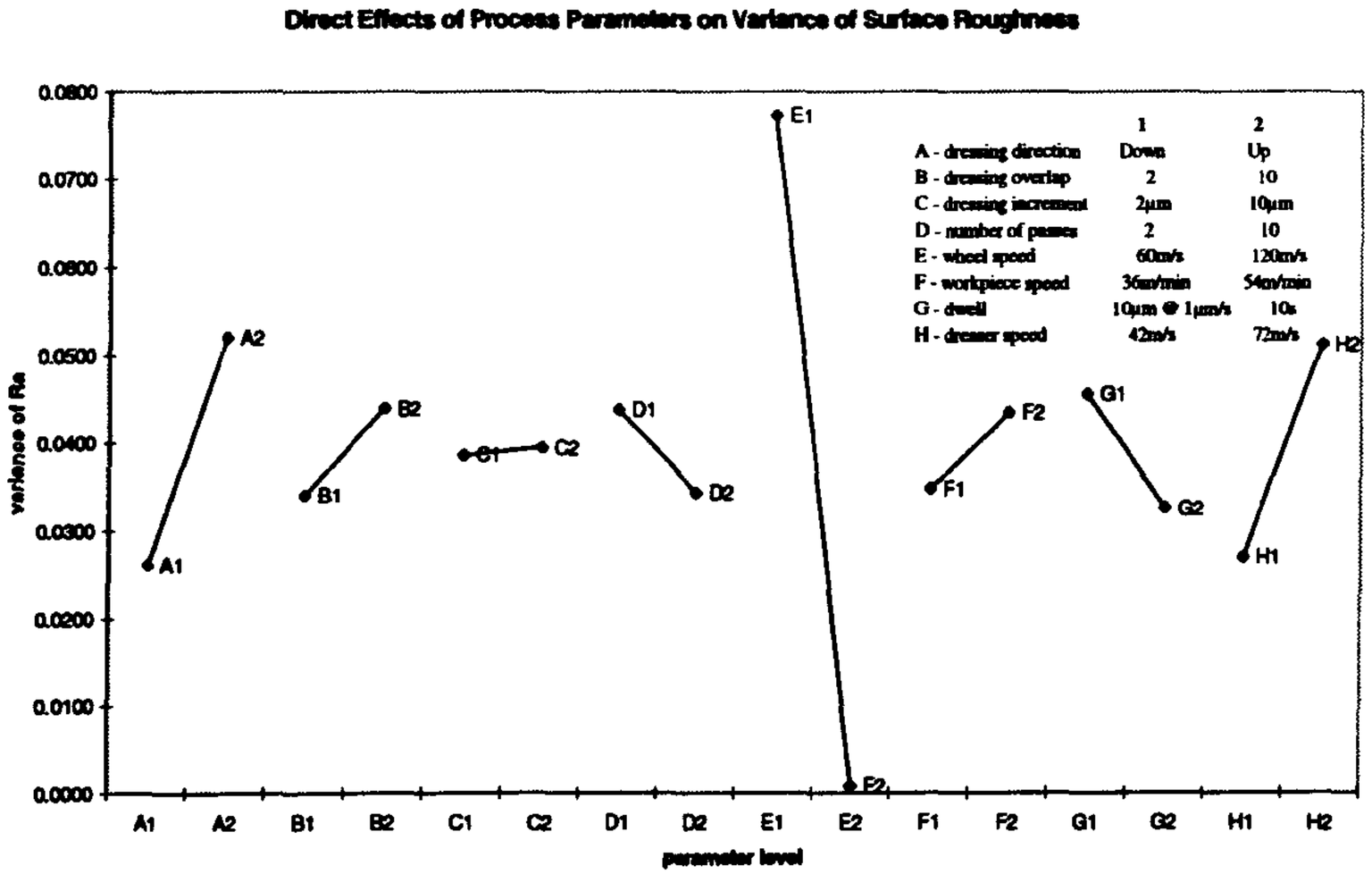

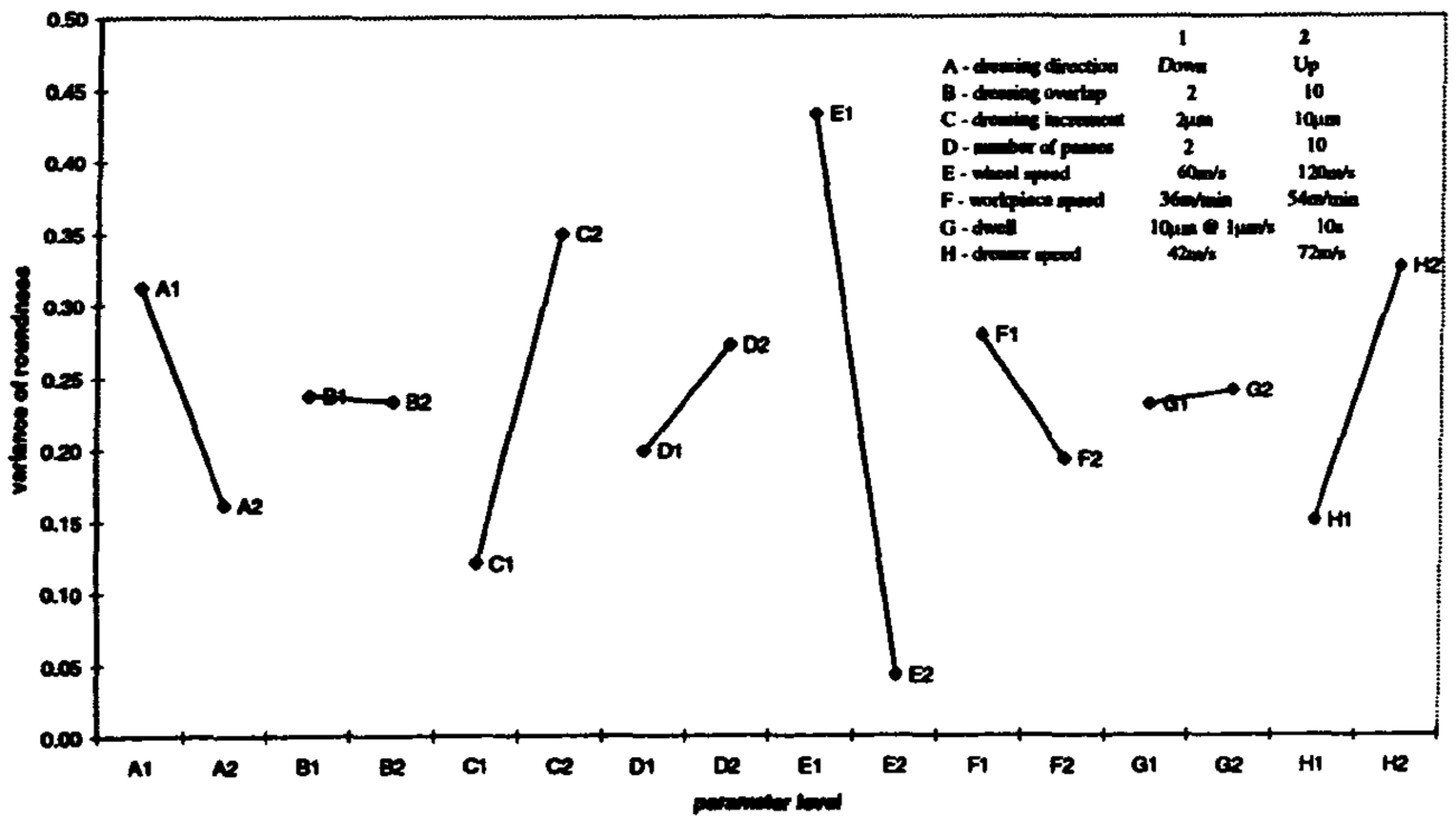

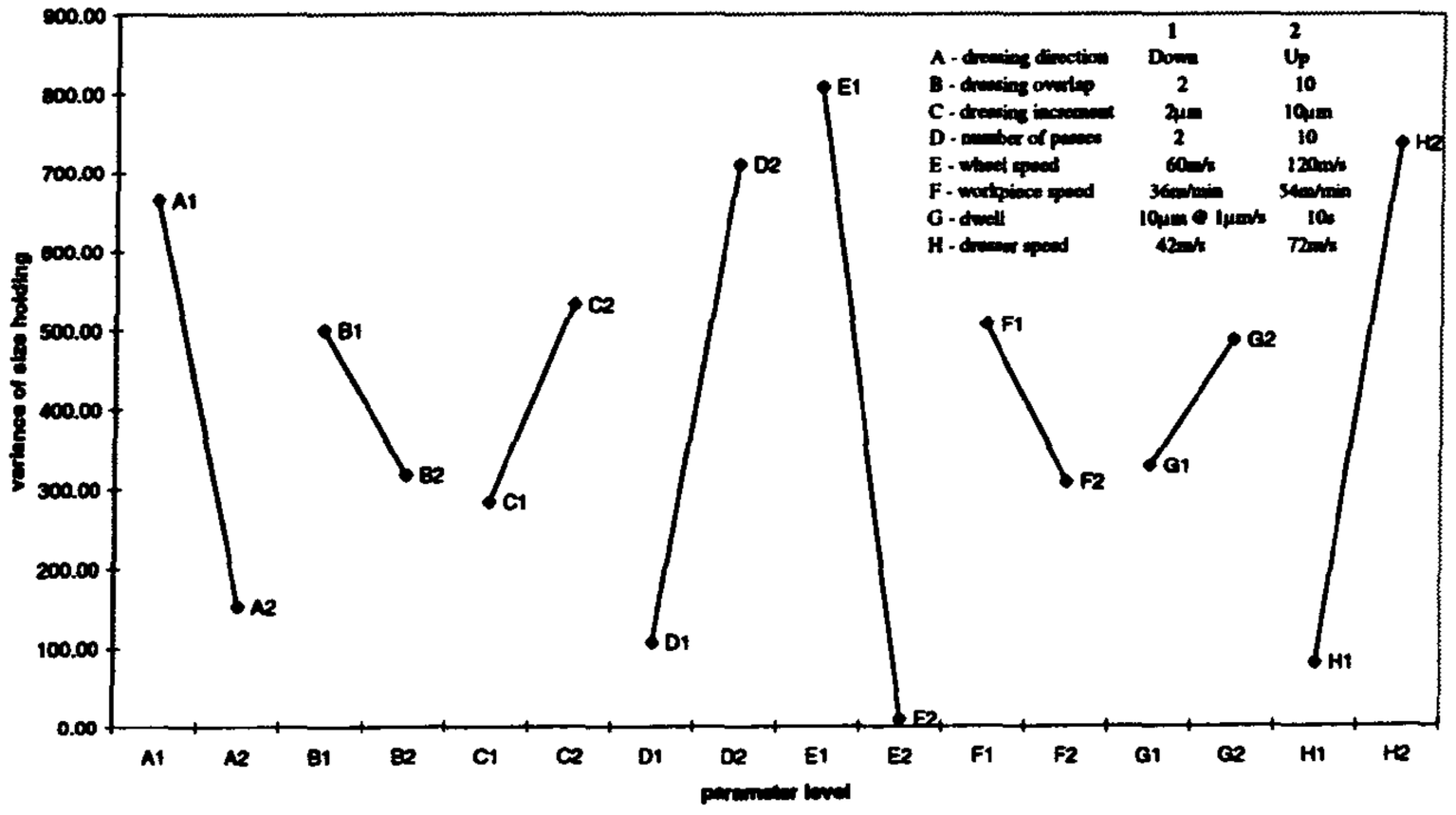

Grinding wheel: Vitrified CBN (B91VR150)
Grinding machine: J&S Suprema

Equivalent diameter: 34mm
Q'_w: 10mm³/mm s (v_f=0.081mm/s)

Coolant type: Castrol Hysol X (10% emulsion)
Coolant delivery: 36 litres/min (30 Bar pump pressure)

APPENDIX B2

Appendix B2. Graphs of results for all sixteen Suprema characterisation trials grinding AISI 52100.

Results for Suprema Characterisation Trial 1 (i.e. 1 of 16) Grinding AISI 52100 With a Vitrified CBN Wheel

<u>Experimental Conditions</u>

- Down dressing
- U_d: 2
- a_d: 2µm
- n_d: 2
- v_s: 60m/s
- v_w: 36m/min
- s:10µm@1µm/s
- v_R: 42m/s
-Q'w: 10mm³/mm s
- Wheel: B91VR150
- Coolant: Hysol X 36 l/min, 30Bar pump pressure

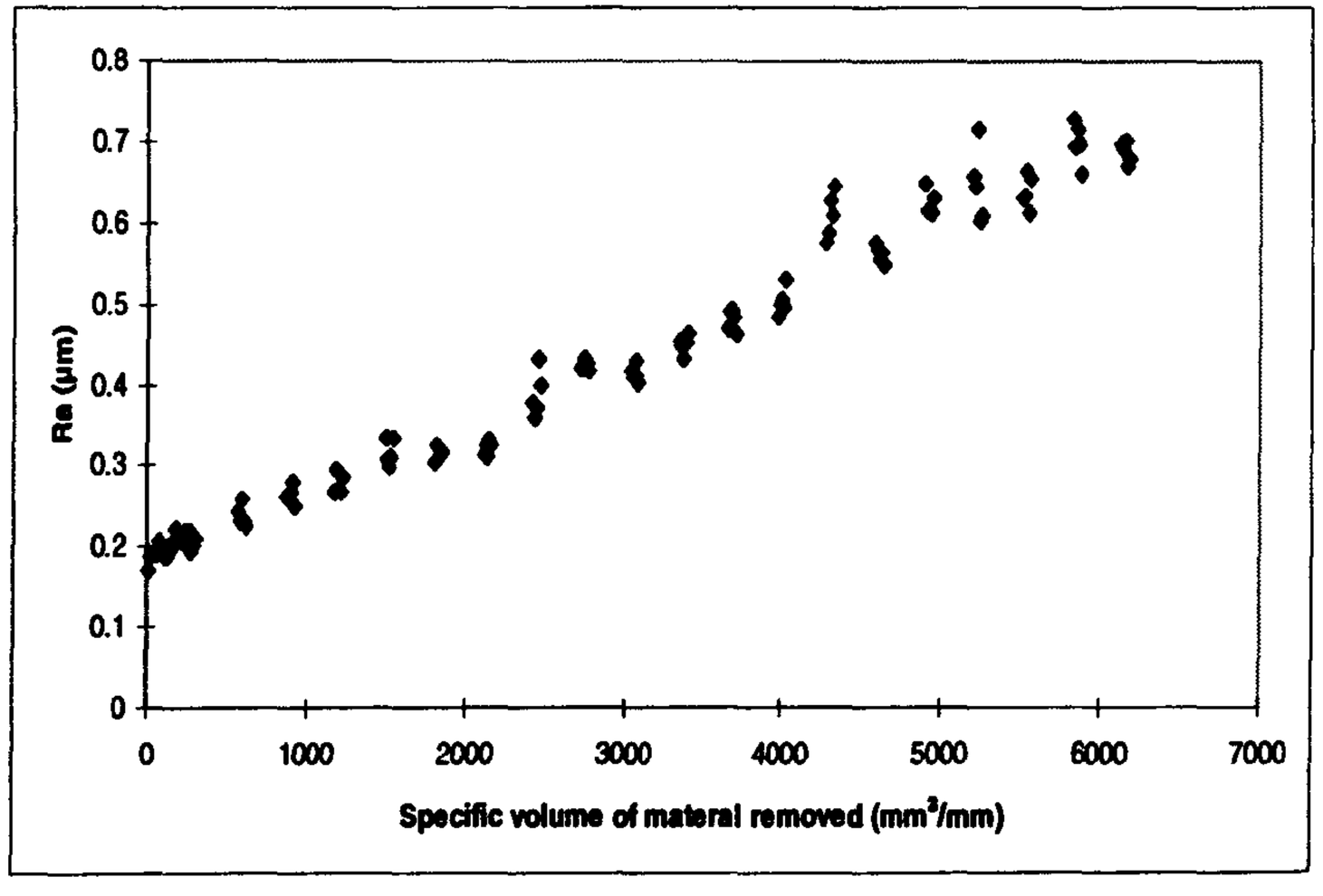

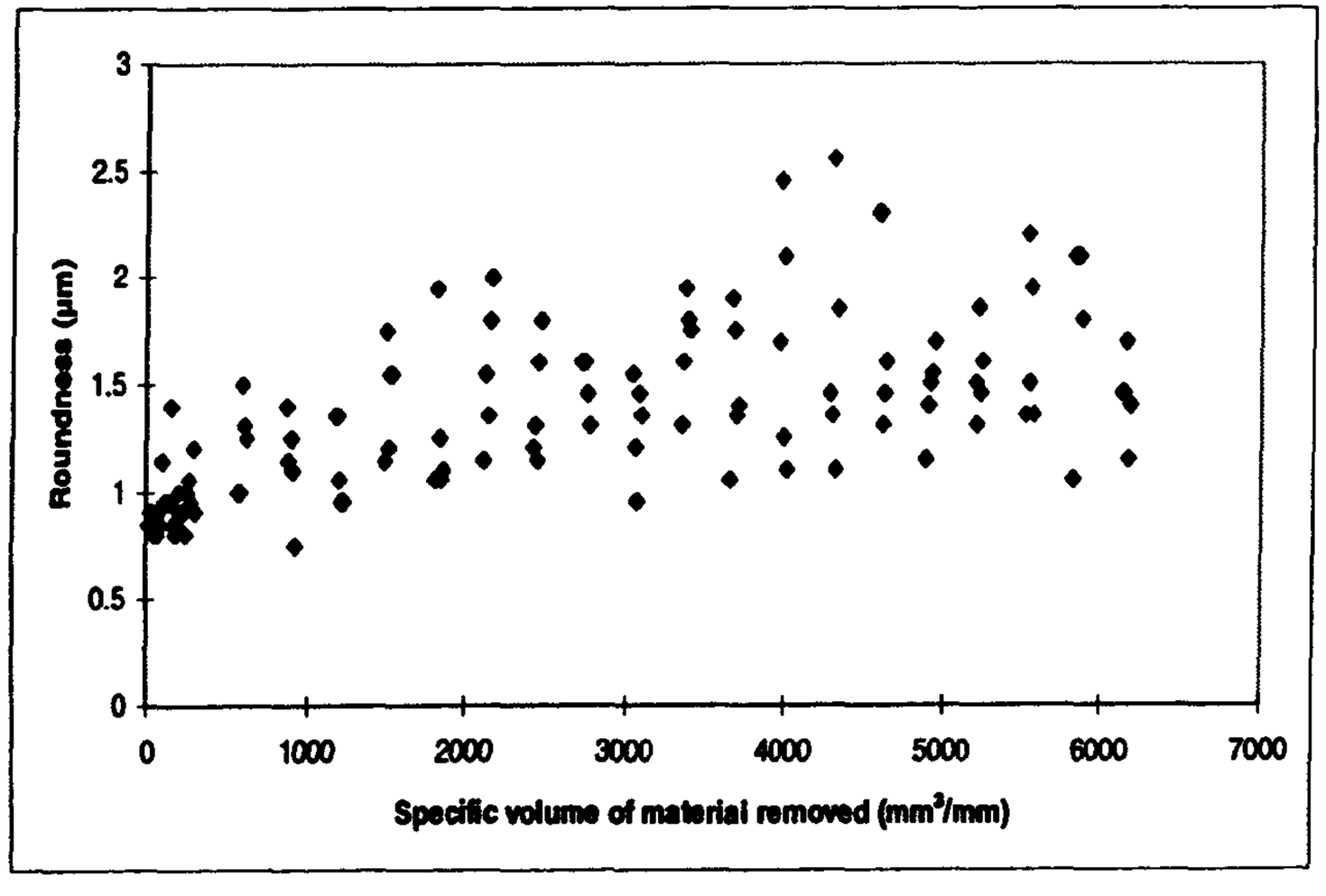

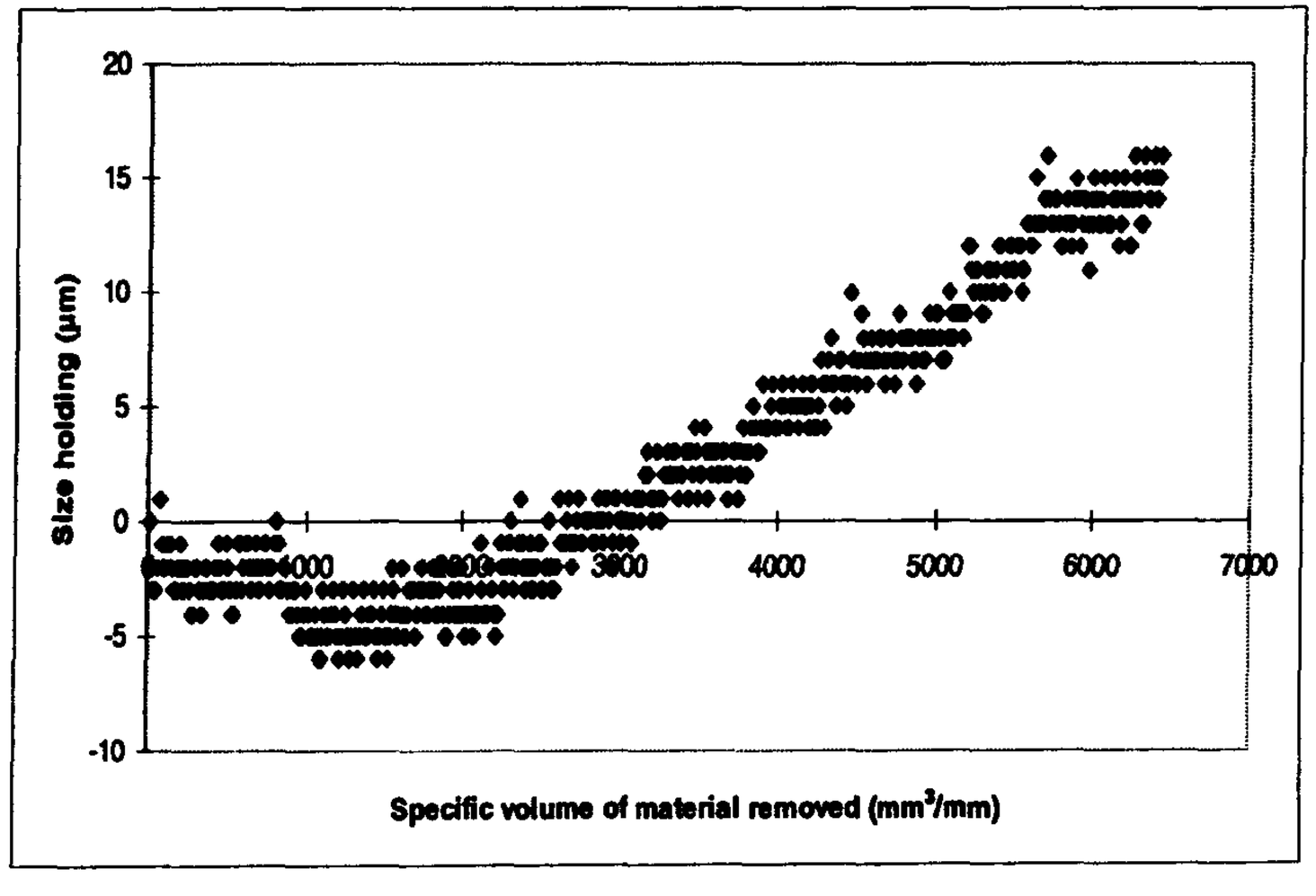

Results for Suprema Characterisation Trial 2 (i.e. 2 of 16) Grinding AISI 52100 With a Vitrified CBN Wheel

Experimental Conditions

- Down dressing
- U_d: 2
- a_d: 2µm
- n_d: 10
- v_s: 120m/s
- v_w: 54m/min
- s:10s
- v_R: 42m/s
-Q'w: 10mm³/mm s
- Wheel: B91VR150
- Coolant: Hysol X 36 l/min, 30Bar pump pressure

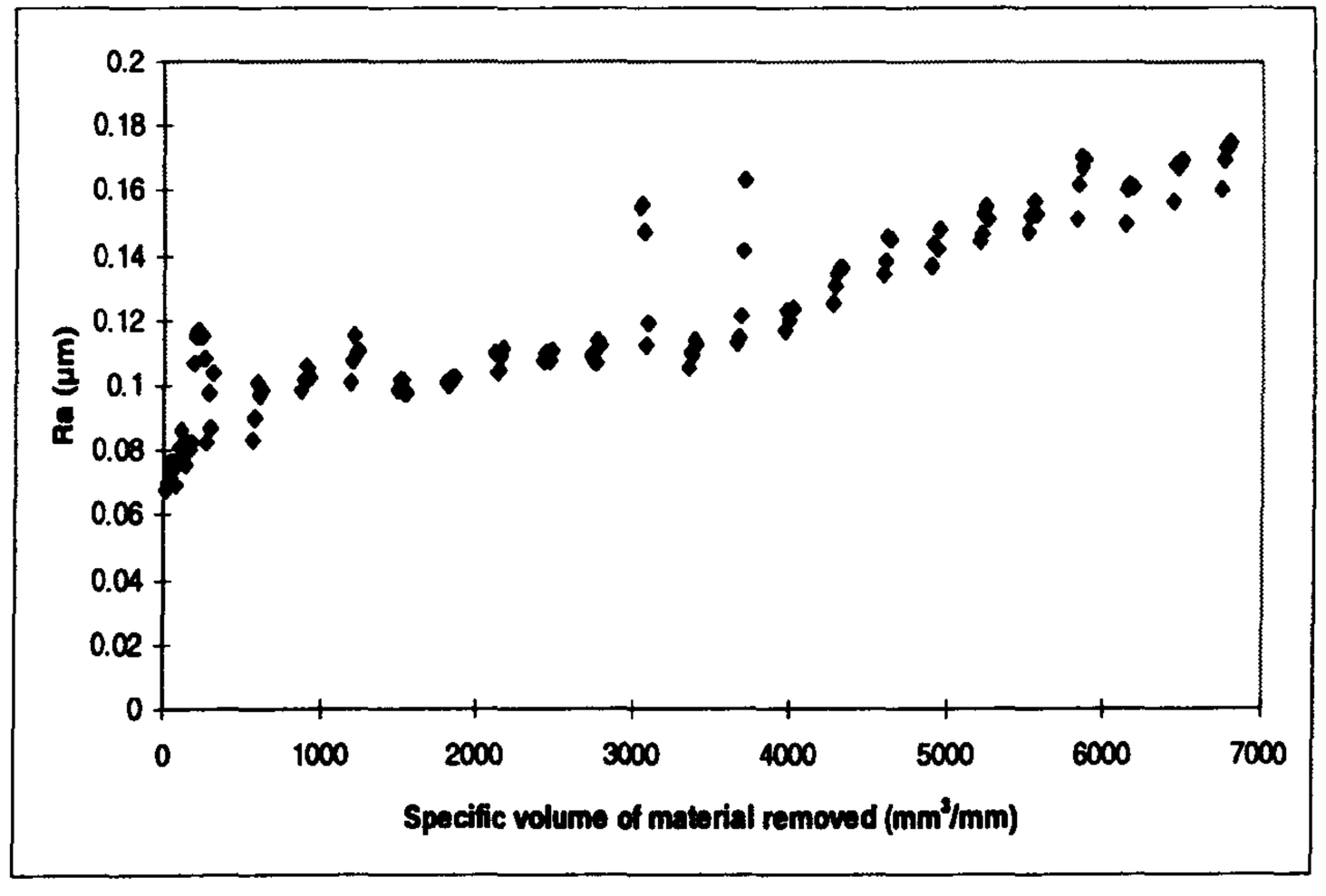

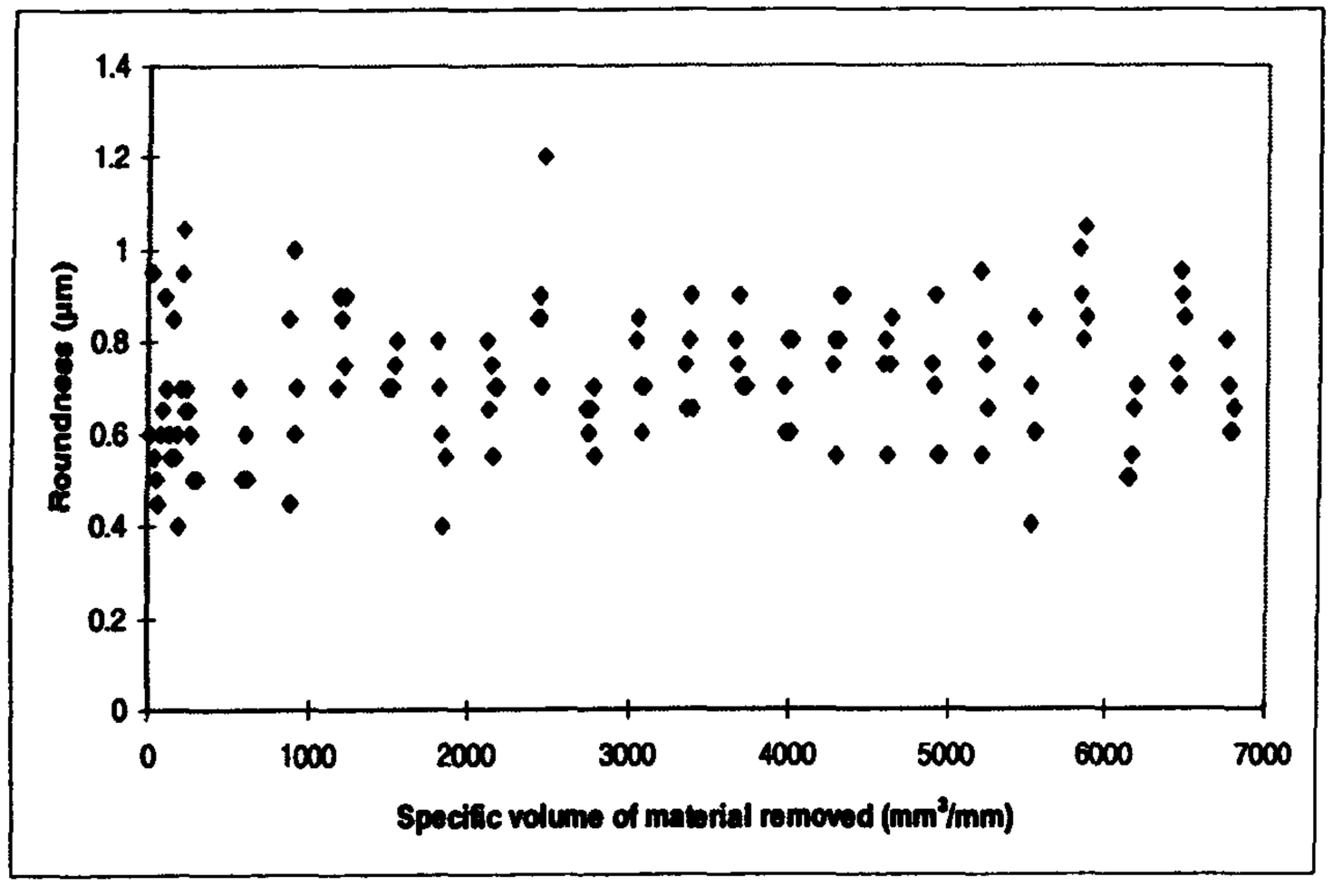

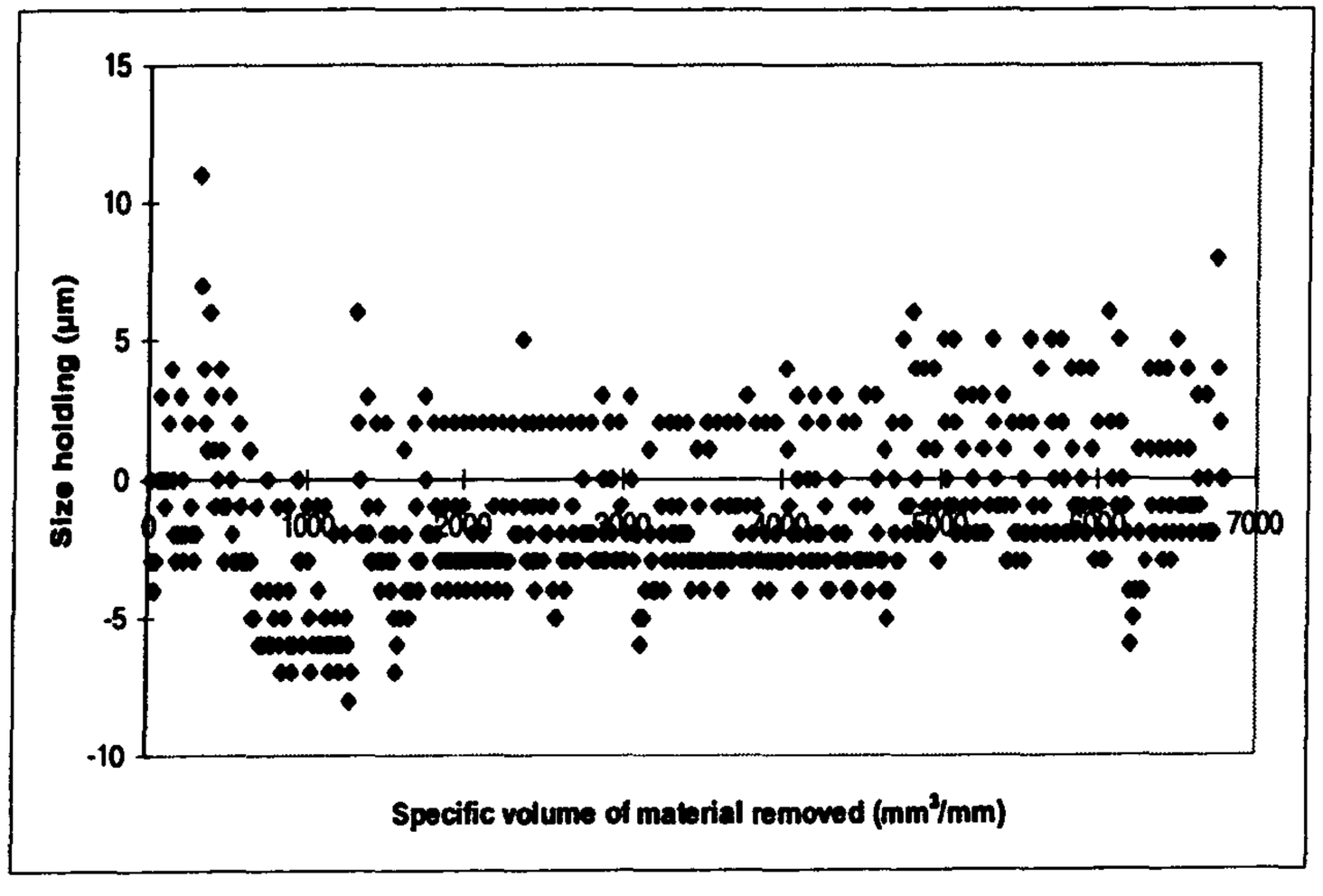

Results for Suprema Characterisation Trial 3 (i.e. 3 of 16) Grinding AISI 52100 With a Vitrified CBN Wheel

<u>Experimental Conditions</u>

- Down dressing
- U_d: 10
- a_d: 10µm
- n_d: 2
- v_s: 60m/s
- v_w: 54m/min
- s:10s
- v_R: 42m/s
-Q'w: 10mm³/mm s
- Wheel: B91VR150
- Coolant: Hysol X 36 l/min, 30Bar pump pressure

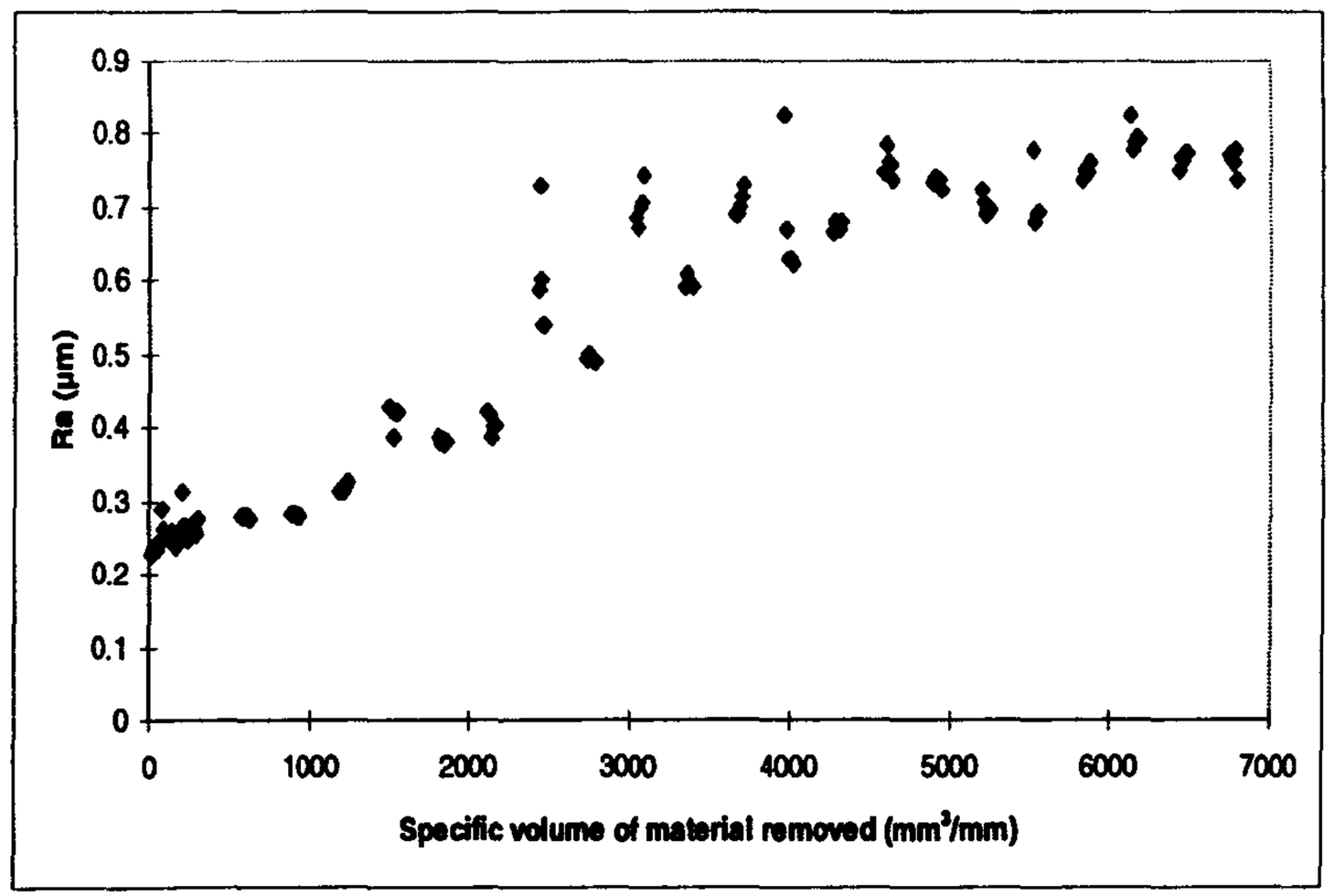

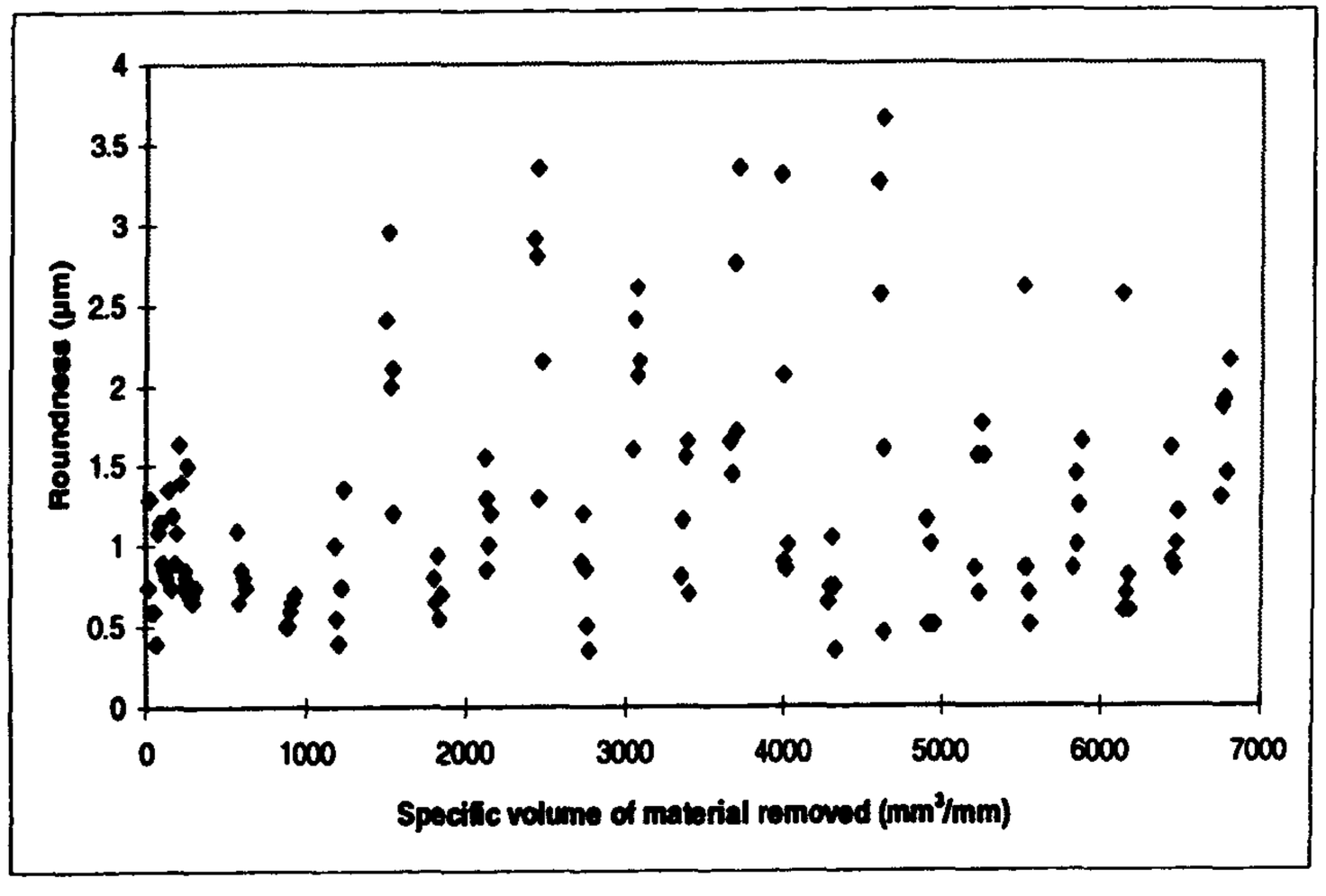

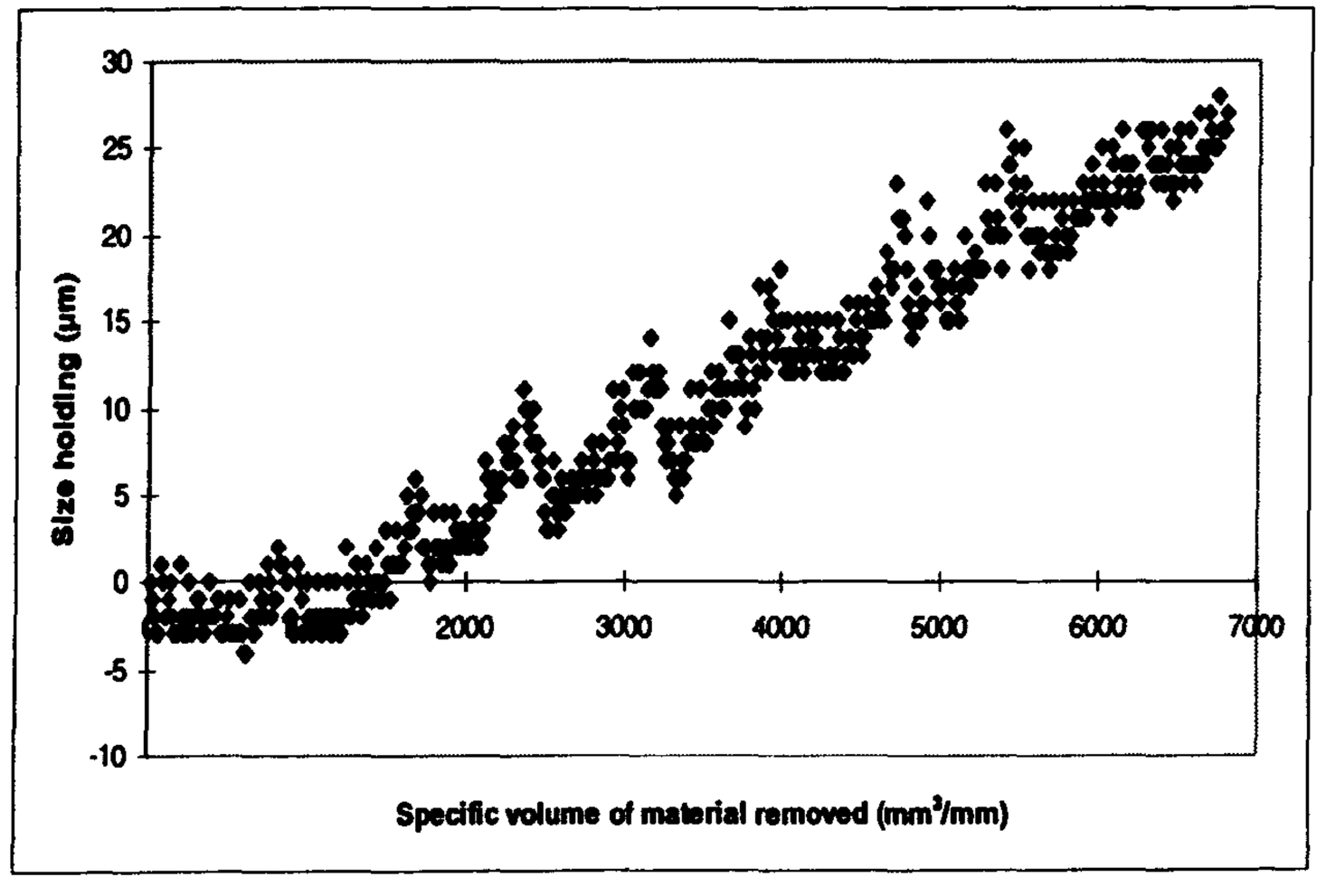

Results for Suprema Characterisation Trial 4 (i.e. 4 of 16) Grinding AISI 52100 With a Vitrified CBN Wheel

Experimental Conditions

- Down dressing
- U_d: 10
- a_d: 10µm
- n_d: 10
- v_s: 120m/s
- v_w: 36m/min
- s:10µm@1µm/s
- v_R: 42m/s
-Q'w: 10mm³/mm s
- Wheel: B91VR150
- Coolant: Hysol X 36 l/min, 30Bar pump pressure

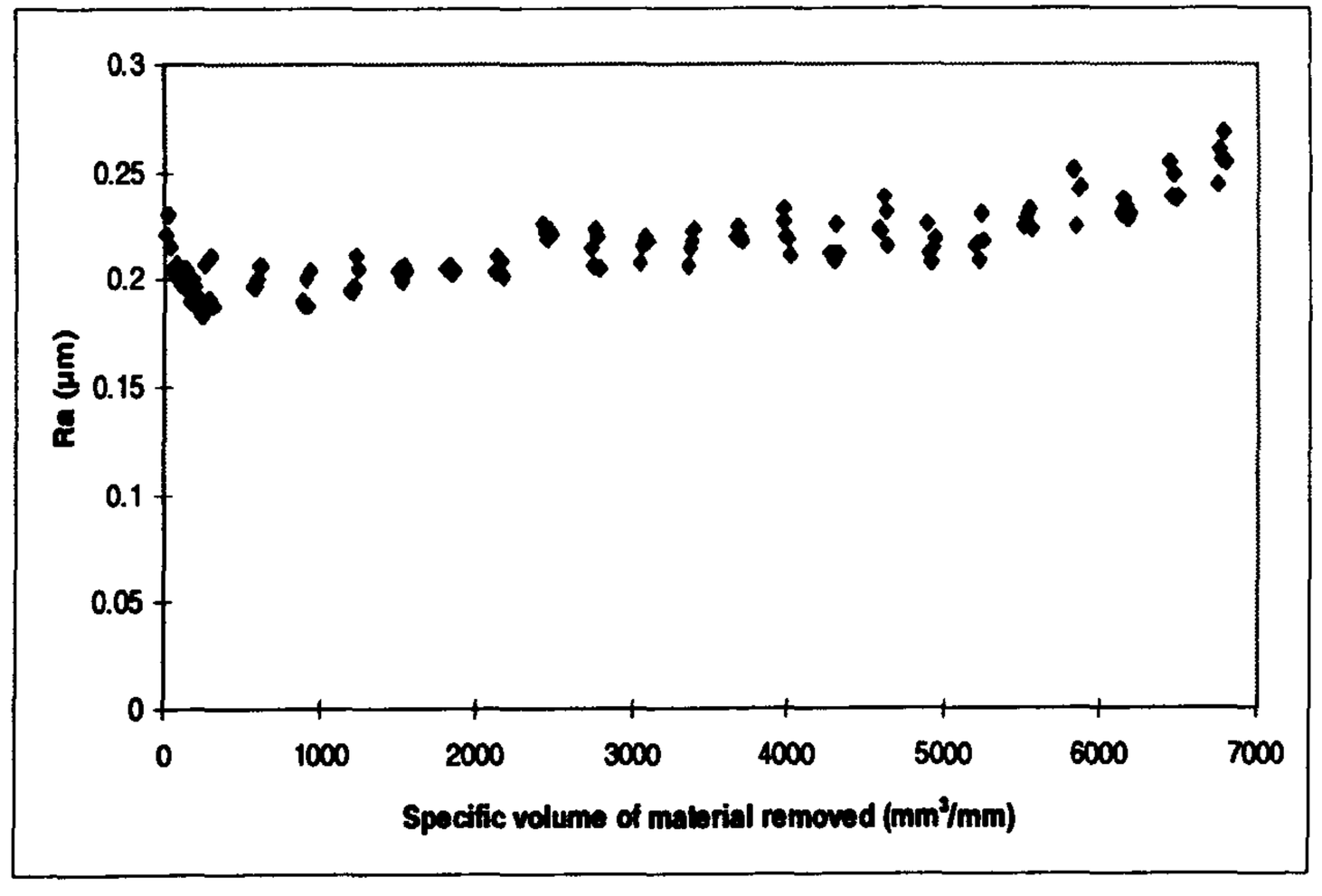

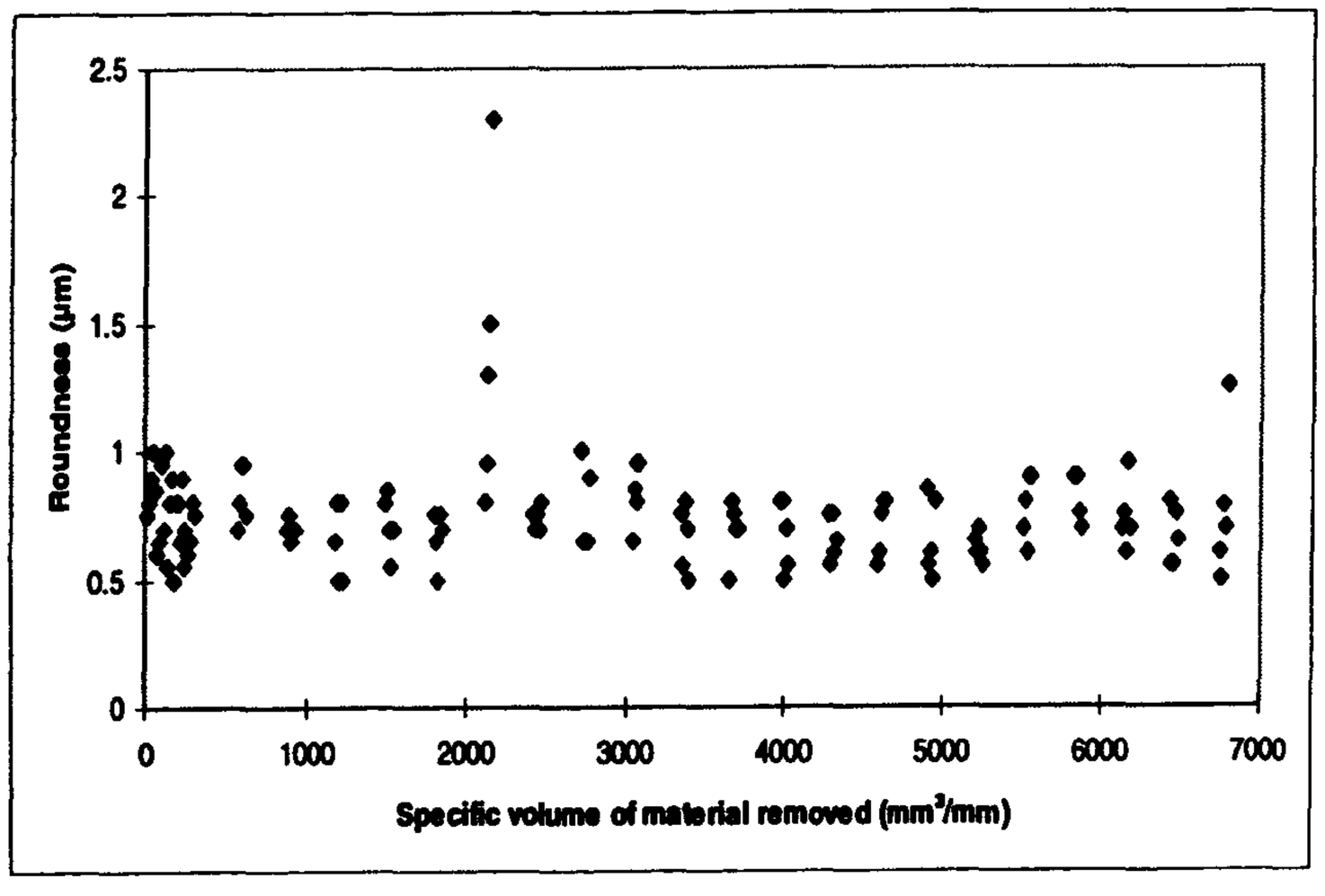

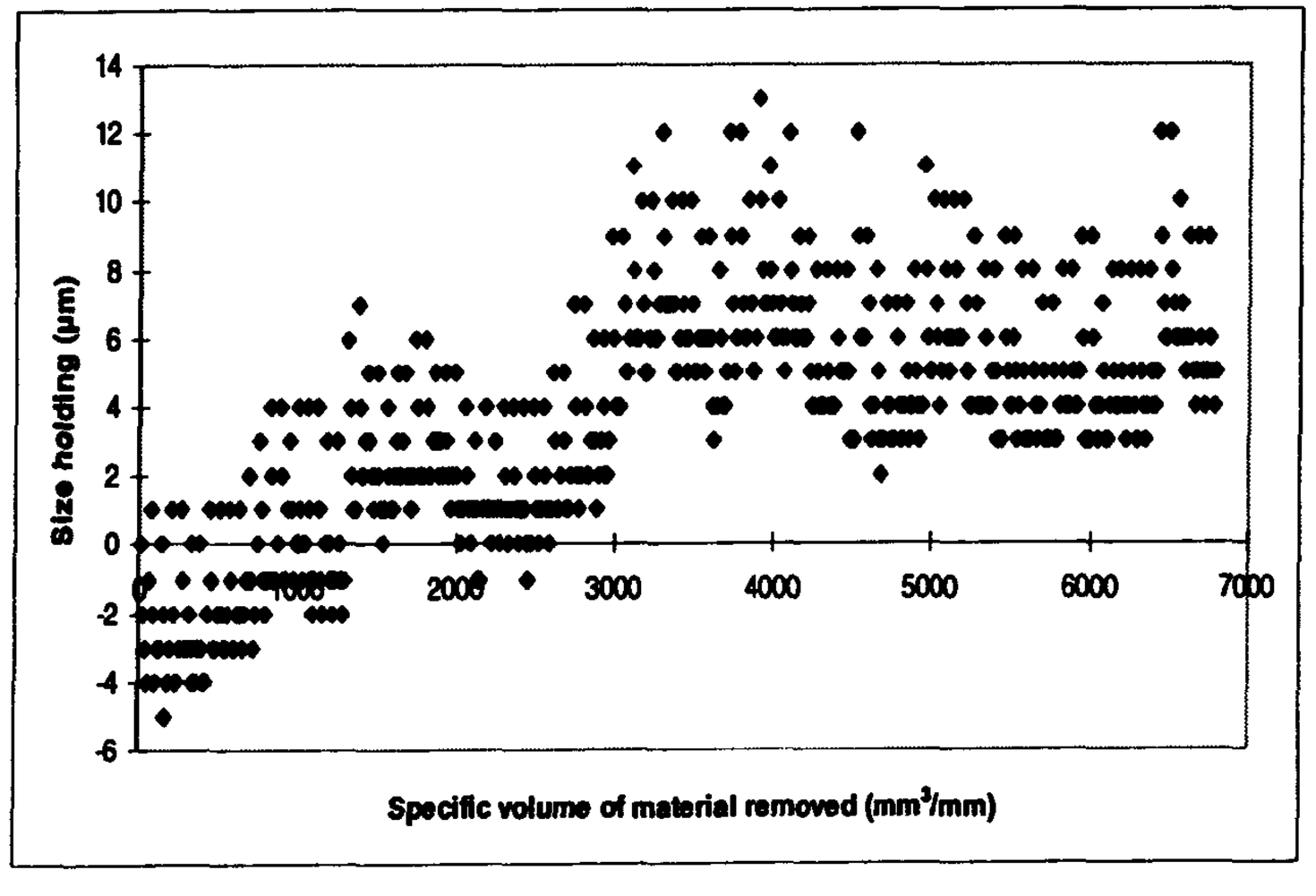

Results for Suprema Characterisation Trial 5 (i.e. 5 of 16) Grinding AISI 52100 With a Vitrified CBN Wheel

Experimental Conditions

- Up dressing
- U_d: 2
- a_d: 10µm
- n_d: 2
- v_s: 120m/s
- v_w: 36m/min
- s:10s
- v_R: 42m/s
-Q'w: 10mm³/mm s
- Wheel: B91VR150
- Coolant: Hysol X 36 l/min, 30Bar pump pressure

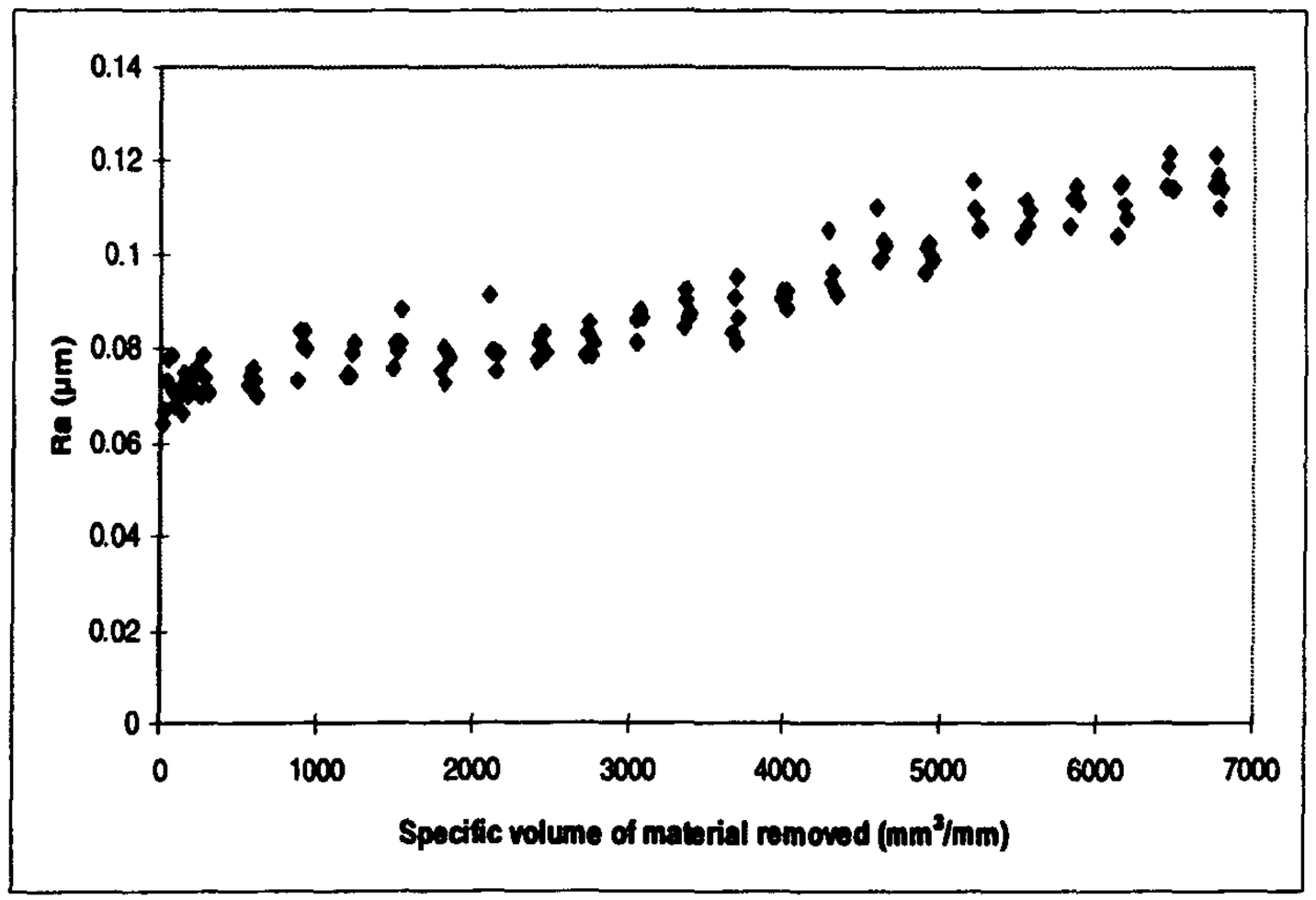

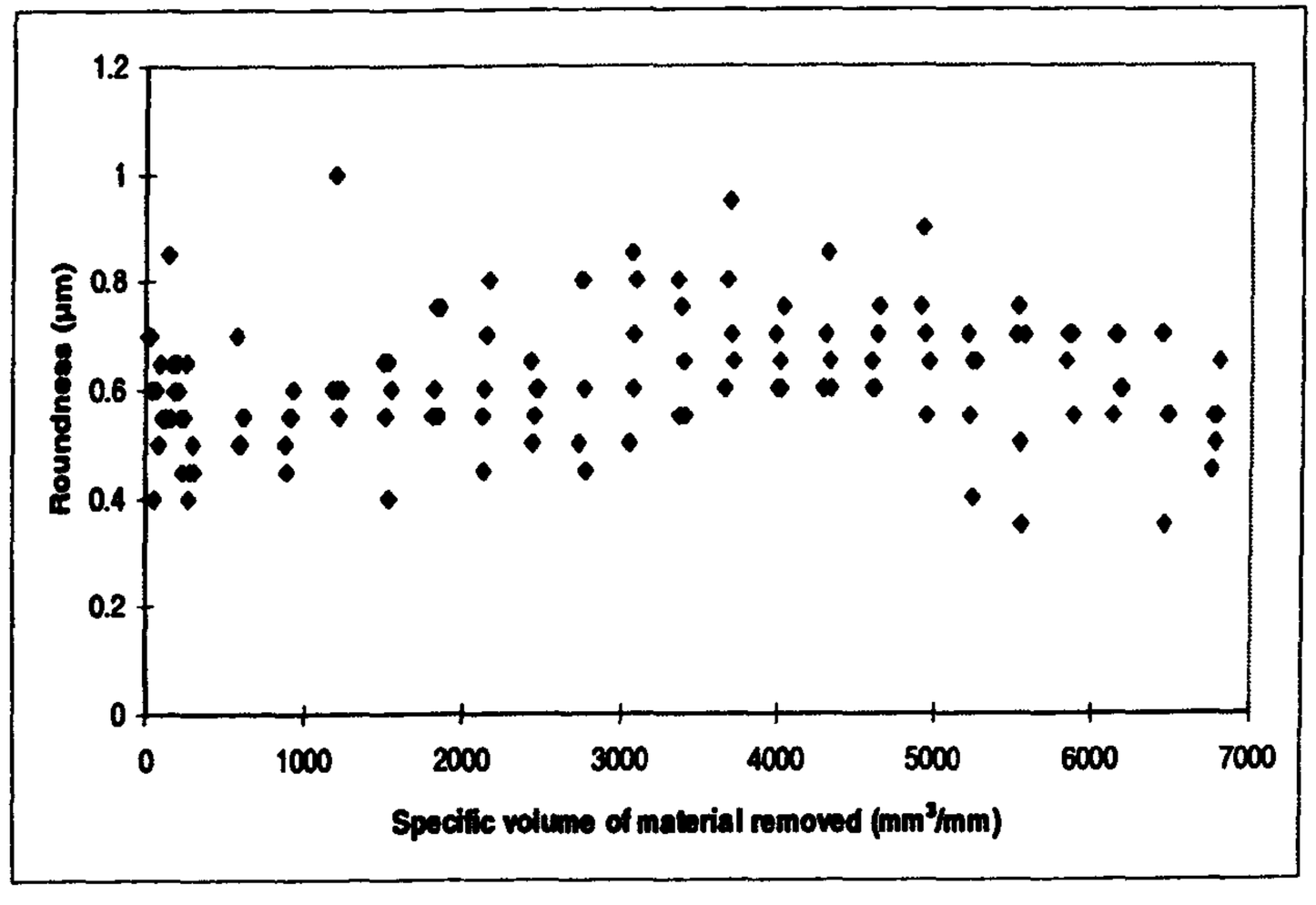

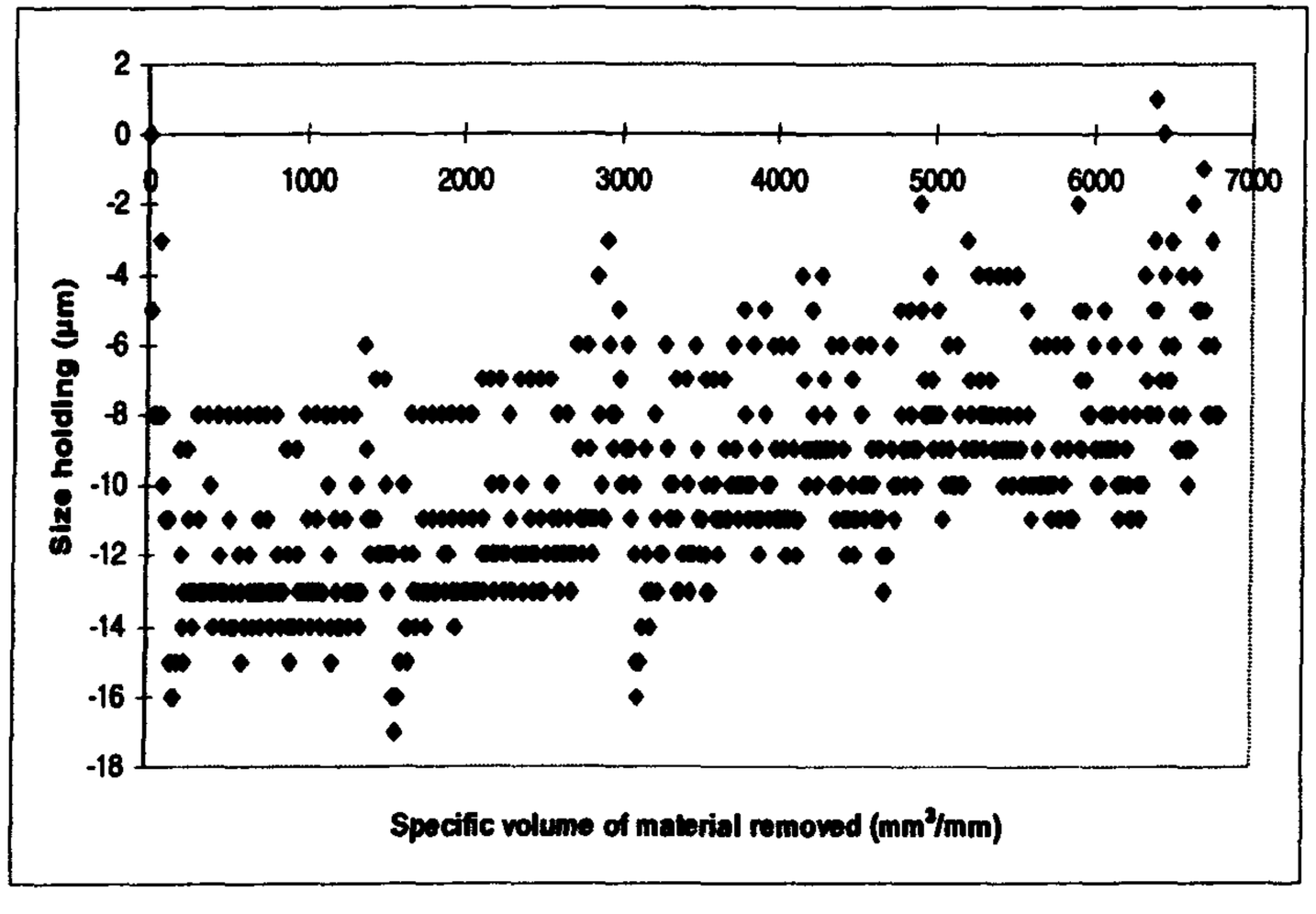

Results for Suprema Characterisation Trial 6 (i.e. 6 of 16) Grinding AISI 52100 With a Vitrified CBN Wheel

<u>Experimental Conditions</u>

- Up dressing
- U_d: 2
- a_d: 10µm
- n_d: 10
- v_s: 60m/s
- v_w: 54m/min
- s:10µm@1µm/s
- v_R: 42m/s
-Q'w: 10mm³/mm s
- Wheel: B91VR150
- Coolant: Hysol X 36 l/min, 30Bar pump pressure

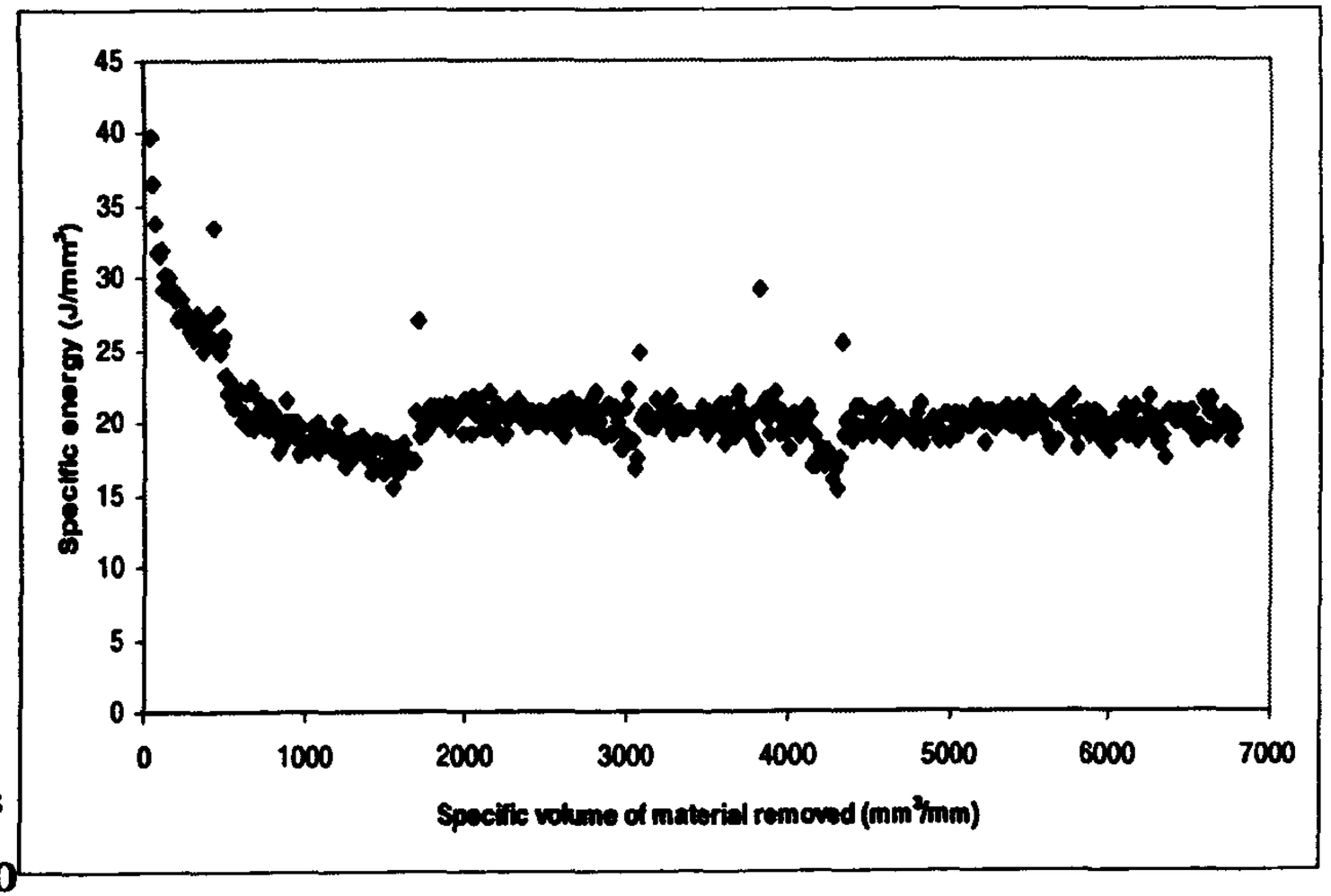

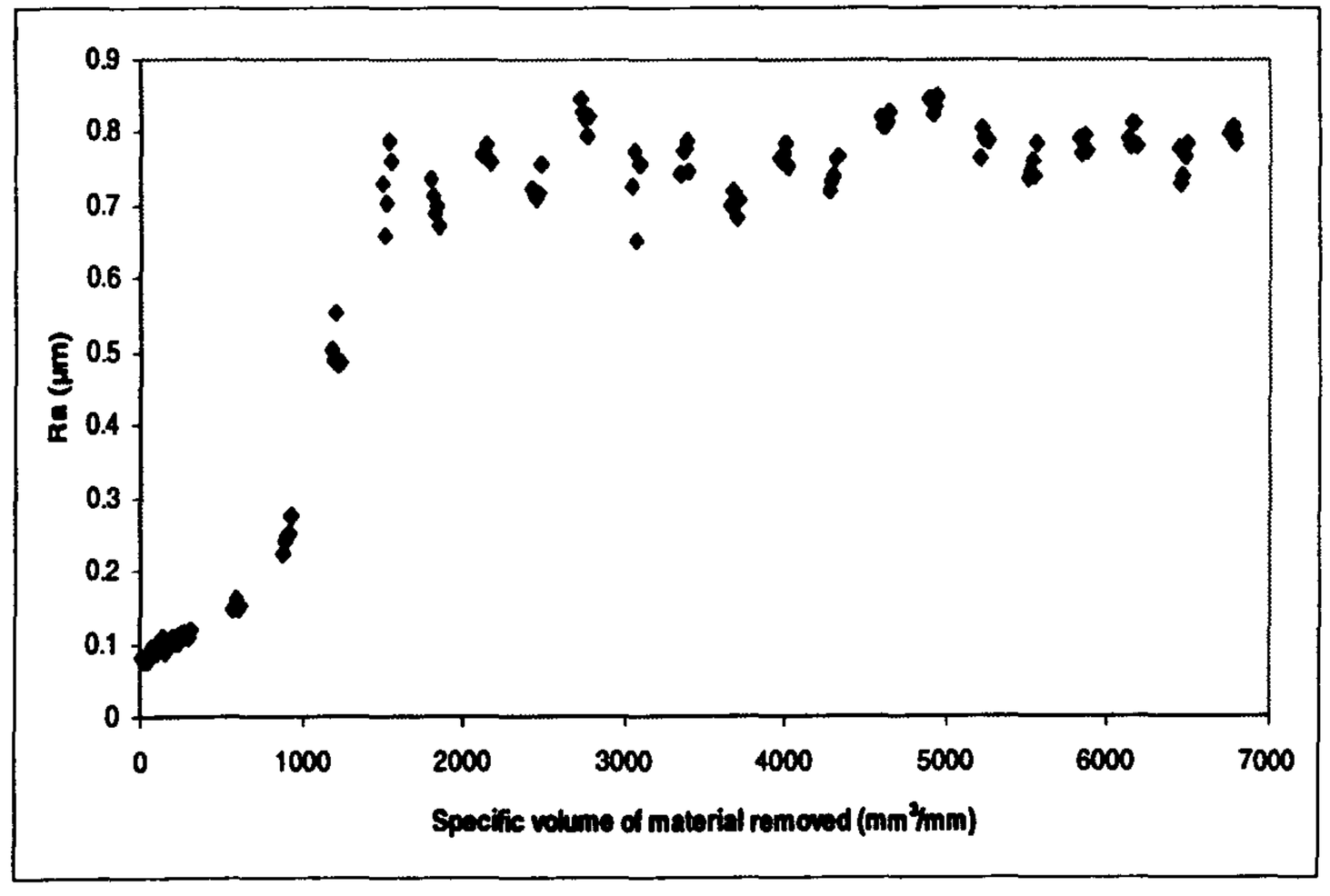

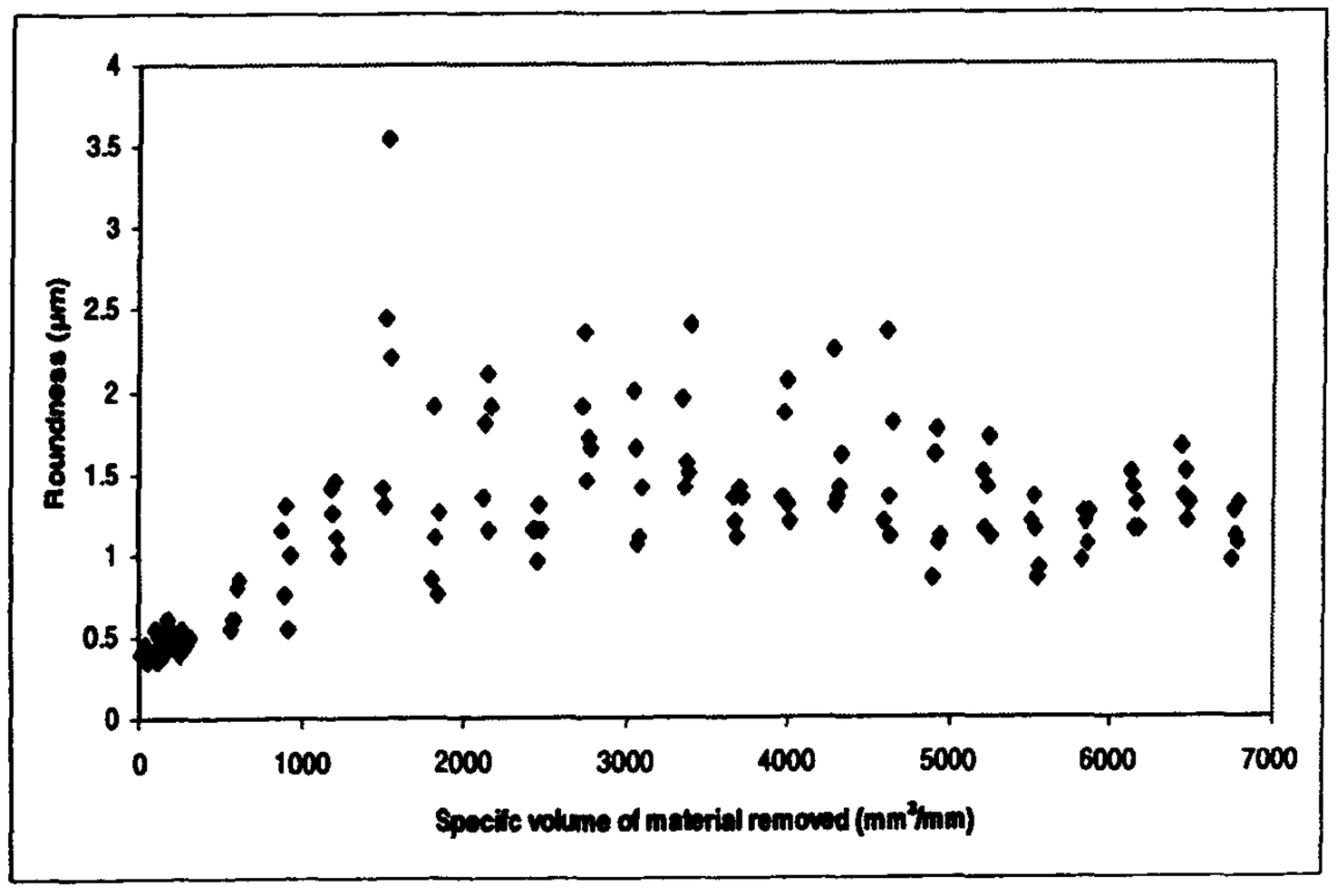

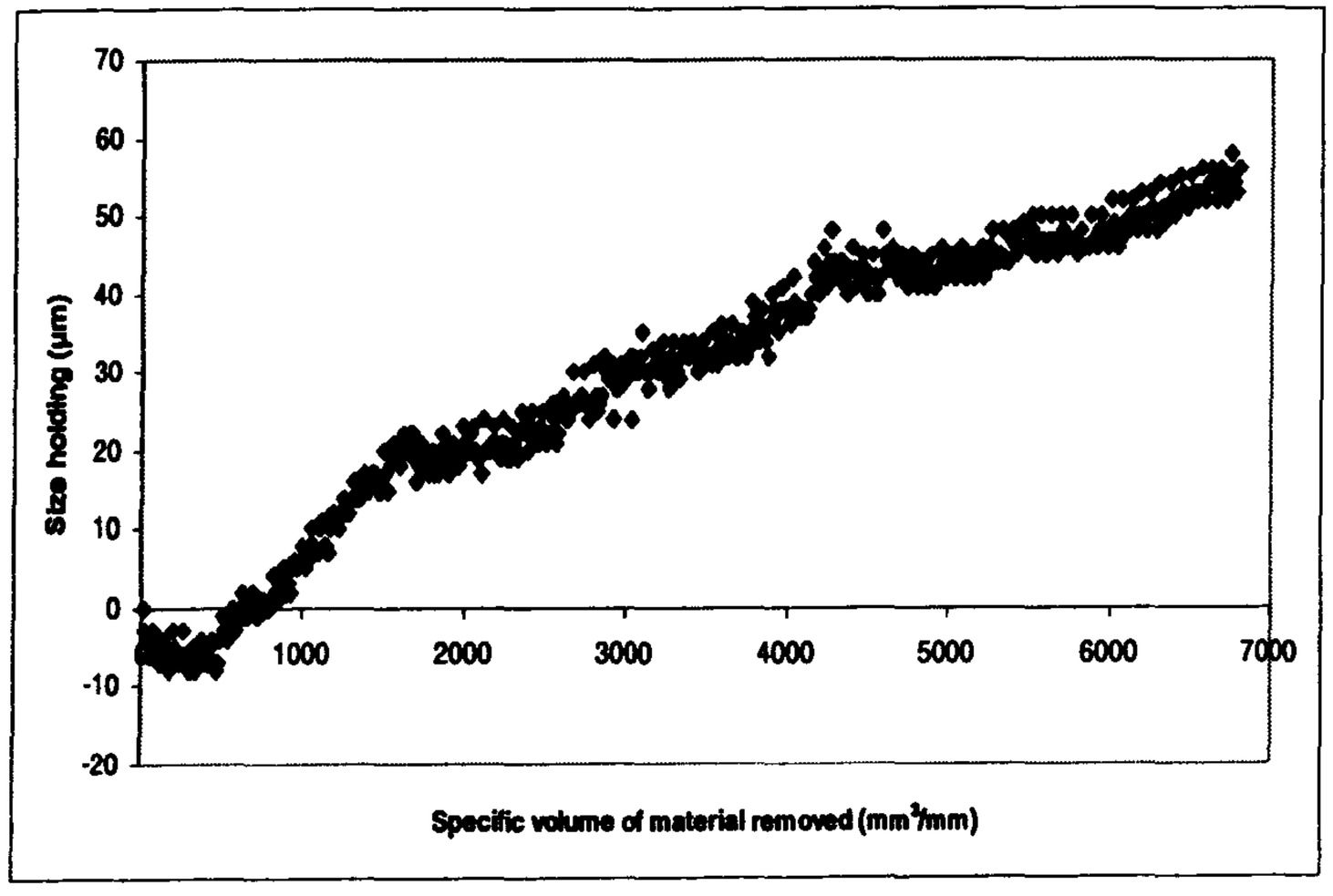

Results for Suprema Characterisation Trial 7 (i.e. 7 of 16) Grinding AISI 52100 With a Vitrified CBN Wheel

<u>Experimental Conditions</u>

- Up dressing
- U_d: 10
- a_d: 2μm
- n_d: 2
- v_s: 120m/s
- v_w: 54m/min
- s:10μm@1μm/s
- v_R: 42m/s
-Q'w: 10mm³/mm s
- Wheel: B91VR150
- Coolant: Hysol X 36 l/min, 30Bar pump pressure

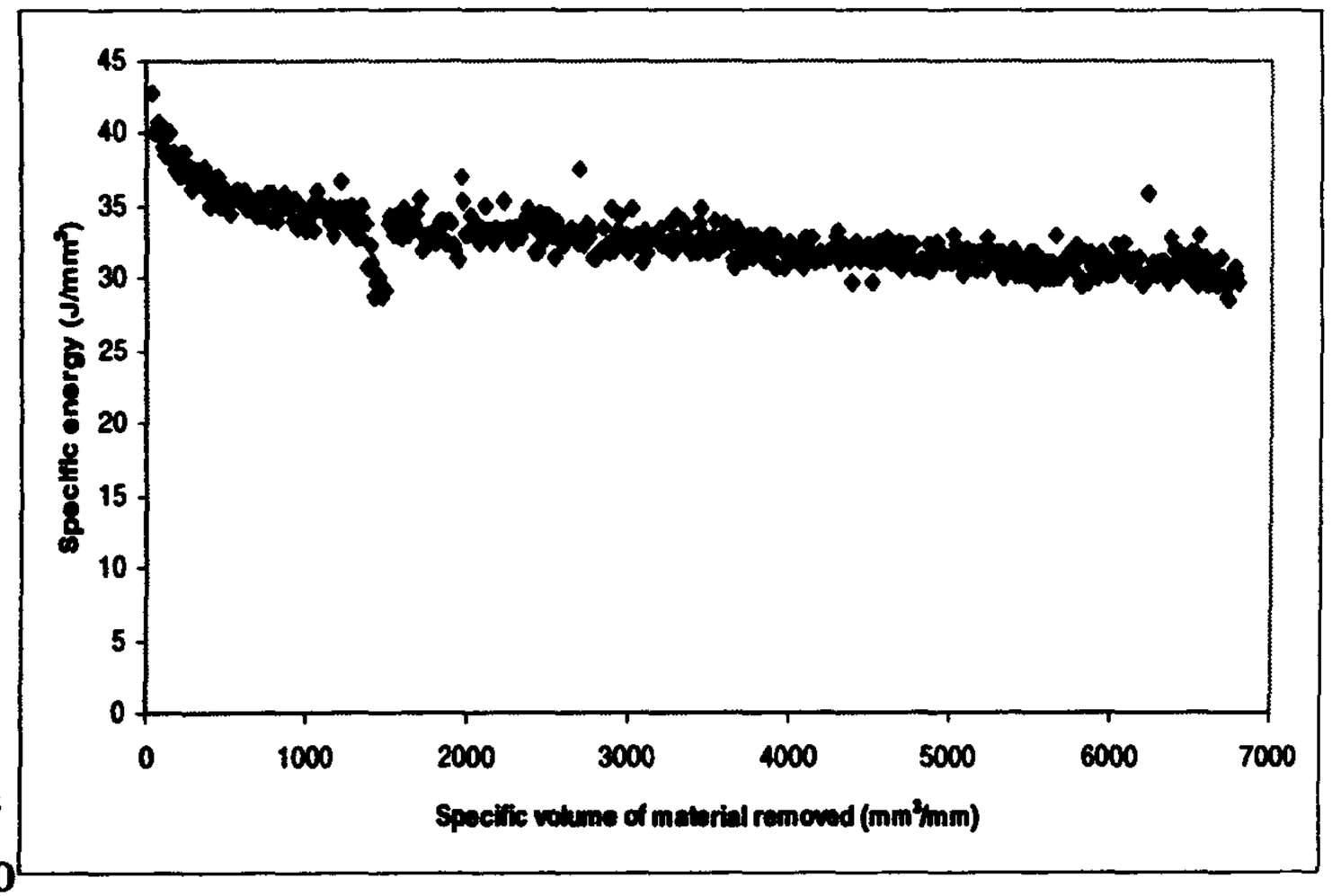

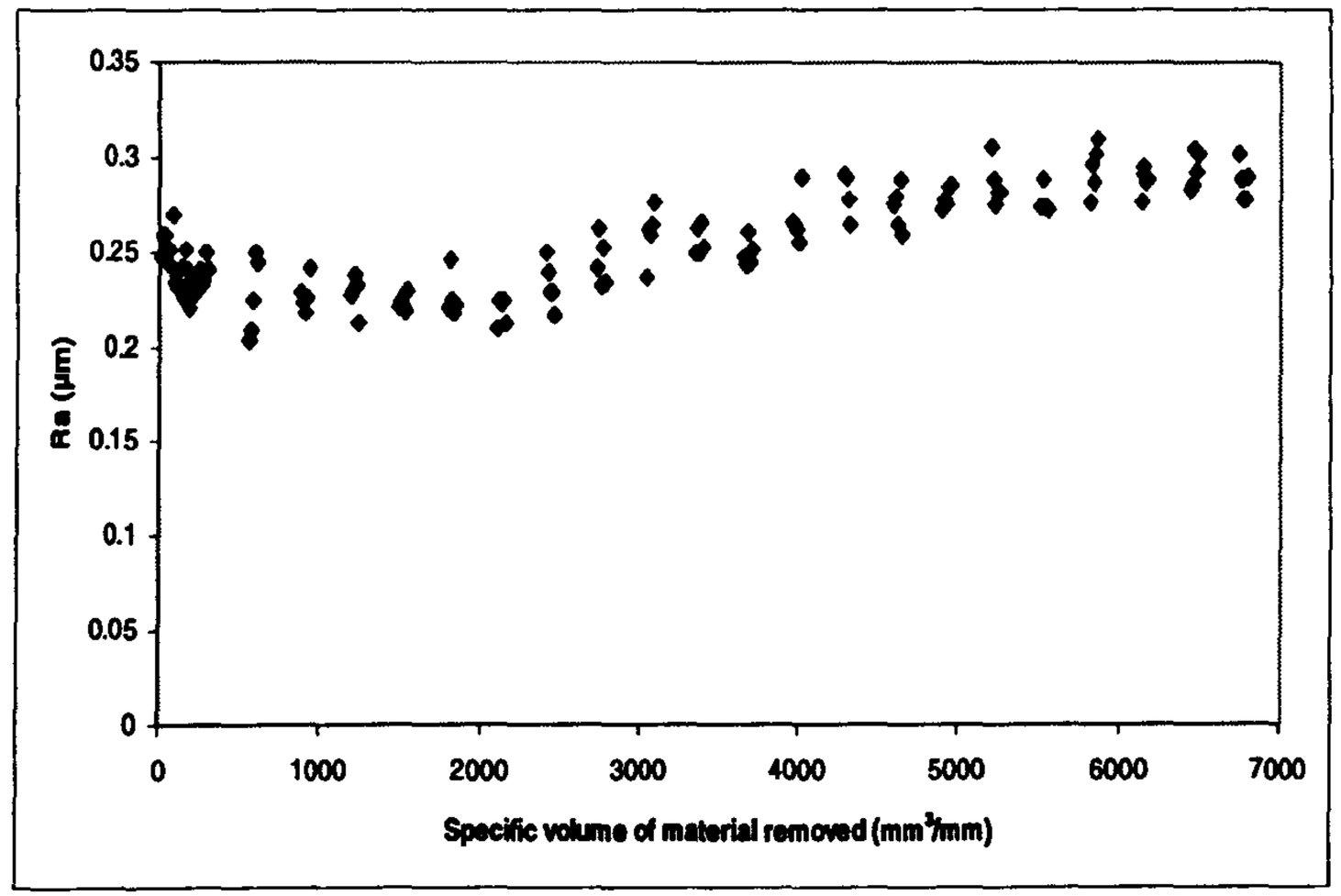

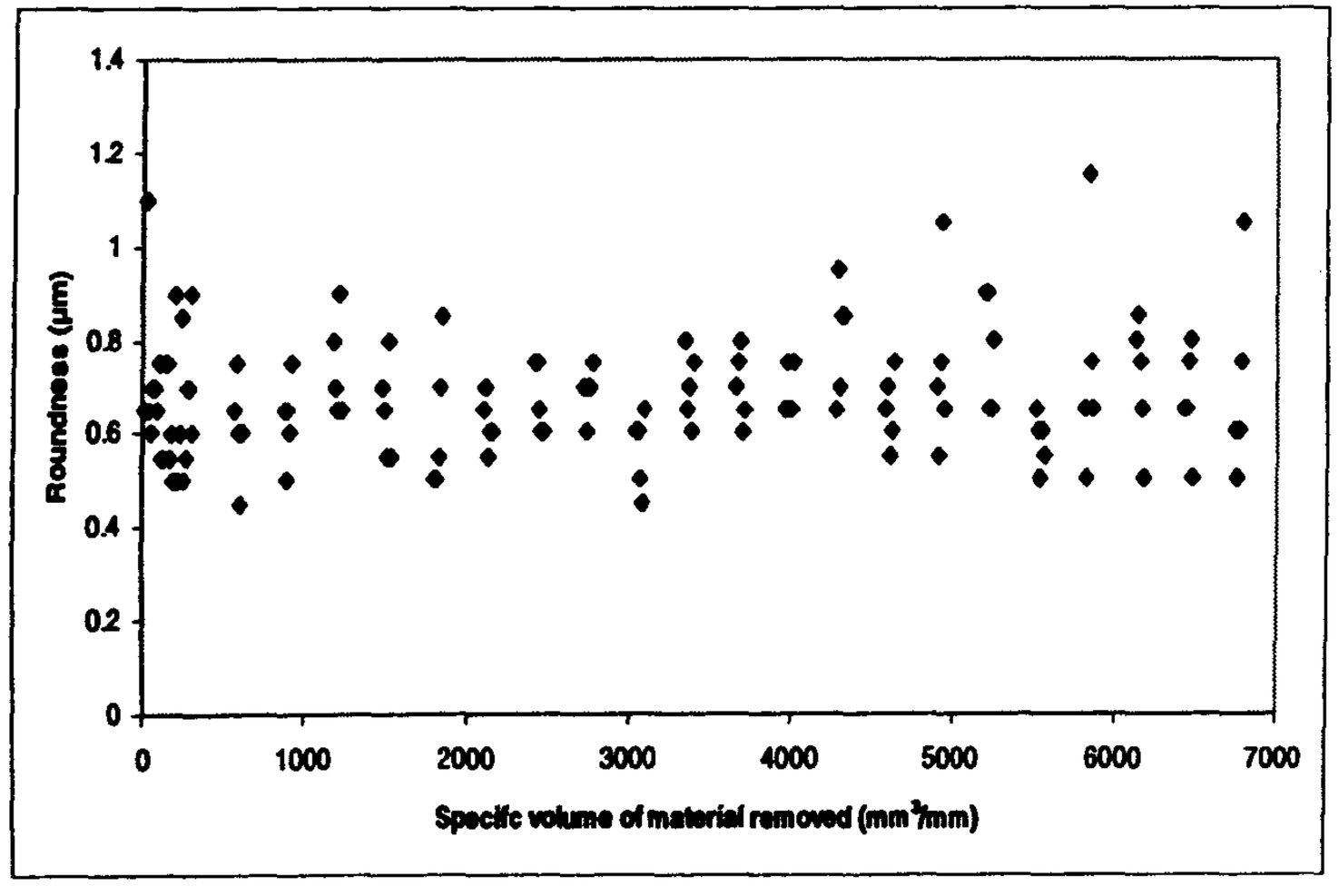

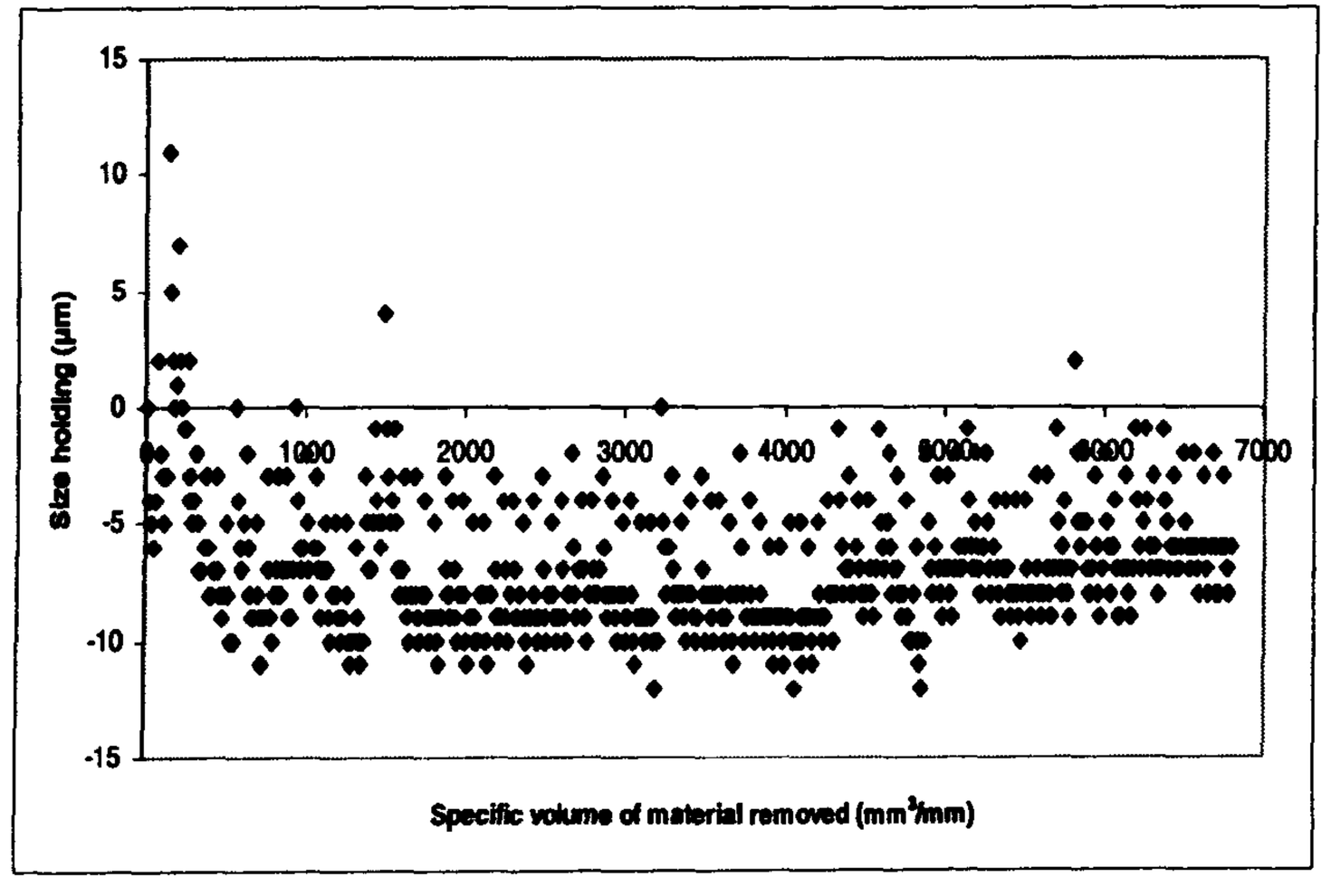

Results for Suprema Characterisation Trial 8 (i.e. 8 of 16) Grinding AISI 52100 With a Vitrified CBN Wheel

Experimental Conditions

- Up dressing
- U_d: 10
- a_d: 2µm
- n_d: 10
- v_s: 60m/s
- v_w: 36m/min
- s:10s
- v_R: 42m/s
-Q'w: 10mm³/mm s
- Wheel: B91VR150
- Coolant: Hysol X 36 l/min, 30Bar pump pressure

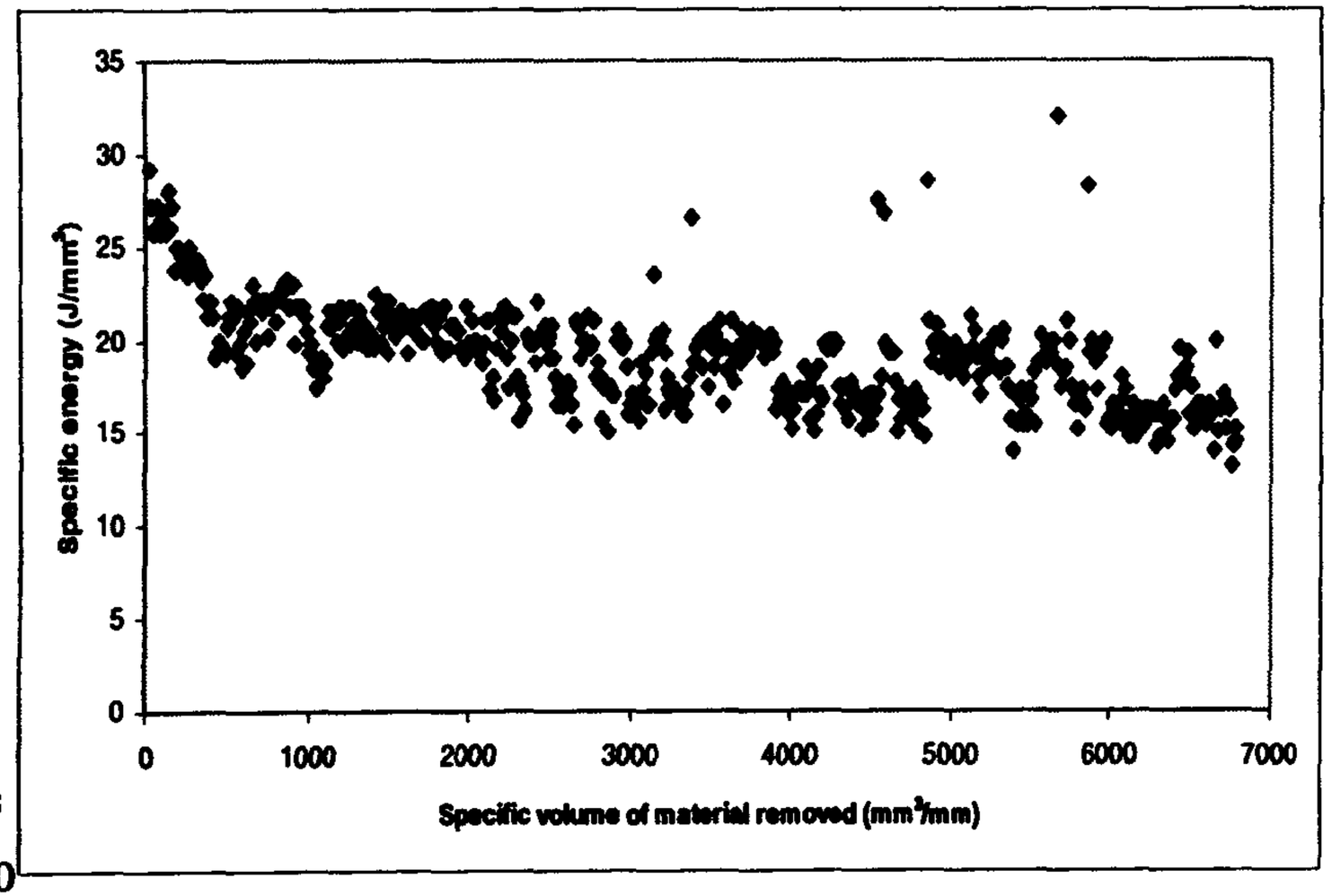

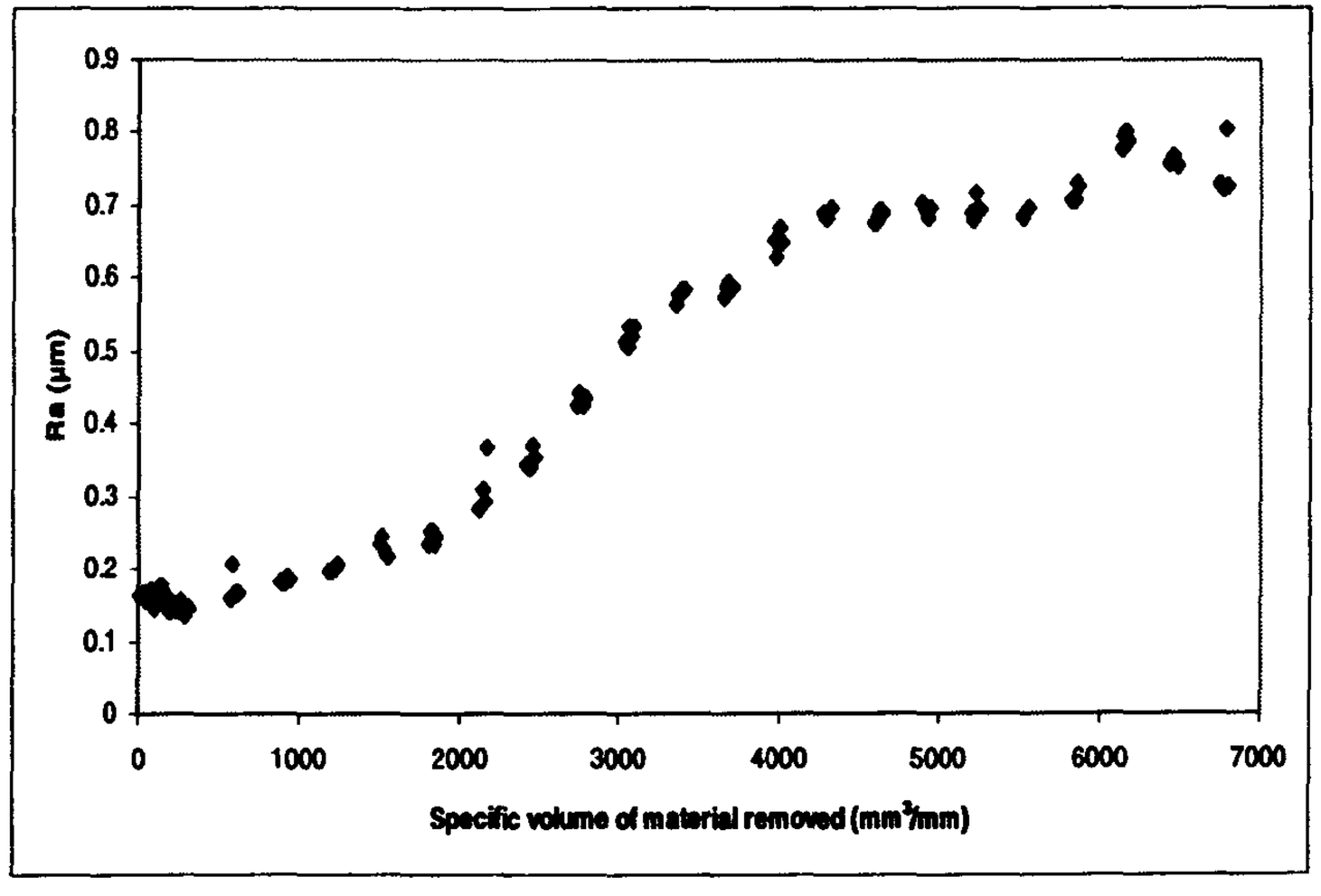

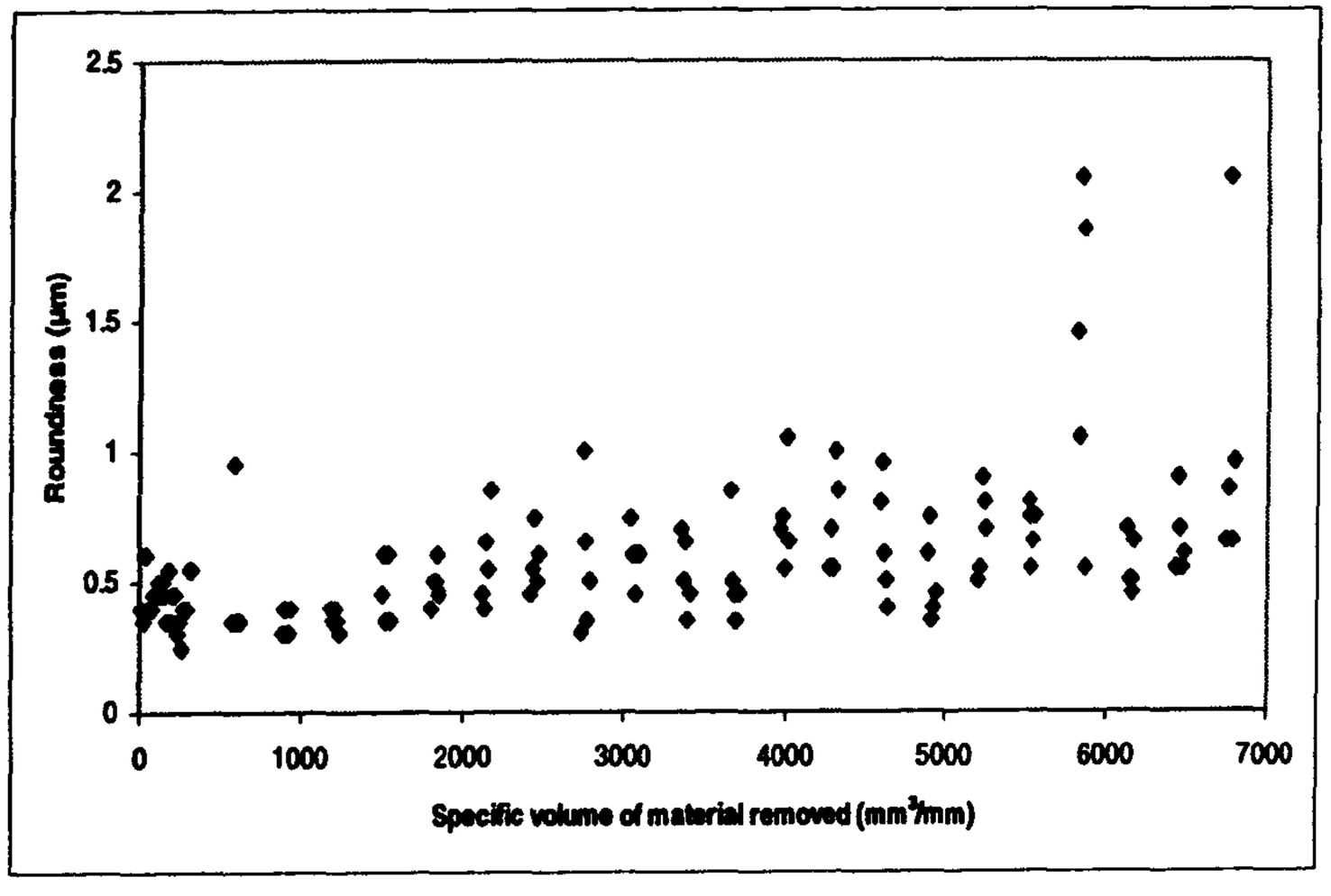

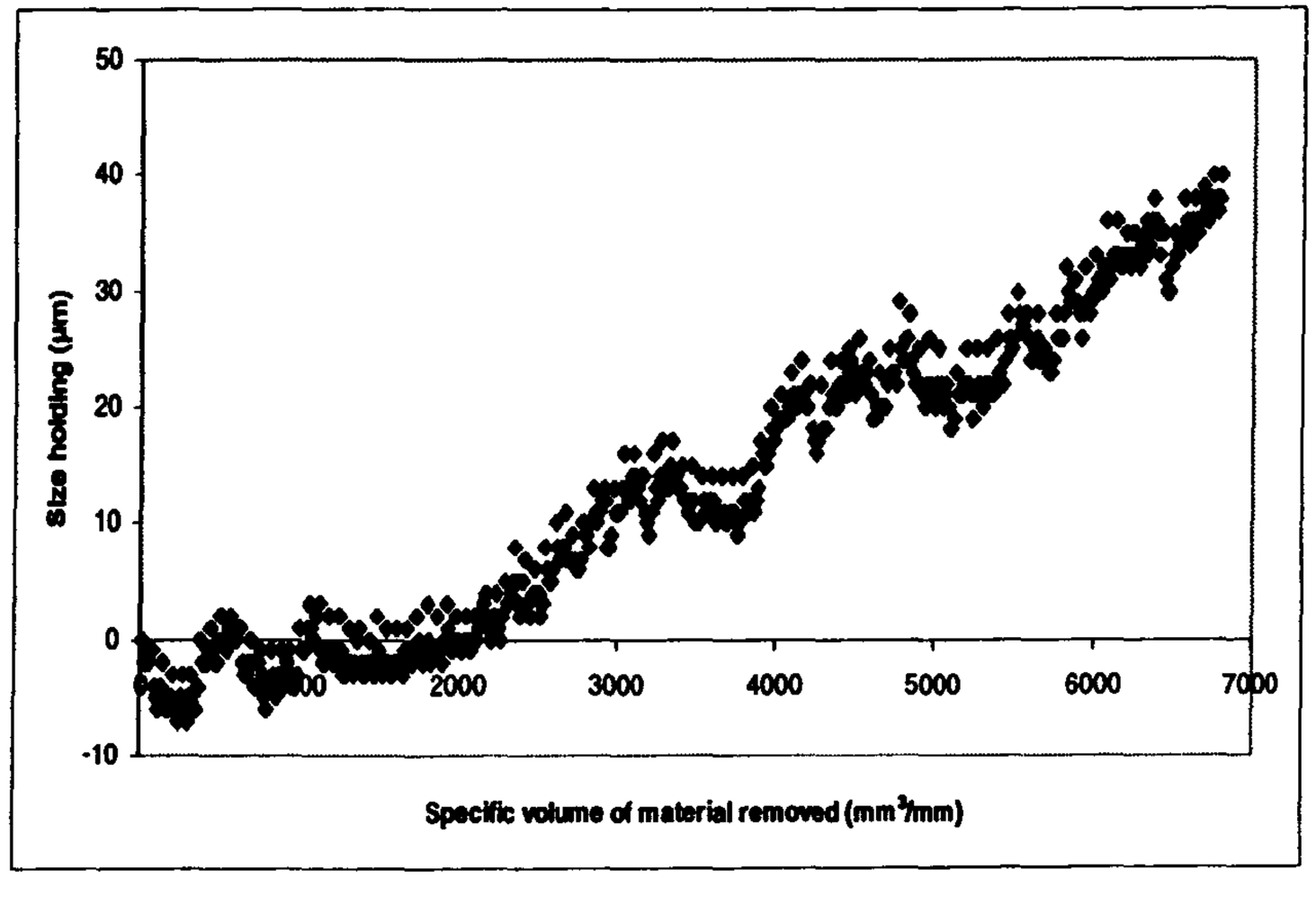

Results for Suprema Characterisation Trial 9 (i.e. 9 of 16) Grinding AISI 52100 With a Vitrified CBN Wheel

<u>Experimental Conditions</u>

- Up dressing
- U_d: 10
- a_d: 10µm
- n_d: 10
- v_s: 120m/s
- v_w: 54m/min
- s:10s
- v_R: 72m/s
-Q'w: 10mm³/mm s
- Wheel: B91VR150
- Coolant: Hysol X 36 l/min, 30Bar pump pressure

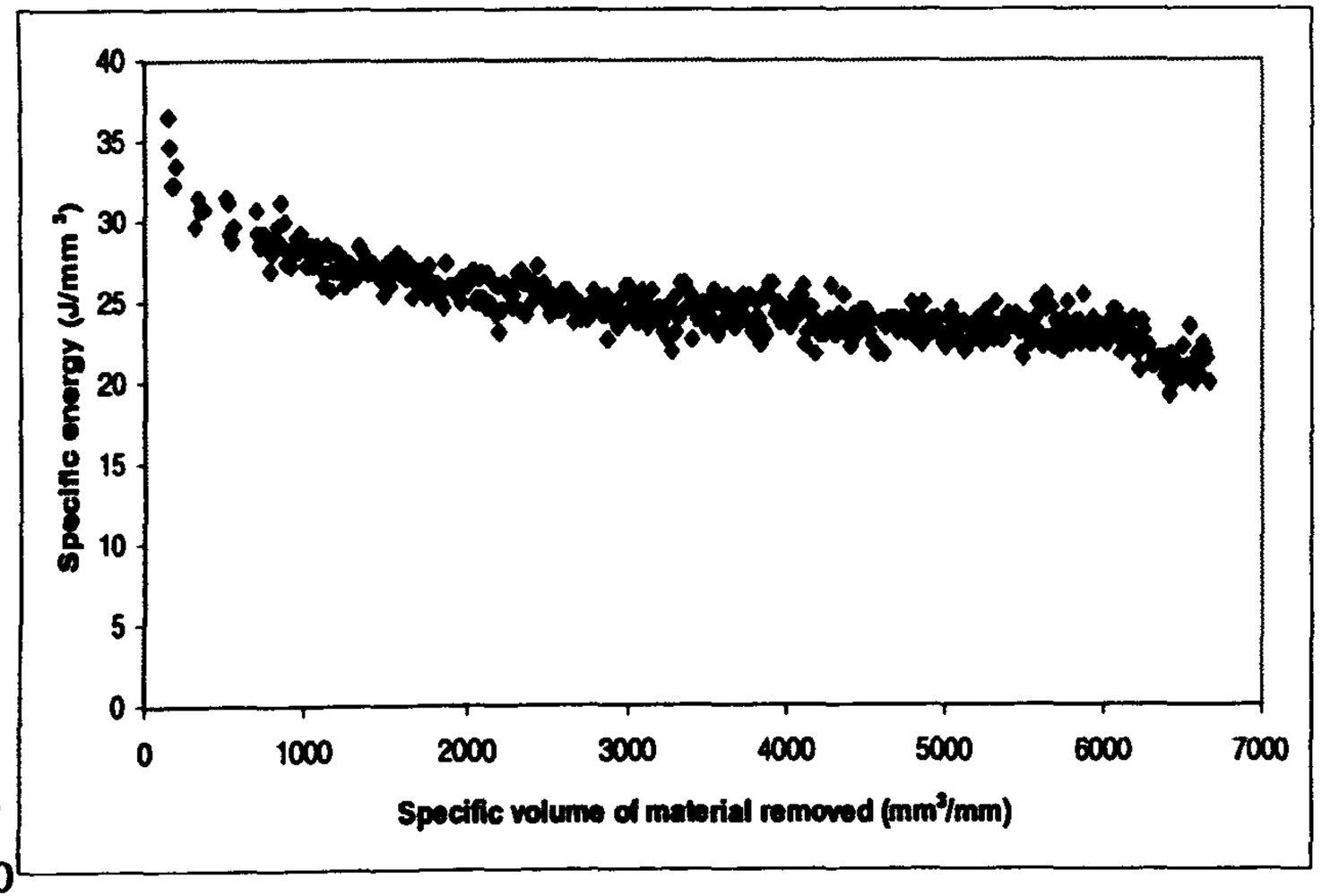

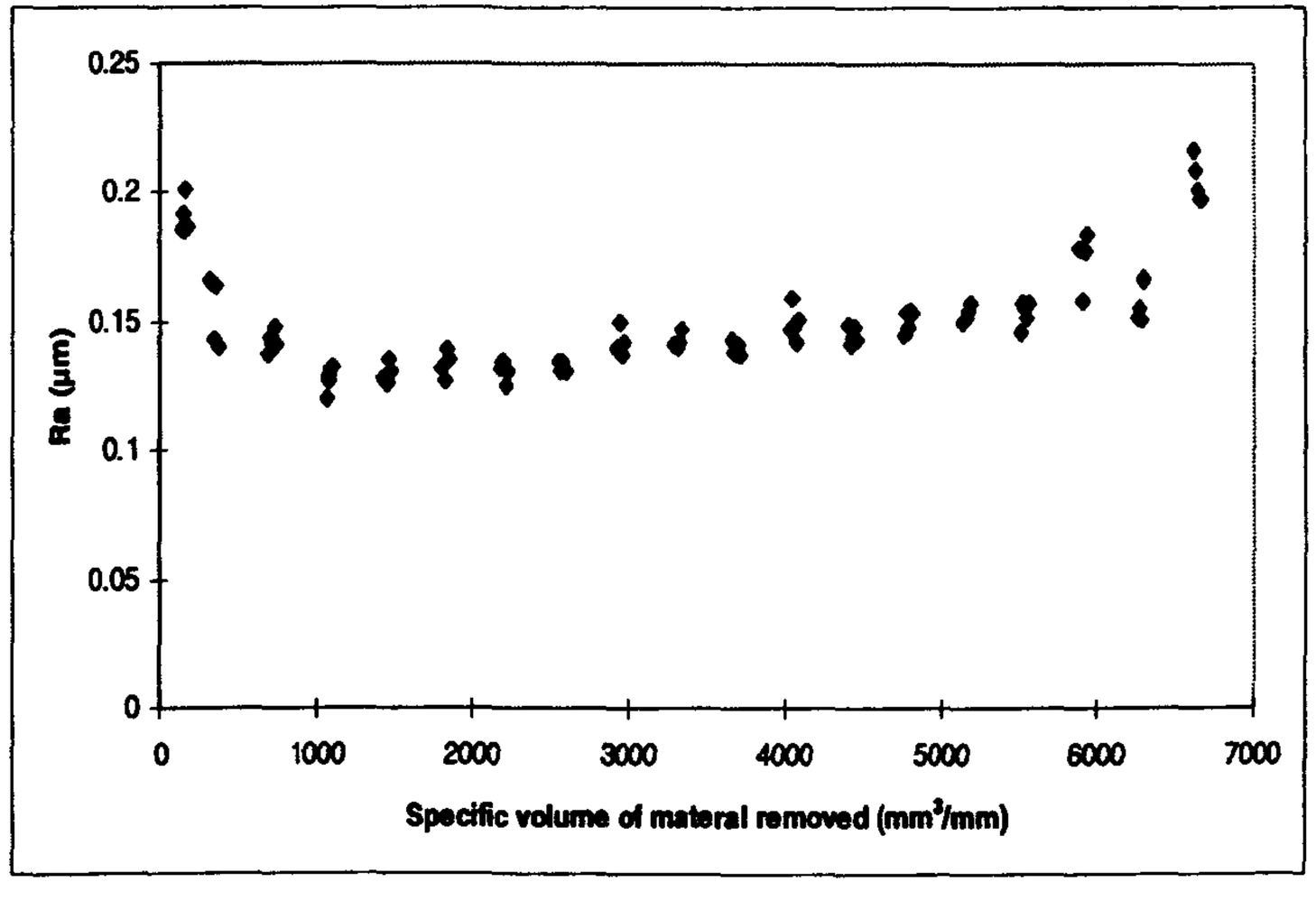

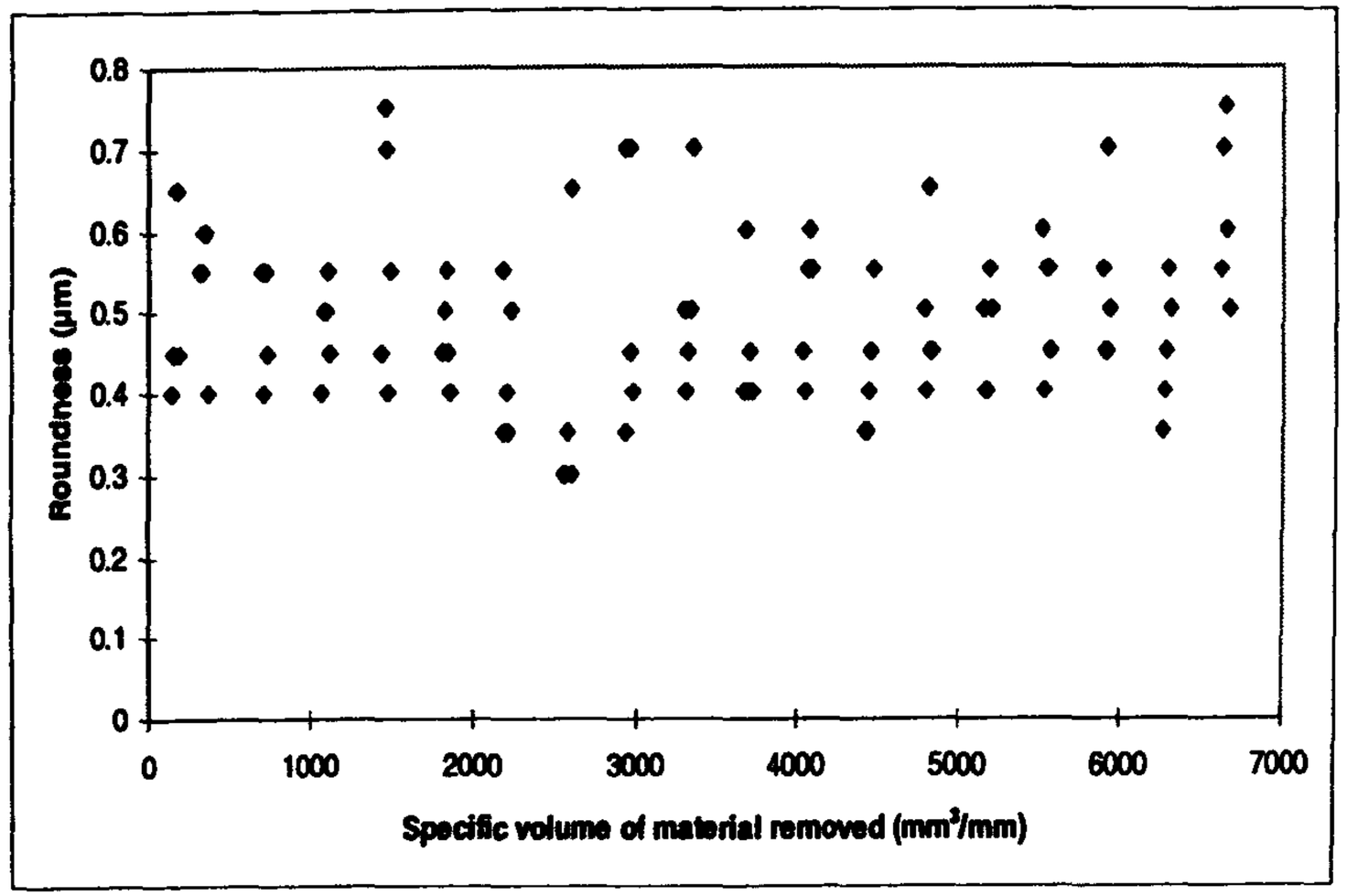

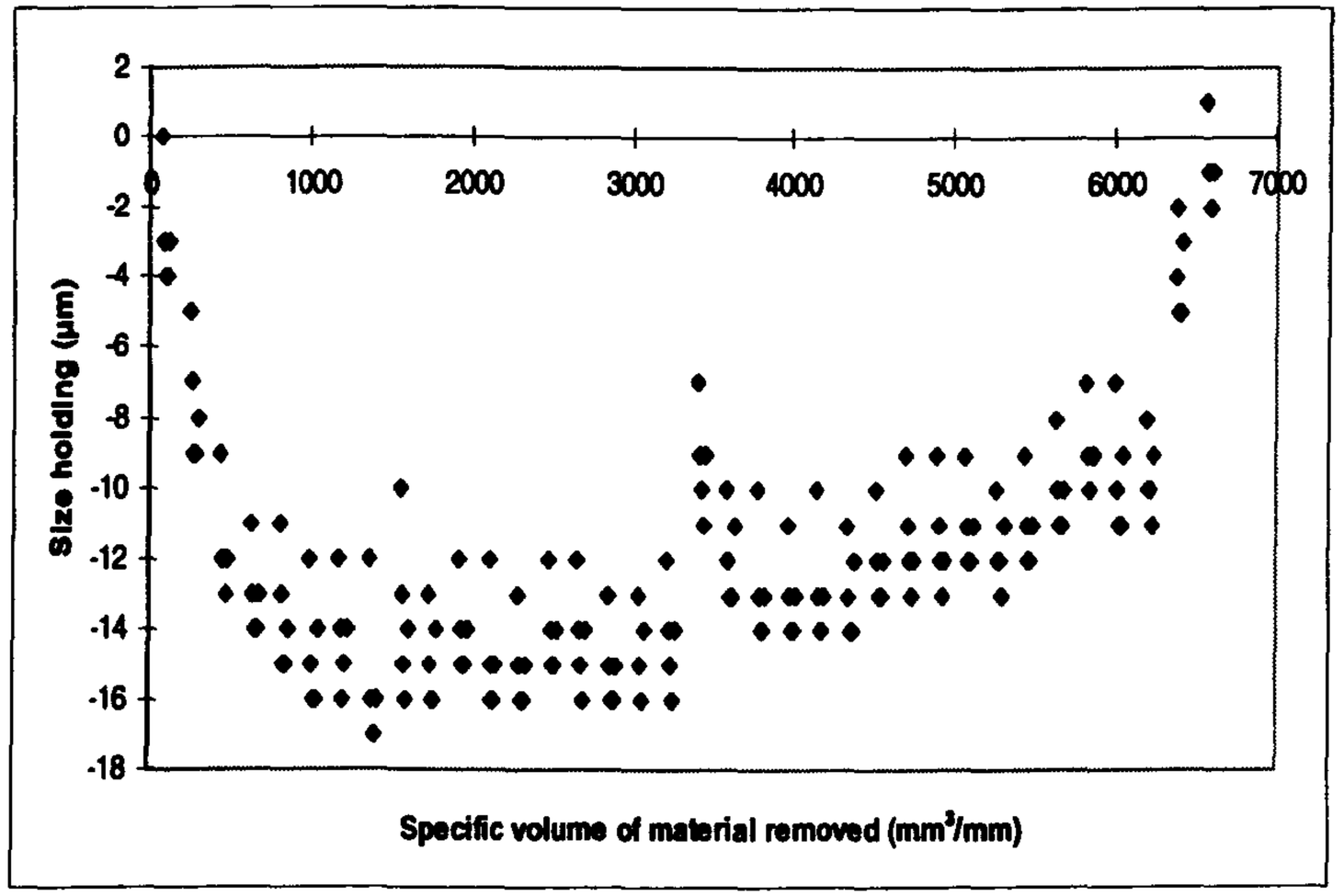

Results for Suprema Characterisation Trial 10 (i.e. 10 of 16) Grinding AISI 52100 With a Vitrified CBN Wheel

<u>Experimental Conditions</u>

- Up dressing
- U_d: 10
- a_d: 10µm
- n_d: 2
- v_s: 60m/s
- v_w: 36m/min
- s:10µm@1µm/s
- v_R: 72m/s
-Q'w: 10mm³/mm s
- Wheel: B91VR150
- Coolant: Hysol X 36 l/min, 30Bar pump pressure

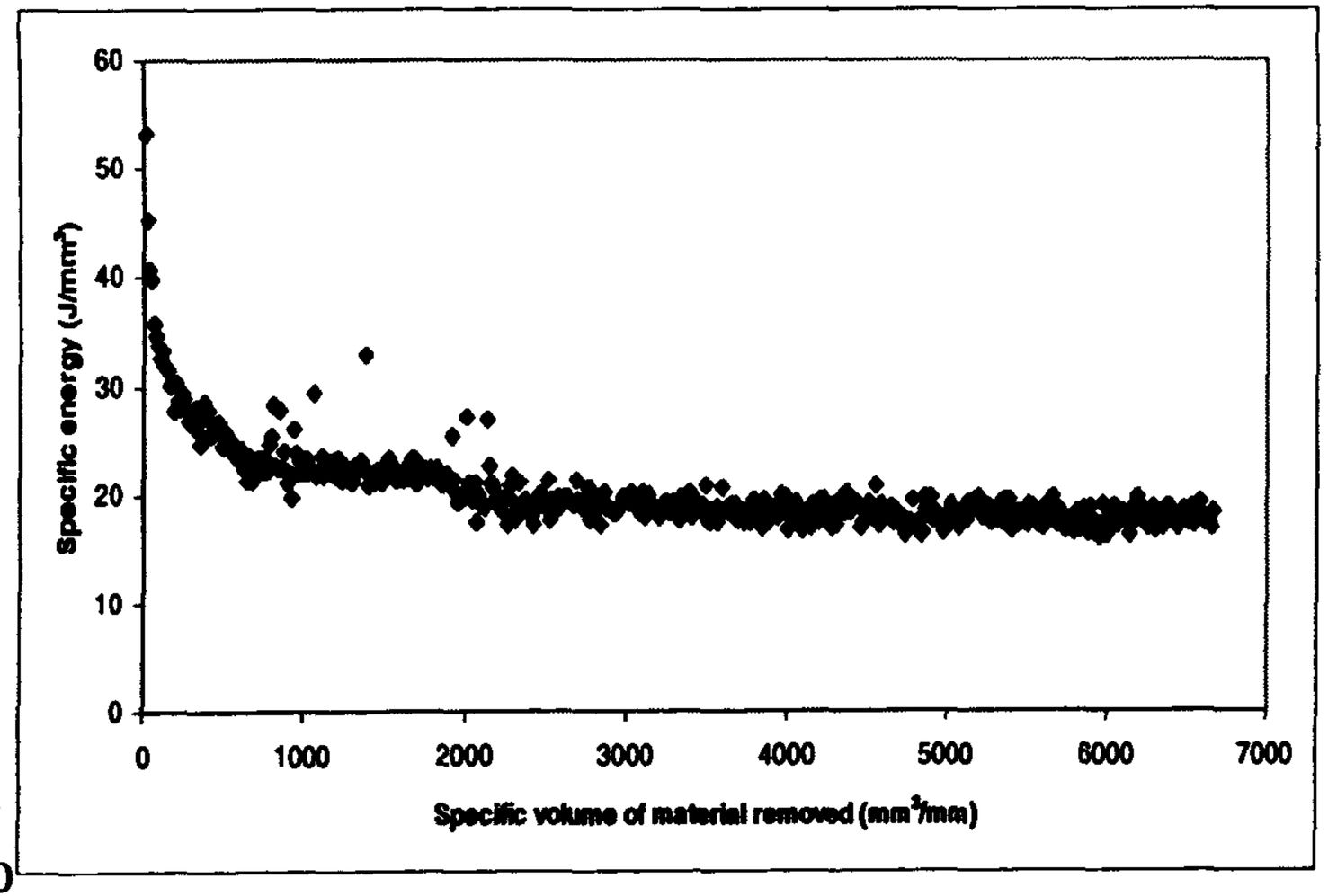

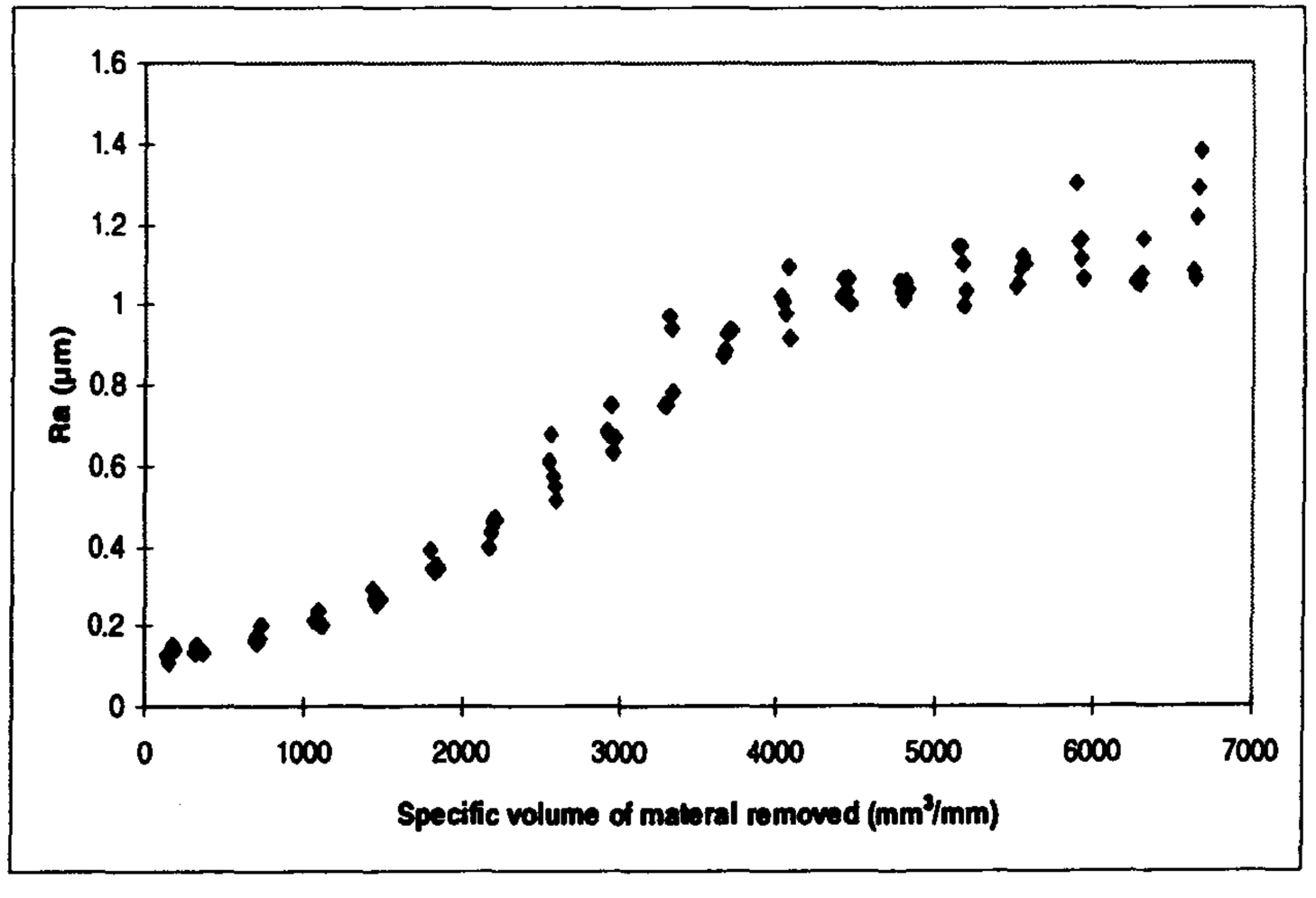

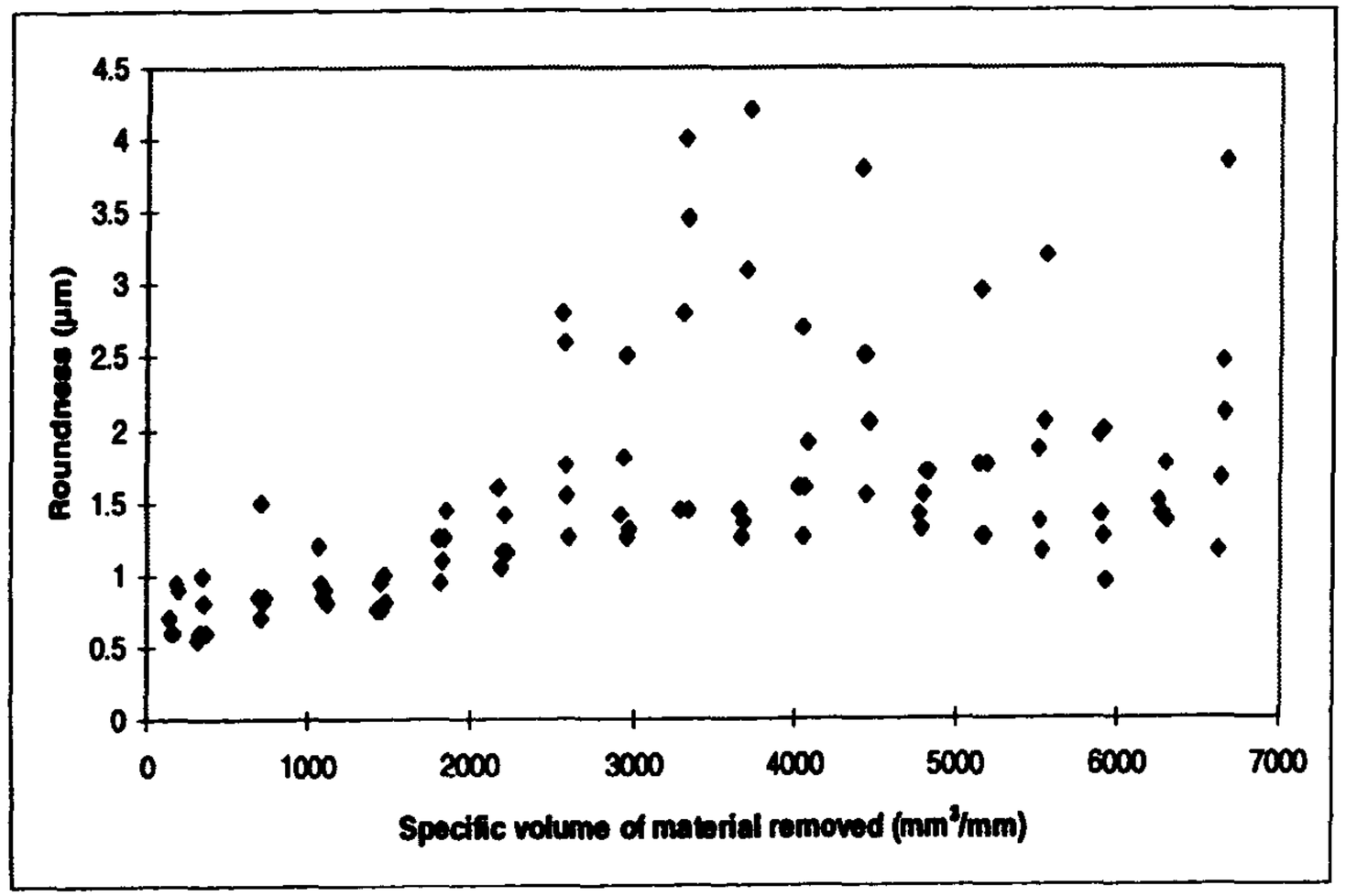

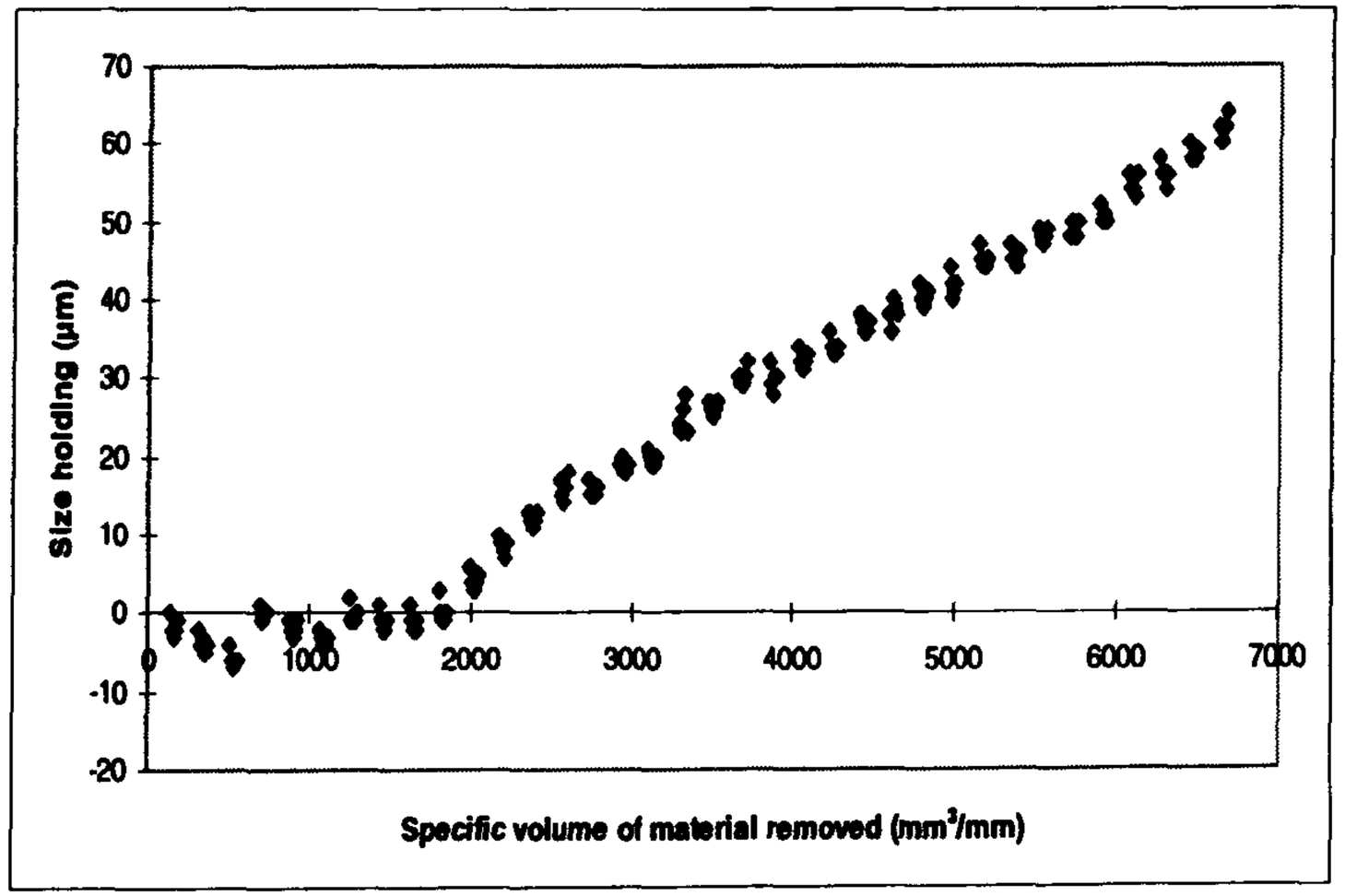

Results for Suprema Characterisation Trial 11 (i.e. 11 of 16) Grinding AISI 52100 With a Vitrified CBN Wheel

Experimental Conditions

- Up dressing
- U_d: 2
- a_d: 2µm
- n_d: 10
- v_s: 120m/s
- v_w: 36m/min
- s:10µm@1µm/s
- v_R: 72m/s
-Q'w: 10mm³/mm s
- Wheel: B91VR150
- Coolant: Hysol X 36 l/min, 30Bar pump pressure

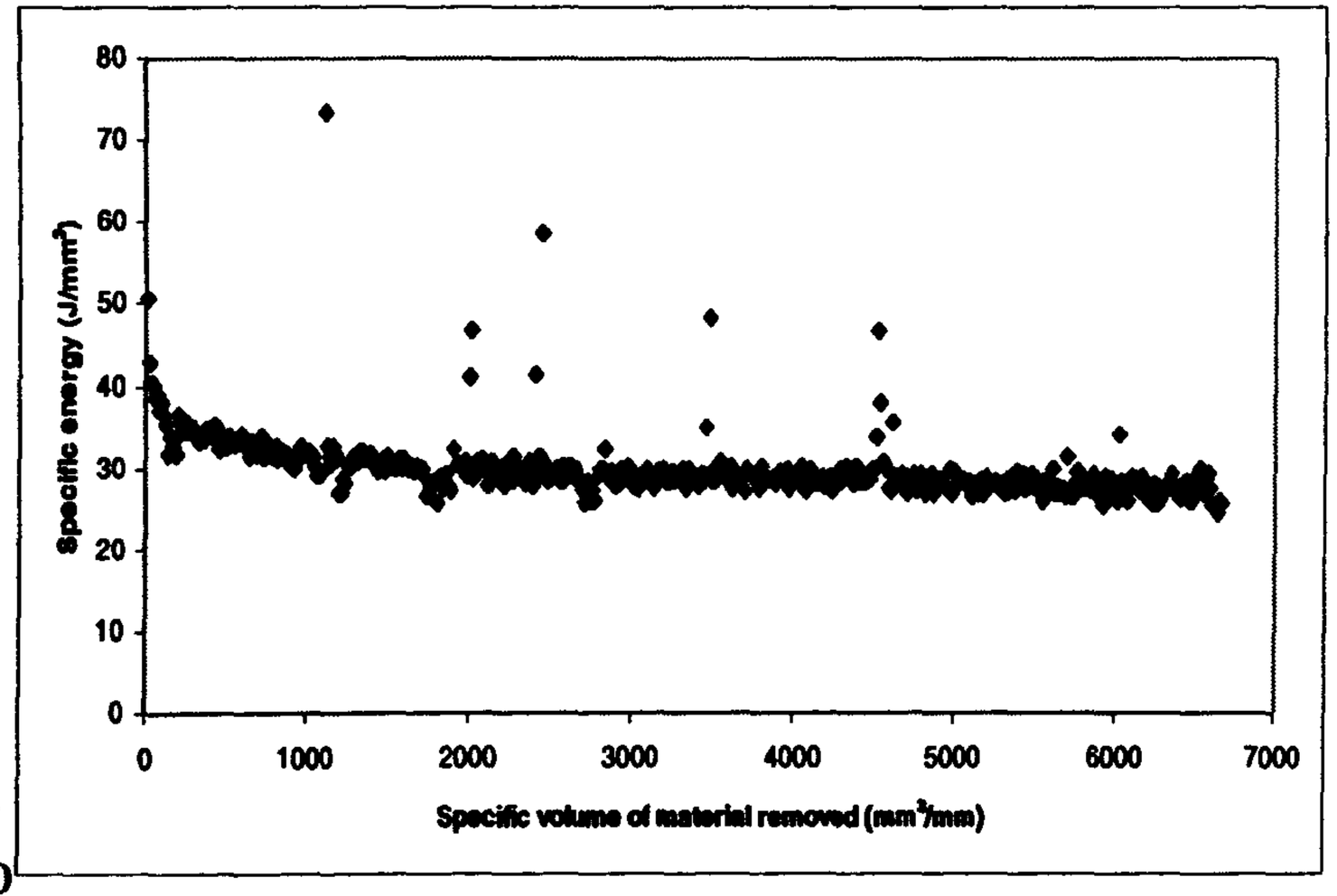

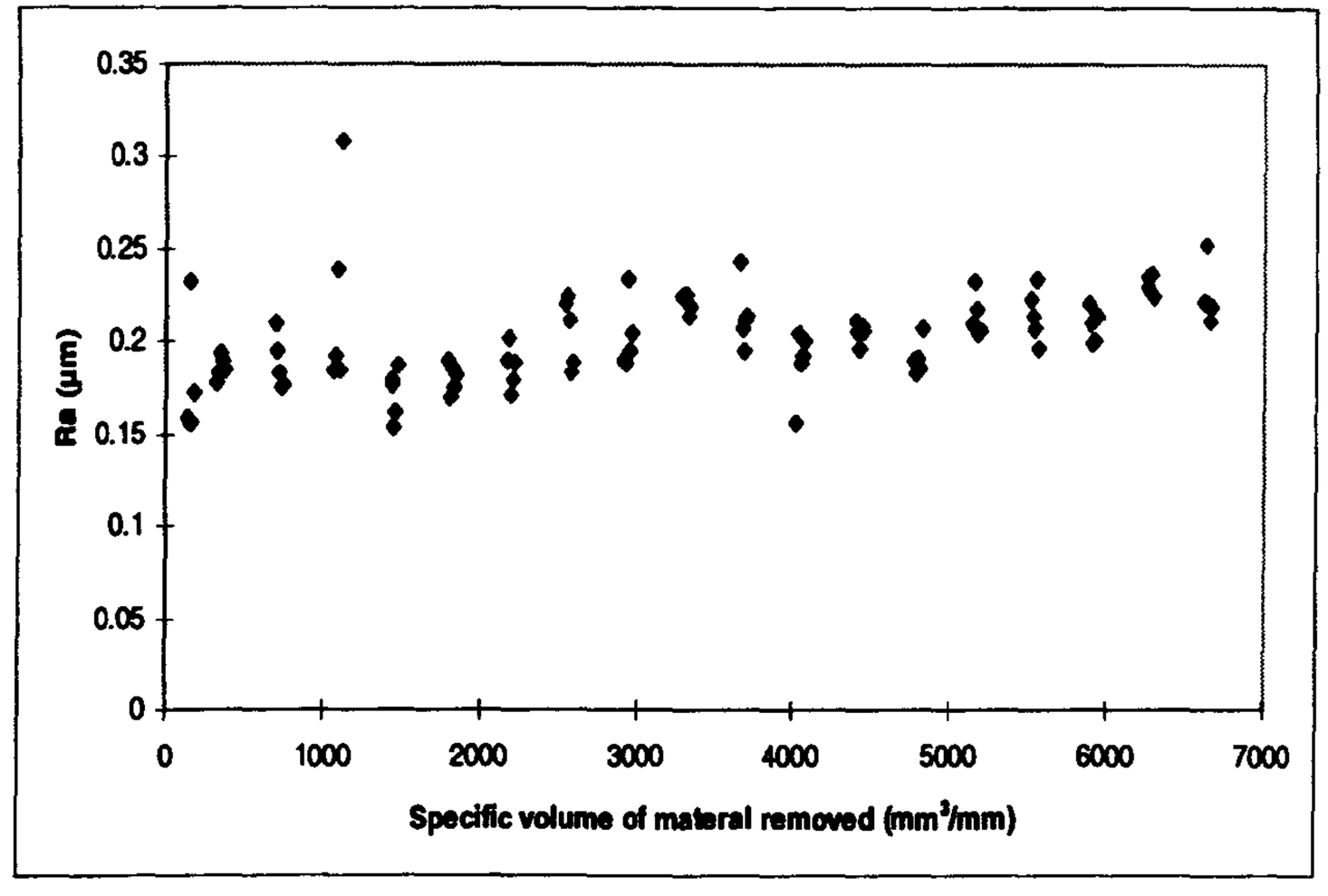

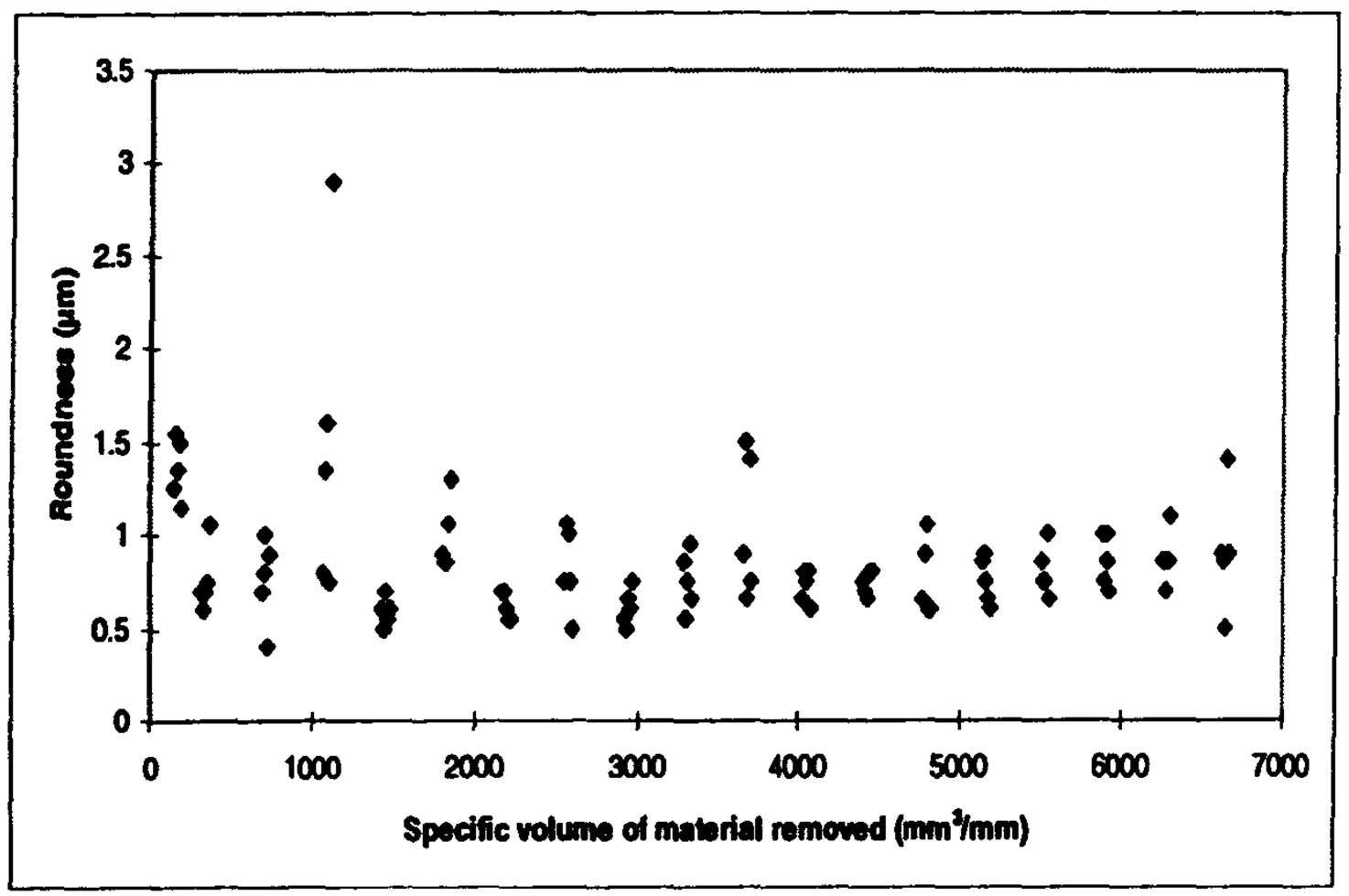

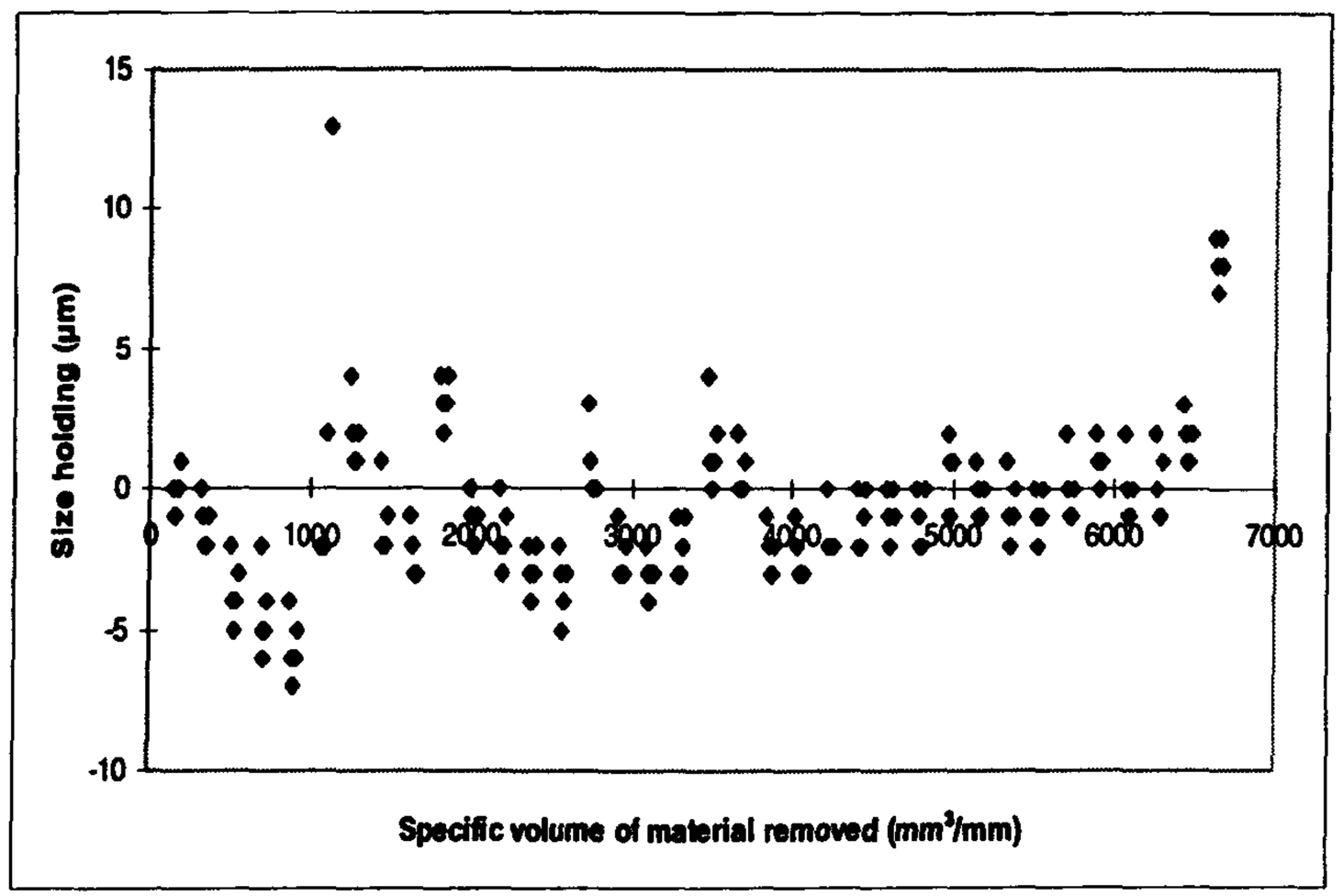

Results for Suprema Characterisation Trial 12 (i.e. 12 of 16) Grinding AISI 52100 With a Vitrified CBN Wheel

<u>Experimental Conditions</u>

- Up dressing
- U_d: 2
- a_d: 2µm
- n_d: 2
- v_s: 60m/s
- v_w: 54m/min
- s:10s
- v_R: 72m/s
-Q'w: 10mm³/mm s
- Wheel: B91VR150
- Coolant: Hysol X 36 l/min, 30Bar pump pressure

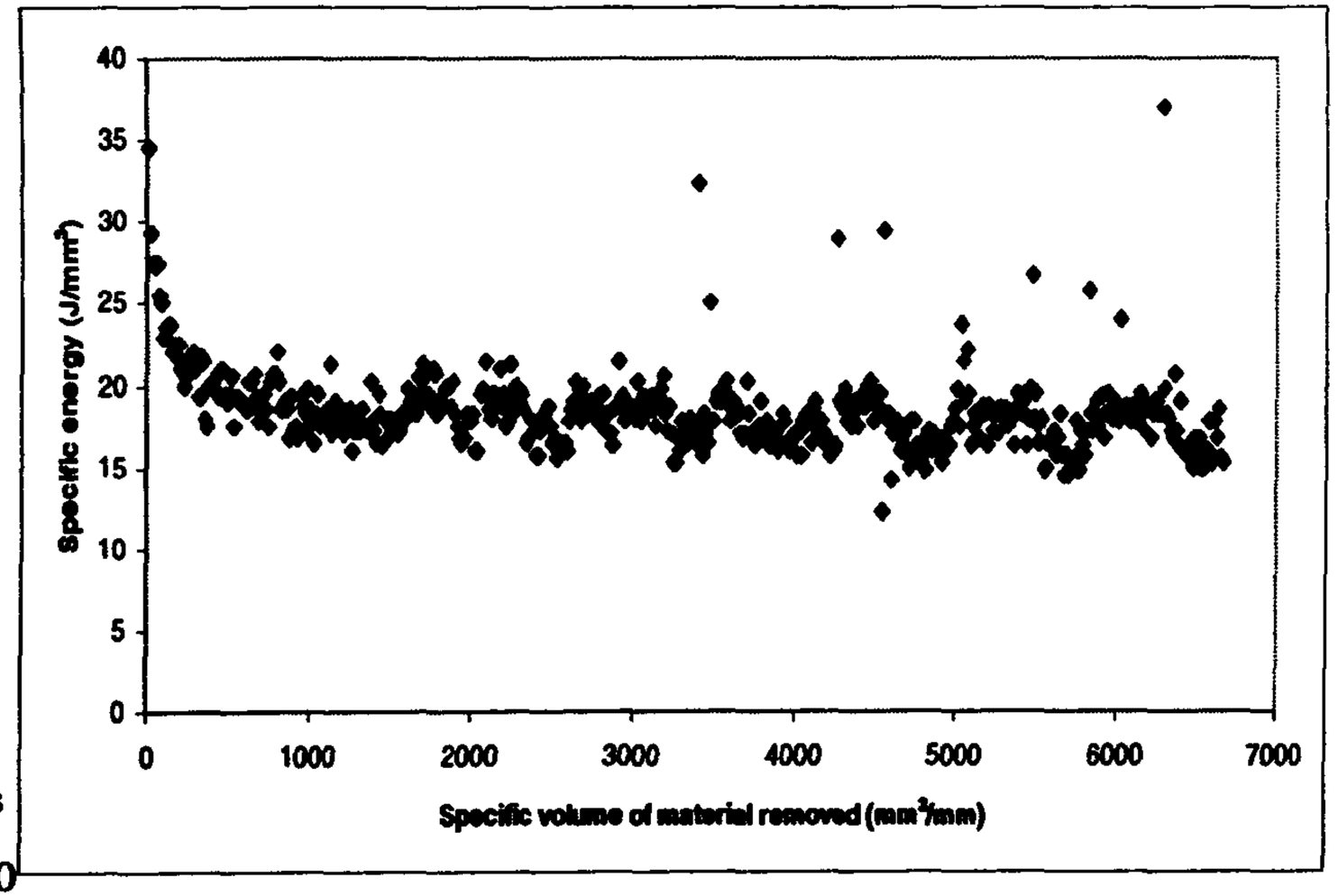

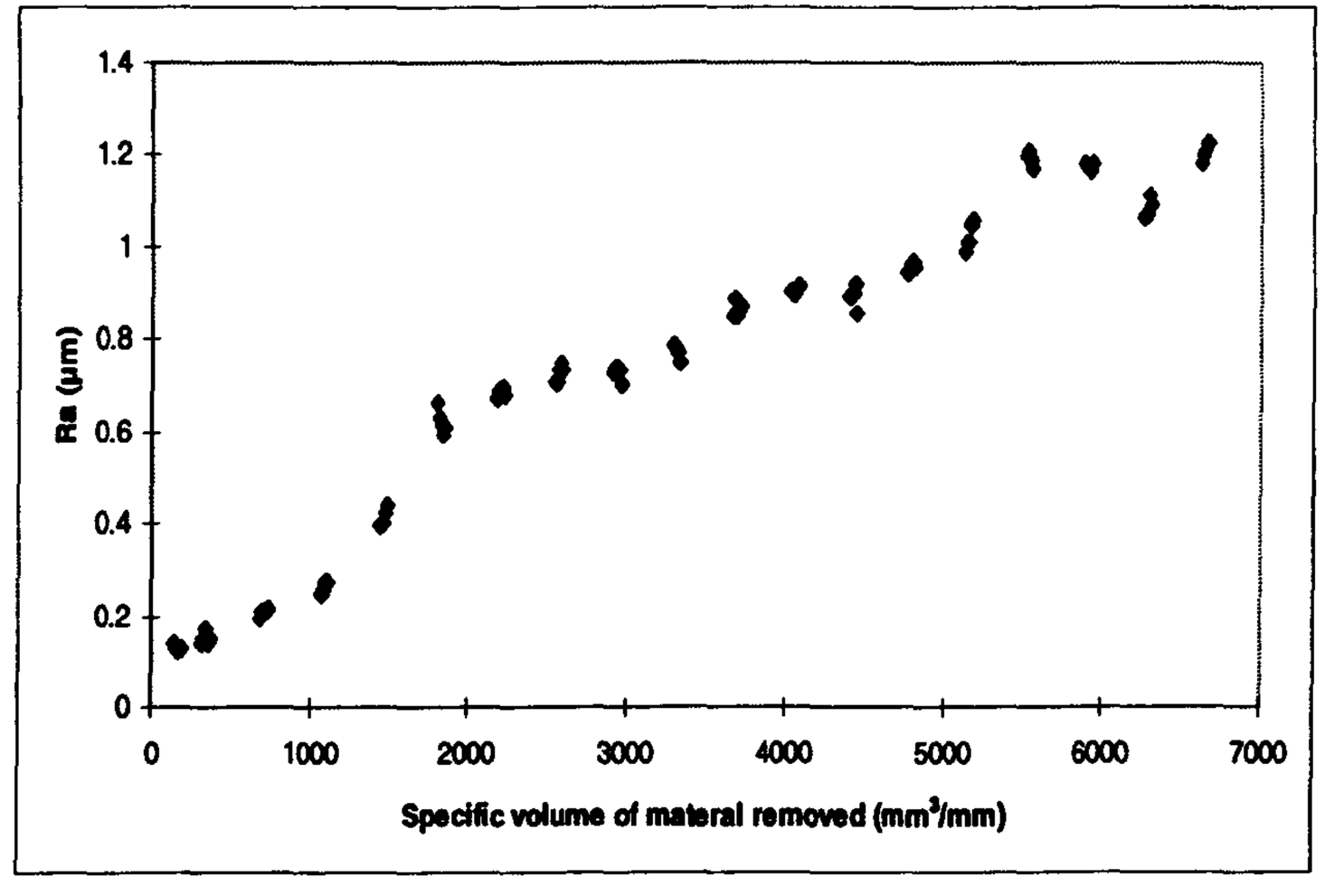

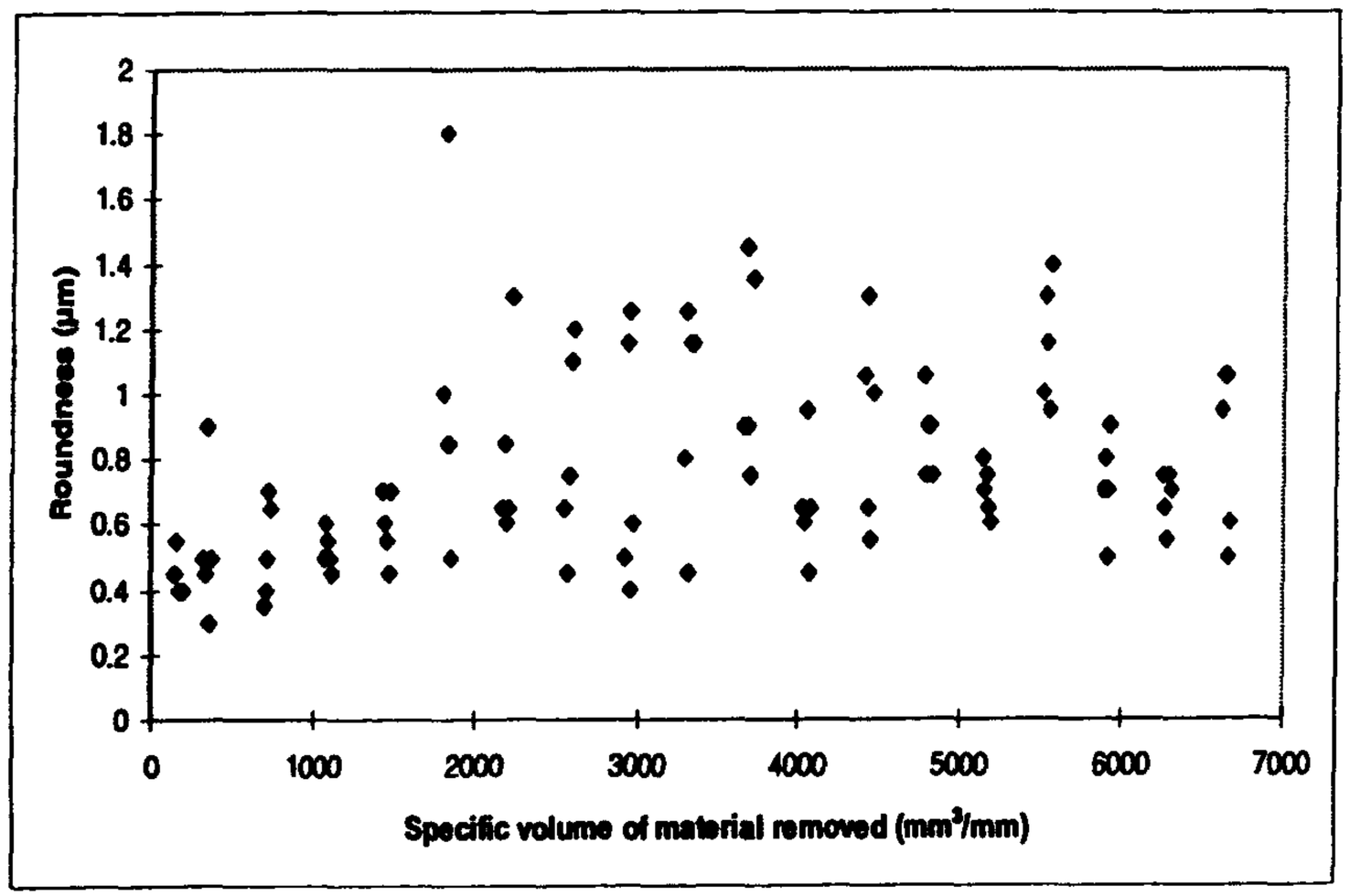

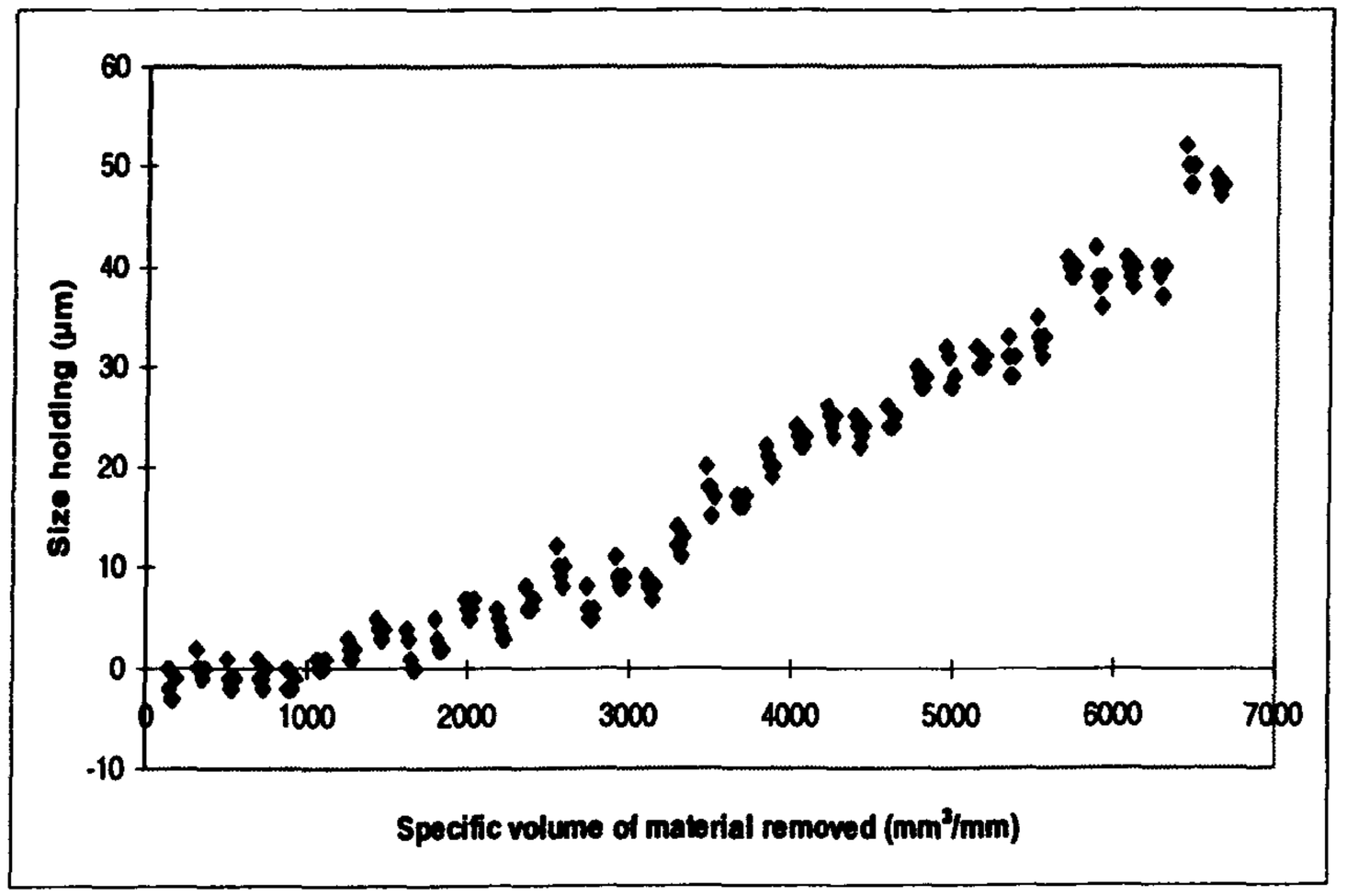

Results for Suprema Characterisation Trial 13 (i.e. 13 of 16) Grinding AISI 52100 With a Vitrified CBN Wheel

Experimental Conditions

- Down dressing
- U_d: 10
- a_d: 2µm
- n_d: 10
- v_s: 60m/s
- v_w: 54m/min
- s:10µm@1µm/s
- v_R: 72m/s
-Q'w: 10mm³/mm s
- Wheel: B91VR150
- Coolant: Hysol X 36 l/min, 30Bar pump pressure

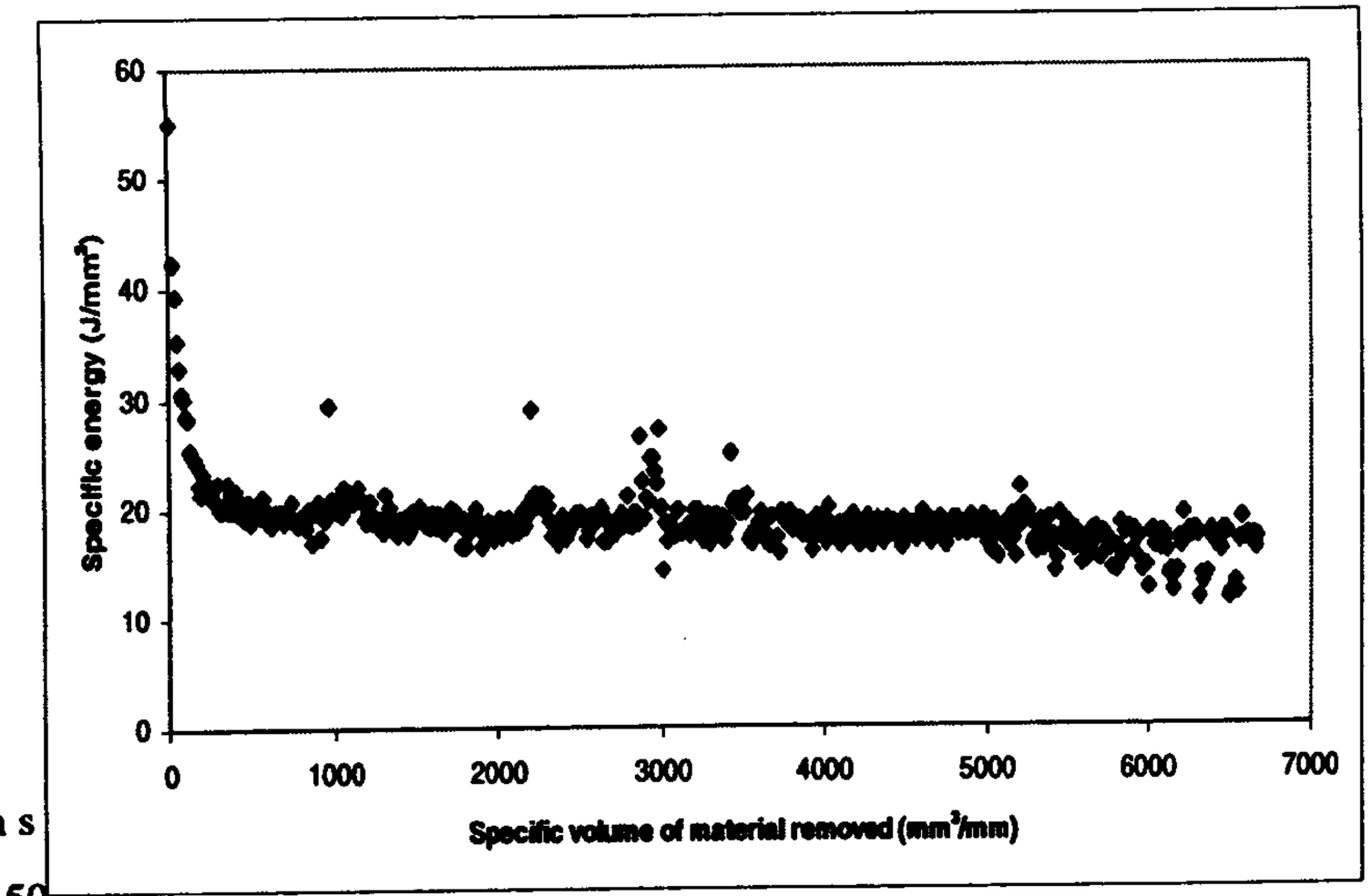

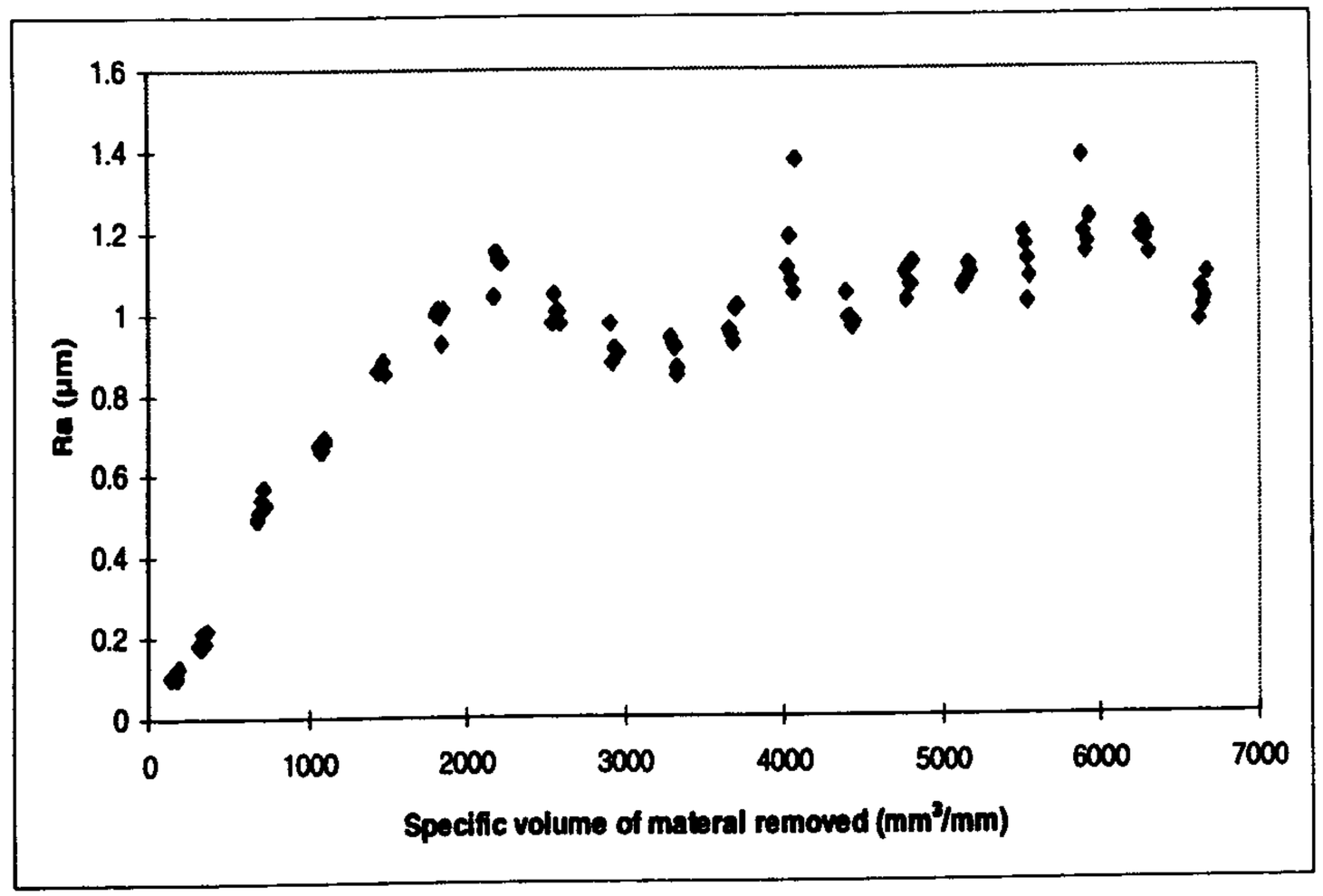

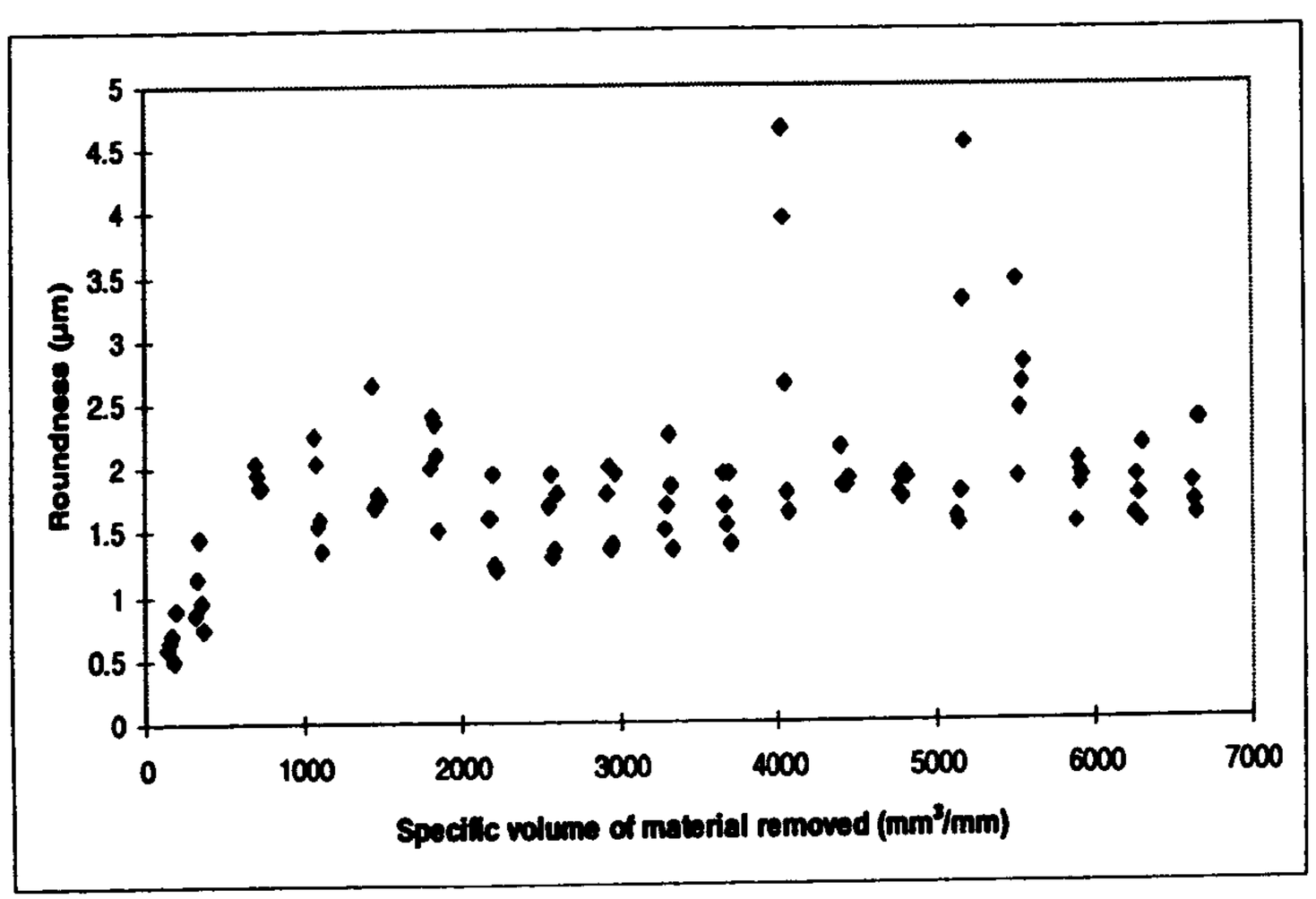

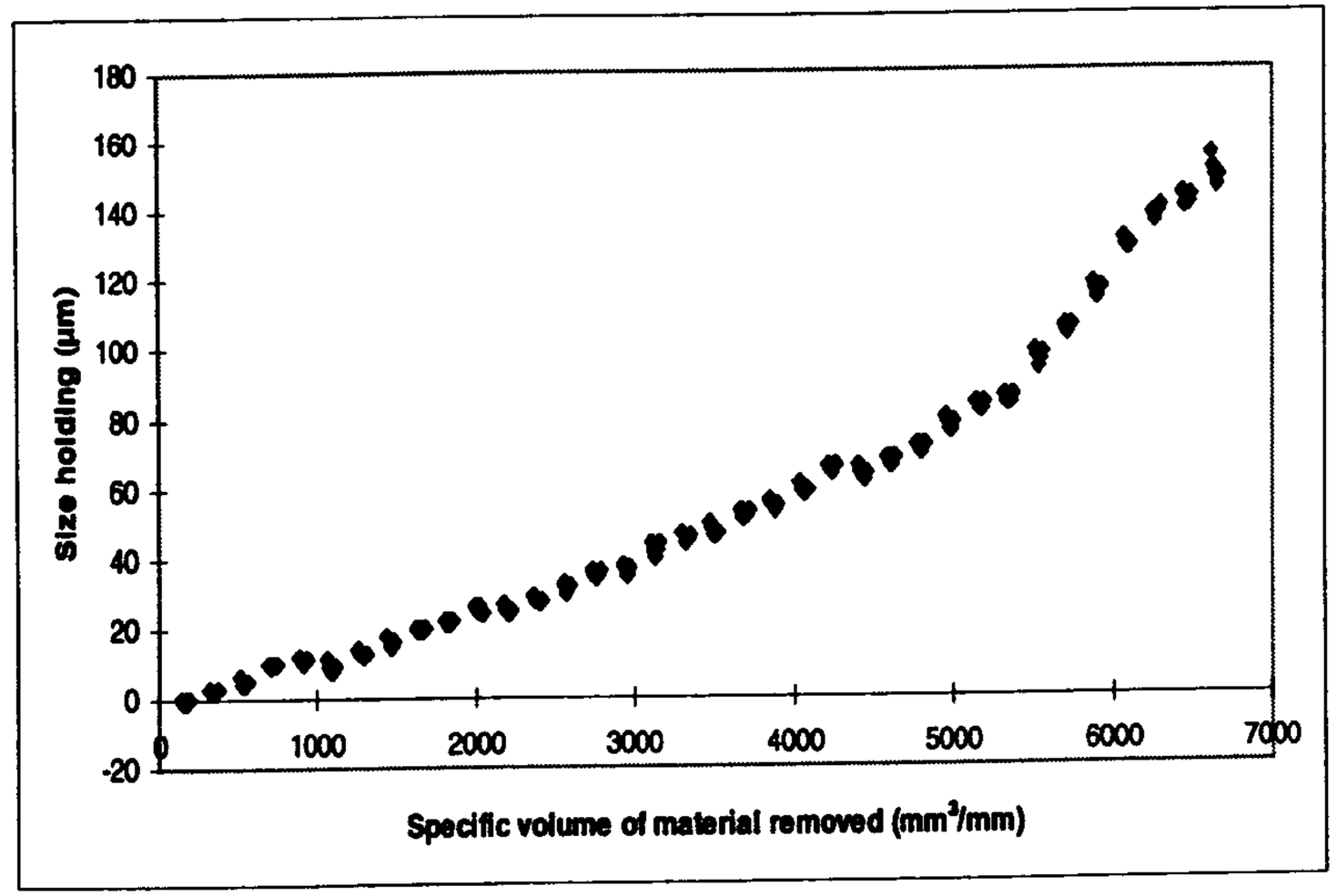

Results for Suprema Characterisation Trial 14 (i.e. 14 of 16) Grinding AISI 52100 With A Vitrified CBN Wheel

<u>Experimental Conditions</u>

- Down dressing
- U_d: 10
- a_d: 2µm
- n_d: 2
- v_s: 120m/s
- v_w: 36m/min
- s:10s
- v_R: 72m/s
-Q'w: 10mm³/mm s
- Wheel: B91VR150
- Coolant: Hysol X 36 l/min, 30Bar pump pressure

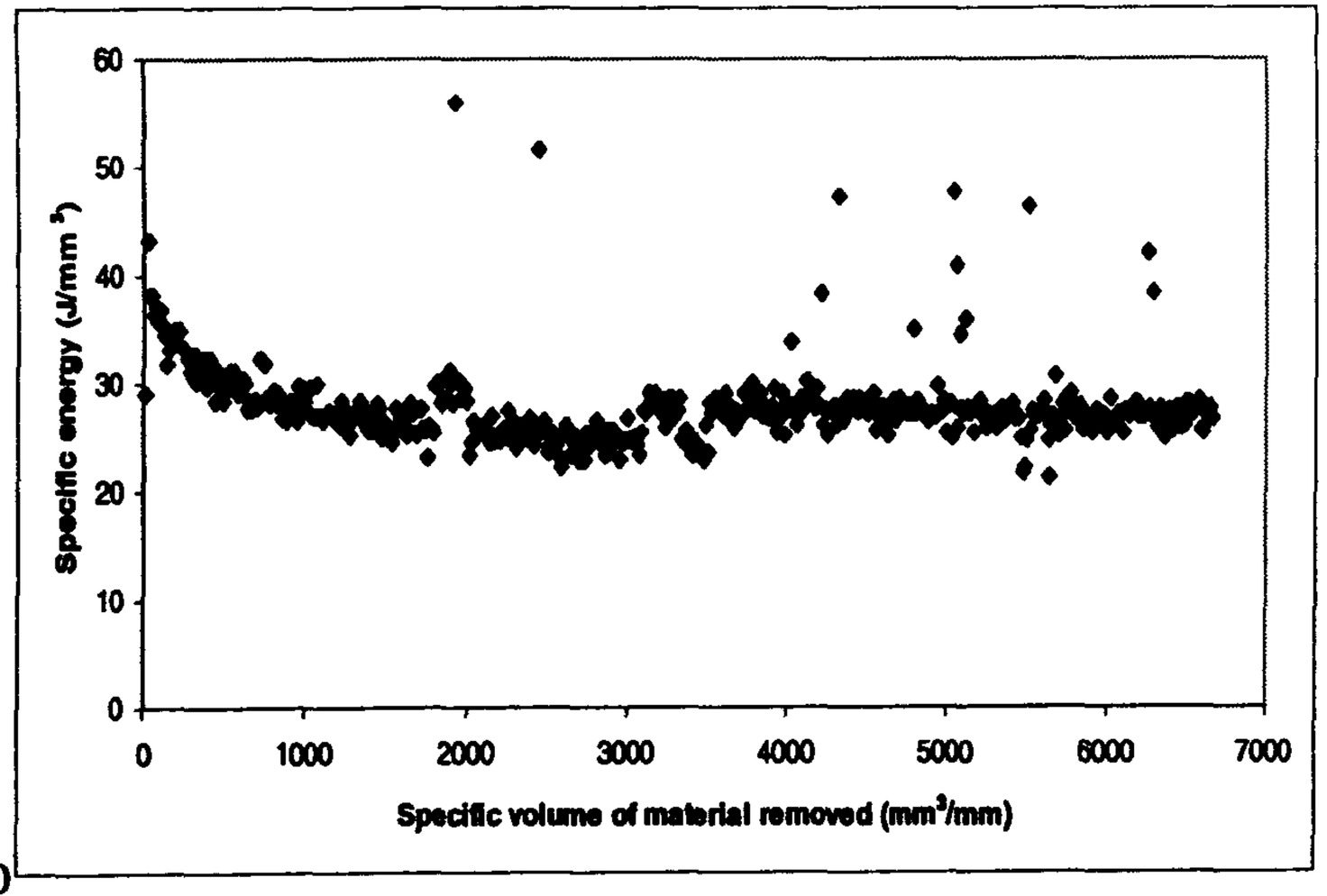

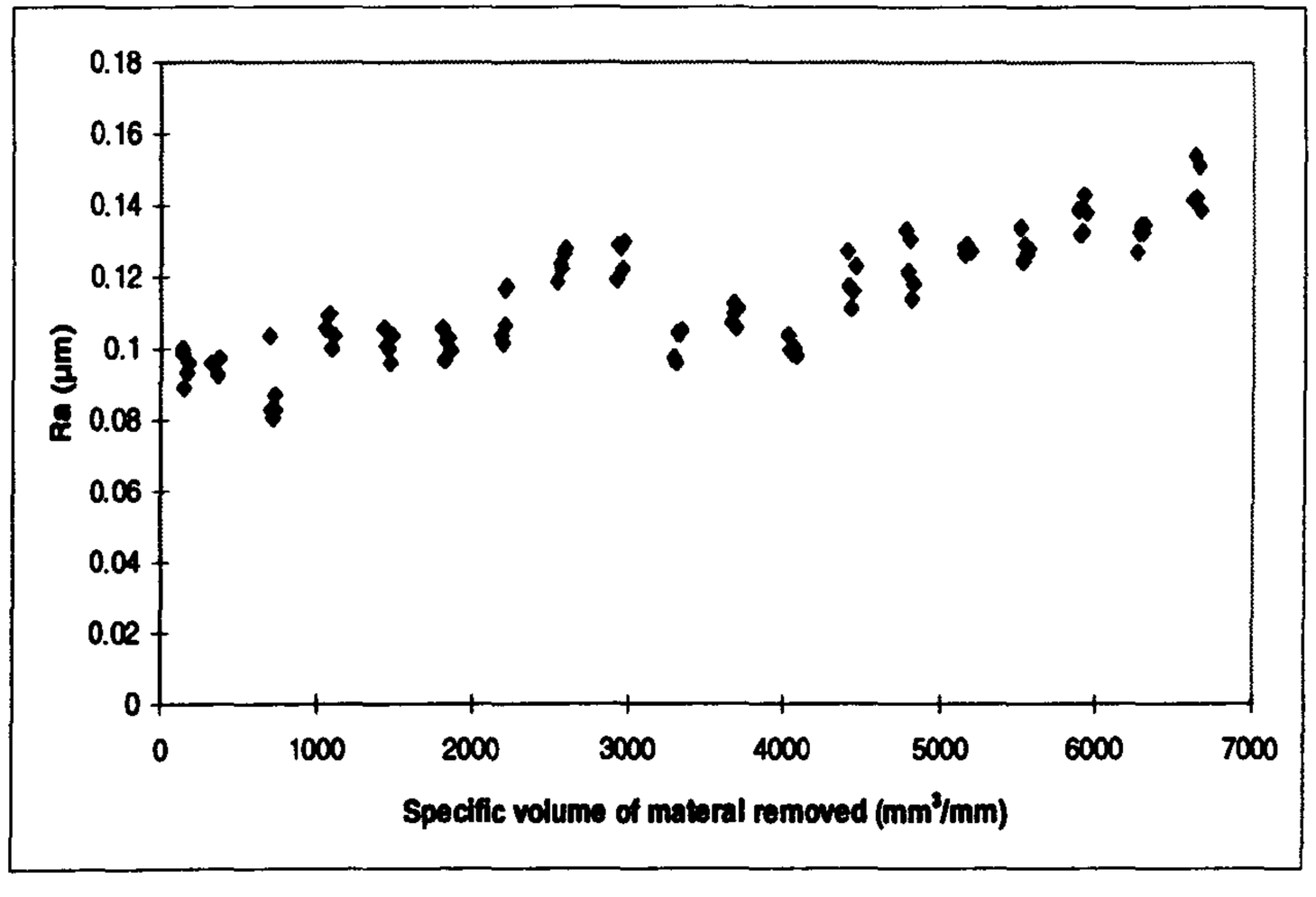

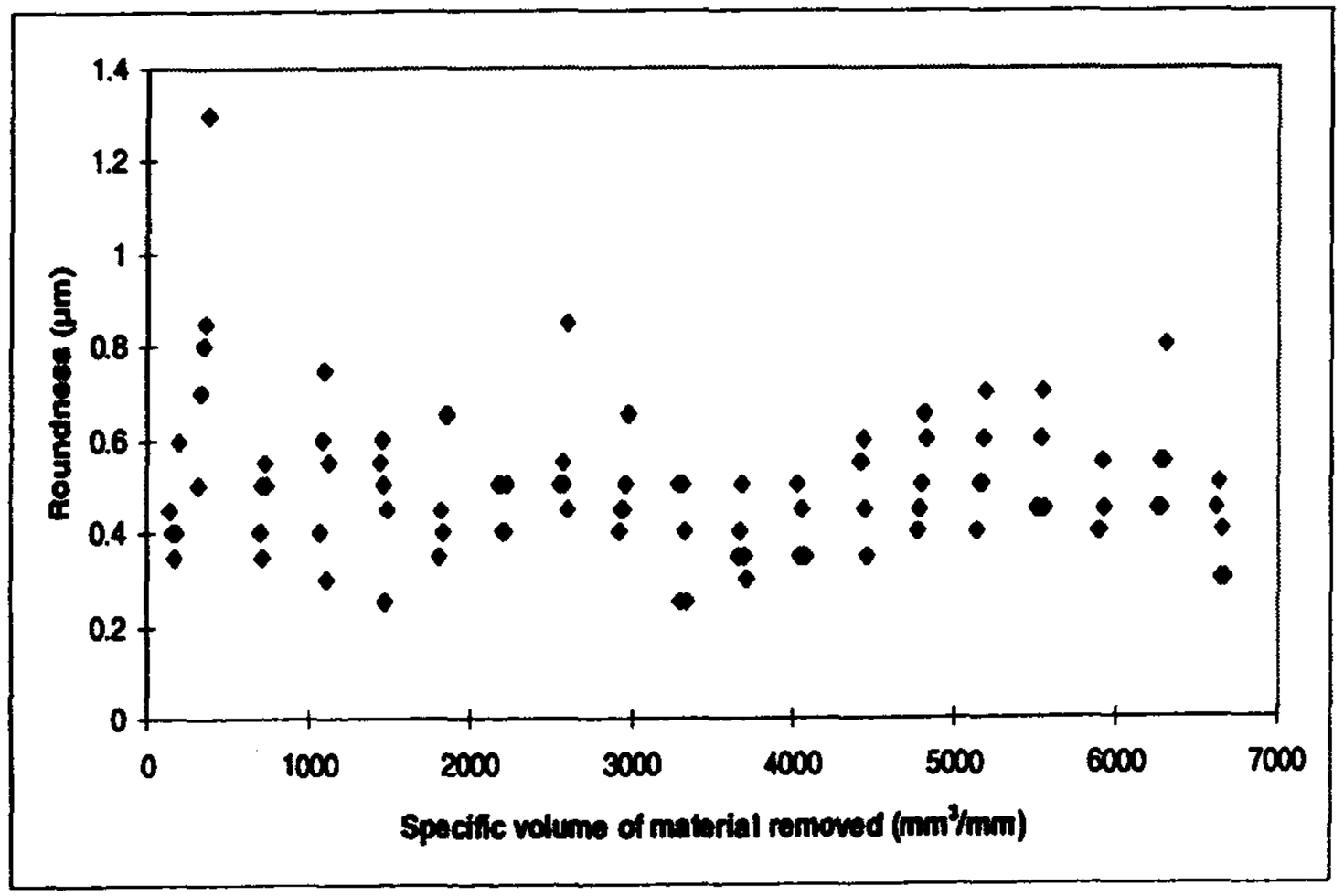

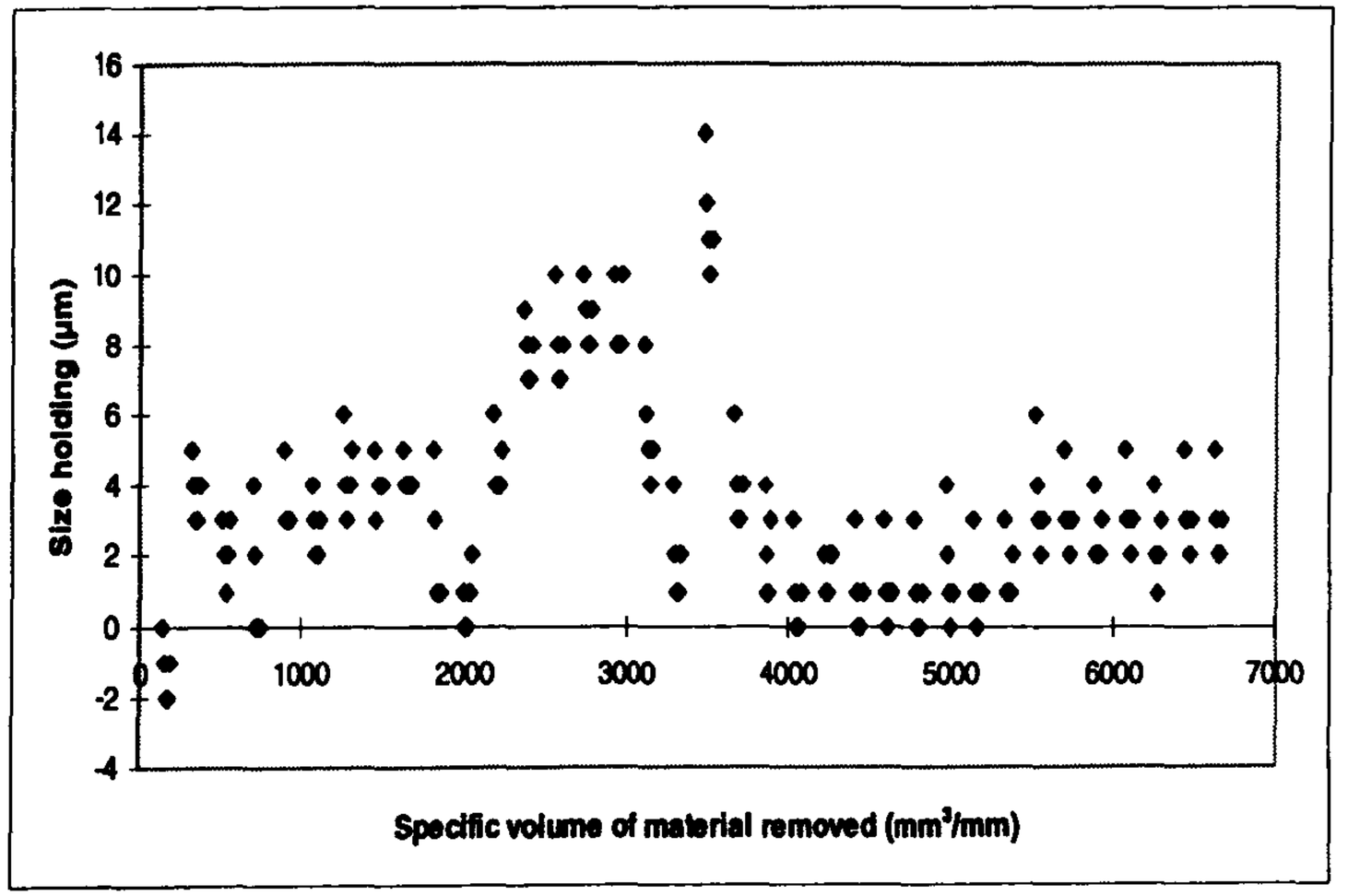

14

Results for Suprema Characterisation Trial 15 (i.e. 15 of 16) Grinding AISI 52100 With a Vitrified CBN Wheel

Experimental Conditions

- Down dressing
- U_d: 2
- a_d: 10µm
- n_d: 10
- v_s: 60m/s
- v_w: 36m/min
- s:10s
- v_R: 72m/s
-Q'w: 10mm³/mm s
- Wheel: B91VR150
- Coolant: Hysol X 36 l/min, 30Bar pump pressure

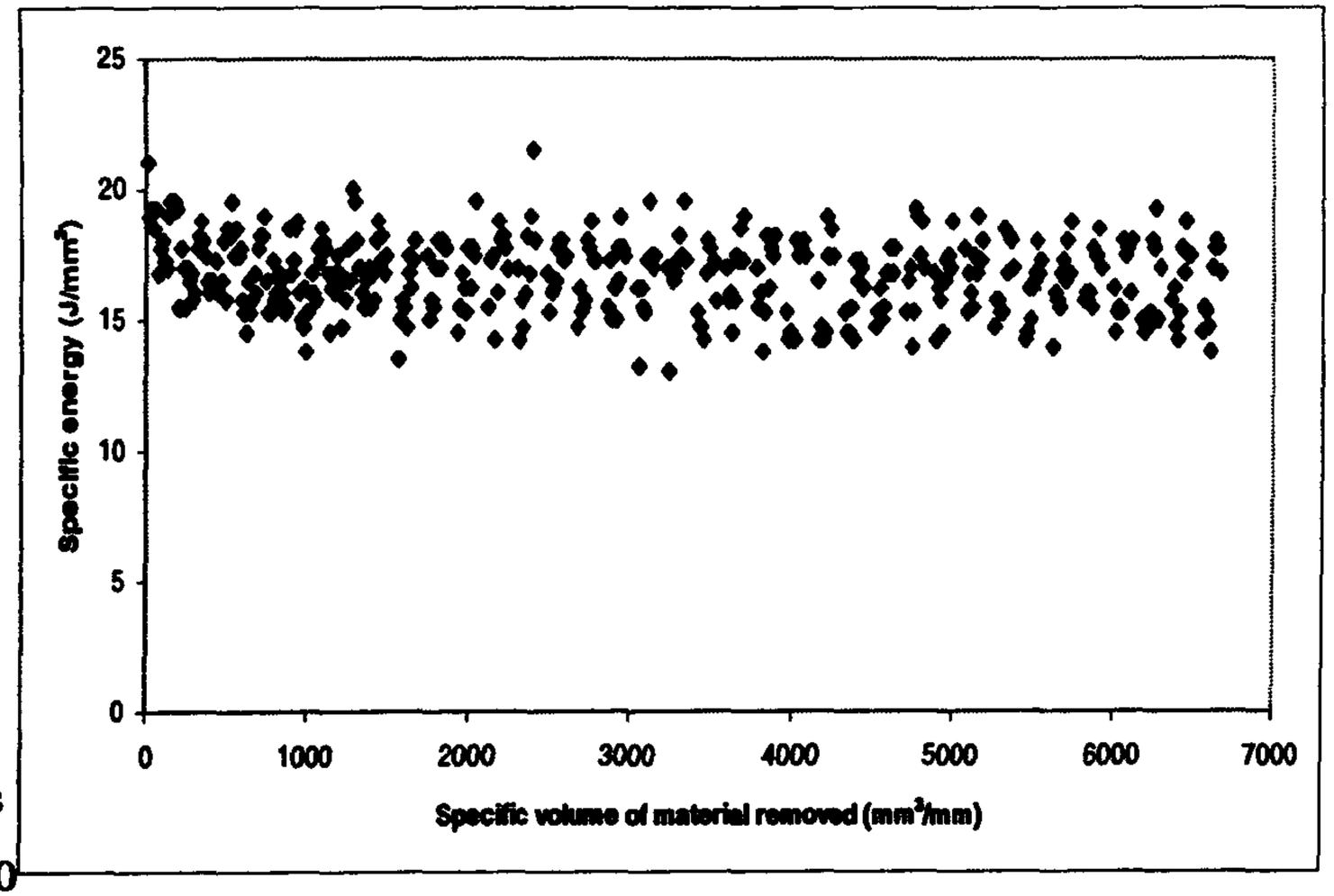

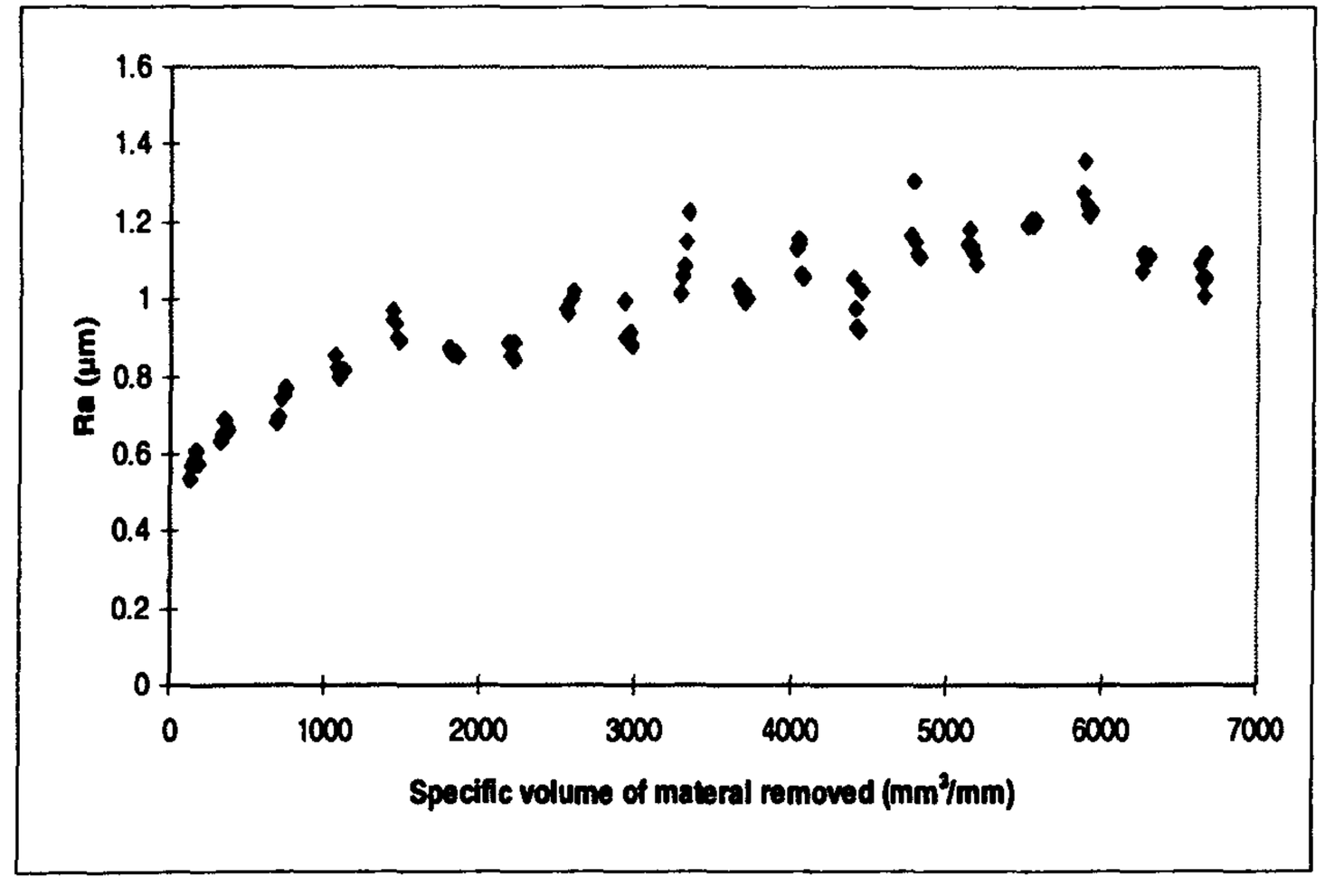

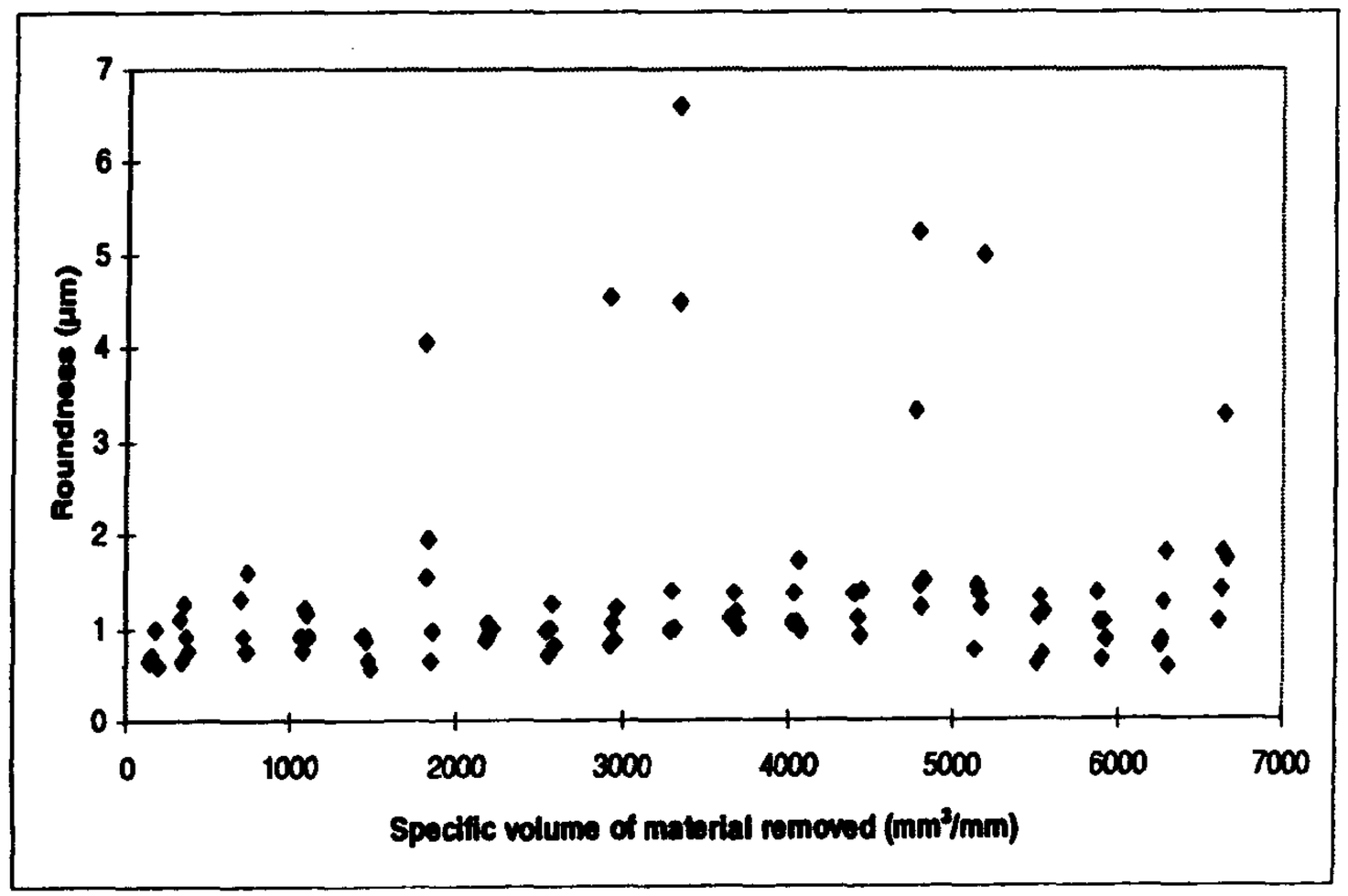

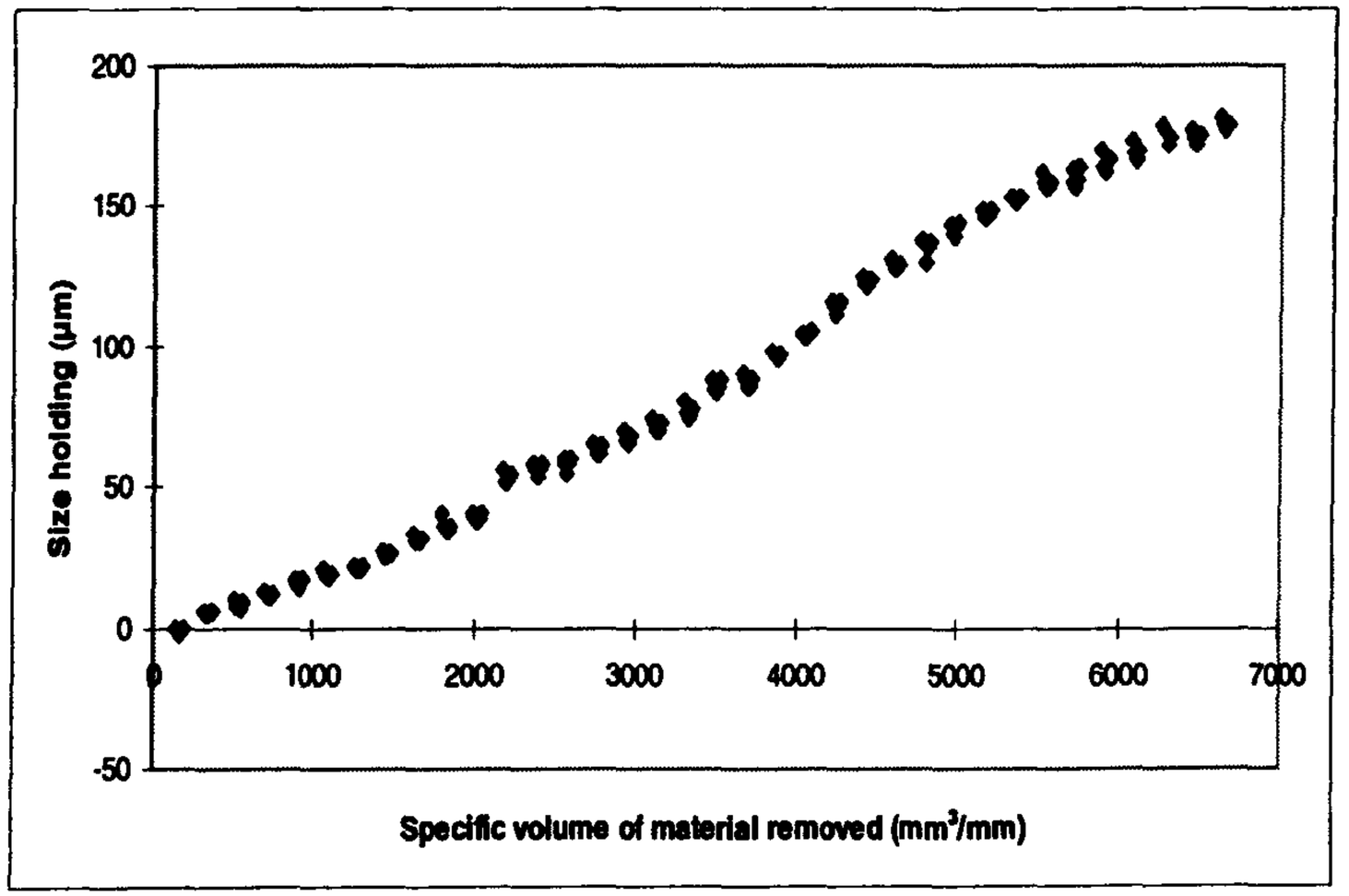

Results for Suprema Characterisation Trial 16 (i.e. 16 of 16) Grinding AISI 52100 With a Vitrified CBN Wheel

Experimental Conditions

- Down dressing
- U_d: 2
- a_d: 10µm
- n_d: 2
- v_s: 120m/s
- v_w: 54m/min
- s:10µm@1µm/s
- v_R: 72m/s
-Q'w: 10mm³/mm s
- Wheel: B91VR150
- Coolant: Hysol X 36 l/min, 30Bar pump pressure

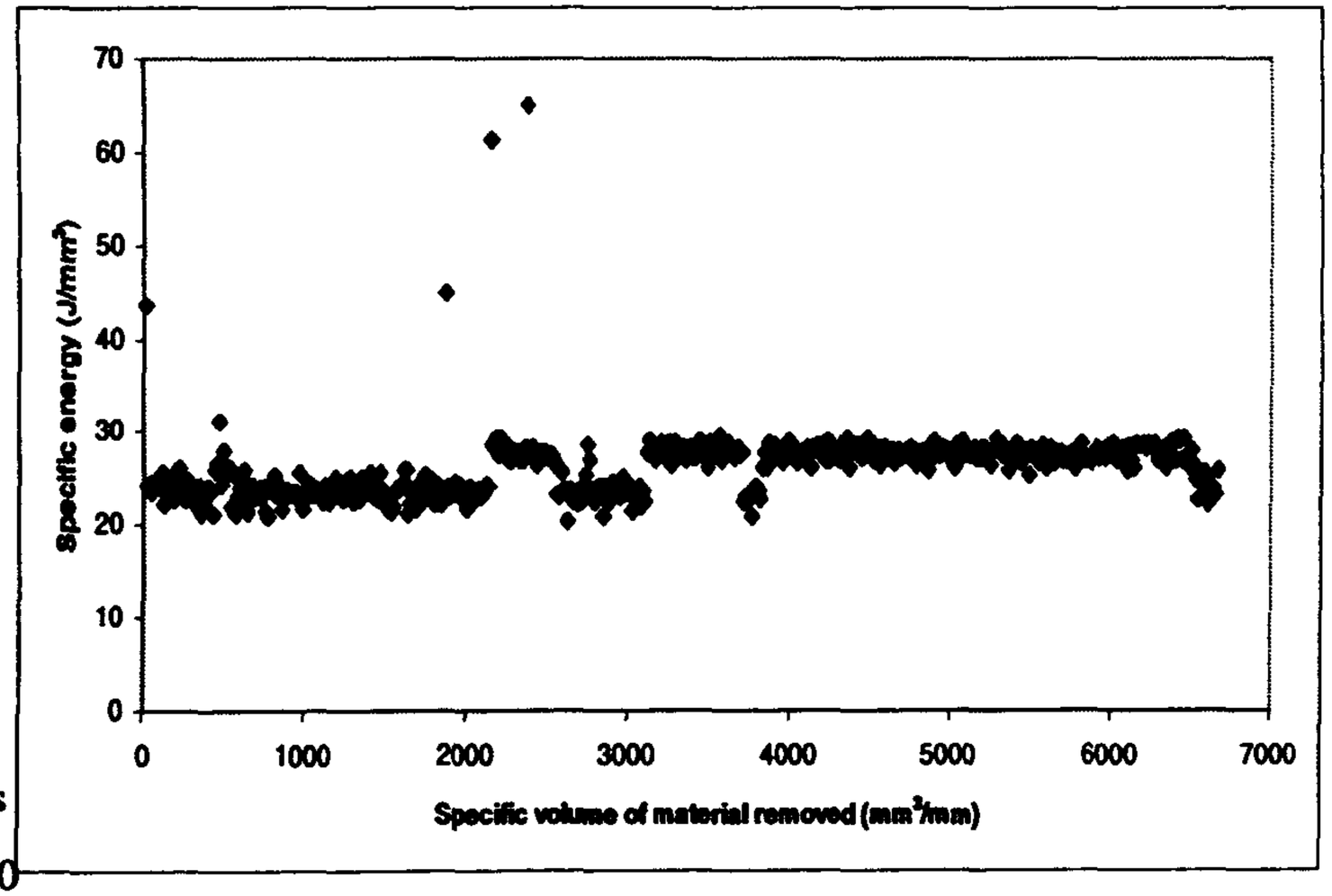

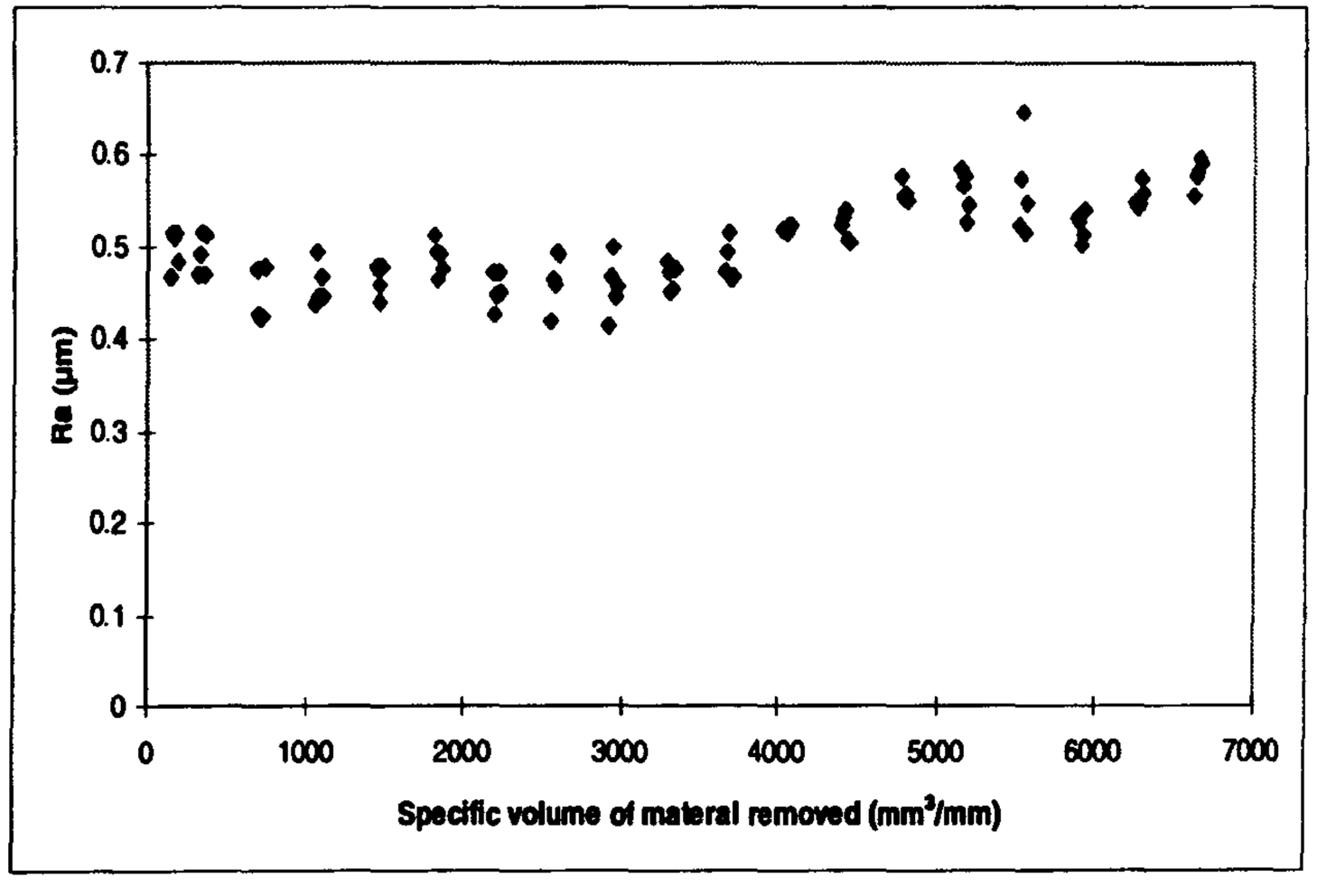

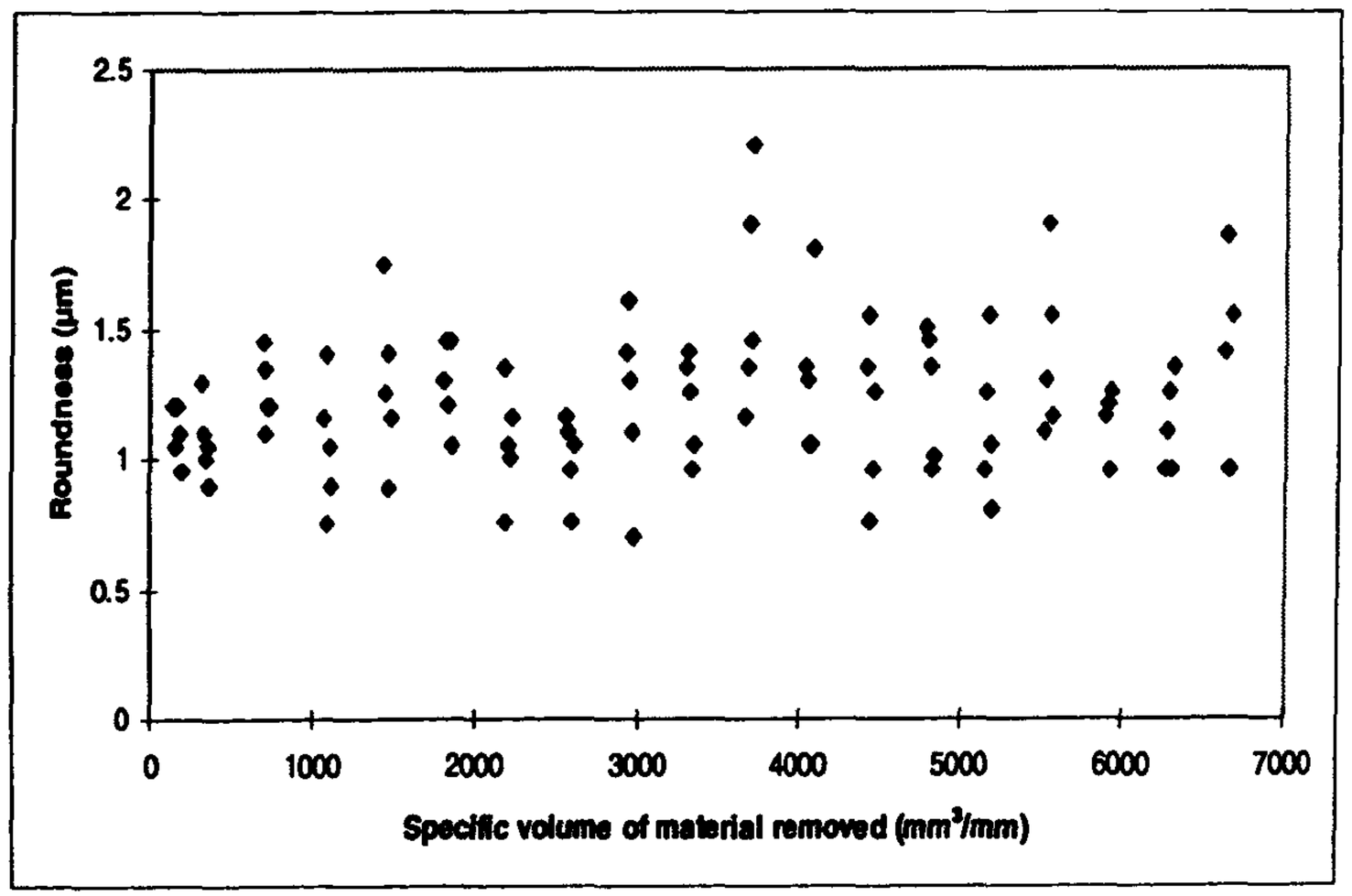

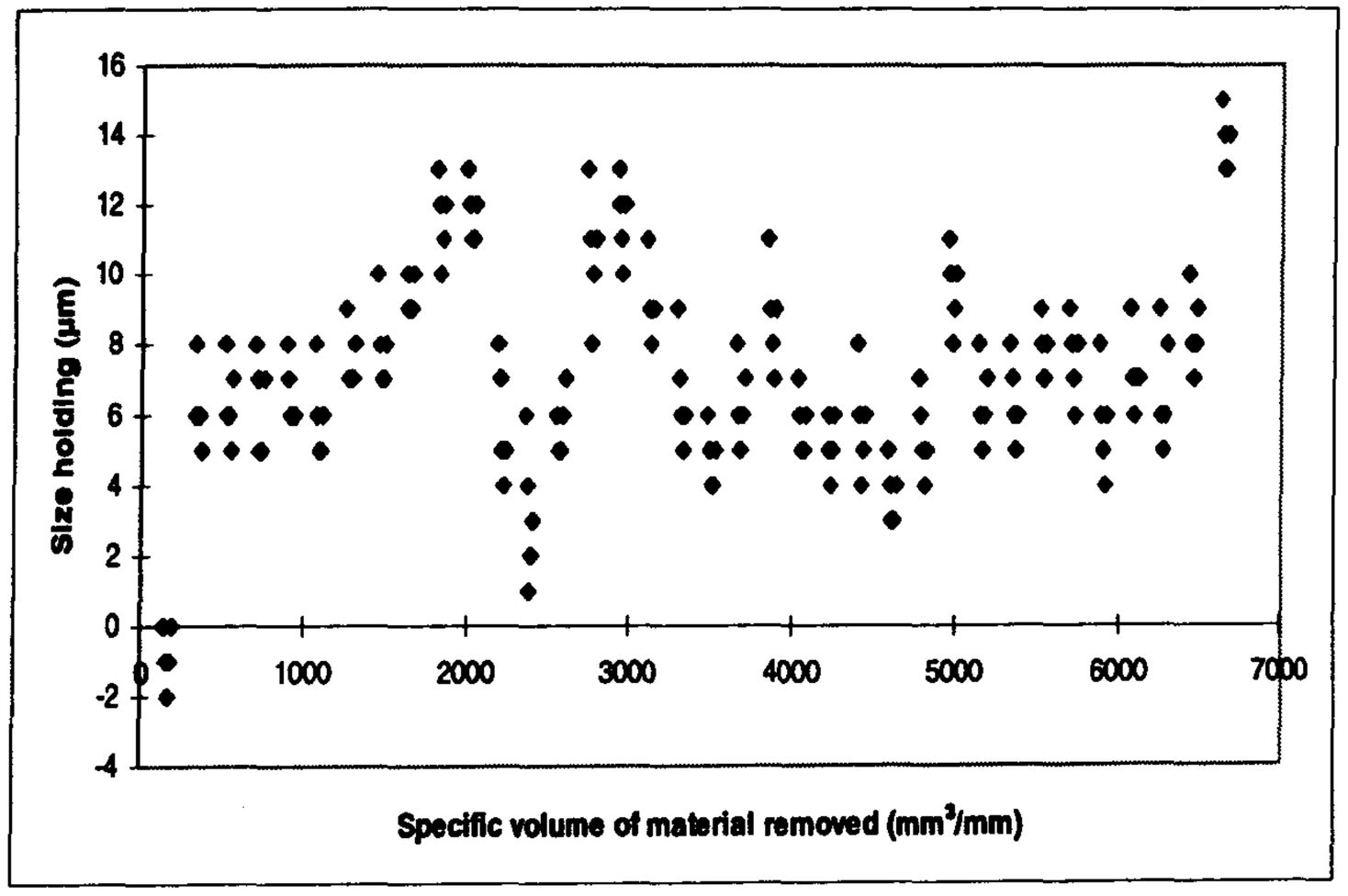

APPENDIX B3

Appendix B3. Graphs of results for all seven Suprema confirmation trials grinding AISI 52100

Graphs Showing Results for Confirmation Trial C1 Grinding AISI 52100 With a Vitrified CBN Wheel on the Suprema

<u>Experimental Conditions</u>

- Up dressing
- U_d: 10
- a_d: 2μm
- n_d: 2
- v_s: 120m/s
- v_w: 36m/min
- s:10s
- v_R: 42m/s
-Q'w: 10mm³/mm s
- Wheel: B91VR150
- Coolant: Hysol X 36 l/min, 30Bar pump pressure

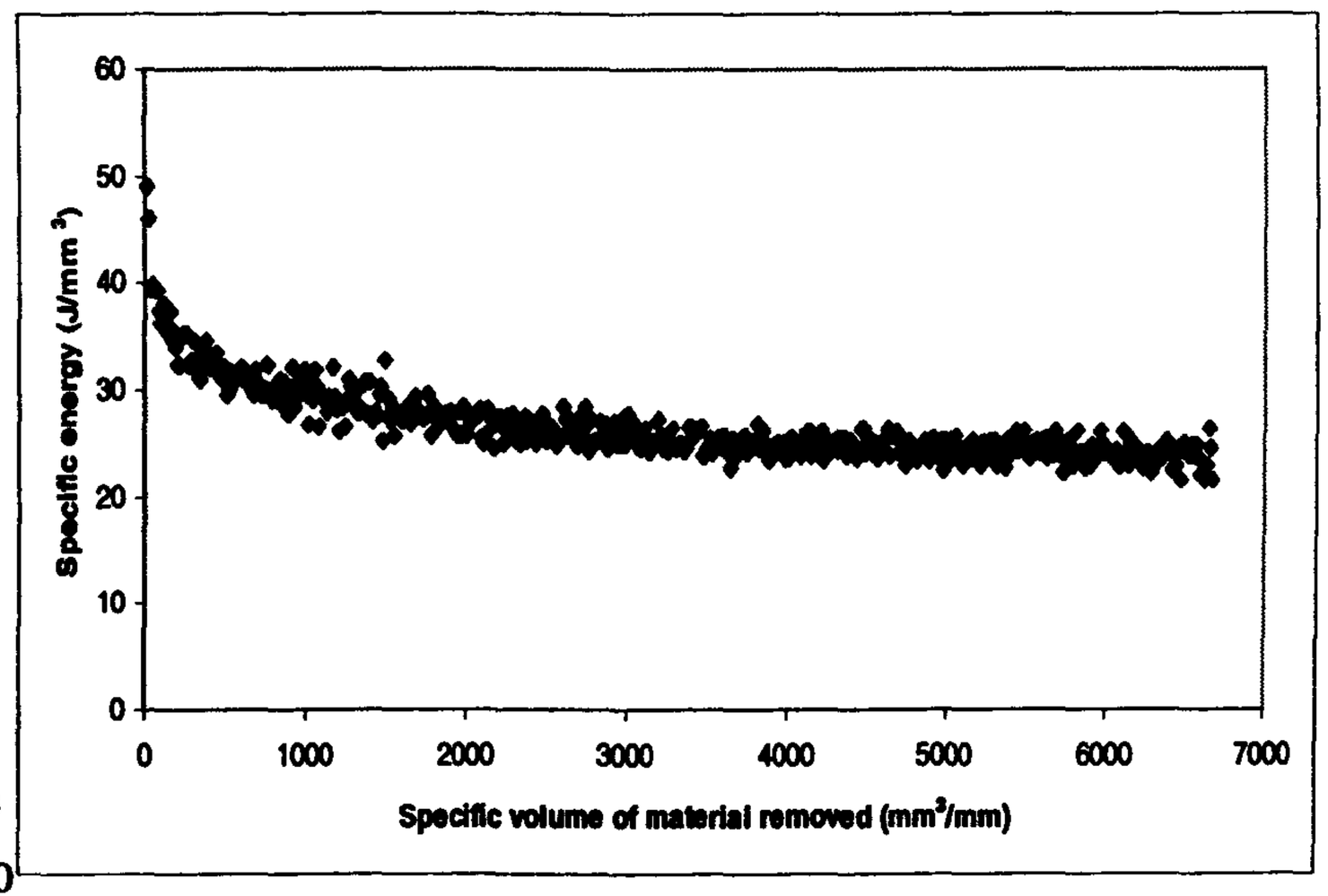

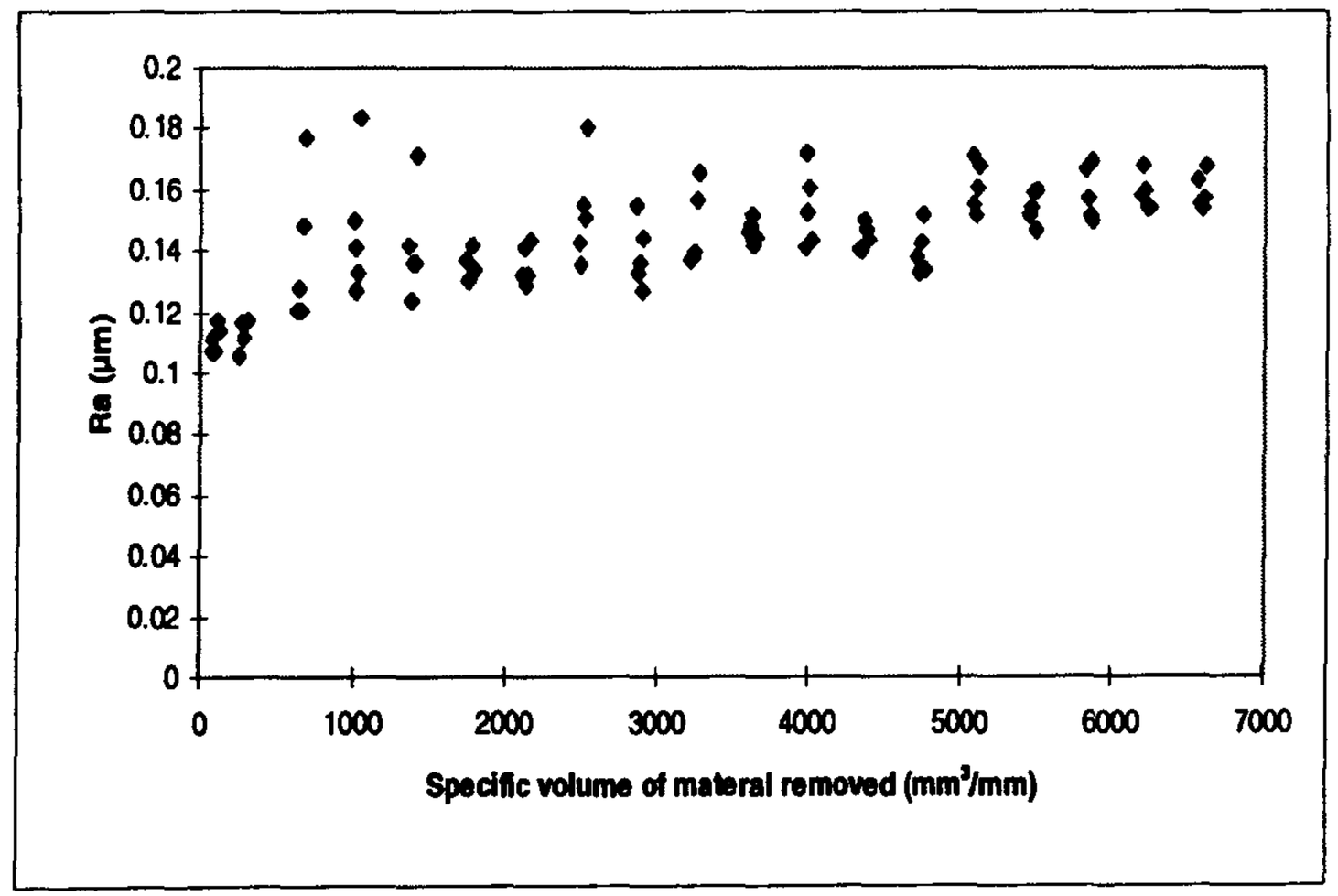

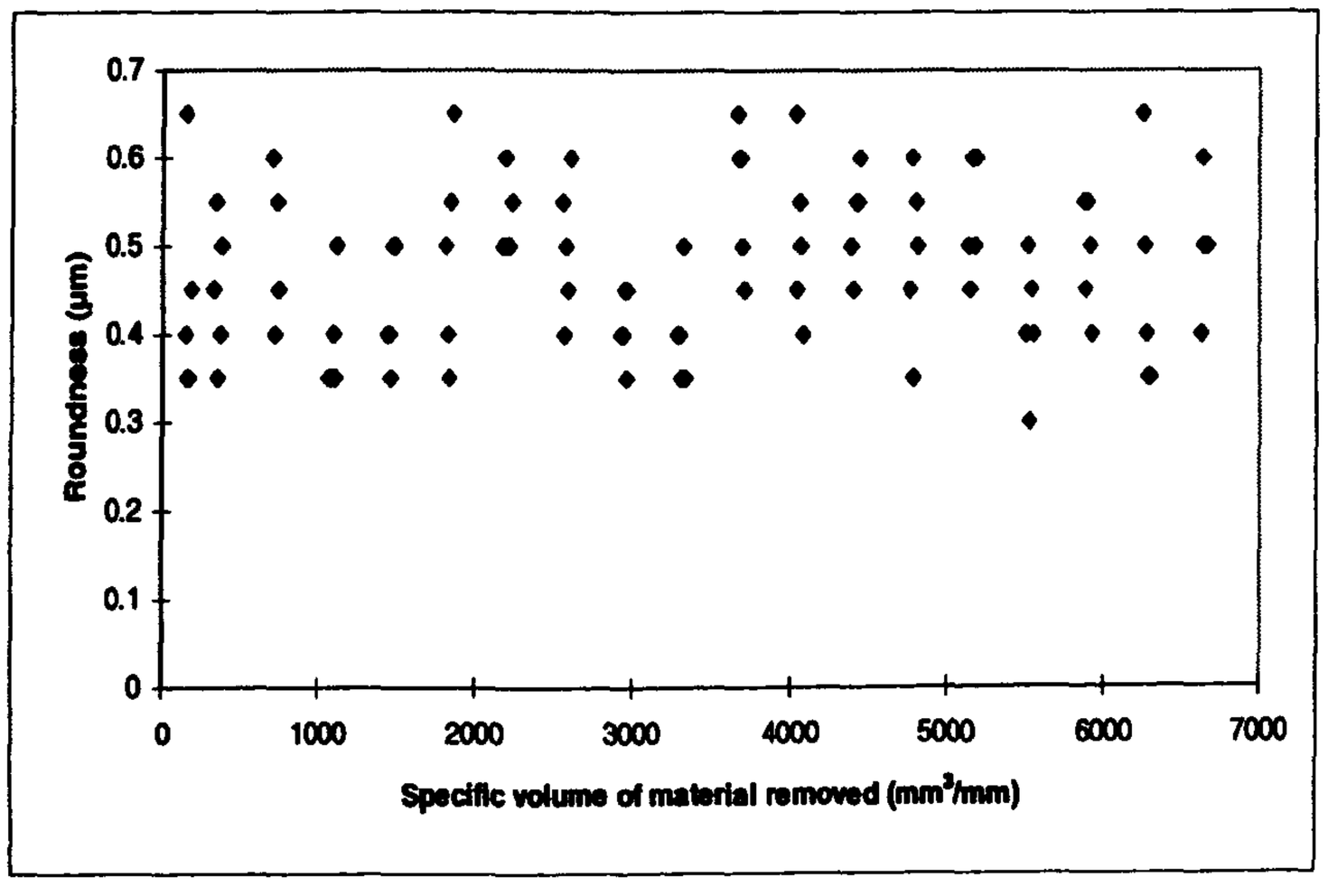

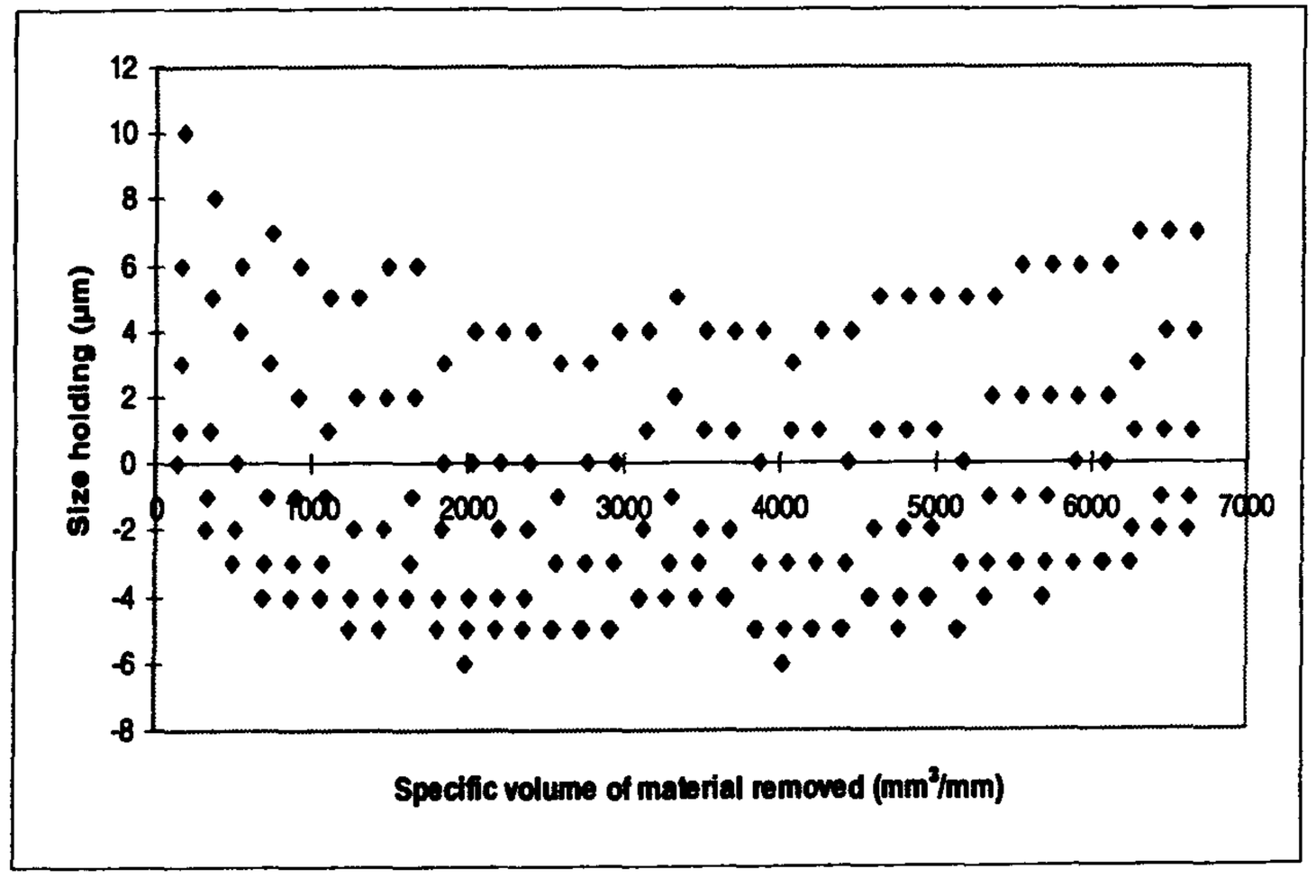

Graphs Showing Results for Confirmation Trial C2 Grinding AISI 52100 With a Vitrified CBN Wheel on the Suprema

<u>Experimental Conditions</u>

- Up dressing
- U_d: 10
- a_d: 2µm
- n_d: 2
- v_s: 120m/s
- v_w: 36m/min
- s: 2s
- v_R: 42m/s
-Q'w: 10mm³/mm s
- Wheel: B91VR150
- Coolant: Hysol X 36 l/min, 30Bar pump pressure

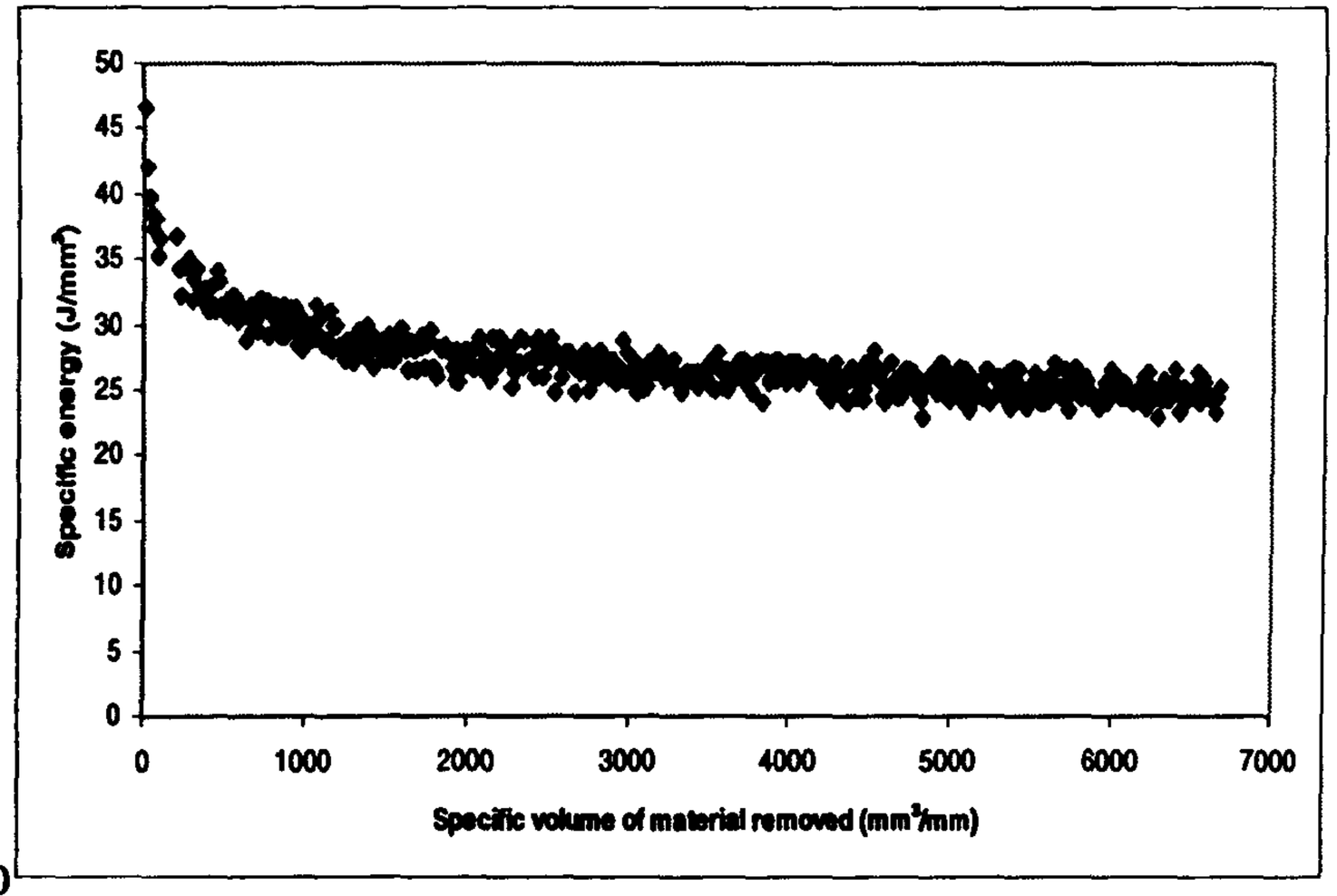

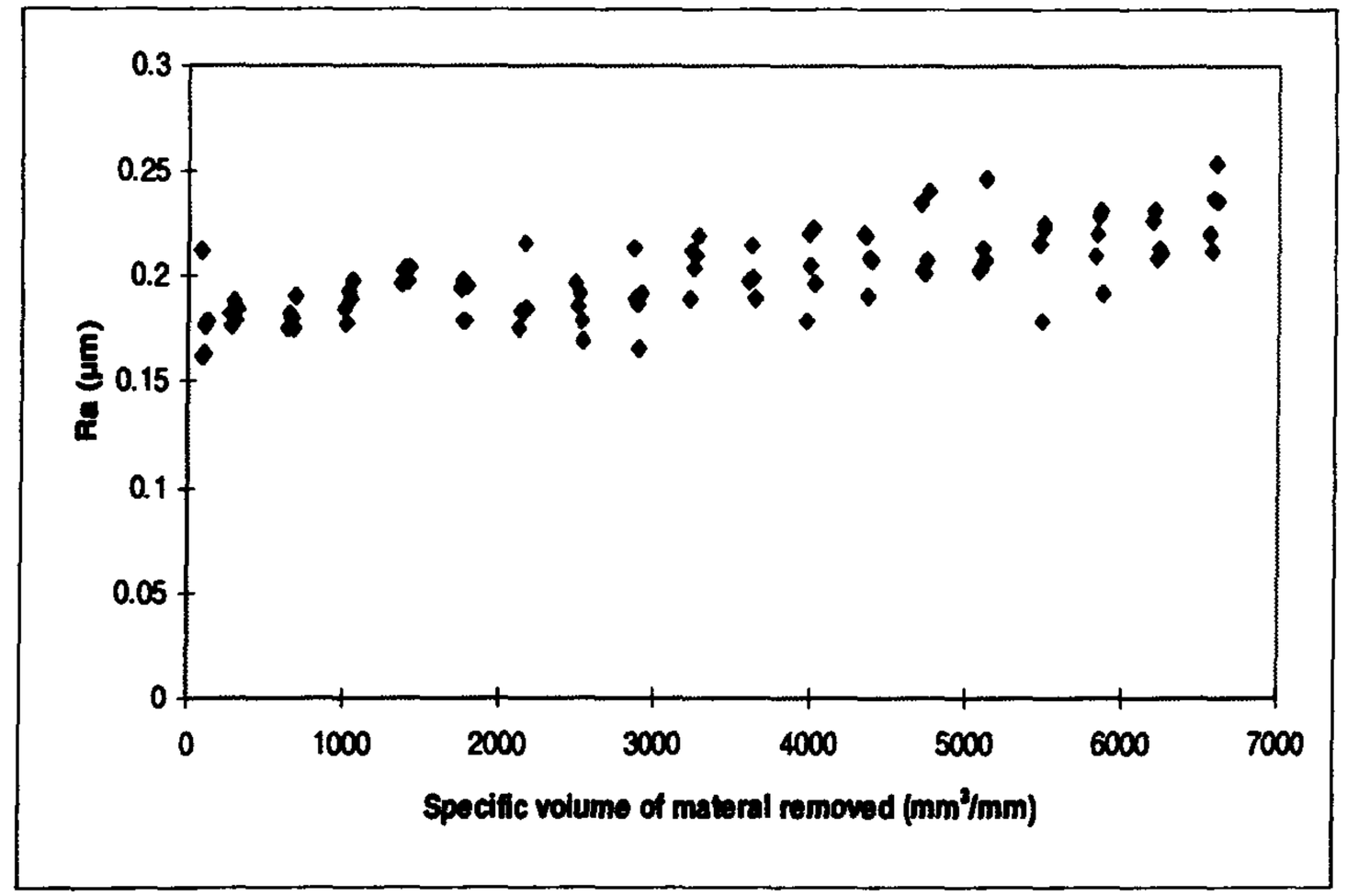

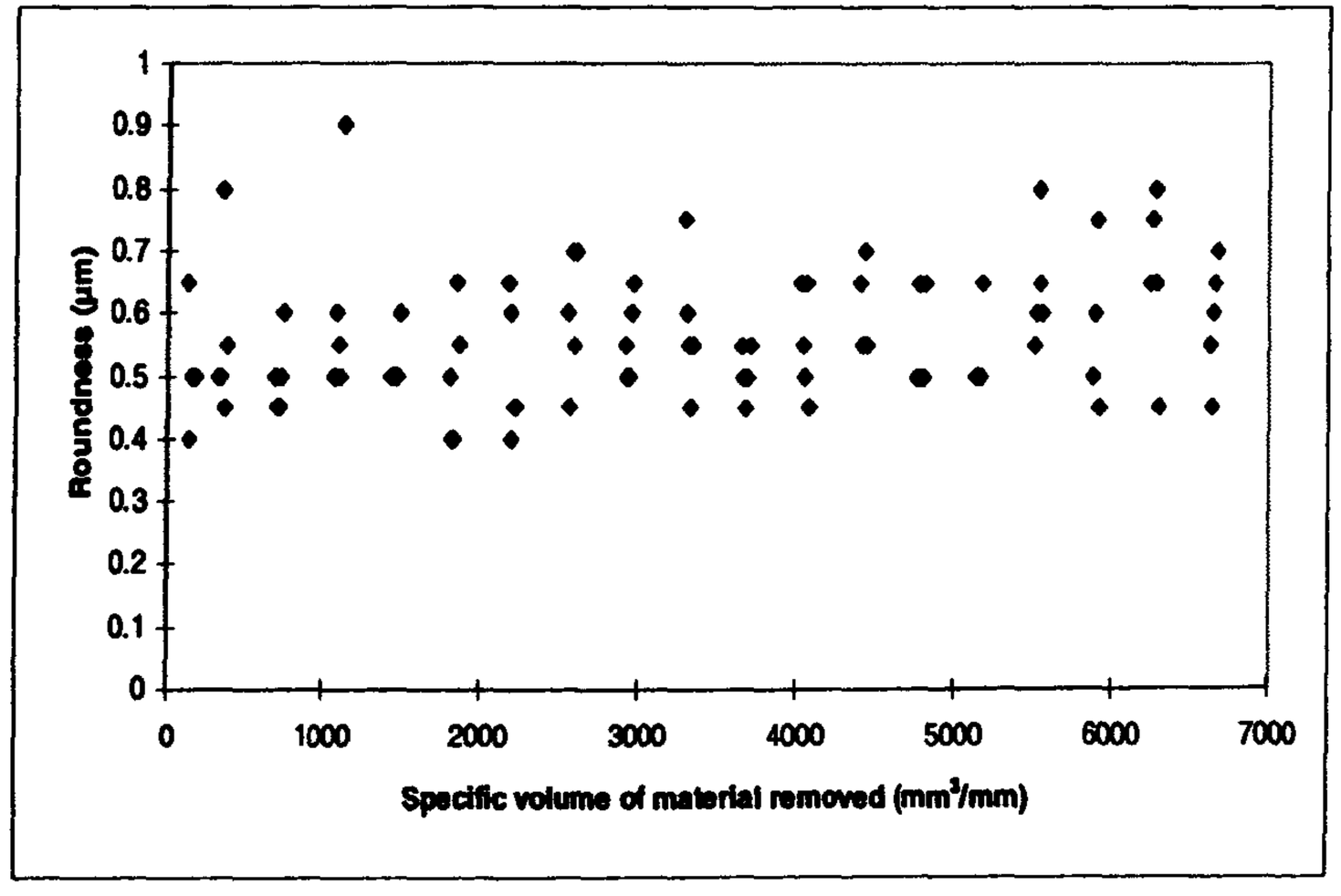

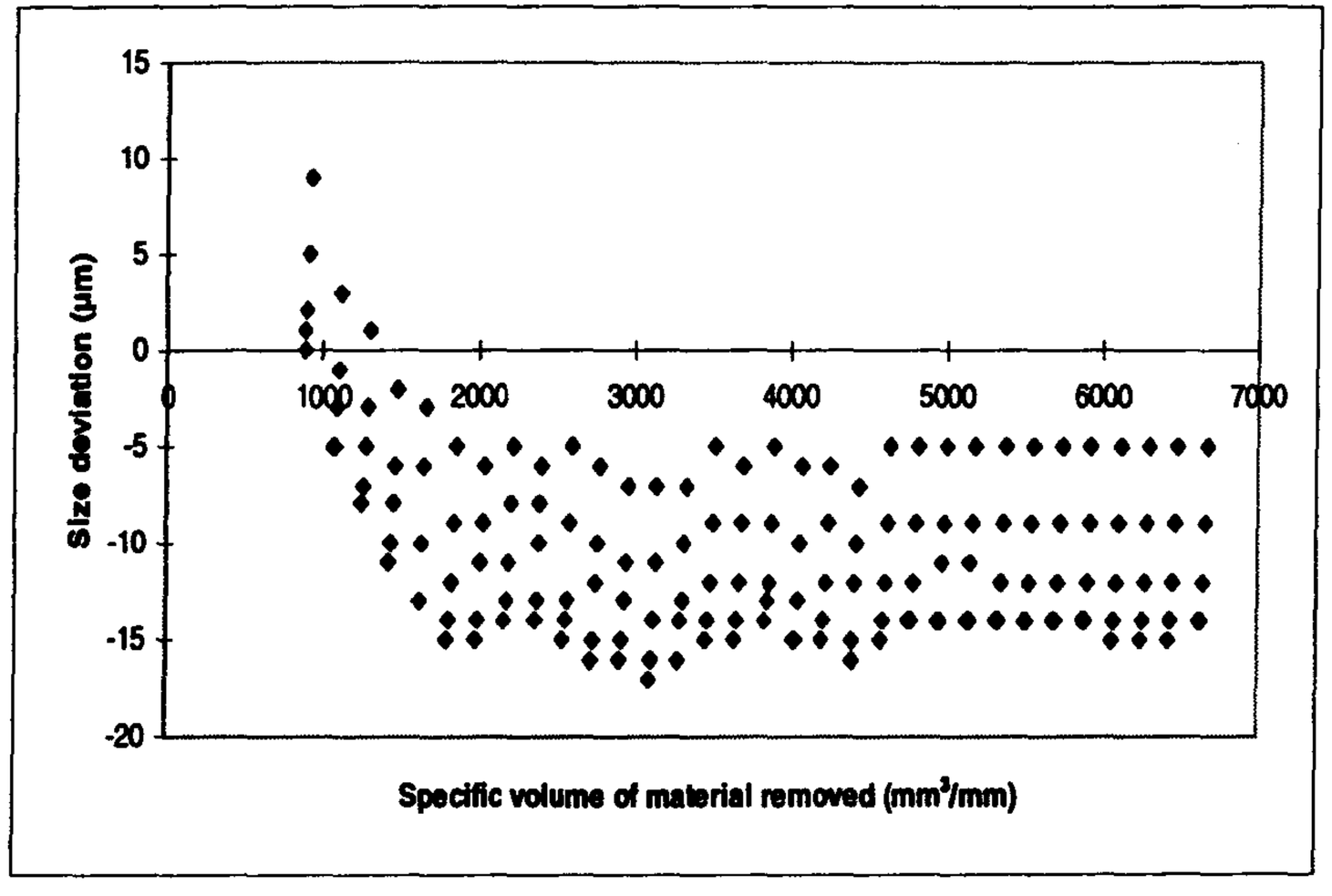

Graphs Showing Results for Confirmation Trial C3 Grinding AISI 52100 With a Vitrified CBN Wheel on the Suprema

Experimental Conditions

- Up dressing
- U_d: 10
- a_d: 2μm
- n_d: 2
- v_s: 120m/s
- v_w: 36m/min
- s: 2s
- v_R: 42m/s
-Q'w: 20mm³/mm s
- Wheel: B91VR150
- Coolant: Hysol X 36 l/min, 30Bar pump pressure

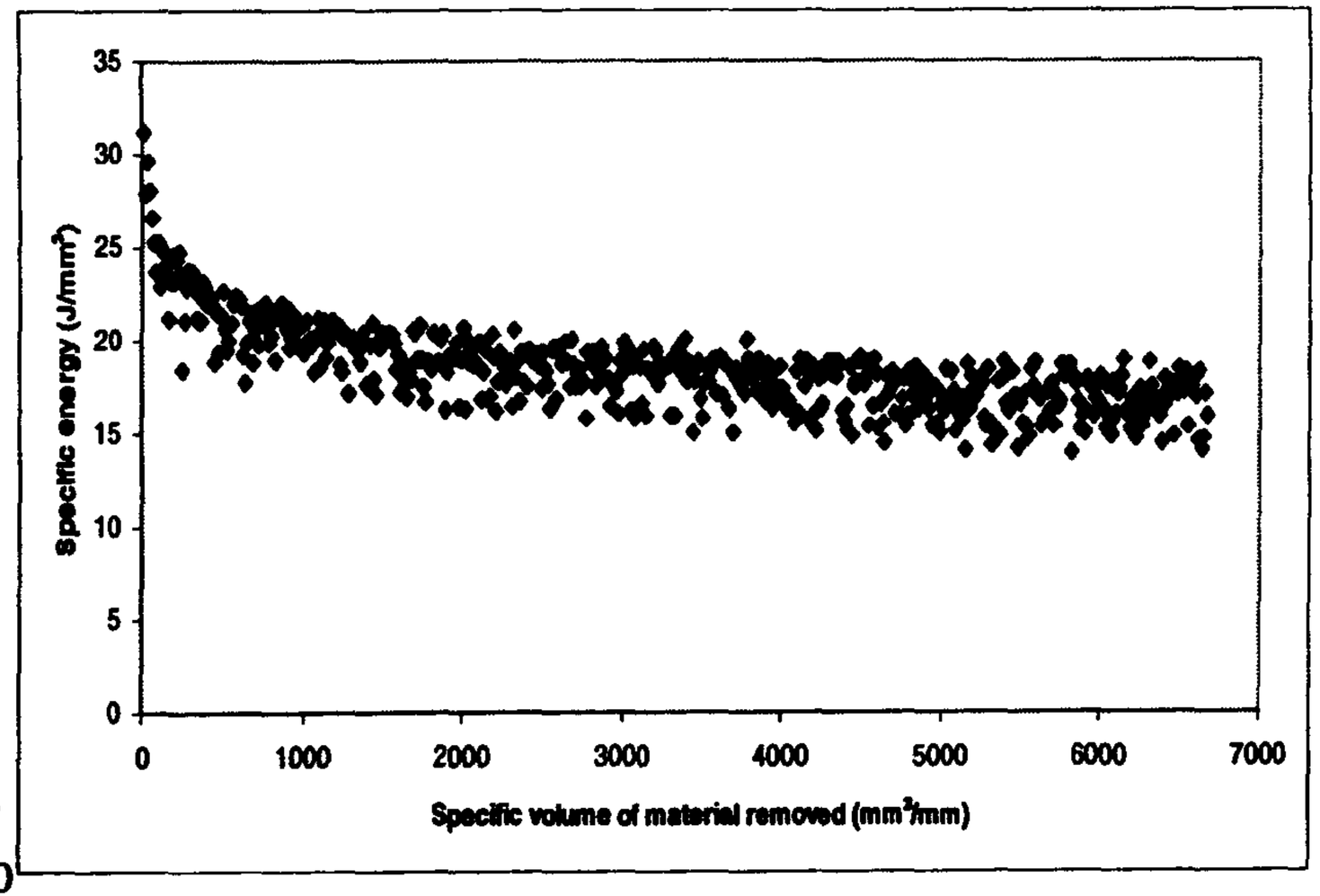

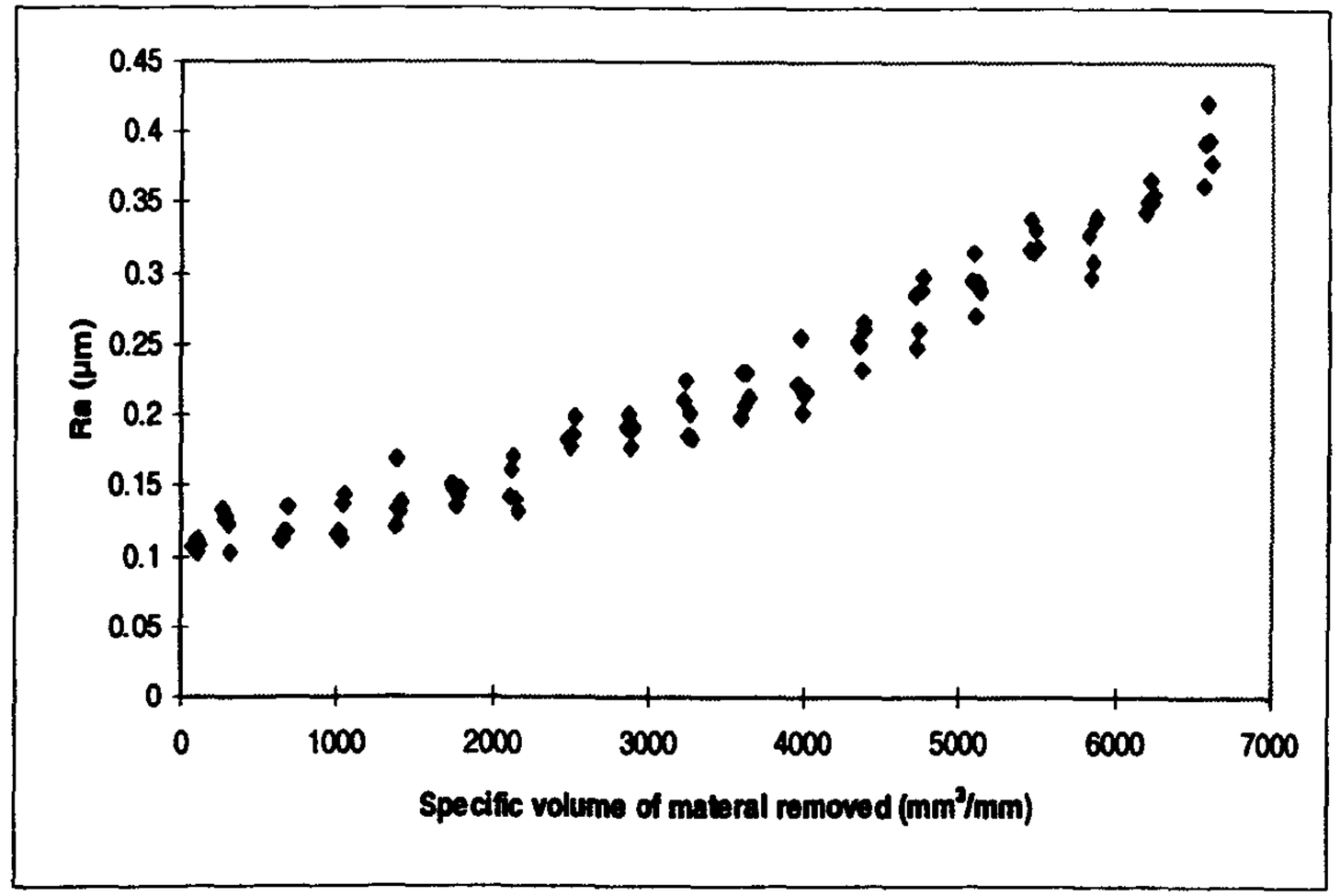

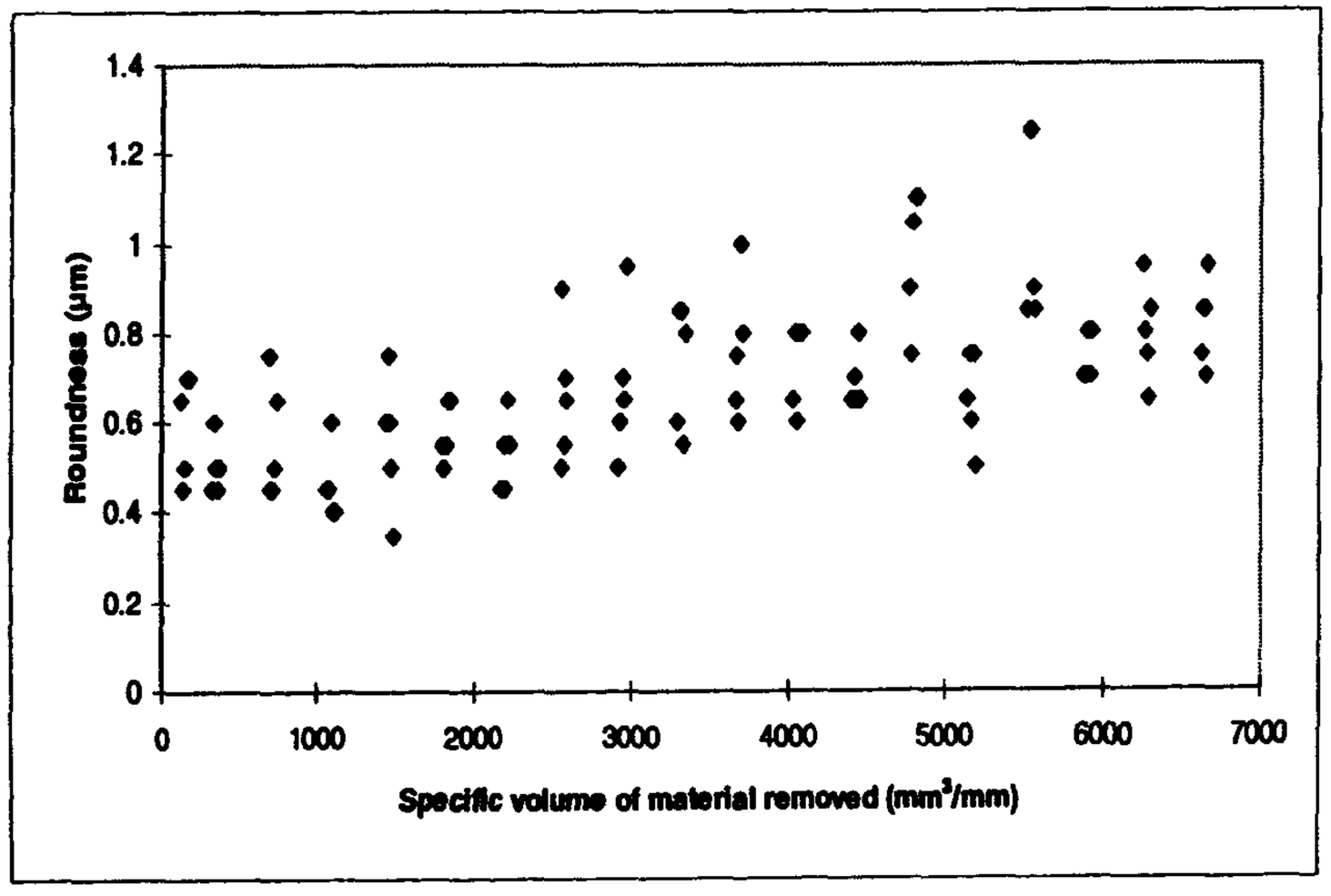

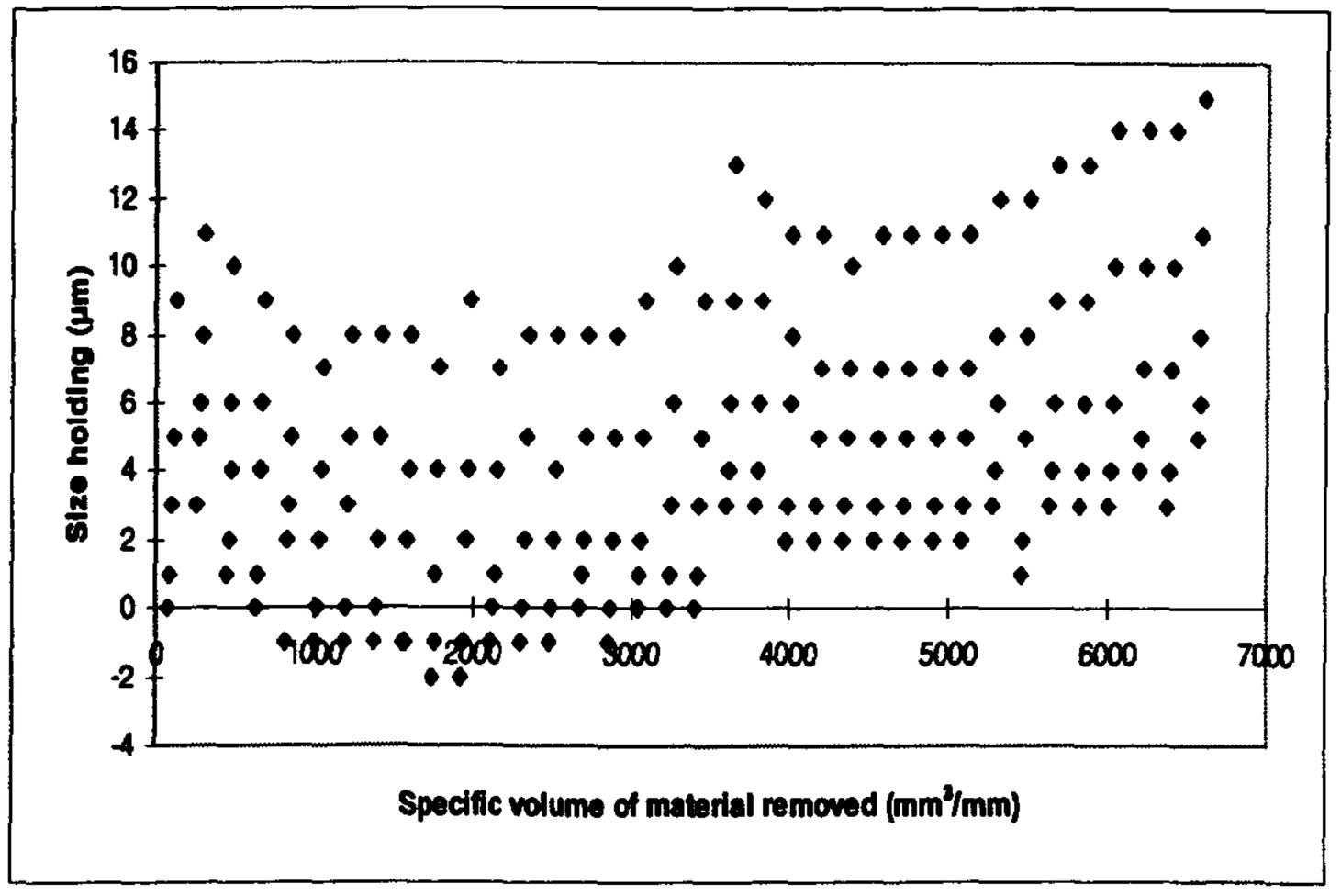

Graphs Showing Results for Confirmation Trial C4 Grinding AISI 52100 With a Vitrified CBN Wheel on the Suprema

<u>Experimental Conditions</u>

- Up dressing
- U_d: 10
- a_d: 2µm
- n_d: 2
- v_s: 120m/s
- v_w: 72m/min
- s: 2s
- v_R: 42m/s
-Q'w: 20mm³/mm s
- Wheel: B91VR150
- Coolant: Hysol X 36 l/min, 30Bar pump pressure

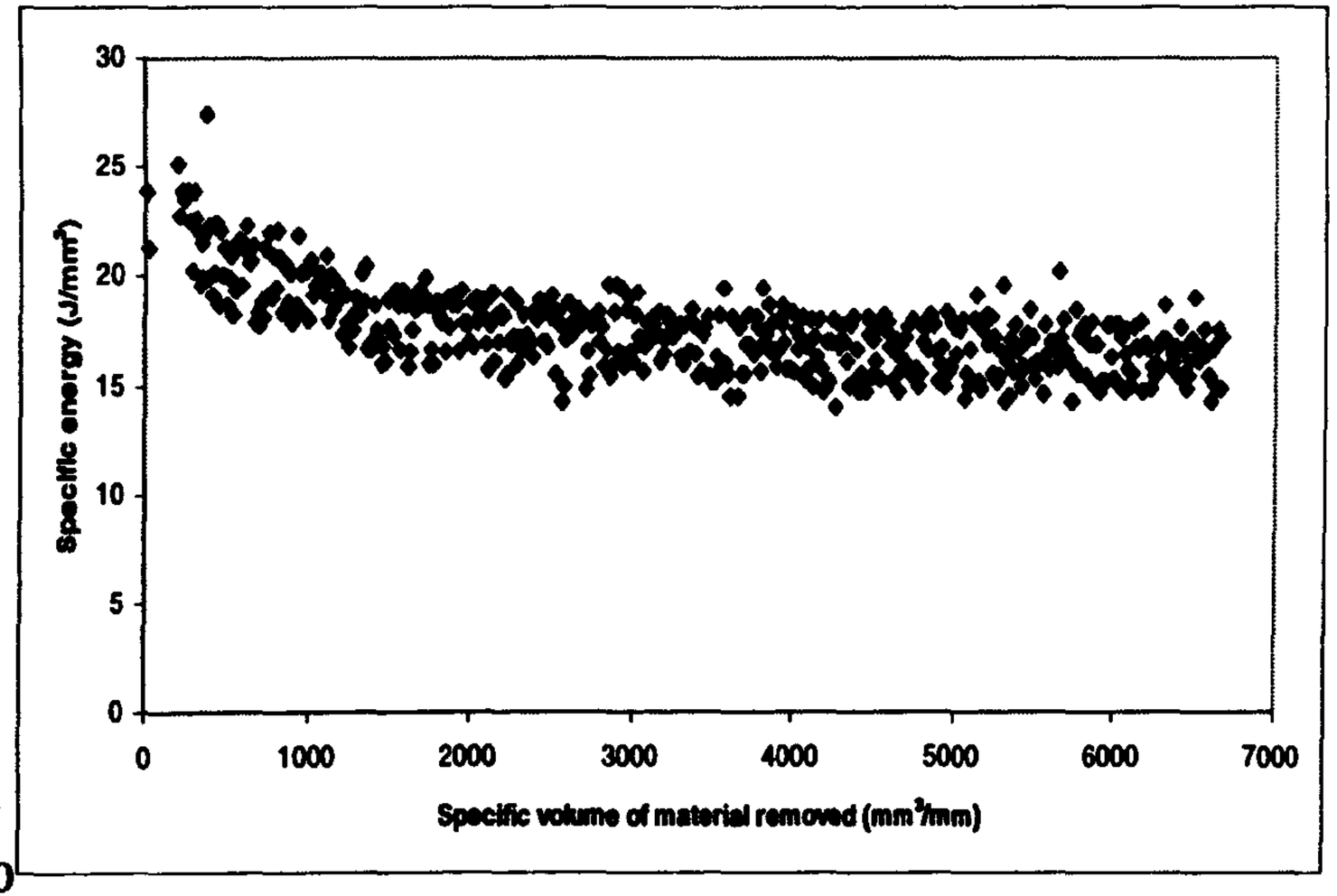

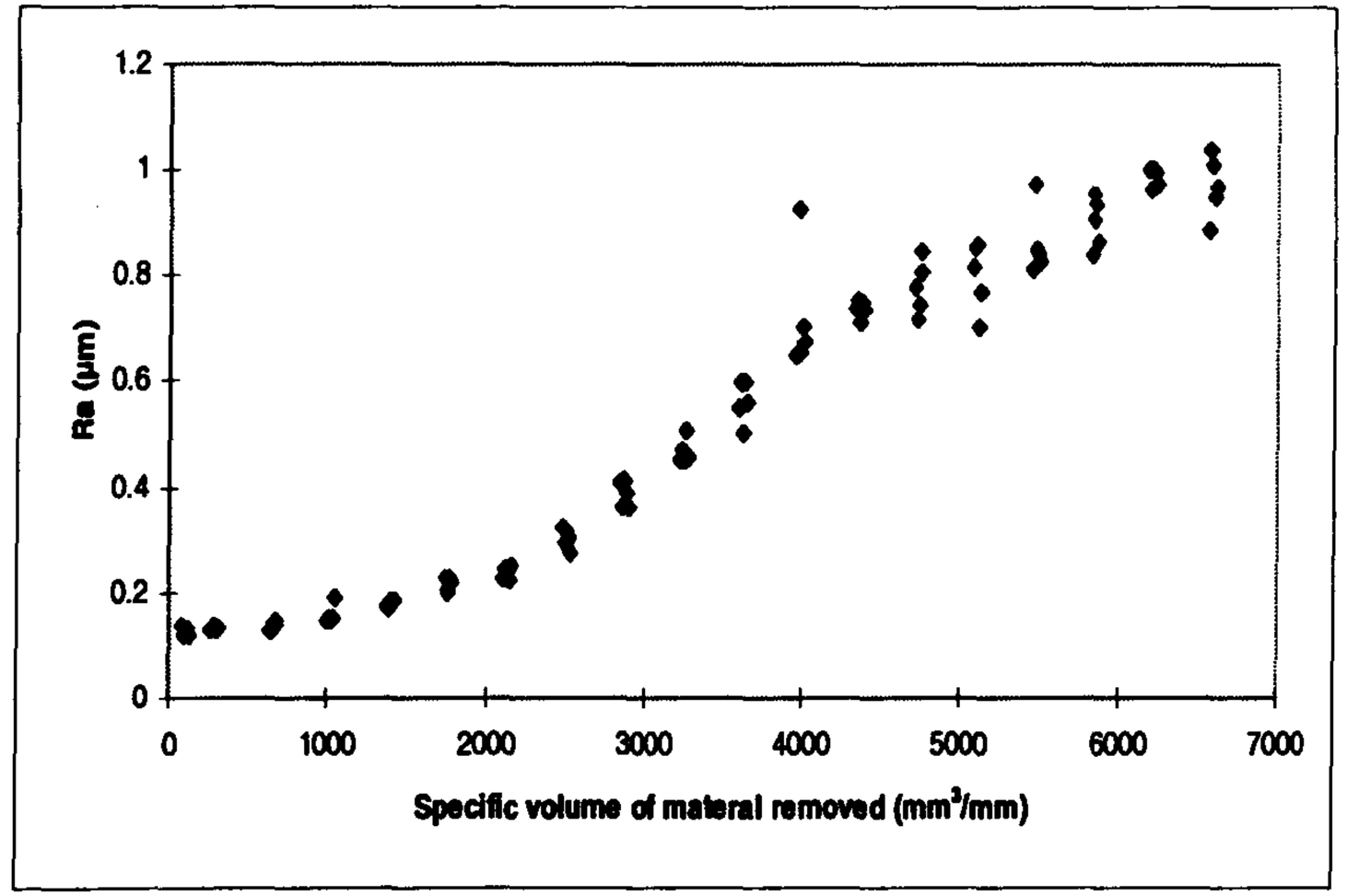

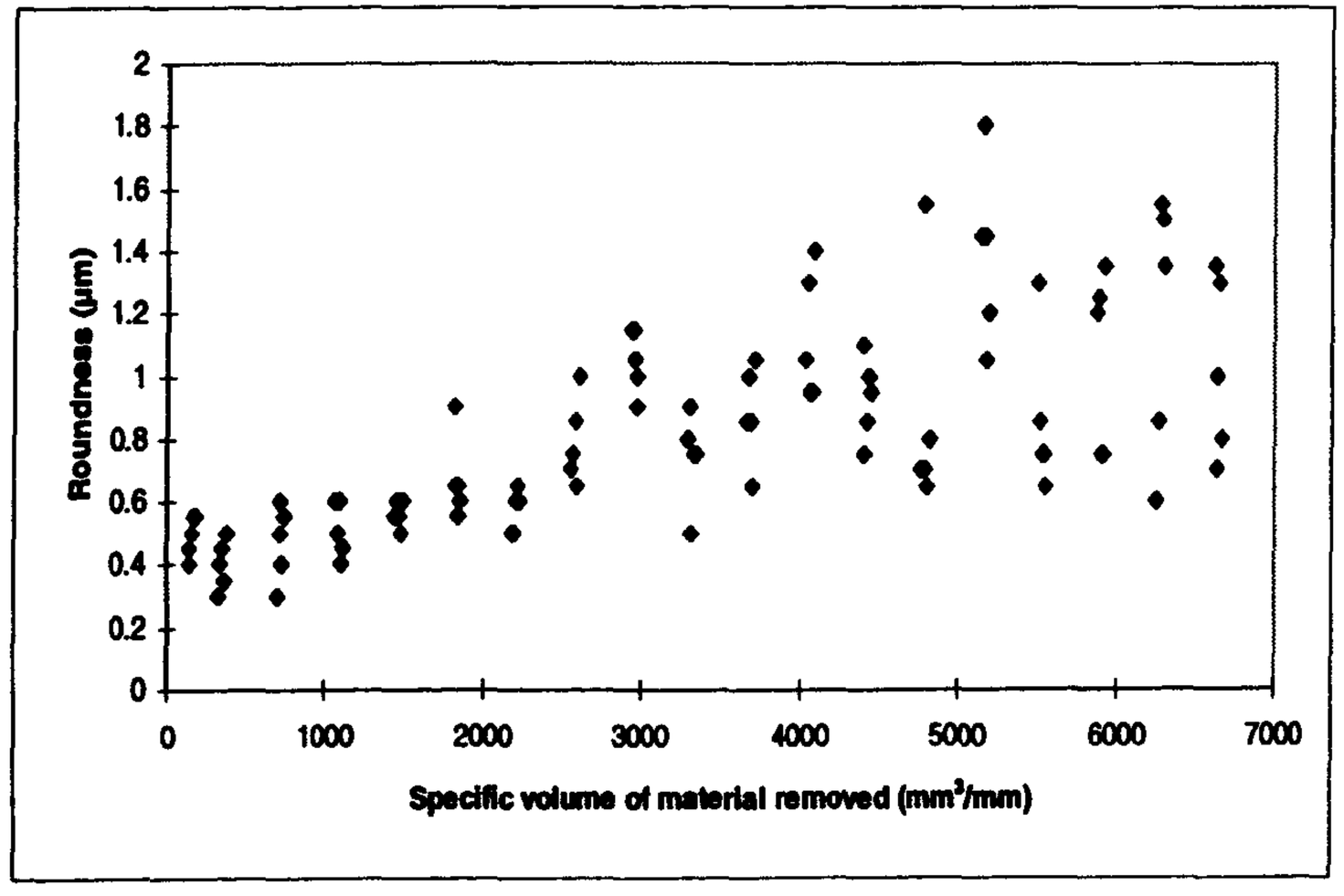

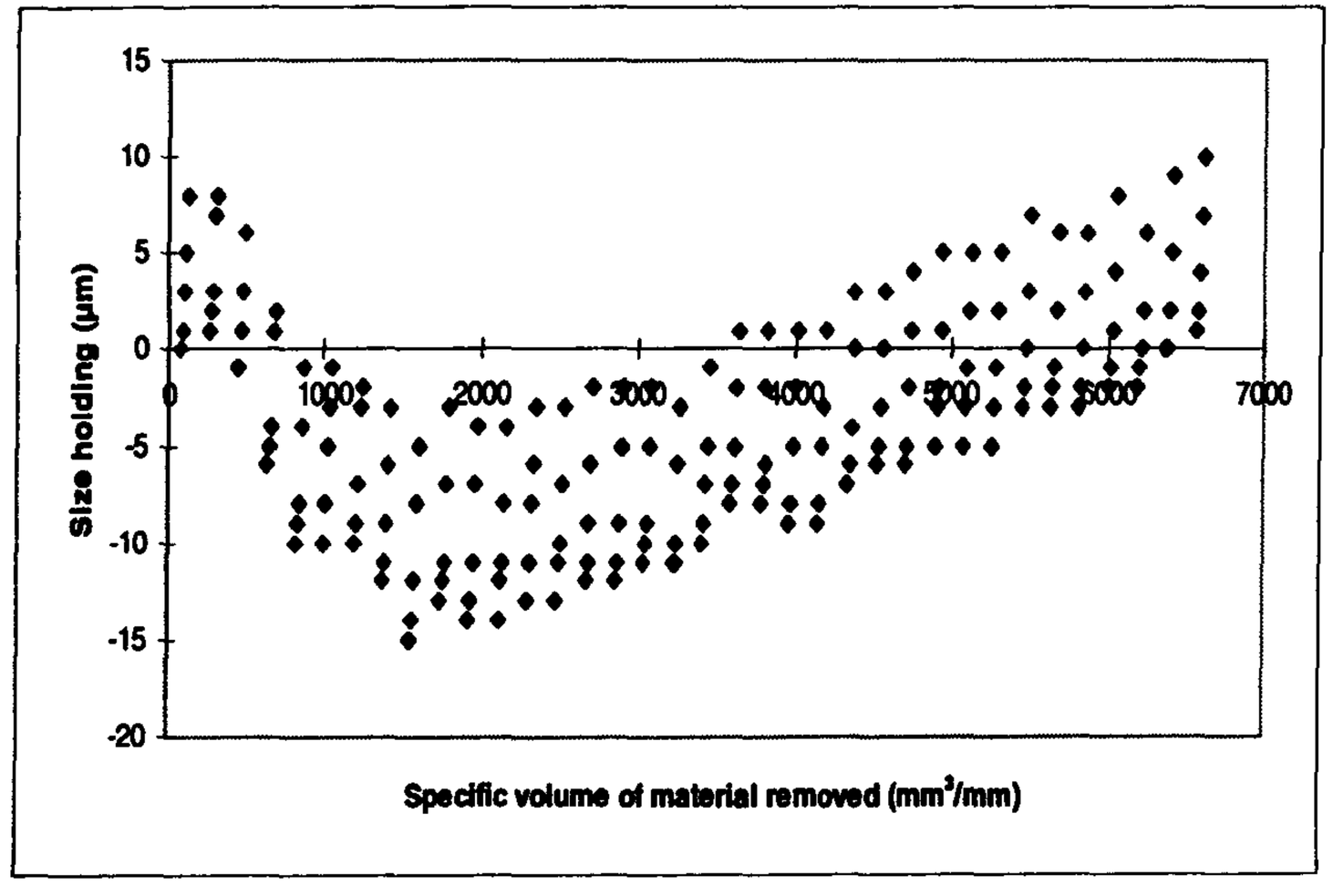

Graphs Showing Results for Confirmation Trial C5 Grinding AISI 52100 With a Vitrified CBN Wheel on the Suprema

<u>Experimental Conditions</u>

- Down dressing
- U_d: 2
- a_d: 10µm
- n_d: 2
- v_s: 120m/s
- v_w: 36m/min
- s: 2s
- v_R: 42m/s
-Q'w: 10mm³/mm s
- Wheel: B91VR150
- Coolant: Hysol X 36 l/min, 30Bar pump pressure

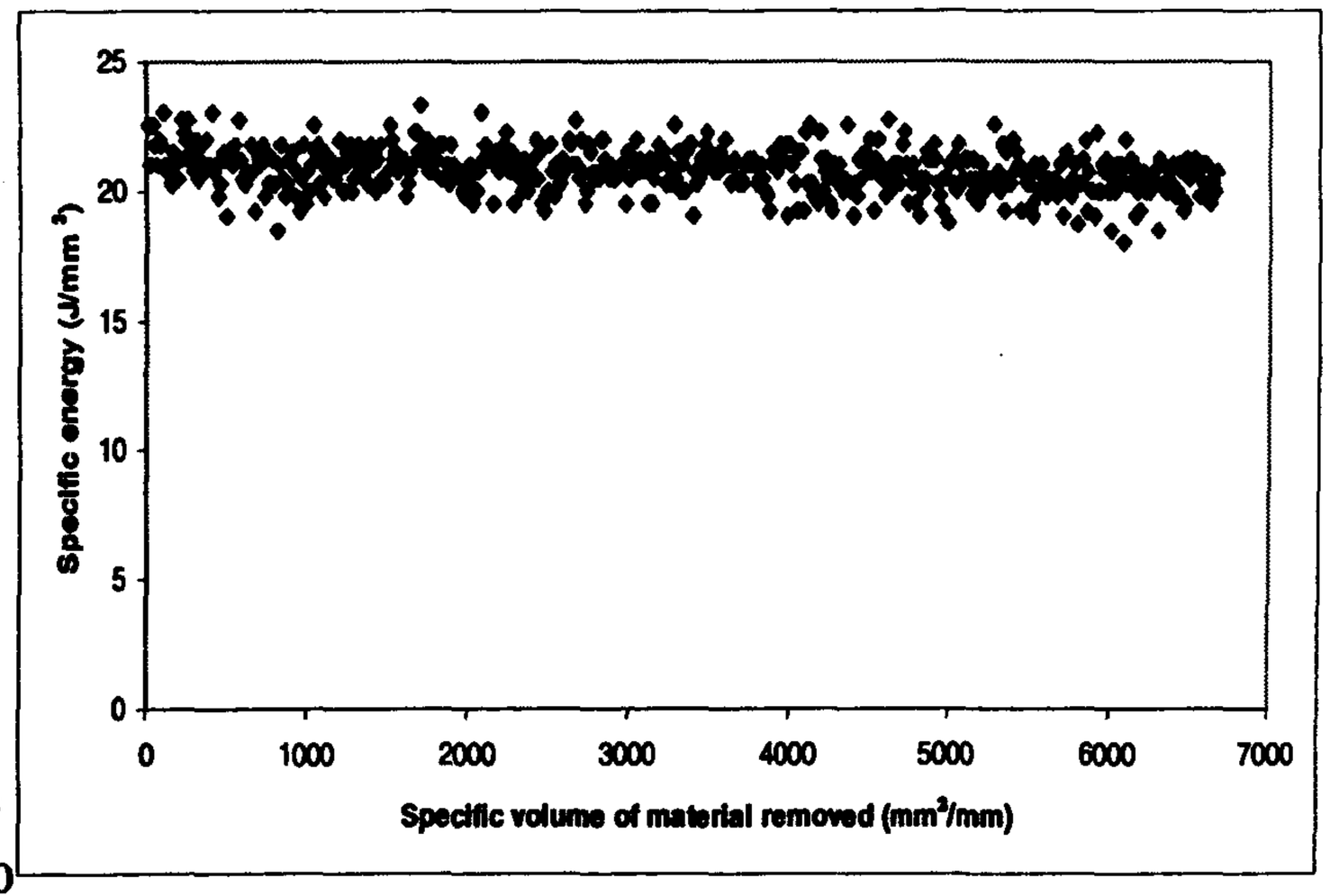

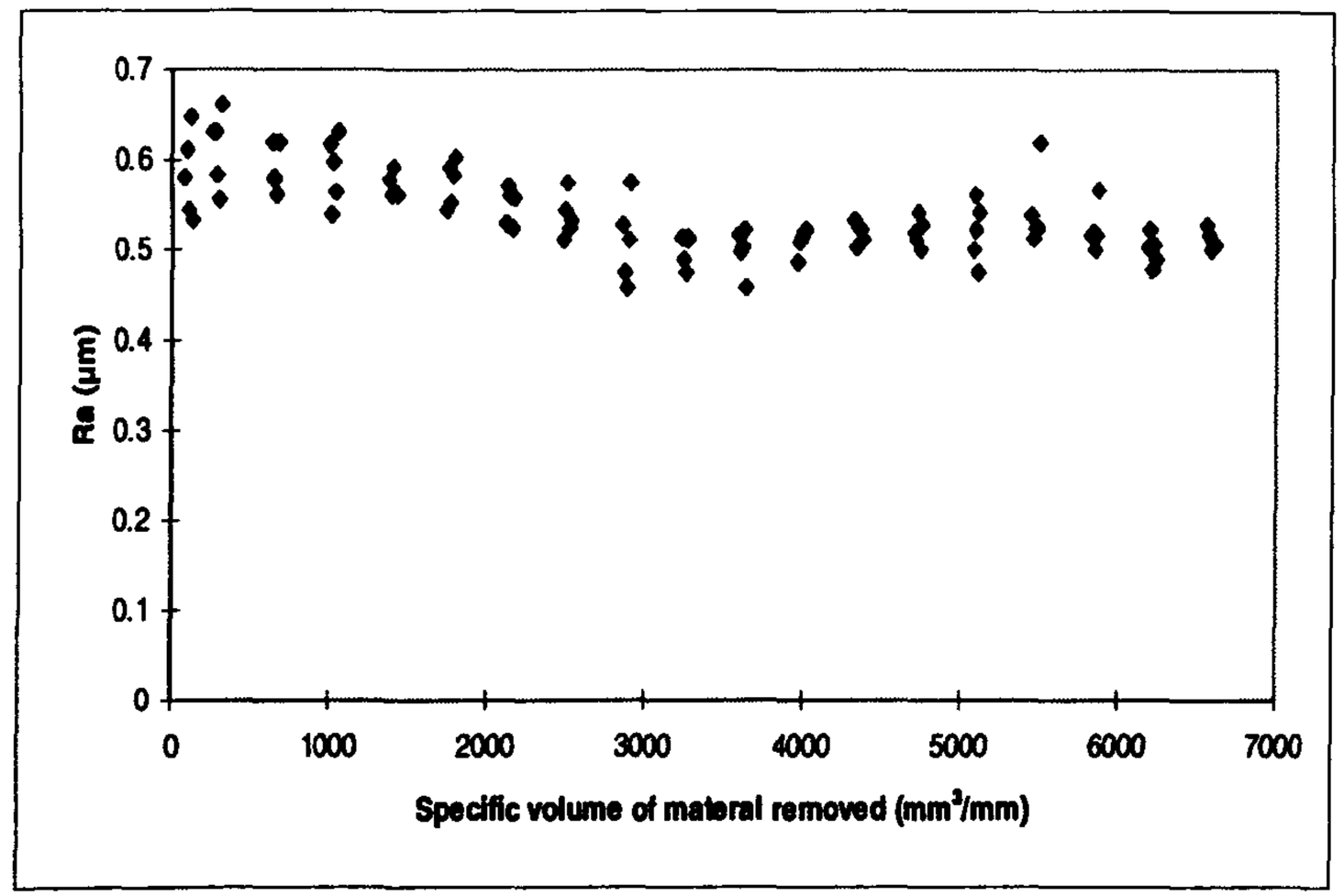

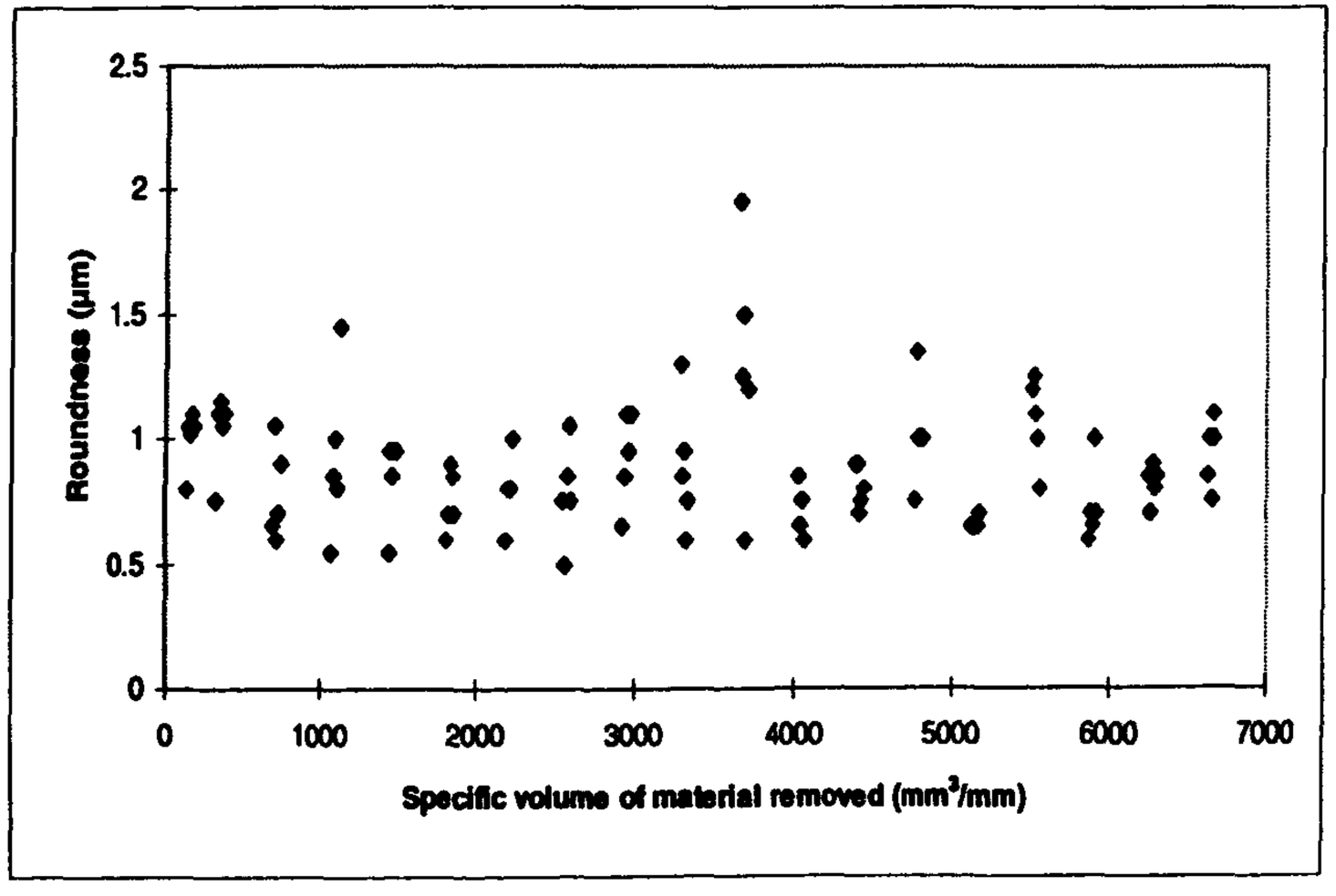

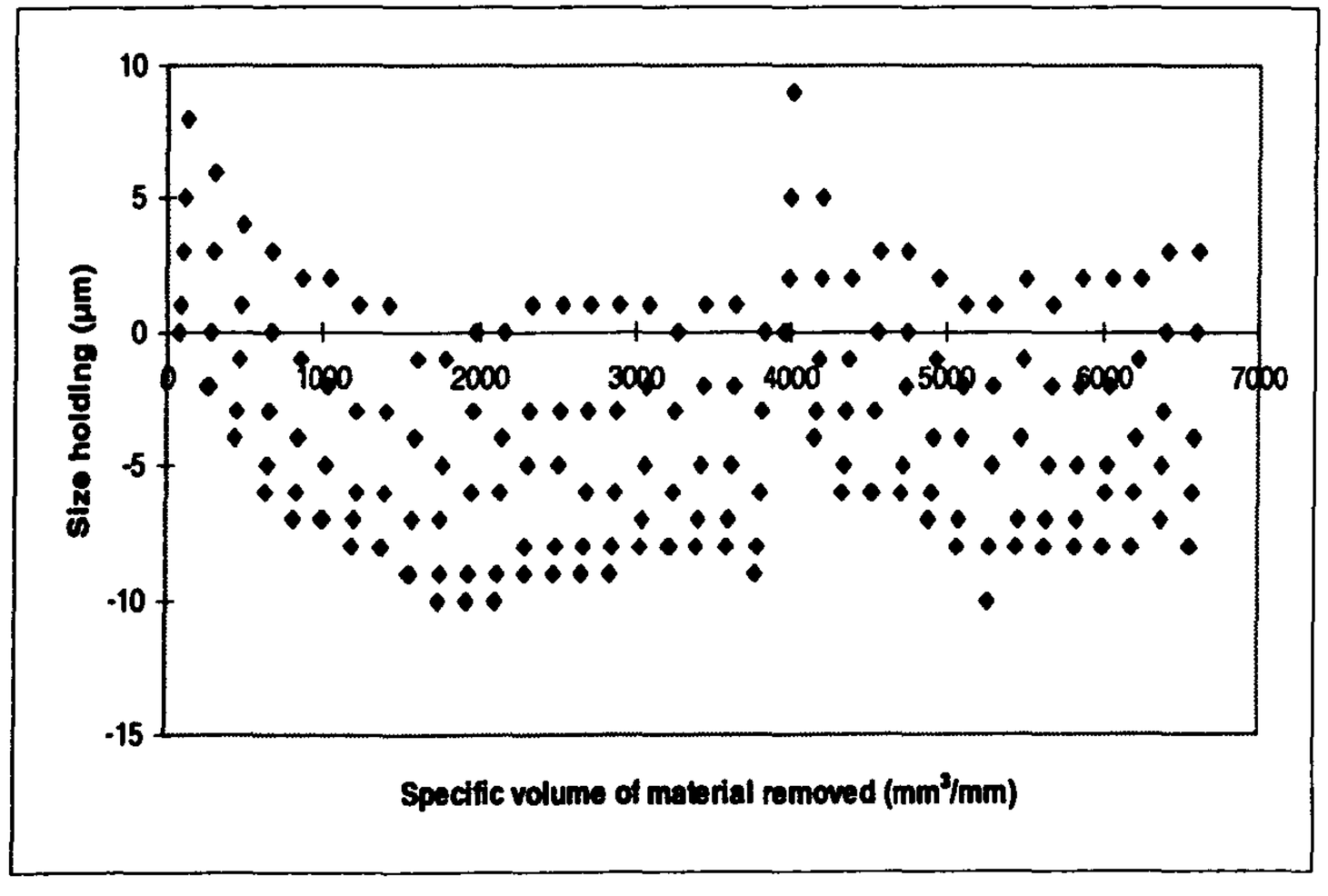

Graphs Showing Results for Confirmation Trial C6 Grinding AISI 52100 With a Vitrified CBN Wheel on the Suprema

<u>Experimental Conditions</u>

- Down dressing
- U_d: 2
- a_d: 10µm
- n_d: 2
- v_s: 120m/s
- v_w: 36m/min
- s: 2s
- v_R: 42m/s
-Q'w: 20mm³/mm s
- Wheel: B91VR150
- Coolant: Hysol X 36 l/min, 30Bar pump pressure

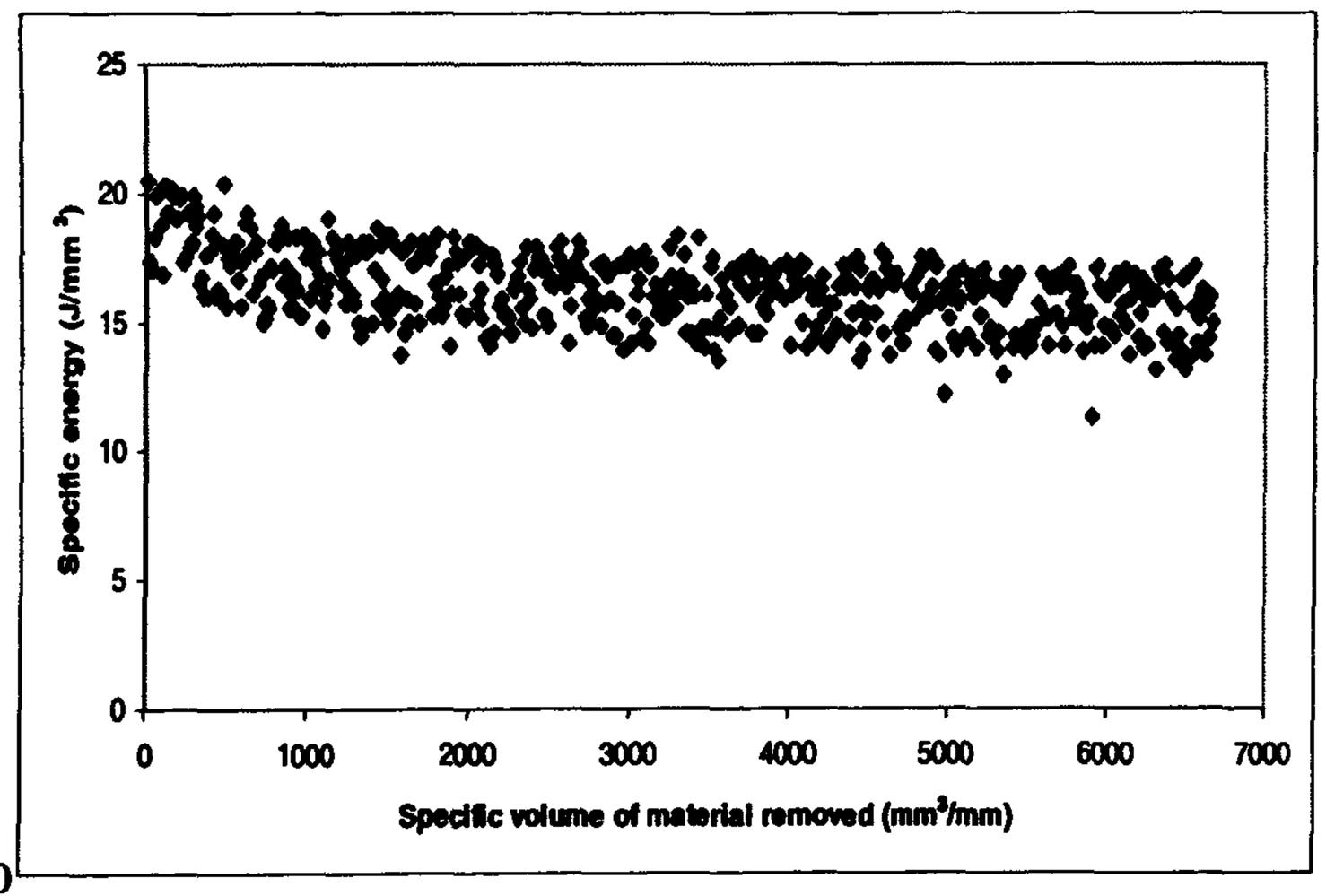

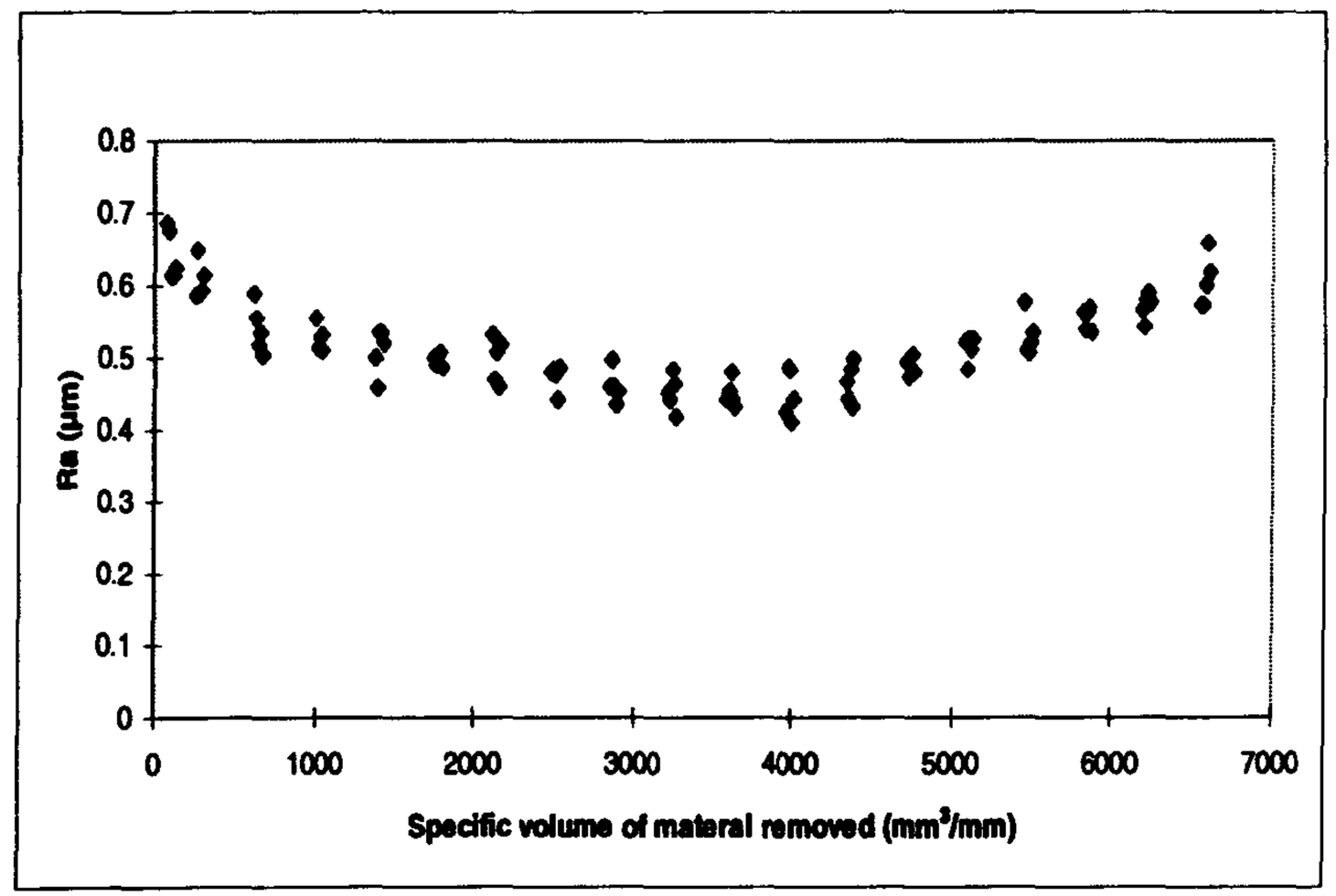

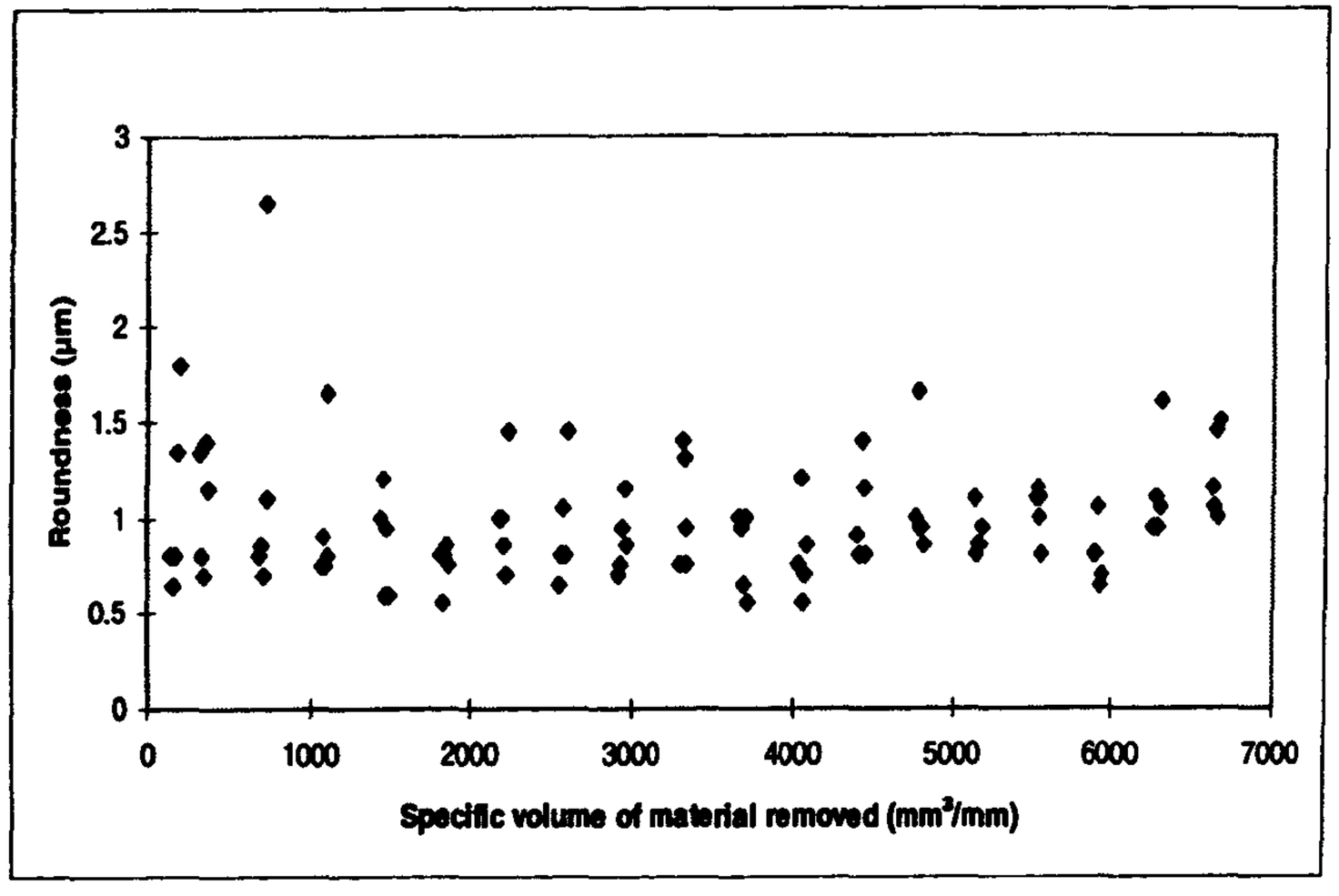

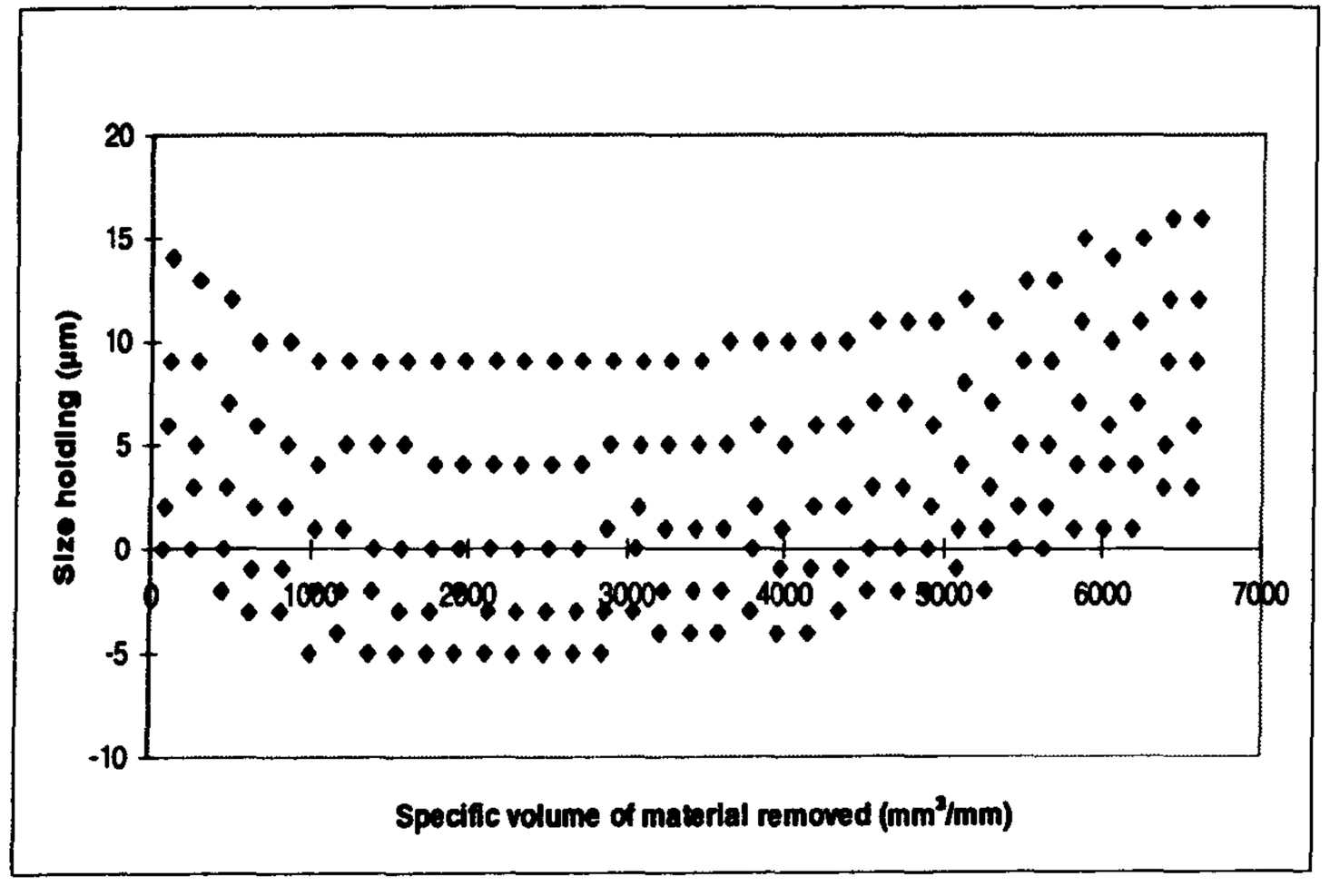

Graphs Showing Results for Confirmation Trial C7 Grinding AISI 52100 With a Vitrified CBN Wheel on the Suprema

Experimental Conditions

- Down dressing
- U_d: 2
- a_d: 10µm
- n_d: 2
- v_s: 120m/s
- v_w: 72m/min
- s: 2s
- v_R: 42m/s
-Q'w: 20mm³/mm s
- Wheel: B91VR150
- Coolant: Hysol X 36 l/min, 30Bar pump pressure

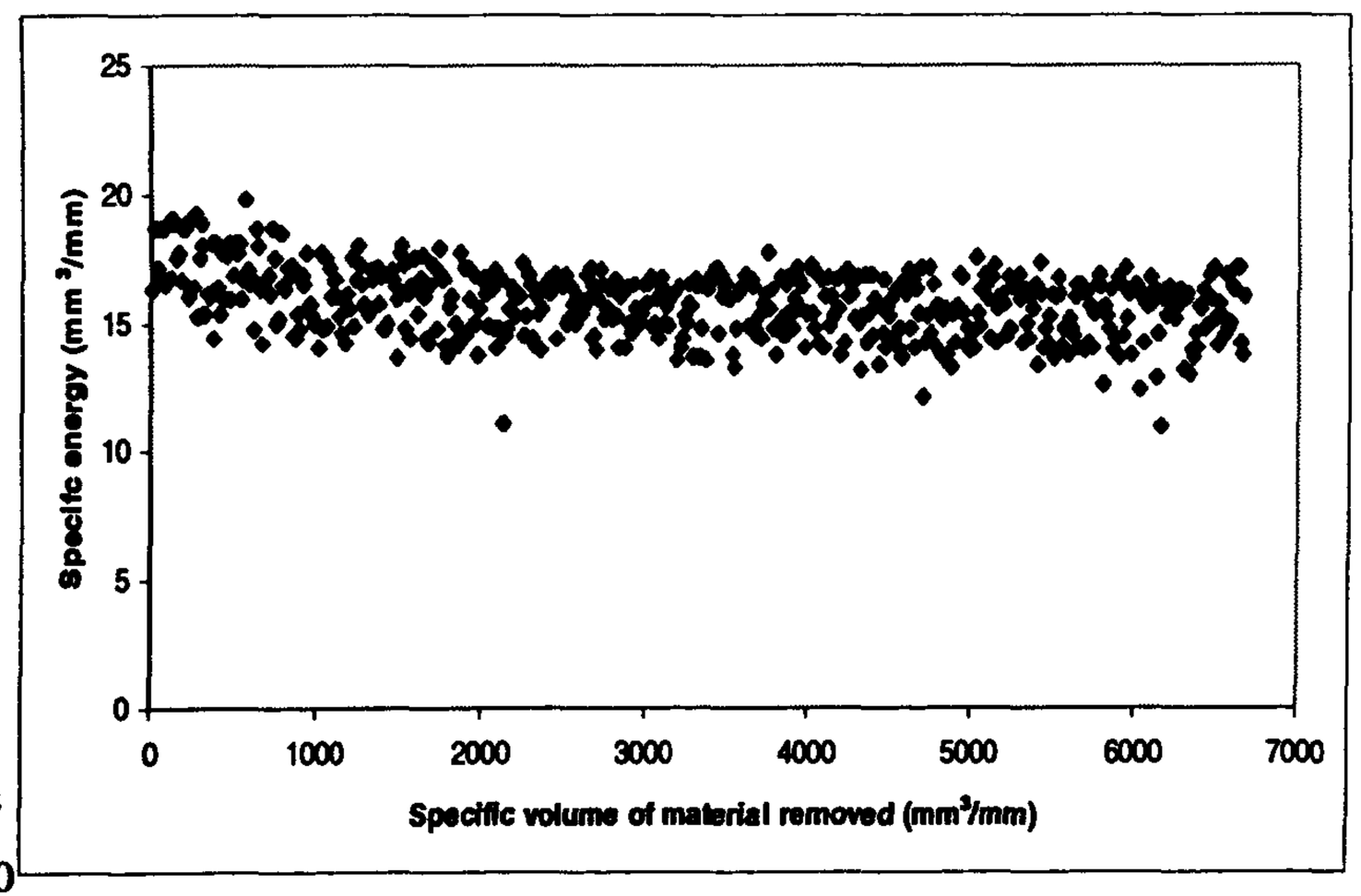

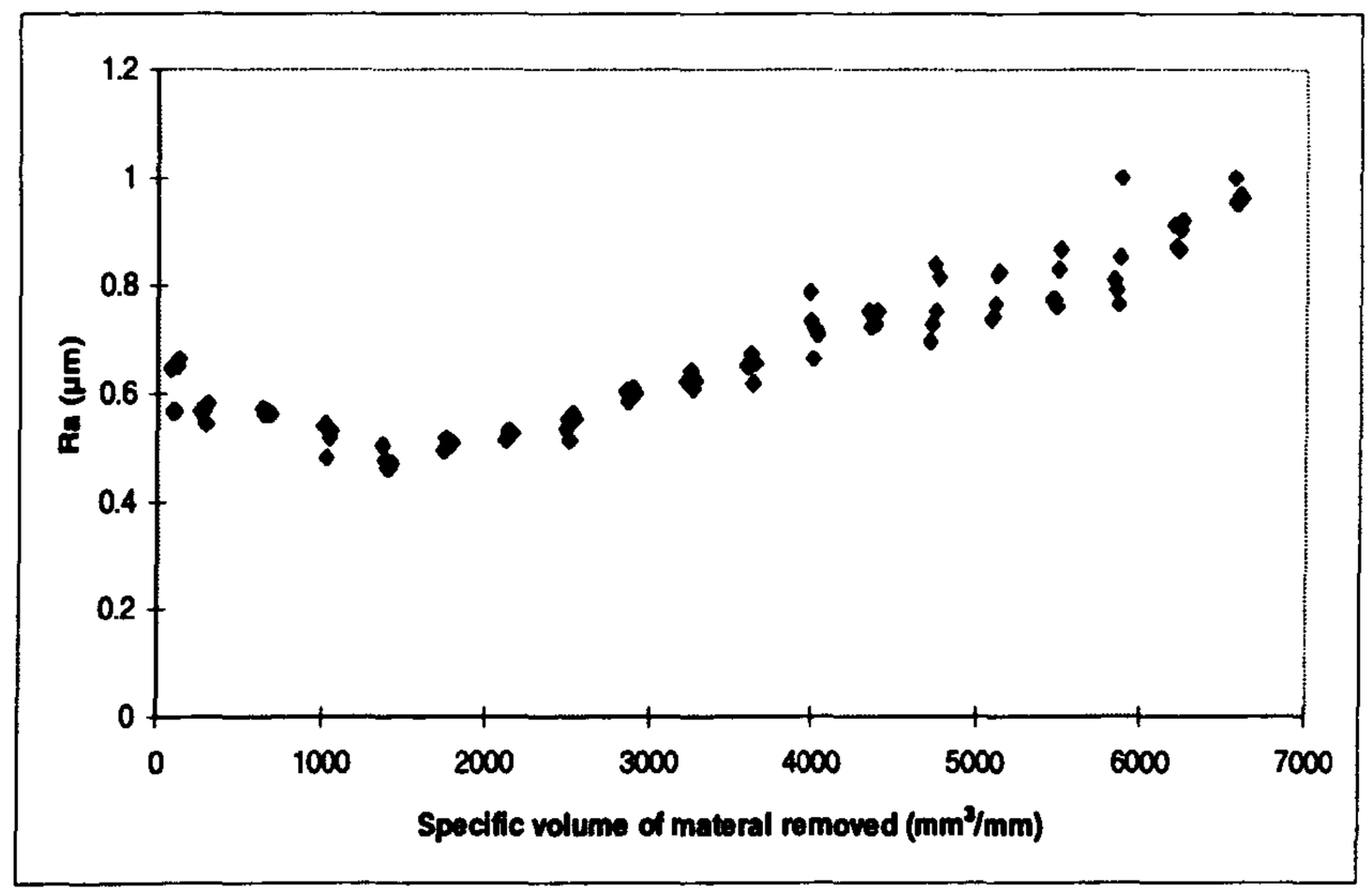

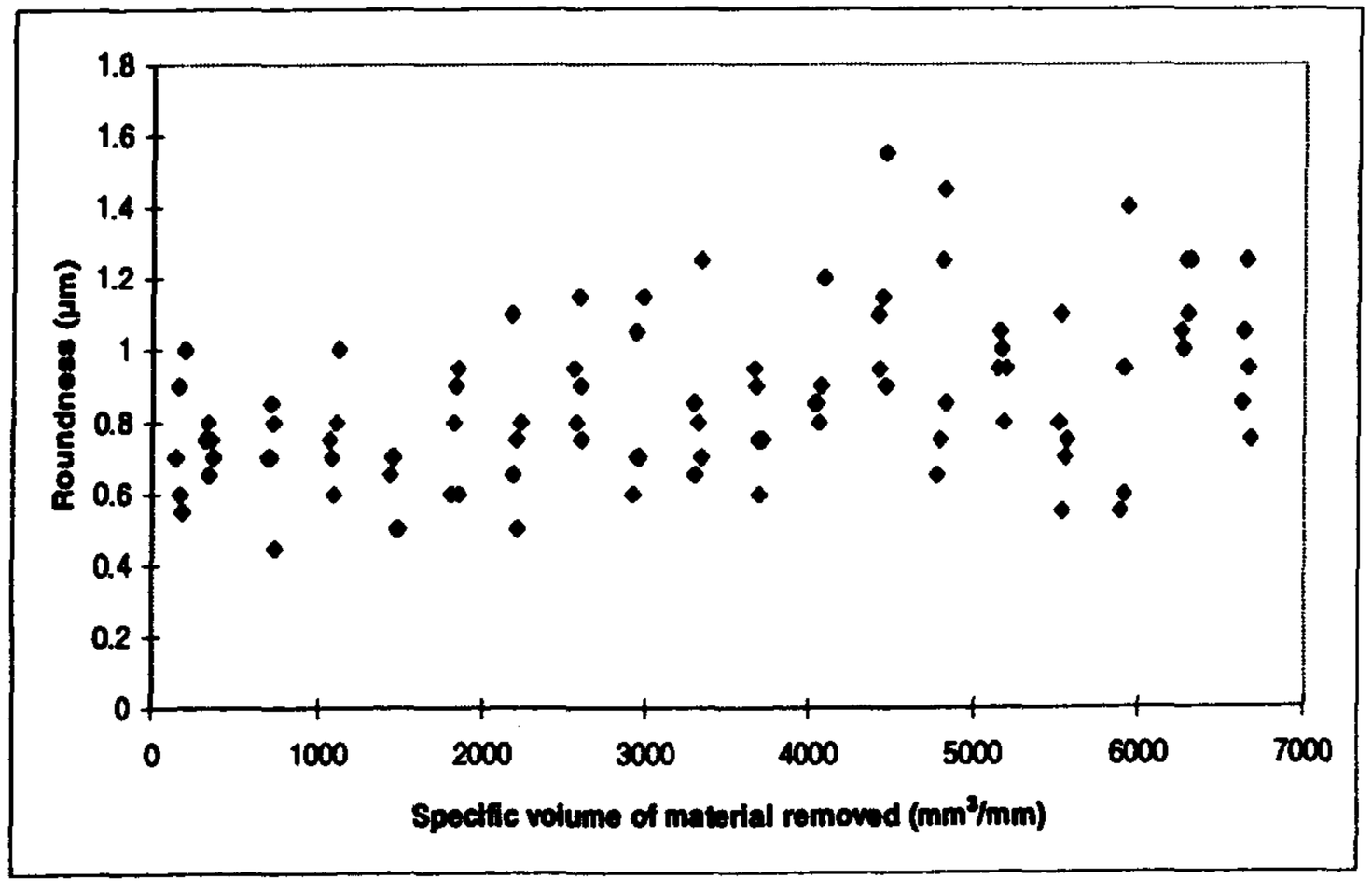

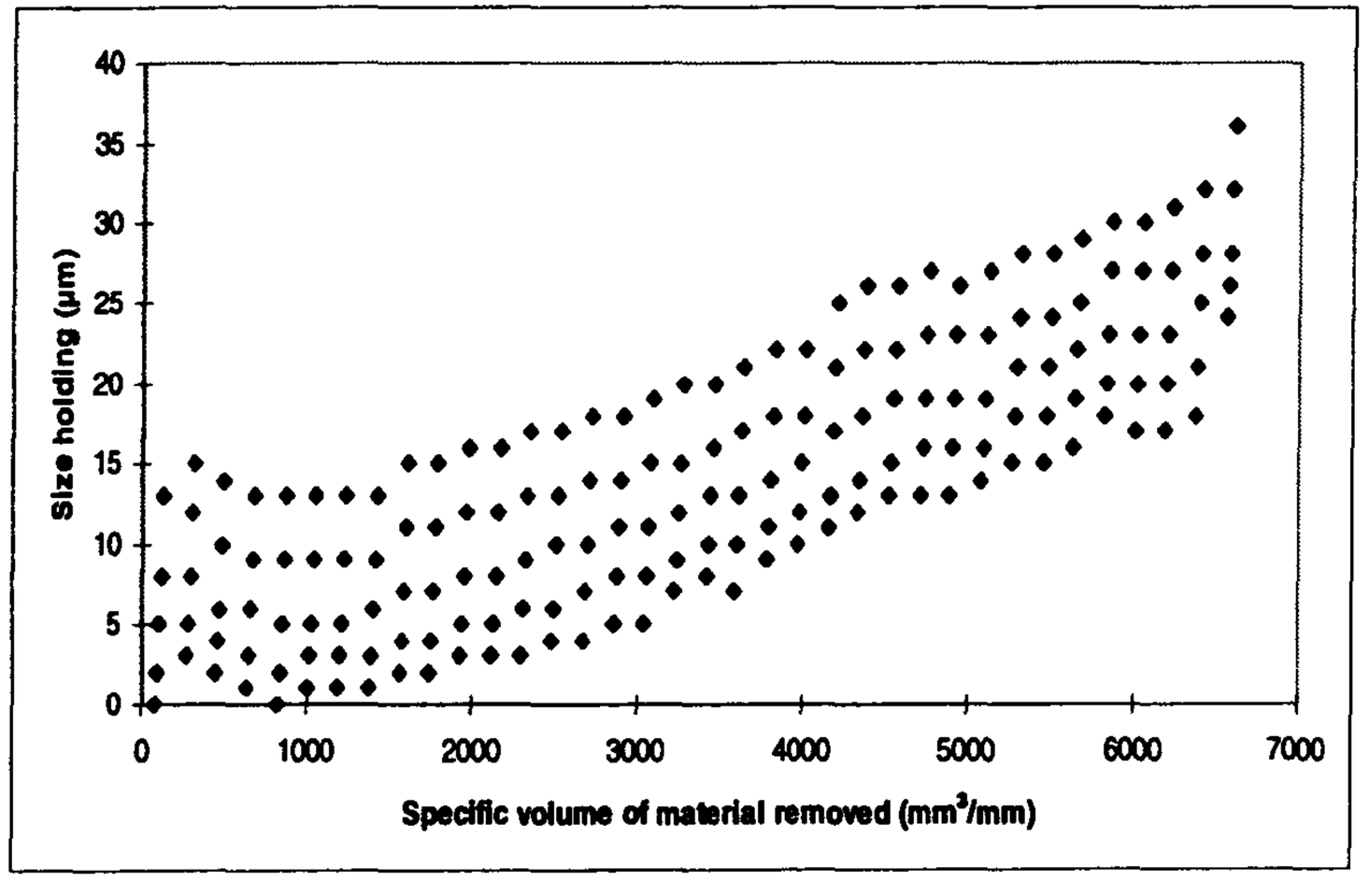

APPENDIX B4

Appendix B4. Graphs of results for all Series 10 benchmark trials grinding AISI 52100.

Results for Benchmark Grinding Trial 1 on the J&S Series 10 Using an Aluminium oxide Wheel to Grind AISI 52100

Experimental Conditions

- U_d: 2
- a_d: 10µm
- n_d: 2
- v_s: 43m/s
- v_w: 21m/min
- s: 10s
- -Q'w: 1mm³/mm s
- Wheel: Universal WA801 J6V
- Coolant: Hysol X 33 l/min, 0.4Bar pump pressure

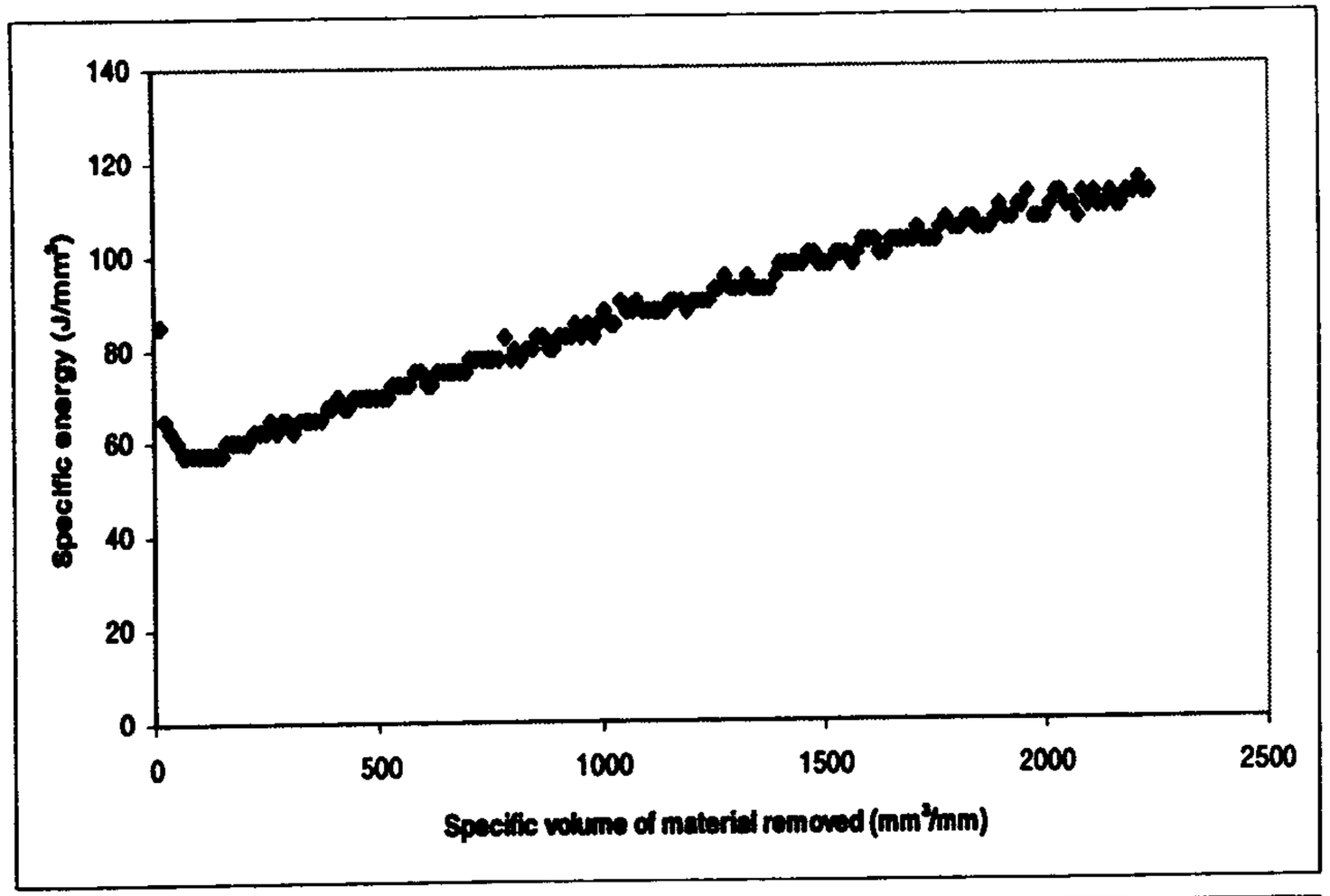

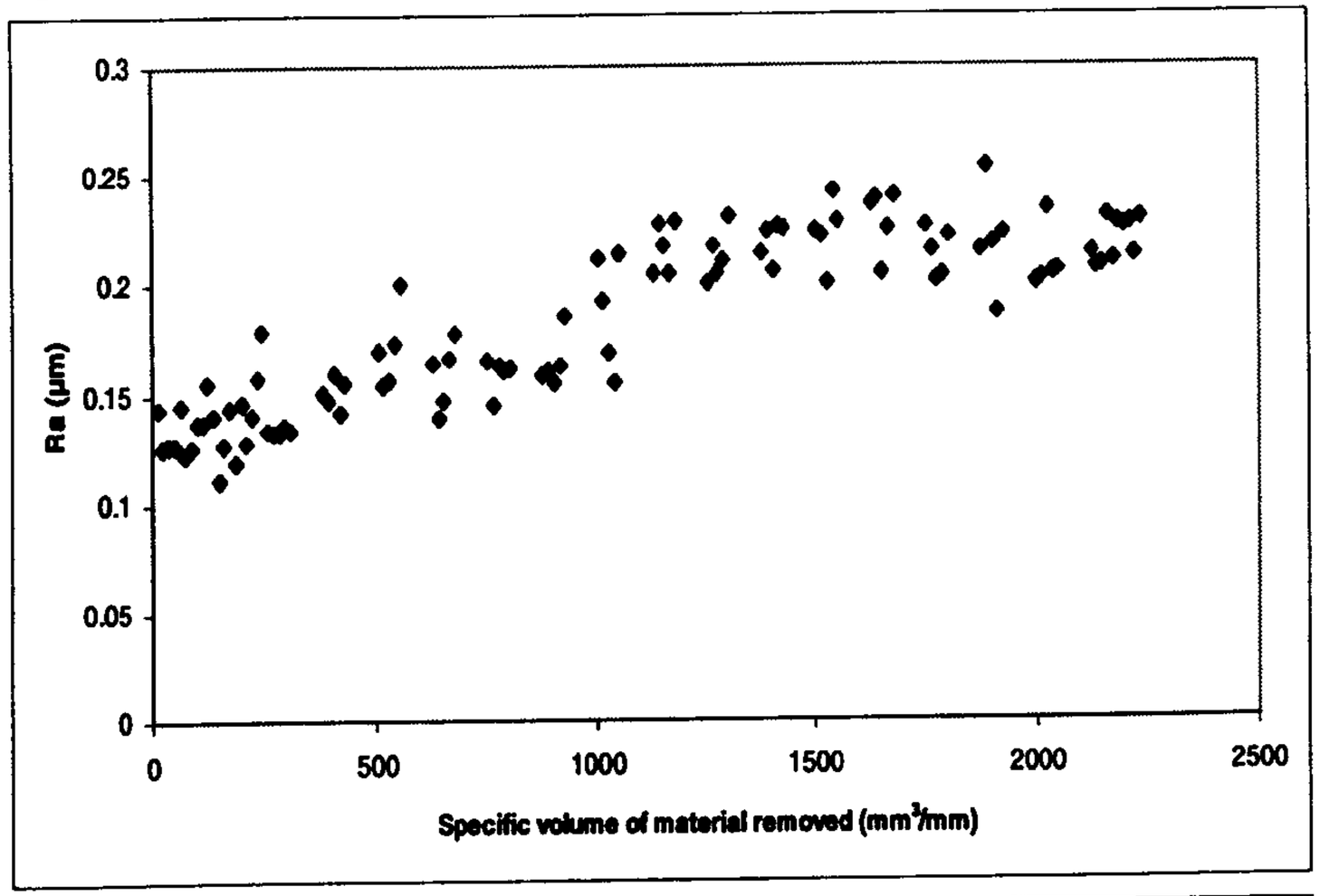

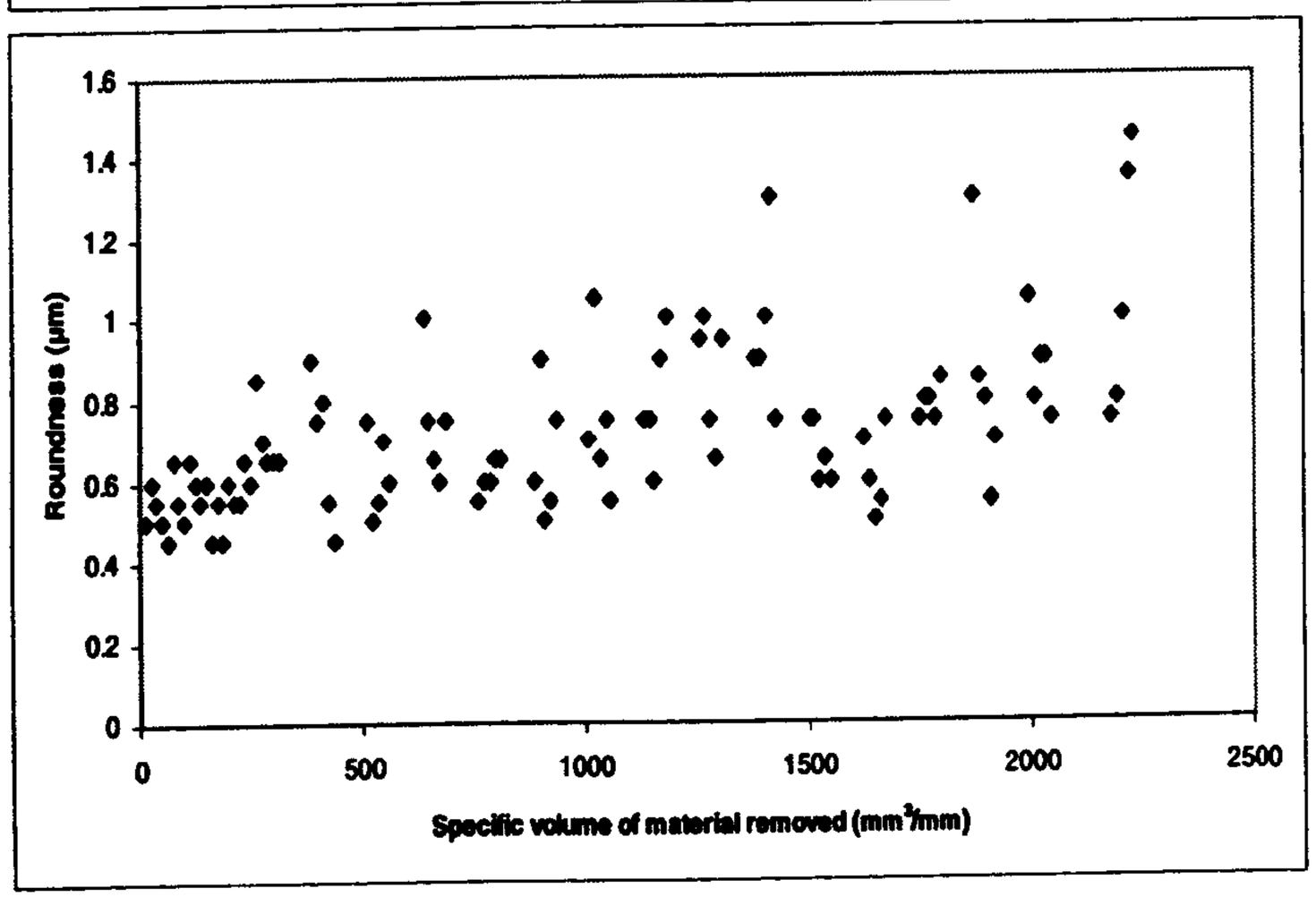

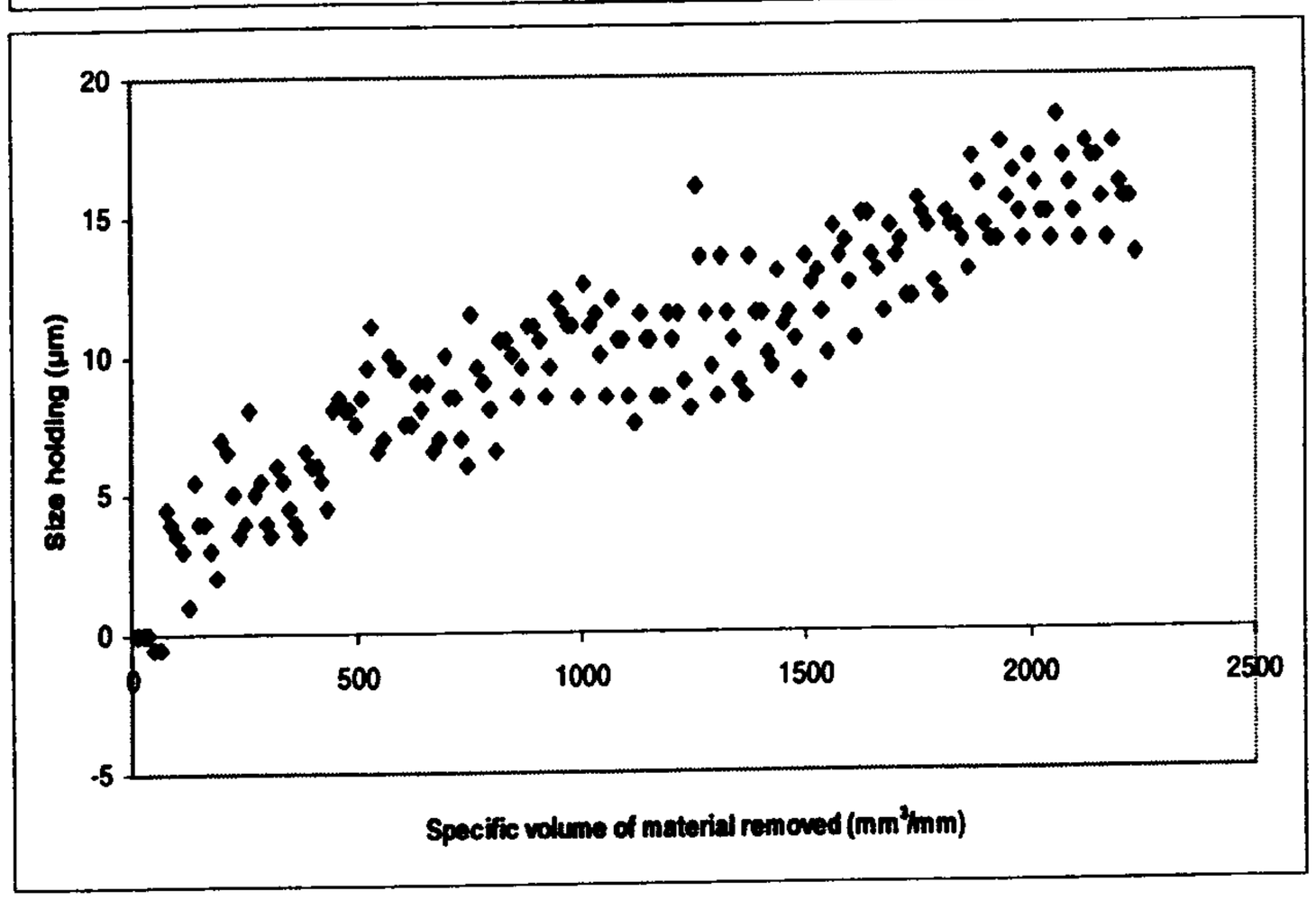

G-Ratio = 260

Results for Benchmark Grinding Trial 2 on the J&S Series 10 Using an Aluminium oxide Wheel to Grind AISI 52100

<u>Experimental Conditions</u>

- U_d: 2
- a_d: 10µm
- n_d: 2
- v_s: 42.4m/s
- v_w: 21m/min
- s: 10s
- -Q'w: 1mm³/mm s
- Wheel: Carborundum A465 K5V
- Coolant: Hysol X 33 l/min, 0.4Bar pump pressure

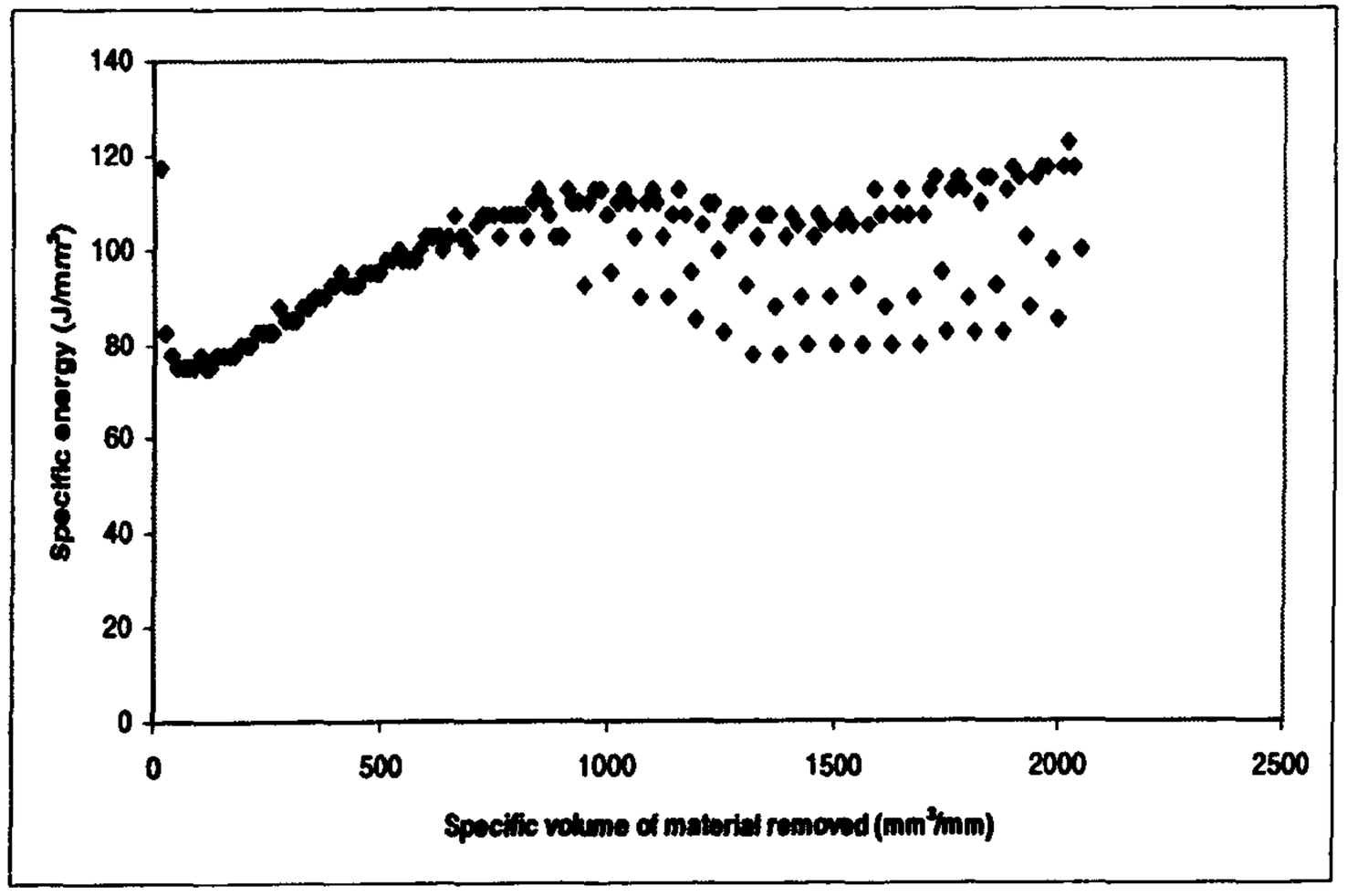

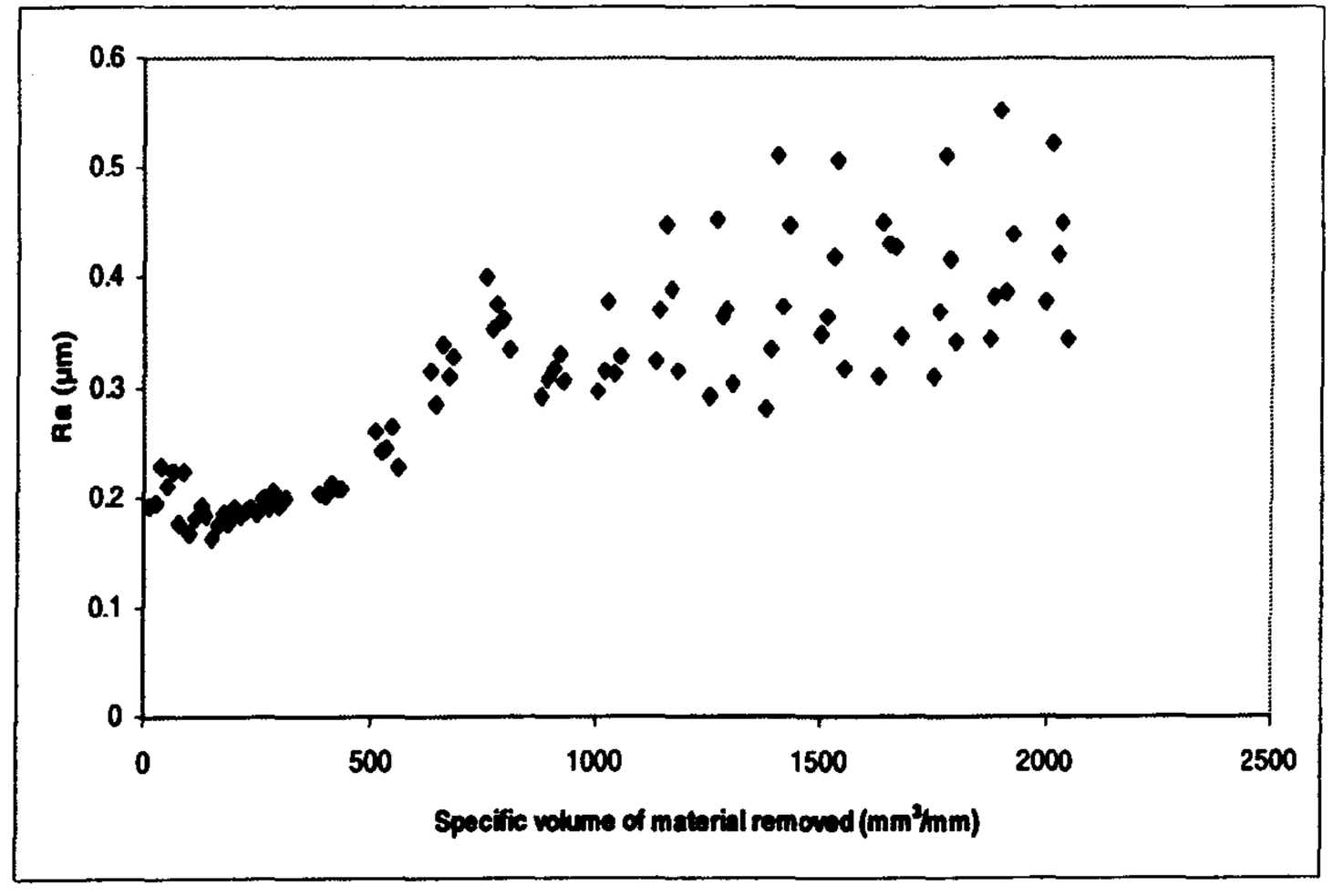

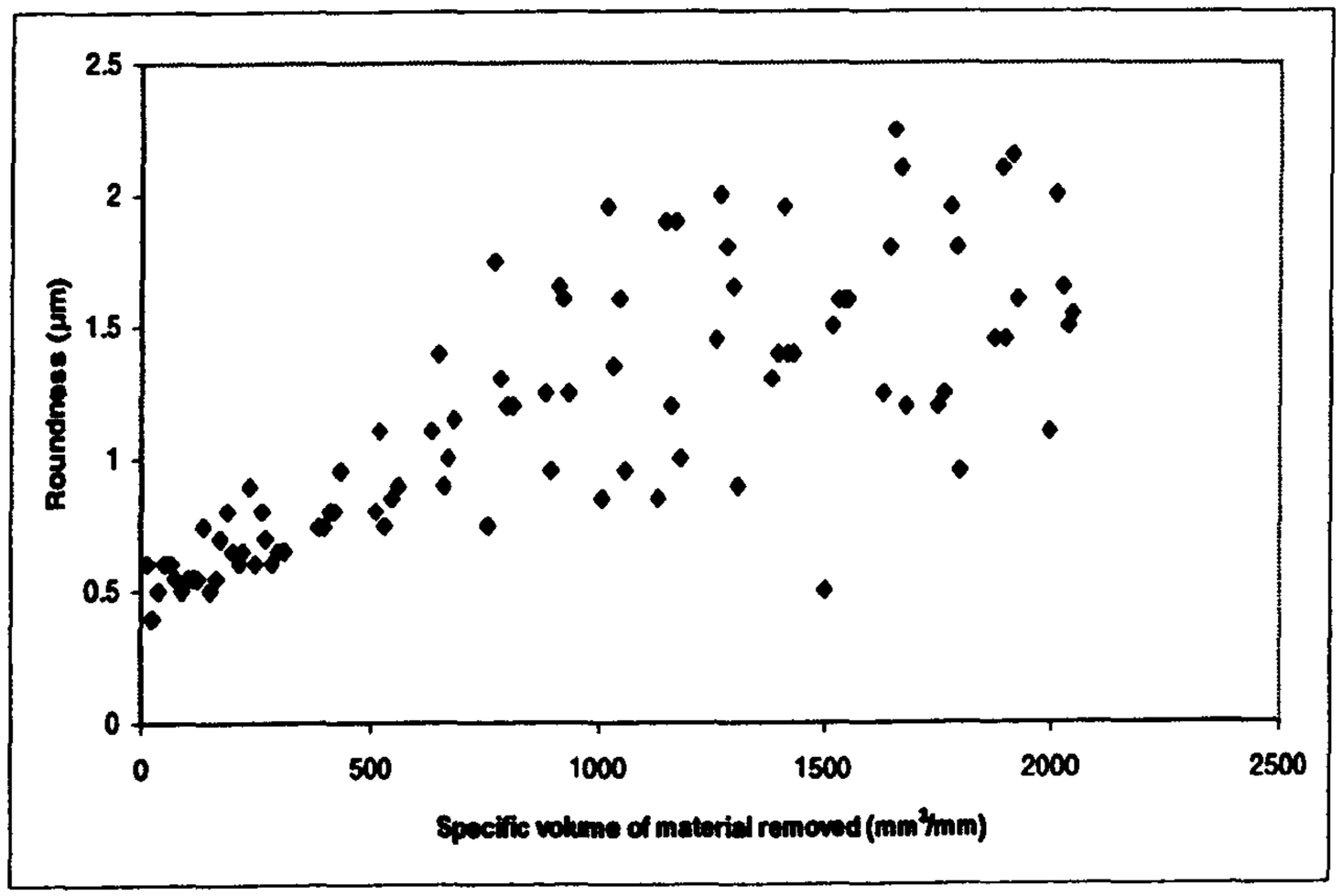

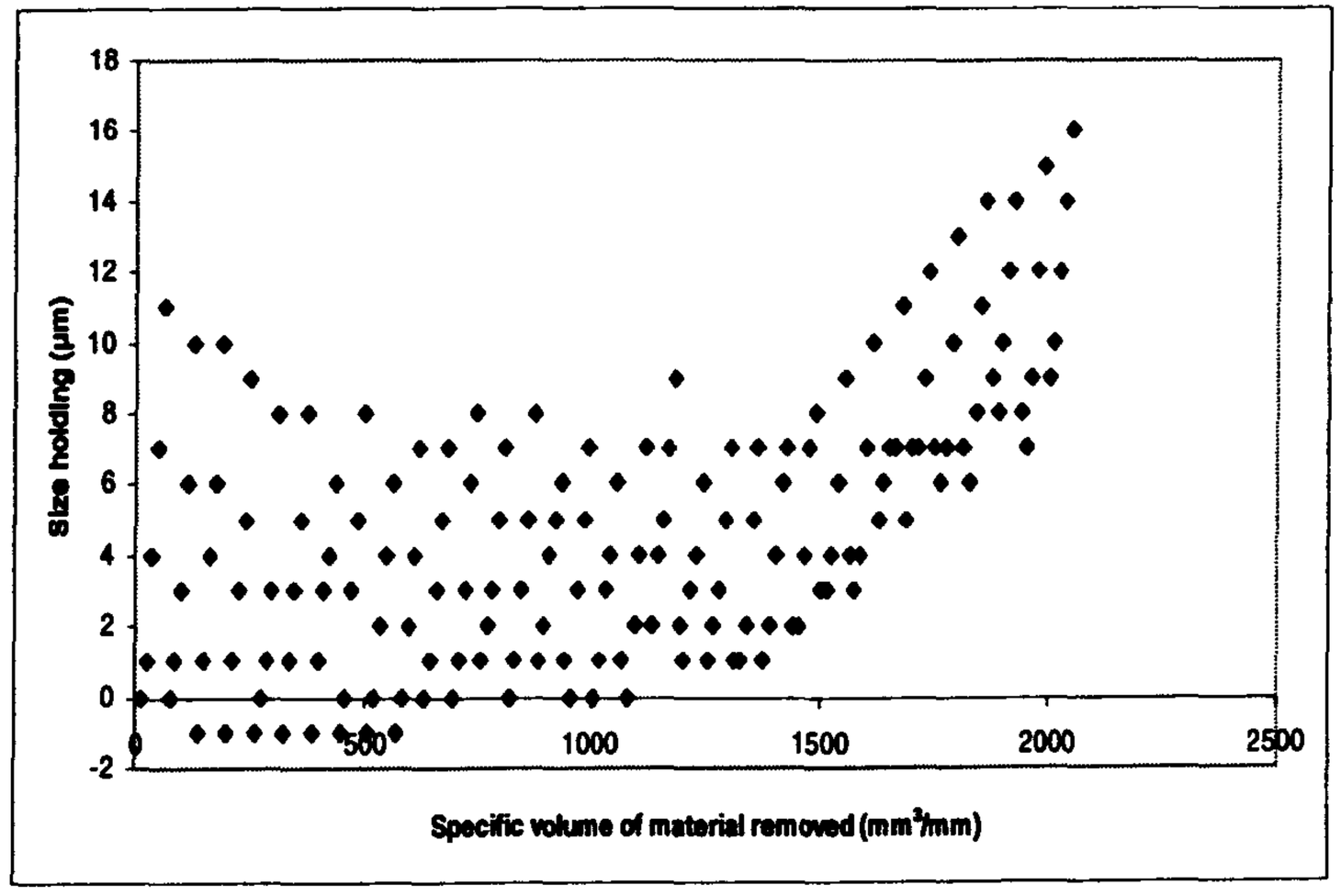

G-Ratio = 126

Results for Benchmark Grinding Trial 3 on the J&S Series 10 Using a Sol Gel Wheel to Grind AISI 52100

<u>Experimental Conditions</u>

- U_d: 2
- a_d: 10μm
- n_d: 2
- v_s: 45m/s
- v_w: 23m/min
- s: 10s
-Q'w: 5mm³/mm s
- Wheel: Universal Sol Gel 73A 601 J8V
- Coolant: Hysol X 33 l/min, 0.4Bar pump pressure

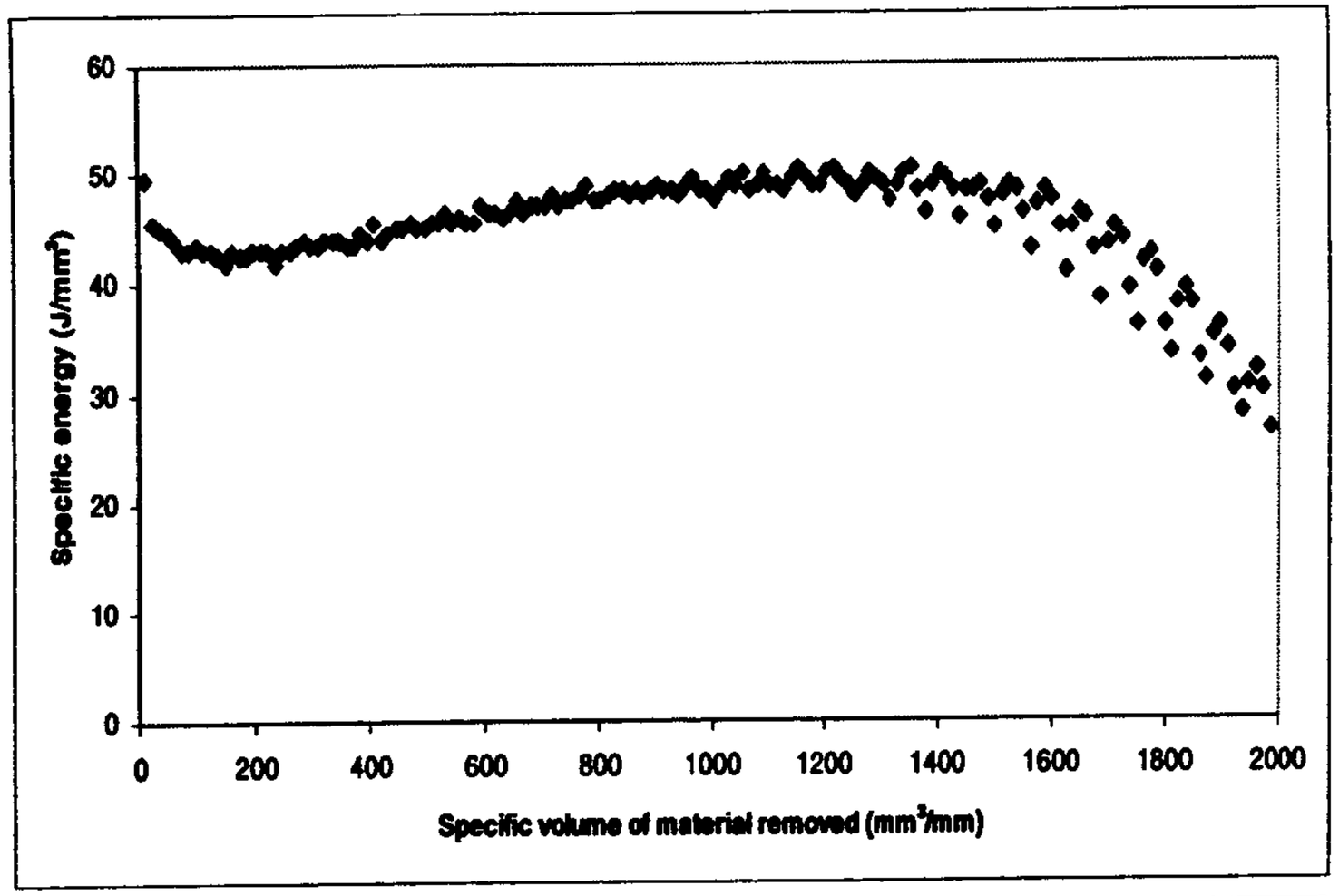

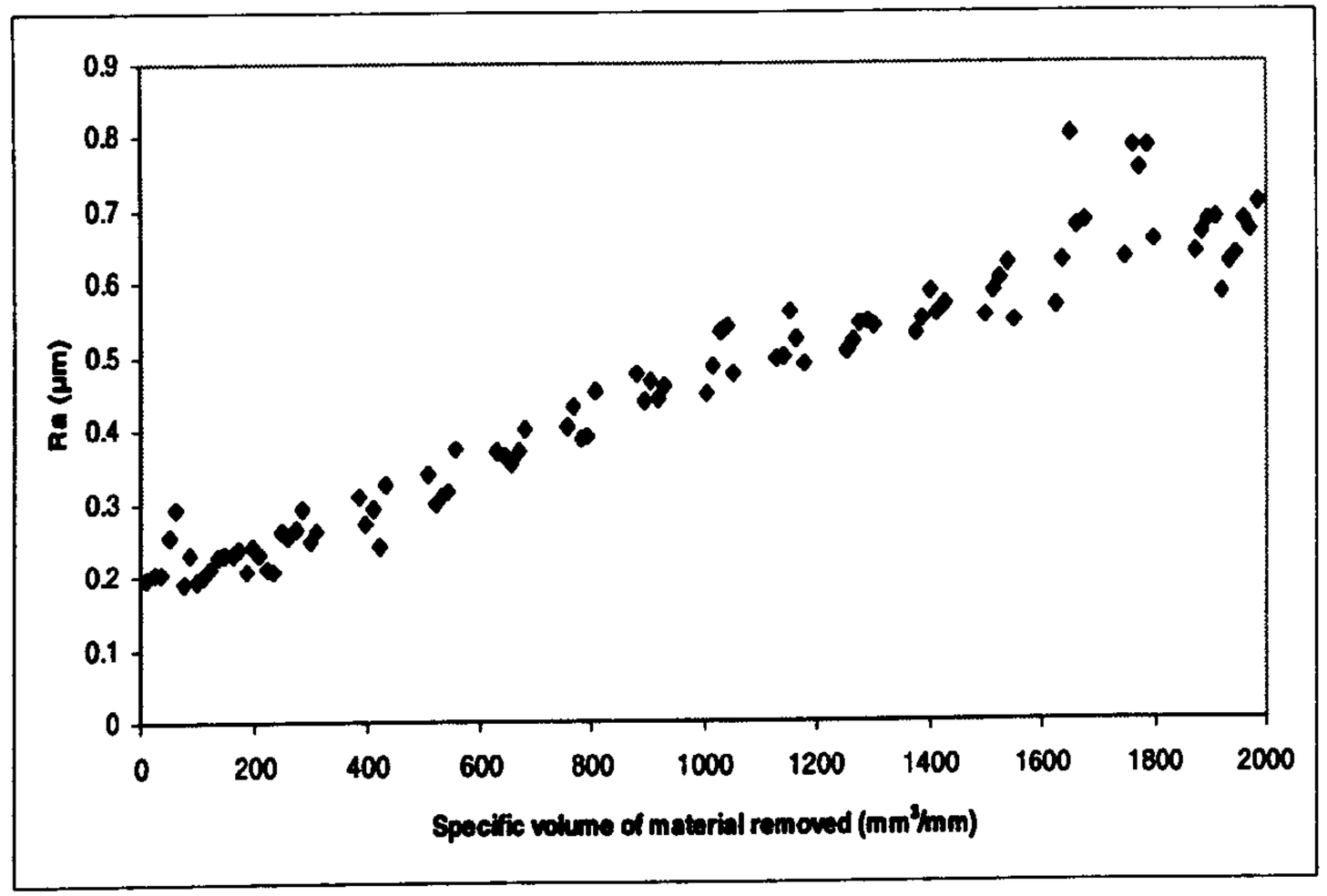

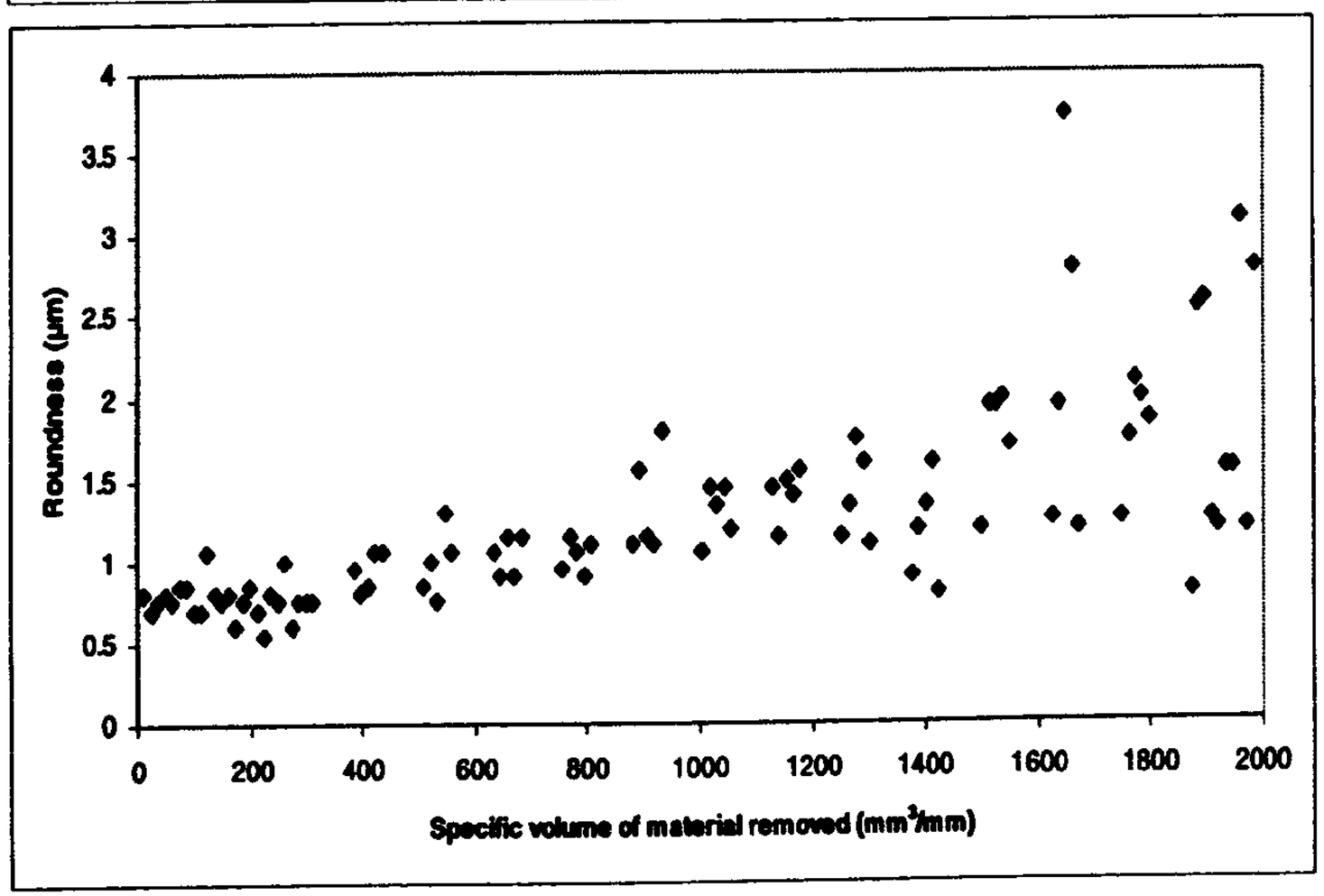

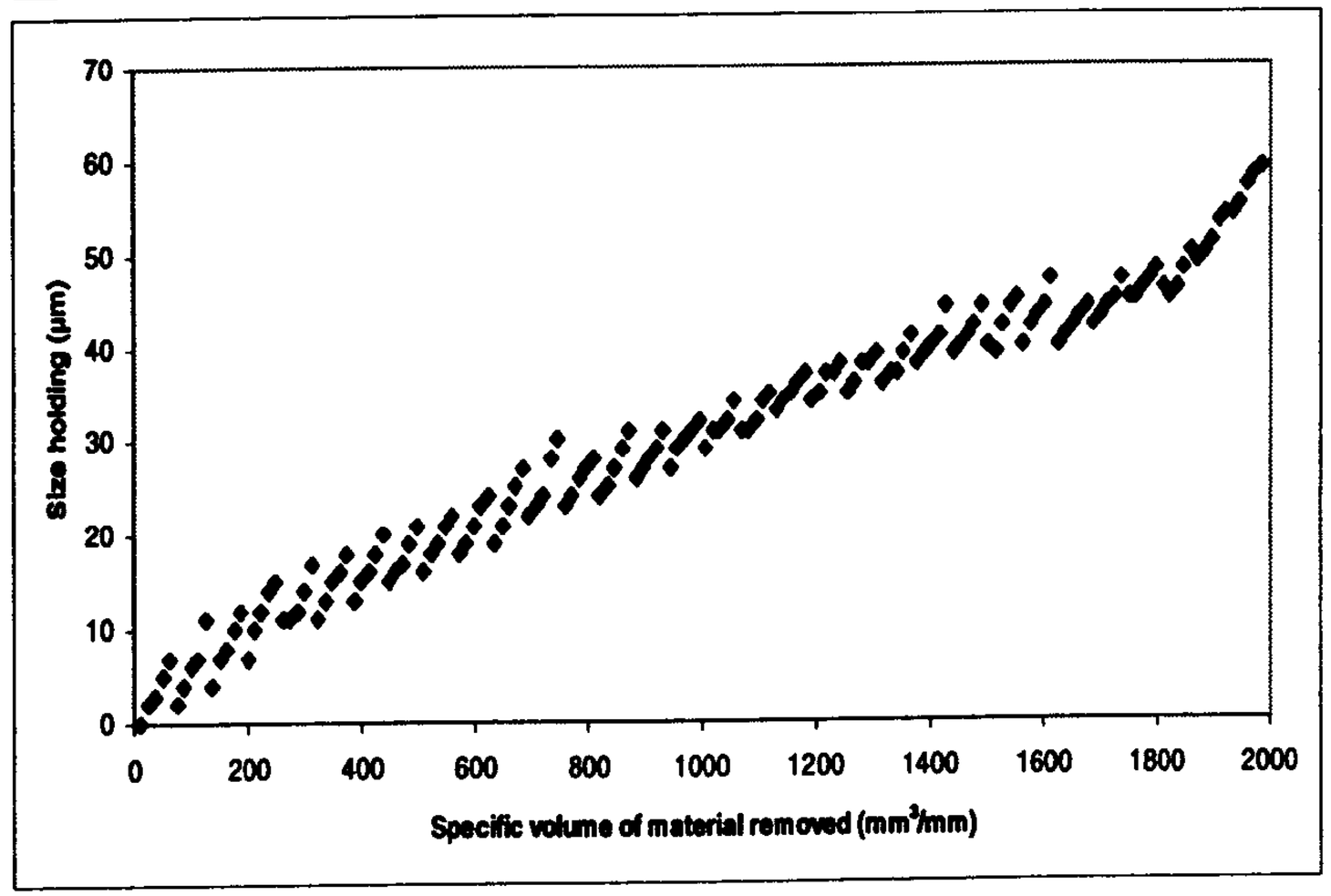

G-Ratio = 87

Results for Benchmark Grinding Trial 4 on the J&S Series 10 Using a Vitrified CBN Wheel to Grind AISI 52100

<u>Experimental Conditions</u>

- Up dressing
- U_d: 2
- a_d: 2µm
- n_d: 2
- v_s: 45m/s
- v_w: 26m/min
- s: 10s
- v_R: 12.6m/s
-Q'w: 7.5mm³/mm s
- Wheel: Saint Gobain B91 ABN500
- Coolant: Hysol X 33 l/min, 0.4Bar pump pressure

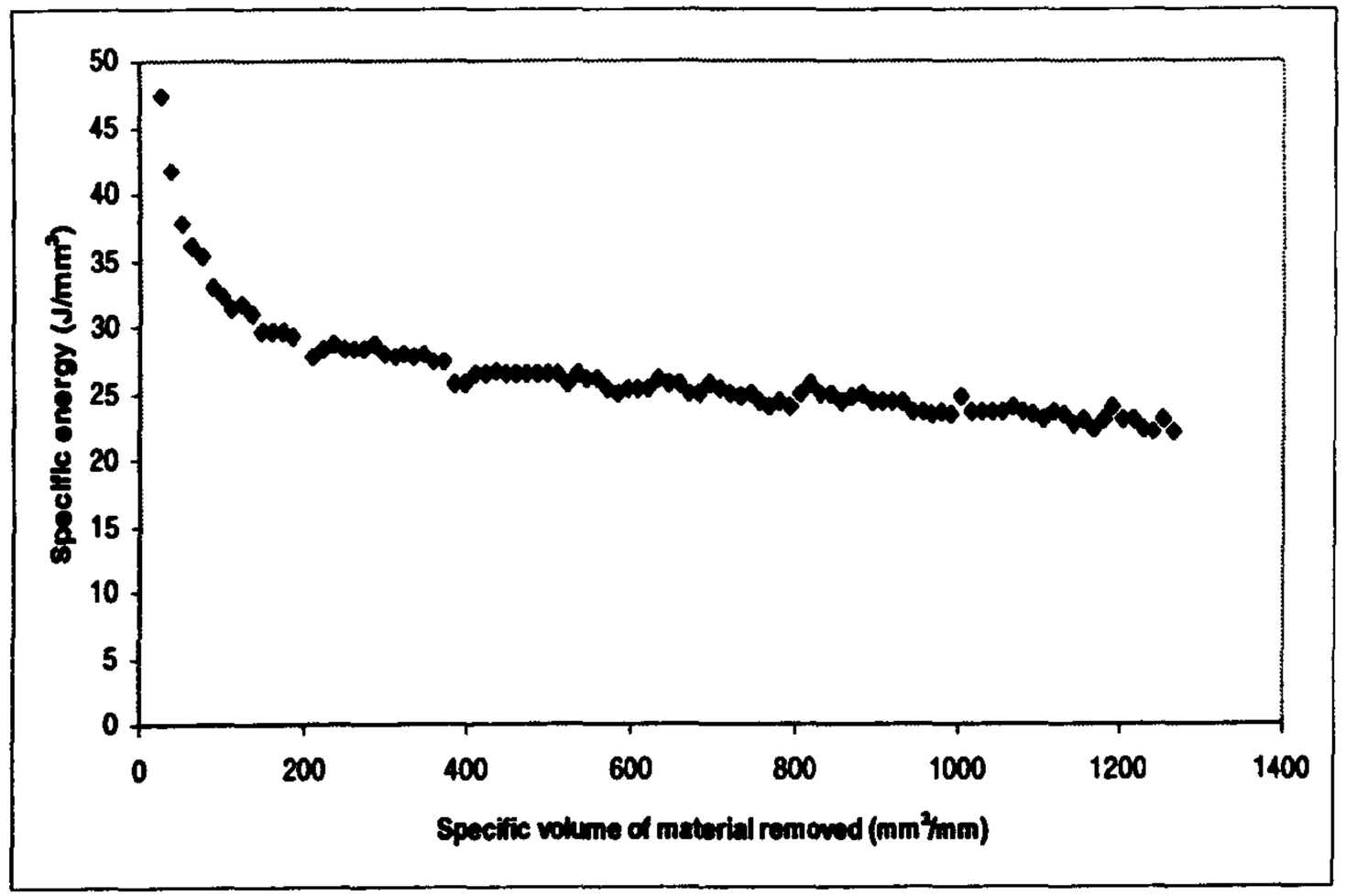

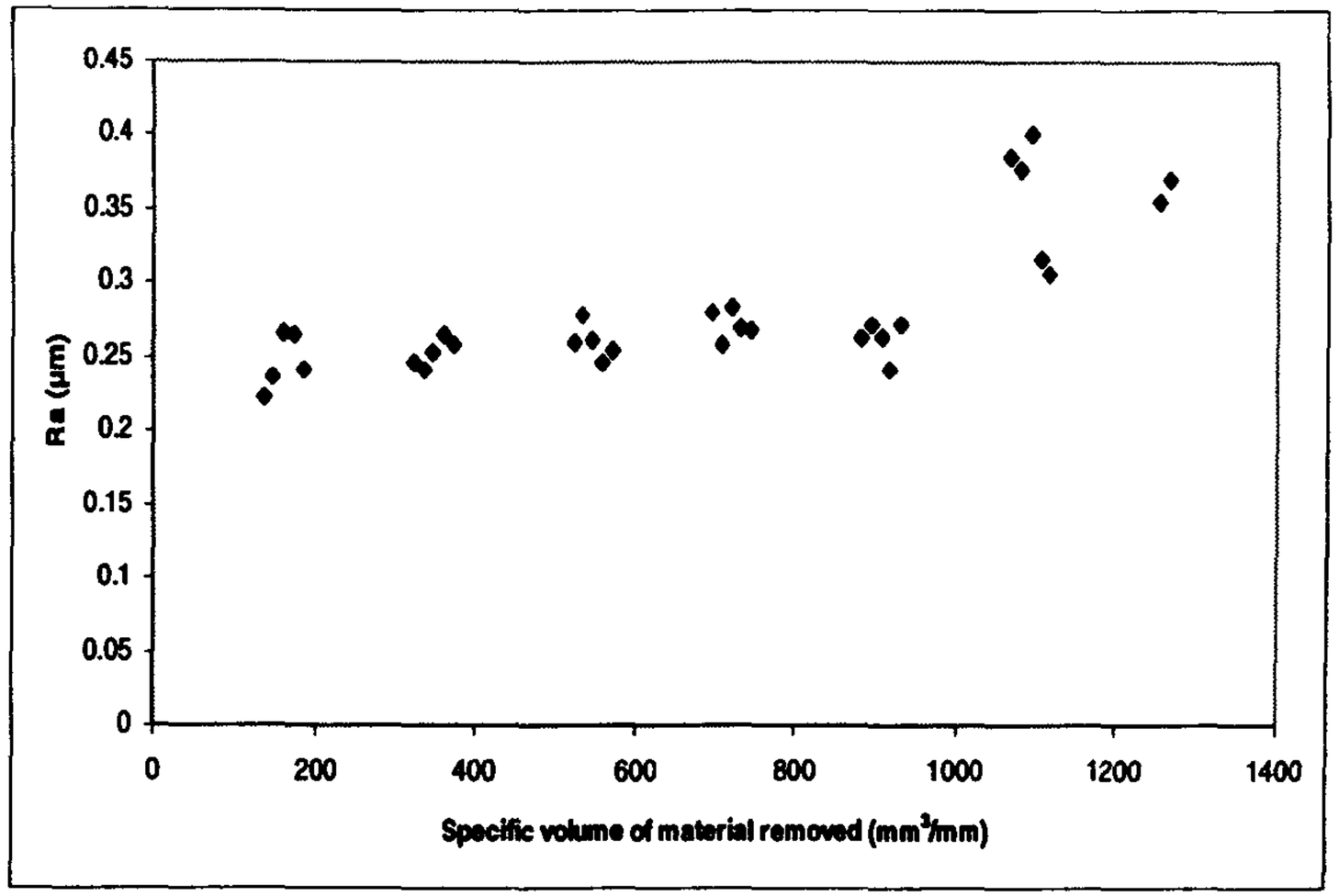

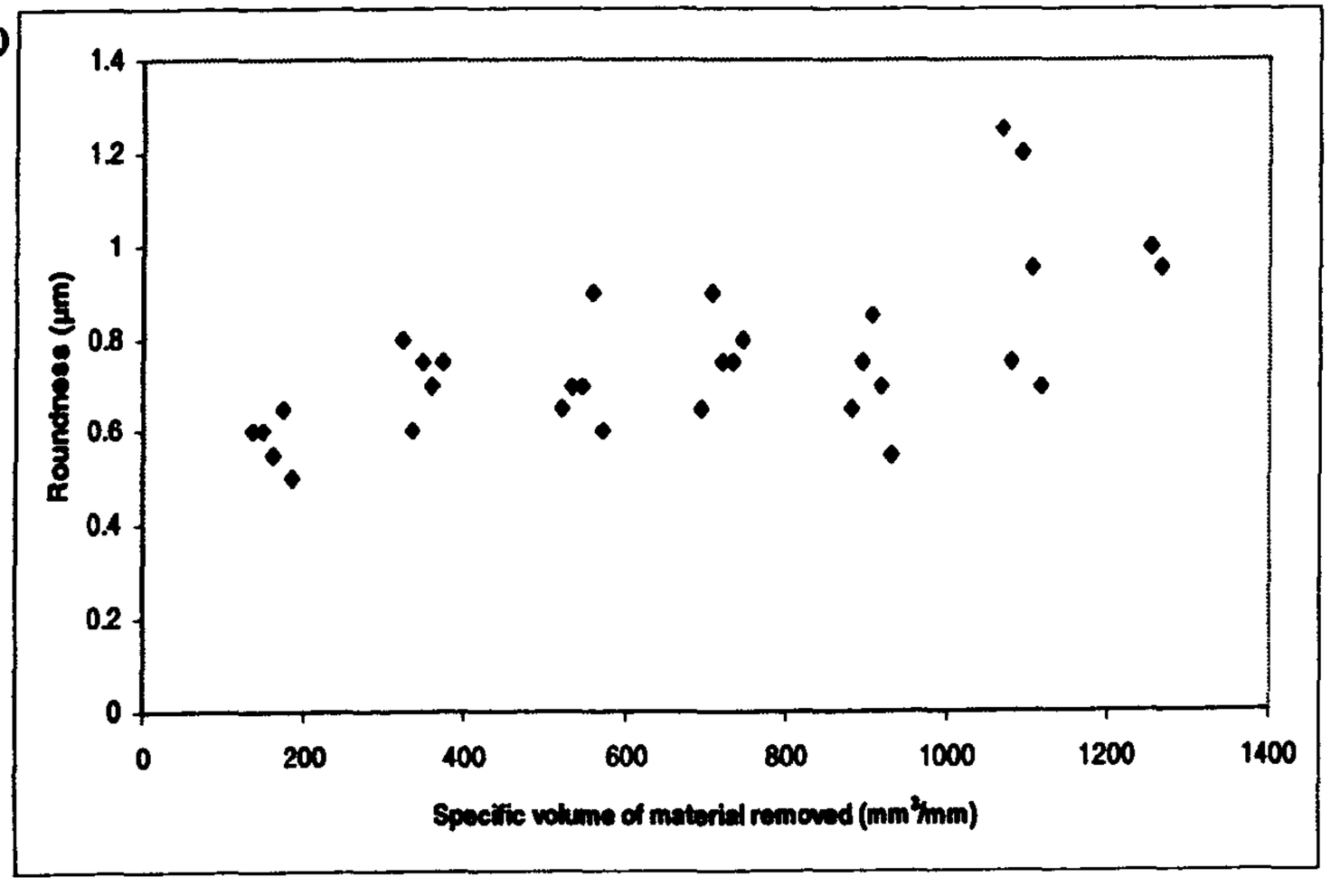

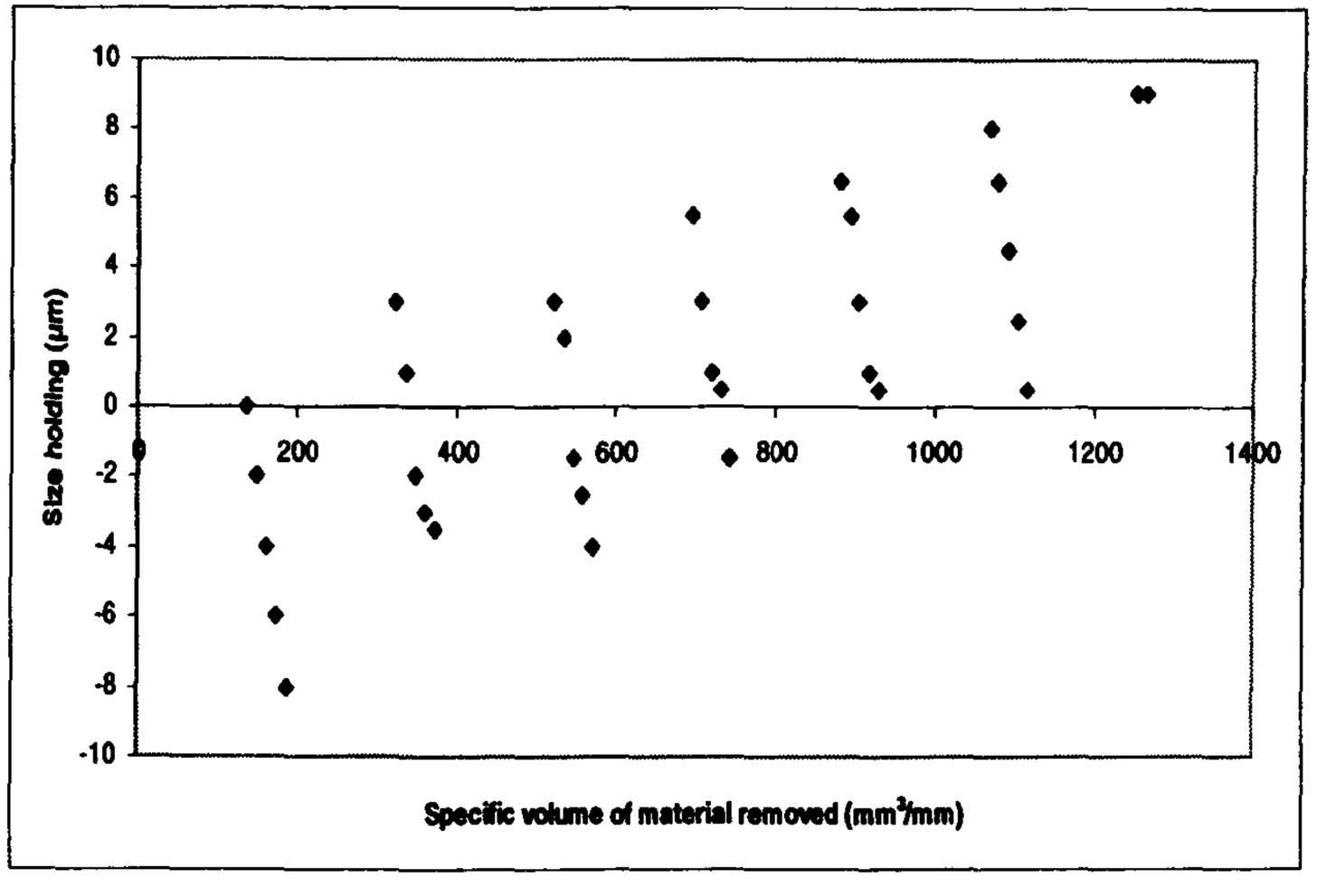

G-Ratio = 205

APPENDIX B5

Appendix B5. Part 1: Breakdown of costs for high-speed Suprema characterisation trials using vitrified CBN to grind AISI 52100.

Part 2: Breakdown of costs for high-speed Suprema confirmation trials using vitrified CBN to grind AISI 52100.

Part 3: Breakdown of costs for conventional-speed Series 10 benchmark trials using aluminium oxide, sol gel and a CBN wheel to grind AISI 52100.

APPENDIX B5

Part 1

Breakdown of costs for high-speed Suprema characterisation trials using vitrified CBN to grind AISI 52100

Factor description	Symbol	Suprema Characterisation Trial 1
Wheel purchase cost (£)	c_s	1700
Maximum wheel diameter (mm)	d_{smax}	250
Minimum wheel diameter (mm)	d_{smin}	240
Radial wheel wear (mm)	r_s	0.01
Depth of dressing increment (mm)	a_d	0.002
Number of dressing passes	n_d	2
Re-dress life (number of parts per dress)	N_d	5
Wheel cost per part (£)	C_s	**0.9520**
Labour cost per hour (£)	c_l	75
Stock removed (mm)	$d_{ww}+d_{ss}$	0.2
Workpiece diameter (mm)	d_w	40
Specific volumetric removal rate (mm^3/mm s)	Q'_w	10
Dwell time (s)	s	5
Wheel width (mm)	b_s	17
Dressing feedrate (mm/s)	v_d	4.235
Labour cost per part (£)	C_l	**0.1900**
Machine purchase cost (£)	c_{mc}	250000
Pay back period (number of hours)	y_t	1920
Machine cost per part (£)	C_{mc}	**0.3298**
Total cost per part, i.e. C_s+C_l (£)	C_t	**1.1420**
Total cost per part including M/C cost, i.e $C_s+C_l+C_{mc}$ (£)	C'_t	**1.4718**
Other factors		
Machine tool used		J&S Suprema
Wheel manufacturer		Wendt
Wheel description		Vitrified CBN
Wheel specifcation		B91
Wheel speed	v_s	60m/s
Workpiece material		AISI52100
Target Ra		0.25µm
Target roundness		1µm

Factor description	Symbol	Suprema Characterisation Trial 2
Wheel purchase cost (£)	c_s	1700
Maximum wheel diameter (mm)	d_{smax}	250
Minimum wheel diameter (mm)	d_{smin}	240
Radial wheel wear (mm)	r_s	0.003
Depth of dressing increment (mm)	a_d	0.002
Number of dressing passes	n_d	10
Re-dress life (number of parts per dress)	N_d	540
Wheel cost per part (£)	C_s	**0.0145**
Labour cost per hour (£)	c_l	75
Stock removed (mm)	$d_{ww}+d_{ss}$	0.2
Workpiece diameter (mm)	d_w	40
Specific volumetric removal rate (mm^3/mm s)	Q'_w	10
Dwell time (s)	s	10
Wheel width (mm)	b_s	17
Dressing feedrate (mm/s)	v_d	8.47
Labour cost per part (£)	C_l	**0.2615**
Machine purchase cost (£)	c_{mc}	250000
Pay back period (number of hours)	y_t	1920
Machine cost per part (£)	C_{mc}	**0.4539**
Total cost per part, i.e. C_s+C_l (£)	C_t	**0.2759**
Total cost per part including M/C cost, i.e $C_s+C_l+C_{mc}$ (£)	C'_t	**0.7299**
Other factors		
Machine tool used		J&S Suprema
Wheel manufacturer		Wendt
Wheel description		Vitrified CBN
Wheel specifcation		B91
Wheel speed	v_s	120m/s
Workpiece material		AISI52100
Target Ra		0.25μm
Target roundness		1μm

Factor description	Symbol	Suprema Characterisation Trial 3
Wheel purchase cost (£)	c_s	1700
Maximum wheel diameter (mm)	d_{smax}	250
Minimum wheel diameter (mm)	d_{smin}	240
Radial wheel wear (mm)	r_s	0.018
Depth of dressing increment (mm)	a_d	0.01
Number of dressing passes	n_d	2
Re-dress life (number of parts per dress)	N_d	3
Wheel cost per part (£)	C_s	**4.3067**
Labour cost per hour (£)	c_l	75
Stock removed (mm)	$d_{ww}+d_{ss}$	0.2
Workpiece diameter (mm)	d_w	40
Specific volumetric removal rate ($mm^3/mm\ s$)	Q'_w	10
Dwell time (s)	s	10
Wheel width (mm)	b_s	17
Dressing feedrate (mm/s)	v_d	1.232
Labour cost per part (£)	C_l	**0.4523**
Machine purchase cost (£)	c_{mc}	250000
Pay back period (number of hours)	y_t	1920
Machine cost per part (£)	C_{mc}	**0.7853**
Total cost per part, i.e. C_s+C_l (£)	C_t	**4.7590**
Total cost per part including M/C cost, i.e $C_s+C_l+C_{mc}$ (£)	C'_t	**5.5443**
Other factors		
Machine tool used		J&S Suprema
Wheel manufacturer		Wendt
Wheel description		Vitrified CBN
Wheel specifcation		B91
Wheel speed	v_s	60m/s
Workpiece material		AISI52100
Target Ra		0.25µm
Target roundness		1µm

Factor description	Symbol	Suprema Characterisation Trial 4
Wheel purchase cost (£)	c_s	1700
Maximum wheel diameter (mm)	d_{smax}	250
Minimum wheel diameter (mm)	d_{smin}	240
Radial wheel wear (mm)	r_s	0.004
Depth of dressing increment (mm)	a_d	0.01
Number of dressing passes	n_d	10
Re-dress life (number of parts per dress)	N_d	540
Wheel cost per part (£)	C_s	**0.0655**
Labour cost per hour (£)	c_l	75
Stock removed (mm)	$d_{ww}+d_{ss}$	0.2
Workpiece diameter (mm)	d_w	40
Specific volumetric removal rate (mm^3/mm s)	Q'_w	10
Dwell time (s)	s	5
Wheel width (mm)	b_s	17
Dressing feedrate (mm/s)	v_d	2.464
Labour cost per part (£)	C_l	**0.1592**
Machine purchase cost (£)	c_{mc}	250000
Pay back period (number of hours)	y_t	1920
Machine cost per part (£)	C_{mc}	**0.2764**
Total cost per part, i.e. C_s+C_l (£)	C_t	**0.2247**
Total cost per part including M/C cost, i.e $C_s+C_l+C_{mc}$ (£)	C'_t	**0.5010**
Other factors		
Machine tool used		J&S Suprema
Wheel manufacturer		Wendt
Wheel description		Vitrified CBN
Wheel specifcation		B91
Wheel speed	v_s	120m/s
Workpiece material		AISI52100
Target Ra		0.25μm
Target roundness		1μm

Factor description	Symbol	Suprema Characetrisation Trial 5
Wheel purchase cost (£)	c_s	1700
Maximum wheel diameter (mm)	d_{smax}	250
Minimum wheel diameter (mm)	d_{smin}	240
Radial wheel wear (mm)	r_s	0.0015
Depth of dressing increment (mm)	a_d	0.01
Number of dressing passes	n_d	2
Re-dress life (number of parts per dress)	N_d	550
Wheel cost per part (£)	C_s	**0.0133**
Labour cost per hour (£)	c_l	75
Stock removed (mm)	$d_{ww}+d_{ss}$	0.2
Workpiece diameter (mm)	d_w	40
Specific volumetric removal rate (mm^3/mm s)	Q'_w	10
Dwell time (s)	s	10
Wheel width (mm)	b_s	17
Dressing feedrate (mm/s)	v_d	12.32
Labour cost per part (£)	C_l	**0.2608**
Machine purchase cost (£)	c_{mc}	250000
Pay back period (number of hours)	y_t	1920
Machine cost per part (£)	C_{mc}	**0.4528**
Total cost per part, i.e. C_s+C_l (£)	C_t	**0.2741**
Total cost per part including M/C cost, i.e C_s+C_l+C_{mc} (£)	C'_t	**0.7269**
Other factors		
Machine tool used		J&S Suprema
Wheel manufacturer		Wendt
Wheel description		Vitrified CBN
Wheel specifcation		B91
Wheel speed	v_s	120m/s
Workpiece material		AISI52100
Target Ra		0.25μm
Target roundness		1μm

Factor description	Symbol	Suprema Characterisation Trial 6
Wheel purchase cost (£)	c_s	1700
Maximum wheel diameter (mm)	d_{smax}	250
Minimum wheel diameter (mm)	d_{smin}	240
Radial wheel wear (mm)	r_s	0.029
Depth of dressing increment (mm)	a_d	0.01
Number of dressing passes	n_d	10
Re-dress life (number of parts per dress)	N_d	50
Wheel cost per part (£)	C_s	**0.8772**
Labour cost per hour (£)	c_l	75
Stock removed (mm)	$d_{ww}+d_{ss}$	0.2
Workpiece diameter (mm)	d_w	40
Specific volumetric removal rate (mm^3/mm s)	Q'_w	10
Dwell time (s)	s	5
Wheel width (mm)	b_s	17
Dressing feedrate (mm/s)	v_d	6.16
Labour cost per part (£)	C_l	**0.1680**
Machine purchase cost (£)	c_{mc}	250000
Pay back period (number of hours)	y_t	1920
Machine cost per part (£)	C_{mc}	**0.2917**
Total cost per part, i.e. C_s+C_l (£)	C_t	**1.0452**
Total cost per part including M/C cost, i.e $C_s+C_l+C_{mc}$ (£)	C'_t	**1.3369**
Other factors		
Machine tool used		J&S Suprema
Wheel manufacturer		Wendt
Wheel description		Vitrified CBN
Wheel specifcation		B91
Wheel speed	v_s	60m/s
Workpiece material		AISI52100
Target Ra		0.25µm
Target roundness		1µm

Factor description	Symbol	Suprema CharacterisationTrial 7
Wheel purchase cost (£)	c_s	1700
Maximum wheel diameter (mm)	d_{smax}	250
Minimum wheel diameter (mm)	d_{smin}	240
Radial wheel wear (mm)	r_s	0.0035
Depth of dressing increment (mm)	a_d	0.002
Number of dressing passes	n_d	2
Re-dress life (number of parts per dress)	N_d	175
Wheel cost per part (£)	C_s	**0.0146**
Labour cost per hour (£)	c_l	75
Stock removed (mm)	$d_{ww}+d_{ss}$	0.2
Workpiece diameter (mm)	d_w	40
Specific volumetric removal rate (mm^3/mm s)	Q'_w	10
Dwell time (s)	s	5
Wheel width (mm)	b_s	17
Dressing feedrate (mm/s)	v_d	1.694
Labour cost per part (£)	C_l	**0.1589**
Machine purchase cost (£)	c_{mc}	250000
Pay back period (number of hours)	y_t	1920
Machine cost per part (£)	C_{mc}	**0.2759**
Total cost per part, i.e. C_s+C_l (£)	C_t	**0.1735**
Total cost per part including M/C cost, i.e C_s+C_l+C_{mc} (£)	C'_t	**0.4494**
Other factors		
Machine tool used		J&S Suprema
Wheel manufacturer		Wendt
Wheel description		Vitrified CBN
Wheel specifcation		B91
Wheel speed	v_s	120m/s
Workpiece material		AISI52100
Target Ra		0.25µm
Target roundness		1µm

Factor description	Symbol	Suprema Characterisation Trial 8
Wheel purchase cost (£)	c_s	1700
Maximum wheel diameter (mm)	d_{smax}	250
Minimum wheel diameter (mm)	d_{smin}	240
Radial wheel wear (mm)	r_s	0.0019
Depth of dressing increment (mm)	a_d	0.002
Number of dressing passes	n_d	10
Re-dress life (number of parts per dress)	N_d	150
Wheel cost per part (£)	C_s	**0.0496**
Labour cost per hour (£)	c_l	75
Stock removed (mm)	$d_{ww}+d_{ss}$	0.2
Workpiece diameter (mm)	d_w	40
Specific volumetric removal rate (mm^3/mm s)	Q'_w	10
Dwell time (s)	s	10
Wheel width (mm)	b_s	17
Dressing feedrate (mm/s)	v_d	0.847
Labour cost per part (£)	C_l	**0.2886**
Machine purchase cost (£)	c_{mc}	250000
Pay back period (number of hours)	y_t	1920
Machine cost per part (£)	C_{mc}	**0.5010**
Total cost per part, i.e. C_s+C_l (£)	C_t	**0.3382**
Total cost per part including M/C cost, i.e C_s+C_l+C_{mc} (£)	C'_t	**0.8392**
Other factors		
Machine tool used		J&S Suprema
Wheel manufacturer		Wendt
Wheel description		Vitrified CBN
Wheel specifcation		B91
Wheel speed	v_s	60m/s
Workpiece material		AISI52101
Target Ra		0.25µm
Target roundness		1µm

Factor description	Symbol	Suprema Characterisation Trial 9
Wheel purchase cost (£)	c_s	1700
Maximum wheel diameter (mm)	d_{smax}	250
Minimum wheel diameter (mm)	d_{smin}	240
Radial wheel wear (mm)	r_s	0.006
Depth of dressing increment (mm)	a_d	0.01
Number of dressing passes	n_d	10
Re-dress life (number of parts per dress)	N_d	540
Wheel cost per part (£)	C_s	**0.0667**
Labour cost per hour (£)	c_l	75
Stock removed (mm)	$d_{ww}+d_{ss}$	0.2
Workpiece diameter (mm)	d_w	40
Specific volumetric removal rate (mm^3/mm s)	Q'_w	10
Dwell time (s)	s	10
Wheel width (mm)	b_s	17
Dressing feedrate (mm/s)	v_d	2.464
Labour cost per part (£)	C_l	**0.2634**
Machine purchase cost (£)	c_{mc}	250000
Pay back period (number of hours)	y_t	1920
Machine cost per part (£)	C_{mc}	**0.4572**
Total cost per part, i.e. C_s+C_l (£)	C_t	**0.3301**
Total cost per part including M/C cost, i.e $C_s+C_l+C_{mc}$ (£)	C'_t	**0.7873**
Other factors		
Machine tool used		J&S Suprema
Wheel manufacturer		Wendt
Wheel description		Vitrified CBN
Wheel specifcation		B91
Wheel speed	v_s	120m/s
Workpiece material		AISI52100
Target Ra		0.25µm
Target roundness		1µm

Factor description	Symbol	Suprema Characterisation Trial 10
Wheel purchase cost (£)	c_s	1700
Maximum wheel diameter (mm)	d_{smax}	250
Minimum wheel diameter (mm)	d_{smin}	240
Radial wheel wear (mm)	r_s	0.034
Depth of dressing increment (mm)	a_d	0.01
Number of dressing passes	n_d	2
Re-dress life (number of parts per dress)	N_d	30
Wheel cost per part (£)	C_s	**0.6120**
Labour cost per hour (£)	c_l	75
Stock removed (mm)	$d_{ww}+d_{ss}$	0.2
Workpiece diameter (mm)	d_w	40
Specific volumetric removal rate (mm^3/mm s)	Q'_w	10
Dwell time (s)	s	5
Wheel width (mm)	b_s	17
Dressing feedrate (mm/s)	v_d	1.232
Labour cost per part (£)	C_l	**0.1757**
Machine purchase cost (£)	c_{mc}	250000
Pay back period (number of hours)	y_t	1920
Machine cost per part (£)	C_{mc}	**0.3050**
Total cost per part, i.e. C_s+C_l (£)	C_t	**0.7877**
Total cost per part including M/C cost, i.e $C_s+C_l+C_{mc}$ (£)	C'_t	**1.0927**
Other factors		
Machine tool used		J&S Suprema
Wheel manufacturer		Wendt
Wheel description		Vitrified CBN
Wheel specifcation		B91
Wheel speed	v_s	60m/s
Workpiece material		AISI52103
Target Ra		0.25µm
Target roundness		1µm

Factor description	Symbol	Suprema Characterisation Trial 11
Wheel purchase cost (£)	c_s	1700
Maximum wheel diameter (mm)	d_{smax}	250
Minimum wheel diameter (mm)	d_{smin}	240
Radial wheel wear (mm)	r_s	0.005
Depth of dressing increment (mm)	a_d	0.002
Number of dressing passes	n_d	10
Re-dress life (number of parts per dress)	N_d	5
Wheel cost per part (£)	C_s	**1.7000**
Labour cost per hour (£)	c_l	75
Stock removed (mm)	$d_{ww}+d_{ss}$	0.2
Workpiece diameter (mm)	d_w	40
Specific volumetric removal rate ($mm^3/mm\ s$)	Q'_w	10
Dwell time (s)	s	5
Wheel width (mm)	b_s	17
Dressing feedrate (mm/s)	v_d	8.47
Labour cost per part (£)	C_l	**0.2402**
Machine purchase cost (£)	c_{mc}	250000
Pay back period (number of hours)	y_t	1920
Machine cost per part (£)	C_{mc}	**0.4169**
Total cost per part, i.e. C_s+C_l (£)	C_t	**1.9402**
Total cost per part including M/C cost, i.e $C_s+C_l+C_{mc}$ (£)	C'_t	**2.3571**
Other factors		
Machine tool used		J&S Suprema
Wheel manufacturer		Wendt
Wheel description		Vitrified CBN
Wheel specifcation		B91
Wheel speed	v_s	120m/s
Workpiece material		AISI52104
Target Ra		0.25µm
Target roundness		1µm

Factor description	Symbol	Suprema Characterisation Trial 12
Wheel purchase cost (£)	c_s	1700
Maximum wheel diameter (mm)	d_{smax}	250
Minimum wheel diameter (mm)	d_{smin}	240
Radial wheel wear (mm)	r_s	0.035
Depth of dressing increment (mm)	a_d	0.002
Number of dressing passes	n_d	2
Re-dress life (number of parts per dress)	N_d	90
Wheel cost per part (£)	C_s	**0.1473**
Labour cost per hour (£)	c_l	75
Stock removed (mm)	$d_{ww}+d_{ss}$	0.2
Workpiece diameter (mm)	d_w	40
Specific volumetric removal rate (mm^3/mm s)	Q'_w	10
Dwell time (s)	s	10
Wheel width (mm)	b_s	17
Dressing feedrate (mm/s)	v_d	4.235
Labour cost per part (£)	C_l	**0.2626**
Machine purchase cost (£)	c_{mc}	250000
Pay back period (number of hours)	y_t	1920
Machine cost per part (£)	C_{mc}	**0.4558**
Total cost per part, i.e. C_s+C_l (£)	C_t	**0.4099**
Total cost per part including M/C cost, i.e $C_s+C_l+C_{mc}$ (£)	C'_t	**0.8657**
Other factors		
Machine tool used		J&S Suprema
Wheel manufacturer		Wendt
Wheel description		Vitrified CBN
Wheel specifcation		B91
Wheel speed	v_s	60m/s
Workpiece material		AISI52105
Target Ra		0.25µm
Target roundness		1µm

Factor description	Symbol	Suprema Characterisation Trial 13
Wheel purchase cost (£)	c_s	1700
Maximum wheel diameter (mm)	d_{smax}	250
Minimum wheel diameter (mm)	d_{smin}	240
Radial wheel wear (mm)	r_s	0.12
Depth of dressing increment (mm)	a_d	0.002
Number of dressing passes	n_d	10
Re-dress life (number of parts per dress)	N_d	15
Wheel cost per part (£)	C_s	**3.1733**
Labour cost per hour (£)	c_l	75
Stock removed (mm)	$d_{ww}+d_{ss}$	0.2
Workpiece diameter (mm)	d_w	40
Specific volumetric removal rate (mm^3/mm s)	Q'_w	10
Dwell time (s)	s	5
Wheel width (mm)	b_s	17
Dressing feedrate (mm/s)	v_d	0.847
Labour cost per part (£)	C_l	**0.4353**
Machine purchase cost (£)	c_{mc}	250000
Pay back period (number of hours)	y_t	1920
Machine cost per part (£)	C_{mc}	**0.7557**
Total cost per part, i.e. C_s+C_l (£)	C_t	**3.6086**
Total cost per part including M/C cost, i.e $C_s+C_l+C_{mc}$ (£)	C'_t	**4.3643**
Other factors		
Machine tool used		J&S Suprema
Wheel manufacturer		Wendt
Wheel description		Vitrified CBN
Wheel specifcation		B91
Wheel speed	v_s	60m/s
Workpiece material		AISI52106
Target Ra		0.25µm
Target roundness		1µm

Factor description	Symbol	Suprema Characterisation Trial 14
Wheel purchase cost (£)	c_s	1700
Maximum wheel diameter (mm)	d_{smax}	250
Minimum wheel diameter (mm)	d_{smin}	240
Radial wheel wear (mm)	r_s	0.003
Depth of dressing increment (mm)	a_d	0.002
Number of dressing passes	n_d	2
Re-dress life (number of parts per dress)	N_d	535
Wheel cost per part (£)	C_s	**0.0044**
Labour cost per hour (£)	c_l	75
Stock removed (mm)	$d_{ww}+d_{ss}$	0.2
Workpiece diameter (mm)	d_w	40
Specific volumetric removal rate (mm^3/mm s)	Q'_w	10
Dwell time (s)	s	10
Wheel width (mm)	b_s	17
Dressing feedrate (mm/s)	v_d	1.694
Labour cost per part (£)	C_l	**0.2615**
Machine purchase cost (£)	c_{mc}	250000
Pay back period (number of hours)	y_t	1920
Machine cost per part (£)	C_{mc}	**0.4539**
Total cost per part, i.e. C_s+C_l (£)	C_t	**0.2659**
Total cost per part including M/C cost, i.e $C_s+C_l+C_{mc}$ (£)	C'_t	**0.7199**
Other factors		
Machine tool used		J&S Suprema
Wheel manufacturer		Wendt
Wheel description		Vitrified CBN
Wheel specifcation		B91
Wheel speed	v_s	120m/s
Workpiece material		AISI52100
Target Ra		0.25µm
Target roundness		1µm

APPENDIX B5

Part 2

Breakdown of costs for high-speed Suprema confirmation trials using vitrified CBN to grind AISI 52100.

Factor description	Symbol	Suprema Confirmation Trial C1
Wheel purchase cost (£)	c_s	1700
Maximum wheel diameter (mm)	d_{smax}	250
Minimum wheel diameter (mm)	d_{smin}	240
Radial wheel wear (mm)	r_s	0.0015
Depth of dressing increment (mm)	a_d	0.002
Number of dressing passes	n_d	2
Re-dress life (number of parts per dress)	N_d	540
Wheel cost per part (£)	C_s	**0.0035**
Labour cost per hour (£)	c_l	75
Stock removed (mm)	$d_{ww}+d_{ss}$	0.2
Workpiece diameter (mm)	d_w	40
Specific volumetric removal rate ($mm^3/mm\ s$)	Q'_w	10
Dwell time (s)	s	10
Wheel width (mm)	b_s	17
Dressing feedrate (mm/s)	v_d	1.694
Labour cost per part (£)	C_l	**0.2615**
Machine purchase cost (£)	c_{mc}	250000
Pay back period (number of hours)	y_t	1920
Machine cost per part (£)	C_{mc}	**0.4539**
Total cost per part, i.e. C_s+C_l (£)	C_t	**0.2649**
Total cost per part including M/C cost, i.e $C_s+C_l+C_{mc}$ (£)	C'_t	**0.7189**
Other factors		
Machine tool used		J&S Suprema
Wheel manufacturer		Wendt
Wheel description		Vitrified CBN
Wheel specifcation		B91
Wheel speed	v_s	120m/s
Workpiece material		AISI52100
Target Ra		0.25µm
Target roundness		1µm

Factor description	Symbol	Suprema Confirmation Trial C2
Wheel purchase cost (£)	c_s	1700
Maximum wheel diameter (mm)	d_{smax}	250
Minimum wheel diameter (mm)	d_{smin}	240
Radial wheel wear (mm)	r_s	0.002
Depth of dressing increment (mm)	a_d	0.002
Number of dressing passes	n_d	2
Re-dress life (number of parts per dress)	N_d	540
Wheel cost per part (£)	C_s	**0.0038**
Labour cost per hour (£)	c_l	75
Stock removed (mm)	$d_{ww}+d_{ss}$	0.2
Workpiece diameter (mm)	d_w	40
Specific volumetric removal rate (mm^3/mm s)	Q'_w	10
Dwell time (s)	s	2
Wheel width (mm)	b_s	17
Dressing feedrate (mm/s)	v_d	1.694
Labour cost per part (£)	C_l	**0.0948**
Machine purchase cost (£)	c_{mc}	250000
Pay back period (number of hours)	y_t	1920
Machine cost per part (£)	C_{mc}	**0.1646**
Total cost per part, i.e. C_s+C_l (£)	C_t	**0.0986**
Total cost per part including M/C cost, i.e $C_s+C_l+C_{mc}$ (£)	C'_t	**0.2632**
Other factors		
Machine tool used		J&S Suprema
Wheel manufacturer		Wendt
Wheel description		Vitrified CBN
Wheel specifcation		B91
Wheel speed	v_s	120m/s
Workpiece material		AISI52100
Target Ra		0.25µm
Target roundness		1µm

Factor description	Symbol	Suprema Confirmation Trial C3
Wheel purchase cost (£)	c_s	1700
Maximum wheel diameter (mm)	d_{smax}	250
Minimum wheel diameter (mm)	d_{smin}	240
Radial wheel wear (mm)	r_s	0.003
Depth of dressing increment (mm)	a_d	0.002
Number of dressing passes	n_d	2
Re-dress life (number of parts per dress)	N_d	330
Wheel cost per part (£)	C_s	**0.0072**
Labour cost per hour (£)	c_l	75
Stock removed (mm)	$d_{ww}+d_{ss}$	0.2
Workpiece diameter (mm)	d_w	40
Specific volumetric removal rate (mm^3/mm s)	Q'_w	20
Dwell time (s)	s	2
Wheel width (mm)	b_s	17
Dressing feedrate (mm/s)	v_d	1.694
Labour cost per part (£)	C_l	**0.0691**
Machine purchase cost (£)	c_{mc}	250000
Pay back period (number of hours)	y_t	1920
Machine cost per part (£)	C_{mc}	**0.1200**
Total cost per part, i.e. C_s+C_l (£)	C_t	**0.0763**
Total cost per part including M/C cost, i.e C_s+C_l+C_{mc} (£)	C'_t	**0.1963**
Other factors		
Machine tool used		J&S Suprema
Wheel manufacturer		Wendt
Wheel description		Vitrified CBN
Wheel specifcation		B91
Wheel speed	v_s	120m/s
Workpiece material		AISI52100
Target Ra		0.25µm
Target roundness		1µm

Factor description	**Symbol**	**Suprema Confirmation Trial C4**
Wheel purchase cost (£)	c_s	1700
Maximum wheel diameter (mm)	d_{smax}	250
Minimum wheel diameter (mm)	d_{smin}	240
Radial wheel wear (mm)	r_s	0.007
Depth of dressing increment (mm)	a_d	0.002
Number of dressing passes	n_d	2
Re-dress life (number of parts per dress)	N_d	180
Wheel cost per part (£)	C_s	**0.0208**
Labour cost per hour (£)	c_l	75
Stock removed (mm)	$d_{ww}+d_{ss}$	0.2
Workpiece diameter (mm)	d_w	40
Specific volumetric removal rate (mm^3/mm s)	Q'_w	20
Dwell time (s)	s	2
Wheel width (mm)	b_s	17
Dressing feedrate (mm/s)	v_d	1.694
Labour cost per part (£)	C_l	**0.0702**
Machine purchase cost (£)	c_{mc}	250000
Pay back period (number of hours)	y_t	1920
Machine cost per part (£)	C_{mc}	**0.1218**
Total cost per part, i.e. C_s+C_l (£)	C_t	**0.0909**
Total cost per part including M/C cost, i.e $C_s+C_l+C_{mc}$ (£)	C'_t	**0.2128**
Other factors		
Machine tool used		J&S Suprema
Wheel manufacturer		Wendt
Wheel description		Vitrified CBN
Wheel specifcation		B91
Wheel speed	v_s	120m/s
Workpiece material		AISI52101
Target Ra		0.25µm
Target roundness		1µm

APPENDIX B5

Part 3

Breakdown of costs for conventional-speed Series 10 benchmark trials using aluminium oxide, sol gel and a CBN wheel to grind AISI 52100.

Factor description	Symbol	Series 10 Benchmark Grinding Trial
M/C & Wheel Combination		Series 10 - A465 K5V
Wheel purchase cost (£)	c_s	200
Maximum wheel diameter (mm)	d_{smax}	450
Minimum wheel diameter (mm)	d_{smin}	350
Radial wheel wear (mm)	r_s	0.012
Depth of dressing increment (mm)	a_d	0.01
Number of dressing passes	n_d	2
Re-dress life (number of parts per dress)	N_d	35
Wheel cost per part (£)	C_s	**0.0037**
Labour cost per hour (£)	c_l	75
Stock removed (mm)	$d_{ww}+d_{ss}$	0.2
Workpiece diameter (mm)	d_w	40
Specific volumetric removal rate (mm^3/mm s)	Q'_w	1
Dwell time (s)	s	10
Wheel width (mm)	b_s	25
Dressing feedrate (mm/s)	v_d	3.18
Labour cost per part (£)	C_l	**0.7413**
Machine purchase cost (£)	c_{mc}	100000
Pay back period (number of hours)	y_t	1920
Machine cost per part (£)	C_{mc}	**0.5148**
Total cost per part, i.e. C_s+C_l (£)	C_t	**0.7449**
Total cost per part including M/C cost, i.e. $C_s+C_l+C_{mc}$ (£)	C'_t	**1.2597**
Other information		
Machine tool used		J&S Series 10
Wheel manufacturer		Carborundum
Wheel description		Aluminium oxide
Wheel specifcation		A465 K5V30W
Wheel speed	v_s	42.4m/s
Workpiece material		AISI 52100
Target Ra		0.25µm
Target roundness		1µm

Factor description	**Symbol**	**Series 10 Benchmark Grinding Trial**
M/C & Wheel Combination		Series10 - WA801 J6V
Wheel purchase cost (£)	c_s	200
Maximum wheel diameter (mm)	d_{smax}	450
Minimum wheel diameter (mm)	d_{smin}	350
Radial wheel wear (mm)	r_s	0.006
Depth of dressing increment (mm)	a_d	0.01
Number of dressing passes	n_d	2
Re-dress life (number of parts per dress)	N_d	75
Wheel cost per part (£)	C_s	**0.0014**
Labour cost per hour (£)	c_l	75
Stock removed (mm)	$d_{ww}+d_{ss}$	0.2
Workpiece diameter (mm)	d_w	40
Specific volumetric removal rate (mm^3/mm s)	Q'_w	1
Dwell time (s)	s	10
Wheel width (mm)	b_s	25
Dressing feedrate (mm/s)	v_d	3.18
Labour cost per part (£)	C_l	**0.7363**
Machine purchase cost (£)	c_{mc}	100000
Pay back period (number of hours)	y_t	1920
Machine cost per part (£)	C_{mc}	**0.5113**
Total cost per part, i.e. C_s+C_l (£)	C_t	**0.7377**
Total cost per part including M/C cost, i.e. $C_s+C_l+C_{mc}$ (£)	C'_t	**1.2490**
Other information		
Machine tool used		J&S Series 10
Wheel manufacturer		Universal
Wheel description		Aluminium oxide
Wheel specifcation		WA801 J6V MRAA
Wheel speed	v_s	43m/s
Workpiece material		AISI 52100
Target Ra		0.25μm
Target roundness		1μm

Factor description	**Symbol**	**Series 10 Benchmark Grinding Trial**
M/C & Wheel Combination		Series 10 - 73A 601 J8V
Wheel purchase cost (£)	c_s	320
Maximum wheel diameter (mm)	d_{smax}	450
Minimum wheel diameter (mm)	d_{smin}	350
Radial wheel wear (mm)	r_s	0.01
Depth of dressing increment (mm)	a_d	0.01
Number of dressing passes	n_d	2
Re-dress life (number of parts per dress)	N_d	25
Wheel cost per part (£)	C_s	**0.0077**
Labour cost per hour (£)	c_l	75
Stock removed (mm)	$d_{ww}+d_{ss}$	0.2
Workpiece diameter (mm)	d_w	40
Specific volumetric removal rate (mm^3/mm s)	Q'_w	2.5
Dwell time (s)	s	10
Wheel width (mm)	b_s	25
Dressing feedrate (mm/s)	v_d	3.18
Labour cost per part (£)	C_l	**0.4309**
Machine purchase cost (£)	c_{mc}	100000
Pay back period (number of hours)	y_t	1920
Machine cost per part (£)	C_{mc}	**0.2992**
Total cost per part, i.e. C_s+C_l (£)	C_t	**0.4386**
Total cost per part including M/C cost, i.e. C_s+C_l+C_{mc} (£)	C'_t	**0.7378**
Other information		
Machine tool used		J&S Series 10
Wheel manufacturer		Univerasl
Wheel description		Sol Gel
Wheel specifcation		73A 601 J8V LRAA
Wheel speed	v_s	45m/s
Workpiece material		AISI 52100
Target Ra		0.25µm
Target roundness		1µm

Factor description	Symbol	Series 10 Benchmark Grinding Trial
M/C & Wheel Combination		Series 10 - Vit. CBN B91
Wheel purchase cost (£)	c_s	3000
Maximum wheel diameter (mm)	d_{smax}	450
Minimum wheel diameter (mm)	d_{smin}	438
Radial wheel wear (mm)	r_s	0.002
Depth of dressing increment (mm)	a_d	0.002
Number of dressing passes	n_d	2
Re-dress life (number of parts per dress)	N_d	75
Wheel cost per part (£)	C_s	**0.0400**
Labour cost per hour (£)	c_l	75
Stock removed (mm)	$d_{ww}+d_{ss}$	0.2
Workpiece diameter (mm)	d_w	40
Specific volumetric removal rate (mm^3/mm s)	Q'_w	4
Dwell time (s)	s	10
Wheel width (mm)	b_s	25
Dressing feedrate (mm/s)	v_d	3.18
Labour cost per part (£)	C_l	**0.3436**
Machine purchase cost (£)	c_{mc}	100000
Pay back period (number of hours)	y_t	1920
Machine cost per part (£)	C_{mc}	**0.2386**
Total cost per part, i.e. C_s+C_l (£)	C_t	**0.3836**
Total cost per part including M/C cost, i.e. $C_s+C_l+C_{mc}$ (£)	C'_t	**0.6222**
Other information		
Machine tool used		J&S Series 10
Wheel manufacturer		Saint Gobain
Wheel description		Vitrified CBN
Wheel specifcation		B91 ABN500
Wheel speed	v_s	45m/s
Workpiece material		AISI 52100
Target Ra		0.25µm
Target roundness		1µm

APPENDIX C

Supplementary graphs for Chapter 7 showing results of confirmation trials for grinding Inconel 718

Figure C1. Results of high-speed CBN (Wendt wheel B151 VR150J) confirmation trials on the Suprema for specific energy, surface roughness, roundness and size holding.

Figure C2. Results of conventional-speed CBN (Wendt wheel B151 VR150J) confirmation trials on the Series 10 machine for specific energy, surface roughness, roundness and size holding.

Figure C3. Results of conventional-speed Al_2O_3 (Winterthur wheel 53A180 L13VPMF) confirmation trials on the Series 10 machine for specific energy, surface roughness, roundness and size holding.

Figure C4. Results of conventional-speed Al_2O_3 (Winterthur wheel 53A80 L15VPMF) confirmation trials on the Series 10 machine for specific energy, surface roughness, roundness and size holding.

Figure C5. Results of conventional-speed Al_2O_3 (Universal wheel WA801 J6VMRAA) confirmation trials on the Series 10 machine for specific energy, surface roughness, roundness and size holding.

Figure C1. Results of Confirmation Trials for grinding Inconel 718 on the Suprema using a vitrified CBN wheel.

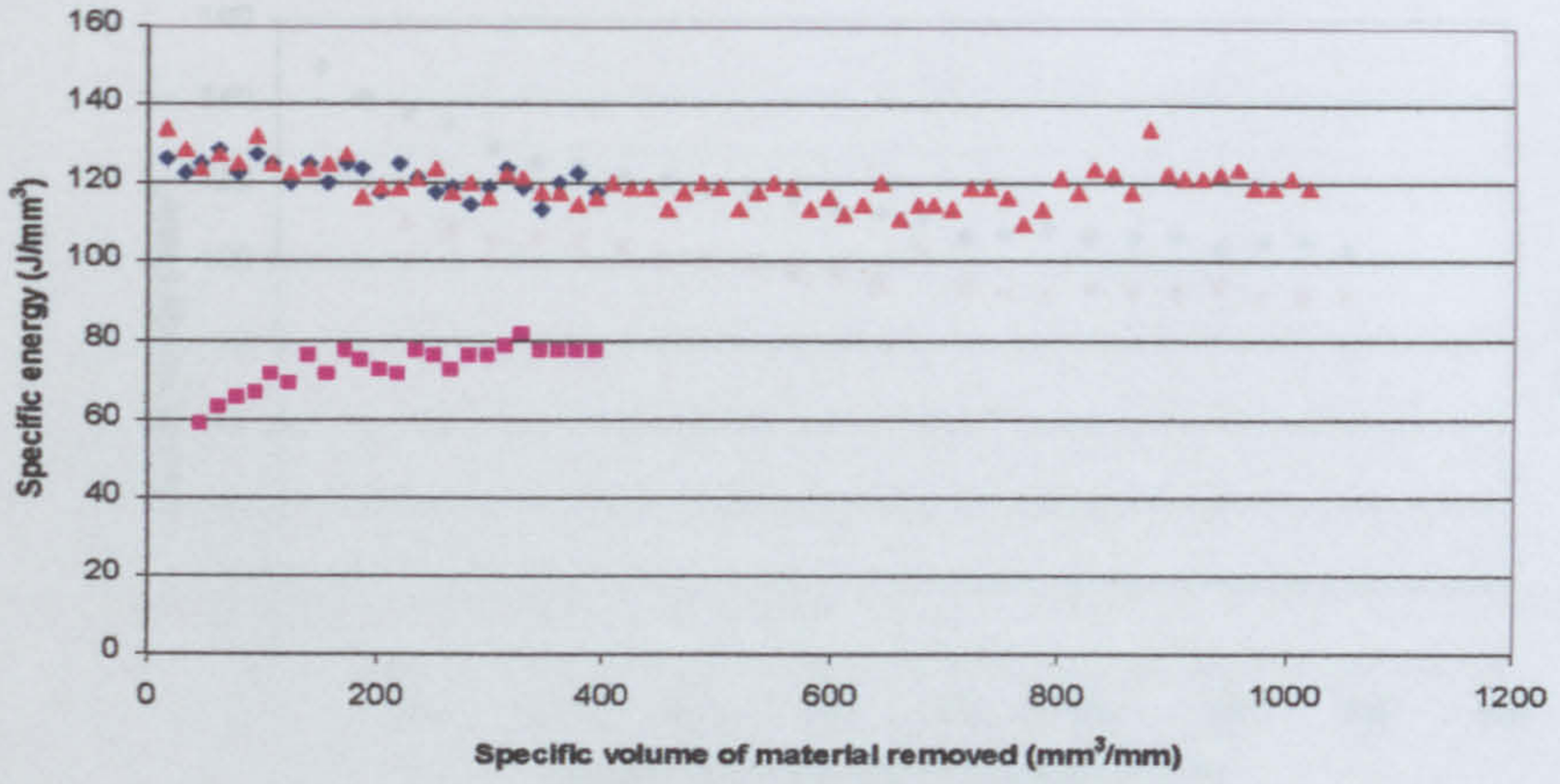

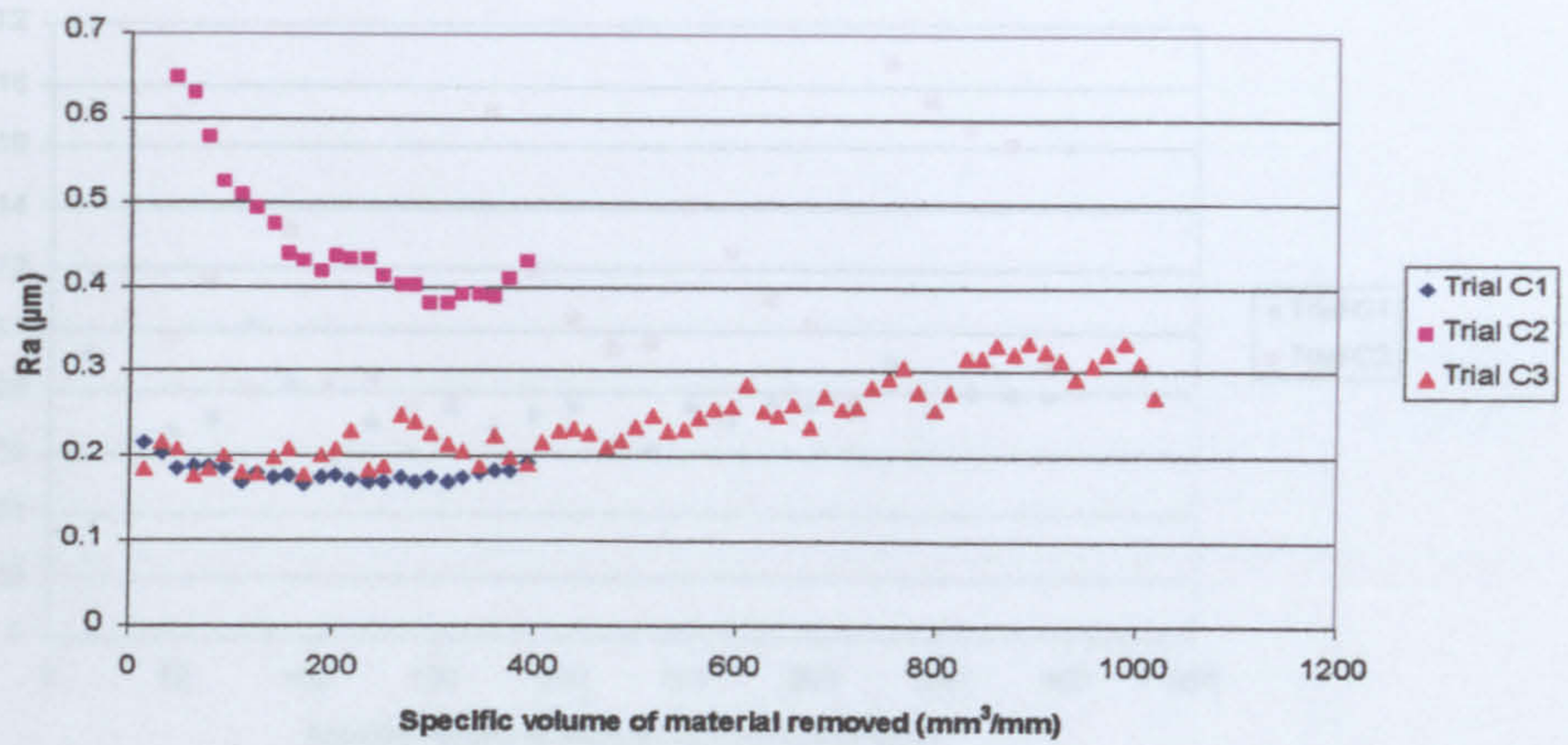

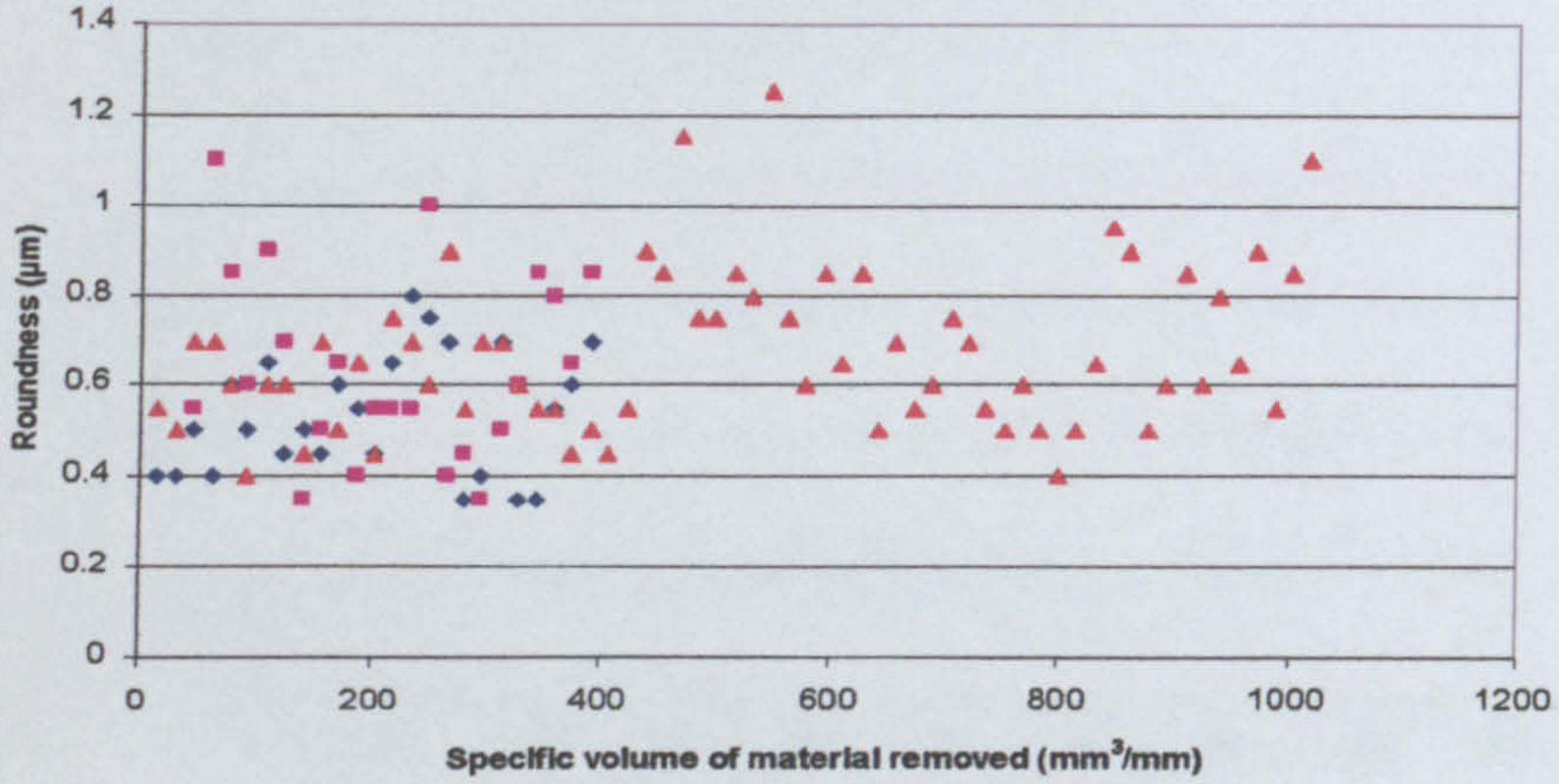

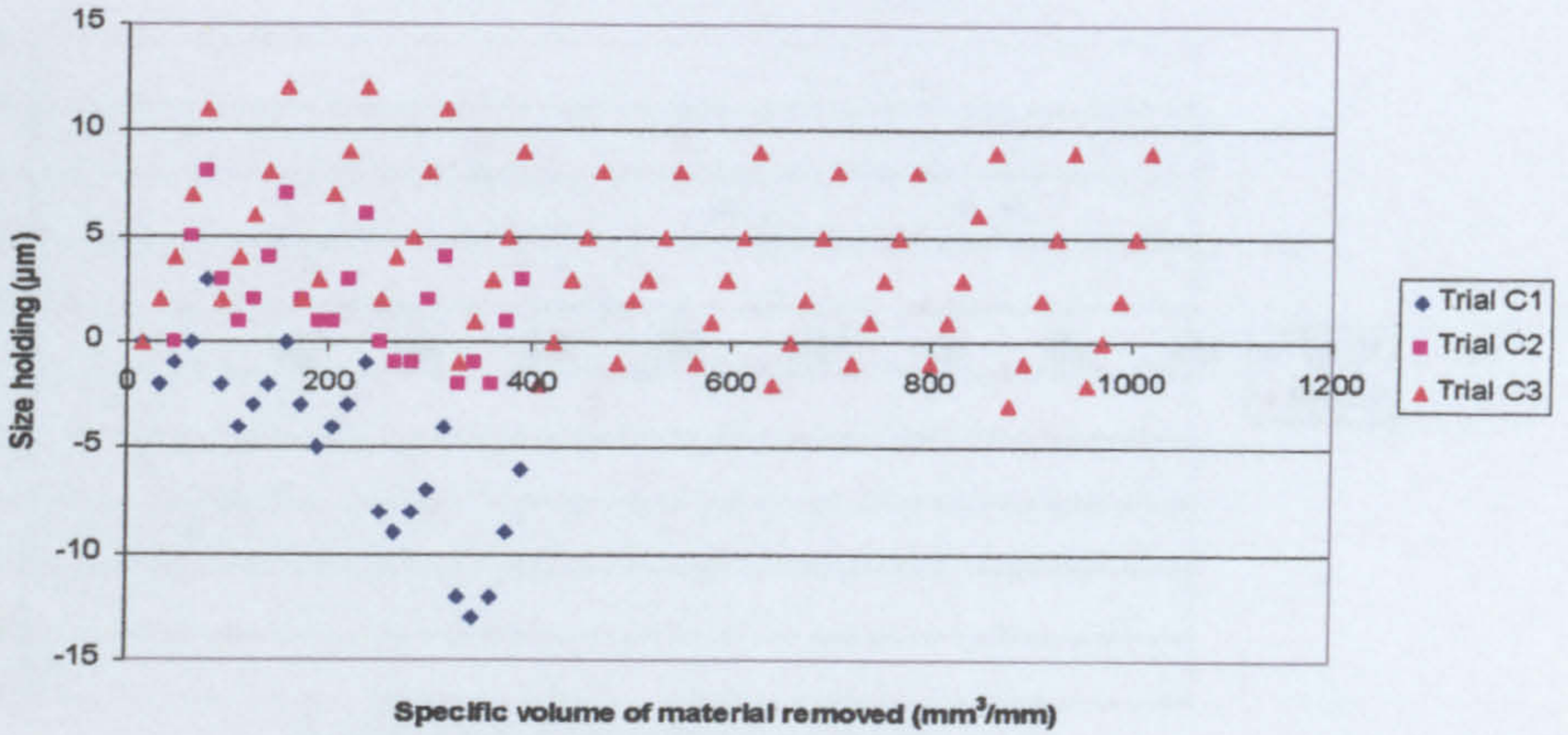

	Dressing Direction	Dressing Overlap	Dressing Increment	No. of Dressing Passes	Wheel Speed	Workspeed	Dwell	Removal Rate
Trial C1:	Up	2	2µm	10	120m/s	36m/min	10s	2mm³/mm s
Trial C2:	Down	2	10µm	2	120m/s	36m/min	10s	2mm³/mm s
Trial C3:	Up	2	2µm	10	120m/s	36m/min	2s	2mm³/mm s

Figure C2. Results of Confirmation Trials for grinding Inconel 718 on the Series 10 using a vitrified CBN wheel.

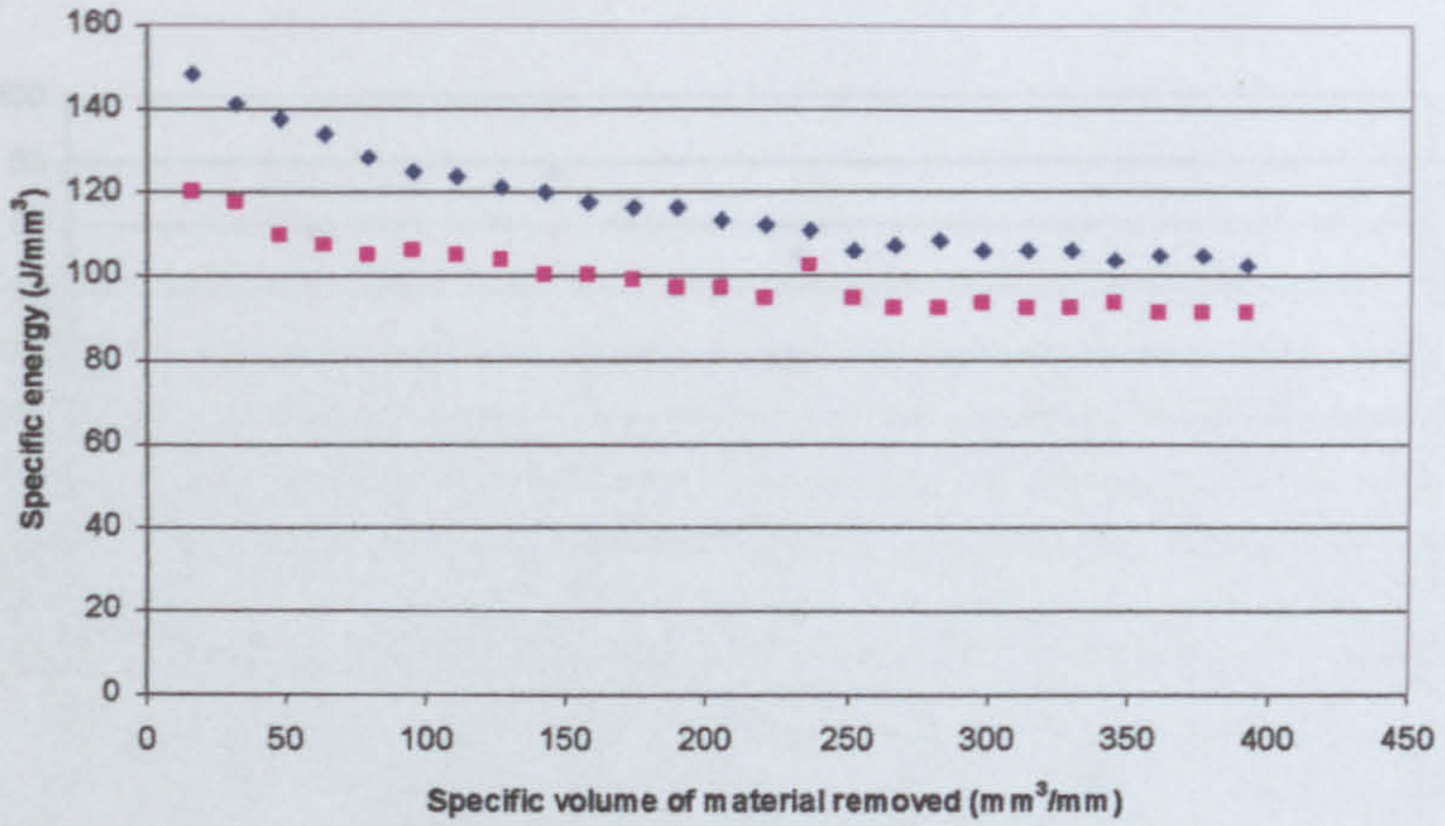

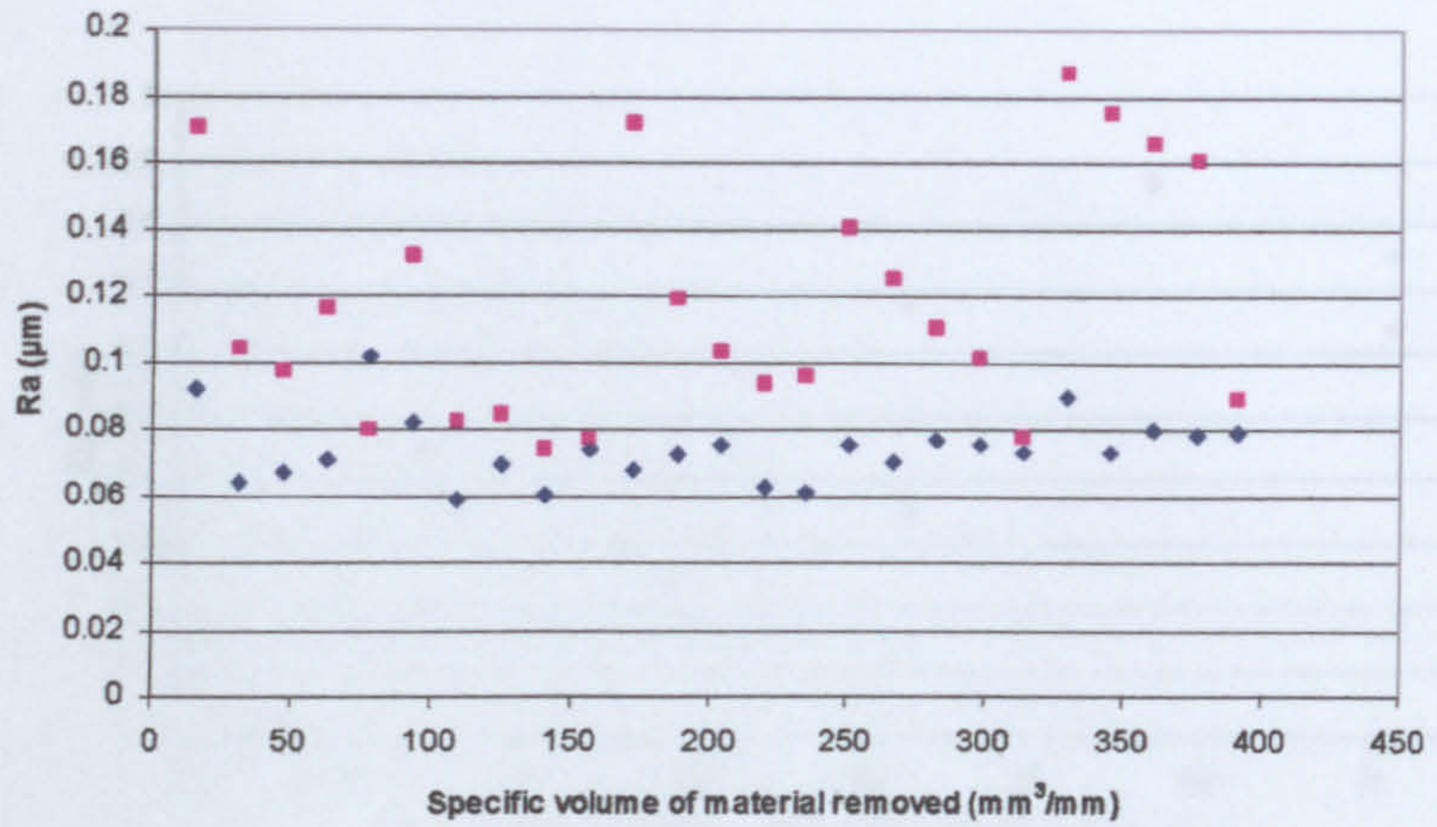

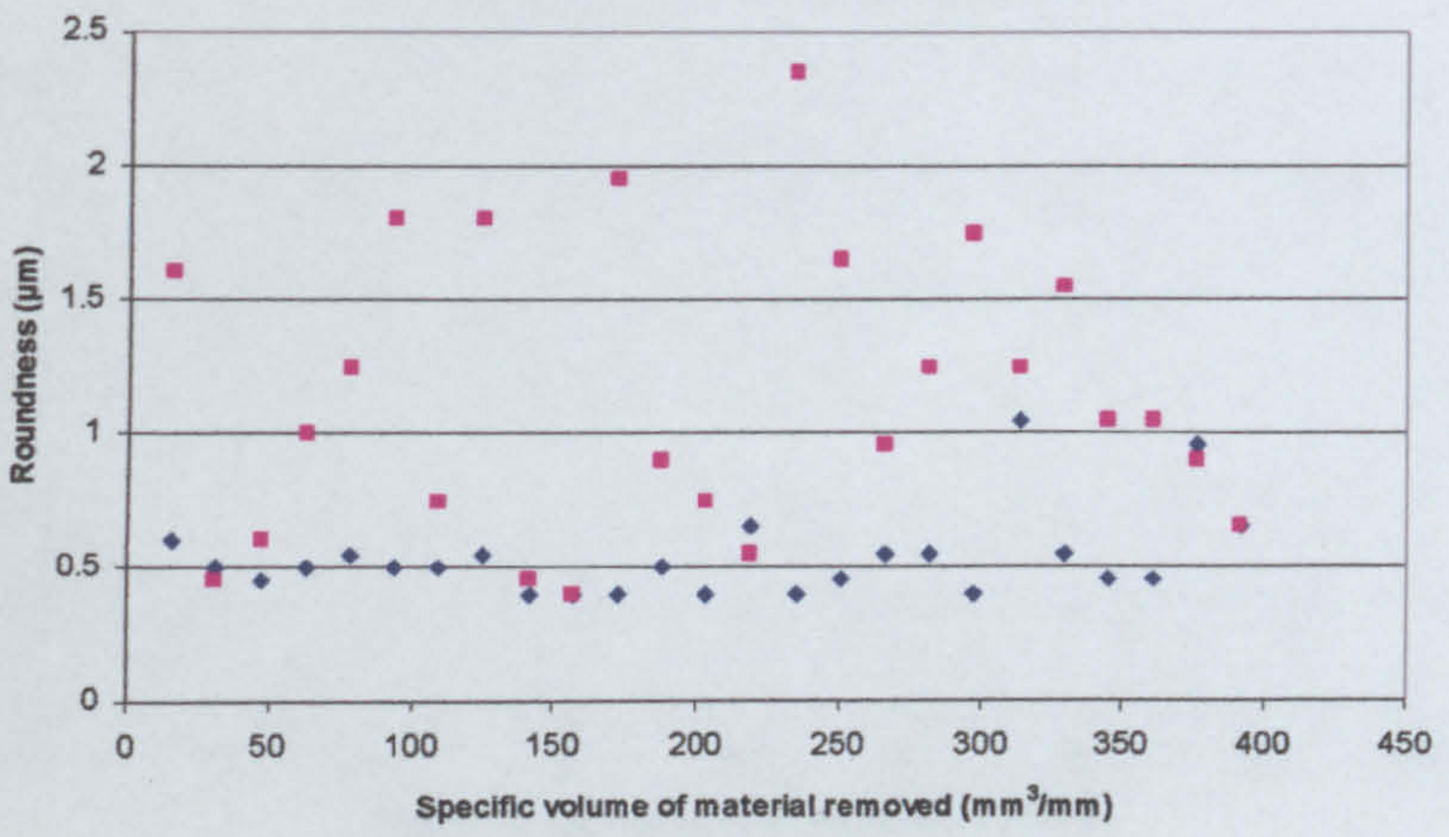

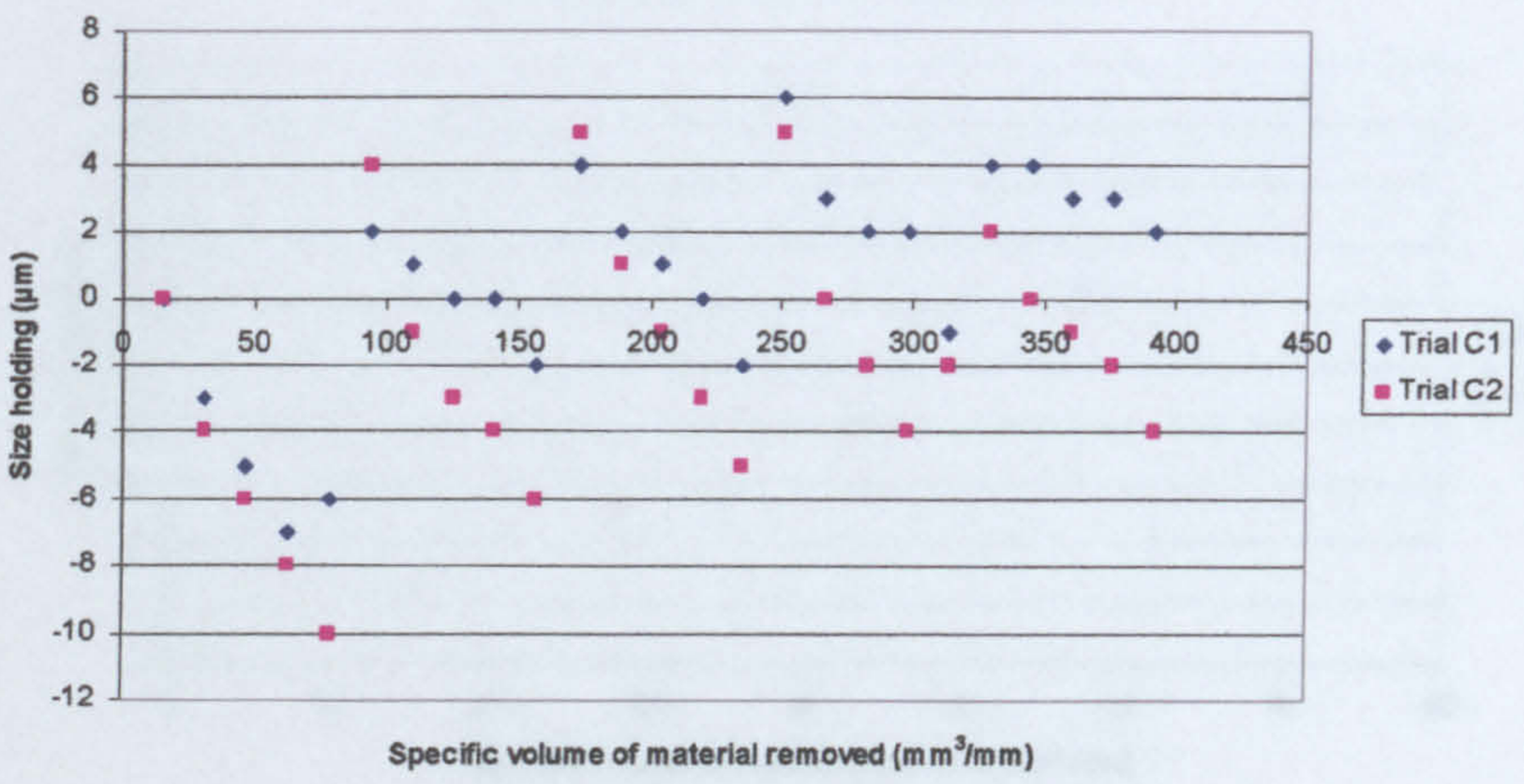

	Dressing Direction	Dressing Overlap	Dressing Increment	No. of Dressing Passes	Wheel Speed	Workspeed	Dwell	Removal Rate
Trial C1:	Up	10	2µm	2	45m/s	20m/min	10s	2mm³/mm s
Trial C2:	Down	2	10µm	2	45m/s	10m/min	2s	2mm³/mm s

Figure C3. Results of Confirmation Trials for grinding Inconel 718 on the Series 10 using a Winterthur 53A180 L13VPMF wheel.

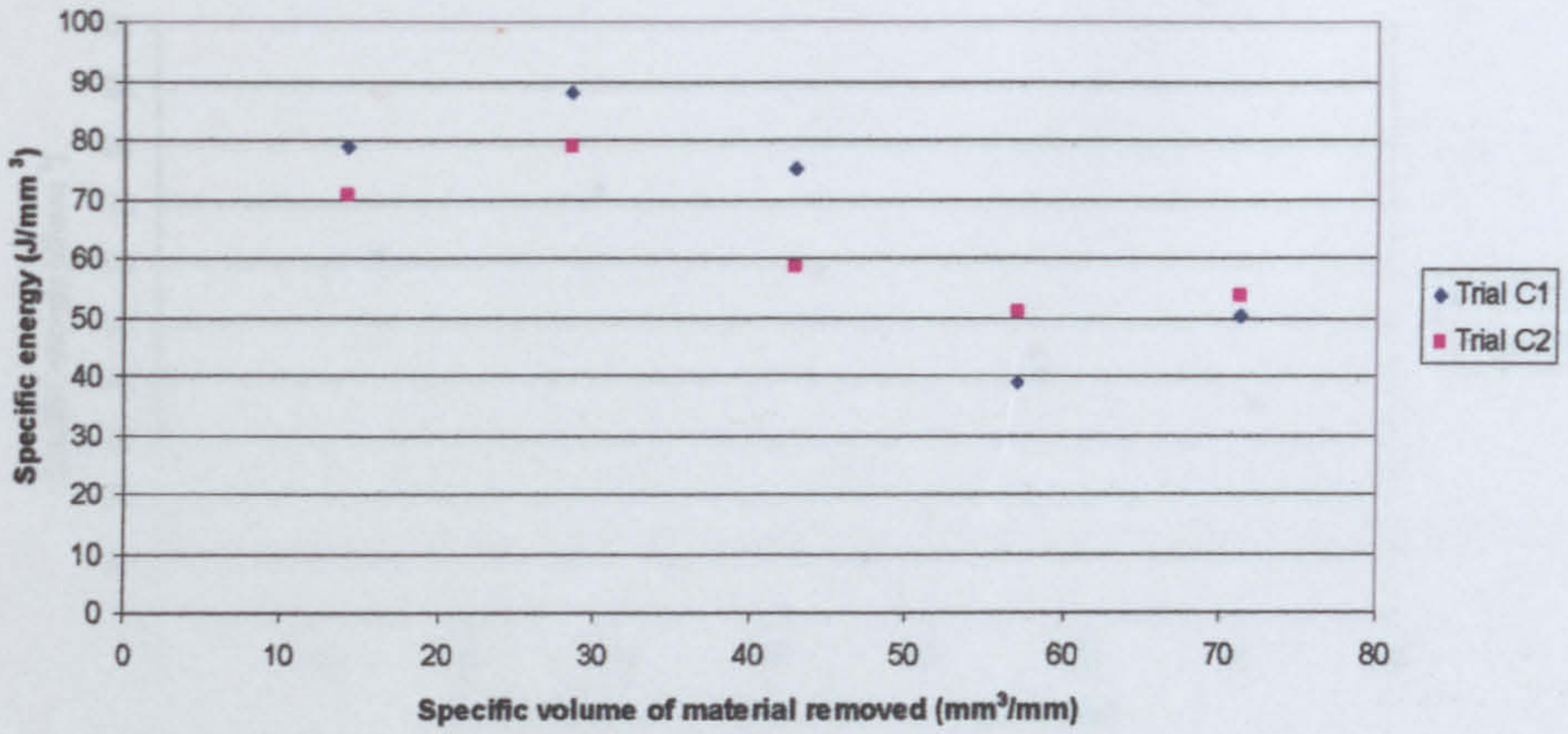

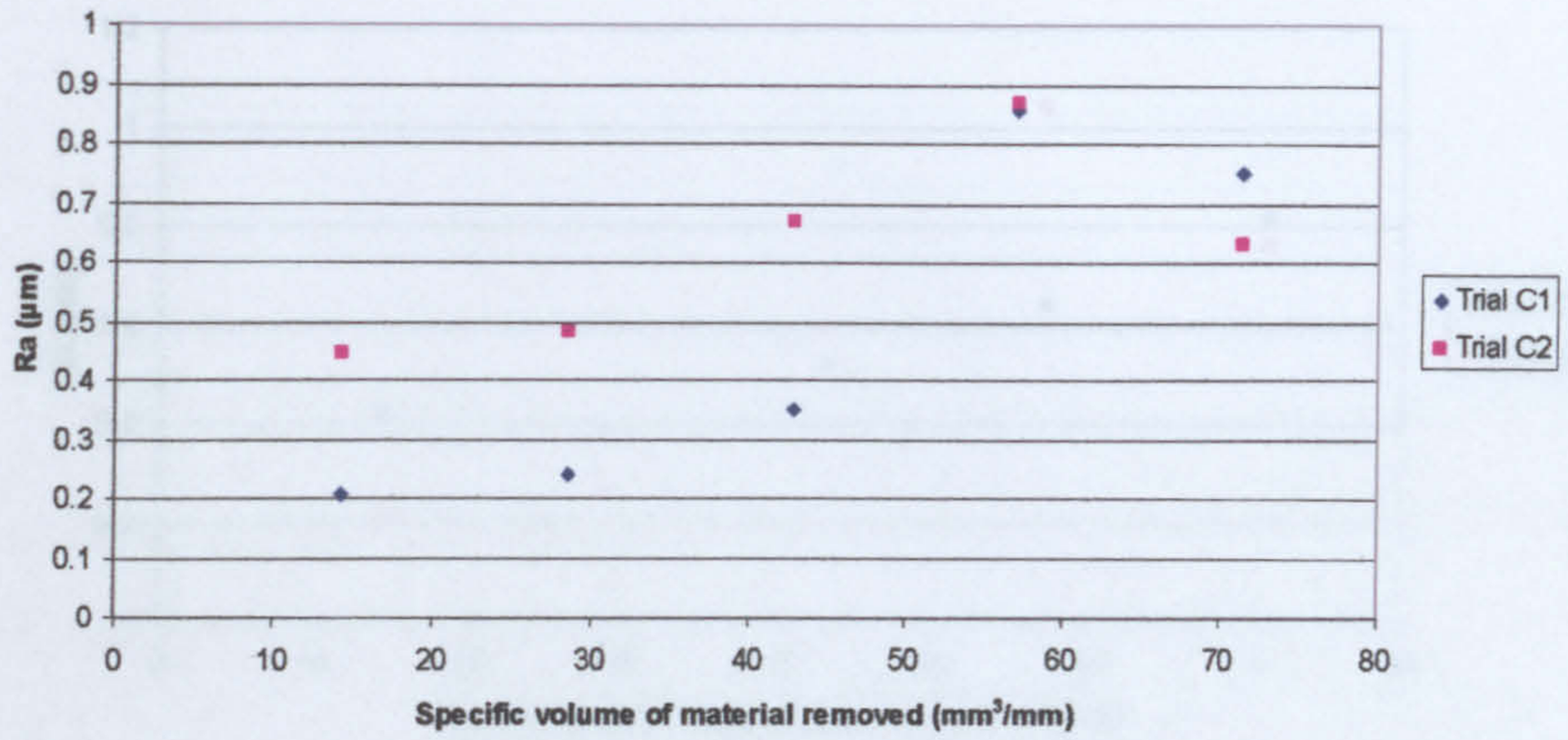

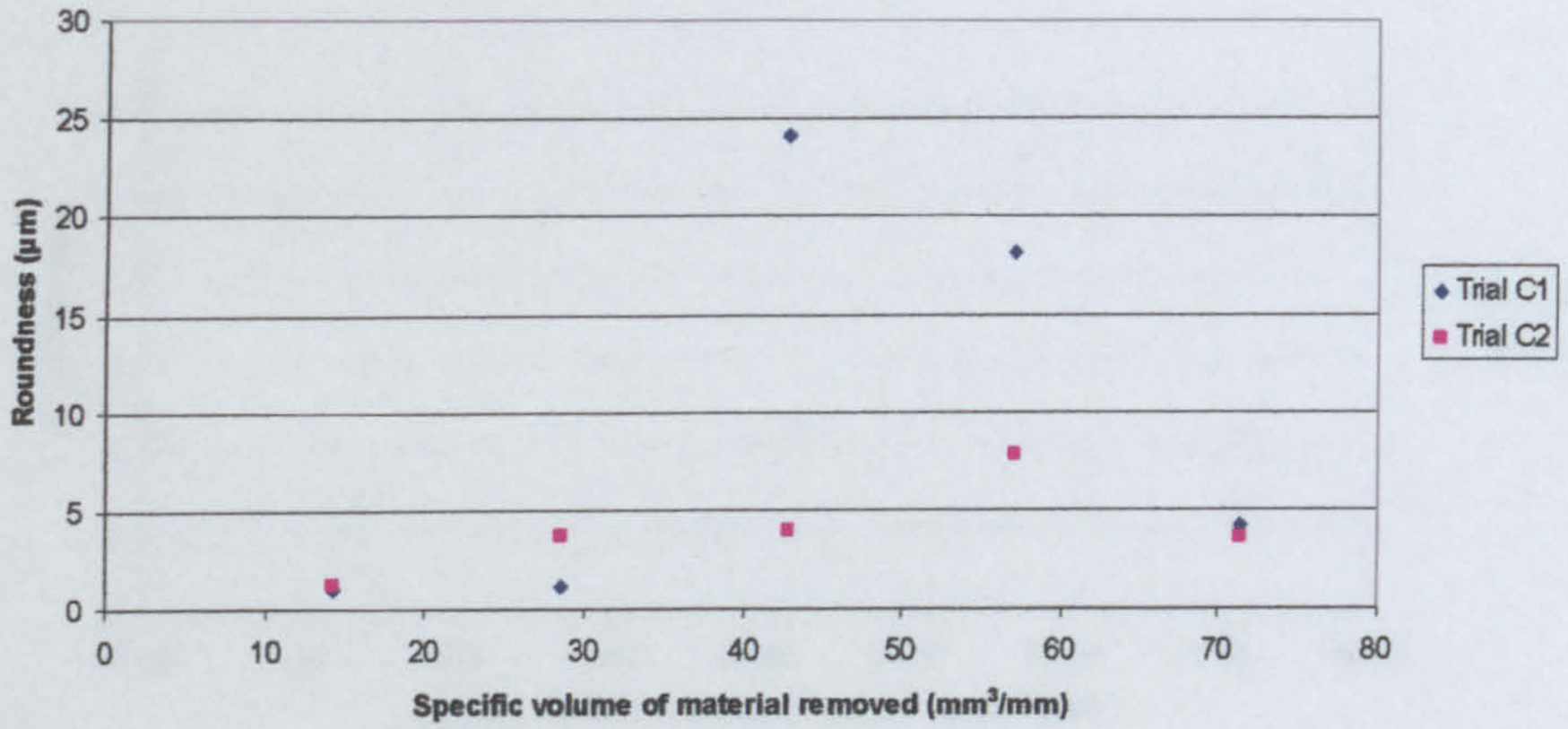

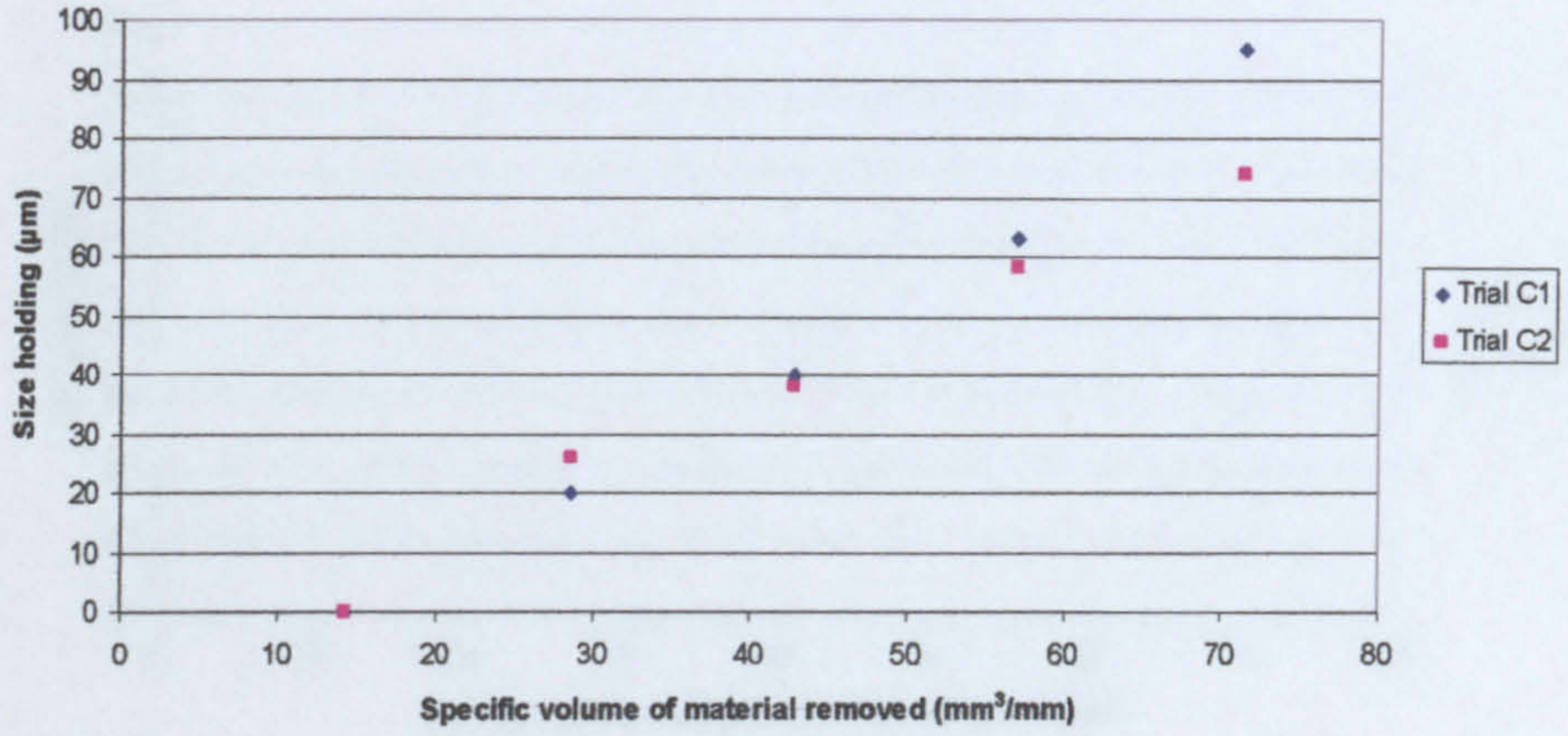

	Dressing Tool	Dressing Lead	Dressing Increment	No. of Dressing Passes	Wheel Speed	Workspeed	Dwell	Removal Rate
Trial C1:	single point diamond	0.05mm/rev	24µm	10	33m/s	10m/min	10s	2mm³/mm s
Trial C2:	single point diamond	0.3mm/rev	24µm	2	45m/s	10m/min	10s	2mm³/mm s

Figure C4. Results of Confirmation Trials for grinding Inconel 718 on the Series 10 using a Winterthur 53A80 L15VPMF wheel.

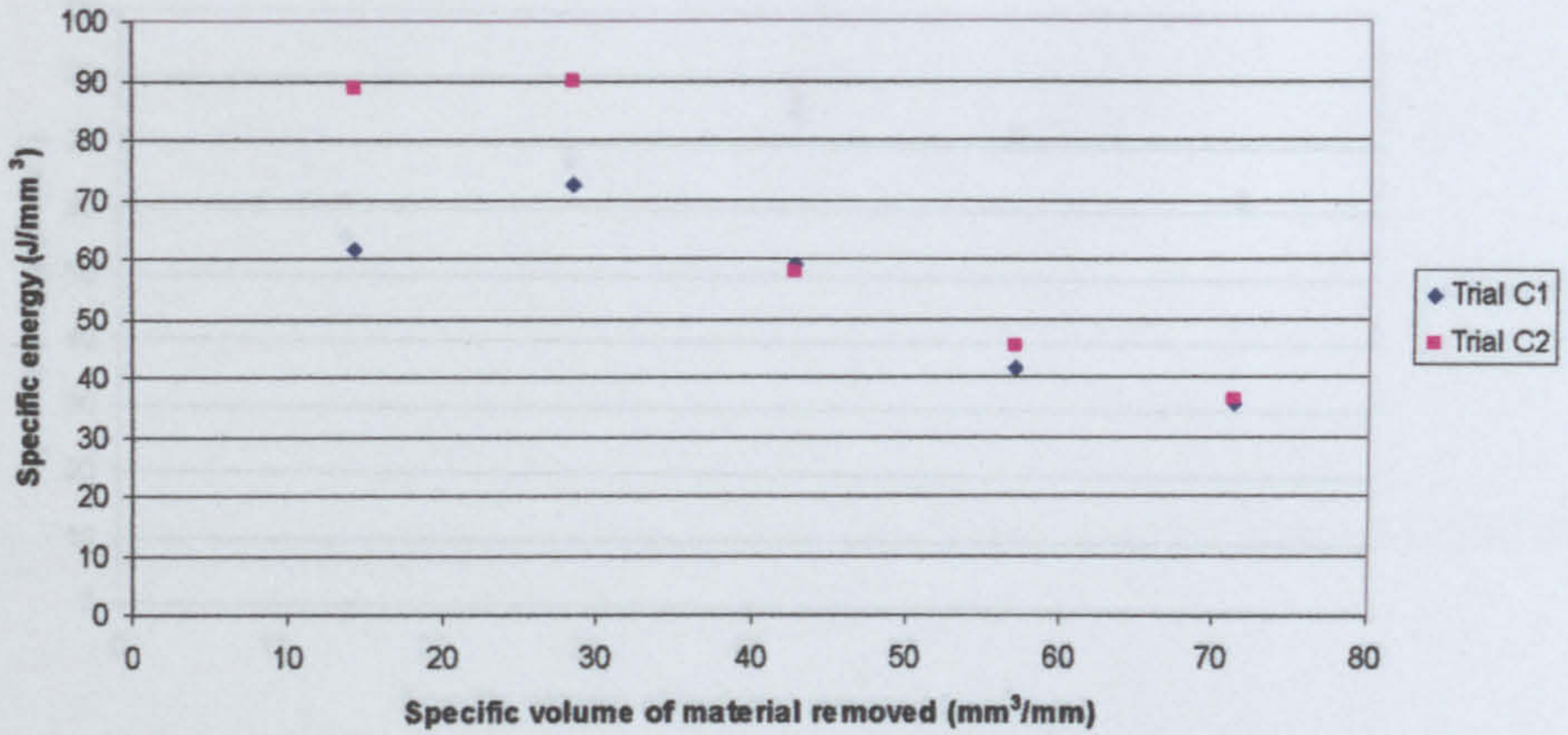

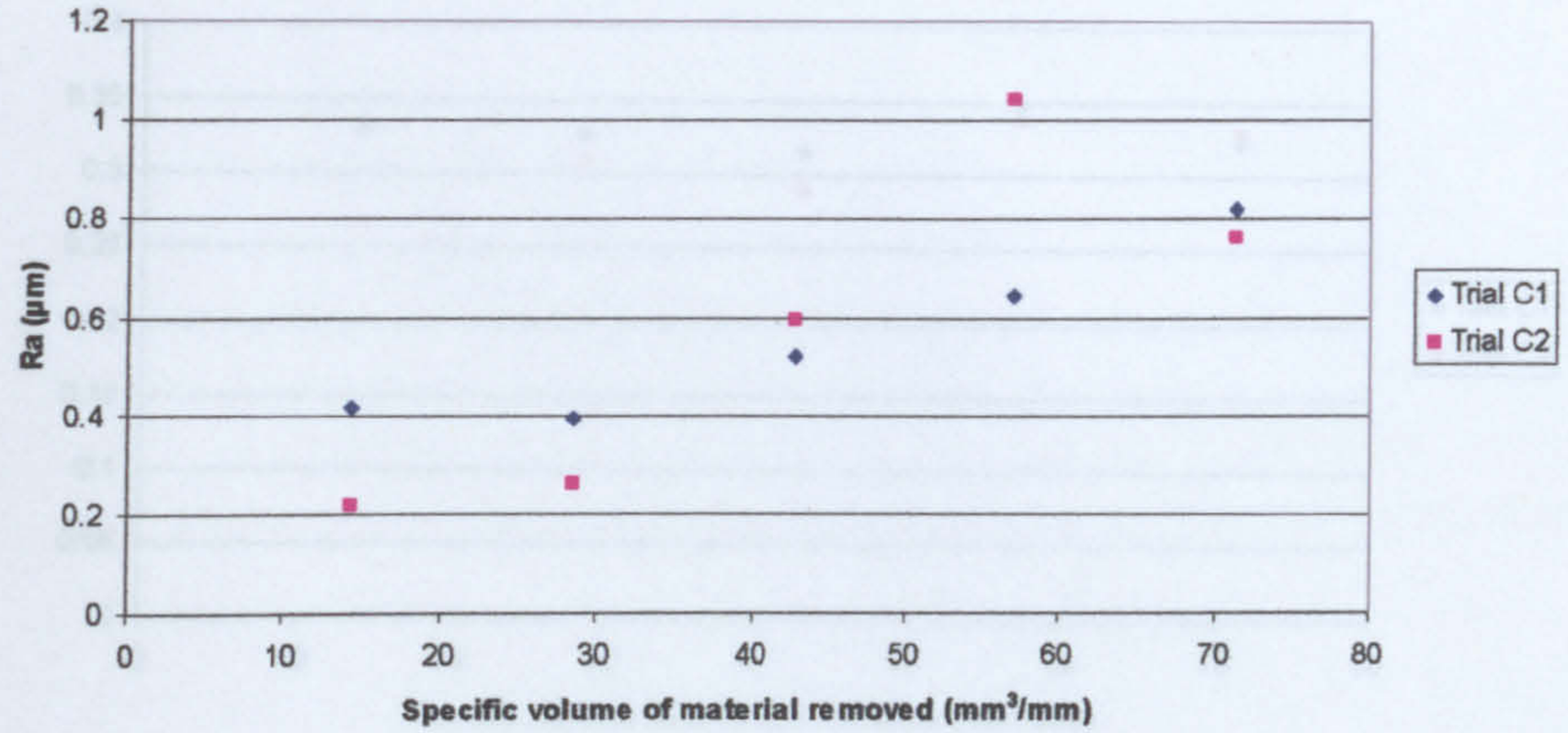

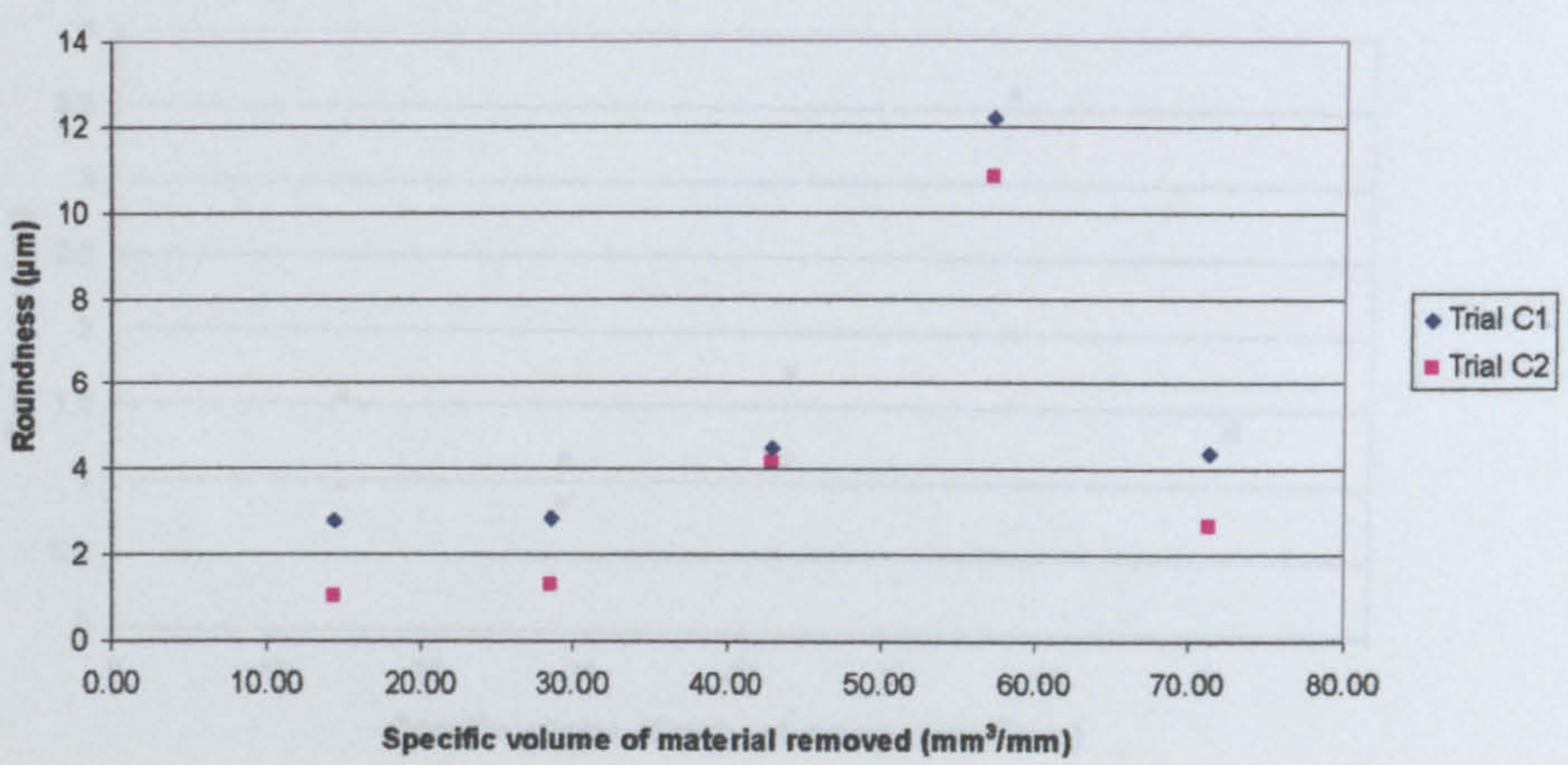

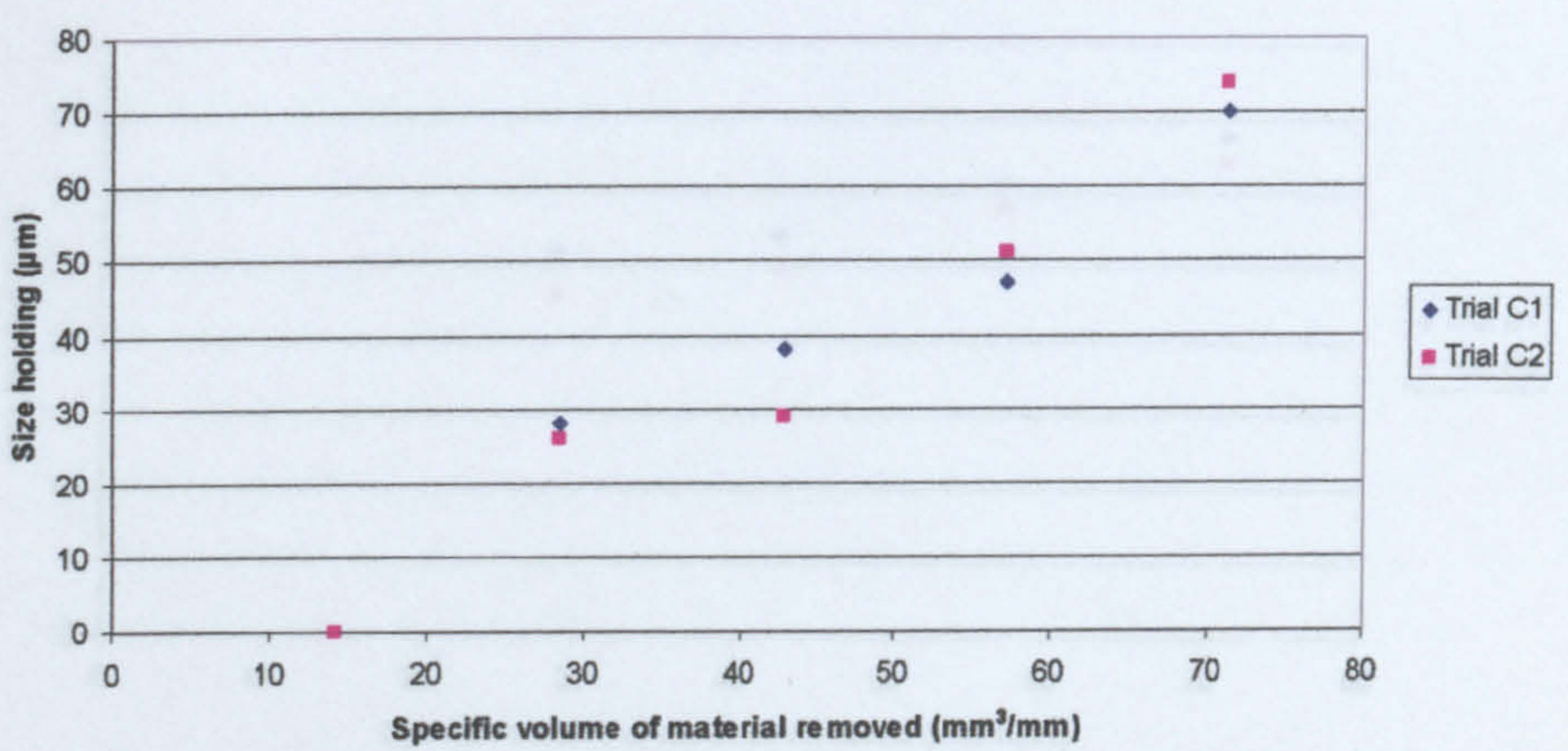

	Dressing Tool	Dressing Lead	Dressing Increment	No. of Dressing Passes	Wheel Speed	Workspeed	Dwell	Removal Rate
Trial C1:	chisel edge diamond	0.3mm/rev	24µm	2	45m/s	20m/min	10s	2mm³/mm s
Trial C2:	chisel edge diamond	0.05mm/rev	24µm	10	45m/s	20m/min	10s	2mm³/mm s

Figure C5. Results of Confirmation Trials for grinding Inconel 718 on the Series 10 using a Universal WA801 J6VMRAA wheel.

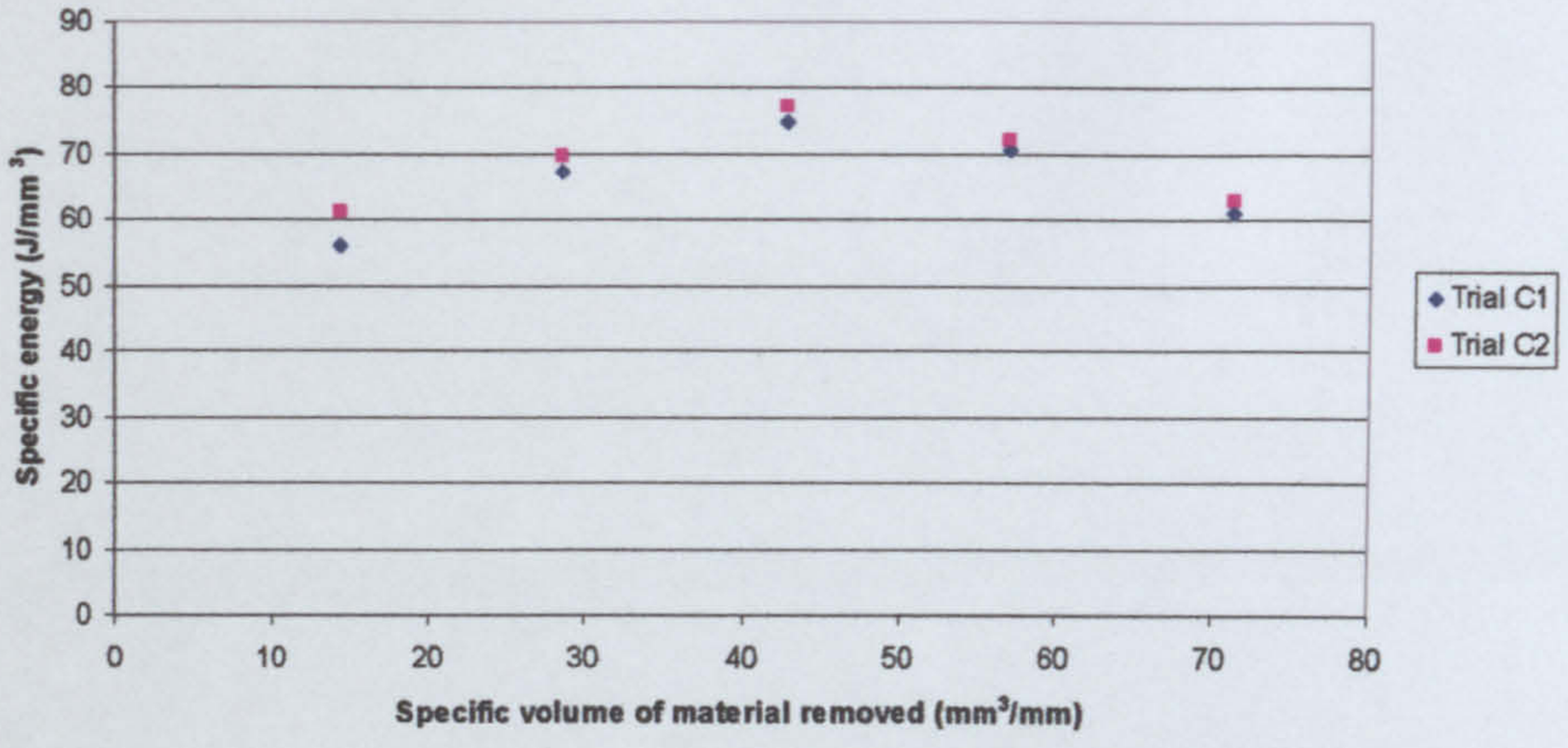

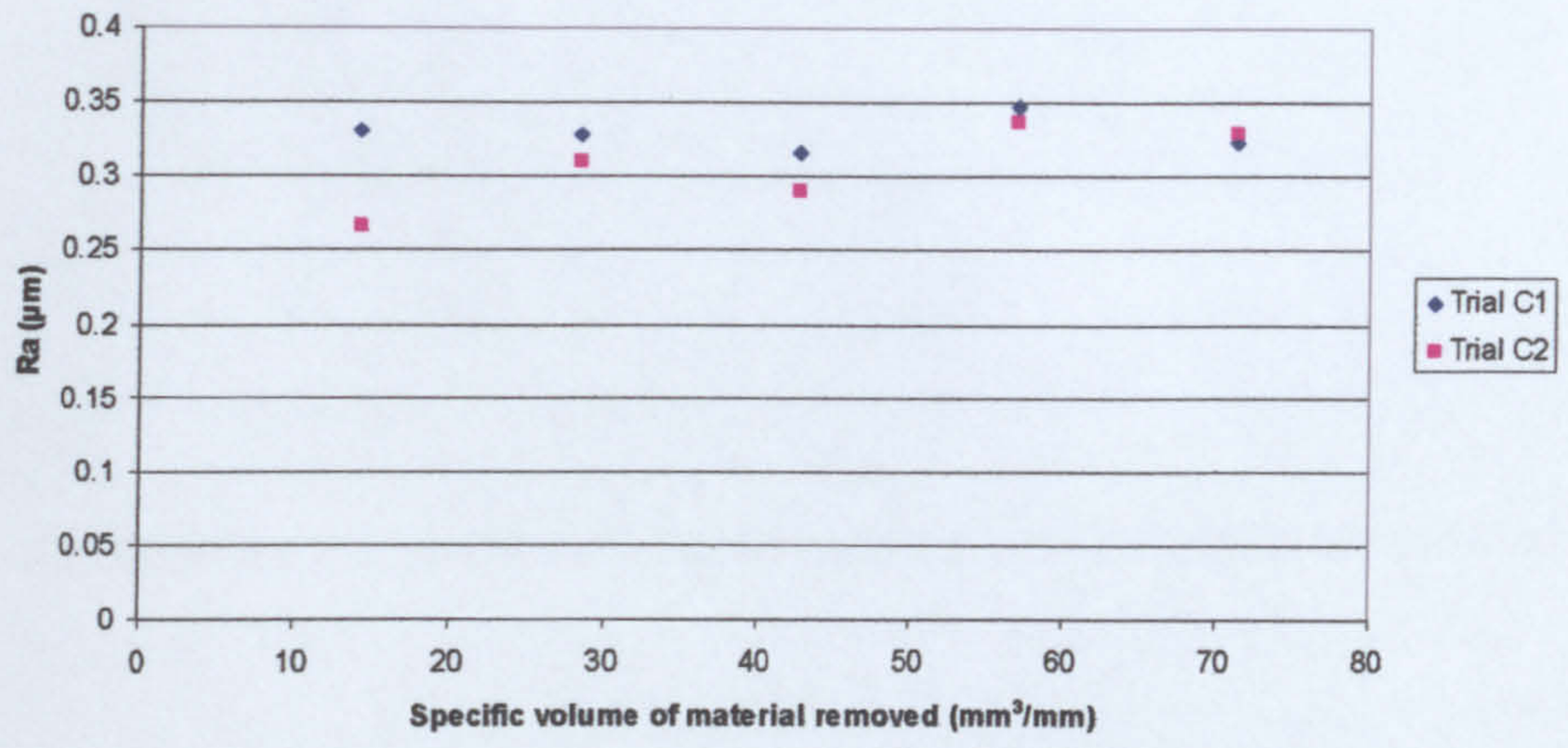

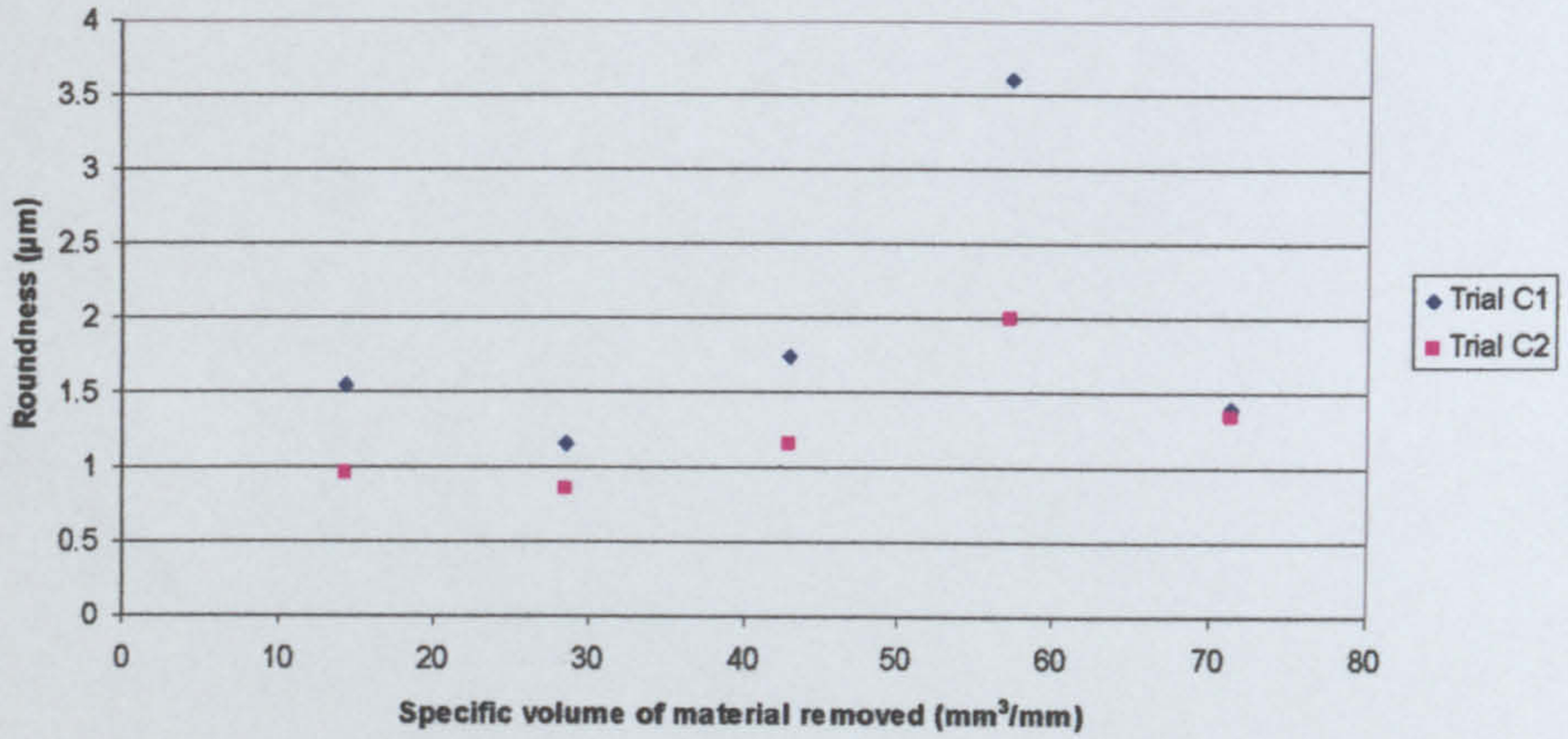

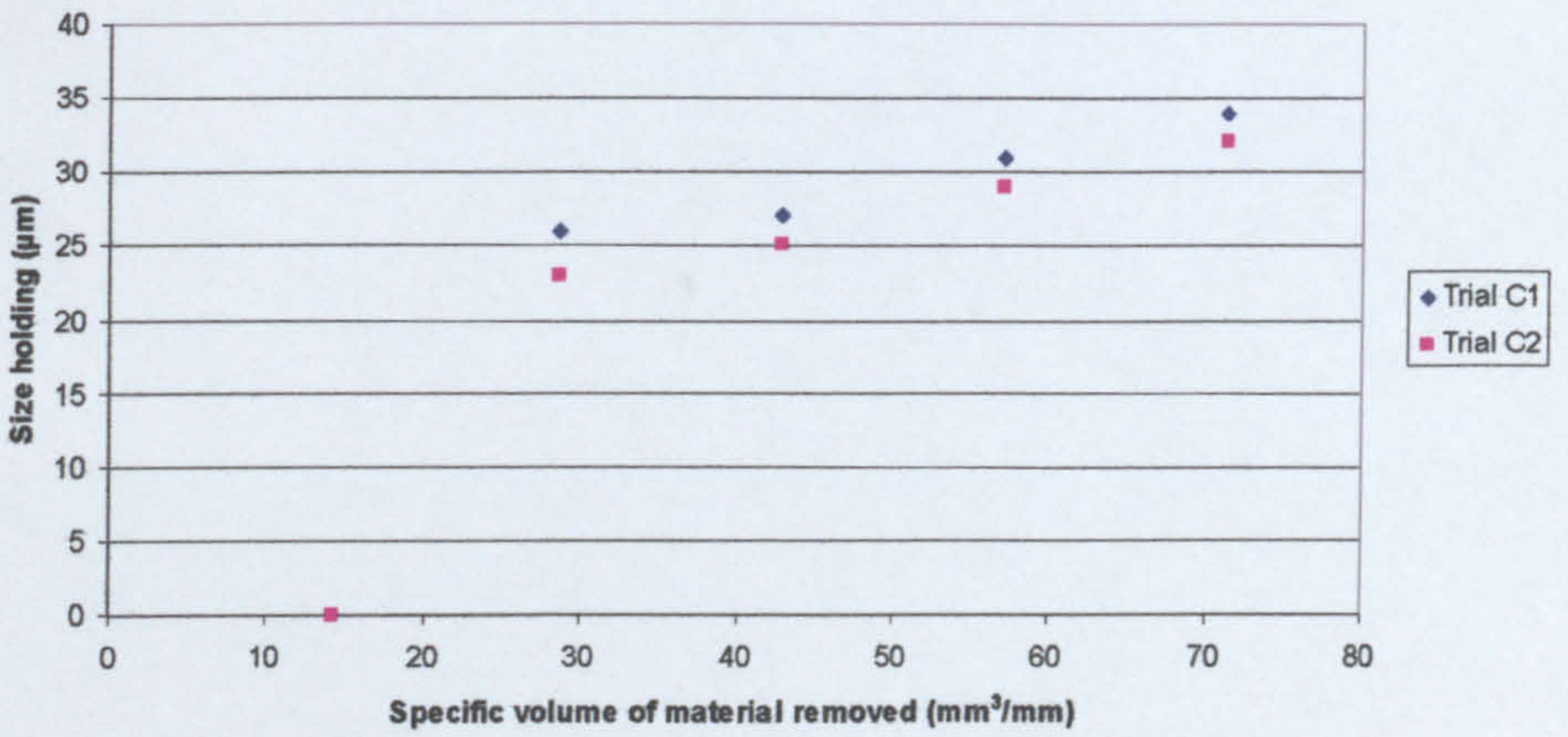

	Dressing Tool	Dressing Lead	Dressing Increment	No. of Dressing Passes	Wheel Speed	Workspeed	Dwell	Removal Rate
Trial C1:	single point diamond	0.3mm/rev	4µm	2	33m/s	20m/min	10s	2mm³/mm s
Trial C2:	single point diamond	0.05mm/rev	24µm	2	33m/s	20m/min	10s	2mm³/mm s